19th Science Council of Asia Conference(2019), Special Issue 2020

Science Council of Asia

19th Science Council of Asia Conference
3-5 December, 2019, Nay Pyi Taw

RESEARCH AND INNOVATION FOR SUSTAINABLE DEVELOPMENT IN ASIA

SUB-THEME I
Revitalize Asian Partnership for Achieving Sustainable Development

Journal of the
Myanmar Academy of Arts and Science
ISSN 2520-0186, LCCN 2003-323143

Special Issue
2020

Journal of the
Myanmar Academy of Arts and Science
ISSN 2520-0186, LCCN 2003-323143

Special Issue
2020

19th Science Council of Asia Conference

3-5 December, 2019, Nay Pyi Taw

SUB-THEME Ⅰ

Revitalize Asian Partnership for Achieving Sustainable Development

Journal of the
Myanmar Academy of Arts and Science **Special Issue**
ISSN 2520-0186 **2020**

Edition

2020, 400 Copies

Published by

Dr Aung Min (00322) Chairman, Journal Publication Committee,
Myanmar Academy of Arts and Science

ISSN 2520-0186
ICCN 2003-323143

Printed by

U Win Aung (00171), Manager
Universities Press, Yangon, Myanmar

FOREWORD

We would like to thank His Excellency Dr. Myo Thein Gyi, Hon'ble Union Minister for Education, for delivering the inaugural address at the Opening Ceremony of the 19th Science Council of Asia Conference, and for the support His Excellency had given for holding this international conference, for the first time, in Myanmar. We are also indebted to express our heartfelt gratitude to His Excellency Dr Wang Xi, Vice Minister, Ministry of Science and Technology of China, President, Science Council of Asia, and Vice President, China Association for Science and Technology (CAST) for his presence at this opening ceremony. We would also like to extend our gratitude to Professor Dr Hiroshi YOSHINO, the Secretary General/Treasurer of SCA. Special thanks would go to Dr Juichi Yamagiwa, the President of SCJ and to all distinguished guests and scholars from SCA member academies who, in one way or the other, contributed to the success of this conference.

MAAS owes its apology to all participants for the delay in producing the papers presented at SCA–19 Conference. The responsibility of opinions, statements, comments, etc. expressed in the papers lie with those of the authors. The views expressed in the papers presented at the conference did not reflect that of MAAS.

Dr Thet Lwin

President, Myanmar Academy of Arts and Science

Contents

Lists of Contributors

Message

It is a great pleasure and inspiring experience to host the 19th Science Council of Asia Conference, held with the theme "Research and Innovation for Sustainable Development in Asia" in Nay Pyi Taw, Myanmar.

This conference is particularly timely as all Member States are unanimously supporting research and innovation to achieve the Sustainable Development Goals (SDGs) of the United Nations 2030 Agenda.

A comprehensive range of the conference sessions reflects a very topical agenda as it provides a wonderful platform and opportunity for several experts, academia, scholars and researchers to exchange their break–through ideas, profound knowledge and invaluable experiences.

I sincerely hope this conference will help to identify ways to bring forward the transformative sustainability agenda and better align research and innovation policies with the SDGs, as set out in the United Nations Agenda 2030 for sustainable development.

To all delegates, I would like to suggest that we adopt innovation in science, technology, engineering and mathematics as integral elements of the strategies for SDGs. I would like to request you to produce action–oriented outcomes of the conference and keep supporting research and innovation for sustainable development in Asia.

Before I conclude, I wish all delegates and participants an enjoyable stay in Myanmar.

Thank you.

Dr Myo Thein Gyi
Union Minister for Education, Myanmar

Message

It is my great pleasure to welcome you all on behalf of Science Council of Asia(SCA) to the 19th SCA conference that brings together experts of scientific organizations to discuss " Research and Innovation for Sustainable Development in Asia". I thank all the local conference hosts in Myanmar and the SCA Secretariat. Thanks to their excellent effort, the SCA19 is organized jointly and successfully.

To a large extent, Asia's rapid economic development and subsequently booming consumption have prompted critical challenge for environment sustainability. Recently, Oxford Dictionaries and Cambridge Dictionary have named "climate emergency" and "upcycling" as their Word of the Year 2019, respectively. Change is necessary.

The 2030 Agenda, adopted at the United Nations Sustainable Development Summit in September 2015, positioned Science, Technology and Innovation as key means of implementation of the SDGs. Also with a new perspective of economic growth, there is a clear shift towards appreciating the adoption of sustainability standards, which has a positive correlation with increased profit as demand for products with sustainable credentials grows.

Many Asian countries have signed up to the SDGs, made growing commitment to address poverty, clean energy and pollution. New science and technology achievements have been applied to solve specific issues, new approaches have been used towards more sustainable activities.

SCA provides such a collaborative platform for member organizations to promote scientific exchange and cooperation, and to reach mutual understanding. We will continue to play a central role to face the common challenges for sustainable development in Asia and lead to a bright future.

Wishing you all a fruitful and joyful stay in Nay Pyi Taw and looking forward to your active participation in the Conference.

With best regards,

Prof. Dr. WANG Xi
President, Science Council of Asia

Message

Millennium Development Goals (MDGs) came to an end in December 2015; certain agenda of MDGs had been left unfinished. In 2015, UN General Assembly adopted the post 2015 Development Agenda and set Sustainable Development Goals (SDGs). The 2030 Global Development Agenda came into effect on 1st January, 2016 with the prospect of covering the five aspects: People, Planet, Prosperity, Peace and Prosperity. The approach to SDGs can be initiated through a different angle. For instance, People: End Poverty and Hunger in all forms and ensure dignity and equality; Planet: Protect our planet's natural resources and climate for future generations; Peace: Foster peaceful, just and inclusive societies; Prosperity: Ensure prosperous and fulfilling lives in harmony with nature.

Living beings inherited the earth, the only planet in the solar system, in which all known life forms can flourish. Human beings are the most intelligent species on earth. Throughout history, they try to change their environment to suit their needs and satisfy their desires. Among the continents, Asia happens to be the most populous region in the world. China and India, each with one billion plus population, have emerged as economic powers. Japan, Korea, Taiwan, and ASEAN TEN too witnessed economic growth. Inventions and innovations contributed to industrial revolutions. The fourth forthcoming inventions of IT and AI are expected to change traditional modes of manufacturing, transportation and urban amenities.

In 21st century, research across various countries in Asia highlight inter-linkages between natural resources and sustainable development goals along with the impact of climate change. The human society is seeking ways to safeguard human's wellbeing and to guarantee the sustainable use of resources. At the same time, it also tries to conserve the environment from natural calamities like floods, earthquakes, volcanic eruptions, drought, etc. so that our future generations will be inherited with green and peaceful environment.

I, on behalf of Myanmar Academy of Arts and Science, would like to express my deep appreciation to all those involved in making the conference a success. Special mention needs to be made to SCJ which co-hosted the SCA19 conference with MAAS for their guidance, support, co-operation and coordination. We fervently believe that the conference will provide our guests a cordial atmosphere for sharing experiences and exchanging views. The deliberations from this conference are expected to bring into light, effective means and ways for resolving common issues people are currently facing in Asia and elsewhere.

Dr. Thet Lwin
President of MAAS

Message

I am pleased to announce that the 19th Science Council of Asia (SCA) Conference is held in Nay Pyi Taw, Myanmar. First of all, I would like to express my sincere gratitude to Myanmar Academy of Arts and Science (MAAS) for its enormous efforts to prepare for this Conference. I also would like to express my deep appreciation to Member Organizations and SCA Secretariat for their cooperation and contribution in organizing this Conference and all the people who support it.

The theme of the 19th SCA Conference is "Research and Innovation for Sustainable Development in Asia". As you might already know, the purpose of SCA established in 2000 is "to facilitate scientific cooperation in Asia towards the progress in science and sustainable development of the region". With this purpose, SCA has contributed to society through the collaboration with academies in the region. Under such circumstances, "Transforming our world: the 2030 Agenda for Sustainable Development" with the 17 Sustainable Development Goals (SDGs) and 169 targets was adopted at the UN General Assembly in 2015. Since then, the efforts to realize the sustainable development in which a key principle is "no one will be left behind" have started at global level. We must continuously and collaboratively address a wide range of issues facing us since they are so challenging in the sense that human beings have never experienced them before.

The 19th SCA Conference is held for 3 days and nearly 180 presentations (oral and poster) are scheduled. I am delighted to know that we have received many applications exceeding our expectation. It indicates a high level of interest in this Conference's theme, "Research and Innovation for Sustainable Development in Asia". In the Conference, there are four (4) sub–themes that are discussed in their respective sessions. The main theme and sub–themes of the Conference have been carefully selected in order to inspire scholars and researchers in Asia to undertake interdisciplinary researches in partnership to contribute to the realization of the 17 SDGs.

This Conference is an advantageous opportunity to build a network of scholars in and outside the country. I am sure that there would be abundant outstanding discussions at this Conference.

Professor Hiroshi Yoshino

Secretary General / Treasure of SCA

The Innovation of Housebuilding Industry in Japan

Kazunobu Minami[1]

Abstract

Following my paper "Adaptable Infill for the Durable and Sustainable Japanese Housing" presented at the last year SCA Conference, the author continues the analysis of the innovations in Japanese house building and construction industry. Recent developments in housing technology has been promoting the longer life for housing and has reduced the material consumption and its environmental impacts. The adaptable infill system preserves building longer by changing its fit out according to the changes of lifestyles of the resident. The number of skilled construction workers in Japan is predicted to fall significantly in the near future. We are conducting the research and development in order to use less manpower for the site works. The use of robots on site works and the use of Artificial Intelligence and BIM in the process of design, building permission, on site construction and maintenance are the main research agenda for the expected innovation of our industry.

This paper analysis the characteristics of the past innovations in Japan and examines the key factors to foster the future innovations. The tradition of the collaborative relation among the government, academia and industry in Japan will be the most effective way to promote new innovation in the housebuilding and construction industry.

Keywords: Innovation, House building industry, Robot, AI, BIM

1. Introduction

In the previous paper "Adaptable Infill for the Durable and Sustainable Japanese Housing [1]" presented at the last year SCA Conference, the author pointed that the continuous research and development of adaptable housing in Japan from KEP, CHS (Century Housing System), KSI (Kodan Skelton Infill) to the establishment of the long fife housing law and the recent development of the zero slope gray water drainage system by the collaboration of the government, private companies and research institutions have been one of the most essential forces for the development of adaptable and sustainable housing in Japan. Based on this, the author tries to find out the necessary collaboration among public and privates sectors for the future innovation of housebuilding and building industries.

2. Methods

Sections 3-1 and 3-2 in this paper are summaries based on references [2] ~ [8] previously presented by the author. Section 3-3 is an examination based on references [9] ~ [10], which contain up-to-date information on technological development in Japan.

[1] Professor, Department of Architecture Shibaura Institute of Technology, k-minami@shibaura-it.ac.jp

3. Results and Discussion

3.1 History of the research and developments of housebuilding industry in Japan

In Japan, research and development has been carried out to improve the adaptability of multi-family dwellings and enable residents to continue living there for a longer period of time. In Japan, such housing units are often demolished after a short period of about 30 years, so efforts have been made to prolong their useful lifetimes by considering environmental and resource problems and economic efficiency.

In Japan, the Japan Housing Corporation, which is now called the Urban Renaissance Agency or UR, has been conducting joint research and development with universities and private companies under the leadership of the national government and the Ministry of Construction. In the early 1970s, their research resolved the problem of housing shortages, and since then it has been improving the quality of housing. Research and development by KEP since the late 1970s and by CHS beginning in the 1980s contributed to the KSI and to the enactment in 2009 of the Act Concerning the Promotion of Long-Life Quality Housing. Many dwellings for family use range in size from 70 to 80 square meters, requiring that they be occupied skillfully or remodeled to keep up with the growth of the children. Our research in housing adaptability is a response to these demands for such housing units in Japan.

The Act Concerning the Promotion of Long-Life Quality Housing was designed to prolong the life of housing units. This law came into effect on June 4, 2009. About 800,000 housing units have been constructed based on technical standards mandated by this law, but almost all were detached houses. Few have been condominiums. Because it must be possible to maintain and replace equipment piping of multi-family dwellings from common corridors, it is difficult for condominiums and apartments to comply with the technical guidelines, preventing the increase in the number of dwellings in compliance with the act.

Technical Guidelines have been enacted under this law. Chapter 3 stipulates ease of maintenance and renewal. Chapter 4 stipulates interior adaptability of dwellings. Vertical sewer pipes need to be easily accessible to allow replacement every couple of decades. The Piping space needs to have additional holes for future replacements.

The first condominium apartment constructed in Japan in compliance with the Act Concerning the Promotion of Long-Life Quality Housing is located in Urawa City. In order to be able to modify the layout of a dwelling, the ceiling and floor slabs of a condominium must ensure at least a vertical distance of 2,650 millimeters. The double floors are 275 millimeters thick. If this dimension is ensured, equipment piping can pass through the double floors, permitting the modification of rooms such as kitchens or bathrooms. Families can create the floor plan they desire by arranging movable storage systems.

3.2 Recent trends in technical developments for collective dwellings

Figure 1 and Figure 2 show a condominium equipped with movable storage walls and movable kitchens developed by Mitsui Real Estate and Haseko Corporation. The bathroom and toilet are installed as a single unit and cannot be moved, but other spaces can be laid out freely. The ceiling inside the room is flat and no columns or beams protrude into the rooms, so the movable storage walls can be installed anywhere without any limitations. The entire unit is double-floored, enabling the location of the kitchen to be changed. The thickness of the double

floor is 130 millimeters and the double ceiling is from 120 to 140 millimeters thick. This space is used to install equipment wiring and piping. Users create the floor plan they desire by arranging the movable storage walls. The kitchen can be relocated. Exhaust from the kitchen can be ventilated above the range to keep the air in the kitchen clean.

The other example of a recent technical development is the zero-slope drainage system. Figure 3 and Figure 4 show a new drainage system based on the siphon principle. The drainage slope is zero in order to fill the interior of the narrow 20-millimeter horizontal pipe with water. The drain pipe fills with water then it flows out under the force of gravity. If a siphonic floor drainage system is installed, the area where the kitchen can be located is greatly expanded. This new drainage system narrows drain pipes and ends the need for a slope. By reducing the height of the double floor, it removes the need for a level difference on the floor, lowering the cost of structure work.

Figure 1. Movable Kitchen System

Figure 2. Wheels for Movable Kitchen System

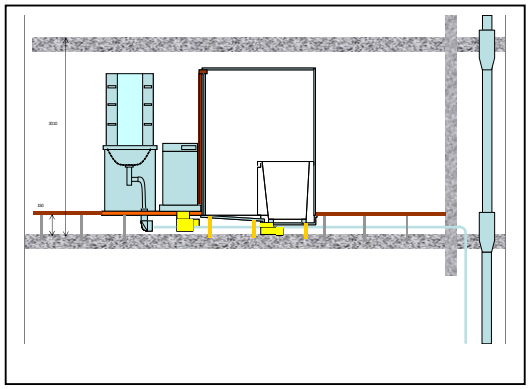

Figure 3. *Diagram of Zero-Slope Drainage System*

Figure 4. Example of Zero-Slope Drainage System

3.3 Strategy for the future technical developments and innovations for building industry

The construction industry in Japan is currently facing a severe shortage of skilled workers, and thus improving productivity is a pressing issue. The construction and housing industry in Japan has so far been improving productivity through innovative refinements to construction methods, in both reinforced concrete as well as conventional wooden structures. The construction industry, which has overcome numerous ordeals, including oil shocks and the collapse of Japan's bubble economy, will likely overcome this shortage of workers to a great

extent through application of robotics, IT (Information Technology) and AI (Artificial Intelligence).

Robotic systems for pulling construction materials have already been introduced in order to reduce the burden of on-site operations on aging workers as well as to improve productivity. Tests have also been conducted on tasking robotic systems with cleaning operations so that workers can focus exclusively on on-site operations during the day. In the near future, it may be possible for workers to commence operations from first thing in the morning thanks to robotic systems conducting cleaning operations at night. It would also likely not be very difficult to repurpose Power Assist Suits, which are used in the distribution industry among others, to be more in line with the characteristics of construction site operations.

The efforts of individual companies and on-site initiatives alone will be insufficient for achieving significant improvements in productivity. It is vital for the industry to engage with the issue collectively. When personnel related to the construction industry were interviewed, personnel in both Design Divisions and Construction Divisions said that, although the in-house inspections, client inspections and government inspections conducted at each stage throughout the construction process are necessary in ensuring construction quality, these inspections are a major time burden. In order to make inspection operations more advanced and streamlined, future developments may be in areas such as laser-based measurements, image recognition technology-based inspections, drone-based layout inspections and photography for construction records. Attaching RFIDs (Radio Frequency Identifiers) to construction materials and architectural parts will likely accelerate on-site confirmation and provide greater accuracy, and may also facilitate confirmation of concealed areas.

Government agencies also likely need to examine ways to streamline various inspection operations for the purpose of improving the productivity of the industry as a whole. For example, in the future, the ratio of existing structures that undergo repair will increase, which means that forming databases and disclosing information on previous building approvals so that clients and designers can clearly determine whether to make use of an existing structure or to rebuild during the initial stages of operational planning will likely lead to smoother project progression and increased productivity.

Utilization of BIM (Building Information Modeling) is expected to improve productivity. Initiatives are progressing in regard to building approvals that utilize BIM, such as standardizing expressions used in drawings and specifications for applications. In the near future, in addition to ensuring consistency between design drawings and application drawings, automatic confirmation will also be conducted for both stand-alone and group regulations relating to various types of area calculations, physical dividers to prevent the spread of fires, fire prevention equipment, measurements of evacuation distances, etc. And this will likely greatly reduce the amount of time necessary for building approvals and for receiving consent from the fire department. Eventually, legality will be automatically checked starting from the basic design stage, and this will likely eliminate the need to redo operations. When it comes to industrialized housing, application of type certification and manufacturer certification systems will streamline building approvals and also simplify on-site inspections. In the field of industrialized housing, which is becoming increasingly componentized, unique CAD systems have been introduced for design, production and construction, so engaging in building approvals that utilize BIM based on these systems will likely be easier than for other general structures. The field of industrialized housing could

become capable of BIM level 3 inspections at a very early stage.

The construction industry in Japan is a mature industry, and it is good at progressively improving productivity. The industry contains companies that have attempted new businesses, such as nursing care and agriculture, by applying their skilled personnel and organizational capacity to these new businesses during periods in which their existing businesses are performing favorably and without falling into 'success traps.' However, due to rapid progress in the fields of IT and AI, companies that are currently aiming to introduce robotics and AI into the construction industry are gaining more and more experience, and this could introduce 'destructive innovation' into the construction and housing industries. In the future, AI technologies will be more advanced, and in terms of architectural designs for residences in particular, this may lead direct connections between clients and production process and cause major changes in business models. In companies that provide industrialized housing, engineers from other fields who graduated from courses other than architecture will be responsible for the information technologies that form the core of production, and educational programs implemented at universities and human resource development programs conducted by companies must stay up-to-date with changes in society.

Achieving further innovation requires 'ambidextrous' administration in which managers search for new businesses while at the same time deepening existing, mature businesses*1. The textile industry in Japan succeeded in shifting its core focus into new fields. But will the constructing and housing industries, for which a drop in domestic demand is unavoidable, also be able to do the same thing?

Komatsu Ltd., a manufacturer of construction equipment, began globalization at an early stage, including entering the Chinese market, and the company has constantly created value through innovation*2, including development of ICT construction equipment, which is increasingly becoming automatized, KOMTRAX, which provides a visual representation of operation status, and SMART CONSTRUCTION, which provides higher level solution businesses. In 2017, through a joint venture with NTT Docomo, SAP Japan and OPTiM Corporation, Komatsu started LANDLOG, an IoT platform for construction sites. This is exactly what Joseph Schumpeter meant by 'new combination' between different industries. Komatsu Ltd., which had previously provided construction equipment for use at construction sites, established a position as a leading company through proactive introduction of IT. And by constructing a platform[*3] that accumulates and processes all types of construction-related data and providing access even to competitors, the company is increasingly becoming the main pillar in the construction solution business.

Even though it is presently limited to the field of civil engineering, including site preparation, etc., it may eventually expand into building construction work. Together with IT, AI and robotics companies, the general construction industry and the housing industry should continue searching for businesses that will create new social value and develop these into their core businesses in the future.

So far, growth of the Japanese economy has been supported by initiatives in which industry, academia and the government are in close cooperation. In terms of technology, further developing the housing and construction industries in Japan, which are already highly advanced, will require not only technological development and technological innovations but also restructuring of social systems to produce new value. It is thought that, in the future as well, the

key to promoting social system reforms and technological innovations in an integrated and effective way will be cooperation between government sectors in charge of policy and private sectors in charge of research and technological development – in other words, the promotion of open innovation in cooperation between industry, academia and the government.

4. Conclusions

Technological developments in the construction and housing industries in Japan during the 1970s and 1980s were promoted through participation by major companies in national technology development projects under government leadership, and these produced results. However, in terms of technological development currently in progress, it is necessary to cooperate with start-up companies in fields other than the construction industry that possess advanced technologies, including IT and robotics. In particular, it is necessary to proceed in a different way than before, including in relation to the state of government subsidies for research and development, etc. In addition, in regard to the ideal state of construction production in the future, it would be preferable to construct a vision that can be shared by society as a whole and to proceed research and development aligned with society as a whole.

Acknowledgements

The author would like to express deep gratitude to all of the researchers who provided advice regarding the writing of this paper.

References

[1] Kazunobu Minami, Adaptable Infill for the Durable and Sustainable Japanese Housing, December 6th, 2018, ORAL presentation at the Conference Strand: 1. Energy, Natural Resources and Built Environment, The 18th Science Council of Asia Conference “Role of Science for Society: Strategies towards SDGs in Asia”, Science Council of Japan (SCJ)

[2] Kazunobu Minami, Japanese Innovation in Adaptable Homes, Loose-Fit Architecture: Designing Buildings for Change AD, pp. 38-45, Willy, September 2017, Alex Lifschutz (Editor) et.al.. Profile 249 Volume 87 No 5

[3] Kazunobu Minami a, The efforts to develop longer life housing with adaptability in Japan, PROCEEDINGS pp.755-766、SBE16 Tallinn and Helsinki Conference; Build Green and Renovate Deep, 5-7 October 2016, Tallinn and Helsinki

[4] Kazunobu Minami b, The Adaptability of Long Life Housing in Japan - Case Studies of Century Housing System (CHS) -, 11th International Symposium on Architectural Interchanges in Asia (ISAIA 2016), September 21st-22nd, 2016

[5] Kazunobu Minami, Long-Term Occupancy Records and Infill Renovation of Housing Designed Based on the Century Housing System, The Future of Open Building Conference 2015, ETH Zurich, September 9-11 2015

[6] Kazunobu Minami, ANALYSES OF LONG TERM OCCUPANCY RECORDS OF PUBLIC HOUSING IN JAPAN, Architecture in the Fourth Dimension Methods + Practices for a Sustainable Building Stock, Proceedings of an International Conference of CIB W104 Open Building Implementation and CIB W110 Informal Settlements and Affordable housing, pp.287-293, November 15th -17th 2011

[7] Kazunobu Minami, The New Japanese Housing Law to Promote The Longer Life of Housing And Exaple of Changes in The Layout of Public Housing Over 40 Years In Japan, Changing Roles; New Roles,

New Challenges, pp.449-455, October 5-9,2009, Noordwijk aan Zee, The Netherlands

[8] Kazunobu Minami, A Study on the Continuous Customization of an adaptable housing by KEP System, Adaptables2006, TU/e, International Conference On Adaptable Building Structures, July,2006,Vol.1, PP.2-101～106

[9] Lead and disrupt: how to solve the innovator's dilemma, Charles A. O'Reilly III and Michael L. Tushman, Stanford Business Books, c2016, Japanese Translation by Noriko Watanabe, Feburary 2019

[10] Komatsu NEWS RELEASE No.017（2852）“DANTOTSU Value-FORWARD Together for Sustainable Growth”, April 26th 2019, https://home.komatsu/jp/press/2019/ management/1202302_1600.html , viewed May 2019

Mold and Dampness in Unplanned Urban Houses in the Hot and Humid Climate of Indonesia

Tetsu Kubota[1], Jumpei Sumi[2], Kresna Bhayu Adinugraha[3] and Usep Surahman[4]

Abstract

Many parts of Indonesian cities comprise unplanned houses, the so-called Kampongs. Most Kampong houses are small detached houses constructed by non-professional workers in densely crowded settlements. Mold and dampness are commonly seen in Kampongs particularly during the rainy season along with seasonal floods, and therefore adverse health effects, especially respiratory diseases, are suspected among residents. We investigated the mold risk using fungal detectors (n=68) and the self-reported prevalence of respiratory diseases using a questionnaire form (ATS-DLD-78) (n=599) in a typical Kampong neighborhood in the city of Bandung, Indonesia during 2018-19. Mainly due to the high humidity conditions, most houses were suffered from severe molds. Approximately 79% of the measured rooms showed a possibility of mold propagation even during the dry season, whereas more than 97% were categorized as severe conditions during the rainy season. Nevertheless, further results showed that the respondents with some symptoms of respiratory diseases tended to be exposed to a lower mold growth index compared to those without any symptoms. The respiratory diseases might be attributed to outdoor air pollutions as well.

Keywords: Mold, Dampness, Health, Tropics, Kampongs

1. Introduction

Microbial pollution involves hundreds of species of bacteria and fungi that grow indoors when sufficient moisture is available. Exposure to microbial contaminations is clinically associated with respiratory symptoms, allergies, asthma and immunological reactions [1]. The presence of many biological agents in the indoor environment is due to dampness and inadequate ventilation [1-2]. Excess moisture on almost all indoor materials leads to growth of microbes, such as mold, fungi and bacteria, which subsequently emit spores, cells, fragments and volatile organic compounds (VOCs) into indoor air [1]. Moreover, dampness initiates chemical or biological degradation of materials, which also pollutes indoor air. Dampness has therefore been suggested to be a strong, consistent indicator of risk of asthma and respiratory symptoms (e.g. cough and wheeze) [1].

Indonesia has a population of more than 150 million as of today and it is still rising particularly in the urban areas. In order to accommodate growing number of urban population, now the central government is highly promoting provisions of affordable housing. But still, many parts of Indonesian cities comprise traditional unplanned houses, the so-called Kampongs. Most Kampong houses are small detached houses constructed by non-professional workers in densely crowded settlements (Fig. 1). Mold and dampness are commonly seen in Kampongs particularly during the rainy season along with seasonal floods, and therefore adverse health effects, especially respiratory diseases, are suspected among residents. We investigated the mold risk

[1] Dr. Associate Professor, Graduate School for International Development and Cooperation, Hiroshima University; Research Institute for Human Settlement and Housing, Ministry of Public Works and Housing, tetsu@hiroshima-u.ac.jp
[2] Graduate School for International Development and Cooperation, Hiroshima University
[3] Graduate School for International Development and Cooperation, Hiroshima University
[4] Department of Architecture, Indonesia University of Education, Indonesia

using fungal detectors and the self-reported prevalence of respiratory diseases using a questionnaire form (ATS-DLD-78) in a typical Kampong neighborhood in the city of Bandung, Indonesia during 2018-19. This paper reports the results of the investigations to analyze an association between the mold risk and the prevalence of respiratory diseases.

2. Methods

A typical Kampong neighborhood, comprising 360 households, was selected in Bandung as a case study area (Fig. 1). After obtaining a consent from the head of the neighborhood association, the field measurements and interviews were conducted during the dry season (October 2018) and the rainy season (March 2019). The subjects investigated include 333 and 266 residents in dry and rainy seasons respectively for the interviews, and 34 and 34 houses for field measurement of air temperature (AT), relative humidity (RH) and mold risk.

The interviews were conducted using a questionnaire form, comprising the American Thoracic Society-Division of Lung Diseases (ATS-DLD-78) [3] and several additional questions, among others: personal attributes, building attributes, cleaning habits, window-opening behavior and smoking habits. The ATS-DLD questionnaire has been validated in many previous studies [4] and commonly used to evaluate general respiratory health. The questionnaire comprises questions for symptoms of cough, phlegm, wheezing, breathlessness, chest colds and chest illnesses. Moreover, occupational history and tobacco smoking habits were additionally asked for adults, among others.

Fungal contamination was predicted by using a fungal detector developed by Abe [5]. The fungal detector encapsulates dried fungal spores and nutrients to measure fungal index. The fungal index, defined by Abe [5], quantifies the capacity for mold growth in an environment being examined, and therefore it is considered one of the useful indices for evaluating microclimates for potential mold growth (Table 1) [6]. The mold measurements were taken at approximately 10 cm above floor in the master bedroom during the dry and rainy seasons, respectively. AT and RH were measured using a small recorder (T&D 72ui, 72wf & 73u) at the same places.

3. Results and Discussion

3.1 Profiles of Respondents

Out of the respective samples (i.e. dry season (n=333) and rainy season (n=266)), there are intersections of 77 respondents. As shown in Table 3, the average age of respondents in dry season is 34.3 years, including 16.5% of children aged 12 years old and below. The majority of respondents are classified as the income group of US$ 150-450 (monthly average). Averagely, they open windows for approximately 8-9 hours in the bedroom and 7-8.5 hours in the living room. They tend to open windows during the daytime. As shown, approximately 69% of the respondents (active; 32%, passive; 37%) are exposed to ETS during the dry season, while more than 98% (50% and 48%) are suspected during the rainy season. Moreover, more than 45% of the respondents (dust; 29%, chemical; 17%) are exposed to dust or chemical fumes during their working time, whereas more than 70% (49% and 22%) are suspected during the rainy season

Table1. Fungal index (6)

Level	Fungal index	Predicted propagation of fungi	Remarks
A	<2	No propagation	Good environment
B	2 – 5	Low possibility of propagation	There is no problem in terms of fungi, but there is a possibility of propagation of mites, which requires countermeasures. Dehumidification is recommended.
C	5 – 15	Possibility of propagation	Fungi prevention measures are recommended. Dehumidification is recommended.
D	>15	High possibility of propagation	Fungi prevention measures are required. Dehumidification is needed for living rooms and regular cleaning is needed for wet areas, such as bathroom.

Figure 1. Kampong houses in the case study area.

Table 2. Number of samples

Samples	Dry season	Rainy season	Total
Questionnaires (ATS-DLD-78)	333	266	599
Measurements (Mold risk)	34	34	68

Table 3. Profile of respondents and overview of building attributes, interior sources and perceived dampness

			Dry season	Rainy season
Personal attributes	Age [%]	Years [mean]	34.3	-
	Gender [%]	Male/ Female	45/55	47/53
	Income (US$) [%]	< 150	36.2	25.9
		150-450	43.6	62.4
		450-750	8.5	9.4
		> 750	4.3	2.4
	Window opening in bedroom	Hours	7.9	8.8
	Window opening in living room	Hours	7.0	8.5
	Smoking behavior [%]	Active	32.3	50.0
		Passive	37.0	48.3
	Work in dusty job	[%]	29.1	49.0
	Exposed to gas or chemical fumes	[%]	16.9	22.3
Health	Asthma	[%]	13.8	6.7
	Eczema	[%]	13.5	-
	Allergy	[%]	13.6	-
	Stress	[mean: 0 = no stress, 10 = very stressful]	1.5	0.9
Building attributes	Age of building	Average age [years]	39.9	41.8
	No. of windows in master bedroom [%]	0	25.9	18.5
		1	50.6	49.2
		>1	23.5	32.3
	No. of windows in living room [%]	0	34.6	22.8
		1	42.0	35.1
		>1	23.5	42.1
	HVAC system [%]	AC	5.6	8.0
		Ceiling / stand fan	50.0	-
		Exhaust fan	21.4	-
	Modification(s)	[%]	-	59.7
	Furniture (units)	Living room [mean]	3.1	-
		Bedroom [mean]	2.4	-
Dampness	Visual mold	[%]	51.3	34.1
	Mite	[%]	17.0	11.0
	Water leakage	[%]	48.3	50.6
	Smell / Odor	[%]	40.9	55.9
	Humidity [%]	0-3: (rather) dry	24.3	28.2
		4-6: neutral	45.2	43.5
		7-10: (rather) humid	30.5	28.2
Perceived IAQ	IAQ [%]	0-3: (rather) clean	35.4	42.0
		4-6: neutral	50.3	44.3
		7-10: (rather) dirty	14.4	13.6
	OAQ [%]	0-3: (rather) clean	28.7	38.6
		4-6: neutral	52.8	46.6
		7-10: (rather) dirty	18.5	14.8
	Annoyance by outdoor air pollution [%]	0-3: not annoyed	57.6	69.4
		4-6: neutral	34.3	18.7
		7-10: annoyed	8.1	11.9
Cleaning behavior	How to clean room	Sweep	95.0	98.9
		Wipe	4.2	1.1
		Vacuum cleaner	0.0	0.0
		Others	0.8	0.0
	How to dry laundries	Indoor	13.7	10.1
		Outdoor	59.8	44.9
		At veranda	9.4	30.3
		Others	17.1	14.6

The average age of buildings is about 40 years in the dry season and 42 years in the rainy season. It should be noted that approximately 26% and 35% of houses do not have any windows in the master bedroom and the living room respectively in the dry season, whereas about 19% and 23% of houses do not have them in the rainy season. Dampness is commonly seen in Kampong houses. As shown in Table 3, visual mold was reported in approximately 51% and 34% of the houses during the dry and rainy season, respectively. About 17% and 11% of the houses reported mite problems in dry and rainy season, respectively. Water leakage was reported particularly in the rain season (51%), and smell and odor were reported more in the rainy season as well (56%). Meanwhile, approximately 14% of the respondents perceived IAQ to be dirty in the both seasons. On the other hand, about 15-19% of the respondents perceived OAQ to be dirty in the two seasons. Approximately 8-12% of the respondents were annoyed by the outdoor air pollutions.

3.2 Self-reported respiratory health: ATS-DLD-78

Magnitude of symptoms on respiratory health (i.e. asthma, cough and phlegm) was evaluated through the ATS-DLD-78 questionnaire (Fig. 2). In the dry season, the percentages of those who have severe symptoms (i.e. sickness) and some degrees of symptoms account for 0.3%/16.1% (asthma), 1.9%/21.9% (cough) and 3.2%/9.6% (phlegm). The percentages are increased in the rainy season especially in persistent cough, and the percentages are 0%/7.6% (asthma), 4.0%/25.4% (cough) and 1.3%/12.7% (phlegm).

3.3 Mold risk

The measured average AT and RH (at the same places of fungal detectors) are summarized in Fig. 3. As shown, in the dry season, the outdoor AT ranges approximately from 21.3-27.3°C with an average of 24.2°C, whereas the corresponding indoor AT ranges from 23.6-26.3°C with an average of 24.9°C. In the rainy season, the outdoor AT maintains almost the same as that of the dry season (approximately 22.1-26.4°C), but indoor AT was averagely increased to approximately 24.7-26.8°C. Meanwhile, in the dry season, the outdoor RH ranges approximately from 56-100% with an average of 81%, whereas the corresponding indoor RH ranges approximately from 71 to 86%. In the rainy season, the outdoor RH is increased to 70-97%, while the indoor RH is averaged at 82%. The results clearly indicate extremely high humidity conditions in Kampong houses even in the dry season.

Mold growth was evaluated in terms of fungal indexes ranging from A to D (see Table 1). The results show that as expected, approximately 79% of the houses are classified as C or D even in the dry season, whereas more than 97% are classified as D, which shows a high possibility of propagation, in the rainy season. It should be noted that in the rainy season, more than 44% of the houses recorded the maximum fungal index of more than 70.

Fig. 5 depicts the relationship between the measured thermal conditions and the mold indexes. As shown, the mold conditions are severe particularly when the indoor RH exceeds 70%. The measured mold indexes slightly vary even when the indoor RH is more than 70% probably due to the other dampness conditions such as water leakage and floods.

3.4. Factors affecting the respiratory health

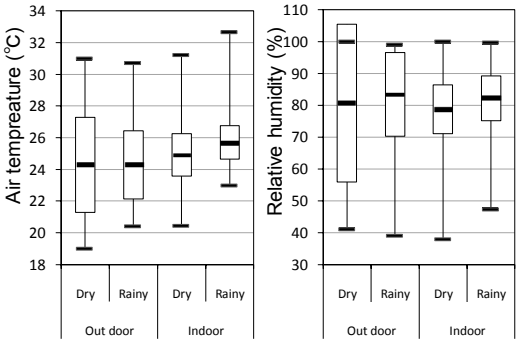

***Figure 2**. Self-reported respiratory health.*

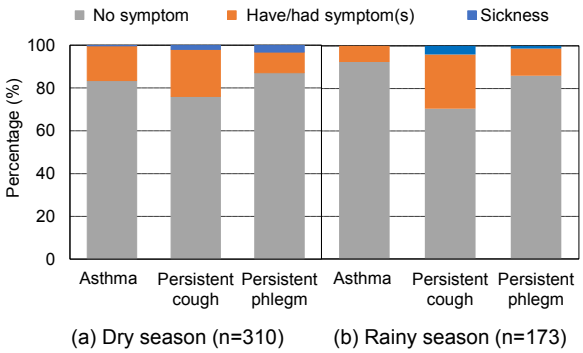

*Figure **3**. Statistical summary of outdoor and indoor AT and RH in dry and rainy season.*

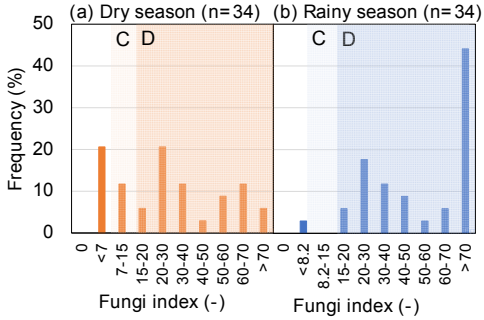

Figure 4. Measured fungal indexes in Kampong houses.

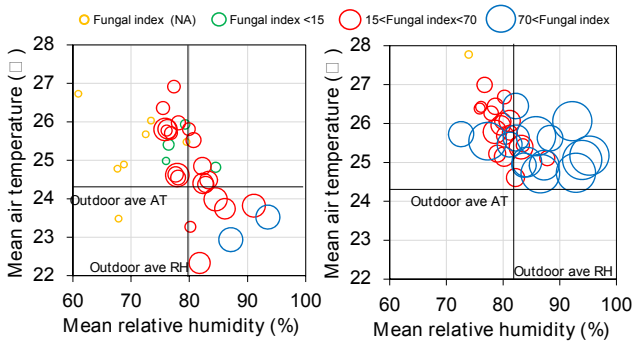

(a) Dry season (b) Rainy season

***Figure 5**. Relationship between thermal conditions and mold risk.*

Table 4. Results of correlation analysis for Respiratory health (dry season)

A: Asthma, C: Persistent cough, P: Persistent phlegm	**A**	**C**	**P**
Personal attributes			
Age group[a]	0.33	0.51	0.29
Gender[a]	0.49	0.34	0.66
Living in home [years][b]	0.09	0.35	0.66
Income[b]	0.38	0.03	0.04
Window-opening_ bedroom[b]	0.97	0.08	0.59
Window-opening_ living room[b]	0.31	0.03	0.08
Active smoking	0.18	0.84	0.47
Passive smoking	0.06	0.35	0.00
Work in dusty job	0.64	0.00	0.22
Exposed to gas or chemical fumes	0.20	0.06	0.33
Health			
Asthma[a]	0.00	0.03	0.03
Eczema[a]	0.42	0.77	0.08
Allergy[a]	0.04	0.02	0.00
Stress[b]	0.25	0.02	0.07
Building attributes			
Age of building [years][b]	0.69	0.66	0.04
No. of windows_bedroom[b]	0.37	0.26	0.60
No. of windows_living room[b]	0.40	0.61	0.07
AC[a]	0.73	0.53	0.61
Furniture living room[b]	0.30	0.94	0.32
Dampness			
Visual mold[a]	0.29	0.45	0.89
Mite[a]	0.91	0.00	0.01
Water leakage	0.42	0.00	0.09
Smell/Odor	0.42	0.55	0.01
Humidity	0.68	0.19	0.28
Perceived IAQ			
IAQ rating[b]	0.26	0.45	0.24
OAQ rating[b]	0.47	0.68	0.48
Annoyance by outdoor air pollution	0.42	0.02	0.05
Creaning behavior			
How to clean room	0.33	0.75	0.00
How to dry laundries	0.14	0.81	0.81

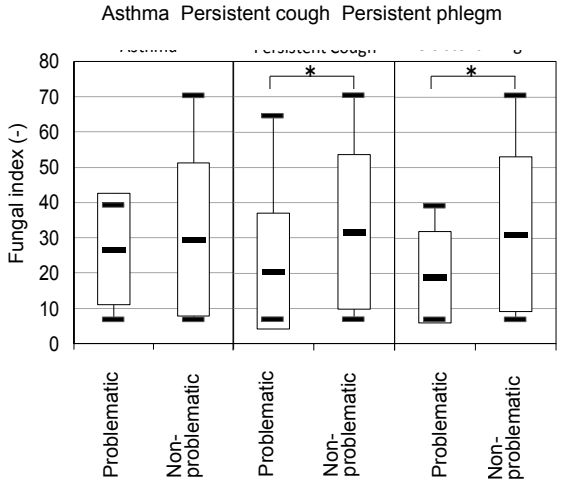

Figure 6. Measured fungal indexes by problematic/ non-problematic respiratory health groups (dry season).

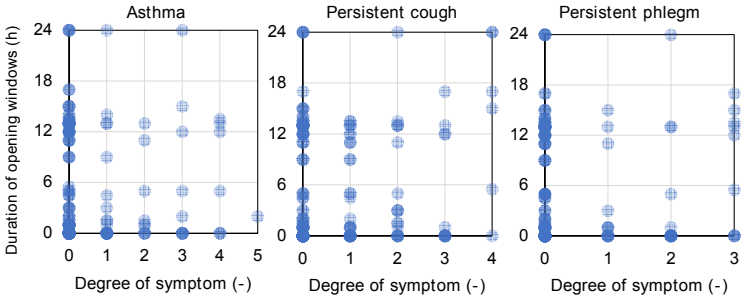

Figure 7. Relationship between duration of opening windows and respiratory health (dry season).

[a] p-value of Chi-Square-Test, [b] p-value of Spearman rho, red: Correlation is significant at the 0.01 level (2-tailed), green: Correlation is significant at the 0.05 level (2-tailed)

By taking the degrees of symptom of respiratory diseases (i.e. ATS-DLD-78) as the target variable, we conducted correlation analyses in order to determine the factors affecting the respiratory health of occupants (Table 4). As shown, the average household income is associated with respiratory health, particularly in terms of cough and phlegm. This may reflect their job occupations and basic sanitary conditions, but further analysis is required. The average duration of opening windows negatively affect the degree of asthma symptoms (the more they open windows the less the symptoms are), but it has positive associations with persistent cough and phlegm. As expected, passive smoking is associated with asthma and persistent phlegm in particular. Meanwhile, those who work in a dusty job tend to have a higher symptom of cough in particular. Previous history of asthma, allergy and stress are also associated with the current symptoms as expected. Furthermore, the age of buildings negatively associates with the phlegm symptoms, which requires further investigation.

Unlike other previous studies, visual mold does not show significant associations with respiratory health in this survey, although other dampness indicators, including mite and water leakage and smell/odor, are associated with persistent cough and/or phlegm. On the other hand, when it comes to the perceived IAQ, it is seen that those who are annoyed by the outdoor air pollutions tend to have higher degrees of persistent cough and phlegm.

We divide the samples into two groups in terms of respiratory health conditions (i.e. problematic and non-problematic groups) and compare the two groups in terms of the measured fungal indexes (Fig. 6). As shown, unexpectedly, those who have no respiratory symptoms tend to be exposed to higher fungal indexes, especially in terms of persistent cough and phlegm. Further investigations are required to clarify the reasons (e.g. it is necessary to identify the species of mold contained in the air). However, the results imply that there is a possibility that respiratory health of these Kampong residents is influenced not only by indoor mold and dampness but also, rather, by outdoor air pollutions, among others. Fig. 7 analyses the respiratory health symptoms by the average duration of opening windows. Interestingly, especially in persistent cough and phlegm, there are two modes in terms of the respiratory health symptoms. The first mode appears when the duration of opening windows is close to zero (i.e. windows are closed for 24 hours), and the second mode is observed when the duration is about 12 hours/day. The results imply that their respiratory health is influenced by the two sources (i.e. indoor sources such as mold and ETS, and outdoor sources such as traffic air pollution) respectively, depending on the window-opening conditions.

4. Conclusions

We investigated the mold risk using fungal detectors and the self-reported prevalence of respiratory diseases using ATS-DLD-78 in a typical Kampong neighborhood in the city of Bandung, Indonesia during 2018-19. The main findings from the investigations are summarized as follows:

- As expected, Kampong houses were suffered from severe mold growths. Even in the dry season, approximately 79% of the houses showed a possibility of mold propagation and 68% were considered to be a high possibility of propagation. In the rainy season, more than 97% of the houses were classified as a high possibility of propagation.
- The possibilities of propagation were mainly due to the very high humidity conditions. The outdoor RH was averaged at 83% while the corresponding indoor RH was averaged at 82% during the rainy season.
- Nevertheless, further results showed that the respondents with some symptoms of respiratory diseases tended to be exposed to lower mold growth conditions compared to those without any symptoms. On the other hand, respiratory health of occupants, particularly persistent cough and phlegm, were associated with average household income, duration of opening windows, passive smoking, working environment (dusty job), medical history such as asthma, eczema and allergy, age of buildings, dampness such as mite, water leakage and smell/odor, and annoyance by outdoor air pollution.
- The results implied that their respiratory health was influenced by the two sources (i.e. indoor sources and outdoor sources) respectively, depending on the window-opening conditions. When they close windows, indoor sources such as mold and ETS may become the main causes of prevalence of respiratory diseases. Meanwhile, if they open windows, then the indoor sources can be less influential, but the occupants are exposed to the outdoor sources more such as traffic air pollutions.

Acknowledgements

This research was supported by a grant from the Sumitomo Foundation. We also would like to sincerely thank the students in Indonesia University of Education (UPI) who supported the surveys in Bandung. We also appreciate the supports from the Laboratory for Mold Prediction in Japan.

References

[1] WHO, "WHO Guidelines for Indoor Air Quality: Dampness and Mould", WHO Regional Office for Europe, 2009.

[2] Olaf C.G. Adan, Robert A. Samson (eds), "Fundamentals of Mold Growth in Indoor Environments and Strategies for Health Living", Wageningen Academic Publishers, 2011.

[3] Ferris B.G., "Epidemiology Standardization Project (American Thoracic Society)", Am Rev Respir Dis, 1978, vol.118, pp.1-120.

[4] Hawari F.I., Obeidat N.A., Ghonimat I.M., Ayub H.S., Dawahreh S.S., "The effect of habitual waterpipe tobacco smoking on pulmonary function and exercise capacity in young healthy males: A pilot study", Respiratory Medicine, 2017, vol. 122, pp. 71-75.

[5] Abe K., "A method for numerical characterization of indoor climates by a biosensor using a xerophilic fungus", Indoor Air, 1993, vol. 3, pp. 344–348.

[6] Laboratory for Mold Prediction, "Additional Guidelines for Fungal Detector", Laboratory for Mold Prediction, Tokyo, Japan, 2004 (in Japanese) (unpublished).

Retail Site Location in Dagon Myothit (North) Township Using GIS

Khin Mi Mi Win[1] , Khin Khin Htay[2], Lae Lae Mon[3]

Abstract

The opening of a new establishment is a critical factor for firms in the retail sector. This article presents the development of a methodology for the process of selecting a retail site location that combines geographic information systems (GIS). The social, economic and environmental impacts of large-scale retail outlets on existing retail and urban systems have been extensively discussed in the planning literature. This article documents the last two decades of transformation in Dagon Myothit (North)'s market sector, which have been characterized by a more organized development of the sector than traditionally existed. Changes in the economy and related legislation prepared a base for the subsequent transformations of that decade, culminating, especially in large cities, in the development of shopping malls as alternative retail spaces to traditional markets and stores on a shopping street. This article may provide implications for urban policy and retail planning in Dagon Myothit (North) Township. The case may also be interesting for urban areas experiencing similar patterns of change and development, that is, where the globalization process in retailing and consumption-related sites began later than in other countries and observed fast-paced development.

Keywords: Retail development, Shopping mall, GIS, Urban policy

1. Introduction

Retailing is defined as the sale of goods and articles individually or in small quantities directly to the consumer, which involves selling relatively large quantities of goods, especially to retailers. Retail location analysis is an important part in site selection of a retail shop. Spatial arrangement of retail shops is one of the most important indicators in the development process of a town. The influences on the location of retail areas, they usually co-vary most closely with population density. This paper presents the development of a methodology for the process of selecting a retail site location that combines geographic information systems (GIS).

The main objectives of this research work are to assess the driving force of the emergence and spatial distribution of retail shop and to analyze the relationship between location of retail shop and urban infrastructure in Dagon Myothit (North) Township.

Dagon Myothit (North) Township is one of 12 townships of Eastern Yangon District in Yangon Region. (Figure. 2) It lies between North latitudes 16° 51′ and 16° 55′ and between East longitude 96° 10′ and 96° 14′. The area of Dagon Myothit (North) is 26.28 square kilometer (10.145 square miles) constituting 27 wards. (Figure 3)

In 2019, the total population was 196199 persons with 92774 males and 103425 females and the average population density was 7465persons per square kilometre. The population distribution in Dagon Myothit (North) is highly uneven. More people are concentrating around the main road and junction's area. East longitude 96° 10′ and 96° 14′. The area of Dagon Myothit (North) is 26.28 square

[1] Dr. Professor, Department of Geography, University of Yangon, Yangon, Myanmar khinmimiwingeog@gmail.com
[2] Department of Geography, Bago University, Bago, Myanmar kkhinhtay.geog@gmail.com
[3] Department of Geography, University of Yangon, Myanmar. laelaemon69@gmail.com

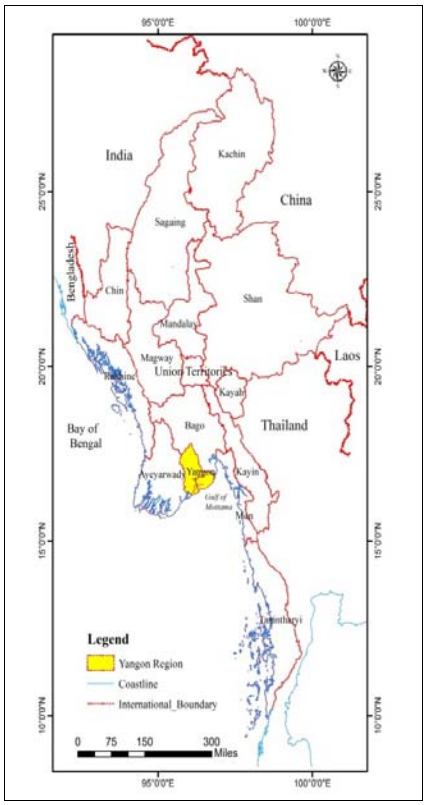

Figure 1. Location of Yangon Regions in Myanmar
Source: UTM Map of Myanmar Survey Department

Figure 2. Location of Dagon Myoyhit (North) Township
Source: Map Based on 1:50000UTM Map No.1696-01

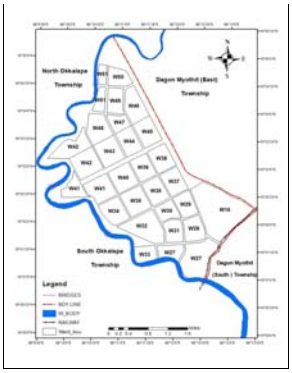

Figure 3. Location of Wards within Dagon Myothit (North) Township
Source: Township General Administrative Department

2. Method

Data processing was done from extracting geographic objects such as ward boundaries roads and streets by using based map of topographic map (1: 63360 and 1:50000) and Google earth images of geographically references data. Retail shops data from field survey (2018), using analysis of geospatial analysis and geostatistical analysis. Location of retail shop is analyzed by nearest neighbor analysis, directional distribution (Standard Deviation Ellipse) and cluster analysis (Anselin Moran I) which are used to present uneven distribution of retail shops.

3. Results and Discussion

For analysis purposes, retail shops can be divided into seven main types in Dagon Myothit (North) Township. They are (I) Food and Beverages, (II) Services, (III) Personal Goods, (IV) Building Material Shop, (V) Grocery Shop, (VI) Fabric shop and (VII) Others. (Table 1) The total number of retail shops was 727 in 2018. In survey 2018, study area of 27 wards found in total retail shop is 727 shops**.** It has 39.61 % of shop type I, 22.42% of shop type II, 15.54 % of shop type III, 7.02 % of shop type IV, 4.40 % of shop type V, 3.58 % of shop type VI and 7.43 % of shop type VII respectively. (Table 2, Figure.4) In the study area, largest retail shop type is type I of food and beverages shop. Retail shops are appears to the increasing population within a short span of time. Retailers are consideration of sold to meet the threshold of customer. Customers are

attracted the retail shops location on basis of accessibility of road side area. High accessibility area are enhances retail shops clustering pattern. Therefore, various types of retail shops were concentrated along the Pyi Htaung Su Road, Pin Lon Road, Bo Hmu Ba Htoo Road and U Wizara Road for having high population density and good accessibility. Among the various types of grocery, food and beverages shops, 75% are dynamic type and include such shops as dry goods, Monghinga and quid of betel, etc. Each of them can move and open easily in every suitable place. Therefore, food and beverages shop, and grocery shops are of footloose and hence have dispersed distribution pattern. Majority of the personal goods and fabric shops are found in linear pattern along the Pinlon Road. Building Material shops have both cluster and dispersed patterns. The building material shops selling likes sand and gravel shops are found along the Ngamoeyeik creek. Distribution pattern of services and other shops are somewhere between the clustered and dispersed pattern due to their type of function. For example, car workshop and car spa shops can be found on either side along the road. Some services like mobile phone services and beauty palor can be found in every ward. (Figure. 5)

Table1. Classification of Retail Shops

Type I	Food and Beverages	Tea shop, Coffee shop, beer station, cold and soft drink, liquor house, restaurant, Monhinga ,Shan noodle food, snack shop, chicken fried shop, rice and curry, Thai food etc,
Type II	Services	Beauty Palor, photo studio, photo copy service, clinic, car workshop, car spa service, T.V repairing service, KTV lounge, lottery shop, phone repairing service, purified drinking water service
Type III	Personal Goods Shops	Gold Smith shop, medicine store, cosmetic store, monk'robe and utensils shop, mobile shop, slipper shop
Type IV	Building Material Shop	Brick and sand shop, ceiling plate shop, timber shop, bamboo shop
Type V	Grocery Shop	Rice and edible oil shop, vegetable shop, ngapi and dried fish shop
Type VI	Fabric Shop	Textile shop, fashion shop, clothes shop
Type VII	Others	Furniture house, animal food shops, banner shop, pet shop, microfinance, floral and gift shop

Source: Field Observation (November, 2018)

Table2. Total Number of Retail Shop by Types (2018)

Types	Name	Number	%
I	Food and Beverages	288	39.61
II	Services	163	22.42
III	Personal Goods	113	15.54
IV	Building Materials	51	7.02
V	Grocery	32	4.40
I	Fabric	26	3.58
VII	Others	54	7.43
	Total	727	100

Source: Field Observation (November, 2018)

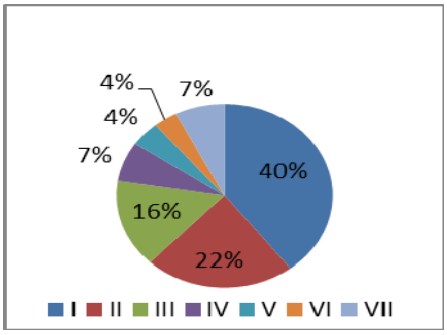

Figure 4. Total Number of Retail Shop by Types (2018)

The nearest neighbor analysis compares the observed average distances between nearest neighboring points and those of a known pattern. This test is required because a point distribution pattern is examined visually whether it is cluster or dispersed or not. It is also explained by computed R scale value. It is difficult to get exact conclusion on clustered or disperse pattern without calculating significant test to accept or reject R value. Therefore, significant test is calculated. The observed average neighbor distance, expected average neighbor distance, nearest neighbor statistics (R), and standardized Z score of the all types of retail shop are calculated to present clustered and dispersed pattern in the study area. According to nearest neighbor statistics, type I, II and III are more clustered than a random pattern since their nearest neighbor value is less than 1. It has been observed that type V is more dispersed pattern then their nearest neighbor value is more than 1. (Table.3)

Table.3 Average Nearest Neighbor Analysis

Types	**Z score**	**P Value Significant Level**	**R value**	**Distribution**
I	-9.037151	0.000000	0.721642	Clustered
II	-5.550311	0.000000	0.772756	Clustered
III	-5.546916	0.000000	0.727239	Clustered
IV	0.671261	0.502054	1.049133	Random
V	1.352297	0.000138	1.352297	Dispersed
VI	0.288505	0.772960	1.029576	Random
VII	0.504186	0.614131	1.035864	Random

Source : Field Survey and NN Analysis

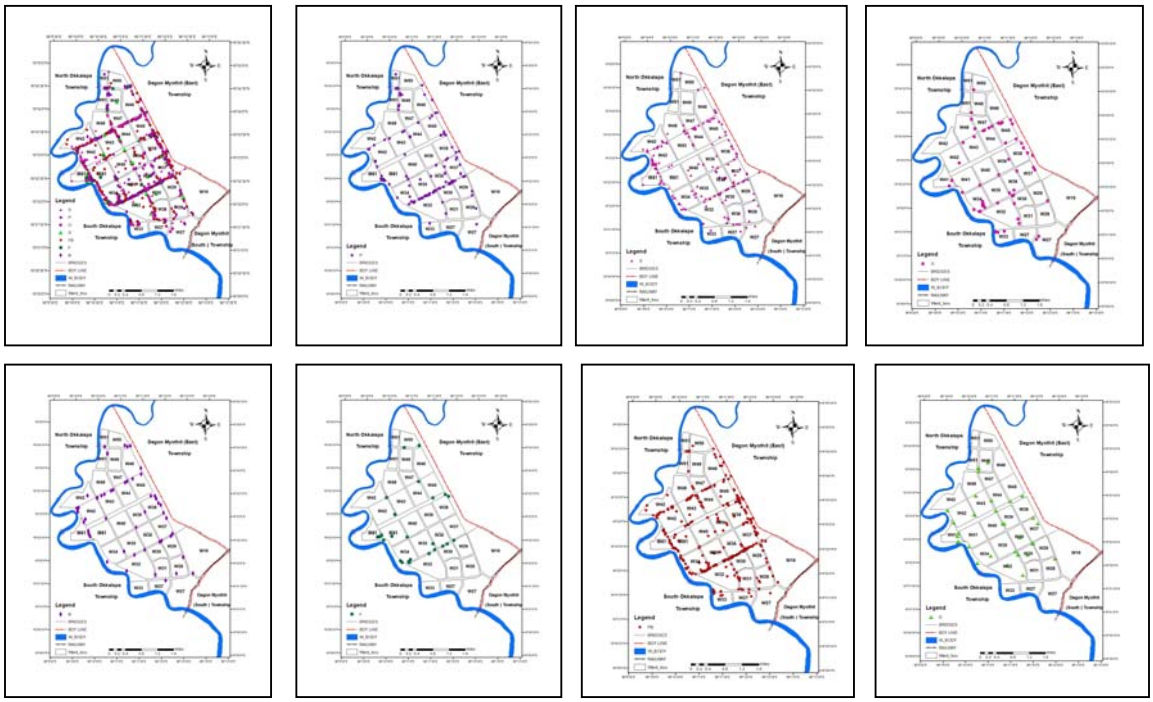

Source: Field Observation (Nov, 2018)

Figure 5. Distribution of Retail Shop by Types in Dagon Myothit (North) Township

Directional Distribution (Standard Deviational Ellipse) measures a distribution of features exhibiting a directional trend. Standard Deviational Ellipse provides information on the directional bias of their locations and also indicates the direction of urban growth. (Figure. 6) The most retail shops are found in southeast and northwest of the area. It is caused by situation of Ngamoeyeik Creek serving as northwest and southeast boundary.

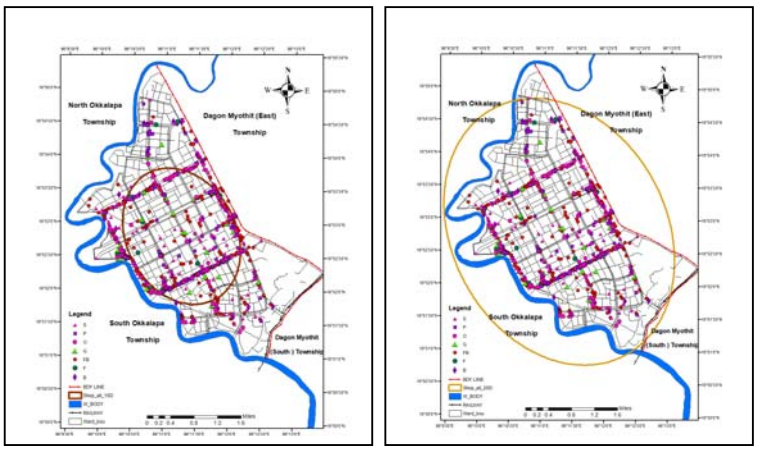

Figure 6. Directional Distribution of All Retail Shop in Dagon Myothit (North) Township

Given a set of weighted features, identifies statistically significant spatial outliers using the Anselin Local Moran's I statistic. Calculates as formula:

$$I = \frac{N\sum_{i=1}^{n}\sum_{j=1}^{n} w_{ij}(x_i - \bar{x})(x_j - \bar{x})}{(\sum_{i=1}^{n}\sum_{j=1}^{n} w_{ij})\sum_{i=1}^{n}(x_i - \bar{x})^2}$$

Where:

N is the number of observations (points or polygons)

Xi is the variable value at a particular location

Xj is the variable value at another location

Wij is a weight indexing location of i relative to j

The most common measure of Spatial Auto Correlation is used for points or polygons. It joins Count Statistic only for polygons. Use for a continuous variable (any value) and join count statistic only for binary variable (1,0)

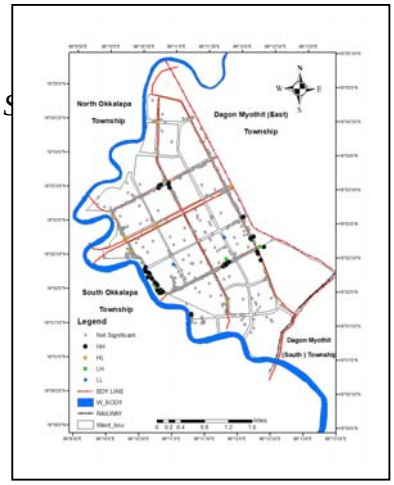

Figure 7. Anselin Local Moran's I Analysis of All Retail Shops

Table.4 Anselin Local Moran's I Analysis of All Retail

Group	Value	Number	Workers
1	HH	50	10-30
2	HL	8	5-10
3	LH	5	3-5

HH=High cluster, High Value

HL=High Cluster, Low Value

LH=Low Cluster, High Value

4. Conclusion

This paper analyzes the retail site location in Dagon Myothit (North) Township by using data obtain from Township Administrative Department and Yangon City Development Committee. To find out the relationship between retail shop and urban infrastructure like main road, Nearest Neighbor Analysis, Directional Distribution and Anselin Local Moran's I Analysis are used. According to the nearest neighbor analysis result is type I, II, III more cluster than the type V, VI and VII. As a result of directional distribution (standard deviation ellipse) of all type of 27 wards northwest and southeast direction are similar to the settlement expansion pattern and road pattern. Result of Cluster and Outlier Analysis (Anselin Local Moran's I) – U Wizara Road, Pinlon Road and Bo Hmu Ba Htoo road are high cluster value of total retail shops in Dagon Myothit (North)Township. (Z score 7.14 & P value 0.00). As a result, retail shop distribution pattern are related to the population density, road network expansion and settlement expansion

pattern. According to geospatial statistics analysis, the large numbers of retail shops are situated at both sides of main road. It shows that transportation roads really have an effect on development of retail shops in this area. Therefore retail site location, shops distribution pattern and trend are indicate the urban development processes.

Acknowledgements

I would like to express my heartfelt thanks to Professor Dr Htun Ko, Head of the Geography Department, University of Yangon for his kind permission and encouragement do this research paper.

Thanks are due to the respective authorizes Dagon Myothit (North) Township Administrative Department and the responsible persons and local people of Township for their ready help in data collection and willing responses to open talk.

References

[1] Aung Kyaw (2006):Spatial Structure of Retail Shops in Loikaw Town, Journal of Myanmar Art & Science, 2006 Vol IV, No 6 (ii)

[2] Khin Khin Htay (2015): Geostatistical Analysis on Retail shops Distribution of 13 wards and Bardo Village in Loikaw Township, Departmental Research Paper, Department of Geography, Loikaw University

[3] Lee,J. and Wong,D.W.S.(2000): Statistical Analysis with Arc View GIS. John Wiley & Son,Inc.New York

[4] Ye Wint Htut (2009): Retail Markets in Dagon Myothit (North) Township, Unpublished MRes: Paper, Submitted to the Department of Geography, Dagon University

Geospatial Analysis of Solid Waste Management in Bago City, Myanmar

Khin Khin Htay[1], Khin Mi Mi Win[2], KhinKhin Han[3], Zaw Zaw[4]

Abstract

Solid waste management of the study area is one of the basic factor to urban development planning of an area because of municipal solid waste is related the systematically collected system. This study only concerns with the urban area covering Bago City which has solid waste collection system and solid waste dump site area in the study area. The primary objective of this study is to practically apply geostatistics tools that can help to improve an evaluation of municipal solid waste for a particular area. A set of geostatistics tools has been applied to the different real data sets which were collected of solid waste form as household, market, commerce, hotel, garden and other waste. There are different methods of data analyses use in this study, which include: (1) spatial source of solid waste, (2) spatial solid waste collection systems, (3) Extend sustainable management of solid wastes, (4) Exploratory Geostatistical Data Analysis. As a result of spatial waste collection system in Bago city and spatial variation dump sites. Conclusion and recommendation of this paper are spatial management of municipal solid collected and sustainability of waste management, encourage people to think about the reduce, reuse and recycle, increase awareness raising the waste management system.

Keywords: Geospatial, Geostatistics, Municipal solid waste, Sustainable

1. Introduction

Solid waste is the useless, unwanted and discarded material resulting from day to day activities in the community. It is widespread problem in both urban and rural areas in many developed and developing countries. Solid waste management may be defined as the discipline associated with the control of generation, storage, collection, transfer, processing and disposal of solid waste. The present paper based on the study carried out on solid waste management practice in Bago City in Myanmar. Bago city is the economic development of lower Myanmar, located between 17° 14′13.59″ North latitude and 17°21′35.56″, between 96°26′15.15″ and 96°30′59.46″ East longitudes. This study was also designed and managing waste sustainably to study the composition of solid waste in Bago city. Municipal solid waste (MSW) collection and disposal is one of the major problems of urban environment in most countries worldwide today. Municipal solid waste management (MSW) solutions must be financially sustainable, technically feasible, socially, legally acceptable and environmentally friendly. Current Municipal Solid Waste Management (MSWM) system in the city of Bago is open dumping system and challenges are insufficient monitoring system, lack of people awareness, law enforcement and lack of research development facilities. In this situation, it is important to understand the current potential of environmental impact of current system in order to set up the new effective management system. Bago City has the 31 wards and central part of the city across the Yangon-Mandalay highway road. There are 53217houses in Bago city and the total population is 222309 in 2018. The average annual rainfall is 285.1 mm in 2018. In this paper, study on the geospatial analysis of municipal solid waste management and sustainable development of solid waste management system in Bago City.

[1] Dr. Associate Professor, Department of Geography, Bago University, Myanmar, kkhinhtay.geog@gmail.com
[2] Department of Geography, University of Yangon, Myanmar, khinmimimwingeog@gmail.com
[3] Professor and Head, Department of Geography, West Yangon University, Myanmar, drkhinkhinhan2013@gmail.com
[4] Assistant Lecturer, Department of Geography, Bago University, Myanmar, Zinlay23837@gmail.com

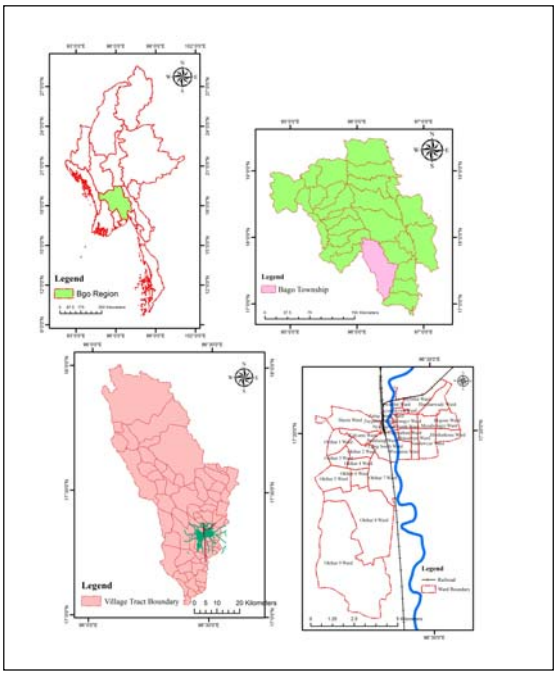

Figure 1. Location of the Study Area

Source: Based on Topographic Map (1:50000) and Google Earth Images (2017)

2. Methods

Garbage truck location data, waste collect sites data and waste collection routes data from Bago City Development Committee (BCDC) and field surveys in 2019. Methodology uses of this paper are geostatistical data analysis of the measures of Incremental spatial autocorrelation and others relevant statistical methods.

3. Results and Discussion

Solid waste can be classified into different types depending on their sources: These are (1) Municipal Solid Waste (MSW), (2) Hazardous Wastes, (3) Industrial Wastes, (4) Agricultural Wastes, (5) Bio-Medical Wastes and (6) Waste Minimization.

In this paper, examine the Municipal Solid Waste Management of the Bago City area. Municipal solid waste (MSW) management solutions must be financially sustainable, technically feasible, socially, legally acceptable and environmentally friendly. Solid waste management issue is the biggest challenge to the authorities of both small and large cities'. Municipal solid waste includes ash generated in thermal or electric power plants, sludge from wastewater treatment plants, animals' farm waste and gangue rocks from mineral extraction.

The activities associated with the management of municipal solid waste from the point of generation to final disposal can be grouped into the six functional elements. These are Waste generation, Storage, Collection, Transportation, Segregation & Processing, and Disposal. These municipal solid wastes including household kitchen waste as well as the domestic food waste from restaurants and markets consist of high lignocellulose materials that could be decomposed and exploited to produce valuable bio-products.

Solid waste management issue is the biggest challenge to the authorities of both small and large cities. Total solid waste generation is 84 tons /day in Bago city. From that solid waste

generation per person is approximately 200 gm/capita/day. Solid waste collection system are three time per day, first time of the day collected the along the Yangon-Mandalay highway road of garbage truck at 7am to 10 am. Second time of day collected the within the Wards at 10 pm to 12. The third time of day is collected the 1 pm to 3 pm. But, collected of car routes are distribute the whole wards except the Okkthar (9) Ward the southern part of City.

Plate 1. Solid Waste collection Sites in Bago City *Source: Field Survey, 2019 August*

Table 1. Sources and Types of Solid Wastes

Source	Typical waste generators	Types of solid wastes
Residential Food	Single and multifamily dwellings	wastes, paper, cardboard, plastics, textiles, eather, yard wastes, wood, glass, metals, shes, special wastes (e.g. bulky items, onsumer electronics, white goods, batteries, il, tires), and household hazardous wastes
Industrial	Light and heavy manufacturing, fabrication, construction sites, power and chemical plants	Housekeeping wastes, packaging, food wastes, construction and demolition materials, hazardous wastes, ashes, special wastes
Commercial	Stores, hotels, restaurants, markets, office buildings, etc.	Paper, cardboard, plastics, wood, food wastes, glass, metals, special wastes, hazardous wastes
Institutional	Schools, hospitals, prisons, government centers	Same as commercial
Construction and demolition	New construction sites, road repair, renovation sites, demolition of buildings	Wood, steel, concrete, dirt, etc.
Municipal services	Street cleaning, landscaping, parks, beaches, other recreational areas, water and wastewater treatment plants	Street sweepings, landscape and tree trimmings, general wastes from parks, beaches, and other recreational area, sludge
Process	Heavy and light manufacturing, refineries, chemical plants, power plants, mineral extraction and processing	Industrial process wastes, scrap materials, off specification products, slag, tailings

Source: World Bank 1999

In the Bago City, the Nearest Neighbour Analysis (NNA) result, garbage truck location pattern is the cluster pattern, Z score values is -6.22 and P value is the 0.000. According to the Nearest Neighbour Analysis (NNA) result, the whole city of garbage site location are near to the

each other's and suited the along the Bago-Yangon highway road and not suited the other parts of the Wards.

Highest population and houses of the Bago City is the Mazin Ward 23124 and 4752 house, Nantawyar Ward as 35076 and 7922 house in 2018 respectively. Mazin Ward is near to the Garbage Truck, Nantawyar Ward is not near the Garbage truck. But collected the waste by car system routes are more the Nantawyar Ward, Ponarsu Ward, Zaypaing, Nyaungwaing-south, Nyaungwaing-north, Zaing-south, Zaing-north, Hintharkone and Bokone Ward. Garbage trucks collected and collected by car of wastes are combined to the site of Sinphyukwin disposal site area. Sinphyukwin disposal site area is only the dump site, not repair the waste.

Plate 2. Classification of Solid waste in Bago City
Source : Bago City Development Committee

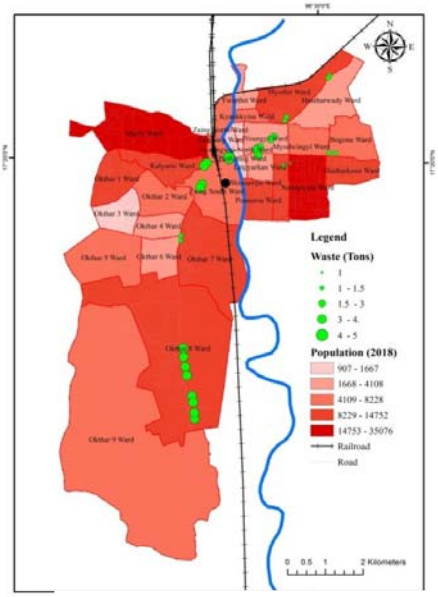

Figure 2. Garbage Truck Location and population in Wards of Bago City
Source : Data from the Bago City Development Committee and Bago Township Administrative

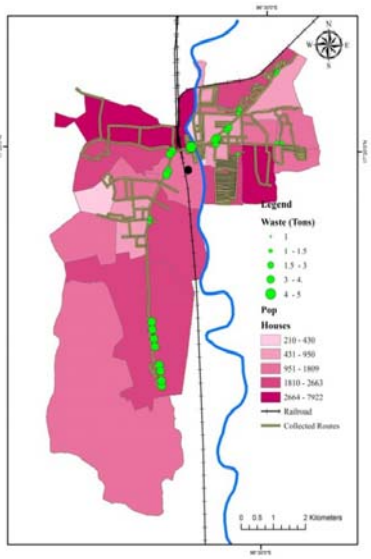

Figure 3. Solid waste collected routes and Houses of Ward in Bago City
Source: Data from the Bago City Development Committee and Bago Township Administrative Office

Measures of Incremental spatial autocorrelation for a series of distances and optionally creates a line graph of those distances and their corresponding z-scores. Z-scores reflect the intensity of spatial clustering, and statistically significant peak z-scores indicate distances where spatial processes promoting clustering are most pronounced. These peak distances are often appropriate values to use for tools with a Distance Band or Distance Radius parameter.

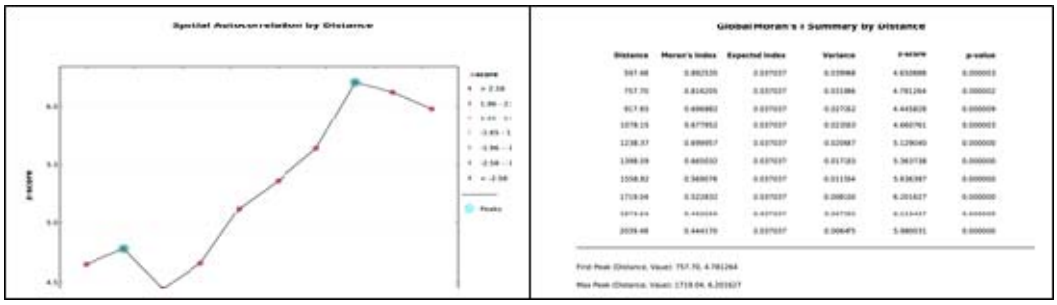

Figure 4. Spatial Autocorrelation by Distance of Garbage Truck Location and Waste tons

Source: Result of the Incremental Spatial Auto correlation

The center of the study area lies between Zaing-south and Shinsawpu Ward which is located the Yangon-Mandalay railroad. All the places of Garbage-truck location are found within the radius of 2100 meter. There are two peaks distance of garbage-truck sites and waste tons within the study area. One peak distance is about 757.70 meter and another is about 1719.04 meter away from the center Figure 5.

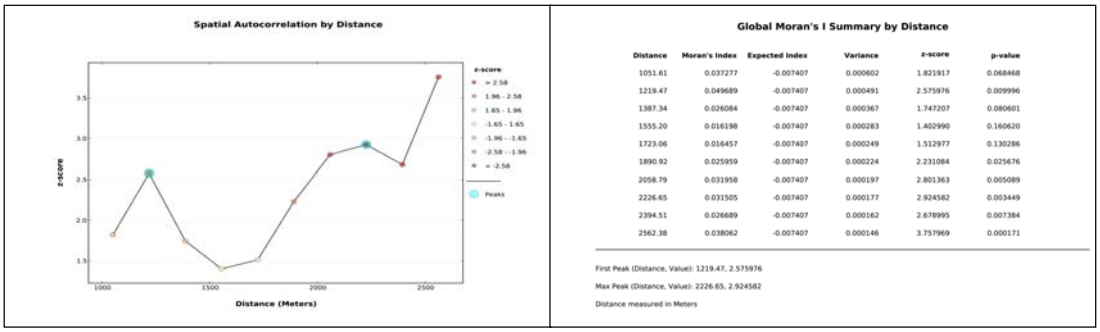

Figure 5. Spatial Autocorrelation by Distance of Solid Waste collected routes and Distance

Source: Result of the Incremental Spatial Auto correlation

The center of the study area lies between Zaing-south and Shinsawpu Ward which is located the Yangon-Mandalay railroad. All the waste collect route location is found within the radius of 2600 meter. There are two peaks distance of garbage-truck sites within the study area. One peak distance is about 1219.97 meter and another is about 2226.65 mete away from the center Figure 5. In 2017, Cooperation of Bago Municipal Development Committee and Green World Energy Co.., Ltd surveyed the waste of City area. In survey, composition Municipal Solid waste were separate of food and garden waste, plastic/rubber, glass, paper, metal, inert and textile. In this survey, food and garden waste is highest collect of 75.87 percent, the second is the plastic/rubber waste is 15.49 percent and the metal waste is lowest collect as 1.78 percent show Figure 6.

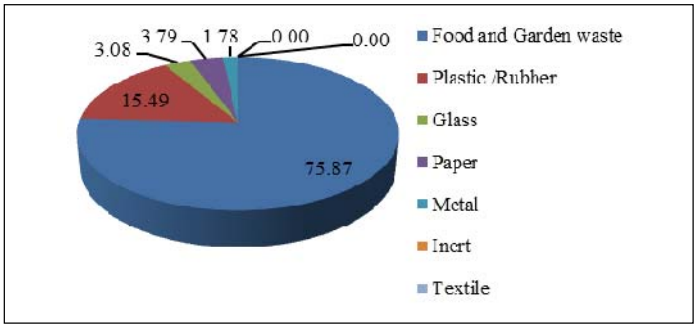

Figure 6. Composition of Municipal Solid Waste in Typical in Bago City Development Committee
Source : Data from Department of Bago Municipal

According to the 2017 survey, Bago Municipal Development Committee has municipal solid collected and sustainability of waste management encourages. It plan will be need the land area about 30 acres. Bago Municipal Development Committee is innovate the people to think about the reduce, reuse, recycle and increase awareness raising the waste management system.

4. Conclusion

The activities associated with the management of municipal solid waste from the point of generation to final disposal can be grouped into the six functional elements. There are Waste generations, Storage, Collection, Transportation, and Segregation & Processing Disposal. In Bago City, BCDC is serves as the waste storage, collection and transportation. The collected data show that the maximum proportion of refuse caused by food and garden wastes, second highest was plastic waste and the third highest was inert material. Percentage of Plastic carry bags was higher, where glass, ceramic and metals were nearly equal with each other in Bago City. As the disposal site is at 6.22 km away the City center and big and smaller vehicle are used for the transportation of solid waste. In Bago City areas: Primary collections are from households and blocks using carts or tricycles. Collectors transport the waste to local depots. Secondary collections use dumper trucks to transport waste from the depots to the disposal sites. Disposal in landfill sites typically 6-8 km from the wards in Bago City. Usually “open dump” sites but there are small engineered landfills in Bago. In the landfill area of advantages are minimizes human contact with the waste, Some potential for energy recovery, no need for separate collections and disadvantages are an expensive solution, more economical at large scale, still some risk of leachate pollution and gas emissions, Sites can be active for many decades, no potential for recycling, leachate and run off a particular problem in the rainy season. Future waste management plan of Bago City, MJT Group of Agricultural Machinery Co., Ltd will start to management of waste. In this project will start to test period at 1.9.2019 to 31.9 2019 the Leikpyarkan, Shinsawpu and Bokone Wards area. It should be done throughout the year. MJT Group plan will collected plastic waste and after renew of plastic seeds and others will make the bio-fertilize. System should be based on Environmental protection rules (reduce, recycle, reuse and recover) Public awareness, political will and public participation as essential for the successful implementation of the legal provisions and to have an integrated approach towards sustainable management of municipal solid wastes. There should be sufficient health and safety provisions for workers at all stages of waste handling. Finally, understand the amounts and composition of solid waste produced in Bago City. Appreciate Myanmar’s waste management

policy and plans. Understand the concept of "stakeholders". Identify the stakeholders involved in waste management in Myanmar people.

Acknowledgements

We would like to express our thanks to Dr Aye Aye Tun, Rector, Bago University for her permission and advice. And then our thanks are also due to Dr Yin Yin Than, Pro-Rector, Bago University for her encouragement and suggestion. I also thanks to Dr Mar Mar Khin, Professor and Head, Department of Geography, Bago University for their suggestion. Moreover, we are greatly thanks to local people in Bago Region and all teachers of Geography Department, Bago University for their help to get the data and conducted field survey.

References

[1] Ashish R et.al, Solid Waste Management – Case Study, International Journal of Research in Advent, Technology, Volume 2, Issues 1, January 2014.

[2] Kurian Joseph, Perspectives of solid waste management in India, International Symposium on the Technology and Management of the Treatment & Reuse of The Municipal Solid Waste, Shanghai, China, 2002.

[3] Hussein Abdel-Shafy, Solid waste issue: Sources, composition, disposal, recycling, and valorization, Egyptian, Journal of Petroleum- 27 (2018) 1275–1290, 2018.

[4] Gaurav K. Singh, Kunal Gupta, and Shashank Chaudhary, Solid Waste Management: Its Sources, Collection, Transportation and Recycling, International Journal of Environmental Science and Development, Vol. 5, No. 4, August 2014.

[5]Mainstreaming Integrated Solid Waste Management in Asia - Solid Waste Management Team, Integrated Solid Waste Management Plan Mandalay, Mainstreaming Integrated Solid Waste Management in Asia, 2016.

[6]Tin Min Htoo, Yoshiro HIGANO, The Environmental Impact Assessment of Current Municipal Waste Management System in Yangon City, Myanmar, Research Paper, 2016

[7]Frank Kreith, Hand Book on Solid Waste Management, The McGraw- Hill Companies, Inc. All rights reserved, Manufactured in the United States of America, 0-07-135623-1, 2002

[8]Bago City Development Committee and Green World Energy C., Ltd, Statistical Analysis Report of Solid Waste management in Bago City, Bago City Development Committee, 2017

Establishment of Sustainable Port Criteria in Myanmar

Mee Mee Soe[1], Min Han Htet[2], Khin Nawarat[3]

Abstract

Moving towards a sustainable port is a balance between the socio-economic development and protection of ecosystems. This paper attempts to establish the appropriate criteria to develop a standard for the sustainable port in Myanmar. It is based on the concrete literature reviews of sustainable principles not only from the Asia but also from all over the world for port development. After that, data collection and analysis step is performed to point out the current situations and challenges of port sector intended for sustainable future in Myanmar. Interviewing with the government agency like Port Authority and stakeholders are comprised to collect the data. Based on these local challenges facing in port industry, opinions from government authorities and stakeholders in combination with the reviews on sustainability principles, the criteria for a sustainable port which is the most promising for Myanmar are established.

Keywords: Challenges in port sector, Sustainable port criteria, Myanmar ports

1. Introduction

Sustainability is "Meeting the needs of the present without compromising the ability of future generations to meet their own needs" by Brundland Report [1]. Sustainability concept consists of environmental, economic and social dimensions and these three dimensions also referred as the triple bottom line of sustainability [2]. Ports are very complicated and combined activities of various services which have a wide range of environmental issues such as water releases, harmful emissions, waste and noise production and pollution [3, 4]. Seaports are notorious to be serious polluting industry; however, they have many opportunities for reducing emissions and pollutions [5]. Sustainability in the port industry is of growing source of fear for port authorities, policy makers, port users and local communities [6]. Therefore, sustainability is one of the important concepts for port industry and implementation of sustainable port development which satisfy economic, environmental and social dimension are intension of current and future generation. To achieve this intension, there are no exact determinations of sustainable port development criteria. To fulfil this gas in the literature, the present study aim to contribute the sustainable port criteria by analyzing the published databases in the literatures and by enquiring some experts and scholars from port related industry.

2. Literature Review

2.1 Sustainable Development – Shipping

Shipping operations interact with environment in many ways, either accidently or intentionally (Talley, 2006a) [7]. Heaver, (2006 b) reported such interactions of shipping operation with environment are generating substantial damages to natural habitats and affecting

[1] Dr, Lecturer, Department of Port and Harbour Engineering, Myanmar Maritime University, meemeesoe@gmail.com
[2] Dr Associate Professor, Department of Marine Engineering, Myanmar Maritime University, mhhtet79@gmail.com
[3] Teaching Assistant, Department of Port and Harbour Engineering, Myanmar Maritime University, khinnawarat.ph.mmu@gmail.com

maritime related economic activities such as ports[8]. Gupta et al. (2005c) studied that the environment is suffering from oil and chemical spills from ships [9]. In these aspects, Yang et al., 2013 suggested shipping firms are increasingly expected to adopt green practices to their system and process that promise environmentally friendly to the international community [10]. Cheng and Tsai (2009 a) also stated that it is a challenge for shipping firms how to perform shipping operations profitably with reducing their negative impacts on the environment [11].

The environmental impact on water quality and atmospheric pollution caused from ship operations were studied by several authors. Frankel (1987 b) included the impact of ballast water on port design and development plan [12]. Maritime operations such as bunkering may cause oil spill risks with potentially terrible impacts on beaches, food chains, sediment and fishing communities (Edoho, 2008; Idemudia and Ite, 2006c)[13,14]. Backhurst and Cole, (2000) concluded that ship operations such as anchoring may damage irreplaceable environments [15]. Gupta et al. (2005) studied various environmental impacts on surface water quality caused by ship and port discharges such as sewage, bilge, sludge, waste, oil discharges and leakages of harmful materials [9].

The emission from ships would affect the air quality in the port and surrounding areas. Zonn (2005b) studied the environmental pollution such as NOx, carbon dioxide (CO_2), sulfur dioxide (SO_2) emission caused by shipping, ports and terminals [16]. It is reported that containerships are by far the most important source of CO_2 emissions in the shipping industry (Psaraftis and Kontovas, 2009b) [17]. Walsh and Bows (2012b) studied the correlation between ship emissions and size as well as ship type [18].

Table 1 . Typical Survey Form which identify the Challenges by Activities with the important level to do the sustainable port development

(for one of challenges: Air Pollution/ Quality (emission of NO_x, SO_x, Black Carbon, PM, VOC's, etc.))

Air Pollution/ Quality (emission of NOx, SOx, Black Carbon, PM, VOC's, etc.)		Important Level				
		I	II	III	IV	V
1	By Land Use	☐	☐	☐	☐	☐
2	By Hinterland Connectivity	☐	☐	☐	☐	☐
3	By Port Structure & Port Construction	☐	☐	☐	☐	☐
4	By Shipping Vessels	☐	☐	☐	☐	☐
5	By Port Vessels	☐	☐	☐	☐	☐
6	By Port Operations	☐	☐	☐	☐	☐
7	By Cargo Handling Equipments	☐	☐	☐	☐	☐
8	By Land Traffic (Truck, Cars, etc.)	☐	☐	☐	☐	☐
9	By Bunkering	☐	☐	☐	☐	☐

Air Pollution/ Quality (emission of NOx, SOx, Black Carbon, PM, VOC's, etc.)		Important Level				
		I	II	III	IV	V
10	By Dredging	☐	☐	☐	☐	☐
11	By Fisheries	☐	☐	☐	☐	☐
12	By Recreation and Tourism	☐	☐	☐	☐	☐
13	By Cargo Storage	☐	☐	☐	☐	☐
14	By Oil and Chemical Spill	☐	☐	☐	☐	☐
15	By Ballast Water Disposal	☐	☐	☐	☐	☐

2.2 Sustainable Development – Port

Ports are considered responsible for a wider set of impacts and seek to resolve short-term views, private and public interests, and commercial and social objectives (Dooms et al., 2012c) [19]. However, (Acciaro et al., 2014a; Dinwoodie et al., 2012d) reported that port activities have adverse consequences on the environment effects [20, 21]. Puig et al., 2014b indicated that port activities would facilitate commercial and economic growth, but also likely cause deterioration of air and marine water quality in the surrounding [22]. In the year of 2015b, Wang et al., investigated port energy efficiency with financial success. They reported a framework of assessing energy efficiency of port operations on the data from public and data base. [23].

Port authorities and administration have to perform sustainable port in a satisfactory of economic demands, environmental and social activities. Daamen's (2007a) investigate port sustainable development in two different geographies to find a new typology and new interpretation of the contemporary port-city interface [24]. Abood K. A. (2007b) made a sustainability framework of New York Port with eight port operational topics such as dredging, ballast water, habitat restoration, air quality, water/energy/material conservation and waste handling [25]. In (2012e) Lam and Van de Voorde made a gap analysis for ports to formulate the concept of green and sustainable port strategy [26]. Jonathan et al. (2014b) propose a sustainable port planning model with the aid of basics of sustainability [27]. Hosseini et al. (2014c) investigated to 381 people to acquire urban sustainable development from citizens' rights point and determined most and least effected identifiers on sustainable port-city development [28]. Kutkaitis et al. (2014d) conducted interviews with practitioners of port and logistics sector to identify the criteria of sustainable port development. Hence, they prepared a set of indicators that determine different levels of sustainability of ports [29]. The decision making process of port authority using the literature review method is suggested by Martino, 2014e [30]. In Roh et al. (2016b) conducted in-depth interviews with Asian port authorities to determine the main factors that shaping sustainable port development. As a result, they identified key elements of sustainable port development from port authorities' perspective [31].

3. Method and Methodology

In this study, proposed indicators of sustainability are air pollution, water pollution, soil pollution, sediment pollution, waste, hazardous waste, noise, habitats loss and so on. The values

and limitations of those indicators have not been measured currently and have not been found in detail in the literatures. Moreover, there is a need to collect in-depth information on people's opinions, particular idea, experiences, desire, and so on. In this regards, a qualitative research technique such as structured-interview- research- methodology was conducted as a data collection (Boyce, C. and Neale, P., 2006d) [32]. For a structured interview, a set of standard, predetermined questions/survey forms are prepared for particular topics in specific orders. For the calculation of weighted values, very high important (I), high important (II), medium important (III), low important (IV) and no important (V) are set up as 5,4,3,2 and 1, respectively. For the interviews, the experts and scholars from port related industry such as Hohai University, Shanghai Maritime University, Myanmar Maritime University, Myanma Port Authority, and Department of Marine Administration in Myanmar have been asked through email using the predetermined survey forms.

4. Results and Discussions

4.1 Current Situations and Challenges

By doing the concrete literature review and discussion with the experiences of port and sustainable fields, the challenges for sustainable port development and port activities which make the challenge can be presented as shown in Table 1. By using this survey form, the opinions can be collected via emails. And then the survey data are weighted and the analysis results of important levels are organized in Table 2. This table can be easily observed by using color cells. Since water pollution/ quality by oil and chemical shows 100% in the color table, it can be clearly assumed that this challenge is the most important one to be performed in achieving the desired sustainable purposes.

The following factors are pointing out the percentage of above 80 percent. Land use, hinterland connectivity, land traffic, oil and chemical spills are the main causes of Air pollution/ quality. The three activities that causes water pollution are land use, dredging and ballast water disposal activities. The activities that causes soil pollution/ contamination are land use, hinterland connectivity and oil and chemical spills. Sediment pollution/ contamination is caused by land use and dredging activities. Waste is formed mainly by land use activities. Hazardous waste is mainly resulted from oil and chemical spills. Noise and higher energy consumption are the results of port structures construction. Land use, hinterland connectivity and land traffic causes traffic congestion. Port structures and dredging causes sedimentation in the vicinity of the port. Land use, hinterland connectivity, oil and chemical spills, ballast water disposal are the main reasons for habitat loss of marine organisms. The challenges concerning with the above mentioned activities are the second important challenges to be performed to achieve sustainable purposes.

The following activities can be performed and solved by taking time since they are 60 to 80 weighted activities. Noise and energy consumption caused by land use and sedimentation/ erosion problems are the activities which are necessary to take actions. Waste and noise resulted from hinterland connectivity should be take into account to meet the sustainable requirements. Air, water, soil and sediment pollution, waste, traffic congestion, erosion and habitat loss caused by type of port structures and construction should be considered to reduce the sustainably against situations. Air and water pollution, various waste, noise and energy consumptions are mainly caused by shipping vessels. And also, air and water pollution, hazardous waste, noise and energy consumption are caused by port vessels. Moreover, air pollution, waste, hazardous waste, noise, energy consumption and traffic congestion are mainly caused by port operations.

The challenges caused by Cargo handling equipment, land traffic, bunkering, dredging , fishery, recreation and tourism, cargo storage, oil and chemical spills, ballast water disposal etc. can be observed in the following color map according to their important level as shown in Table 2.

Table 2. Results of Important level of Activities and Challenges Relationship for Sustainable Port Development

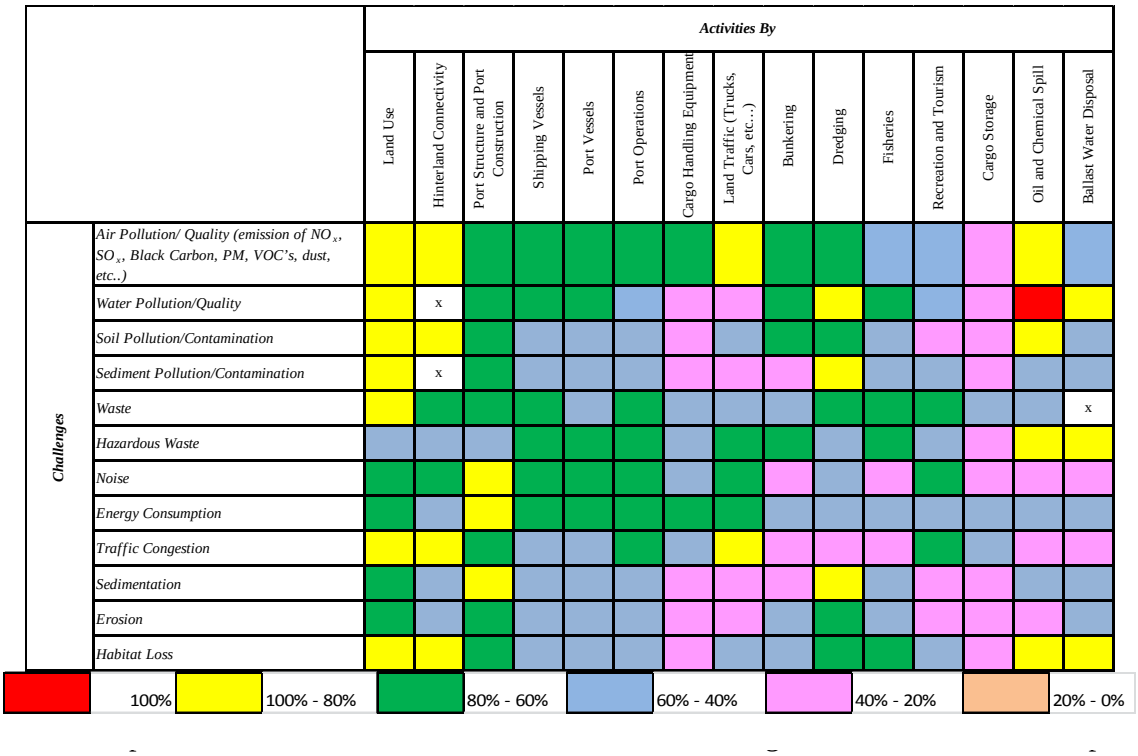

4.2 Sustainable Criteria For Myanmar Port Development

Proposed sustainable criteria based on the review of the guidelines of international ports and the analysis of the port operation experience and challenges with Local Port Authority and stakeholders are listed as follows:

Land use mainly causes pollution and waste. It can also happen traffic congestion, energy consumption, noise, and habitat loss. Effectiveness of existing ports should be promoted with the sustainable practices instead of building a new one. If a new port has to be propose in order to meet the country requirement, a well-made feasibility study should be prepared to choose the location which is the least environmental damage one. Public space and habitat conservation desire should be added in port area planning for the health, recreation and the nature. Port stakeholders' meeting should be held with well-prepared port master plan to decide the land use and local people participation should also be emphasized.

Mode of transport connecting the ports with industrial zone, downtown area and other hubs, etc. should be carefully analyzed in order to avoid the traffic congestion. Transport connectivity plan is vitally needed with the suitable mode of transport. Especially rail transport

network should be arranged with the collaboration of related sectors. So that, the consequences such as time-consuming, feel tired, fuel energy loss and risk of accidents between containers, regular-size cars, slow moving vehicles and people, etc. of uncomfortable transport system can be avoided. Furthermore, Myanmar's inland waterways should be more encouraged doing the investment for cargo and container transportation. This method is cost-effective and it can be reduced the traffic congestion and energy consumption. For the existing ports, current transportation network should be requested to submit and if necessary, appropriate modifications for better network should be done under the charge of the government with the full effort of port owners.

Erosion and sedimentation conditions in water area caused by existing jetty and port structures should be analyzed and informed to the corresponding authorized body. Also the proposed solution to these observed problems should be attached during the inform process. Erosion and sedimentation estimation must be perform before constructing a new structure. The technologies and designs which coincide best to the sustainable requirements should be used during the whole construction process. Sustainable codes for design and construction are also necessary to establish.

Shipping and port vessel causes pollution and waste, energy consumption and noise. The type and size of allowable shipping vessels should be according to the international sustainable criteria. The shipping vessels should follow the rules and regulations which are established according to the international standards. Strict monitoring and actions should be taken for the enforcement of rules and regulations.

Noise and air pollution caused by port operation in port area should be assessed by using monitoring devices. The methods using in the port facilities should coincide with the sustainable needs. Renewable resources such as solar, wind and tidal energy should be replaced in the conventional resources. LED technology should be replaced in lighting inside the port area. Light reduction equipment should be used to reduce annoyance to the nearby residential area [33].

In practice, cargo handling equipment consume large amount of energy. Replacing smart and green cargo handling equipment in port operation can not only reduce the energy consumption but also protect the environment and increase the cost efficiency [34].

Air pollution, traffic congestion, noise and energy consumption can be reduced by establishing good driving practices and applying well trained drivers in land traffic.

Transfer procedures among vessels, bunker stations, bunker vessels, terminal and trucks should be well defined and followed to avoid the pollution and hazardous waste.

In Myanmar, the energy consumption for maintenance dredging works is very large. Dredging is also a major issue to be considered in achieving sustainable requirements. To reduce the energy consumption in dredging works, the location of the deep sea ports should be proposed to an area where dredging works are not necessary. Even if necessary, the proposed site should be chosen wisely where the dredged material can be reused. If disposal of dredged material is unavoidable, the disposal site should be analyzed and allocate carefully.

Since fishery can affect health and environment, good management is required in these fishery ports. Good fishing practice and management should be launched for the reduction of waste. Warning and taking action by using severe penalty system can be used to reduce waste

and noise caused by recreation and tourism. Ballast water disposal can cause the habitat loss of marine organisms. Taking actions in enforcing the existing laws can enhance the protection of the species. If oil and chemical spills occurred, air and water pollution and the habitat loss of marine organisms can happened in serious condition. Therefore, the rules and regulations concerning with oil and chemical spills should be establish precisely and accurately. And also even when spills happened, taking action effectively and removing in a very quick manner should be performed to avoid the unnecessary circumstances.

5. Conclusion

In this paper, we have tried to point out the sustainable challenges by port activities intended for Myanmar ports. The literature was concretely reviewed to identify the activities and challenges. And then the important level of challenges was collected with surveying the experiencers and specialist of port and sustainable fields and it can be seen the colour table to analyze easily. . Later this can be done the large scale for sustainable purpose with more activities and challenges. It was found that land use, hinterland connectivity, are the main activities for sustainable challenges and also port structure and construction, dredging, oil and chemical spill, ballast water disposal cause the challenges This paper proposed some sustainable criteria in accordance of challenges of Myanmar ports such as effective land use, Inland water way transport, Ship size and type limitation, enforcement of rules and regulations.

Acknowledgements

This paper is the first step of our proposing the sustainable criteria for Myanmar port sector and we would like to thank Dr. Tao Aifeng, Dr. Mu Mu Han, Dr. Myo Nyein Aye, Mr. Ye Naing for supporting of their valuable experience.

References

[1] Brundtland, G. H., United Nations,1987a.

[2] Sislian, L., Jaegler, A. and Cariou. P., “Research in Transportation Business & Management,”2016a, 19, 19-26.

[3] Hakam, M. H., “Journal of Service science and Management,” 2015a, 8(01), 14.

[4] Darbra, R. M., “Marine pollution bulletin,” 2005, 50.8: 866-874.

[5] Broesterhuizen, E. F. M., Vellinga, T., Docters van Leeuwen, L., Zwakhals, J. W., Taneja, P. and Nijdam, M. Cesun2012, 2012a.

[6] Acciaro, M., Ghiara, H. and Cusano, M.I., Energy Policy, 2014, 71, 4-12.

[7] Talley, W.K., “Port performance: an economic perspective,” in Brooks, M. R. and Cullinane, K. (eds.), Devolution, Port Governance and Port Performance, Amsterdam: Elsevier Ltd., 2006a, pp. 499-516.

[8] Heaver, T., “The evolution and challenges of port economics,” in Brooks, M.R. and Cullinane, K. (eds.), Devolution, Port Governance and Port Performance, Amsterdam: Elsevier Ltd., 2006b, pp. 11-41.

[9] Gupta, A.K., Gupta, S.K. and Patil, R.S., “Environmental management plan for port and harbor”, Clean Technologies and Environmental Policy, 2005a, Vol. 7, No. 2, pp. pp. 133-141.

[10] Yang, C.S., Lu, C.S., Haider, J.J. and Marlow, P.B. , “The effect of green supply chain management on green performance and firm competitiveness in the context of container shipping Taiwan,” Transportation Research Part E, 2013, Vol. 5, pp. 55-73.

[11] Cheng, Y.H. and Tsai, Y.L., "Factors influencing shippers to use multiple country consolidation services in international distribution centers," International Journal of Production Economics, 2009a, Vol. 122, No. 1, pp. 78-88.

[12] Frankel, E.G., Port planning and development, New York: John Wiley & Sons Inc., 1987b.

[13] Edoho, F.M., "Oil transnational corporations: corporate social responsibility and environmental sustainability," Corporate Social Responsibility and Environmental Management, 2008, Vol. 14, No. 4, pp. 210-222.

[14] Idemudia, U. and Ite, U.E., "Corporate-community relations in Nigeria's oil industry: Challenges and imperatives," Corporate Social Responsibility and Environmental Management, 2006c, Vol. 13, No. 4, pp. 194-206.

[15] Backhurst, M.K. and Cole, R.G., "Biological impacts of boating at Kawau Island, north-eastern New Zealand," Journal of Environmental Management, 2000, Vol. 60, No. 3, pp. 239-251.

[16] Zonn, I., "Environmental issues of the Caspian," in Kostianoy, A. and Kosarev, A. (Eds.) The Caspian Sea Environment, Berlin: Springer, 2005b, pp. 223-242.

[17] Psaraftis, H.N. and Kontovas, C.A., "CO2 emission statistics for the world commercial fleet," WMU Journal of Maritime Affairs, 2009b, Vol. 8, No. 1, pp. 1-25.

[18] Walsh, C. and Bows, A., "Size matters: Exploring the importance of vessel characteristics to inform estimates of shipping emissions," Applied Energy, 2012b, Vol. 98, pp. 128-137.

[19] Dooms, M., Verbeke, A. and Haezendonck, E., "Stakeholder management and path dependence in large-scale transport infrastructure development: the port of Antwerp case (1960-2010)," Journal of Transport Geography, 2012c, Vol. 27, pp. 14-25.

[20] Acciaro, M., Vanelslander T., Sys, C., Ferrari, C., Roumboutsos, A., Giulliano, G., Lam, J.S.L. and Kapros, S., "Environmental sustainability in seaports: a framework for successful innovation," Maritime Policy & Management, 2014a, Vol. 41, No. 5, pp. 480-500.

[21] Dinwoodie, J., Truck, S., Knowles, H., Benhin, J. and Sansom, M., "Sustainable development of maritime operations in port," Business Strategy and the Environment, 2012d, Vol. 21(2), p.111-126.

[22] Puig, M., Wooldridge, C. and Darbra, R.M., "Identification and selection of Environmental Performance Indicators for sustainable port development," Marine Pollution Bulletin, 2014b, Vol. 81, No. 1, pp. 124-130.

[23] Wang, H., Huo, D. and Ortiz. J., Open Journal of Social Sciences, 2015b,3(05), 28.

[24] Daamen. T., In ENHR-conference, 2007a,25-28..

[25] Abood, K. A., In Ports 2007: 30 Years of Sharing Ideas: 2007b,1977-2007.

[26] Lam, J. S. L. and E. Van de Voorde. International Forum on Shipping, Ports and Airports (IFSPA), 2012e, 27-30.

[27] Jonathan, Y. C. E., Kader, A. S. A., Bin Ahmad, Z., Mokhtar, I., "Green and sustainable port project planning: paradigm shift for an integrated container handling system expansion,"2014b.

[28] Hosseini, S. A., Amozad, H. and Mafi, M.K., "European Online Journal of Natural and Social Sciences," 2014c, 3(3), 810.

[29] Kutkaitis, A., Šimanskiené, L.and Burgis, D., "Scientific Papers of the University of Pardubice," Series D, Faculty of Economics & Administration, 2014d, 21(30).

[30] De Martino M., "In Advanced Engineering Forum Trans Tech Publications," 2014e, 11, 87-95.

[31] S. Roh, V.V. Thai and Y.D. Wong. The Asian Journal of Shipping and Logistics, 2016b, 32(2), 107-118.

[32] Boyce, C. & Neale, P., "Conducting in-depth Interviews: A Guide for Designing and Conducting In-Depth Interviews", Pathfinder International Tool Series, 2006d.

[33] Dalwon Kang & Sihyun Kim, "Conceptual Model Development of Sustainability Practices: The Case of Port Operations for Collaboration and Governance", December 2017, 9(12):2333

[34] Jasmine Siu Lee Lam, 'Smart and green cargo handling equipment for port sustainable energy management", October 2018

Effective Control of Hybrid Solar-Hydro Renewable Energy System

Wut Hmone Oo [1], Khin Mar Win [2], Hla Htay Win[3]

Abstract

This research presents the control system of prototype hybrid power driven by two sources of renewable energy which purpose is to provide the continuous electrical power using solar-hydro renewable energy system without causing the environmental pollution. The voltage generated from the solar panel and waPter mill will be stored on a large battery by two different modes, real time mode and switching mode. The real time clock module is used to control the real time data from solar phase during the daytime and a hydro phase is used at night. The solar voltage is recognized as the first priority charging mode from 8:00 a.m. to 5:00 p.m. and the hydro charging mode will start working after solar charging time. Since the availability of voltage from solar and water sources depends on the weather condition, the switching mode needs to be manually changed in the hybrid control system. The hybrid system operates only with higher power source by reading the voltage firstly and then switching the voltage given by higher power plant. The system is constructed with a programmable microcontroller development board, voltage divider circuits, real time clock module, a few input switches and charging control circuit.

Keywords: solar energy, hydro power, hybrid control system, renewable energy sources

1. Introduction

Nowadays, pollution is one of the most serious problems in the world. The best way of reducing CO_2 emission is to use clean source of electrical energy produced from renewable energy. Among these renewable sources, hydroelectric power and solar power are the two most common sources for generating electricity for rural areas. However, these energy sources greatly depend on weather conditions and possess inherited intermittent nature. So, hybrid system, one of the complex control systems due to integration of two or more renewable energy, becomes a solution to those limited conditions [1]. The power generation capacity of hybrid system is more than the power generation capacity of the individual system. The major advantage of solar-hydro hybrid energy system is that when used together, reduces the cost of supplying electricity [2]. In solar-hydro hybrid system, solar panel directly converts solar radiation into electrical energy and hydroelectric system is the process of generating electrical energy by converting kinetic energy of water into mechanical work to turn the turbine [3]. This hybrid power system is suitable for remote places. Rural areas need generation in the form of hybrid power system [4].The scope of the hybrid renewable power system is very high and it is very advantageous for both rural and urban areas [5]. In Myanmar, especially in Tanintharyi Region which lies on the southern part of Myanmar in North Latitude 13° and East Longitude 98°45´, fifth largest region in Myanmar, majority of rural areas are still lack of electricity. Therefore, candles and oil lamps are still being used in those areas. The photograph of the map of Tanintharyi Region is expressed in figure 1 and it is the best location for generating renewable energy such as solar energy from sunlight, and hydro power from water resources. As per annual data recorded from regional department of meteorology and hydrology, both the rainfall (inches) and the sunshine hours in Tanintharyi region is the higher and longer than those in other cities in Myanmar. The Monthly maximum

[1] Department of Physics, Dawei University, Myanmar, hmone1390@gmail.com, +959422203725
[2] Engineering Physics Department, Mandalay Technological University, Myanmar, drkhinmarwin@gmail.com
[3] Department of Physics, University of Bago, Myanmar, hlahtayphy2016@gmail.com

rainfall, Average monthly rainfall, monthly maximum sunshine and average monthly maximum sunshine are illustrated in figures 2-5. So, the effective control of hybrid system is one of the main advantages for rural areas in this region and can provide a good solution for those areas, villages nearby the rivers, streams, mountain, waterfall, and under sufficient sunshine. Furthermore, the system can solve the demand of electricity in regional problem successfully.

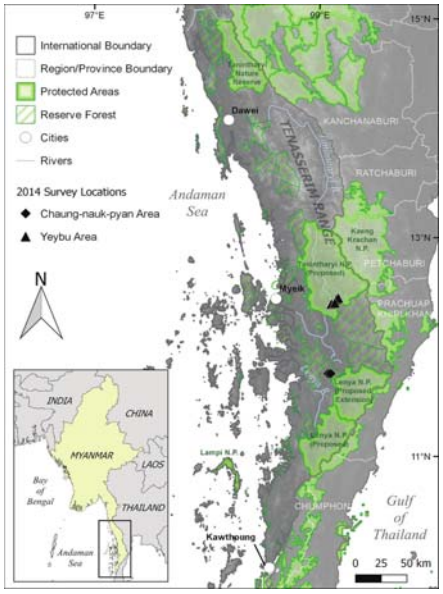

Figure 1. Map of Tanintharyi Region Myanmar [www.researchgate.net]

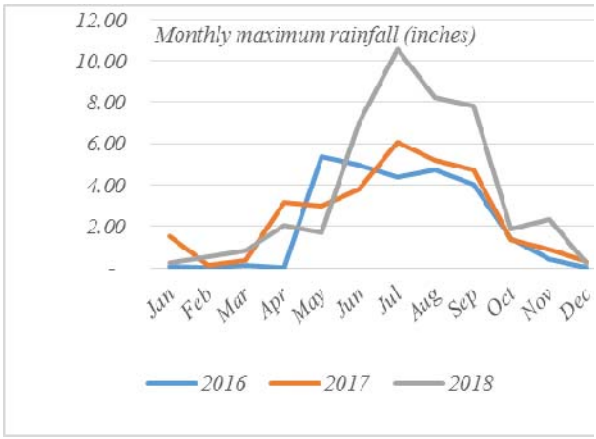

Figure 2. Monthly maximum rainfall

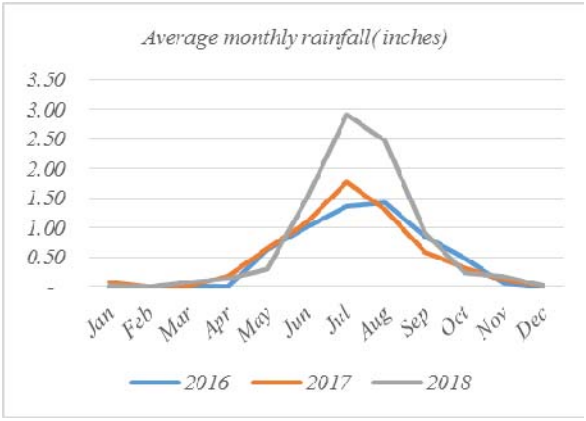

Figure 3. Average monthly rainfall

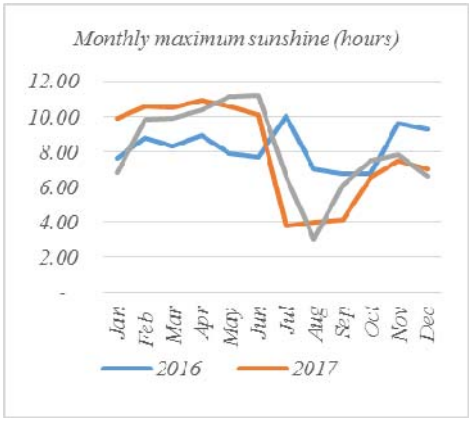

Figure 4. Monthly maximum sunshine

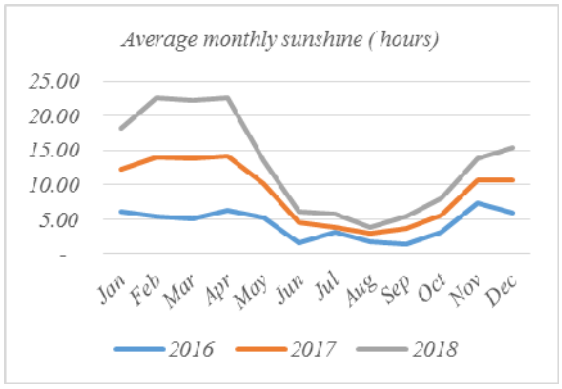

Figure 5. Average monthly maximum sunshine

2. Design and Simulation of Hybrid Power Control System

2.1 Circuit Simulation

The Proteus 8.1 software is a Printed Circuit Board (PCB) design software integrated with the simulation of the circuit design. The main purpose to design with Proteus software is to get the optimum circuit diagram. In this research the circuit design consists of eleven main parts**;** an 8-bit programmable microcontroller (ATmega328p), a crystal oscillator, an alphanumeric liquid crystal LCD display, a few control input switches, a real time clock module, three voltage divider circuits that are used to divide the output voltages of solar plant, hydro plant and storage battery, transistors, relays driver circuits, storage battery, a 5V regulated power supply circuit and a charge controller units. The control system operates together with the two different power plants, charging controller circuit, inverter circuit and storage units. The basic structure of the hybrid system is illustrated with a block diagram in figure 6. The complete schematic diagram of hybrid solar-hydro control system is shown in figure 7.

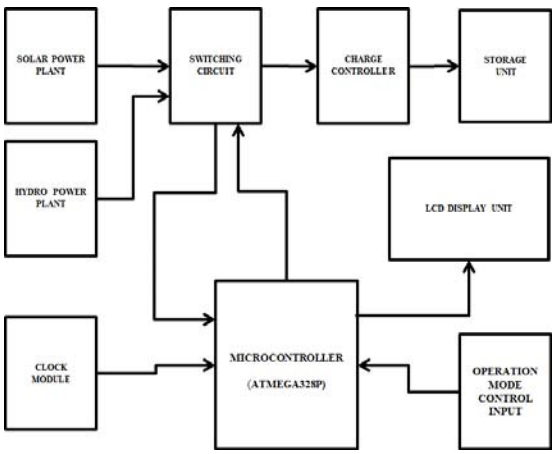

Figure 6. Block diagram of the hybrid solar-hydro power control system

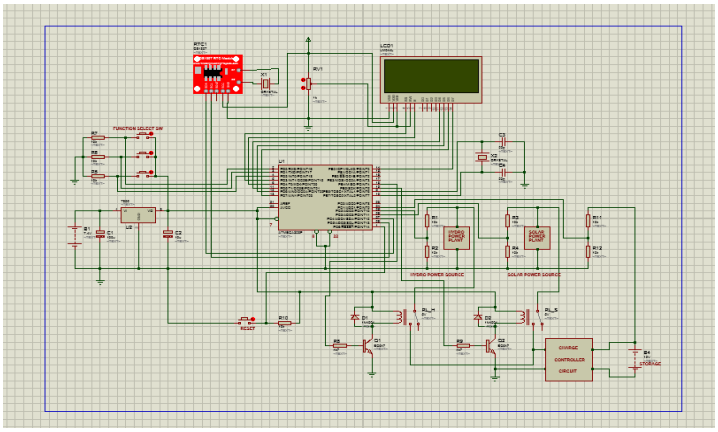

Figure 7. Complete schematic diagram of hybrid power control circuit

2.2 Controller Circuit

The microcontroller is an 8-bit microcontroller and it is Atmega328p. The microcontroller itself cannot operate to run the operation of the circuit; therefore, a program code was created and uploaded into the memory ROM of microcontroller before building the circuit. The program coding was created by using Arduino IDE software. In this circuit design, the program memory in microcontroller cannot execute each instruction without an external clock circuit. In this case, a 16MHz crystal oscillator is connected with the two pins of microcontroller. A real time clock module circuit is included in this circuit design to control the hybrid power system according to the real time data. The real time data can differentiate both day or night and seasonal periods of month within a year. For the experimental process, it is required to create two different circuit boards to complete the prototype design for hybrid power control system since the design of circuit is very complex and consisting of numerous components. The circuits are known as controller circuit and switching circuit. The control circuit consists of four pairs of green terminals, two on the upper edge and other two on the right edge of the circuit. The first terminal on the upper edge is to connect with the solar power plant. The second green terminal is to connect with the hydro power plant. The first green terminal on the right is to connect with battery storage. The second green terminal is to connect with the charge controller circuit. Moreover, there are three voltage divider circuits with three trimmer resistors which are used to divide the voltage of solar power plant, hydro power plant and battery voltages. The control sketch is written in c programming language and the flow chart of the hybrid power control system is as shown in figure 8.

2.3 Switching Circuit

There are two relays and relay driver circuits. Each of the relays cannot be directly operated with a microcontroller since it is a coil device. Therefore, the relays are used to switch the connection between the storage battery and power plants. The common pin of each relays are connected with the solar plant and hydro plant. The normally open pins of relays are connected with the storage battery. There are three control switches on the circuit, and they are wired as active high input switches. They are connected with the three digital pins on the microcontroller. In the moment, only one input switch is used and it is to change the operation mode between real time control (RT CON) and higher voltage control (HV CON). Completely installed and ready to

test circuit board is shown in figure 9 and default operating condition and voltage displays in figure 10.

2.4 Operation of Hybrid Power Control System

The whole circuit will operate with two 3.7V Li-ion batteries. It is not a suitable power supply for the microcontroller and LCD display, real time clock module and relays on the circuit. Therefore, a 5V regulator IC (7805) is utilized to become Vcc voltage level to 5V. When the power supply on/off switch is pressed, the LCD display illuminated the data of clock on the first line. Each voltage level is going to be illuminated on the LCD displays. But the actual maximum input of analog voltage to the microcontroller was limited to 5V. If it is higher than 5V, the microcontroller may damage. Therefore, voltage divider circuits are used in the design. The real time clock function operation is very useful and the system operation can be automatically made by predefined periods. In this design, the default mode operation for hybrid power control system is "RT CON". The operation period predefined for the solar power plant is within a period starting from 8:00 to 17:00 hours. In the display photo as shown in figure the clock is 20 hour, and it is greater than17 hours predefined period, therefore the operation of hydro power plant will be operated. The operation system is predefined for hydro power plant after solar charging time. In this case, the switching on power plant is display on the screen "Hy_P_ON" (hydro power on). If the time is between 8:00 and 17:00, the system will change the solar power plant automatically. In this case, the switching on power plant is display on the screen as "S_P_ON" (solar power on). In switching circuit, voltage divider circuits with blue trimmer resistors are used to divide the input voltages of solar power plant, hydro power plant, and battery voltage terminals.

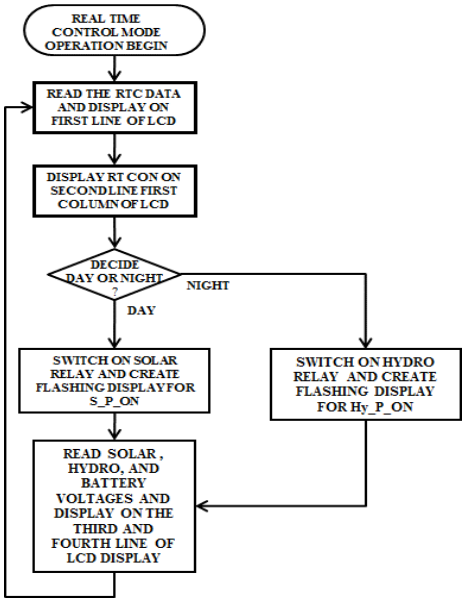

Figure 8. Flow chart of the hybrid power control system

Figure 9. The photograph of the hybrid power control circuit

Figure 10. Default operating condition and voltage display

Figure 11. Calibration of solar power plant voltage

Figure 12. Calibration of hydropower plant voltage

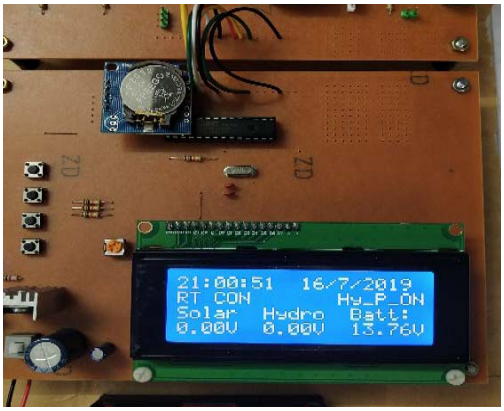

Figure 13. Calibration of storage battery voltage

Figure 14. The selection of operation mode for HV CON

3. Results and Discussion

The solar-hydro hybrid power control system is constructed and the operations have been tested for several times for different results. The hybrid control system is based on ATMEGA328 microcontroller. Moreover, there are two types of relay control pins, relay for hydro power plant and relay for solar power plant. If the power output of solar power plant is higher than input from the other power plant, then the solar relay will operate. If the power output of hydro power plant is higher than input from the other power plant, then the hydro relay will operate. The voltages of each power plant and battery shows 0V, since no power plant and battery are connected on the switching circuit. Therefore, before connecting with any power plants, a variable power supply is

connected instead of solar power plant. Then, the variable power supply is switched on and checks the result display screen on the voltage position of solar power plant. Figure 11 shows the calibration of output solar power voltage plant in hybrid energy system. If the voltage difference between the display of variable power supply and constructed circuit is not equal, it can be adjusted by slowly turning the trimmer resistor with a small flat screw driver. Similarly, the variable power supply is connected on other remaining terminal inputs and calibrated as shown in figure 12 and 13 respectively. The simulation carries out nearly 10 hours between 8:00 and 17:00 hours in a sunny day. In addition, the two power plants are combined with a microcontroller and manage for real time control (RT CON) and higher voltage control (HV CON).So to be able to use effectively higher power source, the manual selection of either “HV CON” from “RT CON” operation mode or “RT CON” from “HV CON” operation mode is required after reading the voltage level. The press of mode switch toggle the two operation mode as shown in figure 14.The availability of the electricity in Tanintharyi Region is only 10.7% and the lowest in Myanmar. According to the results of the proposed research and the above data information shown in the chart, the rainy season is about 6 months and monthly maximum and average rainfall are 10.55 inches and 2.91 inches respectively as shown in figure 2 and figure 3 . Except the rainy period, it is sunny over the course of the year.Monthly maximum and average sunshine are 11.2 hours and 8.48 hours as shown in figure 4 and figure 5.Therefore, the hybrid power control system can be the most suitable hybrid system to solve the lack of electricity and provide continuous power generation in Tanintharyi region especially for rural areas.

4. Conclusions

The use of hybrid power control system is the most effective and efficient ways of generating electrical power. The designed system is intended to reduce the cost of supplying electricity and to solve the power requirement in rural community. Single source system provides discrete power if the source is faced disable conditions. The solar-hydro hybrid system can be used in any region that has the sufficient solar radiation and sufficient kinetic energy of water flow. In such region, the condition of solar power and hydro power will be power complement of each other when the seasonal and variations of the weather condition occur. According to the annual results of weather station of Tanintharyi region figures 2-5, solar-hydro hybrid system should be used rather than other renewable energy generating system. Hybrid system will be able to provide the continuous power generating processes along the coastal region and for sustainable development. Although the system designed is made to be flawless, sudden unexpected changes on weather conditions may arise problem states. But the causes of problem state are negligible comparing with its overall advantages.

Acknowledgements

I would like to express my profound thanks to Professor Dr San San Aye, Head of Department of Physics, and Professor Dr Khin Swe Oo, Department of Physics, Dawei University, for their kind permission to carry out this work. Special thanks are Dr Thiri Khin, Lecturer, Department of Physics, Dawei University, for encouragement and help during this work.

References

Binayak Bhandari, Shiva Raj Poudel, Kyung-Tae. Lee, and Sung-Hoon Ahn, "Mathematical modeling of hybrid renewable energy system: A review on small hydro-solar wind power generation", 2014, Vol.1, pp.157-173.

Bhushan. D. Agarkar and Shivprakash B. Brave, "A review on hybrid solar/ wind/hydro power generation system", 2016, vol.4, pp.188-191.

G. Joga Rao and S.K Shrivastava, "Modeling and implementation of hybrid solar-hydro renewable energy systems", 2016, Vol.3, pp.63-69.

G.Lakshmi,P.V.V. Rama rao, Y.R. Palleswari,"Power Management of Hybrid Renewable Energy System by Frequency Deviation Control",2014,Vol.10,pp.243-251.

Diksha.A. Shinde, "Power quality improvement by solar –hydro hybrid system", 2016, (IJIRST), Vol.3, pp-234-236.

Kavitha Sirasain and S.Y. Kamdi, "Solar wind hydro hybrid energy system simulation", 2013, (IJSCE) Vol.2, pp.500-503.

B.Murali Mohan, S. Muqthiar Ali and P.Manohar, "Designing and control of isolated wind-hydro hybrid system with BEES", 2014, Vol.10, pp.64-70.

Hassan Moghbelli, Hamid Toliyat, Haitham Abu-Rub, "A green hybrid power plant using photovoltaic and wind energy with power quality improvement in Qatar",2011, American Society for Engineering Education, pp-2-14.

Source: MOEE web site: http://www.moee.gov.mm/en/ignite/page/80)

Applying High Performance Seismic Structures to All Asian Countries

Tsutomu Komuro[1], Yozo Shinozaki [2] and Akira Wada[3]

Abstract

In 1868, Japan began importing science and technology from Europe and the USA, which have little experience with severe earthquake disasters. This was the beginning of great changes in Japan's civilization, culture and politics. Over time, vast cities with tremendous numbers of buildings, such as Tokyo, Osaka and Nagoya, became the centers of modern Japanese life. Although Japanese society has always been concerned about earthquakes, people focused more on economic growth during the modernization process than on protecting mega-cities from possible natural disasters. Other Asian countries also have a similar pattern of development.Seismic design codes focus on saving human life, not only in Japan but also in other Asian countries, the USA and some European countries. Regulations generally allow for plastic deformation of building structures in large earthquakes. Under such design standards, it is not necessary to ensure that buildings can continue being used after a major earthquake. However, if too many buildings – governmental, office, factory and residential – become unusable in an earthquake, a city cannot survive and certainly cannot be described as resilient. As society becomes more dense, high-potential and excessively rational, we must develop more reliable structures using current technologies of seismic isolation and passive earthquake control. We would like to introduce some beautiful new buildings constructed with high-performance seismic structural systems to other Asian countries and for Sustainable Development Goals (SDGs).

Keywords: Seismic Design, Human life, Business Continuity, Seismic Isolation, Response Control

1. Introduction

Through the experience of earthquakes over history, the seismic design sections of Japan's building standards law have been continually revised. A new seismic design method enforced in 1981 is the current design code. The basic principle of this code is to limit structural damage to within an allowable range in the case of small and medium earthquakes, while severe damage (plastic deformation) is allowed in the case major earthquakes. The purpose is to prevent buildings from collapsing with the primary purpose of protecting human life. In the 1995 Hyogoken-Nanbu Earthquake (the Kobe Earthquake), many buildings were severely damaged, as shown in Figures 1 and 2. However, damage to buildings designed by the 1981 seismic design code tended to be less than to older buildings, so engineers and bureaucrats believed that the principle of the code was effective. However, the 1981 seismic design code alone is not sufficient from the viewpoint of maintenance or early recovery of building function and the seismic resilience of mega-cities **[1]**.

[1] Dr. Member, Architectural Institute of Japan, Taisei Corporation, komuro@arch.taisei.co.jp
[2] Member, Architectural Institute of Japan, Taisei Corporation, sinozaki@arch.taisei.co.jp
[3] Member, Science Council of Japan, Professor Emeritus, Tokyo Institute of Technology, ada@akira-wada.com

Figure 1. Pancake crushing of Kobe city hall

Figure 2. Building damage scene in Kobe

Since 1995, major earthquakes have occurred in many places in Japan and damage to actual building structures has been reduced. In particular, it has been found that damage to buildings with seismic-isolation structures or response-controlled structures is very small. However, there have been cases where damage to the finish, and to interior fittings, of buildings designed by the current design code but lacking such advanced seismic technologies has had a significant impact on business continuity after an earthquake.

In this paper, we report on several large earthquakes that have occurred in Japan since 1995 and on the behavior of certain buildings. We describe advanced technologies, such as seismic-isolation and damage-controlled structures, that have helped minimize earthquake damage.

2. Nursing Home Facility Hit by Earthquake in 2004

During the period October to November 2004, a series of earthquakes took place about 80km south of Niigata city in Japan's Chuetsu region. The main shock, named the 2004 Mid-Niigata Prefecture Earthquake, occurred on October 23. The magnitude was estimated at M_{JMA}6.8 by the Japan Meteorological Agency (JMA). On the JMA scale of seismic intensity, the earthquake reached level 6+ to 7, which indicate extremely strong motion. Many aftershocks including some of M6 class followed the main shock. The Fire and Disaster Management Agency reported that there were 48 people killed and 634 seriously injured, with 3,181 completely buildings destroyed and 13,531 heavily damaged in Niigata Prefecture.

The nursing home shown in Figure 3 is a five-story reinforced concrete building with a seismic isolation system [2]. It is located in Ojiya city and is about 7 km from the epicenter of the main shock (as shown in Figure 4). This facility was planned in 1995, just after the Hyogo-ken Nanbu Earthquake that seriously damaged many buildings in Kobe city. Considering that damage, the decision was made that the facility should be able to maintain its function as a medical service facility in the case of a major earthquake. Therefore, a seismic isolation system was adopted as the main structural design feature for reducing earthquake damage.

Figure 3. Overview of nursing home

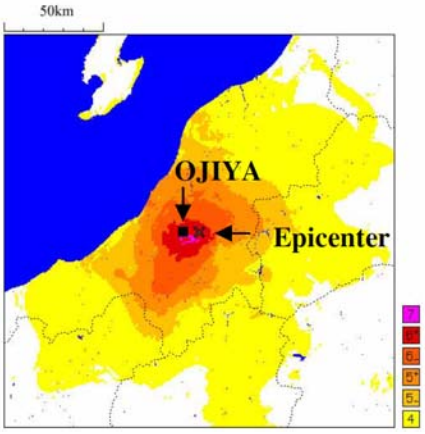

Figure 4. Map of main shock intensity on JMA scale

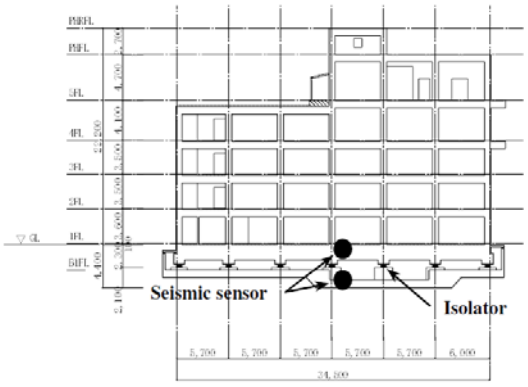

Figure 5. Structural section

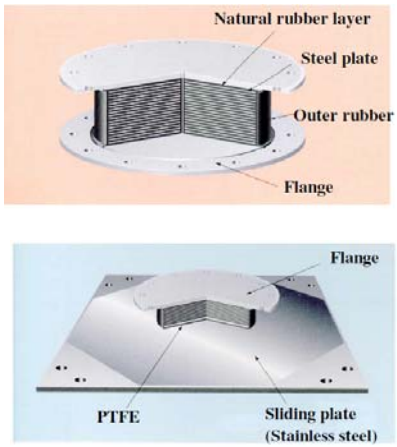

Figure 6. Isolators

(Upper: rubber bearing, lower: slide bearing)

A structural section of the building is shown in Figure 5. The isolation devices (isolators) are installed beneath the first floor. The building is supported by the isolators, 18 sets of rubber bearings and 21 sets of slide bearings. As shown in Figure 6, the rubber bearing consists of thin layers of natural rubber bonded to steel plates and the slide bearing consists of a 3-layer high-damping rubber bearing with a PTFE sliding surface in contact with polished stainless steel.

A field survey of the building was carried out after the main shock. No damage was identified to the exterior wall tiles or the structural members of the building. As Figure 7 shows, there was no falling of objects to the floor. In contrast, some of the wooden houses adjacent to the facility suffered damage and a concrete block wall belonging to a house next door collapsed. The photograph in Figure 8 shows how furniture and household items were thrown around in a building in the neighboring area, giving an indication of the severity of the seismic motion. Taken together, Figures 7 and 8 show the overwhelming difference that a seismic isolation system can make.

Figure 7. Cupboard on 1st floor of the facility after the main shock

Figure 8. Room in neighboring building

3. 2011 Great East Japan Earthquake and Seismic Retrofit of High-rise Building

On March 11 of 2011, a huge earthquake hit the Tohoku district forming the north-eastern part of Japan's main island (the 2011 Off the Pacific Coast of Tohoku Earthquake M_w9.0 (on the moment magnitude scale), sometimes called the 2011 Great East Japan Earthquake). Approximately 16,000 people died and 3,000 people remain missing, mainly due to the tsunami. Figure 9 shows the seismic intensity of this event on the JMA scale [3]. The ground motion was felt across almost the whole of Japan. Figure10 shows a building that toppled in the tsunami. The tsunami-induced meltdowns at Fukushima Daiichi Nuclear Power Plants shocked people around the world while liquefaction in the bay area of Chiba prefecture caused major difficulties to the people living in the region. Buildings were badly shaken, not only in east Japan but also far from the epicenter. High-rise buildings in Tokyo, Osaka and Nagoya experienced strong, long-period motion for several minutes and some residents and office workers in these buildings were quite frightened.

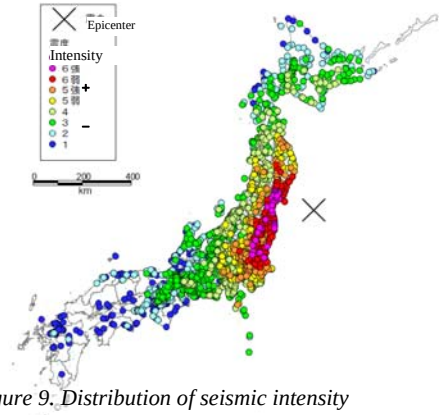

Figure 9. Distribution of seismic intensity of 2011 Great East Japan Earthquake [3]

Figure 10. Building toppled by the tsunami

In 2009, special oil dampers were developed as seismic damage control devices for the retrofitting of old high-rise buildings. They were fitted to an existing 54-story office building (Shinjuku Center Building, as shown in Figure 11, completed in 1979 and located in Shinjuku ward, Tokyo) to suppress vibration during long-period earthquake ground motion [4]. Twelve oil dampers with a deformation-dependent damping characteristic (shown in Figure 12) were fitted on every floor between the 15th and the 39th, for a total of 288 dampers. These floors were

selected because dynamic analysis showed that the story drift and the cumulative plastic deformation ratio of the steel reinforcing bars were relatively large in this range of floors.

The seismic response of the building was recorded in the 2011 Great East Japan Earthquake. Later, simulation analyses were conducted to estimate the performance of the dampers in controlling motion. This modeling work clarified that damping was improved and the response was reduced by 20% as compared to the building without dampers. Figure 13 shows (a) the simulated relative displacement between the roof and the ground floor and (b) the simulated acceleration at the top floor with and without the dampers. The maximum displacement at top floor was 76.4cm without the dampers and this was reduced to 60.8cm with the dampers (the actual observed displacement was 54.2cm). This indicates that the dampers reduced displacement by 20%. The maximum acceleration was 220.3 cm/sec^2 without the dampers and 184.1 cm/sec^2 with them (and the actual observed value was 161.3 cm/sec^2), also about a 20% reduction. This confirmed the value of the seismic retrofitting of this super high-rise building and the analytical results are in good agreement with the observed motion record.

Figure 11. Shinjuku Center Building

Figure 12. Installed oil damper

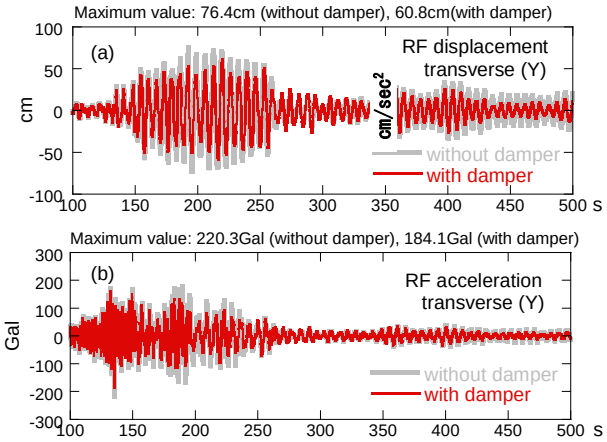

Figure 13. Comparison of simulated response waveforms with/without dampers

3.1 2016 Kumamoto Earthquake and Semiconductor Factory

A series of earthquakes hit the middle of the island of Kyusyu beginning on April 14, 2016, centering on Kumamoto Prefecture, where major damage occurred (the 2016 Kumamoto earthquake, shown in Figures 14[5] and 15). Among the series of events, two major earthquakes occurred at 21:26 on April 14 (foreshock $M_{JMA}6.5$) and at 01:25 on April 16 (main shock $M_{JMA}7.3$). This was the first time in Japan that a seismic intensity of 7 had been recorded twice within two days. The earthquakes caused severe damage not only to the structures of buildings, but also to the contents and the finish (non-structural elements) of buildings and to lifeline in the area.

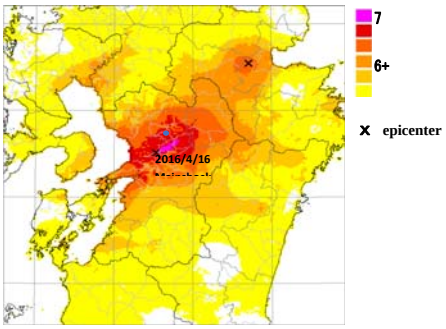

Figure 14. Distribution of seismic intensity of 2016 Kumamoto Earthquake (Main Shock) [5]

Figure 15. Damaged Kumamoto castle

Kumamoto prefecture is home to many factories, including manufacturing facilities for semiconductors. Semiconductor plants include equipment that is sensitive to vibration and also clean rooms that must remain airtight, so they are relatively fragile in the face of a large earthquake. A large earthquake might cause operations to be halted, which leads to opportunity loss. Opportunity losses for semiconductor manufacturers are large and in some cases may exceed actual material losses.

A semiconductor factory (shown in Figure 16) consisting of two buildings of steel structure in Kikuyou town, Kumamoto prefecture, is located 12km away from the epicenter of the main shock. These buildings were designed according to the current seismic design code. The structure, finish and contents of the factory were severely damaged by, principally, the main shock, but there were no injuries or deaths [6]. Brace buckling, bolt fractures and failure of structural member connections were observed. Figure 17 shows the structural damage at the point where the column bases meet the foundation. Figures 18 and 19 show the damage to the finish and to the factory equipment.

Due to the severe damage caused by the main shock, operations at the factory were halted. Full production on all lines resumed by the end of July, about three months after the earthquake. The impact on operating income from the Kumamoto earthquake was estimated at more than 50 billion yen, of which opportunity losses account for about 60%. If recovery could have been hastened, the opportunity losses would have been minimized.

Figure 16. View of factory [6]

Figure 17. Damage to connection of column bases and foundation [6]

Figure 18. Collapse of automatic conveyor rail [6]

Figure 19. Damaged clean room [6]

Figures 16 to 19, Source: Sony Semiconductor Manufacturing

4. Conclusion

Numerous earthquakes, including especially the 2011 Great East Japan Earthquake, have taught us that our goal in seismic design for severe ground motion should evolve from simply the protection of human life to the combined protection of life + property conservation + maintenance of functionality. In other words, we can say our aim should be “resilience”, which is a hot topic these days.

Japan has long made efforts to deliver high seismic performance through the user of seismic isolation and response control technologies. The devices and systems that support these technologies have been improved and have become more reliable and cheaper than in the past. We are now in a position to apply these technologies to a variety of building types in all the countries of Asia for the benefit of the next generation.

References

[1] Wada, A., “From prologue to epilogue in solutions for seismic resilience of mega-city”, Structural Engineering Frontier Conference, March 18-19 2015, Tokyo Institute of Technology, Yokohama, Japan, pp. 323-335.

[2] Komuro, T., Kawamoto, S., Tamari, M., Fukuyama, H., and Iiba, M., “Performance of seismic isolated building under strong earthquakes”, 5th World Conference on Structural Control and Monitoring, 2010

[3] The Headquarters for Earthquake Research Promotion, https://www.jishin.go.jp/main/oshirase/20110311_sanriku-oki.htm, 5 Oct. 2019

[4] Aono, H., Hosozawa, O., Shinozaki, Y., and Kimura, Y., “Seismic retrofit of high-rise building against the long-period ground motions”, 10th U.S. National Conference on Earthquake Engineering Frontiers of Earthquake Engineering, July 21-25, 2014

[5] JapanMeteorological Agency, https://www.data.jma.go.jp/svd/eqev/ data/2016_04_14_kumamoto/ index.html, 5 Oct. 2019

[6] Ito, T., Damages and recovery processes of major semiconductor manufacturers following the Kumamoto earthquake (in Japanese), Matsuyama University Journal, Vol. 29, 2017, pp. 65-96.

Analysis of Some Heavy Metals Concentrations in Muscle Tissue of Three Fish Species and environs, Thanlwin River Segment of Mon State

Yee Yee Win[1] et al

Abstract

The present study was conducted in two different study sites situated on the Thanlwin segment and its tributaries of Mon state. Study period lasted from February 2018 to January 2019. Fish, water and sediment samples were collected seasonally in the study sites. Element concentrations of As, Pb and Cd in extracts were determined by using Flame Atomic Absorption Spectrophotometry (FAAS) (Perkin Elmer AA Analyst 800 and Winlab – 32 s oftware) at University Research Center (URC) in University of Yangon. Concentration of As, Pb and Cd on muscle tissues of three study fish species (*Lates calcarifer*, *Otolithoides pama* and *Polynemus paradiseus*) were analyzed in the study period. Heavy metal concentrations in muscle tissues of all study fish species were below WHO limit. Concentration of As in **water** of study site I in rainy and winter seasons as well as those of study site II in all seasons were found to higher than the WHO limitation. As concentration in **sediment** of study site I in all seasons as well as those of study site II in summer and winter seasons were found to higher than the WHO limitation. In the study site, positive **relationships** between size of fish and heavy metal concentrations were found in *L. calcarifer* while those were negative in *O. pama* and no relation in *P. paradiseus* at study site I. In site II, positive relationships between size of fish and As and Pb concentrations in *L. calcarifer*, As in *O. pama* and Pb and Cd in *P. paradiseus* were observed. However, heavy metal concentrations in muscle tissues of study fish species were not over the WHO MPL. Thus, study fishes from the study area are generally safe for human consumption.

Keyword: fish, arsenic, lead, cadmium, muscle tissue, sediment, water

1. Introduction

Heavy metals are environmentally ubiquitous, readily dissolved and transported by water and readily taken up by aquatic organisms (Alam *et al*., 2002). Fishes are often at the top of aquatic food chain in water ecosystems and fish living in the polluted water may accumulate toxic trace metals (Mansour, and Sidky, 2002).

It is well known that fish, as a regular constituent of the human diet, can represent a dangerous source of certain heavy metals. The discharge of wastewater and industrial effluents whether treated or not can be regarded a constant pollution source that dominate water quality. Water quality parameters can produce an improved understanding of the environmental situation and assist policy makers to design priorities for sustainable water management (Hung *et al*., 2010).

The degree of water quality is determined by the content of physical, chemical and biological parameters available in it. Association between two parameters may cause to increase or decrease in the concentration of others. In this study, concentrations of three metals (arsenic, lead and cadmium) in the three fish species because these fish species have been consumed as food by local people. Water and sediments from Thanlwin river segment of Mon State environs were determined. The muscle is the section of fish that is consumed by human. It is required to verify whether contaminants like heavy metals are within the recommended limits for human consumption. Therefore the metal content in the muscle was analyzed in the present study.

[1] Lecturer, Department of zoology, Mawlamyine University. Myanmar, yeewynn1@gmail.com
2. Kay Lwin Tun 3. Min Thu Aung 4.Cho Cho Thin

Especially, the mean concentrations of test metals were evaluated in terms of international guidelines.

Therefore, present study was chosen to conduct in order to know the following objectives.

- to find out seasonal variation of heavy metals concentration (As, Pb, Cd,) in muscle tissue of study fish species
- to monitor the toxic metals (As, Pb, Cd) concentration in aquatic environs (water and sediment) of the study fish sites
- to investigate relationship between size of fish and metal concentrations in muscle tissue of fish

2. Materials and Methods

The present study will be conducted in two different study sites (Ngan Tae village and Kyauk Tan village) situated on the Thanlwin River segment and its tributaries of Mon states. Ngan Tae village (Lat 16º 28' N and Long, 97º 39' E) and Kyauk Tan village (Lat 16º 24' N and Long, 97º 36' E) were designated as the study site I and II, respectively. Study period lasted from January to December 2018. *Lates calcarifer*, *Otolithoides pama* and *Polynemus paradiseus*,, water and sediment samples were collected monthly in fish landing depots of the study sites. At least seven samples from each fish species were collected. Total length and body weight of specimens were measured. They were dissected using stainless steel scalpels and forceps. A part of the muscle (dorsal muscle) was removed and weighted. Samples were put into an oven (90 ºC) and dried to reach constant weight. After that they were stored at low temperature until digestion. Digestion of the samples carried out according to dry method by using furnace (Model-L-3383).

Element concentrations of As, Pb and Cd in extracts were determined by using Flame Atomic Absorption Spectrophotometry (FAAS) (Perkin Elmer AA Analyst 800 and Winlab-32 software) at Universities Research Center (URC) in University of Yangon. Test results were compared with maximum permissible limit (MPL) designated by WHO.

Functional relationship between size of fish and heavy metal concentrations were analyzed by using regression method with the following formula

$Y = a + bX$

a = Y intercept

b = slope of the line

r = regression coefficient

Fig. 1. Map of the study sites

Cement Factory (near Ngan Tae village)
(site I) Hind view

Industrial Zone (near Kyauk Tan village)
(site II) Hind view

Plate 1. Environs of the study sites

Lates calcarifer

Otolithoides pama

Polynemus paradiseus

Plate 2. Study fish species

3. Results

Seasonal variation of As concentration in muscle tissue of *Lates calcarifer* collected from study site I was -6.296mg/L in rainy season > -6.837 mg/L in summer season > -9.985 mg/L in winter season. Similar results were observed in study site II. As concentration in muscle tissue of *Otolithoides pama* and *Polynemus paradiseus* was summer > rainy season > winter season. As concentration in muscle tissues of three study fish species which collected from study site II were higher than that of study site I in summer season (Table 2).

Lead concentration in muscle tissue of *Lates calcarifer* collected from study site I was -0.873 mg/L in summer season > -0.928mg/L in rainy season > -0.959mg/L in winter season. Similar results were observed in study site II. The same conditions of Pb concentration were found in muscle tissue of *Otolithoides pama* and *Polynemus paradiseus.* However, Pb concentration in muscle tissues of three study fish species which collected from study site II were higher than that of study site I in summer season (Table 2).

Cadmium concentration in muscle tissue of *Lates calcarifer* at rainy season (0.007mg/L) was higher than those of summer season 0.009 mg/L) and winter season (-0.01mg/L) in study site I. Similar results were observed in study site II. The same conditions of Cd concentration were found in muscle tissue of *Otolithoides pama* and *Polynemus paradiseus.* However, Cd concentration in muscle tissues of *Lates calcarifer, Otolithoides pama* and *Polynemus paradiseus* which collected from study site II were higher than that of study site I (Table 2).

Arsenic concentration in water and sediment at winter season (1.003mg/L in water and 74.64mg/L in sediment) was higher than those of rainy season (0.134mg/L in water and 26.43mg/L in sediment) and Summer season (-0.326mg/L in water and 99.36mg/L in sediment)

in study site I. Similar results were observed in study site II. However, As concentrations in water which collected from study site II was higher than that of study site I although As concentrations in sediment which collected from study site I was higher than that of study site II (Table 3, 4).

Lead concentration in water at winter season (1.003mg/L in water and 74.64mg/L in sediment) was higher than those of rainy season (0.134mg/L in water and 26.43mg/L in sediment) and summer season (- 0.326 mg/L in water) but summer season was the most higher (99.36 in sediment) in study site I. Similar results were observed in study site II. However, Pb concentrations in water and sediment which collected from study site I were higher than that of study site II in summer season (Table 3, 4).

Cadmium concentration in water and sediment at rainy season (-0.005mg/L in water and 0.02mg/L in sediment) was higher than those of summer season (-0.011mg/L in water and 0.025mg/L in sediment) and winter season (-0.008mg/L in water and 0.029mg/L in sediment) in study site I. Similar results were observed in study site II. However, Cd concentrations in water and sediment which collected from study site I were higher than that of study site II in summer season (Table 3, 4).

WHO maximum permissible limit of As, Pb and Cd in muscle tissue of fish are 0.01 mg/L, 1 mg/L and 0.2 mg/L, respectively. Concentrations of As, Pb and Cd in muscle tissues of study three fish species were not found over the maximum levels permitted by WHO (Table 2).

Positive relationships between length of fish and concentrations of As ($y = 0.380x – 16.67$, $r = 0.868$), Pb ($y= 0.009x - 1.135$, $r = 0.955$) and Cd ($y = 0.002x - 0.049$, $r = 0.959$) were found in *L. calcarifer* while those were negative in *O. pama* ($y = -1.543x +33.13$, $r = 0.740$), Pb ($y= -0.020x – 0.380$, $r = 0.828$) and Cd ($y = -0.003x + 0.091$, $r = 0.530$) and no relation in *P. paradiseus* ($y = -0.094x – 3.426$, $r = 0.045$), Pb ($y= -0.010x – 0.765$, $r = 0.232$) and Cd ($y = 0.001x - 0.021$, $r = 0.161$) at study site I (Table 5). Similar results were observed between body weight of fish and metal concentrations (Table 5).

In the study site II, positive relationships between size of fish and As and Pb concentrations in *L. calcarifer*, As in *O. pama* and Pb and Cd in *P. paradiseus* were observed (Table10, 11).

Table 1. Mean total length and body weight of fish for seasonal analysis of metal concentration in site I and site II

Study area	Species	Summer		Rainy		Winter	
		TL(cm)	Weight(g)	TL(cm)	Weight(g)	TL(cm)	Weight(g)
Site I	*Lates calcarifer*	18.7 ± 2.71	78.4 ± 39.3	27.7 ± 2.32	263.1 ± 52.46	23.3 ± 1.08	191.4 ± 35.5
	Otolithiodes pama	26.7 ± 0.37	137.1 ± 6.21	24.58 ± 1.57	102.2 ± 20.92	26.58 ± 1.4	127.3 ± 3.97
	Polynemus paradiseus	16.2 ± 0.71	24.73 ± 2.67	16.22 ± 0.67	25.33 ± 3.3	17.78 ± 0.97	4.39 ± 5.46
Site II	*Lates calcarifer*	18.5 ± 2.3	82.5 ± 42	18.7 ± 1.86	94.82 ± 34.05	27.8 ± 3.97	225.4 ± 22.05
	Otolithiodes pama	20.3 ± 0.55	57.05 ± 5.02	21.67 ± 0.37	64.22 ± 5.53	24.83 ± 1.28	96.42 ± 13.13
	Polynemus paradiseus	16.3 ± 1.42	25.06 ± 7.6	18.38 ± 0.7	46.23 ± 10.2	15.06 ± 0.8	20.33 ± 2.82

MPL = Maximun permissible limit

Table 2. Variation of heavy metals concentration (mg/L) in studied species at two different study sites

Species	**Element**	**Site I**			**Site II**			**MPL**
		Summer	**Rainy**	**Winter**	**Summer**	**Rainy**	**Winter**	
Lates calcarifer	As	-6.837	-6.296	-9.985	-6.296	-6.051	-10.24	0.26
	Pb	-0.873	-0.928	-0.959	-0.769	-0.799	-0.843	1
	Cd	0.009	0.007	-0.01	0.019	0.01	0.011	0.2
Otolithiodes pama	As	-4.872	-6.207	-9.637	-6.67	-5.255	-6.17	0.26
	Pb	-0.893	-0.917	-0.952	-0.788	-0.818	-0.859	1
	Cd	0.008	0.008	-0.005	0.023	0.011	0.011	0.2
Polynemus paradiseus	As	-3.379	-5.112	-6.55	-7.221	-4.431	-5.196	0.26
	Pb	-0.902	-0.96	-0.984	-0.785	-0.829	-0.862	1
	Cd	0.006	0.001	-0.008	0.022	0.008	0.013	0.2

MPL = Maximun permissible limit

Table 3. Variation of metal concentrations in water of two different study sites at Thanlwin River

Sr No.	Elements	Site I			Site II			MPL
		Summer	Rainy	Winter	Summer	Rainy	Winter	
1	Arsenic	-0.326	**0.134**	**1.003**	**0.329**	**0.356**	**0.978**	0.01
2	Lead	-0.445	-0.487	-0.518	-0.537	-0.57	-0.599	0.01
3	Cadmium	-0.011	-0.005	-0.008	-0.013	-0.016	-0.022	0.003

Table 4. Variation of metal concentrations in sediment of two different study sites at Thanlwin River

Sr No.	Elements	Site I			Site II			MPL		
		Summer	Rainy	Winter	Summer	Rainy	Winter	TEC	MEC	PEC
1	Arsenic	99.36	26.43	74.64	43.54	0.235	**29.75**	9.8	21.4	33
2	Lead	-0.514	-0.467	-0.477	-0.549	-0.572	-0.507	36	83	130
3	Cadmium	0.025	0.02	0.029	0.023	0.023	0.028	0.99	3	5

MPL = Maximun permissible limit

TEC = Threshold effect concentration

MEC = Midpoint effect concentration

PEC = Portable effect concentration

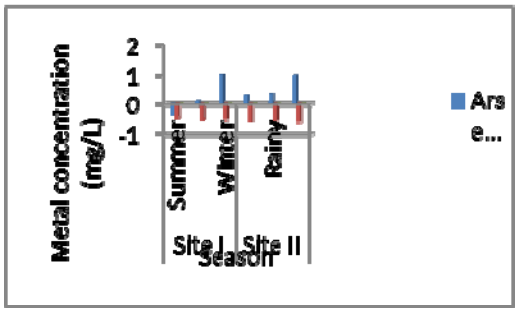

Fig. 2. Variation of metal concentrations in water of two different study sites at Thanlwin River

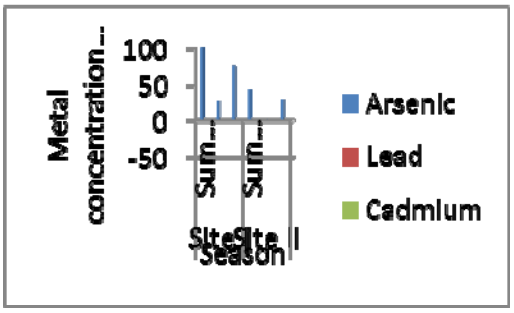

Fig. 3. Variation of metal concentrations in sediment of two different study sites at Thanlwin River

Table.5.Relationship between body length(cm) and weight(g) of fish and heavy metal concentrations in muscle tissue of fish at study site I and Site II

Species	Heavy	Site I				Site II			
		Length		Weight		Len		Weig	
		Linear equation	Remark	Linear equation	Remark	Linear equation	Remark	Linear equation	Remark
Lates calcarifer	As	y=0.380x-16.67 R^2=0.753 r=0.868	Positive relation	y=0.018x-10.98 R^2=0.743 r=0.862	Positive relation	=0.247x-12.9 ^{2}=0.313 =0.559	Positive relation	y=0.0018x-9.952 R^2=0.369 r=0.607	Positive relation
	Pb	y=0.009x-1.135 R^2=0.912 r=0.955	Positive relation	Y=0.000x-0.999 R^2=0.919 r=0.959	Positive relation	=47.24x-1305 ^{2}R=0.266 =0.516	Positive relation	Y=3.474x-747.8 R^2R=0.320 r=0.566	Positive relation
	Cd	Y=0.002x-0.049 R^2R=0.919 r=0.959	Positive relation	Y=0.000x-0.017 R^2R=0.913 r=0.956	Positive relation	=-0.000x=0.0024 ^{2}R=0.324 =0.569	Negative relation	y=-3E-05x+0.017 R^2R=0.270 r=0.520	Negative relation
Otolithoides pama	As	y=-1.543x+33.13 R^2=0.548 r=0.740	Negative relation	y=-0.0120x-7.766 R^2=0.773 r=0.879	Negative relation	=0.247x-11.54 ^{2}=0.635 =0.979	Positive relation	y=0.029x-8.177 R^2=0.746 r=0.864	Positive relation
	Pb	y=-0.020x-0.380 R^2=0.685 r=0.828	Negative relation	y=-0.0001x-0.731 R^2=0.879 r=0.938	Negative relation	=0.005x-0.949 ^{2}=0.138 =0.371	No relation	y=0.000x-0.853 R^2=0.066 r=0.257	No relation
	Cd	y=-0.003x+0.091 R^2=0.281 r=0.530	Negative relation	y=-0.000x+0.040 R^2=0.514 r=0.717	Negative relation	=-0.000x+0.030 ^{2}=0.052 =0.228	No relation	y=-0.000x+0.023 R^2=0.118 r=0.344	No relation
Polynemus paradiseus	As	y=-0.094x-3.426 R^2=0.002 r=0.045	No relation	y=-0.120x=7.766 R^2=0.773 r=0.879	Negative relation	=-0.850x+8.479 ^{2}=o.989 =0.994	Negative relation	y=0.029x-8.177 R^2=0.746 r=0.864	Positive relation
	Pb	y=-0.010x-0.765 R^2=0.054 r=0.323	No relation	y=-0.001x-0.909 R^2=0.031 r-0.176	No relation	=0.015x-1.086 ^{2}=0.473 =0.688	Positive relation	y=0.002x-0.895 R^2=0.668 r=0.817	Positive relation
	Cd	y=0.001x-0.021 R^2=0.026 r=0.161	No relation	y=-0.000x-0.008 R^2=0.047 r=0.217	No relation	=0.004x-0.055 ^{2}=0.999 =0.999	Positive relation tion	y=0.000x-0.001 R^2=0.965 r=0.982	Positive relation

Discussion

Toxic metals are very harmful because of their potential to absorb, accumulate and concentrate in different body parts. Heavy metals, such as As, Pb and Cd are dangerous for human health because of their accumulation properties in the body parts (Tressou *et al*., 2004). Metals bioaccumulation through aquatic food webs to fish, human and other piscivorous animals are environmental and human health concern (Dehn *et al*., 2006).

Arsenic is released in the environment through natural processes such as weathering, and may circulate in natural ecosystems for long time (Mol *et al*., 2010).Toxic effects appear when arsenic is ingested in excess for long periods resulting in cancer, cutaneous malignancies, etc.Lead is toxic metal and non-essential element for human body as it causes a rise in blood

pressure, kidney damage and miscarriage (Kiran *et al*., 20111).Cadmium injures the kidney, poor reproductive capacity, hypertension, tumors and hepatic dysfunction.

Khin Thida Kyaw (2008) stated that in the Daydaye Thilawar fisheries, seasonal variation of toxic metals (As, Pb and Cd) concentration in three fish species were higher in summer and rainy season than those of winter. However, Cho Cho Thin (2017) stated that the concentration level of As in muscle tissues of fish in Ayeyawady River segment of Salay environ were found over the WHO limit but Khin Myint Mar(2011) studied that the concentration of heavy metals in studied species were lower than WHO limit. Thus, present findings were not agreed with the findings of above authors and potential danger may not be occurred for the consumption of study fish species from the present study area.

In the present study, arsenic, concentration in water of study site I in rainy and winter seasons as well as those of study site II in all seasons were found to higher than the WHO limitation. In the present study, arsenic, concentration in sediment of study site I in all seasons as well as those of study site II in summer and winter seasons were found to higher than the WHO limitation. Arvind (2002) also stated that metal content of fish increases with the increment of metal level in water, sediment and food organism. Present findings were agreed with the findings and potential danger may be occurred for water and sediment. In the present study, concentrations of As, Pb and Cd in muscle tissues of three study fish species which collected from study site I and II were not over the MPL recommended by WHO. However, near the study sites, cement factory, machine cleaning workshop and industrial zone were established in 2014. The accumulation trend of As was approximately summer> winter>rainy. The elevation of these metals accumulation in this study may be due to industrial and sewage wastes. Therefore, As in fish will be expected over the MPL in the future study.

In the present study, positive relationships between size of fish and heavy metal concentrations were found in *L. calcarifer* while those were negative in *O. pama* and no relation in *P. paradiseus* at study site I. In the study site II, positive relationships between size of fish and As and Pb concentrations in *L. calcarifer*,As in *O. pama* and Pb and Cd in *P. paradiseus* were observed. However, heavy metal concentrations in muscle tissues of study fish species were not over the WHO MPL. Thus, study fishes from the study area are generally safe for human consumption.

Acknowledgements

I am greatly indebted to Dr Thida Lay Thwe Professor/Head and Dr Aye Mi San Professor. My profound gratitude goes to Dr Kay Lwin Tun, Professor, Department of Zoology, Yangon University and Dr Min Thu Aung, Professor, Department of Zoology, University of Pathein, for their kind support, guidance and supervision.

References

Alam, M. G. M., Tanaka, A., Allinson, G., Laurenson, L. J. B., Stagnitu, F., Snow, E. T., "A comparison of trace element concentrations in cultured and wild carp (*Cyprinus carpio*) of Lake Kasumigaura, Japan. *Ecotox. Environ."* 2012. *Safe*., 53:348-354.

Arvind, K., "*Ecology of polluted waters"*, A. P. H Publishing Corporation, New Delhi. 2002.

Cho Cho "Thin, Relation of some essential and Toxic elements Ayeyawady on different feeding types of some freshwater fishes along the Ayeyawady River segment, Salay Environs". *PhD Thesis*, Department of Zoology, University of Yangon. 2017

Dehn L.A.,Follman E. H., Thomas D. L.,Sheffield G.G., Rosa C., Duffyl.K.,O.Harat.M., "Trophic relationships in an Arctic food web and implication for trace metal transfer". Science of the Environment. 2006. 362,103.

Hung, H., Kallenborn, R., Breivik, K., Su, Y., Brorström-Lundén, E., Olafsdottir, K., Thorlacius, J. M., Leppänen, S., Bossi, R., Skov, H., Manø, S., Patton, G. W., Stern, G., Sverko, E., Fellin., "Atmospheric monitoring of organic pollutants in the Arctic under the Arctic Monitoring and Assessment Programme". *Sci Total Environ* Kiran, 2010. 408: 2854-2873.

Khin Thida Kyaw, "Analytical studies on toxic metals (A, Cd, Pb, and Hg) concentrations in Nga-dan (*Pangasius pangasius)*, Ka-kadit (*Lates calcarifer)*, and Nga-yant (*Channa striata*) samples", *PhD Thesis*. Department of Chemistry, University of Yangon. 2008. 61-104 pp.

Khin Myint Mar, "Uptake of heavy metals and its relationship to feeding habit of selected fish species in Ayeyawady River, Mandalay and Magway segments", *PhD Thesis*. Department of Zoology, University of Mandalay. 2011.

Kiran, Y. K., Mir, A. K., Rabia, N., Mamoona, M., Hina, F., Nighat, S., Tasmia, B., Ammarah, K., "Element content analysis of plants of genus *Ficus* using actomic absorption spectrometer". *African Journal of Pharmacy and Pharmacology* 5 2011. (3): 317-321.

Mansour. S. A., Sidky, M. M., "Ecotoxicological studies 3. Heavy metals contaminating water and fish from Fayoum Governorate, Egypt". *Food Chemistry*, 2002. 78(1):15-22.

Mol ,O, Ozden and S.A. Oymak. Turkish J. Fish. Aqua. Sci., "Determination of Heavy Metals in Fish Tissues, Water and Sediment from Epe and Badagry Lagoons, Lagos, Nigeria",2010. 10:209-213,

Tressou J., Crepet A., Bertail P., Feinberg M.H.., Leblanc J. Ch., Probalistic exposure assessment to food chemicals based on extreme value theory. "Application to heavy metal from fish and sea products". Food and Chemical Toxicology. 2004. 42,1349.

Analysis of Elemental Concentration in Kye Pè (*Plukenetia volubilis* L.) Samples by Using WDXRF Technique

Khin Shwe Tint[1]

Abstract

In this research work, we have been analyzed the concentration elements in three kinds of samples which are fruits (M1), leaves (M2) and stems (M3) for KyePè or Sacha Inchi plant. The concentration elements in these samples were determined by using WDXRF (wavelength dispersive X-rays fluorescence) technique. All measurements have been done in drying condition. According to the experimental results, eighteen elements are contained in fruits sample and stems samples, seventeen elements are contained in leaves samples. These elements are Magnesium (Mg), Aluminum (Al), Silicon (Si), Phosphorus (P), Sulfur (S), Chlorine (Cl), Potassium (K), Calcium (Ca), Titanium (Ti), Vanadium (V), Manganese (Mn), Iron (Fe), Nickel (Ni), Copper (Cu), Zinc (Zn), Rubidium (Rb), Strontium (Sr) and Lead (Pb) elements in fruits sample (M1) and stems sample (M3) and then Nickel (Ni) is not contain in leaves sample (M2). The concentration of Silicon (Si) is large in leave (M2) samples. The concentration of Potassium (K), Calcium (Ca) and Magnesium (Mg) are largest in this research samples. The concentration element in Kye Pè can be prevented diabetes, hypertension, cancer cell and heart disease. Health benefits of Kye Pè include improving digestion, aiding in weight loss, managing diabetes and stimulating cognition. Kye Pè plant is a medicinal plant.

Keywords: WDXRF technique, elemental concentration, Kye Pè plant.

1. Introduction

Everybody, human health is very important. If everybody has good health, everybody will make everything. Nowadays, people would like to use fresh air, clean water, hygienic food and good medicine for health but human activities are causing harm. Plants are not only the major source of energy-rich foods in our societies, but are also an indispensable source of vitamin and other substances promoting healthy growth. They have played an important role in traditional medicine in Myanmar since ancient time. Human health, natural safeguard and minimizing the damages of human activities to Earth are the environmental study today. The aim of this research is to analysis of the concentration of elements in Sacha inchi or Kye Pè samples by using WDXRF (wavelength dispersive X-rays fluorescence) technique. We have collected the fruits, leaves and stems of Sacha inchi or Kye Pè plant. These samples were collected from KyunHla village, Myittha Township, Mandalay Region.

2. Experimental Procedure

2.1 Sample Collection

In this research, we analyzed the three samples in Sacha inchi or Kye Pè plant samples by using WDXRF. We collected three samples which are fruits, leaves and stems. To analysis the elemental concentration of these samples, they were sent to Department of Chemistry, Yadanabon University. The concentrations of elements contained in three samples were analyzed by WDXRF technique.

[1] Dr. Lecturer, Department of Physics, Yadanabon University, Myanmar, physdrshwe@gmail.com

Sample Preparation

Sample preparation is very important process to experiment. In the first step, three samples were dried under the shade of any roof. These samples were ground in order to get fine powders. The lists of sample are shown in Table (1).

Table 1. The list of samples.

Local Name	Kye Pè
English Name	Sacha inchi, sacha peanut
Scientific Name	*Plukenetia volubilis L*
Family Name	Euphorbiaceaes
First sample code	M1 (fruits)
Second sample code	M2 (leaves)
Third sample code	M3 (stems)

The characters of three samples are shown in Figure 1 to Figure 4.

Figure 1. The Kye Pè plants from Myittha Township, KyunHla village, Mandalay region.

Figure 2. The photograph of dried fruits (M1) and fine powder in Kye Pè plant.

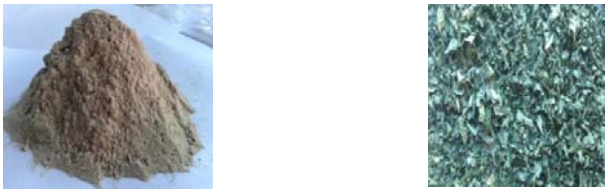

Figure 3. The photograph of dried leaves (M2) and fine powder in Kye Pè plant.

Figure 4. The photograph of dried cortices (M3) and fine powder in Kye Pè plant

These powders were sent to Experimental Laboratory, Department of Chemistry, Yadanabon University. Sample preparation is important in the WDXRF analysis because it is required to get flat, smooth and homogeneous samples for best results. To obtain reliable results in X-ray emission spectrometry, proper sampling is taken and sample storage and sample preparation prior to measurement are conducted. Then hydraulic press machine and a 32 mm diameter die set including a die body, base and two polished metal disks were used for pellet sample in our research work. Prior to pelletizing all parts of the die set was carefully cleaned with methylated spirit to prevent contamination. Initially each sample was weighed using digital balance to obtain the needed amount (5g). Binding agent is added to form stable pellet of the samples. Therefore, binder (1g) was added to the samples (5g) and they were mixed to homogenize with each other. After that weighed sample were poured into the die set (mould) and pressed with 25 tons for 15 minutes by using hydraulic press machine. The pellet was then removed from the die set, taking care not to creak it in the process. After getting the pellet, each of these samples is weighed again and whose weight is exactly 5g is used in this experiment. In making pressed pellets for each sample, these samples were weighted by using the digital balance. The density of each pellet is 0.2 gcm^{-3}.X-ray fluorescence technique is a multi-elemental quantities determination and it can provide concentration of many elements contained in the sample by a single measurement. Three samples were analyzed by using energy dispersive X-ray fluorescence system. All of the pellet samples were analyzed 600 sec for four secondary targets system and the measurement of atmosphere is helium purge. It is used 50 kV bias voltage and tube current is automatically adjusted by hardware. The analyzed range is 0-50 keV. The X-ray spectrum is analyzed with the help of computer to obtain the concentration of each element in the sample. This research was done with WDXRF technique in Experimental Laboratory, Department of Chemistry, Yadanabon. The wavelength dispersive spectrometer is usually coupled with a SEM imaging system and requires dedicated instruments designated by electron microprobe micro-analyzer (EPMA). The spectrometer uses diffraction to sort by wavelength the characteristic. X-rays emitted by the sample. The X-rays are selected using analytical crystals with specific lattice spacing positioned at specific θ angles. Only the wavelengths that satisfy Bragg's law are allowed to pass on the detector. The analytical crystals are bent in order to focus the X-ray beam on the sample and on the detector. These are situated in the Rowland circle to maximize the collection efficiency of the spectrometer. The function of diffraction is shown in Figure (5).

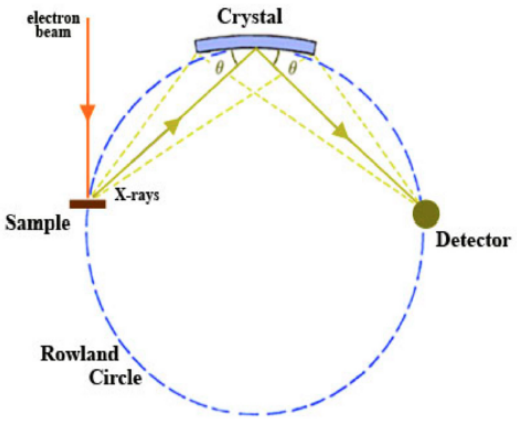

Figure 5. The function of diffraction in WDXRF technique

Each element produces a unique set of characteristic X-rays when bombarded with electros. Each X-ray will have a specific energy and wavelength. Wavelength dispersive spectrometers (WDS) sort the X-rays based on their λ. WDS system use X-ray diffraction as the means by which they separate X-rays. The spectrometer consists of the crystal and diffract will enter the detector. An X-ray photon will diffract, depending on its wavelength, the orientation of the crystal and the crystal's lattice spacing. Only X-ray of a given wavelength will enter the detector at a given time. To measure X-rays of another wavelength, the crystal and the detector are moved to a new position. Since a specific WD spectrometer can measure only one X-ray wavelength at a time. It is important that a WDXRF system has an array of spectrometers in order to work efficiency. Electron microprobes typically have up to five elements simultaneously. Each spectrometer typically has between two and four analyzing crystals, each with a different lattice spacing, because each type of crystal can diffract only a given wavelength. WDXRF requires standard reference materials in concentrations similar to the materials to investigate and is typically used for quantitative spot analysis. The composition of unknown samples is determined by comparing the intensities obtained from studied samples with those from the reference standard materials.

3. Results and Discussion

In this research work, three samples of fruits (M1), leaves (M2) and stems (M3) for *Plukenetia volubilis L.* or Kye Pè or Sacha Inchi were analyzed with WDXRF (wavelength dispersive X-rays fluorescence)technique in the Experimental Laboratory, Department of Chemistry, Yadanabon University. Elemental concentrations of sample contained in the three samples were measured by WDXRF technique and their results are expressed in Table (2). The graphs of these samples are shown in Figure (6).

The concentration of elements was analyzed for three samples. The three samples are M1, M2 and M3. The concentration of elements for three samples is shown in Table (3). According to the experimental results, the sample of fruit (M1) is contained eighteen kinds of elements. They are Magnesium (Mg), Aluminum (Al), Silicon (Si), Phosphorus (P), Sulfur (S), Chlorine (Cl), Potassium (K), Calcium (Ca), Titanium (Ti), Vanadium (V), Manganese (Mn), Iron (Fe), Nickel (Ni), Copper (Cu), Zinc (Zn), Rubidium (Rb), Strontium (Sr) and Lead (Pb) elements. According to the experimental results, Lead (Pb) element is minimum concentration. The samples of leaf (M2) are contained seventeen kinds of elements. According to the experimental results, Bromine (Br) element is very small concentration. The samples of stem (M3) are contained eighteen kinds of elements. They are Magnesium (Mg), Silicon (Si), Aluminum (Al), Phosphorus (P), Sulfur (S), Chlorine (Cl), Potassium (K), Calcium (Ca), Vanadium (V), Copper (Cu), Zinc (Zn), Bromine (Br), Rubidium(Rb), Manganese (Mn), Titanium (Ti), Iron (Fe), Strontium (Sr) and Lead (Pb) elements. According to the experimental results, the concentration of Bromine (Br) element is very small in M3 samples.

Table (2) The comparison of elemental concentration in M1, M2 and M3 samples.

Symbol	Concentration (ppm)			Symbol	Concentration (ppm)		
	M1	**M2**	**M3**		**M1**	**M2**	**M3**
K	42800.00	43200.00	53700.00	Zn	39.00	42.00	36.00
Ca	8290.00	54600.00	21500.00	Ti	24.00	93.00	50.00
Mg	3700.00	4400.00	5400.00	Mn	23.00	86.00	39.00
P	3120.00	2660.00	3160.00	Cu	20.00	23.00	17.00
S	2680.00	4090.00	1840.00	Sr	17.00	139.00	50.00
Si	1450.00	32200.00	2940.00	Rb	10.00	7.00	10.00
Al	655.00	1450.00	1140.00	V	3.00	-	4.00
Cl	203.00	377.00	390.00	Ni	3.00	-	-
Fe	173.00	462.00	245.00	Pb	2.00	4.00	4.00

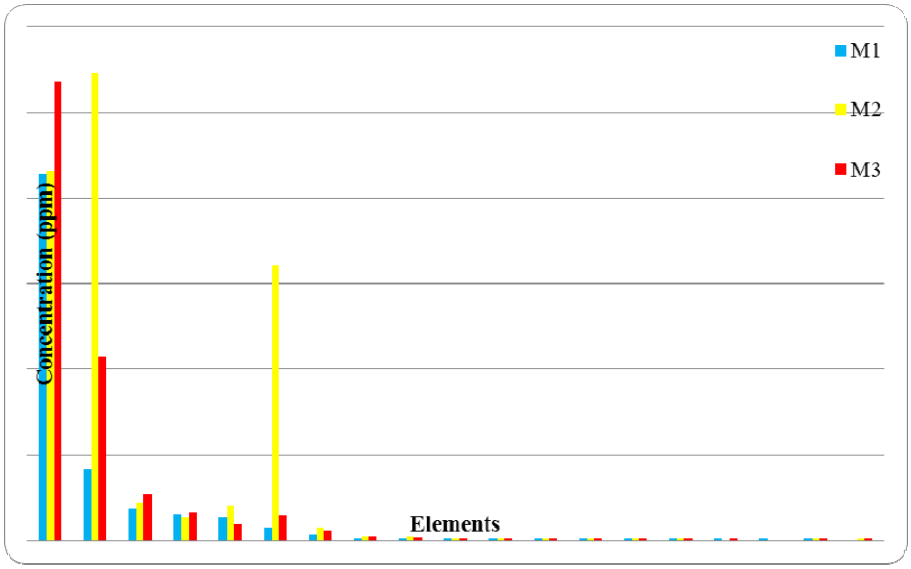

Figure 6. The experimental results of elemental concentration in M1, M2 and M3 samples.

4. Conclusion

According to the experimental result, the concentration of potassium (K) is larger in sample M3 than M2 and M1. The potassium is highest concentration in M3. This element is needed for many essential process including enzyme activation photosynthesis. Potassium is one of the seven essential macrominerals. Potassium (K) participates actively in the maintenance of the cardiac rhythm. High levels of potassium in the blood have been linked to pressure, heart and kidney disorders, and other health problems.

The concentration of calcium (Ca) measured in M1 is small and measured in M2 is larger than M3. Calcium is the main constituent of the skeleton, bone and dental health and important for regulating many vital cellular activities such as nerve and muscle function and lowers the blood pressure. The concentration of magnesium (Mg) measured in M3 is large and measured in

M2 and M1 is small. Magnesium is essential for both plant and animal growth and health. Magnesium is also included in some remedies for heartburn and upset stomach due to acid indigestion. The concentration of phosphorus (P) measured in M1 and M3 is large and measured in M2 is small. Phosphorus is required in most of the body's bio-chemical process including cell growth and converting food to energy is also required for metabolism of fats and carbohydrate to produce energy. The main function of P is to bind with calcium to make healthy teeth and bones.

It is also necessary for the synthesis of protein for repair and growth of tissue and cells. Other key functions help the body to utilize vitamin B complex and support proper nerve and muscle functioning, maintaining, calcium balance and preventing high blood calcium levels. The concentration of sulfur (S) measured is larger in sample M2 than M1 and M3 is smaller than M1. This element aids the liver in bile secretion and maintains oxygen balance for proper brain function and is involving in the clotting of blood. It assists in the fight against bacterial infection by disinfecting the blood helping the body resist bacterial, and protecting. The concentration of Iron (Fe) measured in M1 and M3 is smaller than M2. This element is an essential element for human beings and animals and component of hemoglobin. It facilitates the oxidation of carbohydrates, protein and fat to control body weight, which is very important factor in diabetes.

The concentration of Lead (Pb) measured in three samples is very small. Lead is a useful and common metal that has been used by humans for thousands of years. Lead in the body is distributed to the brain, liver, kidney and bones. It accumulates over time. Lead in bone is released into blood during pregnancy and becomes a source of exposure to the developing fetus. The concentration of Potassium (K), Calcium (Ca) and Magnesium (Mg) are largest in this research sample. The concentration element in Kye Pè can be prevented diabetes, hypertension, cancer cell and heart disease. Health benefits of Kye Pè include improving digestion, aiding in weight loss, managing diabetes and stimulating cognition. Kye Pè plant is a medicinal plant.

Acknowledgements

I would like to express my heartful thanks to Dr Mg Mg Naing, Rector, Dr Tint Moe Thuzar and Dr Si Si Khin, Pro-Rector of Yadanabon University for giving permission and encouragement. I wish to express my gratitude of Professor Dr.Yi Yi Myint, Head of Physics Department, Yadanabon University, for her valuable advice in this research work.I am also grateful to Professor Dr May Thida Win, Physics Department, Yadanabon University, for her advice and suggestions.

References

[1] Guillen, MariaD*et al.,* "Characterization of SachaInchi (*Plukenetia Volubilis L.*) Oil by FTIR spectroscopy and LH NMR.Comparison with Linseed Oil".Journal of the American Oil Chemists' Society. 80(8): 755-762, (2003).

[2] Hla Hla Than, Dr., "Analysis of Traditional Medicine", University of Yangon (2000).

Hufstader. Chris. "Looking to SachaInchi for their Future". Oxfam Exchange, (2009).

[3] Ministry of Health, Department of Trditional Medicine, "Collection of Commonly Used Herbal Plants" (1982).

[4] L. friberg*et al*., "Handbook on the Toxicology of metals" Elsever, Amsterdan (1979).

[5] Win Myint, Dr., "A Study on Combined Effects of TMF-27 and TMF-35 on Plants with Type 2 Diabetes Mllitus", University of Trditional Medicine, Mandalay (2012).

Importance of Soil Moisture Balance and Soil texture in Yields of Crop: A Case Study of Thayetlaypin Village Tract in Magway Township

Hlaing Myo Myo Htay[1], Win Win Maw[2], Si Si Wai[3], Hnin Khaing Aye[4]

Abstract

Climate, soil moisture and soil texture interact with each other for crops growth. The main issue is crop yield deterioration in Magway Township. It is necessary to know the nature of soil water in the area for future utilization in agriculture. The aim of this research is to investigate the effect of soil moisture balance and texture on crop yields of Magway Township. Soil moisture balance was calculated by CW Thornthwaite method to estimate the balance of soil water in the soil. Soil water content is controlled by the soil texture. Soil texture was analyzed by biker method. Soil textural class is determined by USDA soil textural triangle, 1987. The main types of soil texture are sandy loam, loamy sand and sandy soil. The relative yields of sesame and groundnut are 25.67% and 78.38% respectively. Soil moisture deficiency is 538.10 mm/month in 2018. According to the ratio of evapotranspiration and rainfall, the study area needs the water supply or rain fall. The variables can effectively explain the yield together with other variables as correlation. As a result, the yields of sesame and groundnut related to these soil properties but not significantly.

Keywords: soil moisture balance, soil texture, crop yields

1. Introduction

The soil moisture budget refers to water in the soil as moisture, as it is the term most commonly used by scientists who study the subject from the agronomist‘s point of view. A fundamental concept of physical geography is that the availability of water to plants and animals is more important in the environment than precipitation itself (Fundamental of physical geography). Field capacity of a given soil depends largely on its texture. Soil texture influences on the availability of water to the plant. Soil texture also impacts organic matter levels; organic matter breaks down faster in sandy soil than in fine texture soil (www.ristormwatersolutions.). Soil texture is composition of size of soil particles that is sand, silt, clay. Soil texture can be classified by the percentage of sand, silt and clay into loam, silty loam, loamy sand, sandy loam, silty clay loam, etc. (www.ristormwatersolution.org). The importance of soil texture determines different methods and management decisions in cultivation. There are also subclass in sand and silt. Sand is divided into very coarse sand, coarse sand, medium sand, fine sand and very fine sand (USDA, 1987). Density of soil porosity, water holding capacity, organic matter content and susceptibility to erosion are controlled by soil texture (Daji et al 1996; Biswas and Mukherjee, 1994). Sandy soil is suitable for maize, groundnut potato and grapes (USDA,1987). The relationship between crop yield and soil is very complex and depends on complex interaction between physical and chemical properties of soil and other external natural factors’(Sys et al,1991). The soil quality should be tested before cultivation; does soil have problems? Does the crop need water? How much should you apply? Therefore, soil analysis is very important for to farmers. In this paper, soil texture, moisture and basic analysis of soil properties such as pH, and

[1] Dr., Professor, Department of Geography, University of Magway, Myanmar, myomyo67.hh39@gmail.com
[2] Assistant Lecturer, Department of Geography, University of Magway, Myanmar, winwinmaw.mdy.24@gmail.com
[3] Assistant Lecturer, Department of Geography, University of Magway, Myanmar, sisiwai.mdy.26@gmail.com
[4] Dr., Lecturer, Department of Geography, University of Magway, Myanmar, ,hninkhineaye@gmail.com

organic matter were studied preliminarily for suitable crops cultivation and also to sustain the crop productivity base on moisture conditions.

Aim and Objectives

The aim of this paper is to investigate the effect of soil moisture balance and texture on crop yields of Magway Township. The objectives are as follows:

1. To measure the ratio between precipitation and evapotranspiration
2. To analyze the soil moisture budget
3. To determine the soil textural categories and
4. To find out the relationship between soil properties and crop yields

2. Materials and Methods

This research was done based on the primary data. The soil samples were collected by grid method in field area. With the sample collection, land owners were interviewed in detail as well as their suggestions regarding crop yield. Selection of study area, literature survey, and selection of soil samples location in grid methods have been done before going to the field. Soil texture has been tested by biker method in study room. Soil moisture balance was analyzed by CW Thornthwaite method. After that soil test data are plotted on map by GIS 10.0.The estimation of evaporation was used by Penman coefficient equation.Finally, interpretation and analyzing was done by using MS-Excel 2007.

2.1 Study Area

Magway Township is one of the significant oil crops areas in Central Myanmar. Sesame and groundnut are predominantly cultivated crops in this area. The Thatyetlaypin village tract consisting of the oil pots in Magway Township was chosen as a case study to explore relation between the soil texture, moisture and crops. The study area is located at between latitude 19 ^{0} 45′ North and latitude 20 ^{0} 21′ North and between longitude 94 ^{0} 54′ East and longitude 96^{0}18′ East. The total area is 11007acres on which 5142 acres is cultivable land, actually in Thatyetlaypin Village Tract.

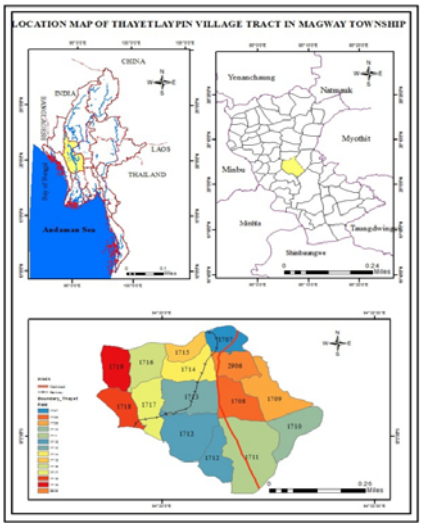

Figure 1. Thatyetlaypin Village Tract.

3. Results and Discussions

3.1 Relationship between precipitation and evapotranspiration

Potential evapotranspiration is a maximum water loss and it measures the moisture demand for regions, (CW Thornthwaite, 1948) and also the ratio of precipitation to potential evapotranspiration. This ratio may be less than 0.1 for these regions; water must be supplied at potential rate. The ratio of precipitation to evapotranspiration ranges from 0.2 to 0.6, again indicating a need for irrigation water in crop production. The range is from 0.8 to 1.6, indicating a rather well balanced situation and in some cases, water surplus. In the study area, the ratio of precipitation to evapotranspiration lying within 0.8 to 1.6, indicates rather well balanced situation and in some cases, water surplus.

3.2 Soil moisture budget analyze in study area

The annual water budget of the soil concerned with the storage of water in soil, runoff and deficiency for plant growth. The basic soil moisture balance equation is as follows: P=E+G+R (CW Thorn Thwaite, 1948) Where P = Precipitation, E = Evapotranspiration, G = Change in soil moisture storage, R = Runoff. The water balance has been calculated the water balance for each month singly and for the year as a whole. As a result, precipitation varies are less than actual evapotranspiration value. In this case, very high potential evapotranspiration is occurred. When Ep (Potential Evapotranspiration) exceed P (precipitation), the plant must draw up moisture stored in the soil as an attempt to sustain as rapid growth as possible at all time. P is measurable in small amount in most months. The values of Ep are always larger. Consequently soil moisture deficiency (D) prevails throughout all months of the year although the storage of moisture is larger than 300 mm. Therefore, crops thrive without irrigation and yields are high in some years.(Table-1)

Table (1) The equation of Soil moisture budget analysis of study area

Rainfall	AET	G(-)	G(+)	R	PET	D=PET-AET
91.95	46.66		45.29		66.66	20
0	58.22	-58.22			83.18	24.95
0	80.3	-80.3			114.72	34.42
6.1	89.78	-83.68			128.26	38.48
172.97	96.11		76.86		137.3	41.19
491.99	84.83		77.07	330.09	121.18	36.35
99.06	87.17	11.89			124.53	37.36
182.12	83.24		98.88		118.92	35.68
15	80.39	-65.39			114.84	34.45
117.1	69.57	47.53	17.71		99.39	29.82
0	54.71	-54.71			78.15	23.45
15	47.93	-32.93			68.46	20.54
1191.29	878.9	-315.81	315.81	330.09	1255.58	376.67

Source: Meteorology and Hydrology Department, Magway Region

3.3 Soil textural classes of study area

According to the experimental results, soil textural classes were determined by the ratio of sand silt and clay. In the study area, the soil textural class is moderately coarse textures are loamy sand, sandy loam and sand respectively. The common names are sandy soils and texture are coarse texture .Size of grain size is involved in the group of 2-0.05 mm (USDA 1987). In the study area, sandy loam 70%, loamy sand 20%, sand texture 10 % is occurred. Spatial distribution of Soil texture classes were shown in figure(2).The result show that the loamy sand contains 87.5% of sand, silt 8.3 %and clay 4.2%. The sandy loam types contains sand 68%,silt 21% and clay 11%.

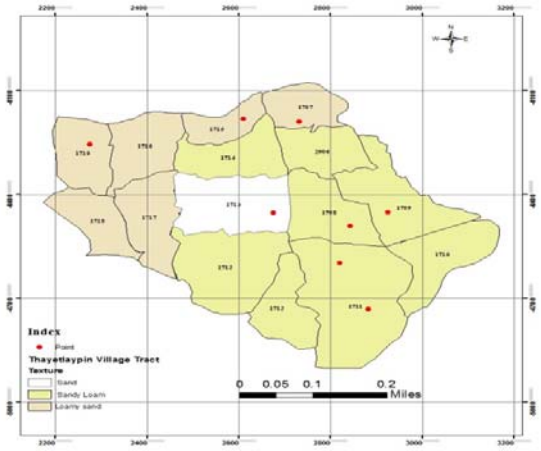

Figure 2. Spatial distributions of soil texture classes of study area

3.4 Soil water content

The soil water content is the amount of water held in the soil at any given time. Average water content for various soils textural classes are shown with organic carbon, pH and humus in table (3). According to table 3, soil water holding capacity was observed with soil texture. The correlation coefficient(r) between the percent of sand content in soil samples and water holding capacity(WHC) is positive correlation (r= 0.54).It is 74% significantly. Moreover, the correlation between clay content in soil samples and WHC is assessed by regression method .The correlation value is (r= 0.59). The relation of silt content in soil samples and WHC is positive correlation (r= 0.47).So, Soil texture controls the water holding capacity. Furthermore, the organic matter carbon is very low and low value in the study area. There are positive correlation between organic carbon and WHC (r=0.02). So, the study area is not sufficient in organic carbon in the soil. Organic matters retain the soil moisture. So it is suggested that providing the soil organic matter increases the soil water holding capacity.

Table (3) Soil Water holding capacity and properties of soil with texture in study area

Soil texture	field capacity	available water	organic carbon	PH	Humus
sandy loam	21	12	0.3	7.29	0.47
loamy sand	19	11	1.4	8.0	2.5
sandy loam	21	12	0.3	6.3	0.5
sandy loam	21	12	0.4	6.5	0.6
sandy loam	21	12	0.4	6.7	0.6
sandy loam	21	12	0.3	6.5	0.6
sandy loam	21	12	0.3	6.7	0.5
loamy sand	19	11	1.4	8.0	2.4
sandy	12	7	0.3	8.0	2.5
sandy loam	21	12	0.2	6.3	0.6

Source: USDA (1987) and field data

3.5 The relative crop yields

The sesame and groundnut yields were collected from each sample field. Therefore, The potential of crop production cannot be equaled in actual because of other factors. Therefore, raw yield data (survey) was calculated by relative crop yield (pp.435,Katalin Jushos, Szilard Szaabo, and Marta Ladanyi, September,2015). The data were calculated by using the relative yield of each crop as follows: $RY_p = Y_p / Y_{max}$ RY_p is the relative yield of plot *p*(a value between 0 and 1), Y_p = the yield of plot p (t/h^{-1}), Y_{max} = maximum yield the total research site over all plots (t/h^{-1}).According to the indices of yield, the relative yield of sesame is less than the relative yield of groundnut. The largest yields of sesame and groundnut indices value are 1, 1 are found in sandy loam type respectively. The yield variability of sesame and groundnut are 63.17% and 27.84%. Table (4) shows the Indices of crop relative yield of plot. As a result, the sandy loam type and sandy soil are more suitable for sesame crop and for groundnut.

Table (4) Indices of crop relative yield of plot

sample soil type	yields/Acres sesame	Yield /Acres groundnut	Relative Yield (Sesame)	Relative yield (Groundnut)
sandy loam	8	6	1	0.60
loamy sand	6	4	0.8	0.40
sandy loam	5	8	0.6	0.80
sandy loam	6	6	0.8	0.60
loamy sand	6.7	5.3	0.8	0.53
sandy loam	6	8	0.8	0.8
sandy loam	6	5	0.8	0.50
loamy sand	4.4	5.4	0.6	0.54
sand	5	10	0.6	1.00
sandy loam	5	4	0.7	0.64

Sources; Field survey

3.6 An analysis of importance of Soil properties on crop yields

Based on the soil moisture balance and soil texture, soil water, field capacity, organic, pH, humus is studied for the crop yields. These factors were analyzed by regression analysis method. As a result, the relative of sesame yield / acres are relations the available water in soil due to the r value=0.47, as well as significant level p=0.16(84%). Similarly, the yields of groundnut were observed with percent of water available in the soil, it is also correlated to the available of water in soil due to the significant level 0.07(93%). In the analysis of oil crop relationship, field capacity and yields of sesame are correlations due to the correlation coefficient r=0.47. Moreover, the confident level is 0.16(84%).The relationship between groundnut and field capacity were occurred significantly by p value is 0.08(91%).Furthermore, the relation between sesame yields and the percent of sand content in the soil samples were observed due to the coefficient correlation r=0.58. Moreover the relationship between sesame and pH value is very strong correlation (r=0.92).However, the relationship between pH in the samples and groundnut yields is very weak(r=0.26).The pH value also is correlation significantly with the humus in the sample soil due to the r value (r=0.91). All these variables are also controlled by soil texture. Therefore, the others factors have to consider for the increase of crop yields.

4. Conclusion

According to the relationship between precipitation and evapotranspiration, the value of ratio is indicating to the good water balance situation for plant growth in the study area. Whereas the conditions of moisture balance, the crop can grow without irrigation because of the storage of moisture larger than 300 mm. Furthermore, the common type of soil is sandy soil and the basic soil classes are sandy loam, loamy sand and sandy soil. Soil texture classes are more suitable for in sesame and groundnut. The basic type of soil textural classes determines the water for plant growth. As a result, the yields of sesame and groundnut are related to these physical and chemical properties but it is not significantly related. However, the soil moisture, texture and properties are not only important but also need to test before crop cultivation for soil quality. Therefore, it is suggested that other external factors have to be considered in the crop cultivations.

Acknowledgements

We deeply indebted to Dr Khin Maung Oo, Rector of University of Magway, for his kind permission to do this research. We also thank to Dr Khin Myo Myo Chun, (Professor and Head, Department of geography, University of Magway) for her recommendation. Finally, we acknowledge to Science Council of Asia and all respectable teachers for call paper and encouragement.

References

[1] Maurice Amooh,Kwame Nkrumoh ,University of Science and Technology, Effects of Soil Texture and Organic matter in Evaporative loss of soil moisture, August, 2015.

[2] Surinda Jalota and Seven authors,Punjab Agriculture University, Soil Texture, Climate and Management effect on plant growth, grain yield and water use by rainfed maize-wheat cropping system: field and simulation study.

[3] Katain Jushos, Szilard Szaabo,and Marta Ladanyi, Influence of soil Properties on Crop Yield: a multivariate statistical approach. September,2015

[4] Kshudiram Chakraborty& Biswranjan Mistri, Importance of soil texture in sustenance of agriculture: A study in Burdwan-I C.D Block, Burdwam, West Bengal,Vol XXINo1 Jan, 2015,ISSN 0973-7642

[5] T.N.Nath,Int.J.chem.sci.: Soil Texture and Total Organic Matter content and Its Influences on Soil Water Holding Capacity of Some Selected Tea Growing Soils in Sivasagar District of Assam,India,12(4),2014,1419-1429,ISSN 0972-768X,www.sadgurupublication.com,

[6] Zachary M.Easton, Assistance Professor and Extension Specialist,Virginia Cooperative Extension,Virginia Tec.Virginia University, Soil and Soil Water Relationships ,PSE-194P,

Operation Models of Mini-Grid in Myanmar: The Case of Shan State

Kensuke Yamaguchi[1], Hiroshi Komikado[2]

Abstract

In Myanmar, rural electrification by mini-grids is necessary for its balanced development. This paper examines the effectiveness of each operation model in conflict areas in Shan State. There are four operation models: utility-operator; private-operator; community; and hybrid model. First, focus group interviews were conducted to sample representative cases of each model. Next, a survey was conducted on each operator about energy capacity, energy resources, tariff, owner, and maintenance. Finally, semi-structured interviews were conducted on members of the Parliament and the state assembly and the chief of the ward. Three main points were found out: (i) When the private enterprise operates, the tariff can be reduced through the economy of scale. But the private have low incentives to enter conflict areas. (ii) When the local leader is responsible, people enjoy relatively cheap electricity with stable supply, which eventually benefits anti-government armed forces. (iii) When the community both constructs and operates, the tariff is highest due to its high initial cost, which widens inequality in the community. In the conflict areas, a hybrid model—mini-grids initially built by governments, then transferred to communities—is most feasible. To scale up this model, a rural development fund is recommended to subsidize initial costs.

Keywords: Rural electrification, Mini-grid, Operation model, Rural Development Fund, Myanmar

1. Introduction

In Myanmar, there is an unbalanced situation in the use of electricity between urban and rural areas. People living in urban areas enjoy electricity with heavily subsidized tariff, while people in rural areas face much higher tariff, and often do not have access to electricity. Since the beginning of the rule by Burmese people in 1948, ethnic minorities, most of whom live in rural areas, have increasingly suffered from this unfair situation. As a consequence, severe poverty still remains among minorities while the urban development is rapid.

As a counter, lots of ethnic groups formed armed forces and they began incidents with the national army. Electrification in rural areas is essential to correct the gap among ethnic groups and achieve balanced development over the nation (Noah and Yamaguchi, 2017; Yamaguchi et al., 2018ab; Yamaguchi, 2019). Especially in conflict areas, expansion of the national grid has a huge risk, and then the development of mini-grids has its significance for electrification. This paper examines the effectiveness of each operation model of mini-grids in Shan State with contentious conflicts area.

2. Methods

There are several key issues for mini-grids, such as who should manage and own them. As the initial and running costs of mini-grids are far larger than the cost of a small power management system such as SHS, their business sustainability needs to be considered carefully (ERIA, 2018; GNESD, 2014; Seguin, 2014). An analysis using the business operator model

[1] Project Assistant Professor, Institute of Future Initiatives, The University of Tokyo, yamaguchi@ifi.u-tokyo.ac.jp; +81-(0)3-5841-0933
[2] Research Assistant, Institute of Future Initiatives, The University of Tokyo, komikadohiroshi@gmail.com

gives an effective view of the discussion (Safdar, 2017). Focusing on operators of mini-grids makes it possible to analyze the structure of the business, the flow of funds, among others. Although there is no universal solution for electrification by mini- grids, an appropriate business model can be chosen based on the advantages and disadvantages for business operators, and the situations where mini-grids are introduced. There are four models of mini-grids operators: Utility operator model; Private operator model; Community model; Hybrid model (European Union Energy Initiative Partnership Dialogue Facility, 2014; Shirley, 2018). Based on the advantages and disadvantages mentioned in previous papers, mini-grids in Shan State are analyzed in this paper.

Data used in the analysis were collected from the field survey conducted by authors from October to December in 2018. There were three surveys in the field survey. The first survey is focus group interviews with five informants on Shan State, including a member of Kachin Democratic Party, members and an advisor of Union Parliament. It was conducted to sample six representative towns with mini-grids in Shan State, considering the operator model of operators of mini-grids. The second is a questionnaire survey on each operator of the six representative town to collect basic information, such as tariff, energy capacity, energy resources, owner, and people in charge of maintenance. The third is semi-structured interviews with 12 stakeholders related to each mini-grid, including members of the Parliament, members of a state assembly, and the chief of the ward. It was conducted to collect information about the advantages and disadvantages of each model to clarify detail information of each case.

3. Results and Discussion

First, focus group interviews picked up six representative cases of mini-grid. Real names and locations of the cases are not used to protect personal information and the towns are re-named Town A, Town B, Town C, Town D, Town E, and Town F. It was clarified that the six representative cases can be divided into four models. Private Operator Model (Private enterprise); Private Operator Model (Local leaders and armed ethnic groups); Community Model; Hybrid Model (Community transfer). Unlike the previous paper, it was clarified that there was no utility-operator model, but that private-operator model can be divided into two models: Private enterprise; Local leaders and armed ethnic groups.

Basic information of each case and model, such as tariff and energy capacity, was clarified by the questionnaire survey. Table 1 summarizes the result. Information about scale (Energy capacity), tariff, operator, owner, and maintenance are described in each case.

Table1. Mini-grid in Shan State, Myanmar

Private	Private enterprise	Town B	6,300 kW	Illumination: MMK100/kWh Industry:	Private enterprise	Four stockholders	Private enterprise
		Town E	20 MW	MMK65/kWh	Private enterprise	Private enterprise, government	Private enterprise
	Local leader	Town C	640 kW	MMK35/kWh	Private enterprise	Armed ethnic group	Private enterprise
		Town F	75 and 65 kW	MMK500 /bulb	Private enterprise	Local leader	Private enterprise
Community	Community burden	Town D	160 kW	MMK100–200/kWh	Community (government loan)	Community	Community
Hybrid	Community transfer	Town A	5 kW	MMK1000 /month	From DRD to Community	Community	Community

Source: Based on interviews conducted by authors

Private Operator Model (Private enterprise) is observed in Town B and Tow E. Private companies contract with the government to invest and manage the business In Town B, private companies and residents are communicating each other and both are satisfied. However, in rural areas, residents are dissatisfied with electricity charges because they do not know the pricing system. Private Operator Model (Local leaders and armed ethnic groups) is observed in Town C and Town F, where armed forces are involved in electricity distribution. Armed groups invest in a power generator for electricity supply as company shareholders. The private company by the armed forces that set up the system is given overall control by the local government and taxes are paid to the federal government. In some cases, the community is involved in system administration because the armed forces are closely related to the community.

Community Model is observed in Town D, and the government provides loans to residents for an initial investment. The mini-grid is owned by the community and is managed by several residents. The initial cost is borne by the residents. Hybrid Model (Community transfer) is observed in Town A, allowing low-cost operation by the community. The initial cost of the mini-grid was borne by government agencies and foreign funds, and its operation will be handed over to the community. Japan International Cooperation System transfers human resources to the community through the Department of Rural Development (DRD). The community owns and manages the mini-grid. This system is expected to reduce electricity costs because it only recovers the lowest operational costs.

As a result, the following three points became clear. First, as the private operator model, not only private companies but also local leaders are often business operators. When the operators are private enterprises, the average energy capacity is ten times bigger than that of other models. On the other hand, if the operator is a local leader, the tariff is cheaper than other

models, but the owner is an anti-government army. Second, the tariff of the Community Model was from three to five times than that of other models. Third, as the Hybrid Model (Community transfer), transfers of mini-grid facilities from the Department of Rural Development to communities are observed. In this model, energy capacity is much smaller than that of other models.

Based on the results, an appropriate model of mini-grids is discussed for rural electrification. If the private enterprise is responsible for an operation of mini-grid, there is an advantage that the economy of scale can be pursued and the price can be reduced. On the other hand, these private-sector businesses have low incentives to enter areas with frequent conflicts and poor purchasing power because there is a possibility that they cannot recover their cost. Then, areas, where the private enterprise wants to introduce mini-grids, are limited and, that is, Private Operator Model (Private enterprise) is limited in scale. If the local leader is responsible for operation, people may be able to receive power supply at a cheap price, but there is a concern that it will be a source of anti- government armed forces. In other words, the patron-client relationship in local politics is strengthened through the mini-grids. Conflicts between armed ethnic forces and the national force will happen more often and they will be more serious. Private Operator Model (Local leaders and armed ethnic groups) will be deepen the gap between people in urban areas and in rural areas, which is originally planned to be solved. When the community takes charge of construction and operation, mini-grids have high initial costs, which leads to high prices. There is a possibility that the people with purchasing power and the people without it will be divided. Moreover, the transfer of knowledge about construction and operation of mini-grid is another challenge for replication of mini-grids with Community Model.

Based on the discussion above, a hybrid model can be expected to be an efficient solution for electrification in conflict areas where purchasing power is often scarce because it will reduce risks for private enterprises to enter the mini-grid business, because it will not be a resource for anti-governmental armed forces, and it gives all residents an access to electricity with relatively low tariff.

4. Conclusions

This paper examines the effectiveness of each model of the Shan state mini-grid. Rural electrification is expected to correct the disparity between ethnic groups and achieve balanced development across the country. Particularly in conflict areas, the expansion of the national grid presents significant risks, and the development of mini-grids is very important for electrification. Analyses employed the framework of business operator model to discuss the appropriate model. Data was collected from a field survey conducted by the author in 2018. There were three surveys: focus group interview, questionnaire survey, and semi-structured interview. The survey clarified the mini-grids in Shan State can be classified into four models and details of each models. Considering each advantages and disadvantages and current situation in Myanmar, Hybrid model (Community transfer) is appropriate for replications of mini-grids because there is a possibility that Hybrid model can solve the problems the other models have.

Finally, following three points are proposed to promote replications of mini-grids of

Hybrid model (Community transfer). First, if DRD is in charge of construction, scalability is limited. Therefore, it is highly expected to leave some of constructions to private enterprises, but, at the same time, a public subsidy needs to be provided so that they can recovered cost by operation for a fixed period. Second, a fund under on the village development law, which is about to be approved, can be utilized for such subsidies. For example, a gasoline tax may be collected to make the fund managed sustainably. Third, it is better for DRD to carry out electrification within the Ministry of Electricity and Energy with not only on-grid but also off-grid electrification, although it is currently in charge of only off-grid solutions and oversees the above-mentioned village development law. Carrying out the proposals above, mini-grid developments with the electric power company model, which was not seen this time, can be expected.

1. Recommendations

To secure government support in a significant scale, a public financing mechanism such as fund is needed.

Where a banking sector is not mature in a country such as Myanmar, fund mechanism is important to achieve a certain multi-year target. Currently, a rural development law legalizing rural development fund is in its final deliberation. As the law articulates that the fund can be used for rural infrastructure such as electrification, it is reasonable and realistic to utilize this fund mechanism to support mini-grids by community.

The source for the fund could be secured as an ear-marked tax system such as gasoline tax.

The initial cost of the mini-grid is required to be subsidized, especially for this community model. The current public support for one project by DRD is around 0.18mil USD. As the Minister of MOEE states, 2,000 villages need mini-grid solution in peripheral regions. A rough calculation shows around 360 million USD to achieve mini-grid targets in conflict-prone areas. Referring to the case in Thailand (i.e. Energy Conservation Fund, ENCON Fund), a petroleum tax is one of the feasible options. Assuming the surging transportation usage in urban areas, imposing an approximately 5% tax rate both on gasoline and on diesel is sufficient as this fund source.

A certain institutional reform among relevant line-ministries is favored to diffuse mini-grid systems in a large scale.

Currently, Ministry of Energy and Electricity (MOEE) is in charge of on-grid electrification while Ministry of Agriculture and Livelihood (MoALI) conducts the off- grid electrification projects such as the “60-20-20” program. As MoALI is not an “energy” Ministry, the program remains at a small scale. To expand the scale and integrate off-grid systems with on-grid ones, an institutional reform between MOEE and MoALI is required for deeper integration and coordination. Ultimately, an integrated policy and planning bodies such as National Energy Management Committee (NEMC) as under the previous government is required with more authority.

Acknowledgements

The authors thank Myo Zaw Shein and Mitasu Company for its research assistance, anonymous reviewers, and seminar participants at Yangon Technical University and the University of Tokyo for useful comments. This research was partially supported by the Ministry of Education, Science, Sports and Culture, Grant-in-Aid for Research Activity Start-up (17H06582, Kensuke Yamaguchi). The authors also gratefully acknowledge financial support from the Economic Research Institute for ASEAN and East Asia (ERIA).

References

[1] ERIA, “Electricity futures in the Greater Mekong Sub region: Towards sustainability, inclusive development, and conflict resolution”, ERIA, 2018

[2] European Union Energy Initiative Partnership Dialogue Facility, “Mini-grid Policy

Toolkit”, European Union Energy Initiative Partnership Dialogue Facility, 2014

[3] GNESD, “Renewable energy-based rural electrification: The mini-grid experience from India”, GNESD, 2014

[4] Yamaguchi, K., “Why economic sanctions in Myanmar is a bad idea”, PacNet: Pacific Forum CSIS, 2019

[5] Yamaguchi, K., Kittner, N., Del-barrio, D., Yoshikawa, H., and Kammen, D., “Energy for Peace in Myanmar: a sustainable and inclusive strategy”, Myanmar Times, 2018a (Burmese)

[6] Yamaguchi, K., Kittner, N., and Yoshikawa, H., “Energy for Peace: ミャンマーにおける水力ダム開発”, エネルギー・資源, 39(4), 247-251, 2018b (Japanese)

[7] Kittner, N., and Yamaguchi, K., “Hydropower threatens peace in Myanmar -- but it

doesn't have to”, Nikkei Asian Review, 2017

[8] Safdar, T., “Business models for mini-grids”, Smart Villages, 2017

[9] Seguin Robert, “Economic feasibility of rural electrification projects”, In Side Event at the High-Level Meeting of the Africa-EU Energy Partner- ship. Addis Ababa, 2014 [10] Shirley, R., “Fact Sheet: Mini-Grids in India: Mini-Grid Finance and Business Models”, Power for All, 2018.

Health Risk Assessment of Soil and Water Pollution near Public Dug Wells along Shwe-Ta-Chaung Creek in Mandalay City

Aye Myat Mon[1]

Abstract

The objective of this research is to determine the environmental pollution in the four public dug wells located adjacent to the Shwe-Ta-Chaung Creek in Tanpawaddy Quarter, Mandalay, Myanmar. Four water samples from four dug wells, named Yarma, Coco-plant, Cow Lake and Salty Water along the creek were examined with Public Health Laboratory to determine the contamination of surface associated with waste water. The water chemical analysis reports for twelve water quality posts of measurement in Coco-plant and Salty Water dug wells are chemically potable and the other two dug wells are chemically unpotable. Eight soil samples near each dug well and relevant creek were determined with Rigaku EDXRF spectrometer to estimate the elemental pollution in the soil. Modified degrees of contamination and pollution load index for soil pollution were analyzed. The water supply wells are impacted by contamination associated with waste water. Soil around Yarma Dug Well and Salty Water Dug Well are more polluted than the other two dug well regions along the creek.

Keywords: Yarma Dug Well, Coco-plant Dug Well, Cow Lake Dug Well, Salty Water Dug Well, Shwe-Ta-Chaung Creek

1. Introduction

The quality of the water in the wells can impact human health even if it is not consumed, due to the contamination of surfaces with chemicals or pathogenic microorganisms through improper installation of wells, or being in close proximity to sources of pollution such as sewage or lands fills. The main ways a home has access to water is either through a municipal water supply from a major city or through wells. Wells exist in two forms, dug wells and tube wells. It is hypothesized that the sewage migrates through the soil and will decrease the water quality of the groundwater. Soil pollution as part of land degradation is caused by the presence of human-made chemicals or other alteration in the natural soil environment. It is typically caused by industrial activity, agricultural chemicals, or improper disposal or waste. Soil Pollution can have a number of harmful effects on ecosystems and human, plants and animal health. Health consequences from exposure to soil contamination vary greatly depending on pollutant type. Industrial or man-made concentrations of naturally occurring substances, such as nitrate and ammonia associated with livestock manure form agricultural operations, have also been identified as health hazards in soil and groundwater.

It is suspected that the waste water from the Shwe-Ta-Chaung Creek may be contaminating the dug wells degrading the water quality. Thus, this research is to determine the impact of the creek on environment near four public dug wells by the analysis of four water samples and eight soil samples collected at four sites next to the creek during the dry season in 2018.

[1] Dr Lecturer, Department of Physics, Banmaw University, Myanmar, ammon37@gmail.com,+9592017813

2. Materials and Methods

2.1 Description of Research Area

Yarma Dug Well (W_1), Coco-plant Dug Well (W_2), Cow Lake Dug Well (W_3) and Salty Water Dug Well (W_4) are located in the Tanpawaddy, Chanmyatharsi Township, Mandalay district, Myanmar and situated beside Mandalay-Sagaing-Shwebo Road.

2.2 Sample Location (Sampling Site), Collection and Preparation

Yarma Dug Well (W_1), Coco-plant Dug Well (W_2), Cow Lake Dug Well (W_3) and Salty Water Dug Well (W_4) were constructed over 100 years ago. The well-bases of four wells are about 30 feet, 9.5 feet, 45 feet and 36.5 feet away from the creek during the dry season. A garbage area is about 75 feet, 15 feet, 95 feet and 65 feet away from each well-base. The diameter of the four wells are 6.5 feet, 4.9 feet , 4 feet and 4 feet .The thickness of the four wells are 1.5 feet, 10 inches, 11 inches and 10 inches which are constructed with a brick lining. The heights of their well bases are 1.5 feet, 5 inches, 9 inches and 1 foot above the ground. The depth to water from the top of the four wells casing are 20.5 feet, 17 feet, 21 feet and 19 feet in March 2018. The widths of the creek near the four wells are about 25 ft, 25ft, 20 ft and 22 ft. Raw sewage from downtown Mandalay flows into the creek. The creek adjacent to W_1 and W_2 are not lined by concrete. Waste water is in direct contact with the ground in the creek. The creek adjacent to W_3 and W_4 are lined by concrete. Waste water is not in direct contact with the ground in the creek. W_1 region is located adjacent to the rubbish filter site along the creek. There is vegetation between W_4 and the creek. The photographs of the four dug wells beside the Shwe-Ta-Chaung Creek are shown in Figure 1, 2, 3 and 4. Photograph of location map of eight research sites in Tanpawaddy Township, Mandalay is represented in Figure 5.

Four water samples were collected with one litre bottle each from the four wells during period in March, 2018. Eight soil samples were collected from the creek at the same time. The sample codes for eight soil samples are listed in Table 1. These soil samples from eight research sites were each collected with two inches in diameter PVC pipe which is one feet long. The small trashes in these samples were cleaned and dried under the room temperature. And then it is needed to grind the soil powdered samples and to get very fine powders. The soil powder samples were passed through 325 mesh sieve of the samples. After getting very fine powder, the sample was weighted nearly 5g. Sample preparation is an important role in X Ray Fluorescence (XRF) measurement.

2.3 Public Health Laboratory, Ministry of Health and Sports

The water quality parameters (Appearance, Colour, Turbity, pH value, Total Solids, Total Hardness, Total Alkalinity, Ca, Mg, Cl, SO_4 and Fe) in four water samples of Yarma Dug Well (W_1),Coco-plant Dug Well (W_2), Cow Lake Dug Well (W_3)and Salty Water Dug Well (W_4) were tested at Public Health Laboratory, Ministry of Health and Sports, Mandalay.

Experimental Procedure for Rigaku X-ray Spectrometer

The EDXRF machine (Rigaku) at the University Research Centre, Taunggyi University is used for determination of elemental concentration in the sample of interest.

Contamination Factor (CF) and Modified Degree of Contamination (mC_d)

The level of metal contamination was expressed by the contamination status of sediment in the current research. CF and mC_d were calculated according to the equation described as

$$CF = \frac{MC}{BC} \qquad \text{and} \qquad mC_d = \frac{1}{N}\sum_{i=1}^{N} CF$$

.

Pollution Load Index (PLI)

Pollution Load Index (PLI) was used to evaluate the extent of pollution by metals in the environment.

$$PLI = (CF_1 \times CF_2 \times CF_3 \times ..... \times CF_n)^{1/n}$$

where n is the number of metals and CF is the contamination factor.

.

Figure.1 Yarma Dug Well beside the creek

Figure.2 Coco-plant Dug Well beside the creek

Figure.3 Cow Lake Dug Well beside the creek

Figure.4 Salty Water Dug Well beside the creek

Figure.5 Location Map of four dug wells in Tanpawaddy Township,Mandalay District,Myanmar

Table.1 Sample Codes for eight soil samples

Sample Code	Soil Samples
S_1W_1	Soil sample near Yarma Dug Well (W_1)
S_1C_1	Soil sample adjacent to Shwe -Ta- Chaung Creek around W_1
S_2W_2	Soil sample near Coco-plant Dug Well (W_2)
S_2C_2	Soil sample adjacent to Shwe -Ta- Chaung Creek around W_2
S_3W_3	Soil sample near Cow Lake Dug Well (W_3)
S_3C_3	Soil sample adjacent to Shwe-Ta-Chaung Creek around W_3
S_4W_4	Soil sample near Salty Water Dug Well (W_4)
S_4C_4	Soil sample adjacent to Shwe-Ta-Chaung Creek around W_4

3. Results and Discussions

The water chemical analysis for twelve water quality posts of measurement in four dug wells are listed in Table 2.Total solids and total alkalinity are greater than maximum permissible level in W_1 and W_3.Other parameters are under the maximum permissible level. The remarks of water chemical analysis report for W_1 and W_3 are chemically unpotable and W_2 and W_4 are chemically potable. The depth to water from the top of the well casing of W_1 and W_3 are greater than the other two dug wells. The water from the four dug wells is now used for taking baths, washing clothes and cleaning dishes. It is not used for drinking purpose now.

Modified Degree of contamination (mC_d) and pollution load index (PLI) of metal contaminates in soil pollution near four dug wells were calculated in Table 3. The comparison of mC_d for soil pollution near four dug wells is shown in Figure 6. The comparison of mC_d for soil pollution in the bank of the creek near four dug wells is also shown in figure 7. Figure 8 gives the comparison of PLI for soil pollution near four dug wells. Figure 9 gives the comparison of PLI for soil pollution in the bank of the creek near four dug wells. The mC_d for soil near W_1 and in the bank of the creek near W_1 is moderate degree of contamination. The mC_d results for soil near W_2 is moderate degree of contamination and in the bank of the creek near W_2 is low degree of contamination. The result of mC_d for soil near W_3 and in the bank of the creek near W_3 is very low degree of contamination. The mC_d results for soil near W_4 is very low degree of contamination and in the bank of the creek near W_4 is very high degree of contamination.

Pollution Load indices (PLI) for soil near the four dug wells are moderately polluted and would indicate deterioration of site quality. The PLI for soil in the bank of the creek near W_1, W_2 and W_3 are moderately polluted and near W_4 is strongly polluted. The PLI for soil in the bank of the creek near the four dug wells would indicate deterioration of site quality. Although the creek near Yarma Dug Well (W_1) and Coco-plant Dug Well (W_2) are not lined by concrete and the creek near Cow Lake Dug Well (W_3) and Salty Water Dug Well (W_4) are lined by concrete.

According to the results, soil around W_1 and W_4 are more polluted than the other two dug well regions along Shwe-Ta-Chaung Creek. There is more pollution at Yarma Dug Well (W_1) because there are many trash and garbage near in it. And there are many cash crop eugenia trees near the Salty Water Dug Well (W_4). Therefore, there are heavy pollutions because of fertilizer insecticide from the plantations adjacent to creek around W_4 region.

Table.2 Water chemical analysis in four dug wells

No.	**Parameter**	**W_1**	**W_2**	**W_3**	**W_4**	**Maximum Permissible Level [WHO]**	**Unit**
1	Appearance	Slightly Turbid	Slightly Turbid	Clear	Slightly Turbid	-	-
2	Colour (Platinum, Cobolot Scale)	7	6	6	6	50	Units
3	Turbidity (Silcoda Scale Unit)	-	-	-	-	25	NTU
4	PH value	7.1	7.1	7.3	7.3	6.5 to 9.2	-
5	Total Solids	1571	1109	1808	1109	1500	mg/l
6	Total Hardness (as $CaCO_3$)	310	270	230	260	500	mg/l
7	Total Alkalinity (as $CaCO_3$)	1105	715	1495	780	950	mg/l
8	Calcium as Ca	112	80	84	96	200	mg/l
9	Magnesium as Mg	7	17	5	5	150	mg/l
10	Chloride as Cl	140	100	120	60	600	mg/l
11	Sulphate as SO_4	147	147	49	118	400	mg/l
12	Total Iron as Fe	Nil	Nil	0.01	Nil	1	mg/l

Table.3 Modified Degree of Contamination (mC_d) and Pollution Load Index (PLI) for soil pollution near four dug wells

Sample Location	S_1W_1	S_1C_1	S_2W_2	S_2C_2	S_3W_3	S_3C_3	S_4W_4	S_4C_4
mC_d	3.128	2.713	2.530	1.994	1.447	1.279	1.363	11.362
PLI	1.879	1.941	1.743	1.845	1.397	1.256	1.340	3.045

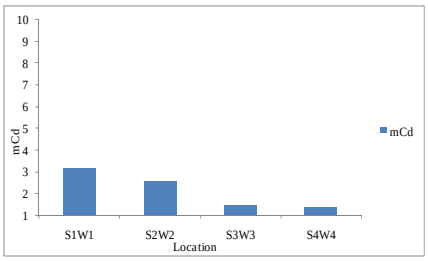

Figure.6 Comparison of mC_d for soil pollution

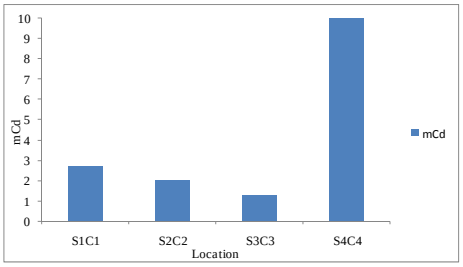

Figure.7 Comparison of mC_d for soil pollution in the bank of the creek near four dug wells

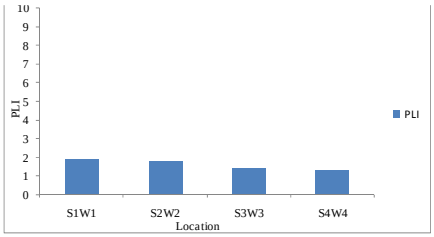

Figure.8 Comparison of PLI for soil pollution near four dug wells

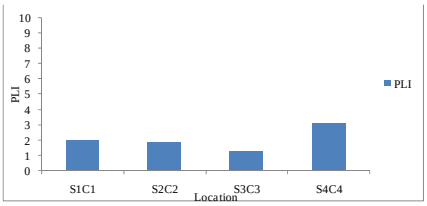

Figure.9 Comparisons of PLI for soil pollution

4. Conclusion

It is indicated that the water supply wells are impacted by contamination associated with waste water. It is recommended that the municipality declare a policy to reduce the pollution and educate the public to have a cleaner environment. The water in Coco-plant (W_2) and Salty Water (W_4) dug wells for twelve water quality posts of measurement are chemically potable and the other two dug wells are chemically unpotable. Soil around Yarma Dug Well (W_1) and Salty Water Dug Well (W_4) are more polluted than the other two dug well regions along Shwe-Ta-Chaung Creek. The pollution around Yarma Dug Well (W_1) is due to garbage landfills. The pollution around Salty Water Dug Well (W_4) is due to excessive fertilizers and pesticides used in agriculture. The waste water creek should be reconstructed with appropriate protection. Humans and animals should not use the wells located near the waste water canal for any purpose. To protect public welfare, safety and health, the water from public dug wells located beside Shwe-Ta-Chaung Creek should not be used long-term.

Acknowledgements

First and foremost I would like to express my gratitude to Dr Aung Kyaw Tin , Rector of Banmaw University, for his kind permission to carry out this work. I am also grateful to Professor Dr Than Than Lwin, Head of Physics Department, Banmaw University for her valuable suggestions.

References

[1] Angelidis T.N,(1997), Water Air Soil Pollution, pp 99-179

[2] Foster S.D & P.J Chilton, (2004), Hydrogeology Journal, pp12-15

[3] Lawrence A R et al., (2000), Hydrogeology Journal, pp 8- 564

[4] Lorna Fewtrell, (2004), Environmental Health Perspectives, Vol. 112,pp 1371-1374

Health Risk Assessment of Heavy Metals via Consumption of Vegetables

Me Me Nyunt[1]

Abstract

Vegetables are an important part of a healthy and balanced diet. They could be contaminated by heavy metals in many ways. Health risk assessment is a very good technique to regard heavy metal contamination in vegetables. The main objective of this paper is to estimate the risk to human health by heavy metals (Mn, Fe, Cu, Zn, Sr and Pb) through the intake of five common vegetables (lettuce, mustard, radish, roselle and water spinach) grown near the drain in Taungthaman lake at Amarapura township by using indexes for vegetables. The elemental concentrations of samples were checked by EDXRF method. Then the indexes for vegetables were calculated. The condition of risk is determined by health risk index (HRI). If the HRI value is less than one, there will be no observed risk. An index more than one is considered as not safe for human health. According to the calculated results, all analyzed vegetable samples except water spinach were not found to cause any risk to the consumer. Water spinach had greatest potential to pose health risk to the consumers. It may be due to the higher absorptivity of heavy metals than the other samples because of its soft and spongy stem.

Keywords: Vegetables, Contamination, Heavy Metals, EDXRF, Indexes for Vegetables

1. Introduction

Vegetables are widely used as food due to their high nutrition values and are edible plants or parts of a plant; they are herbaceous plants whose parts are eaten as supporting food or main dishes. The nutrient content of different types of vegetables varies considerably. Human beings are encouraged to consume more vegetables and fruits due to their richness in vitamins, minerals, fibers and anti-oxidative effects. The fruits and vegetables are important components of a healthy diet and their consumption could prevent a wide range of diseases. However, plants take up metals by absorbing them from contaminated soil as well as from deposits on parts of the plants exposed to the air from polluted environments.

Heavy metals are generally used to describe chemical elements with a specific gravity that is at least 5 times the specific gravity of water. Heavy metals such as manganese (Mn), iron (Fe), copper (Cu) and zinc (Zn) are essential in plant nutrition, however many heavy metals do not play a significant role in the plant physiology. Plants cultivated in polluted environments can accumulate these toxic metals at a high concentration causing serious risks to human health when consumed. Moreover potentially harmful metal contents in soils may come not only from the bedrock itself, but also from the anthropogenic sources like liquid or solid waste deposits, agricultural inputs, fallout of industrial and urban emissions. The use of polluted soils mainly results in decrease the growth of vegetables. Moreover, the heavy metals in soil reduce the yield of vegetables because of disturbing the metabolic processes of plants. Heavy metals contamination is a major problem of our environment and they are also one of major contaminating agents of our food supply. This problem is receiving more and more attention all over the world.

[1] Dr. Lecturer, Department of Physics, Yadanabon University, Myanmar. memeamarapura@gmail.com

Human health are directly affected through intake of vegetables grown in polluted soils. Since heavy metals in the nutrient cycle have seriously threatened health and environmental integrity, more research work is still needed to be done on all species of vegetables grown and consumed. Thus this study was designed to assess the level of some heavy metals (Mn, Fe, Cu, Zn, Sr and Pb) in five vegetable samples (lettuce, mustard, radish, roselle and water spinach) grown near the drain in Taungthaman lake, Amarapura.

2. Methods

2.1 Collection and Preparation of Vegetables

In the present work, the vegetable samples had been collected from the fields near the drain of Taungthamanlake during the period in December 2018. The field is located in the east part of Taungthamanlake of Amarapura Township in Myanmar. To grow the plants, the farmers use the water in drain. The water in the drain is mixed with rainwater, water from the river and the waste water of industries. The industries from the industrial zone used to discard their waste products into the drain. The photograph of the sampling area is shown in *Figure 1*.

The five vegetable samples collected are lettuce, mustard, radish, roselle and water spinach shown in *Figure 2 (a)*. After collecting, the freshly vegetable samples were washed with tap water thoroughly to remove the attached dust particles, soil, unicellular algae, etc. Then they were washed with distilled water. The washed vegetables were passed through filter papers to remove surface water. After that the edible parts were chopped into small pieces. All wet vegetable samples were dried with natural air in room temperature and the drying process was continued until the constant weight had been obtained as shown *Figure 2 (b)*. The dry pieces of samples were crushed into powder using a porcelain mortar and pestle. Then, powder samples were passed through the mesh to get homogeneous powder. The resulting powder samples shown in *Figure 2 (c)* were kept in air tight polythene packet before being taken to the laboratory for metal analyses.

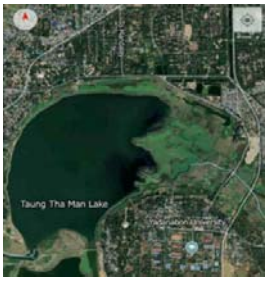

Figure 1. Photograph of sampling area

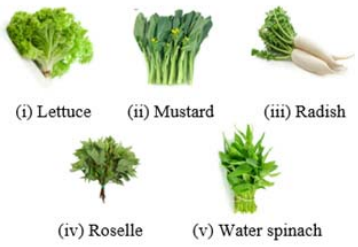

(a)

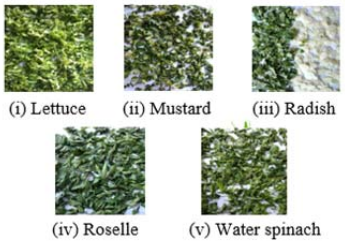

(b)

(c)

Figure2(a.) Photographs of analyzed samples, (b) Sample preparation for fresh condition, (c) Sample preparation for dry and powder condition

2.2 Health risk assessment

Food safety is a major public concern worldwide. The index for food and foodstuff are required to know the information about heavy metal concentration in food products and their dietary intake is very important for assessing their risk to human health. There are many indexes for food and foodstuff according to the field of the study area. In this work, the three indexes associated for food and foodstuff will be discussed, these indexes are (i) the metal pollution index MPI, (ii) daily intake for metal DIM and (iiii) health risk index HRI.

2.3 Metal pollution index (MPI)

Metal pollution index is one of the indexes associated to food and foodstuff which is to determine overall trace elements concentrations in different foodstuff analyzed. This index is obtained by calculating the mean concentration of all the metals in different foodstuff as follow.

$$\text{Metal Pollution Index MPI (mg/kg)} = (Cf_1 \times Cf_2 \times ... \times Cf_n)^{1/n} \quad (1)$$

Where Cf_n = concentration of n^{th} metal in a given foodstuff

Metal pollution index is suggested to be a reliable and precise method for metal pollution monitoring of wastewater irrigation areas. Leafy vegetables are found to contain higher MPI value than which are may be due to the uptake of higher amount of heavy metal available from polluted soil.

2.4 Daily intake of metal (DIM)

The potential health risks of heavy metal consumption through vegetables were assessed based on the daily intake of metal (DIM) and health risk index (HRI). To averagely estimate the daily metal loading into the body system of a specified body weight of a consumer, the daily intake of metal was calculated based on the formula below:

$$\text{Daily Intake of Metal} = \frac{C_{metal} \times C_{factor} \times Con \times EF \times ED}{B_w \times AT} \quad (2)$$

Where C_{metal} = the concentration of heavy metal in vegetable (mg/kg)

C_{factor} = conversion factor from fresh to dry vegetable weight = 0.085

Con = daily average consumption of vegetable in the region (kg person^{-1} day^{-1})

EF = exposure frequency (37 days/year)

ED = exposure duration (65 years, equivalent to the average lifespan)

AT = average time (ED × 365 days/year)

B_w= average body mass of the consumer (kg/person)

The average daily vegetable intakes for a person vary according to locality and their life style. For this present work, the average daily vegetable intake of adult for lettuce and roselle were considered to be 0.165 kg person^{-1} day^{-1}and that for mustard, radish and water spinach were to be 0.345kg person^{-1}day^{-1}(expressed as fresh weight). The average body weight was taken as 70kg for adults according to the World Health Organization (WHO 1993).

Health Risk Index (HRI)

Health risk index HRI is the ratio of daily intake of metal DIM to the reference dose RD, and it is defined as the maximum tolerable daily intake of a specific metal that does not result in any harmful health effects. If the value of HRI less than one, the exposed local population (consumers) is said to be safe and if greater than one indicating that there is a potential risk associated with that metal and not safe for human health. The health risk index HRI was calculated by using the following equation

$$\text{Health Risk Index HRI} = \frac{\text{Daily intake of metal DIM}}{\text{reference dose RD}} \qquad (3)$$

3. Results and Discussion

3.1 Results for metal pollution index: The EDXRF measurement of the vegetable samples gives the elemental concentration of the metal in each sample. The detectable percentage forms of the concentration for each sample have been transformed into the form of milligram per kilogram (mg/kg) scale. The metal pollution index (MPI) for each sample has been calculated by using equation (1). The calculated result of metal pollution index was shown in Table 1.

Table 1. Metal pollution indexes for vegetable samples

Sample	Number of elements (n)	MPI values (mg/kg)
Lettuce	21	447.127
Mustard	23	664.449
Radish	23	485.671
Roselle	21	622.901
Water Spinach	23	3992.254

Results for daily intake of metal : The concentrations of some heavy metals: Mn, Fe, Cu, Zn, Sr and Pb were presented in Table 2. Concentration of heavy metals were in the increasing order: Fe>Zn>Cu>Mn,Sr>Pb. The daily intake of metal (DIM) for a person has been calculated by using equation (2). For DIM calculation, heavy metal concentration, the conversion factor from fresh vegetable to dry vegetable, the daily average consumption of vegetable, exposure frequency, exposure duration, average time and the average body weight were used. In calculation, daily intakes of vegetable per person for lettuce and roselle were used as 0.165 kg and that for mustard, radish and water spinach were 0.345 kg for fresh condition. The average body weight of a person was taken as 70kg for adults according to World Health Organization (WHO, 1993). In this present work, the daily intakes of metal indexes were estimated for six heavy metals. The calculated result data of DIM values for all samples was shown in Table 3. The DIM values of Fe are the highest and that of Pb are least in all samples.

Table 2. Heavy metal concentrations in vegetable samples

Elements	**Heavy Metal concentration (mg/kg)**				
	Lettuce	**Mustard**	**Radish**	**Roselle**	**Water Spinach**
Mn	117	180	150	216	25100
Fe	1050	2410	1830	3170	152000
Cu	173	761	724	797	49000
Zn	305	988	778	814	54400
Sr	134	281	135	169	4190
Pb	23	51	65	63	2500

Table 3. Daily intake of metal (DIM) values for vegetable samples

Elements	**Daily intake of metal (DIM) values (mg/kg/day)**				
	Lettuce	**Mustard**	**Radish**	**Roselle**	**Water Spinach**
Mn	0.0024	0.0077	0.0064	0.0043	1.0659
Fe	0.0214	0.1023	0.0777	0.0644	6.4549
Cu	0.0035	0.0323	0.0307	0.0162	2.0809
Zn	0.0062	0.0420	0.0330	0.0166	2.3102
Sr	0.0027	0.0119	0.0057	0.0034	0.1780
Pb	0.0005	0.0021	0.0028	0.0013	0.1062

Results for health risk index : By using daily intake of metals (DIM) and reference oral dose for each metal, the important index called the health risk index (HRI) can be calculated by applying equation (3). The oral reference dose values for analyzed heavy metals Mn, Fe, Cu, Zn, Sr and Pb are 0.014, 0.7, 0.04, 0.3, 0.6 and 0.004mg kg^{-1} day^{-1}respectively. If the HRI value is less than one, there will be no observed risk. An index more than one is considered as not safe for human health. The calculated result data of HRI values were shown in Table 4. According to these results, HRI value of water spinach is greater than one for almost all heavy metals except strontium.

Table 4. Health risk index (HRI) values for vegetable samples

Elements	Health risk index (HRI) values				
	Lettuce	**Mustard**	**Radish**	**Roselle**	**Water Spinach**
Mn	0.1697	0.5460	0.4550	0.3134	76.1368
Fe	0.0304	0.1462	0.1110	0.0919	9.2213
Cu	0.0879	0.8079	0.7687	0.4047	52.0217
Zn	0.0206	0.1399	0.1102	0.0551	7.7006
Sr	0.0045	0.0199	0.0057	0.0057	0.2966
Pb	0.1168	0.5415	0.0028	0.3199	26.5417

3.2 Discussion

In the present research, five kinds of vegetable samples have been observed. In these samples, lettuce, mustard, roselle and water spinach are the types of leaf vegetables and radish is the type of storage root vegetable. According to Table (1), water spinach and mustard have the highest MPI value while lettuce has the lowest MPI value among the samples. Higher MPI of water spinach and mustard suggests that these vegetables may cause more human health risk due to higher accumulation of heavy metals in the edible portion. Therefore, the leaf vegetable is found to contain higher MPI value than the other types of vegetable which may be due to the uptake of higher amount of heavy metals available from soil and photosynthesis process takes place in the leaf.

To assess the health risk associated with heavy metal contamination of plants grown locally, estimated exposure of tested vegetables (daily intake of metal) and risk index were calculated. The health risk index results showed that Mn, Fe, Cu, Zn and Pb in water spinach had greatest potential to pose health risk to the consumers. It may be due to the higher absorptivity of heavy metals than the other samples because of its soft and spongy stem. The HRI values for analyzed heavy metals in other samples are lower than one. Therefore, it can be said that all analyzed vegetable samples except water spinach were not found to cause any risk to the consumer in the present study.

4. Conclusion

The higher health risk index of heavy metals in water spinach also suggests that there may be potential for human health risk due to consumption. Therefore, it can be concluded that consumption of foodstuff with elevated levels of heavy metals may lead to high level of accumulation in the body causing related health disorders. Long term consumption of heavy metal contamination may be leading to health risk of consumers. Moreover, waste water irrigation for vegetables should be discouraged as it serves as the major route for heavy metal accumulation in vegetables. Further research has to be carried out of determine the concentration of heavy metals in this environment.

Acknowledgements

I would like to express thanks to my students, HninPwintWai and WahWahNaing, atDepartment of Physics, Yadanabon University for theirhelpsin collecting the samples to do this research work.

I would like to express gratitude to my colleagues at the Department of Physics, Taunggyi University for their helps in checking the EDXRF results.

References

[1] Chauhan, G. and Prof. Chauhann, U. K.,"Human health risk assessment of heavy metals via dietary intake of vegetables grown in wastewater irrigated area of Rewa, India", International Journal of Science and Research Publication, Volume 4, Issue 9, September 2014

[2]Duruibe, J. O., Ogwuegbu, M. O. C and Egwurugwa, J. N., "Heavy metal pollution and human biotoxic effects", International Journal of Physical Science Vol. (2), May 2007

[3] Ramteke, S., Sahu, B. L., Dahariya, N. S., Patel, K. S., Blazhev, B. and Matin, L., "Heavy metal contamination of Vegetables", Journal of Environmental Protection, 2016

[4] Singh, A., Sharma, R. K., Agrawal, M. and Marshall, F. M., "Health risk assessment of heavy metals via dietary intake of foodstuffs from the wastewater irrigated site of a dry tropical area of India", Food and Chemical Toxicology, 2010

[5] Adedokun, Aderinola Hannah; Njoku, Kelechi Longinus; Akinola, ModupeOlatunde; Adesuyi, Adeola Alex; Jolaoso, AnuoluwapoOmosileola "Potential human health risk assessment of heavy metals intake via consumption of some leafy vegetables obtained from four market in Lagos Metropolis, Nigeria", J. Appl. Sci. Environ. Manage. Vol (20), Sept. 2016

PC-Based Ultrasound Object Detection System

Aung Naing Oo[1] , Mar Mar Cho[2]

Abstract

To determine the presence of object and to search the object when it moves from its initial position, the object detection system by using ultrasound transducers is constructed. The PIC microcontroller (PIC16F628A) is programmed to generate the required driving clock frequency for ultrasound transmitter (T40-16). The echo sent back from the detected object is received by the ultrasound receiver (R40-16). Then, the received echo pulse is amplified and transformed into digital signal by dual audio operational amplifier (LM833) and low power dual voltage comparators (LM393). Three receiver modules are constructed to sense the movement of the object. The receiver which accepts the echo sent back from the object is identified. The CMOS quad 2-input NAND schmitt triggers (CD4093B) is used to produce the proper logic level of signal receiver which receives the echo. The camera takes the picture of the object and sends to the monitor via VLC media player software. The stepper motor performs the movement of the constructed system either clockwise or counter clockwise direction. The operation of the system is controlled by the written program in Visual C Sharp programming language.

Keywords: PIC microcontroller, ultrasound transmitter, ultrasound receiver, Visual C Sharp programming language.

1. Introduction

Ultrasonic waves are mechanical waves that consist of oscillations or vibrations of the atomic or particles of a substance about the equilibrium positions of these particles. Ultrasonic waves behave essentially the same as audible sound waves. They can propagate in an elastic medium, which can be solid, liquid or gaseous, but not in a vacuum.

To find a barrier in the path or to avoid from the obstacles, ultrasonic transducers are used to detect the presence of object. In this work, 40 kHz driver circuit is constructed by PIC microcontroller (PIC16F628A). This frequency is sent to the ultrasonic transmitter circuits. The ultrasonic transmitter (T40-16) produces the ultrasound. When the transmitted ultrasound detects the object, echo is appeared. The ultrasonic receiver (R40-16) accepts the echo that falls on to it. The signal is amplified by dual audio operational amplifier (LM833). The amplified signal is sent to the low power dual voltage comparators (LM393) to be free from the noise interference. After that the output voltage from LM393 is changed to digital logic level of HIGH or LOW corresponding on the existence of object or not. Then, the logic level is sent to the personal computer via line printer terminal. The written program controls the operation of stepper motor depending on the logic level sent along the line printer terminal. The PC camera mounted on the circuit board sends the photographs of objects that lie in front of it. These photographs are shown on the monitor.

2. PIC Microcontroller

A microcontroller is an inexpensive single-chip computer. The PIC16F628A is 18-pin flash-based member of the versatile PIC microcontroller. It is complementary metal oxide semiconductor and has high performance. It employs an advanced RISC architecture. The

[1] Dr. Lecturer, Department of Physics, Yadanabon University
[2] Dr. Lecturer, Department of Physics, Yadanabon University

PIC16F628A has enhanced core features, eight-level deep stack, and multiple internal and external interrupt sources. The separate instruction and data buses of the Harvard architecture allow a 14-bit wide instruction word with the separate 8-bit wide data. The two-stage instruction pipeline allows all instructions to execute in a single-cycle, except for program branches. A total of 35 instructions are available, complemented by a large register set. Fig. (1) shows the photograph and pin diagram of PIC16F628A microcontroller.

Figure1. The photograph and pin diagram of PIC16F628A microcontroller

2.1 Ultrasonic Transducer (TR40-16)

The T40-16 and R40-16 are matched pair ultrasonic transmitter and receiver respectively operated at 40 kHz center frequency. This transducer utilizes the piezoelectric properties of engineering ceramic that provides high sound pressure and high sensitivity. Fig. (2) shows the photograph of ultrasonic transducer (TR40-16).

Figure2. Photograph of ultrasonic transducer (TR40-16)

2.2 Stepper Motor

A stepper motor is an electromechanical device which converts electrical pulses into discrete mechanical movements. The shaft or spindle of a stepper motor rotates in discrete step increments when electrical command pulses are applied to it in the proper sequence. The motor rotation has several direct relationships to these applied input pulses. The sequence of the applied pulses is directly related to the direction of motor shafts rotation. The speed of the motor shafts rotation is directly related to the frequency of the input pulses and the length of rotation is directly related to the number of input pulses applied. The photograph of stepper motor is shown in Fig. (3).

Figure 3. Photograph of stepper motor

2.3 Design and Construction

To find the barrier in path or to know the disappearance of the object, object detection systems are constructed. In these systems, infrared sensor or ultrasonic transducers are used. This work is intended to detect an object which is placed in front of the detector. In this work, ultrasonic transducers are used to detect the object.

The block diagram of the constructed system is shown in Fig. (4). The system is composed of seven main parts. They are power supply unit, oscillator unit, ultrasonic transmitter unit, ultrasonic receiver unit, level comparator unit, interfacing unit and stepper motor control unit.

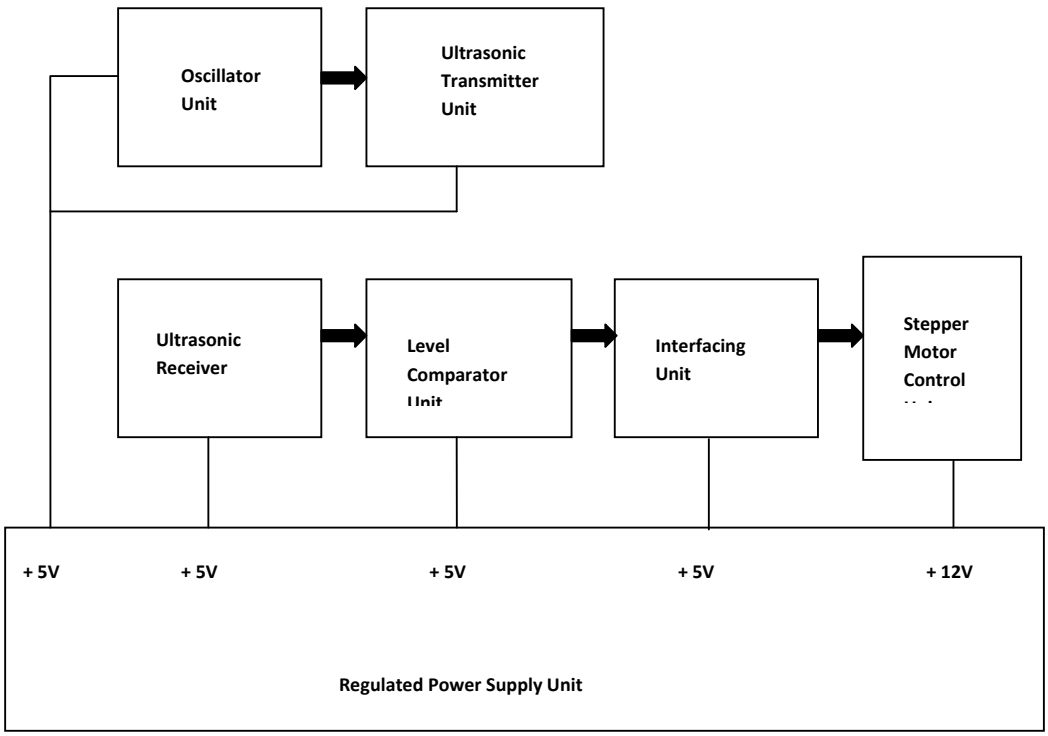

Figure 4. Block diagram of the constructed system

The oscillator circuit composed of PIC microcontroller (PIC16F628A) is used to generate the required driving clock frequency. The ultrasonic transmitter unit and ultrasonic receiver unit are constructed by using ultrasonic transmitter (T40-16) and ultrasonic receiver (R40-16). To get the noise free voltage level, level comparator circuits are constructed by using low power dual voltage comparators (LM393). For interfacing with the personal computer, the interfacing circuit using CMOS quad 2-input NAND schmitt triggers (CD4093B) is also attached. When the object is disappeared, the transducer units are needed to rotate either in clockwise or counter clockwise direction in searching the object. Therefore, stepper motor control circuit is also constructed. To show the object on the monitor, a camera is also fixed in this system. Fig. (5) shows the ultrasonic transmitter and receiver transducers array.

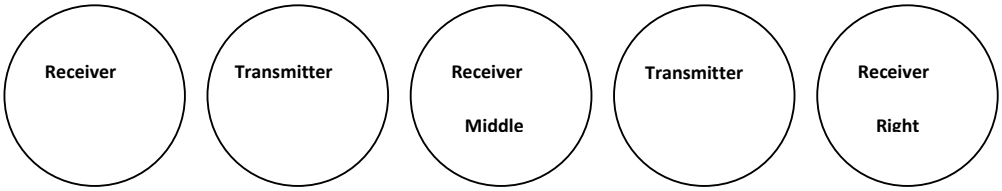

Figure 5. The ultrasonic transmitter and receiver transducers array

3. Results and Discussion

The oscillator produces the required clock frequency. The ultrasonic transmitter (T40-16) uses this frequency and sends out the ultrasound. When the ultrasound hits the object, the echo is appeared. This echo is received by the ultrasonic receiver circuit and sent to the personal computer. The written program determines the presence of object. If there is no object, no echo is appeared. Since there are three receivers for middle, left and right positions, the movement of the object from its initial position can be known. The written program also drives the stepper motor to rotate in clockwise or counter clockwise direction until the system finds the object. The function of the constructed system is shown in Fig. (6).

The photograph of constructed circuit is shown in Fig. (7). Fig. (8) shows the complete circuit diagram of the constructed circuit.

Ultrasonic Receiver			**Stepper Motor Rotation**
Left	**Middle**	**Right**	
OFF	ON	OFF	Stationary (No Rotation)
ON	OFF	OFF	Counter Clockwise Rotation
OFF	OFF	ON	Clockwise Rotation

Figure 6. The function of the constructed system

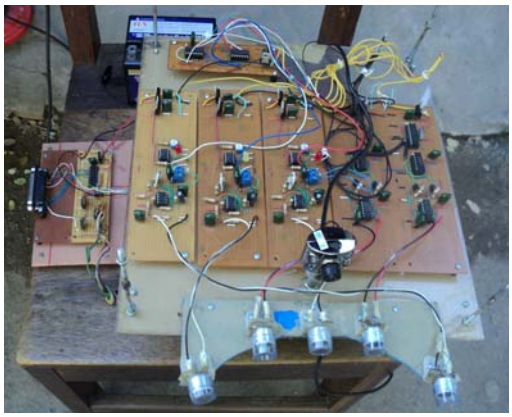

Figure 7. Photograph of constructed circuit

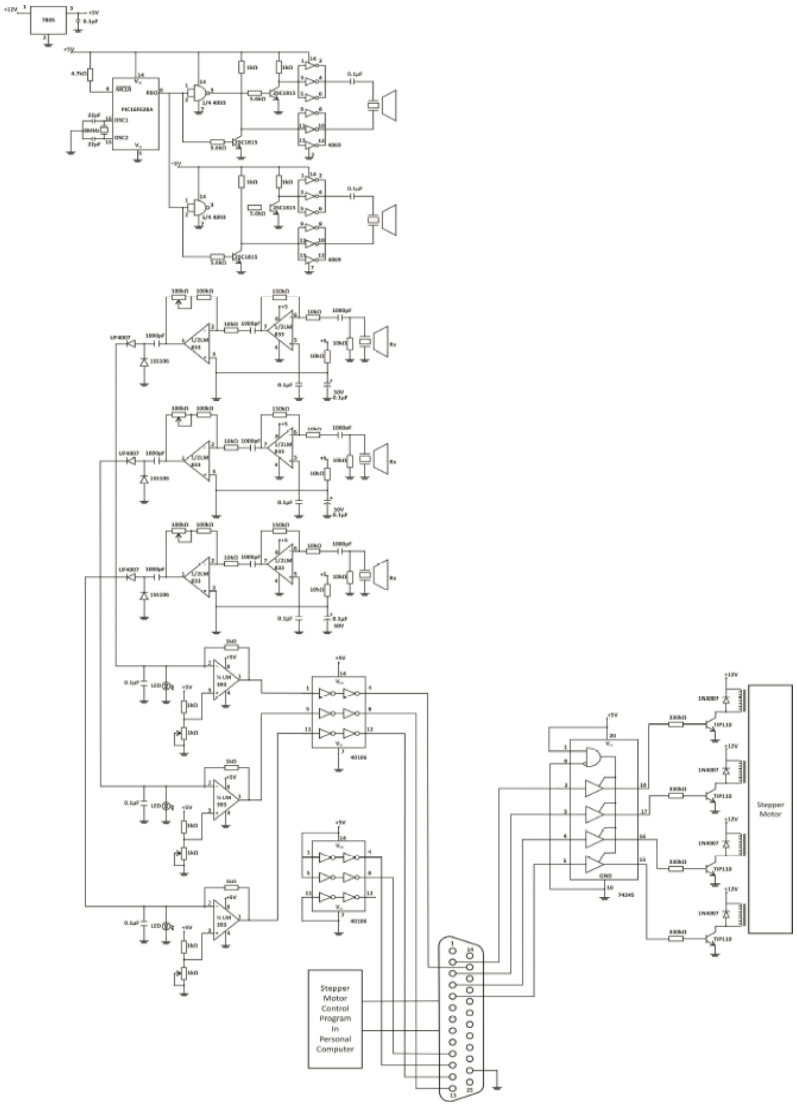

Figure 8. Complete circuit diagram of the constructed circuit

4. Conclusion

In this work, three ultrasonic receivers (R40-16) are used to detect the movement of object. Each ultrasonic receiver is needed to get the noise free echo for the exact object location. So, the voltage gain from dual audio operational amplifier (LM833) is limited even though the operational amplifier has very high open loop gain. Therefore, the constructed work is effective in detecting the object in short range.

Circuit design and programming for PIC microcontroller and personal computer is also very important in carrying out this work. The enhancement of knowledge of application of PIC microcontroller, interfacing with the personal computer is the great advantage of this work.

Acknowledgements

We would like to express our gratitude to Dr Maung Maung Naing, Rector, Dr Si Si Khin, Pro-Rector and Dr Tin Moe Thuzar, Pro-Rector of Yadanabon University for their suggestion and permission to perform this project work. We would also like to express our great thanks to Dr Yi Yi Myint, Professor (Head of the Department), Dr May Thida Win, Professor and all the teachers and staff from the Department of Physics, Yadanabon University for their help and discussion throughout this research work.

References

[1] J. David N. Cheeke, “Fundamentals and Applications of Ultrasonic Waves”, CRC Press LLC, United States of America (2002).

[2] Parallax Inc., “Detect Distance With The Ping))) Ultrasonic Sensor”, http://www.parallax.com (2005).

[3] Waitrony, “Ultrasonic Transducer (TR40-16)”, http://www.ic-on-line.cn (2003).

[4] R. A Penfold, “Easy PC Interfacing”, Bernard Babani Ltd., England (1995).

[5] S. Mueller, “Upgrading and Repairing PCs”, 14th Edition, Que, Indiana (2003).

[6] J. Iovine, “PIC Microcontroller Project Book”, McGraw-Hill, New York (2000).

[7] Microchip Technology Inc., “PIC16F627A/628A/648A Data Sheet”, United States of America (2004).

[8] Stmicroelectronics, “LM393”, http://www.st.com (2011).

[9] National Semiconductor Corporation, “LM7805”, http://www.national.com (2006).

[10] National Semiconductor Corporation, “LM833”, United States of America (1995).

[11] Texas Instruments, “CD4093B”, Dallas (2003).

[12] Philips Semiconductors, “HEF40106B”, http://www.datasheetcatalog.com (1995).

[13] Texas Instruments, “SN74LS245A”, Dallas (2003).

Green Synthesis and Characterization of Chitosan-Copper Nanoparticle Used as Antimicrobial and Antitumor Activities

Aung Than Htwe[1], Thinzar Nu[2], Cho Cho[3]

Abstract

This work is an attempt to aim to synthesize, characterize and apply of eco-friendly green synthesized copper - chitosan nanoparticles (Cu-NPs). In this work the environmentally friendly synthesis of stable Cu chitosan NPs through green route with chitosan as a stabilizer and or reducing agent was synthesized. The synthesized copper nanoparticles were confirmed by the change of colour after addition of chitosan into the Copper (II) sulphate solution. The biosynthesized CuNPs were characterized by using UV-Vis, Fourier Transform Infrared (FTIR), X-ray diffraction analysis (XRD) and Scanning Electron Microscopy (SEM). Average crystalline size of the nanoparticles was estimated from the Debye- Scherrer's equation. The antimicrobial activity of the nanoparticles were investigated using six microorganisms of interest, including *Staphylococcus aureus, Bacillus subtilis, Pseudomonas aeruginosa, Bacillus pumilus, E-coli and Candida albicans*. The effect of a chitosan medium on growth of the microorganism was studied, and this was found to influence growth rate. The antitumor activities of the synthesized CuNPs were investigated by Potato Crown Gall teat and these activities were found to be within 5-7 days by the dose of 0.05, 0.1 and 0.15 g of CuNPs. Finally, the present study provided to full fill the scientific evidence, become a new trend to save and reduce environmental pollution and safety in bactericidal, wound healing and other medical applications.

Keywords: Chitosan, Cu-NPs nanoparticles, antimicrobial activity, antitumor activity

1. Introduction

Bacterial and fungus infection is a problem in all over the world. So this chitosan-copper nanoparticles (CuNPs) is to solve and reduce this problem.

Metal nanoparticles have attracted considerable attention in many fields, such as catalysis, optoelectronics, photovoltaic technology, information storage, environmental technology, engineering, biosensors development, medicine, and so on [1]. Among nanomaterials, nanoparticles have been contributing to the progress in this field. In particular, therapies using nanoparticles have widely been achieved for the treatments of cancer, diabetes, allergy, infection and inflammation [2]. Generally, metallic nanoparticles show antibacterial and antifungal activity, even though there are environmental and human safety concerns regarding the release and consumption of metal nanoparticles which are yet to be explored. Excessive release of silver, for example, causes environmental pollution which in turn makes silver harmful to human and animals. An excess of copper in the human body leads to generation of the most damaging radicals, such as the hydroxyl radical [3]. Nanomaterials are widely used in various technological applications viz. refrigeration systems, medical imaging, drug targeting and other biological applications, and catalysis [4].

[1] Dr Assistant Lecturer, Department of Chemistry, University of Yangon, Myanmar, e-mail: aungthanhtwe76@gmail.com

[2] Associate Professor, Department of Chemistry, University of Yangon,Myanmar, e-mail: thinzarnu50@gmail.com

[3] Professor, Department of Chemistry, University of Yangon, Myanmar, e-mail: chocho.urc@gmail.com

Environmentally friendly solvents, reducing agents are used with enormous potential as part of a responsible green approach for the development of nanotechnology. Biocompatible and nontoxic polymers (e.g. chitosan) as a reducing and stabilizing agent of metal nanoparticles is suggested [1]. Copper nanoparticles (CuNPs), due to their excellent physical and chemical properties and low cost for preparation, have been of great interest [5].

Chitosan is a natural product derived from chitin, a polysaccharide present in the exoskeletons of shellfish such as shrimps and crabs. It is a cationic polysaccharide composed of β-(1-4)-linked D-glucosamine and N-acetyl-D glucosamine units. Environmental-friendly material with many superior properties with momentous amounts of amine and hydroxyl groups that can be easily engineered [6]. The antimicrobial action is influenced by intrinsic factors such as the type of chitosan, the degree of chitosan polymerization, the host, the natural nutrient constituency, the chemical or nutrient composition of the substrates or both, and the environmental conditions (e.g. substract water activity or moisture or both) [7]. The NPs generated are strongly attached to the chitosan due to the chemical bond between the electron rich nitrogen present in the amino groups of the polymer and copper. The use of biopolymer as capping and or reducing agents represents an environmentally friendly alternative to hazardous organic solvents [8].

The present work deals with environmentally friendly synthesis of stable chitosan-copper nanoparticles through green route with chitosan as a stabilizer and or reducing agent. The synthesized NPs were characterized by UV-Visible spectrometry, SEM, and XRD. Their antimicrobial properties were tested using microorganism such as fungi, algae and some bacteria. Finally, antitumor activities were investigated.

2. Methods

2.1 Synthesis of Chitosan-Copper Nanoparticles (CuNPs)

In a typical one-step synthesis, 50 mL of 1 % (w/v) chitosan solution was prepared by using 1 g of chitosan(CS) was dissolved in 100 mL of 1 % acetic acid solution. 50 mL of 1 % CS solution and 25 mL of 0.05 M $CuSO_4.5H_2O$ were then mixed and stirred on magnetic stirrer at 80 °C for 12 h till the reaction was completed. After 12 h the colloid was centrifuged at 7,000 rpm for 20 mins to separate particles from suspension. The precipitate was re-suspended in acetone (90%, v/v) and the centrifugation was repeated three times to remove unreacted reagents. Finally, the precipitate was dissolved in water, dried under vacuum overnight and stored.

2.2 Characterization of Cu NPs

UV-visible spectra were recorded using a Shimadzu UV-Vis1800 Spectrophotometer for the confirmation of NP formation. The structural features of Cu-Chitosan NPs were performed in a PerKinElmer GX system FT IR spectrometer in a range from 400 to 4000 cm^{-1}. The size and morphology of the Cu-Chitosan NPs were examined by SEM (JEOL model JSM 5610 LV scanning microscope). X-ray diffraction studies were performed with an X-ray diffractometer (Rigaku Ultima III XRD) with Cu Kα1 radiation to determine the structure of a sample. The X-ray source was operated at 40 kV and 40 mA. Diffraction intensity was measured in the reflection mode at a scanning rate of 2°/min for 2θ=10-70°.

2.3 Determination of Antimicrobial Activity

The CuNPs was tested with *Bacillus subtilis, staphylococcus aureus, Pseudomonus aeruginosa, Bacillus pumalis, Candida albican and E. coil* species to investigate the nature of antimicrobial activity. After preparing the bacteriological media, the dried films were placed on the agar with flamed forceps and gently pressed down to ensure proper contact. The plates were incubated immediately or within 30 min after incubation [9, 10]. After overnight incubation at 37 ºC, the results are shown in Table 1 and Figure 1.

2.4 Screening of Antitumor Activity by Potato Crown Gall Test or Potato Disc Assay

Tumor producing bacteria, *Agrobacterium tumefacien*, was used in this study. All of these strains have been maintained as solid slants under refrigerator. For inoculation of potato discs, 48 h broth cultures containing $5\times 10^7 - 5\times 10^9$ cell/mL were used. *Agrobacterium tumefaciens* strain was cultured on Luria-Bertani (LB) agar medium which was prepared by dissolving a mixture of yeast extract (1 g), peptone (1 g), NaCl (0.5 g) and agar (2 g) in distilled water (100 mL). Single colony was transferred into LB broth and incubated at 30 °C for 48 hours in the shake. Six to seven loops of bacterial suspensions (1.0×10^9 cfu) were transferred into sterilized phosphate buffer saline (PBS) and this was used during antitumor assay inoculums. The antitumor activity was examined by observation of tumor produced or not.

3. Results and Discussion

The formation of Cu-NPs was observed in a series of colour changes. The addition of Cu^{2+} solution to CS solution resulted in the appearance of a light blue which indicates the formation of a $[Cu (CS)]^{2+}$ (aq) complex figure 1. The reduction of metal ion is one of the most convenient and promising synthetic approaches to obtain metallic nanoparticles with relatively inexpensive setups. Cu-NPs are very difficult to obtain by simple reduction of copper salts in aqueous solution where copper is oxidized to CuO and Cu_2O [6].

chitosan solution | *$CuSO_4.5H_2O$ (aq)* | *$[Cu(CS)]^{2+}$* | *[Cu(CS)]NPs*

Figure 1: Photographs of the sample at the different stages of synthesis showing colour variations

3.1 UV-visible Spectrophotometric Analysis

The observation of the absorption spectra of different aliquots overtime containing copper sulphate (50 mM) in chitosan (0.75% w/v) showed major peak in the range 500-600 nm , thus revealing the formation of Cu-NPs. The colloidal Cu-NPs prepared at 12 h at 70 °C showed a characteristic single absorption peak at 536 nm (Figure 1), which indicates the decrease of reactants Cu^{2+} ions in the presence of chitosan to the formation of large amount of monodisperse NPs. The present finding was in agreement with the blue shift of the surface plasmon resonance

(SPR) of the metallic NPs with their decreasing size. Nanosized Cu particles exhibited a SPR at around 500-600 nm. This shows that copper ions was added to the chitosan solution. This is to indicate that Cu^{2+} ions are attached to chitosan macromolecules by electrostatic interactions. The electron-rich oxygen atoms of polar hydroxyl and ether groups of chitosan are responsible to interact with electropositive metal cations. It has been reported that chitosan acts as a controller of nucleation as well as a stabilizer [8].

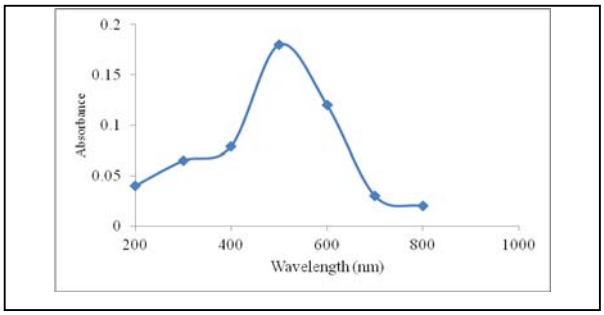

Figure 2: UV- visible spectrum of synthesized copper-chitosan nanoparticle

3.2 FTIR Analysis

FTIR analysis was conducted to determine the molecular interactions between chitosan and the synthesized NPs. The chitosan spectrum in figure 3(b) illustrates an amide I C = O vibration band at 1633.94 cm^{-1}. The spectrum also dhows transmissions at 3303.19 cm^{-1} assigned to the overlap of O-H and N-H stretching vibrations, 1633.94 cm^{-1} and 1537.88 cm^{-1} to -NH_2 bending, 1336.57 cm^{-1} to C-H bending and 1064.11 cm^{-1} to -C-O skeletal stretching. A similar trend was observed in CuNPs spectrum (figure 3(c)). For instance, a general decrease in band with a blue shift was noticed (from 1633.94 to 1632.60, 1537.88 to1531.25 and 1064.11 to 1063.68 cm^{-1}). The peak at 611.7 cm^{-1} evidence the interaction between CuNPs and CS media which indicates a reaction between the CuNPs surface, and the CS amino and hydroxyl group [3, 11].

The experiments described above indicate the importance of chitosan in the performed synthesis. Chitosan, as a biopolymer, has a significant content of primary amines and hydroxyl groups and possess a strong affinity towards metal ions, which are incorporated by simple chelation by ion exchange, thereby making it an excellent support for nucleation of Cu-NPs. The generation of $[Cu\ (CS)]^{2+}$ complexes in solution enables metal ion reduction. From these results, it can be envisaged that the biopolymer plays an important role as polymeric capping agent (Stabilizer) [1].

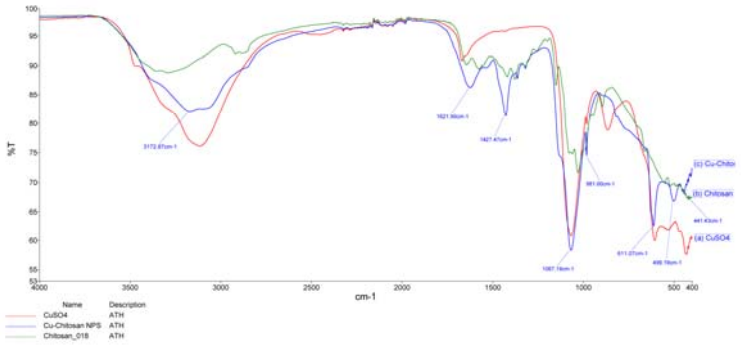

Figure 3. FT IR Spectrum of synthesized copper-chitosan nanoparticle

3.3 Powder X-ray Diffraction Analysis

The solid state or crystallinity of the synthesized CuNPs was characterized by X-ray diffractometry. The XRD diffractogram of the CuNPs are shown in figure 4. The XRD pattern for CuNPs exhibited two crystalline peaks at 2θ angles of 36.628 ° and 50.141° respectively. The prominent diffraction peaks observed are indexed to (111) and (200) reflections. This confirms that the resultant nanoparticles are face centered cubic (fcc) of metal nanoparticles. The highest intense peak for fcc materials is generally (111) reflection and this was observed in the synthesized nanoparticles. These planes observed were compared with the standard powder diffraction card of JCPDS copper file No. 78-0428 and copper X-ray diffraction reference No. 85-1326. The absence of any noticeable peaks in the pattern resulting from the sample suggests that the sample is free from impurities such as CuO and Cu_2O. The average crystalline size of the CuNPs obtained was estimated to be in the range of 28.221 nm using Debye-Scherrer equation is given as: $D = \frac{K\lambda}{\beta \cos\theta}$, where D is the mean nanoparticles diameter (Particle size), K is a constant with value 0.94, λ is the wavelength of X-ray (0.154), β is full width at half maximum and θ is the differential angle [12].

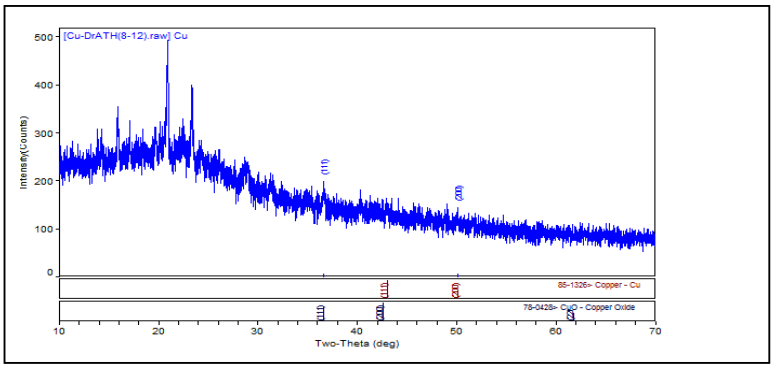

Figure 4. XRD diffractogram of synthesized copper-chitosan nanoparticle in chitosan media

3.4 SEM

The surface morphology of synthesized CuNPs was examined and the thickness of these particles was determined by JEOL scanning electron microscopy. The thickness was approximately 10 μm. The micrograph of the cross-section surface structure of CuNPs was shown in figure 5. From the micrographs the CuNPs found to be made up of the slightly

aggregated due to the absence of strong surface protecting ligands and found to be irregular in shape.

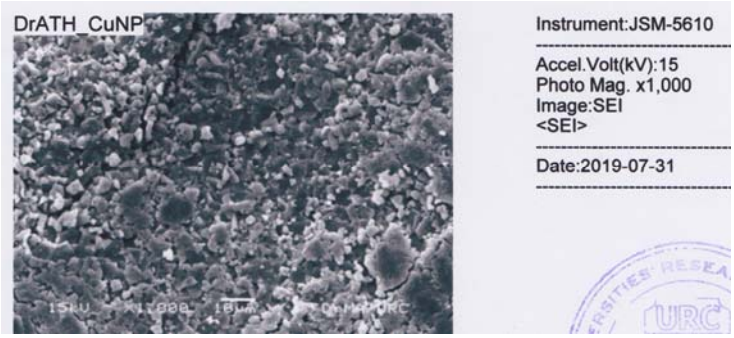

Figure 5. SEM micrograph of synthesized copper-chitosan nanoparticle

3.5 Antimicrobial Activity of CuNPs

Antimicrobial activity of CuNPs are shown in Table 1. Tested organisms were *Bacillus subtitles*, *Staphylococcus aurous*, *Pseudomonas aeruginosa*, *Bacillus pumalis*, *Candida albican* and *E.Coli*. As seen in figure 6, antimicrobial test of CuNPs was used the agar medium cultivation. According to the experimental results, the prepared CuNPs was really effective to antimicrobial activity. The cell wall is more exposed to nanoparticles through the outer bacterial membrane. The unique high surface to volume ratio of CuNPs enables them to interact with the bacterial cell membrane through its surface, which leads to the death of the bacterium. Therefore, the size of the nanoparticles is important for antimicrobial activity [3]. It was observed that CuNPs was bactericidal and fungicidal against both gram-positive and gram-negative bacteria and fungus.

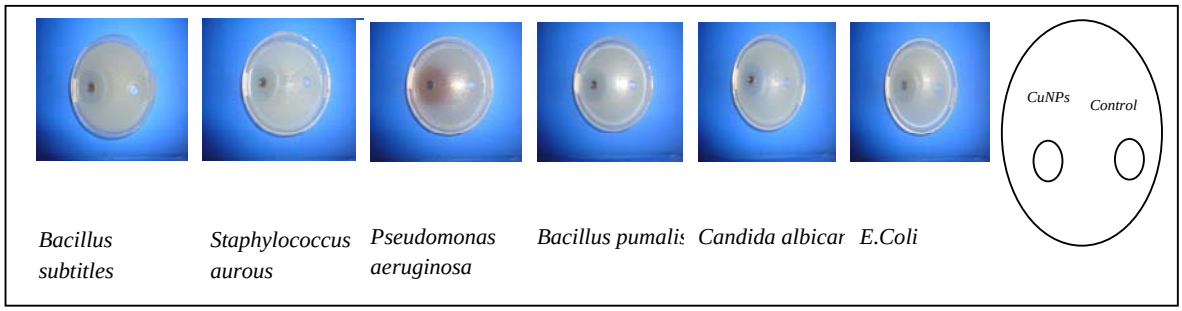

Figure 6. Antimicrobial activities of synthesized copper-chitosan nanoparticle

Table 1. Antimicrobial Activity of CuNPs by Agar Disc Diffusion Method

Sample	***Microorganism***					
	Bacillus subtilis	***Staphylococcus aureus***	***Pseudomonas aeruginosa***	***Bacillus pumilus***	***Candida albican***	***E-coil***
CuNPs	25 mm (+++)	20 mm (+++)	13 mm (+)	16 mm (++)	23 mm (+++)	21 mm (+++)

Agar well 10 mm, 10 mm-14 mm (+), 15 mm-19 mm (++), 20 mm above (+++)

3.6 Antitumor Activity of CuNPs

The antitumor activity of CuNPs was investigated by using PCG test with bacterium *A. tumefaciens*. For inoculation of the potato disc, 48 h broth cultures containing 5× 10^9 cells/mL were used. The tested sample was dissolved in DMSO, diluted and mixed with the bacterial culture for inoculated on the cleaned and sterilized potato discs, and incubated for 7 days at room temperature. After that, the tumors were appeared on potato disc and checked by staining the knob with Lugol's (I_2-KI) solution. In the control the formation of while knob were on the blue background indicated the presence of tumors cell because there is no protein in tumor cells. The tested sample did not form any tumors on the potato discs and its surface remained blue. Form this experiment, it was found that CuNPs was not significantly inhibited the formation of tumor cell with the dose of 0.1, 0.2 and 0.3 g/disc. These results are shown in Table 2 and figure 7.

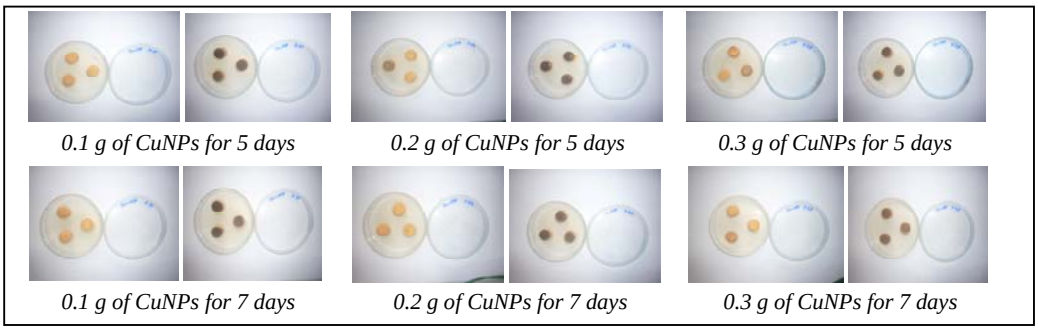

Table 2. Antitumor activity of CuNPs

sample	**Days**	**Concentration/disc (mg)**		
		0.1 g	**0.2 g**	**0.3 g**
CuNPs	**5**	+	+	+
	7	+	+	+
Control	++			

Tumor inhibition:

(++) = non activity

(+) = less activity

4. Conclusion

The present study indicates that of CuNPs with a size of 28.22 nm have been successfully synthesized in the presence of a biowaste polymer chitosan. The synthesized NPs were characterized by UV-Vis, FTIR, XRD and SEM analyses. From FTIR analysis, the peaks of the CuNPs are attributed to N-H, O-H, C=O, C-O, C-OH, CH and Cu-O stretching and bending vibrations. The average crystalline size of CuNPs nanoparticle is 28.22 nm and agglomerate porous and crystalline nature. The chitosan plays the main role of chelating with metal ions. The synthesized CuNPs exhibited good antimicrobial and antitumor activity. The present synthetic method represents a simple, convenient, cost-effective and environmental-friendly. The main contribution of the present work producing chitosan-copper nanoparticles could promote to a certain extent of sustainable development and foster innovation toward and may be used for pharmaceutical and biomedical application.

Acknowledgements

The authors feel indebted to Professor and Head Dr. Ni Ni Than, Department of Chemistry, University of Yangon, Yangon, Myanmar, for his stimulating suggestions. I would like to express my deepest gratitude to Science Council of Asia (SCA) and Myanmar Academy of Arts and Science for this conference.

References

[1] Katarzyna Tokarek, Jose L Hueso, Piotr Kustrowski, Grazyna Stochel, Agnieszka Kyziol, "Green synthesis of chitosan-stabilized copper nanoparticles", European Journal of Inorganic Chemistry, 2013, vol.28, pp. 4940-4947.

[2] Sachiko Kaihara Nitta, Keiji Numata, "Biopolymer-based nanoparticles for drug/gene delivery and tissue engineering", International Journal of Molecular Science, 2013, vol. 14, pp. 1629-1654.

[3] Muhammad Sani Usman, Mohamed Ezzat EI Zowalaty, Kamyar Shameli, Norhazlin Zainuddin, Mohamed Salama and Nor Azowa Ibrahim, "Synthesis, characterization, and antimicrobial properties of copper nanoparticles", International Journal of Nanomedicine, 2013, vol. 8, pp. 4467-4479.

[4] Marimuthu Nidhin, Ramasamy Indumathy, Kalarical Janardhanan Sreeram, Balachandran Unni Nair, "Synthesis of iron oxide nanoparticles of narrow size distribution on polysaccharide templates" , Bulletin of Materials Science, 2008, vol. 31(1), pp. 93–96.

[5] Muhammad Sani Usman, Nor Azowa Ibrahim, Kamyar Shameli, Norhazlin Zainuddi, Wan Md Wan Yunus, "Copper nanoparticles mediated by chitosan: synthesis and characterization via chemical methods", Molecules, 2012, vol. 17, pp. 14928-14936.(DOI: 10 3390/molecules 171214928)

[6] Kaushik Mallick, Mike J. Witcomb, Mike S. Scurrell, "In Situ synthesis of copper nanoparticles and poly (o-toluidine): a metal-polymer composite material", European Polymer Journal, 2006, vol. 42, pp. 670-675.

[7] Entsar I. Rabea, Mohamed E. T. Badawy, Christian V. Stevens, Guy Smagghe and Walter Steurbaut, "Chitosan as antimicrobial agent: Applications and Mode of Action", Biomacromolecules, 2003, vol. 4 (6), pp. 1457-1465.

[8] Appu Manikandan and Muthukrishnan Sathiyabama, "Green synthesis of copper-chitosan nanoparticles and study of its antibacterial activity", Journal of Nanomedicine & Nanotechnology, 2015, vol. **6**(1), pp. 1-5. (DOI: 10.4172/2157-7439.1000251)

[9] Norashikin Mat Zain, Andrew G. F. Stapley, Gilbert Shama, "Green synthesis of silver and copper nanoparticles using ascorbic acid and chitosan for antimicrobial applications", Carbohydrate Polymers, 2014, vol. 112, pp. 195-202.

[10] Aung Than Htwe, Sandar Tun, Khin Aye May, Kyaw Myo Naing, "Studies on preparation, characterization and application of pH-sensitive biodegradable chitosan-polyvinyl alcohol hydrogel", Jour. Myan. Acad. Arts & Sc., 2013, vol. XI (1), pp. 127-140.

[11] Thi My Dung, Thi Thu Tuyet Le, Eric Fribourg-Blanc, Mau Chien Dang, "The influence of solvents and surfactants on the preparation of copper nanoparticles by a chemical reduction method", Advances in Natural Science: Nanoscience and Nanotechnoloty, 2011, vol. 2, pp. 1-7.

[12] Krithiga N, Jayachitra A. Synthesis of copper nanoparticle by chemical method and analysis, its significant antibacterial activity. International Journal for Research in Applied Sciences and Biotechnology, 2014, vol. 1(1), pp.22-27.

Determination of Ion Occupation Model in Spinel Lettice

Aye Aye Thant[1], Thet Phyu Phyu Naing[2]

Abstract

Ferrite materials have exploited for a number of extensive applications in non-reciprocal devices at microwave frequencies. Ferrite samples with the chemical composition $Ni(Gd_xFe_{1-x})_2O_4$ (x = 0.0125, 0.0250, 0.0375 and 0.0500) were prepared by Conventional Ceramic Method. By introducing a relatively small amount of Gd^{3+} ions instead of Fe^{3+} ions, the crystallization of these dopants in the mother system was investigated. The structural analyses were performed via X-ray diffraction (XRD) and Scanning Electron Microscope (SEM). The partial substitution of Gd^{3+} ions in the place of Fe^{3+} ions was confirmed by the decrease in the lattice parameter with the Gd^{3+} concentration. The formation of small crystallite and grains are responsible for the increase of coercivity with Gd^{3+} ion substitution. The model of ion occupation among the available tetrahedral (A) and octahedral (B) sites of spinel was estimated by the obtained magnetic moment per unit cell and the Bohr magneton of each ion in the lattice according to spin quantization.

Keywords: nickel ferrite, Gd^{3+} ion, conventional, coercivity, ion occupation

1. Introduction

Spinel ferrite in general and magnesium-manganese in particular have extensive applications in construction of non-reciprocal devices at microwave frequencies [1]. Ferrimagnetic cation substituted spinal ferrites are technologically versatile materials [2]. The interesting physical and chemical properties of ferrospinels arise from their ability to distribute the cations among the available tetrahedral (A) and octahedral (B) sites [3]. The addition of trivalent ions in ferrites influences the electric and magnetic properties of the system; density, crystallite size, grain size, residual macrostress and initial permeability [4], [5]. The rare earth oxides are becoming the promising additives for the improvement ferrite properties [6], [7]. In the case of advanced functional materials, doping with small concentration of rare earth is a well-known versatile way to tune the desirable physical properties of ferrites not only because of the lanthanide contraction which induces monotonic change of ionic radii, but also because of the different stable oxidation states and the periodical variation in magnetic moments coming from the sequential filling of electrons in their 4f shells [8]. To date very few literature is available reporting the effect of rare earth atom on the properties of ferrite. In this background, nickel ferrite doped with gadolinium ions was prepared by conventional ceramic technique to provide an accurate understanding of the changes caused by the substitution.

2. Materials and Methods

Specimens of the Gd doped Ni ferrites, Ni $(Gd_xFe_{1-x})_2O_4$, where x = 0.0125, 0.0250, 0.0375 and 0.0500, were grounded in an Agate mortar for 4 h. The mixture was pre-sintered at 1000 ºC for 4 h with heating rate of 20 ºC /min, and cooled to room temperature with the same rate. The mixture was ground with an Agate mortar for 1 h. A few drops of PVA binder were added to the powder and the powder was pressed into pellets by uniaxial hydraulic press at a pressure of 150MPa. The final sintering was performed at 1100 ºC for 10 h with the heating rate

[1] Dr. Professor, Department of Physics, University of Yangon, Myanmar, ayeayethant@uy.edu.mm
[2] Yangon, Myanmar, thetzin18@gmail.com

of 20 ºC/min. The pellets were well polished for further characterizations. The phase formation of the sintered ferrite pellet was checked using XRD. The morphology of the samples was examined by using SEM. The magnetic properties were also measured and the model of ion occupation among the available tetrahedral (A) and octahedral (B) sites of spinel was estimated in this work.

3. Results and Discussion

3.1 Structural Analysis by XRD

After preparing Gd doped Nickel Ferrite, Ni $(Gd_xFe_{1-x})_2$ O_4, by Conventional Ceramic Method, the structural characteristics of these samples were analyzed by XRD method. The XRD patterns of the samples with compositions (x = 0.000 and 0.0125) show the formation of single phase cubic spinel while the samples with (x =0.025, 0.0375 and 0.0500) involved a secondary phase at around 2θ value of 32º in addition to spinal phase as shown in Figure 1. Among the XRD patterns of the samples with gadolinium (Gd) dopants, only the sample with compositions (x = 0.0125) exhibited single phase cubic structure while the samples with (x =0.025, 0.0375 and 0.0500) involved a secondary phase at around 2θ value of 32º in addition to spinal phase.

According to the literature, the secondary phase may be identified as $GdFeO_3$ phase. The initial sample $NiFe_2O_4$ is inverse spinel and Gd^{3+} ions preferentially occupy the B-sites. It was estimated from the present study that the Gd^{3+} ions preferentially occupy the B-sites at Gd concentration x > 0.0125 while small fraction of it also entered into the A-sites.

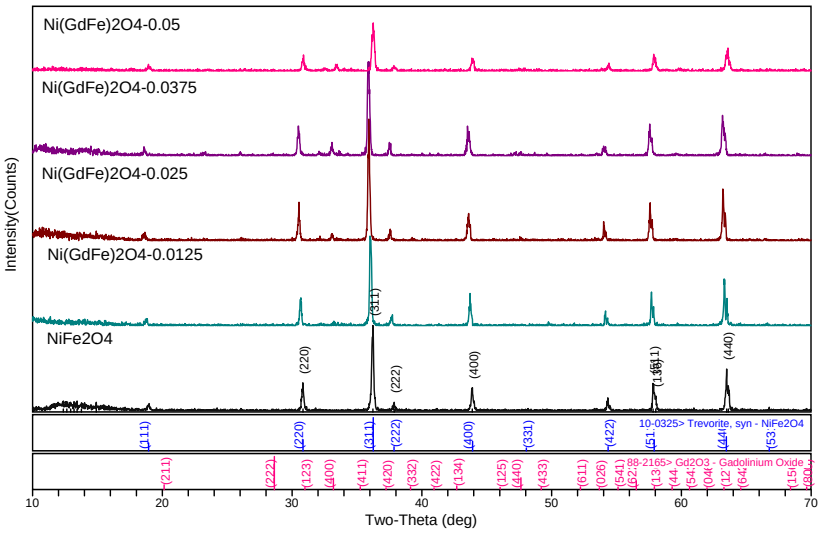

Figure 1. XRD patterns of $Ni(Gd_xFe_{1-x})_2O_4$, where x = 0.0125, 0.0250, 0.0375 and 0.0500.

3.2 Estimation of Lattice Parameter and Crystallite Size

The values of lattice constant were determined from the XRD data and presented in Table 1. The lattice constant slightly increases with increase in Gd-content. The increase of the lattice constants with increasing Gd concentration is strongly related to the relative ionic radius of Fe^{3+} and Gd^{3+} ions. The ionic radius of Fe^{3+} (0.64 Å) is smaller than that of Gd^{3+} (0.94 Å). It shows the increase of the crystalline lattice parameters. If the ionic radius of the impurity ion is larger

than that of the displaced ion, the lattice expends and the lattice constant increases. However, the lattice parameter again decreased with the Gd concentration x=0.0500 which is the largest value in this system. This observation again confirms the partial substitution of Gd ions in the place of Fe ions. The crystallite size was calculated from the XRD peak broadening of the (311) peak using Scherrer formula and presented in Table 1. It is observed that the crystallite size increased with the substitution of small amount of Gd^{3+} ions in $NiFe_2O_4$. However, the size became smaller with the increase in Gd dopants beyond x=0.0250. This may be due to the presence of secondary phase in the samples with larger amount of dopants. Moreover, the broad peaks in XRD patterns are due to fine crystallite size of the ferrite particles. The crystallite sizes of Ni $(Gd_xFe_{1-x})_2\ O_4$ were found to be in the range of 41 to 32 nm.

3.3 Structural Analysis by SEM

SEM investigations was conducted mainly on sample surfaces to obtain information with respect to grain morphology and bonding characteristics. SEM micrographs of Ni $(Gd_xFe_{1-x})_2\ O_4$ samples are shown in Figure 2. As shown in SEM micrographs, the grains are found to be in spherical shape. However, the grains become smaller and the pores between the necks of the grains become bigger with increasing Gd^{3+} ions substitutions. It reveals that the average grain size ranges from 1.07 μm to 1.66 μm for sintering at 1100 ºC.

Table 1**.** Lattice parameter, crystallite size as a function of the concentration of Gadolinium

Gd content (x)	**Ferrite**	**Lattice constant (nm)**	**Crystallite size (nm)**	**Average grain size (μm)**
0.0000	$Ni\,Fe_2O_4$	8.21	33.39	2.783
0.0125	$Ni(Gd_{0.0125}\,Fe_{0.9875})_2O_4$	8.26	32.64	2.466
0.0250	$Ni(Gd_{0.0250}\,Fe_{0.9750})_2O_4$	8.28	40.73	2.425
0.0375	$Ni(Gd_{0.0375}\,Fe_{0.9625})_2O_4$	8.29	33.74	2.183
0. 0500	$Ni(Gd_{0.0500}\,Fe_{0.9500})_2O_4$	8.21	34.37	2.151

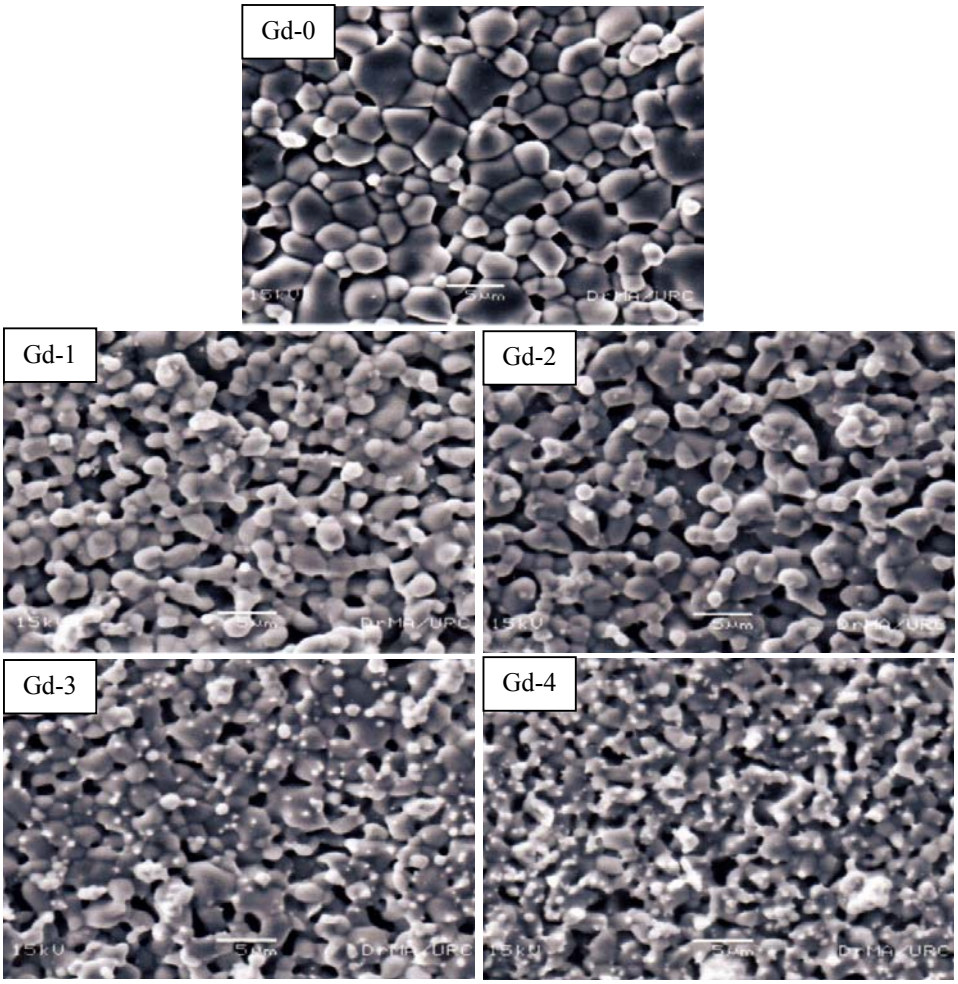

Figure 2. SEM micrographs of $Ni(Gd_xFe_{1-x})_2O_4$, x = 0.0000 (Gd-0), 0.0125 (Gd-1), 0.0250 (Gd-2), 0.0375 (Gd-3) and 0.0500 (Gd-4)

3.4 Analysis on Magnetic Hysteresis Loop

The most interesting characteristics in ferrite are the behavior of mixed ferrites with different non-magnetic ion concentrations. As the values of magnetization can be conveniently varied by suitable substitution, Gd^{3+} ions were substituted for Fe^{3+} ions in $NiFe_2O_4$ and the magnetizations were obtained for different compositions. The hysteresis loops Ni $(Gd_xFe_{1-x})_2$ O_4 are shown in Figure 3. From the hysteresis loops, the coercivity (H_c), saturation magnetization (M_s), magnetic moment (n_B) and remnant flux density (B_r) of the samples were calculated and presented in Table 2.

The increase in Gd^{3+} ion concentration leads saturation magnetization and saturation moment to be decreased. Gd^{3+} ion with ionic radius of 0.94 Å may prefer to occupy B site while Ni ions with ionic radius of 0.78 Å may enter both A site and B site. Since the resultant magnetization is the difference of B site magnetization and A site magnetization, the decrease in saturation magnetic moment pointed out that the magnetization resulted from the simultaneous increase of Gd^{3+} ion and decrease of Fe ions in B site is smaller than that from the decrease of Ni

ions and increase of Fe ions in A site. H_c shows an increase with increasing Gd^{3+} ions substitution. One important effect on H_c is the microstructural behavior. Therefore, the formation of small crystallite and grains are responsible for the increase of coercivity with Gd^{3+} ion substitution.

Table 2. Coercivity (Hc), the residual flux density (Br), saturation magnetization (Ms) and magnetic moment (nB) of $Ni(Gd_xFe_{1-x})_2O_4$

Gd contents (x)	Coercivity, H_c (O_e)	Saturation flux density, B_s (Gauss)	Residual flux density, B_r (Gauss)	Saturation magnetization, M_s (emu/g)	Magnetic moment, n_B (μB)
0.0000	5.90	893.19	803.87	70.64	2.9647
0.0125	9.56	738.45	521.26	58.03	2.4618
0.0250	12.12	617.82	376.06	48.22	2.0267
0.0375	14.20	551.26	413.45	42.75	1.8527
0.0500	14.81	403.50	238.43	30.94	1.3549

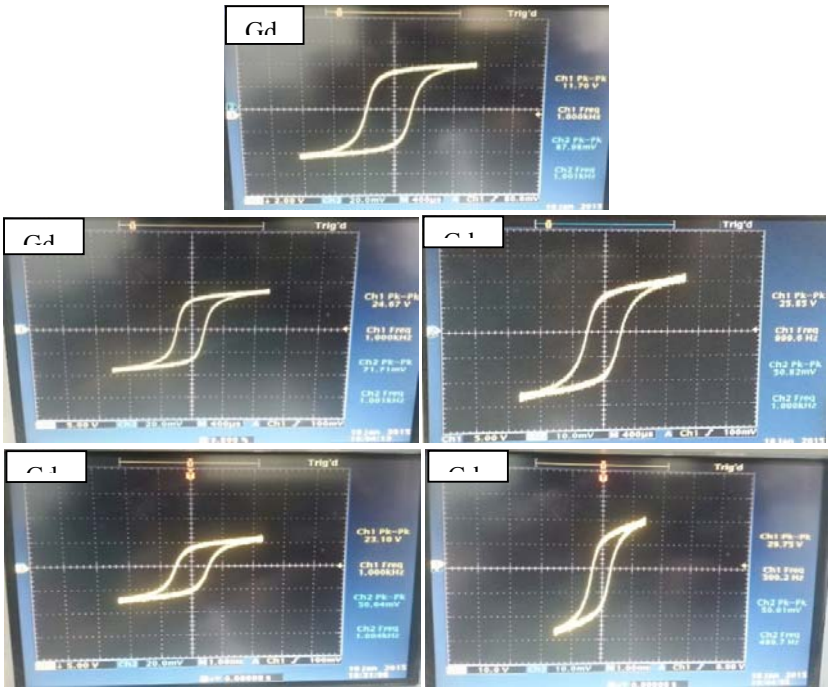

Figure 3. Hysteresis loops of $Ni(Gd_xFe_{1-x})_2O_4$, x = 0.0000 (Gd-0), 0.0125 (Gd-1), 0.0250 (Gd-2), 0.0375 (Gd-3) and 0.0500 (Gd-4)

3.5 Ion Occupation in Ni $(Gd_xFe_{1-x})_2O_4$

It is generally known that the divalent ions are generally larger than the trivalent ions. This is because the larger charge in the trivalent ion produces greater electrostatic attraction and so pulls the outer orbit inward. In the unit cell of the spinel lattice, the radius of octahedral site is apparently larger than that of the tetrahedral site. Particularly, in $NiFe_2O_4$ ferrite, the tetrahedral site has a radius of 0.57 Å and octahedral site has a radius of 0.73 Å. Therefore, it would be reasonable to suggest that the trivalent ions, Fe^{3+} prefer to go into the tetrahedral A-sites while the divalent Ni^{2+} and Gd^{3+} ions into the octahedral B-sites.

The most interesting characteristic in this study is the behavior of cation distribution in the mixed ferrites. Based on the site preference of ions, the crystal structure of spinel and the reported work on the distribution of $NiFe_2O_4$, a model of ion occupation in Gd doped $NiFe_2O_4$, Ni $(Gd_xFe_{1-x})_2O_4$, is proposed in this work.

For $NiFe_2O_4$ spinel lattice,

$$(Ni^{2+}{}_{\delta}\ Fe^{3+}{}_{1-\delta})_{A\text{-site}}\ [Ni^{2+}{}_{1-\delta}\ Fe^{3+}{}_{1+\delta}]_{\ B\text{-site}}O_4$$

where δ = the mole of the Ni^{2+} ions. On the other hand, for the Ni $(Gd_xFe_{1-x)2}\ O_4$ spinel lattice, the model for cation distribution is proposed as:

$$(Ni^{2+}{}_{y+\delta}\ Fe^{3+}{}_{1-x-\delta})_{\ A\text{-site}}\ [Ni^{2+}{}_{1-y-\delta}\ Fe^{3+}{}_{1-x+\delta}Gd^{3+}{}_{2x}]_{\ B\text{-site}}O_4$$

The magnetic moment of a unit cell of Ni $(Gd_xFe_{1-x})_2\ O_4$ferrite was calculated by using the following equation.

$$n_B = [m_{Ni}\,(1\text{-}y\text{-}\delta) + m_{Fe}\,(1\text{-}x +\delta) + m_{Gd}\,2x]_B - [m_{Ni}\,(y+\delta) + m_{Fe}\,(1\text{-}x\text{-}\delta)]_{\ A}$$

The net magnetic moment of Gd^{3+} ion (61 electrons in the electronic shells); m_{Gd} is 7 μ_B, that of Ni^{2+} ion (26 electrons in the electronic shells); m_{Ni} is 2 μ_B and Fe^{3+} ion (23 electrons in the electronic shells); m_{Fe} is 5 μ_B.

This proposal is supported by the resultant magnetization of the Gd doped nickel ferrite samples which has been observed in hysteresis measurement. According to the above estimation, the added Ni^{2+} ions replaced Fe^{3+} ions in A-sites while Gd^{3+} ions replaced Ni^{2+} ions in B sites preferably as simplified in Table 4.

Table 4. Occupation of cations in $Ni(Gd_xFe_{1-x})_2O_4$

Ferrite	A-site	B-site
$NiFe_2O_4$	$Ni^{2+}{}_{0.16}\ Fe^{3+}{}_{0.84}$	$Ni^{2+}{}_{0.84}\ Fe^{3+}{}_{1.16}$
$Ni(Gd_{0.0125}Fe_{0.9875})_2O_4$	$Ni^{2+}{}_{0.71447}\ Fe^{3+}{}_{0.67303}$	$Ni^{2+}{}_{0.28553}$ $Fe^{3+}{}_{1.30197}$ $Gd^{3+}{}_{0.0250}$
$Ni(Gd_{0.0250}Fe_{0.9750})_2O_4$	$Ni^{2+}{}_{0.61279}\ Fe^{3+}{}_{0.76221}$	$Ni^{2+}{}_{0.38721}$ $Fe^{3+}{}_{1.18779}$ $Gd^{3+}{}_{0.0500}$
$Ni(Gd_{0.0375}Fe_{0.96250})_2O_4$	$Ni^{2+}{}_{0.55462}\ Fe^{3+}{}_{0.80788}$	$Ni^{2+}{}_{0.44538}$ $Fe^{3+}{}_{1.11712}$ $Gd^{3+}{}_{0.0750}$
$Ni(Gd_{0.0500}Fe_{0.9500})_2O_4$	$Ni^{2+}{}_{0.44249}\ Fe^{3+}{}_{0.90751}$	$Ni^{2+}{}_{0.55751}$ $Fe^{3+}{}_{0.99249}$ $Gd^{3+}{}_{0.1000}$

4. Conclusion

The Ni $(Gd_xFe_{1-x})_2O_4$ (x= 0.0000, 0.0125, 0.0250, 0.0375, 0.0500) spinel ferrite system was synthesized successfully using Conventional Ceramic method. The XRD analysis confirmed that all Gd^{3+} substituted ferrite was obtained a single spinel phase in the range of x=0.0000-0.0125. The lattice parameter showed an increase with Gd^{3+} substitution until x = 0.0375 and decrease up to x=0.0500, because of the formation of the secondary phase of $GdFeO_3$. However, the particle size decreases with increase of Gd^{3+} content due to hindrance of grain boundary mobility. The saturation magnetization decreased and coercivity H_c increased with increasing Gd^{3+} ions substitution due to the formation of small crystallite and grains with Gd ion substitution. Importantly, a model of ion occupation in Ni $(Gd_xFe_{1-x})_2O_4$ was estimated by the obtained magnetic moment per unit cell and the Bohr magneton of each ion in the lattice according to spin quantization.

Acknowledgements

The authors are grateful to the Department of Physics and Universities' Research Centre, University of Yangon for the supports with research facilities.

References

[1] Anjana Dogra, M. Singh and Ravi Kumar, "50MeV Li^{+3} ion irradiation induced modifications in dielectric properties of Al^{+3} substituted Mg-Mn ferrite", Nucl. Instr. and Meth. B, 2003, vol. 207, pp. 296-300.

[2] S K Sharma, Ravi Kumar, Shalendra Kumar, M Knobel, C T Meneses, V V Siva Kumar, V R Reddy, M Singh and C G Lee, "Role of interparticle interactions on the magnetic behavior of $Mg_{0.95}Mn_{0.05}Fe_2O_4$ ferrite nanoparticles", J. Phys.: Condens. Matter, 2008, vol. 20, pp. 235214.

[3] A. A. Pandit, A. R. Shitre, D. R. Shengule and K. M. Jadhav, "Magnetic and dielectric properties of $Mg_{1+x}Mn_xFe_{2-2x}O_4$ ferrite system" J. Mater. Sci., 2005, vol. 40, pp. 423-428.

[4] Mohd Hashim, SS Meena, RK Kotnala, Sagar E Shirsath, Aashis S Roy, Ameena Parveen, Pramod Bhatt, Shalendra Kumar, RB Jotania, Ravi Kumar, "Study of structural, electrical and magnetic properties of Cr doped Ni–Mg ferrite nanoparticle", Journal of Alloys and Compounds, 2014, vol. 602, pp. 150-156.

[5] M Singh, SP Sud, "Controlling the properties of magnesium–manganese ferrites", Mater. Sci. Engng. B, 2001, vol. 83, pp. 180.

[6] Balwinder Kaur, Monita Bhat, F. Licci, Ravi Kumar, S.D. Kulkarni, P.A. Joy, K.K. Bamzai and P.N. Kotru, "Modifications in magnetic anisotropy of M-type strontium hexaferrite crystals by swift heavy ion, irradiation", J. Magn. Magn. Mater, 2006, vol. 305, pp. 392.

[7] M Hashim, SS Meena, RK Kotnala, SE Shirsath, AS Roy, A Parveen, "Study of structural, electrical and magnetic properties of Cr doped Ni–Mg ferrite nanoparticle", Journal of Alloys and Compounds, 2014, vol. 602, pp. 150-156.

[8] Pardavi-Horvalh M., "Microwave applications of soft ferrites" J. Magn. Magn. Mater., 2000, vol. 171(83), pp. 215-216.

A Study on Structural Properties and Biological Response of HAP/β-TCP

Nay Win Tun[1], Win Kyaw[2], Aye Aye Thant[3]

Abstract

Hydroxyapatite ($Ca_{10}(PO_4)_6(OH)_2$) is used in many biomedical applications including bone graft and joint replacements. Due to its structural and chemical similarities to human bone mineral and teeth, HAP promotes growth of bone tissue directly on its surface. In this research, hydroxyapatite was prepared by precipitation method to provide an accurate understanding of the behavior of biphasic biomaterials with hydroxyapatite (HAP) and beta-tricalcium phosphate (β-TCP). Raw materials of calcium sulphate dihydrate ($CaSO_4.2H_2O$, or Gypsum) and di-ammonium hydrogen phosphate ($(NH_4)_2HPO_4$) solution were used as the starting materials to synthesize high purity hydroxyapatite in the first step. The effect of reaction temperature on conversion efficiencies of gypsum to HAP and reaction kinetics were investigated. After calcination at 1000 ℃, HAP ($Ca_{10}(PO_4)_6(OH)_2$) converted partially into beta-tricalcium phosphate (β-TCP, $Ca_3(PO_4)_2$). Fourier Transform Infrared Spectroscopy (FTIR) analysis clearly revealed the presence of various vibrational modes corresponding to phosphate and hydroxyl groups. Besides porosity were measured at different sintering temperatures, the theoretical density was calculated from X- Rays Diffraction (XRD) results. Finally, the bone bonding ability was evaluated by examining the formation of the new apatite layer on the surface after immersing in Simulated Body Fluid (SBF).

Keywords: calcium sulphate, HAP,βTCP, FTIR, XRD, SBF

1. Introduction

Among all biomaterials, hydroxyapatite; the mineral component of hard tissues in vertebrates, is the most biocompatible material able to be used in clinical applications of conservation and restoration because of its excellent features such as biocompatibility and bioactivity. Hydroxyapatite shows excellent biocompatibility not only with hard tissue but also with soft tissue [1]. This material is capable of integrating biologically when directly implanted into a bone defect; furthermore, it produces no harmful effect on the immune system and features of an osteoconductive behavior. Tricalcium phosphate is also one of the most important biomaterials based on phosphates, currently recognized as ceramic material that significantly simulates the mineralogical structure of bone. β-TCP is found to be resorbable in vivo with new bone growth replacing the implanted β-TCP. Theoretically, resorbable β-TCP is an ideal implant material [2].

2. Materials and Methods

2.1 Experimental Procedure

Laboratory grade gypsum ($CaSO_4.2H_2O$) was used for starting material to synthesize hydroxyapatite (HAP) in the first stage. HAP synthesized from gypsum powder was achieved by precipitation method at 90 ℃. This reaction conversion was achieved according to the reaction below.

$$10CaSO_4.2H_2O + 6(NH_4)_2\,HPO_4 \rightarrow Ca_{10}(PO_4)_6(OH)_2 + 6(NH_4)_2SO_4 + 4H_2SO_4 + 18H_2O$$

1.6 M of gypsum solution was prepared with 11.5 g of gypsum and 40 ml of deionized water. Then the gypsum solution was mixed with 40 ml of 1 M - $(NH_4)_2HPO_4$ solution in conical flask with water bath at the reaction temperature of 90° with magnetic stirring. The reaction time was lasted for 4 hours. At the end of the reaction period, the solid products were washed with DI-

[1] Department of Physics, Dagon University, naywinhtun747@gmail.com
[2] Department of Physics, Pyay University, wkyaw08@gmail.com
[3] Department of Physics, University of Yangon, ayeayethant@uy.edu.mm

water for 5 times and filtered to eliminate any water soluble remains. After washing, the solid residue was put in drying oven operating at 75 ℃ for 24 hours. Again, the dry powder was heat-treated at 500 ℃, 800 ℃, 1000 ℃, 1100 ℃ and 1150 ℃ for 2 hours each in a furnace. The HAP phase was formed at 500 ℃ and 800 ℃ for 2 hours. However, HAP converts into β-tricalcium phosphate (β-TCP) at 1000 ℃ and beyond. After sintering 1200 ℃ of HAP/β-TCP pellet partially converts into biphasic HAP/α-TCP. The α-TCP is brittle and more soluble than HAP and β-TCP. Therefore, this research focuses on biphasic HAP/β-TCP.

3. Results and Discussion

3.1. Formation of Dentures with HAP, HAP/β-TCP and β-TCP

Titanium-Chromium alloy was used as base of the denture. Bricera vacuum porcelain body A-3 from Brident Inc, USA was placed above the base. Then, HAP, HAP/β-TCP and β-TCP powder which were mixed with DI water was placed above the porcelain layer as enamel. The heat-treatment was conducted into the Automatic Programmable Vacuum Porcelain Furnace at 930 ℃ for 15 minutes. The denture obtained by using this method is shown in Figure 1.

Figure 1. The formation of dentures with HAP, HAP/β-TCP and β-TCP at different calcination temperatures.

3.2. Bioactivity Test

The bone-bonding ability of a material is often evaluated by examining the ability of apatite to form on its surface in a Simulated Body Fluid (SBF) with ion concentrations nearly equal to those of human blood plasma. Haemo-A (Aeonmed Co., Ltd) was mixed with Haemo-B (Aeonmed Co., Ltd) in 1:1.2 ratio to form Simulated Body Fluid (SBF). This solution was mixed with DI water in 1:32.8 ratio. Each of this solution (5 ml) was put into 25 ml of three glass beakers. HAP, HAP/β-TCP and β-TCP pellets were put into the SBF solution in each beaker. The beakers were put into an incubator and set the temperature at 37 ℃ for 14 days. Then, the pellets were dried in desiccator for 2 days. These dried pellets were analyzed by SEM. SEM micrographs obtained from pellets before SBF test and after SBF test were compared.

3.3. Analysis on Molecular Vibration by FTIR

The FTIR analysis strongly supports the XRD result in this work. FTIR spectroscopy has been performed in order to investigate the functional groups presented in hydroxyapatite synthesized by precipitation method. The functional groups present in hydroxyapatite clearly revealed the presence of various vibrational modes corresponding to phosphate and hydroxyl groups. Chemical groups with vibration bands are confirmed by the FTIR transmission bands of synthesized HAP and β-TCP.

In HAP and β-TCP, PO_4^{3-} group formed intensive IR absorption bands at 502 cm^{-1} and at 1000 – 1100 cm^{-1}. Adsorbed water band was relatively wide, from 3600 to 2600 cm^{-1} indicating the symmetric stretching and asymmetric stretching vibrations of water. In FTIR spectra of HAP and β-TCP, the characteristic absorption bands at 3435 and 3428 cm^{-1} were attributed to υ_3 mode (asymmetric stretching) of water. The bands at 900-1200 cm^{-1} were the stretching mode of PO_4^{3-} group. The sharp peaks at 608 and 677 cm^{-1} represented the vibrational peaks υ_4 mode of PO_4^{3-}

in both HAP and β-TCP. The characteristic bands due to vibration of PO_4^{3-} group appeared at 595, 604, 606, 608, 615 and 677 cm^{-1}. Five IR bands were detected peaking at 2132, 2133, 2135 and 2137 cm^{-1} for soluble CO_2 (gas) in the ceramic materials. The peaks at 2137 cm^{-1} were formed at the two calcination temperatures at 500 ℃ and 800 ℃. FTIR results are similar to the literature data [3].

Figures 2 shows the FTIR results obtained at different calcination temperatures. All spectra show the characteristic band of adsorbed water, hydroxyl and phosphate species. The peaks in the spectrum and their association to respective chemical groups are summarized in Table 1.

3.4. Porosity Measurement

The values of apparent porosity of HAP, HAP/β-TCP and β-TCP at different sintering temperatures were estimated by the equations using Archimedes' method and are shown in Table 2. In this study, for three different sintering temperatures, the porosity of sintered pellets rapidly increased to the highest percentage, 63.63% when sintered at 1200 ℃ compared to other temperatures.

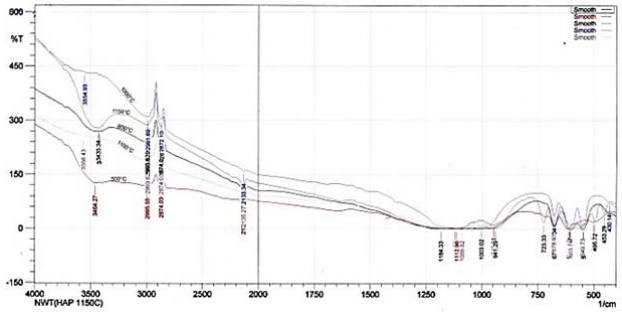

Figure 2. The FTIR spectra of HAP, HAP/ β-TCP and β-TCP prepared at different calcination temperatures of 500 ℃, 800 ℃,1000 ℃, 1100 ℃ and 1150 ℃

Table 1. The FTIR transmission bands of HAP, HAP/ β-TCP and β-TCP at calcination temperatures of 500 ℃, 800 ℃, 1000 ℃, 1100 ℃ and 1150 ℃

Chemical Group	Transmission Band (cm-1)					Vibrational Mode (cm^{-1})
	500 ℃	800 ℃	1000 ℃	1100 ℃	1150 ℃	
PO_4^{3-}	949	941	ND	ND	ND	υ_1 Symmetric Stretching
	502	453 496	430 550	ND	ND	υ_2 Bending
	1113	1003 1184	1090	1090	1119	υ_3 Dipole
	606 677	615 677 723	615 677	595 604 679	595 608 677	υ_4 Polarization

Chemical Group	Transmission Band (cm-1) 500 ℃	800 ℃	1000 ℃	1100 ℃	1150 ℃	Vibrational Mode (cm^{-1})
H-O-H	2874	2870	2872	2874	2874	υ_1 Symmetric Stretching
	2996	2994	2992	2994	2994	
	ND	ND	ND	ND	ND	υ_2 Bending
	3464	3435	3555	3568	3428	υ_3 Asymmetric Stretching
CO_2	2137	2137	2133	2135	2132	

ND= Non Detected

Table 2. The variation of Apparent Porosity and Theoretical Density of HAP, HAP/β-TCP and β-TCP at three different sintering Temperatures

Sintered Temperature (℃)	Dry Weight, D (g)	Soaked Weight, W (g)	Suspended Weight, S (g)	Apparent Porosity (%)	Theoretical Density (g/cm3)
900	1.63	1.78	1.42	41.66	3.38
1100	1.58	1.72	1.45	51.85	3.17
1200	1.23	1.30	1.19	63.63	3.23

3.5. Apatite Formation in Simulated Body Fluid (SBF)

The SEM images for the pellets before and after immersing in SBF are presented in Figures 3 to 5. It is worth to note that the morphology of the pellets immersed in SBF was changed distinctly. As seen in the SEM images the formation of apatite layers on each surface of HAP, HAP/β-TCP and β-TCP pellets was confirmed by the difference in the surface texture of the sample. Importantly, the β-TCP exhibited the faster rate of formation of apatite layer compared to the pure HAP and biphasic HAP/β-TCP. Based on the SEM analysis, β-TCP seemed to have better bioactivity than HAP in this work. The apatite layer formed on the surface of the HAP, HAP/β-TCP and β-TCP can bond to living bone. Therefore, the HAP, HAP/β-TCP and β-TCP prepared in this research have potential biomaterials which can be applied for bone replacement.

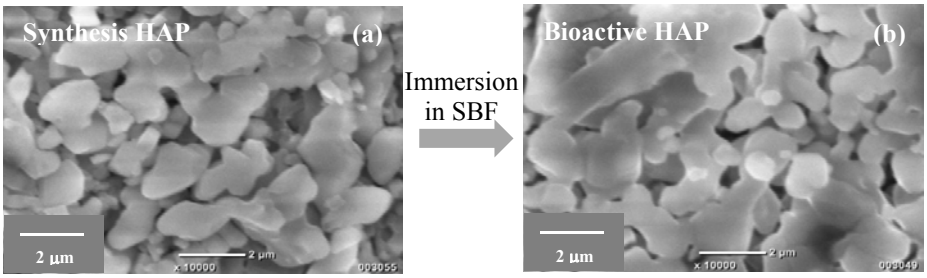

Figure 3. SEM micrographs of HAP pellets at the calcination temperature of 900 ℃ in 10 K × magnification (a) before and (b) after immersion in SBF.

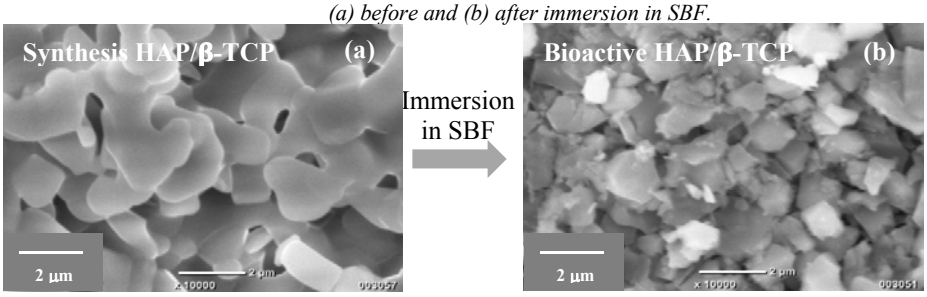

Figure 4. SEM micrographs of HAP/β-TCP pellets at the calcination temperature of 1100 ℃ in 10 K × magnification(a) before and (b) after immersion in SBF.

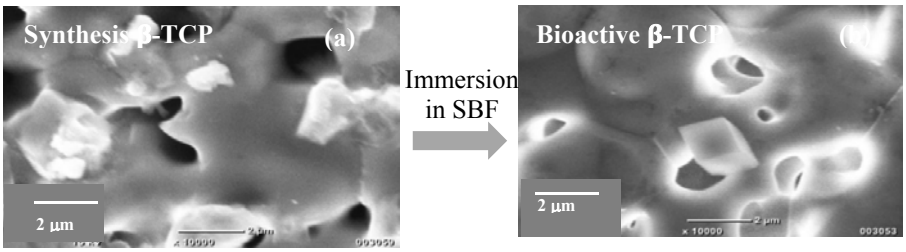

Figure 5. SEM micrographs of β-TCP pellets at the calcination temperature of 1200 □ in 10 K × magnification (a)before and (b) after immersion in SBF

4. Conclusion

Hydroxyapatite, $Ca_{10}(PO_4)_6(OH)_2$ was prepared from gypsum by precipitation method. The raw materials were well characterized prior to the preparation of HAP. A single phase structure of HAP from gypsum was successfully formed via the precipitation method after heat-treated at 500 ℃ and 800 ℃ for 2 hours. It is worth to note that some parts of HAP converted to β-TCP phases after heat-treated at 1000 ℃ for 2 hours. It is interesting to note that transformation to β-TCP started by calcination at 1000 ℃ and the transformation rate increased with increase in temperature. FTIR data clearly revealed the presence of various vibrational modes corresponding to phosphate and hydroxyl groups. The porosity of sintered pellets rapidly increased to the highest percentage, 63.63% when sintered at 1200 ℃ compared to other temperatures. The SBF soaking results revealed that all the studied materials are biologically active which confirmed its application as bone in living things.

Acknowledgements

The authors are grateful to the Department of Physics and Universities' Research Centre, University of Yangon for the supports with research facilities.

References

[1] Angelescu, N., Ungureanu, D.N., Anghelina F.V. "Synthesis and Characteristic of Hydroxyapatite Obtained in Different Experimental Conditions", 2011, Valahia University of Targoviste, Romania.

[2] Bahman Mirhadi, Bahman Mehdikhani , Nayereh Askari, "Sintering effects on the hardness of β-TCP", Journal of Ceramic Processing Research, 2012, vol. 13, No.4.

[3] Maisara S.M. Arsad, Pat M.Lee, Lee Kong Hung, "Synthesis and Characterization of Hydroxyapatite Nanoparticles and β-TCP Particles", 2011, IPCBEE vol.7.

[4] Hitachi High-Tech Science Corporation, "Thermal Analysis of Gypsum", 1985, Tokyo, TA No.22.

[5] Kim, S.R., Lee, J.H., Riu, D.H., Jung, S.J., Lee, Y.J., Chung, S.C., Kim, Y.H., "Synthesis of Si, Mg substituted hydroxyapatite and their sintering behaviors", Biomaterials, 2003, vol. 24, pp. 1389-1398.

[6] Kannan,S., Lemos,I.A.F., Rocha, J.H.G., Ferreira, J.M.F. "Synthesis and characterization of magnesium substituted biphasic mixtures of controlled hydroxyapatite/beta-tricalcium phosphate ratios", 2005, Department of Ceramics and Glass Engineering, University of Aveiro, Portugal.

[7] Onur Rauf Bingöl, Caner Durucan, "Hydrothermal Synthesis of Hydroxyapatite from Calcium Sulfate Hemihydrate", 2011, Department of Metallurgical and Materials Engineering, Middle East Technical University, Ankara, Turkey.

[8] Orlovskii, V.P. et al., "Hydroxyapatite and Hydroxyapatite-Based Ceramics", Inorganic Materials, 2002, vol. 38.

Characterization & Morphological Analysis of Nanostructured Material Images by Image Processing

Khin Khin Win[1], Zin Min Tun[2], Zin Min Myat[3], Thidar Pyone[4] Thazin Khaing[5]

Abstract

This paper aims to analyse and characterize the nanostructured material images obtained from SEM (Scanning Electron Microscopy) technique at the morphological aspect. State-of-the-art techniques for these purposes are complex and complicated given the variability of the different image acquisition modalities, different synthesis parameters and material composition. Image processing is a potential tool to characterize and analyse the properties of nanoscale images in terms of data acquisition, pre-processing, filtering, classification, surface morphology, particle size, porosity measurement which is enable to use in many areas. The morphological analysis of nanoscale images is an important research area in Materials Science to characterize their properties for many applications in the area of materials science and solid state physics. This work has carried out the characterization and morphological analysis of titanium dioxide (TiO_2) nanostructured material images at different temperatures by utilizing the image processing methods. The results show that current approach is capable of characterizing complex morphological characteristics of the subtle nanostructured SEM images. The analysis of nanostructured materials is easy to perform for well-behaved samples which have been described using simple functions of existing MatLab software packages (R2019b). This paper compares and presents the results of previous works. It is found that the present work can be able to perform more efficient and effective methods to analyse and characterize the nanostructured material images. Moreover, this research work is enabling to address the issues and challenges of nanostructured materials image characterization and analysis.

Keywords: SEM (Scanning Electron Microscopy), pre-processing, edge detection, morphology,

1. Introduction

This paper aims to address some problems and state-of-the-art techniques encountered in image processing for material analysis and design. Current methods for this purpose are a complex task given the variability of the different image acquisition modalities, different synthesis parameters and material composition. This paper presents an overview of techniques that have been and are currently developed to address this diversity of problems, such as segmentation, texture analysis, multi scale and directional features extraction, stochastic models and rendering, among others. Finally, it provides references to enter the issues, challenges and opportunities in materials characterization for Nanostructured Material Images.

1.1 Scanning Electron Microscope (SEM)[1]

The Scanning Electron Microscope (SEM) is a tool for visualizing the surface of solid samples, with a resolution (depending on the application) that can approach 1nm. Energy-dispersive X-ray analysis can be used to analyze volumes with dimensions of around 1 micron with a sensitivity of about 0.2wt%, while back-scattered electron imaging allows the

[1] Dr, Professor & Head, Department of Physics, University of Yangon, khinkhinwin@uy.edu.mm
[2] Dr, Assistant Lecturer, Department of Physics, West University of Yangon
[3] Dr. Assistant Lecturer, Department of Physics, University of Yangon
[4] PhD Candidate, Lecturer, Department of Physics, University of Yangon,
[5] PhD Candidate, Assistant Lecturer, Department of Physics, Bamaw University,

visualization of regions of different composition. Crystallographic orientation and structure can be examined using electron backscatter diffraction (EBSD) analysis, though sample preparation requirements for this technique are very stringent and limit the number of samples that can be studied in this way.

In principle, the SEM generates a primary focused electron beam in a vacuum chamber and raster scans the beam over a sample surface. The incident primary electrons interact with the atoms in the surface of the sample. Some of the primary electrons excite the sample to emit secondary electrons while some are being scattered back. A secondary electron detector or a backscattered electron detector collects and converts the secondary electrons or the back scattered electrons into high resolution images.

Secondary electrons are emitted by atoms near the surface of a sample material when their electrons become excited and have sufficient energy to escape the sample surface. Secondary electrons carry information about morphology and surface topography of the sample. The contrast is dominated by the so-called edge effect: more secondary electron can leave the sample at edges for reduced material retardation and adsorption and thus can lead to increased brightness.

A highly sensitive backscatter electron detector captures composition, topography, and shadow images. Elements of higher atomic number will backscatter electrons more strongly than those of lower atomic numbers. Backscatter imaging allows for improved image contrast for compositional images as well as topographical images. Therefore, backscatter detectors are used to detect areas of varying chemical compositions. Backscattered electron imaging of nonconductive, uncoated samples shows composition by contrast; higher atomic number regions are brighter, while lower atomic number regions are darker.

1.2. Nano structured materials images and Features

The possibility of designing, analysing and modelling materials from images (or generally two- or three dimensional modalities) reveals important contributions in this area. As mentioned, the appearance of nano structured materials images changes significantly with imaging processing techniques, the scale of analysis, image qualities and settings, physical properties and sample preparation methods of materials. Understanding these aspects turns out to be crucial for material analysis and modelling. In particular, we face challenges regarding the characterization of the physical assembly process of materials, the formation process of images, of imaging techniques interacting with materials (geometry, transmission, illumination, reflection, scattering). Answering these questions is important to separate the material appearance from its intrinsic morphology and properties. This paper aims to report on issues from image feature extraction to image simulation with the challenges and emerging trends in material analysis and modelling that are likely to pose challenges to image processing, through the diversity of types of materials, acquisition techniques and applications. Most likely traditional such as human vision-based interpretation of materials image can be misleading, as illustrated in Figure 1. Fully taking into account physical properties and laws is at the heart of successful image analysis in material science.

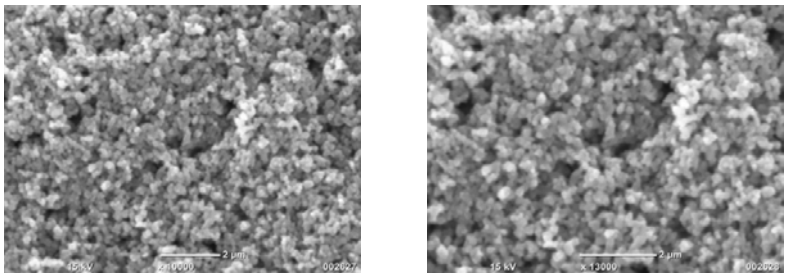

Figure 1 Images at 400℃ *and* 500℃ *temperature treatment*

2. Methods and Outputs

Figures 2 represent a sample of images acquired and problems for material analysis. It illustrates the cracks (black), partially filled pores (rounded dark grey shapes with white spots) and zeolite inclusions (scattered or aggregated white dots) in a neutral substrate. Its characteristics relate to the efficiency of a spherical catalyst used in refining for the conversion of hydrocarbons into chemical products. Such images raise different problems at different scales of observations, from isolated objects to scattered phases, requiring different segmentation tools. Figure 3 results from optical microscopy. The thickness of the crusts may be measured by electron probe microanalysis. It directly correlates with catalyst activity. Resorting to image processing techniques to automate the measurement of crust thickness avoids invasive probe techniques, and hastens the conception of new catalysts. It can use local orientation estimates for 2D and 3D texture segmentation. The goal is to infer bounds on the effective properties of materials by dealing with three-dimensional, computational microstructure simulations. It combines a multiscale approach with homogenization techniques. The same goal is pursued in the nanometric scale that illustrates a mixture of a crystalline and an amorphous material. The periodicity of the first one, and the lack of long-term regularity of the second one, drives the use of local Fourier attributes.

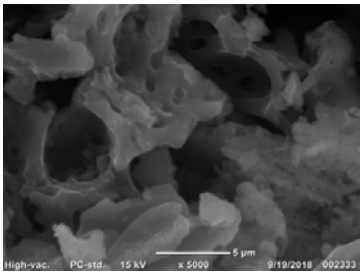

Figure 2 Sample acquired image

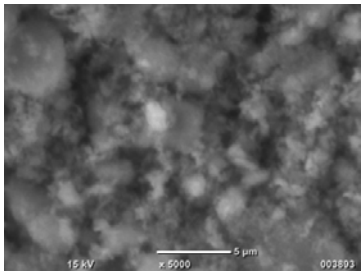

Figure 3 Sample Image from Optical Microscopy

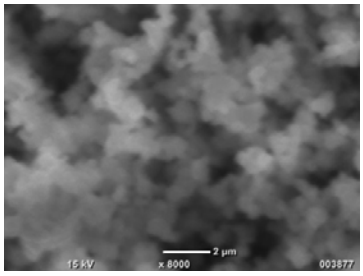

Figure 4 CaTiO3 Image at 1100℃

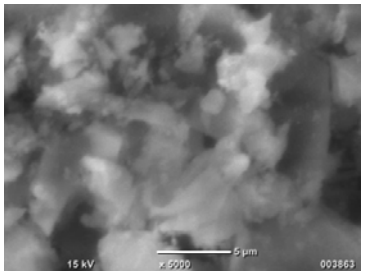

*Figure 5 SiO2 Image at 8*00℃

3. Image processing: issues and challenges

Classical approaches and techniques may define a relatively standard work-flow for image processing in materials science. It includes the following steps: Image acquisition or reconstruction Depending on the resolution of interest, different equipments may be used, for instance optical microscopes (mm-µm), scanning electron microscopes or SEM (µm) and transmission electron microscopes or TEM (nm-˚A) for 2D acquisitions. Turning to 3D acquisitions, one observes a frequent use of X-ray tomography (mm-µm) and electronic tomography (nm) based on TEM projections. Some techniques deal with the reconstruction of surface topography [20].

Enhancement and filtering: This step (Fig. 2, with bilateral filtering) relates to image improvement from a noise level or homogeneity point-of-view. One is primarily interested in noise filtering techniques permitting only minimal modifications in the structures of interest, or drift or background correction. Techniques for artifact corrections, specific to the acquisition process, include for instance ring artifact suppression (X-ray tomography), sample impregnation or encasement in colourless resin (causing effects akin to cast shadows), mechanical or ionic surface polishing.

Segmentation: This step encompassing dimensionality reduction, classification and model fitting, simplifies rich images into a few meaningful intensities or components. It aims at the recovery of the border of the objects of interest. When the colour intensity level is directly related to object properties (topography, like in secondary electron SEM, or chemical structure, like in back-scattered electron SEM), global histogram segmentation methods (inter-class variance maximization, entropy, Expectation-Maximization) are complemented by criterion-based segmentation (object length, surface, tortuosity). This combination permits the elimination of non conform or non interesting elements, sometimes mere residuals of a previous processing sequence. For images whose intensity is less directly related to properties, extraction of local morphology or contours may be performed using global optimization approaches such as geodesic active contours and regions, maximum flows approaches and/or mathematical morphology operations such as top-hat filtering or watershed transformations. Analysis Image structures can be described without an explicit segmentation of the objects of interest using multi scale image representations based on morphological decompositions or wavelet-based multi scale representations. Once simplified, objects of interest may be characterized by numbers, shapes and spatial distribution among others. Stereology, stochastic modelling (spatial moments, such as the covariance, and spatial distributions) and the use of distance functions (inter-object, geodesic length, tortuosity) provide the main sources of algorithms. Multi-modality It involves image regularization and segmentation of multi-modal/multichannel/multi scale images acquired from the same samples. In order to deal with this kind of data, some pre-processing steps such as registration, denoising and image fusion are required. In addition to extract relevant information from complex data sets integrating various acquisition techniques, it is useful to use dimensionally reduction techniques, from classical PCA to modern nonlinear manifold learning.

Microstructure stochastic modelling: This step (with 3D modelling from 2D images) may use input characteristic data either from segmentation or analysis. It consists in estimating a stochastic, geometric model (Boolean random functions, reaction-diffusion or dilution models, dead leaves tessellations), representing the microstructure of the observed material. It serves the purposes of inferring the potential 3D structure from 2D cuts, or of obtaining structure variations

through model parameter modifications, hence of “numerical material by design”. Finally, this step may even replace the segmentation step, when individual objects can not, or need not, be individualized.

Segmentation and analysis are sometimes merged. “Texture approaches” aim at extracting image characteristics without resorting to individual or excessively precise object separation. Morphological metrics are extracted, with the help of 2D/3D models. Machine learning techniques are also emerging, typically to automate supervised/unsupervised classification problems. Meaningful characteristics may be enriched by combining or merging different acquisition techniques. Acquisitions may consider different scales of observation (multiscale fusion approaches), or different modalities (multi-modal fusion approaches), or both. Such techniques, very common in medical or satellite imaging, are increasingly being used in materials design, combining for instance topographic and physico-chemical information (via secondary electron and back-scattered SEM or Energy-Dispersive Spectroscopy). With 3D or 3D+time imaging [9], an important effort is dedicated to processing performance, especially algorithm acceleration. Materials science processing work-flows are increasingly carried out, with reduced cost, with CPU/GPU optimization. For instance, tomographic reconstruction is typically now faster than acquisition. Similar performance increases are being pursued with filtering or segmentation techniques, toward integrated high-throughput materials science and engineering.

4. Conclusions

Among the challenges proposed before, and the ones recently exposed in [9], we retain the attention on the following four:

• multi-step: to produce a complete pipe-line or work-flow of image analyses and simulations, from sample acquisition to the estimation of physical properties;

• data-flow: to manage raw and simulated data and acceleration of the aforementioned work-flows from high throughput screening of materials with ever increasing amounts of numerical information;

• multi-modality (or synergy): to employ as much as possible the potentialities to retrieve information on materials from different acquisition sources, with novel fusion/combination techniques improving characterization or providing access to novel properties;

• reverse engineering: to help in computational material design, by orienting the synthesis or manufacturing process of novel materials, desired or predicted (e.g. graphene).

A successful application of more standard image processing thus requires a better integration of known techniques, as well as the deployment of image analysis not used in materials science yet, with the new challenges raised by its variety of data and physical models.

Acknowledgements

Author would like to thank all concerns from Ministry of Education (MOE), Department of Higher Education (MOE), Myanmar Academy of Arts & Science (MAAS), Science Council of Asia and Japan Science Council (JSC) for their permission, supporting and all round assisting to carry out this paper.

References

[1] R. E. Hummel, “Understanding Materials Science: History, Properties, Applications”, Springer, 2nd edition, 2004.

[2] J. A. Mathews, “The steel age—1876 to 1926,” Ind. Eng. Chem., vol. 18, no. 9, pp. 913–914, 1926.

[3] P. Ball, Madeto Measure: NewMaterialsforthe21stCentury, PrincetonUniversity Press, 1999.

[4] Y. Br´echet, “Materials science: from materials discovered by chance to made-tomeasure materials,” Coll`ege de France, 2013.

[5] J. P. Davim and C. A. Charitidis, Eds., “Nanocomposites: materials, manufacturing, and engineering, Advanced Composites”, Walter De Gruyter, Berlin Boston, 2013.

[6] Y. Liu and X. Zhang, “Met materials: a new frontier of science and technology,” Chem. Soc. Rev., vol. 40, no. 5, pp. 2494, 2011.

[7] J. W. Gibbs, “On the equilibrium of heterogeneous substances”, Trans. Connect. Acad. Arts Sci., vol. III, pp. 108–248 and 343–524, 1875 to 1878.

[8] L.Wojnar, “Image analysis. Applications in materials engineering”, CRCPress,1999.

[9] I. M. Robertson, C. A. Schuh, J. S. Vetrano, N. D. Browning, D. P. Field, D. J. Jensen, M. K. Miller, I. Baker, D. C. Dunand, R. Dunin-Borkowski, B. Kabius, T.Kelly,S.Lozano-Perez,A.Misra,G.S.Rohrer,A.D.Rollett,M.L.Taheri,G.B. Thompson, M. Uchic, X.-L. Wang, and G. Was, “Towards an integrated materials characterization toolbox,” J. Mater. Res., vol. 26, no. 11, pp. 1341–1383, Jun 2011.

[10] D. Salomon and G. Motta, Handbook of Data Compression, Springer, 2009.

[11] B. K. Gunturk and X. Li, Eds., “Image Restoration: Fundamentals and Advances, Digital Imaging and Computer Vision”, CRC Press, 2012.

[12] J. Chanussot, C. Collet, and K. Chehdi, Eds., Multivariate Image Processing, ISTE Ltd and John Wiley & Sons Inc., 2009.

[13] J. Ohser and K. Schladitz, “3D Images of Materials Structures: Processing and Analysis”, Wiley-VCH, 2009.

[14] A.Depeursinge,A.Foncubierta-Rodriguez,D.VanDeVille, and H.M¨uller, “Three dimensional solid texture analysis in biomedical imaging: Review and opportunities,” Med. Image Anal., vol. 18, no. 1, pp. 176–196, 2014.

[15] H. H. Bauschke, R. S. Burachik, P. L. Combettes, V. Elser, D. R. Luke, and H. Wolkowicz, Eds., “Fixed-Point Algorithms for Inverse Problems in Science and Engineering”, Springer, 2011.

[16] M.L. Comer and E.J.Delp, “The EM/MPM algorithm for segmentation of textured images: analysis and further experimental results,” IEEE Trans. Image Process .,vol. 9, no. 10, pp. 1731–1744, 2000.

[17] C. Chaux, A. Jezierska, J.-C. Pesquet, and H. Talbot, “A spatial regularization approach for vector quantization,” J. Math. Imaging Vis., vol. 41, no. 1-2, pp. 23–38, 2011.

[18] C. Park, J. Z. Huang, J. X. Ji, and Y. Ding, “Segmentation, inference and classification of partially overlapping nanoparticles,” IEEE Trans. Patt. Anal. Mach. Int.,vol. 35, no. 3, pp. 669–681, 2013.

[19] M. Petrou and P. G. Sevilla, Image processing: dealing with texture, John Wiley & Sons, Ltd, 2006.

[20] R. Leach, Ed., “Characterisation of Areal Surface Texture”, Springer, 2013.

[21]S. T. Ali, J.-P. Antoine, and J.-P. Gazeau, “Multidimensional Wavelets and Generalizations”, pp. 411–456, Theoretical and Mathematical Physics. Springer-Verlag, Aug. 2014.

[22] S. Torquato,“Random Heterogeneous Materials: Microstructure and Macroscopic Properties”, Springer, 2002.

Formation of Calcium Hydroxide ($Ca(OH)_2$) Nanorods for CO_2 Adsorption

Nwe Ni Hlaing[1], Srimala Sreekantan[2], Hirofumi Hinode[3], Winarto Kurniawan[4],

Aye Aye Thant[5]

Abstract

Carbon dioxide (CO_2) is one of the major contributors to the global warming and climate change. Hence, mitigate towards the emission of CO_2 into an atmosphere, various types of adsorbents were reported. Recent years, nanostructured calcium hydroxide ($Ca(OH)_2$) has been proposed as a potential calcium oxide (CaO) based adsorbent for CO_2 adsorption. In this study, $Ca(OH)_2$ samples were synthesized via simple precipitation method by using cetyltrimethyl ammonium bromide (CTAB) as a surfactant. The effect of CTAB concentration (0.01-0.03 mol) on the structure and morphology of synthetic $Ca(OH)_2$ samples were investigated by X-ray diffraction and field emission scanning electron microscopy (FESEM). From XRD and FESEM results, the formation of $Ca(OH)_2$ nanorods with an average diameter of 80-100 nm was observed at 0.03 mol of CTAB. The CO_2 adsorption capacities of CaO derived from synthetic $Ca(OH)_2$ samples were studied by thermogravimetric analysis (TGA). The TGA results demonstrated that CaO derived from $Ca(OH)_2$ nanorods exhibited CO_2 adsorption capacity of 0.75 g-CO_2/g-adsorbent which was higher than those of CaO derived from irregular and hexagonal shapes $Ca(OH)_2$ samples synthesized at 0.01 and 0.02 mol of CTAB, respectively.

Keywords: calcium hydroxide, nanorods, carbon dioxide, adsorption capacity, XRD, TGA

1. Introduction

Mitigate towards the emission of carbon dioxide (CO_2) from the combustion of fossil fuel burning has been worldwide concerns due to their adverse effect towards the heath of mankind and environment. Carbon dioxide capture, utilization and storage (CCUS) technology is a reasonable technology that prevents the release of large quantities of CO_2 into the atmosphere by capturing CO_2 and transporting it to where it can be useful. The first step of CCUS technology is carbon dioxide capturing process and hence, researches are focused on the investigation of materials and techniques which can capture large amount of CO_2 [1,2].

Among numerous gas separation technologies which have been attempted to capture CO_2 from flue gas, adsorption using solid materials is one the most promising methods due to some advantages of solid adsorbents including low energy requirement, cost advantage, and the ability to use over a wide range of temperatures and pressures. Different solid adsorbents including metal organic frameworks (MOFs), grapheme organic frameworks (GOFs), zeolites, activated carbons, clays, calcium oxide, etc have different capability to adsorb CO_2 and cyclic stabilities. Among various materials, calcium oxide (CaO) based adsorbent is one of the promising material

[1] Department of Physics, Taunggyi University, 06013, Taunggyi, Myanmar, nwenihlaing76@gmail.com
[2] School of Materials and Mineral Resources Engineering, Engineering Campus, Universiti Sains Malaysia, 14300 Nibong Tebal, Penang,
[3] Department of Transdiciplinary Science and Technology, School of Environment and Society, Tokyo Institute of Technology, 2-12-1 Ookayama, Meguro-ku, Tokyo, Japan
[4] Department of Transdiciplinary Science and Technology, School of Environment and Society, Tokyo Institute of Technology, 2-12-1 Ookayama, Meguro-ku, Tokyo, Japan
[5] Department of Physics, University of Yangon, 11041 Kamayut, Yangon, Myanmar

because of the advantages such as high CO_2 adsorption capacity, low material cost and reversible carbonation/calcination cycles [2,3].

Calcium hydroxide ($Ca(OH)_2$) is one of the materials that can be used as CaO-based adsorbent for the capture of CO_2 because of its excellent properties such as high reactivity and fast reactions [4,5]. Some researchers synthesized $Ca(OH)_2$ by various methods including water-in-oil (W/O) microemulsions [6], sonochemical [7], hydrogen plasma-metal reaction [8] and wet chemical method [9]. However, some of these methods require high temperature or complicated equipment [6-8]. Therefore, the development of a simple method with low-temperature is highly desirable for the synthesis of $Ca(OH)_2$.

Recent years, high aspect ratio one dimensional (1D) nanostructures including nanowires, nanorods, and nanotubes have attracted attention owing to their chemical, mechanical, electrical, and optical properties and their promising applications in in different types of applications. Up to now, a variety of synthetic approaches including precipitation, hydrothermal, solvothermal, spray pyrolysis, thermal hydrolysis and sol-gel methods have been developed to synthesize one dimensional nanostructures [10-12].

In this study, $Ca(OH)_2$ nanostructures were synthesized by a simple precipitation method using calcium acetate hydrate as calcium (Ca) source. The formation of $Ca(OH)_2$ nanorods were studied by varying the concentration of cetyltrimethyl ammonium bromide (CTAB). The obtained samples were characterized by X-ray diffraction (XRD) and scanning electron microscopy (SEM). The CO_2 adsorption capacities of the synthetic $Ca(OH)_2$ nanostructures were investigated by thermogravimetric analysis (TGA).

2. Methods

A 0.01 mol of cetyltrimethyl ammonium bromide, CTAB (Merck) was added to the 0.16 mol of sodium hydroxide, NaOH (Aldrich) aqueous solution. This solution was stirred for 30 min. A 0.02 mol of calcium acetate hydrate, $Ca(CH_3COO)_2.H_2O$ (Merck) was dissolved in 100 ml distilled water and then dropped slowly into the previously stirred solution. This mixed solution was heated to 40°C and vigorously stirred for 30 min. White precipitates were formed and subsequently centrifuged and then dried in an oven at 70°C for 24 hours. The same procedures were performed for preparing other samples with different moles of CTAB (0.02-0.03).

The obtained samples were characterized by X-ray diffraction (XRD) with a Bruker AXS D8 Advance X-Ray Diffractometer and field emission scanning electron microscopy (FESEM, Carl Zeiss SUPRA 35 VP). The thermal behaviors and CO_2 adsorption capacities of CaO derived from synthetic $Ca(OH)_2$ samples were studied by a Rigaku thermogravimetry-differential thermal analysis (TG-DTA) apparatus with Thermoplus 2 software. A small amount of $Ca(OH)_2$ sample (~ 6.5 mg) was placed in a platinum crucible and heated from room temperature to 700°C at a heating rate of 10°C/min under 100% N_2 gas flow. After that, carbonation process was performed for 30 min under 100% CO_2 gas flow. The constant gas flow rate for CO_2 and N_2 was 40 ml/min. The CO_2 adsorption capacity was calculated by using the following equation.

$$CO_2 \text{ Adsorption Capacity} = \frac{W_n - W_i}{W_i}$$

where, W_n is the weight of the carbonated sample after carbonation process and W_i is the initial weight of the calcined sample.

3. Results and Discussion

Figure 1(a-c) shows the XRD patterns of the synthetic samples obtained by a simple precipitation method. All the major diffraction peaks could be indexed to the hexagonal structure $Ca(OH)_2$ (calcium hydroxide) phase, according to the standard data (JCPDS No. 78-0135). The peaks at 2θ value of 28°, 34°, 47°, 50°, and 54° were corresponded to the reflection from (100), (011), (012), (110) and (111) planes of $Ca(OH)_2$ phase, respectively. Moreover, minor diffraction peaks belong to the calcite ($CaCO_3$,) phase with rhombohedral structure (JCPDS No. 05-0586) were also observed.

In the XRD pattern of $Ca(OH)_2$ sample prepared with 0.01 mol of CTAB (Figure 1(a)), the high intensity diffraction peak was found at 2θ value of 29° which was corresponded to the reflection from (104) plane of calcite phase. In the XRD patterns of $Ca(OH)_2$ samples prepared with 0.02 mol and 0.03 mol of CTAB, the intensities of the characteristic diffraction peaks of calcite (at 2θ value of 29°) decreased. On the other hand, the intensity of characteristic diffraction peak of $Ca(OH)_2$ phase at 2θ=34° increased. The results showed that the concentration of CTAB influenced the contents of calcite phase in the synthetic $Ca(OH)_2$ samples.

The crystallite sizes of $Ca(OH)_2$ samples were calculated by well-known Scherrer's equation ($D = k\,\lambda/\beta \cos\theta$), where D is crystallite, k is Scherrer's constant (typically between 0.85 and 0.99), λ is the wavelength of the incident X-rays, θ is the angle of diffraction and β is full width at half maximum (FWHM). The calculated crystallite sizes of $Ca(OH)_2$ samples prepared with 0.01 mol, 0.02 mol and 0.03 mol of CTAB were 42.07 nm, 45.54 nm and 56.04 nm, respectively. The results showed that the crystallite size and crystallinity increased with increasing the concentration of CTAB.

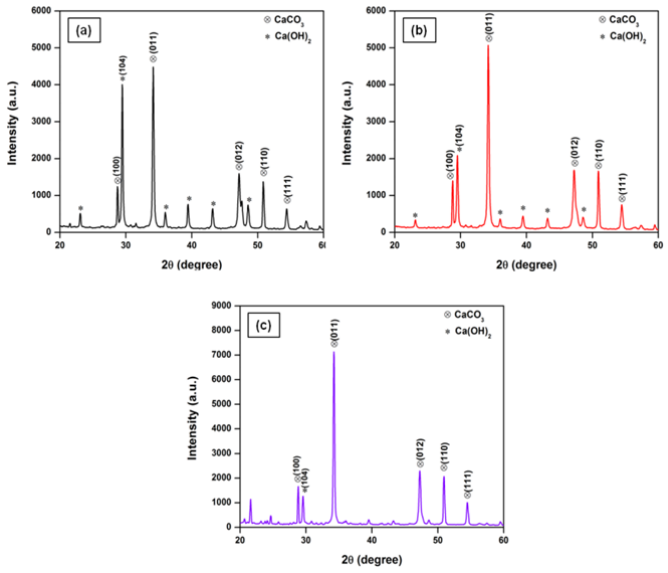

Figure 1. XRD patterns of calcium hydroxide samples synthesized with (a) 0.01 mol, (b) 0.02 mol and (c) 0.03 mol of CTAB

Figure 2(a-c) displays the FESEM images of synthetic $Ca(OH)_2$ samples prepared with 0.01 mol, 0.02 mol and 0.03 mol of CTAB. In the FESEM image of $Ca(OH)_2$ sample prepared with 0.01 mol of CTAB (Figure 2(a)), irregular shaped and irregular sized micro/nano particles were observed. When CTAB was increased to 0.02 mol, micro/nano hexagonal plates with non uniform sizes were seen in Figure 2(b). With 0.03 mol of CTAB, the formation of $Ca(OH)_2$ nanorods with an average diameter of 80-100 nm was observed (Figure 2(c)). FESEM images revealed that the concentration of CTAB played a critical role to control the formation of $Ca(OH)_2$ nanorods.

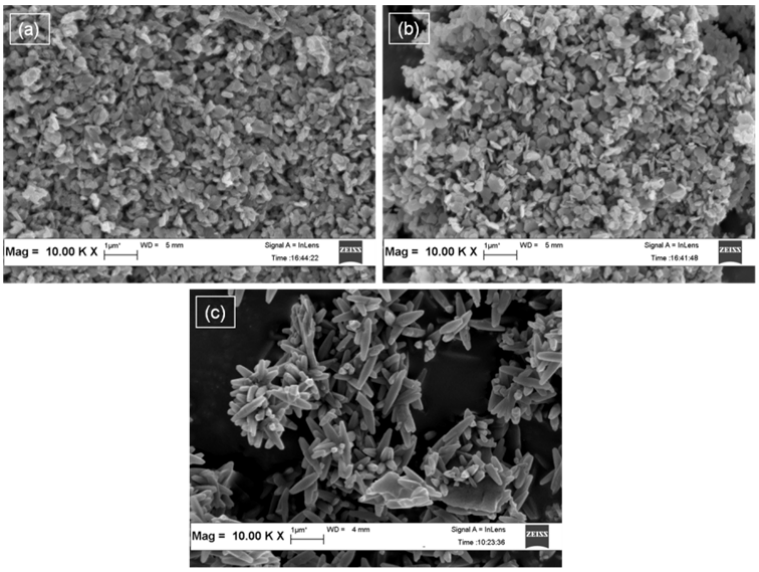

Figure 2. FESEM images of calcium hydroxide samples synthesized with (a) 0.01 mol, (b) 0.02 mol and (c) 0.03 mol of CTAB

TG/DTA analysis was carried out to examine the conversion process of synthetic $Ca(OH)_2$ sample during calcination process. Figure 3(a-b) shows the TG and DTA curves of synthetic $Ca(OH)_2$ sample prepared with 0.03 mol of CTAB. Three weight-loss steps were observed in the TGA curve shown in Figure 3(a). The first step occurring in the temperature range from 50°C to 300°C was attributed to the physical water evaporation of $Ca(OH)_2$ sample. The second step between 360°C and 460°C was ascribed to the chemical dehydration of $Ca(OH)_2$, which are confirmed by the sharp endothermic peak at 430°C in DTA curve (Figure 3(b)). The weight loss of this step was about 20%. The third step between 550°C and 680°C was attributed to the decomposition of $CaCO_3$. The weight loss 6% in this step was consistent with the XRD result shown in Figure 1(c), indicating that calcite was a minor phase.

The synthetic $Ca(OH)_2$ samples were used as calcium oxide (CaO) based adsorbents for carbon dioxide (CO_2) adsorption. The CO_2 adsorption capacities of CaO derived from synthetic $Ca(OH)_2$ samples were determined by TGA. Figure 4(a) shows the TGA profile of two consecutive carbonation/calcination cycles of CaO derived from synthetic $Ca(OH)_2$ sample prepared with 0.03 mol of CTAB in weight percentage. When synthetic $Ca(OH)_2$ sample was heated from room temperature to 700°C under 100% N_2 gas, dehydration of $Ca(OH)_2$ and decomposition of $CaCO_3$ were observed. Then, the temperature was maintained at 700°C for 6 min to ensure complete decomposition of $CaCO_3$ to CaO. After that, the reaction atmosphere was

switched to 100% CO_2, the carbonation reaction of CaO took place to form the carbonated $CaCO_3$. This step was followed by the next calcination reaction whereby the carbonated $CaCO_3$ converted to CaO under 100% N_2 gas.

The CO_2 adsorption capacities of CaO obtained from synthetic $Ca(OH)_2$ samples prepared with 0.01 mol, 0.02 mol and 0.03 mol of CTAB were calculated from the TGA profile. The calculated results are presented in Table 1 and Figure 4(b). As seen in Table 1 and Figure 4(b), CO_2 adsorption capacities of CaO derived from $Ca(OH)_2$ samples increased with increasing of CTAB concentration. In comparison with CaO derived from irregular-shaped and hexagonal-shaped $Ca(OH)_2$ samples prepared with 0.01 mol and 0.02 mol of CTAB, the capacity of CaO derived from one dimensional (1D) nanorods $Ca(OH)_2$ sample prepared with 0.03 mol of CTAB after 1st cycle was higher (0.75 g-CO_2/g-adsorbent), which approached to the theoretical adsorption capacity of CaO (0.78 g-CO_2/g-adsorbent).

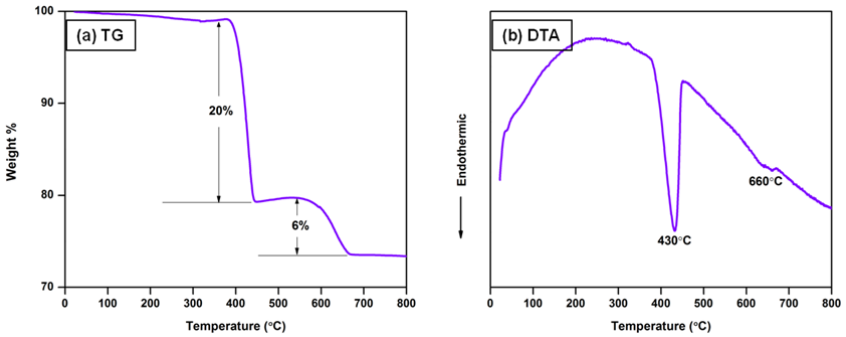

Figure 3. (a) TG and (b) DTA curves of calcium hydroxide sample synthesized with 0.03 mol of CTAB

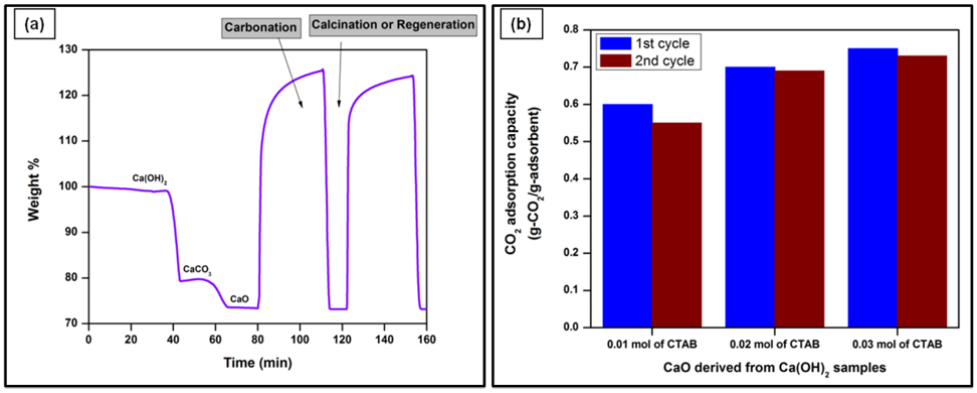

Figure 4. (a) TGA profile $Ca(OH)_2$ sample synthesized with 0.03 mol of CTAB and

(b) CO_2 adsorption capacity of CaO derived from $Ca(OH)_2$ samples

Table 1. CO_2 adsorption capacities of CaO derived from $Ca(OH)_2$ samples

No	Sample	CO_2 adsorption capacity (g-CO_2/g-adsorbent)	
		First cycle	Second cycle
1	CaO derived from $Ca(OH)_2$ sample prepared with 0.01 mol of CTAB	0.60	0.55
2	CaO derived from $Ca(OH)_2$ sample prepared with 0.02 mol of CTAB	0.70	0.69
3	CaO derived from $Ca(OH)_2$ sample prepared with 0.03 mol of CTAB	0.75	0.73

4. Conclusion

In this study, nanostructured calcium hydroxide ($Ca(OH)_2$) samples were synthesized via a simple precipitation method at the temperature 40°C by varying the concentration of cetyltrimethyl ammonium bromide (CTAB). The formation of one dimensional $Ca(OH)_2$ nanorods was investigated. FESEM images exhibited that $Ca(OH)_2$ samples synthesized with 0.01 mol of CTAB resulted in irregular shaped and sized micro/nano particles, with 0.02 mol of CTAB resulted in micro/nano hexagonal plates with non uniform sizes, with 0.03 mol of CTAB resulted in nanorods with an average diameter of 80-100 nm, respectively. Based on FESEM images, it could be concluded that the concentration of CTAB played a critical role to control the formation of $Ca(OH)_2$ nanorods. The TGA results showed that the CO_2 adsorption capacity of CaO derived from synthetic $Ca(OH)_2$ nanorods sample (0.75 g-CO_2/g-adsorbent) was higher than those of CaO derived from irregular and hexagonal shapes $Ca(OH)_2$ samples.

Acknowledgements

The authors thank the AUN/SEED Net Project under the Grant no. 304/6050219 and JICA for financial support and greatly acknowledge to Universiti Sains Malaysia and Tokyo Institute of Technology for facility support. The authors are grateful to Dr Mu Mu Myint, Rector and Dr Win Win Ei, Pro-Rectors, Taunggyi University for their permission to submit this paper. The authors grateful to Dr Khin Khin Htoot, Head of Department of Physics and Professor Dr Nwe Nwe San, Department of Physics, Taunggyi University for encouragement to submit this paper.

References

[1] Luís Quesada Carballo, María del Rosario Perez, David Cantador Fernández, Alvaro Caballero Amores, and José María Fernández Rodríguez , "Optimum particle size of treated calcites for CO_2 capture in a power plant", Materials, 2019, vol.12, pp.1-17.

[2] Muhammad Awais Naeem, Andac Armutlulu, Qasim Imtiaz, Felix Donat, Robin Schäublin, Agnieszka Kierzkowska and Christoph R. Müller, "Optimization of the structural characteristics of CaO and its effective stabilization yield high-capacity CO_2 sorbents", Nature communications, 2018, 9:2408, pp.1-11.

[3] Qiang Wang, Jizhong Luo, Ziyi Zhong and Armando Borgna, "CO_2 capture by solid adsorbents and their applications: current status and new trends", Energy Environ. Sci, 2011, vol.4, pp. 42-55.

[4] Chiung-Fang Liu, Shin-Min Shih, and Tsai-Bang Huang, "Effect of SO_2 on the reaction of calcium hydroxide with CO_2 at low temperatures", Ind. Eng. Chem. Res. 2010, vol.49, pp.9052-9057.

[5] Wu, S.F, T. H. Beum, J. I. Yang, and J. N. Kim, "Properties of Ca-base CO_2 sorbent using $Ca(OH)_2$ as precursor", Ind. Eng. Chem. Res, 2007, vol. 46, pp. 7896-7899.

[6] Nanni, A. and L. Dei, "$Ca(OH)_2$ nanoparticles from W/O microemulsions", Langmuir, 2002, vol.19, pp. 933-938.

[7] Amin Alavi, M. and A. Morsali, "Ultrasonic-assisted synthesis of $Ca(OH)_2$ and CaO nanostructures", Journal of Experimental Nanoscience, 2010, vol. 5, pp. 93-105.

[8] Tong Liu, Yarong Zhu, Xuanzhou Zhang, Tongwen Zhang, Tao Zhang, Xingguo Li, "Synthesis and characterization of calcium hydroxide nanoparticles by hydrogen plasma-metal reaction method", Materials Letters, 2010, vol. 64, pp. 2575-2577.

[9] Rodriguez-Navarro, C, A. Suzuki, and E. Ruiz-Agudo, "Alcohol dispersions of calcium hydroxide nanoparticles for stone conservation", Langmuir, 2013, vol. 29, pp. 11457-11470.

[10] Yanlong Xing and Petra S. Dittrich, "One-dimensional nanostructures: microfluidic-based synthesis, alignment and integration towards functional sensing devices", Sensors, 2018, vol.18:134, pp.1-21.

[11] Maithri Tharmavaram, Deepak Rawtani and Gaurav Pandey, "Fabrication routes for one-dimensional nanostructures via block copolymers", Nano Convergence, 2017, vol. 4:12, pp.1-13.

[12] Rui Chen, Zuoshan Wang, Qingqing Zhou, Juan Lu and Min Zheng, "A template-free microwave synthesis of one-dimensional Cu_2O nanowires with desired photocatalytic property", Materials, 2018, vol.11: 1843, pp.1-11.

The Updated Probabilistic Seismic Models 2018 for Mitigation of Seismic Risks in Myanmar

Myo Thant[1], Maung Thein[2]

Abstract

The seismic hazard assessment of Myanmar was firstly carried out by Gorshkov (1959), and the seismic hazard model was then continuously updated by Mg Thein in 1985 and 2001, and Maung Thein et al. in 2003 and 2005. All of those seismic hazard models based on the previous major events, it means that the models were developed by using deterministic seismic hazard assessment (DSHA) methodology. The seismic hazard maps and information are very important for a country in seismic risk reduction processes. In recent years, all of the scientists accept that only deterministic seismic hazard model is not sufficient for conducting the seismic risk reduction processes, and the seismic hazard models constructed by using probabilistic seismic hazard assessment (PSHA) method. Therefore, the probabilistic seismic hazard maps of Myanmar were developed in 2012 by Myo Thant et al. In developing those maps, the seismic sources are modeled as areal seismic sources for the subduction zone domain of Indian-Australia Plate beneath Burma Plate, in the west of country and the collision zone domain of Indian-Australia Plate and Eurasia Plate, in the north-west. Moreover, the Eastern Highland region is also modeled as the areal seismic sources due to the unavailability of the sufficient fault parameters, even though there are several strike-slip faults in that region (e.g. Moemeik Fault, Nampon Fault, Shweli Fault, Kyaukme Fault, and Nam Ma Fault, etc.). The 2012 seismic sources were remodeled especially the areal seismic sources of subduction and collision zones, and Eastern Highland, and the new probabilistic hazard models are proposed for Myanmar in 2018. In those models, the seismic hazard calculations are for 10% and 2% probability of exceedances in 50 years as the previous one. The resulted seismic hazard maps of Myanmar are peak ground acceleration (PGA) maps, spectral acceleration (SA) maps for the period 0.2 s and 1.0 s, and peak ground velocity (PGV) maps. In this work, we try to understand the seismic risk of Myanmar based on the available demographic and other related information, and the modified seismic hazard models, especially for the major cities as Yangon, Mandalay, Sagaing, Bago, etc. Moreover, we also make the seismic hazard model for 10% probability of exceedance in 50 years simple to understand by public for self-realization of risk condition, and the public can prepare themselves for seismic risk reduction purposes.

Keywords: probabilistic seismic hazard maps, peak ground acceleration, spectral acceleration, peak ground velocity, seismic risk reduction.

1. Introduction

Myanmar is the earthquake disaster prone country since it lies along one of the major earthquake belts of the world, Alpide earthquake belt. With respect to the tectonics of the country, the convergence of Indian-Australia Plate in the south with the Eurasia Plate in north is the major cause of the earthquakes in Myanmar and surrounding regions. The crustal faults present in Myanmar can be assumed due to this tectonic process. One of the major active faults is the right-lateral, strike-slip, Sagaing Fault passing through near or on the major cities of Myanmar such as Naypyitaw, Yangon, Mandalay, Bago, and Sagaing, etc. The others are Kabaw Fault, Mrauk-U Fault, Gwegyo Fault, West Bago Yoma Fault in central and western parts of Myanmar; Lashio

[1] Dr Professor, Department of Geology, University of Yangon, myothant05@gmail.com
[2] Dr Professor, Ret., Department of Geology, University of Yangon

Fault in the Eastern Highland; NW-SE trending Three Pagodas Fault, and Papun Fault in Tanintharyi Region. From the point of view of earthquake experiences, the country has experienced several large earthquakes such as 1839 Ava (Innwa) Earthquake, 1912 Maymyo Earthquake, 1929 Swa Earthquake, 1930 Bago Earthquake, 1930 Phyu Earthquake, 1956 Sagaing Earthquake, 1991 Tagaung Earthquake, etc. Among them th deadliest and the most damaged events are 1930 Bago Earthquake originated from Sagaing Fault, which struck on May 5 with the magnitude of 7.3 M, causing 550 deaths and several buildings were damaged in Bago and Yangon, while the other is 1839 Ava (Innwa) event that caused 400 casualties in Innwa and surrounding areas with several buildings damages especially pagodas, and monasteries. The most recent events are 2011 Tarlay Earthquake, 2012 Thabeikkyin Earthquake, 2016 Chauk Earthquake and 2017 Taikkyi Earthquake.

It can, therefore, be clearly seen that earthquake disaster of Myanmar is quite high, and the earthquake disaster mitigation processes are required to continuously carry out. Among those processes, the seismic hazard assessment is the essential and initial step. Therefore, seismic hazard assessments had been carrying out since eighteen century, e.g. Gorshkov (1959) [1], Mg Thein (1985, 2001) [2, 3], and Maung Thein et al. (2003, 2005)[4,5] based on the deterministic methodology. In 2012, Myo Thant et al. [6] carried out seismic hazard assessment of Myanmar by using the probabilistic seismic hazard assessment (PSHA) approach, then they modified in 2018 again.

2. Probabilistic Seismic Hazard Assessment Methodology and Applied Data

The methodology used in the seismic hazard assessment of Myanmar by Myo Thant et al. (2018) is probabilistic seismic hazard analysis defined by Cornell (1968) [7], and the basic steps are briefly described as four steps (Reiter, 1990; Cramer, 1996) [8, 9]. The earthquake sources identification is the first step of the method, in which the seismic sources are identified as being of uniform earthquake potential throughout the sources that can be range from planar faults to large seismotectonic provinces. The second step is definition of seismicity recurrence characteristics for each seismic source, by earthquake recurrence relationship giving the chance of an earthquake of a given size to happen in the source during a specific period of time, considering all of the upper limits of earthquakes. The simple earthquake recurrence relationship is Log N= a - bM, in which N is the cumulative number of earthquakes of a given magnitude or larger that can be expected to happened during a specified time period; a and b are the constants of earthquake occurrence, M is the earthquake magnitude, normally moment magnitude. Estimation of the earthquake effect is the step, and the attenuation of ground motion expected from the earthquakes in different magnitude range with distance, mostly represented nowadays by means of ground motion prediction equations. The last step is determining the seismic hazard at the site, i.e. the probability that the ground motion parameter (for example: ground acceleration, ground velocity and spectral acceleration) will be exceeded during a specified time period is calculated by considering the uncertainties in spatial and temporal earthquake occurrences, earthquake size, and ground motion prediction, etc.

The data and information applied in the seismic hazard calculation are the combined information of seismic sources model (2012) and the modified 2016 seismic sources model, and the seismicity information (Figure 1). The seismic sources are modeled as areal seismic sources for the subduction zone domain of Indian-Australia Plate beneath Burma Plate, in the west of country and the collision zone domain of Indian-Australia Plate and Eurasia Plate, in the north-

west. Moreover, the Eastern Highland region is also modeled as the areal seismic sources due to the unavailability of the sufficient fault parameters, even though there are several strike-slip faults in that region (e.g. Moemeik Fault, Nampon Fault, Shweli Fault, Kyaukme Fault, and Nam Ma Fault, etc.). The 2012 seismic sources were remodeled especially the areal seismic sources of subduction and collision zones, and Eastern Highland, and the new probabilistic hazard models are proposed for Myanmar in 2018.

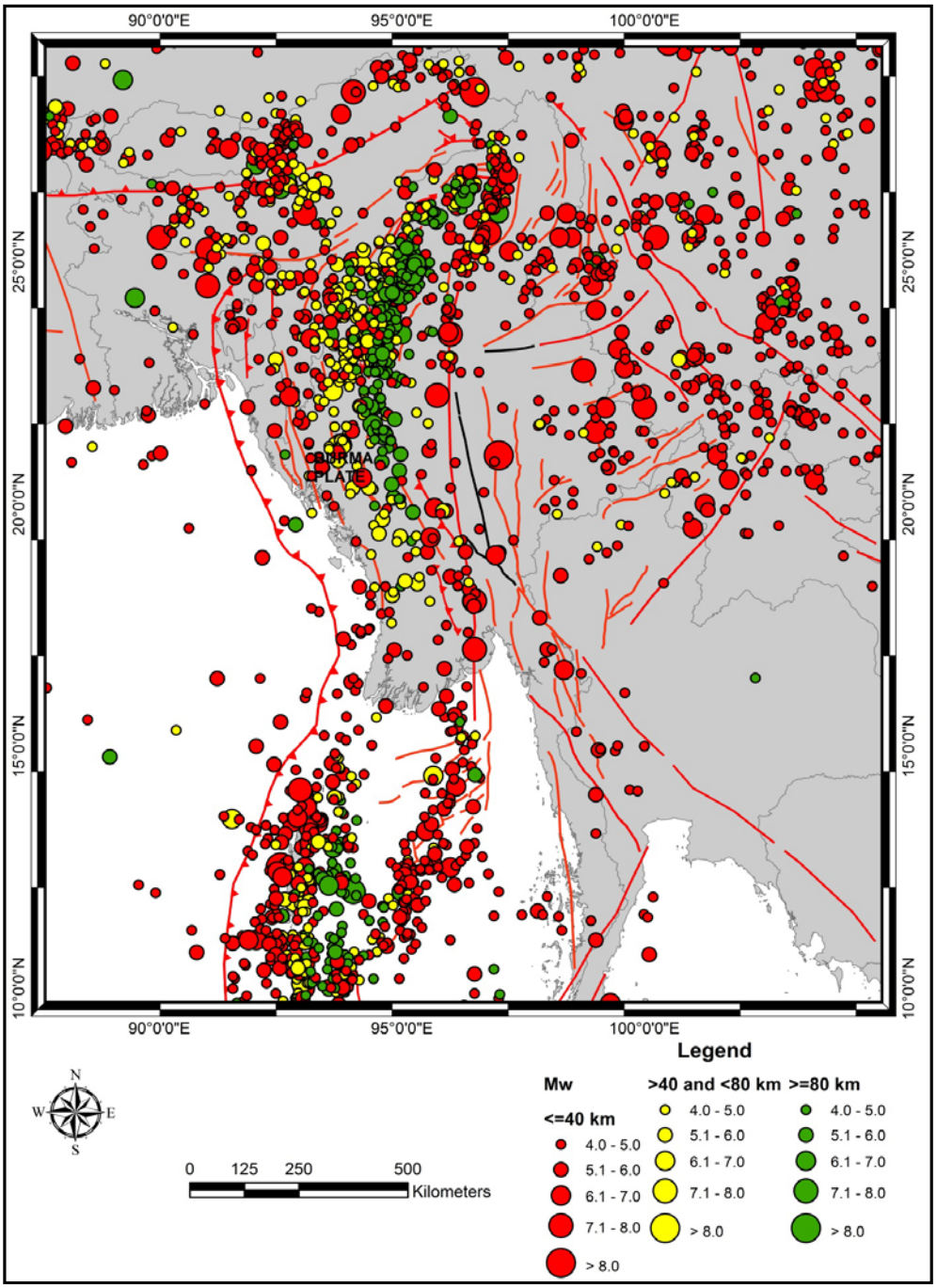

Figure 1. Map presenting the seismicity of Myanmar region (ISC earthquake catalog, 2011) after declustering.

3. Results and Discussion

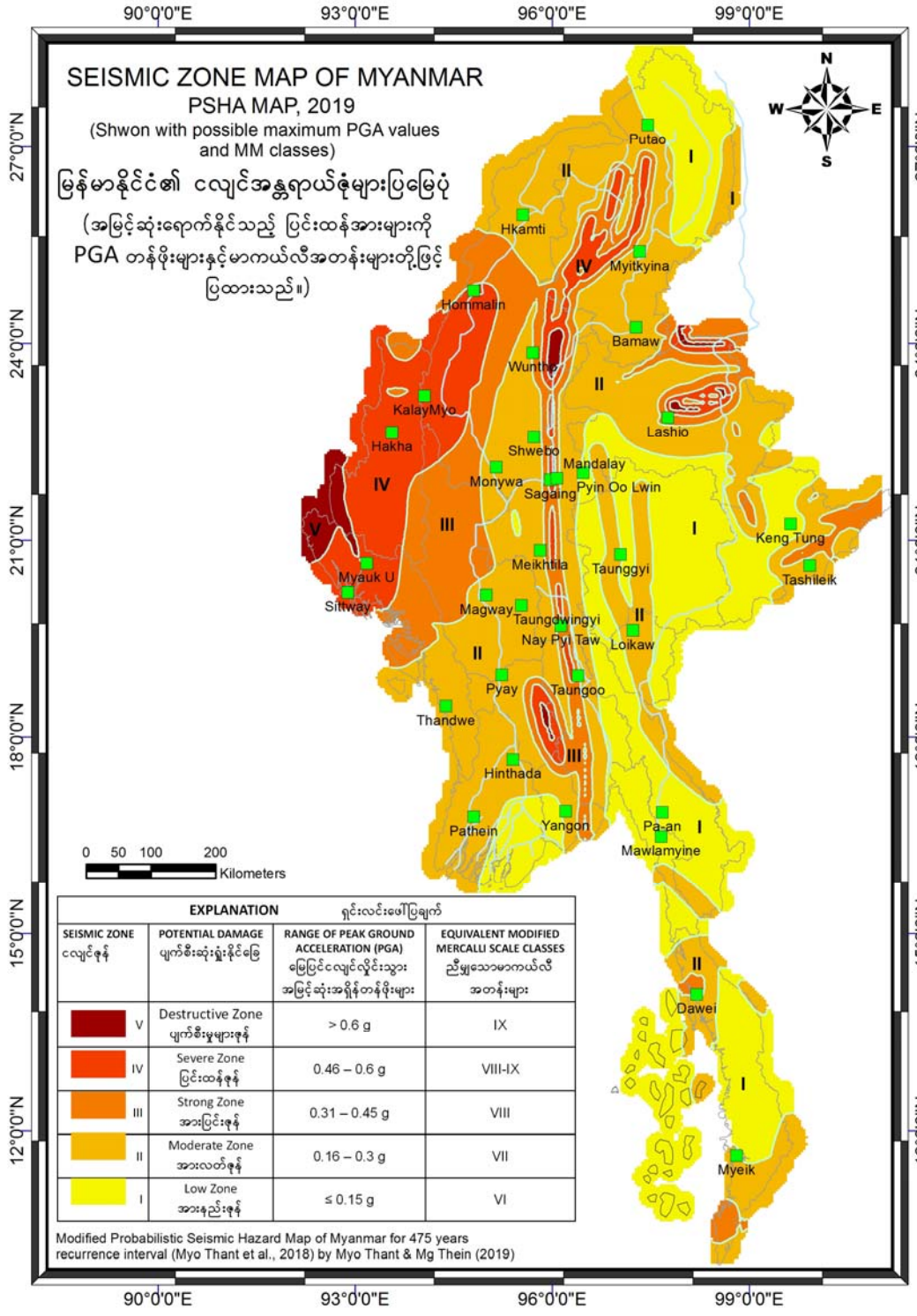

Figure 2. Seismic zone map of Myanmar, modified probabilistic seismic hazard map of Myanmar for 475 years recurrence interval (Myo Thant et al., 2018) by Myo Thant and Mg Thein (2019)

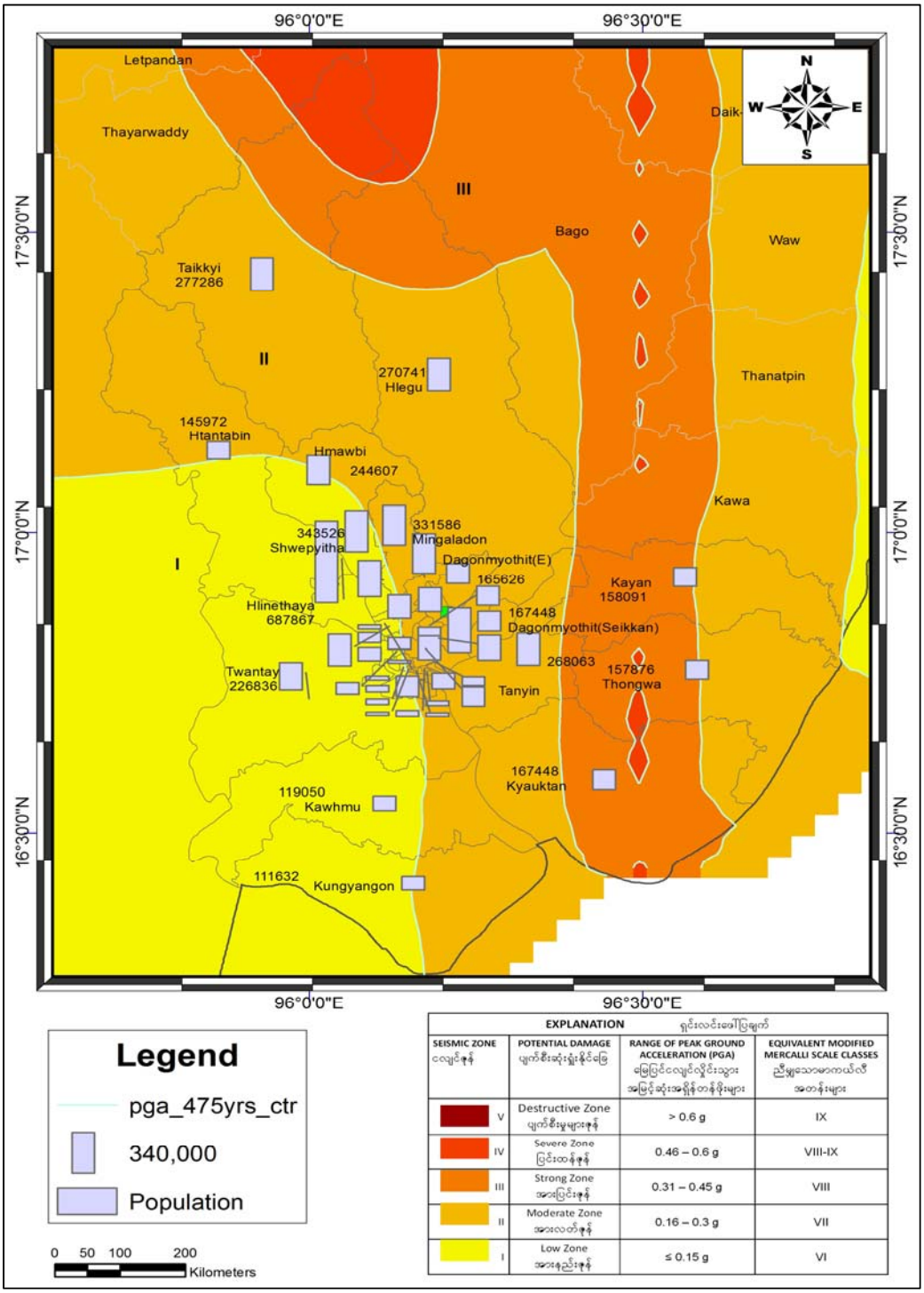

Figure 3. Seismic zone map of Yangon Region, modified probabilistic seismic hazard map of Myanmar for 475 years recurrence interval (Myo Thant et al., 2018) by Myo Thant and Mg Thein (2019)

Myo Thant et al. (2018) [10] constructed the probabilistic hazard maps of Myanmar for 10% and 2% probability of exceedance in 50 years and seismic hazards are illustrated in terms of peak ground acceleration (PGA), peak ground velocity (PGV), and spectral acceleration at the periods of 0.2 s and 1.0 s. In here, we modified the seismic hazard map for 10% probability of exceedance in 50 years (Figure 2) and the seismic hazards are presented by dividing different

zones in terms of peak ground acceleration (PGA), Modified Mercalli (MM) scale and potential damages. Five seismic zones are identified based on the range of PGA in which Seismic Zone I comprises Low Zone of Potential Damage with PGA value of ≤ 0.15 g and MM scale of VI; Seismic Zone II as Moderate Potential Zone with PGA range of 0.16 -0.3 g and MM scale VII, Zone III as Strong Potential Damage Zone with PGA range 0.31 – 0.45 g; Zone IV as Severe Potential Damage Zone with PGA range of 0.46 – 0.6 g and MM scale VIII-IX; and Seismic Zone V as Destructive Zone with PGA range ≥ 0.6 g and MM scale IX (Figure 2). The western part of Myanmar as northern Rakhine, Chin, northern Magway, western Sagaing are located in Seismic Zone III, IV and V. Four major regions/states as Yangon, Bago, Mandalay, Kachin also occur in Zone III, IV and V. Most of the major cities such as Mandalay, Sagaing, Naypyitaw, Bago, Taungoo, and Wuntho correspond to the seismic zones of III and IV while the city Yangon belongs to seismic zone of II. However, it should be noted that this seismic zone map is probabilistic seismic hazard map of 10% probability of exceedance in 50 years (475 years recurrence interval) and the site condition is considered as the bedrock. If the reference seismic hazard is for 2% probability of exceedance in 50 years (2475 years recurrence interval) and the site conditions are considered based on the soil properties, the hazard values will be higher than the present one and the hazard distributed areas will also be wider.

With regards to Yagon Region, The central and eastern part of the region belongs to the seismic zones of Zone II to III and some are of Seismic Zone IV such as Thongwa and Kyaukktan, Tanyin, Taikkyi and Hlegu Townships. Based on the population of Yangon City, Most of the high populated townships, e.g. Dagonmyothit (S), Myaukokkalar, Mingaladon, Thakeda, Thingankyun, Dagonmyothit (N), Dagonmyothit (Seikkan), Dagonmyothit (E) Tamwe, Taungokkalar, comprise of Seismic Zone II. As mentioned previously, This also bases on the seismic hazard information of 10% probability of exceedance in 50 years and bedrock condition, if the hazard information based on 2% probability of exceedance in 50 years and the detailed soil condition, the seismic hazard will be higher and the area of distribution will be wider.

The seismic hazard assessment plays an important role for earthquake disaster mitigation processes that will include application in seismic resistance design calculation (for engineering purposes, the seismic zone factor will be included in National Building Code), land-use plan, seismic risk assessment, and other mitigation purposes. Moreover, the public must understand the seismic risk condition of their buildings and areas, the development of seismic zone map by translation the estimated seismic hazard is therefore very important, especially for the public. Based on these information, they can carry out earthquake disaster preparing processes and the concerned ministries, departments and organizations can also use for various purposes.

References

[1] Gorshkov, G. P. "Problems of Seismotectonics and Seismicity – Zoning of the Territory of the Union of Burma". (Mineographed Manuscript), 1959.

[2] Maung Thein. "Mitigation of Earthquake Hazards in Myanmar (in Myanmar Language)", Working People Daily, 18 Nov., 1985.

[3] Maung Thein. "Mitigation of Earthquake Hazard in Myanmar (in Myanmar Language)", Jour. Myan. Acad. Tech., Vol. 1., No. 2, P. 124 – 134.

[4] Maung Thein, Tint Lwin Swe and Tin Htay Mu. "Seismic Zone Map of Myanmar", With an Explanatory Note (9 pg.), 2003.

[5] Maung Thein and Tint Lwin Swe. "The Seismic Zone Map of Myanmar", Myanmar Earthquake Committee, Myanmar Engineer Society, 2005.

[6] Myo Thant, Nwai Le' Ngal, Soe Thura Tun, Maung Thein, Win Swe, Than Myint**.** "Seismic Hazard Assessment For Myanmar**",** Report to Myanmar Earthquake Committee and Myanmar Geoscience Socity, P58., 2012.

[7] Cornell, C. A. "Engineering Seismic Risk Analysis", Bulletin of the Seismological Society of America, Vol. 58, 1583-1606, 1968.

[8] Reiter, L., "Earthquake Hazard Analysis- Issues and Insights", Columbia University Press, New York, 254pp., 1990.

[9] Kramer, S. L. "Geotechnical Earthquake Engineering", Prentice-Hall International Series in Civil Engineering and Engineering Mechanics, 653 pp., 1996.

[10] Myo Thant, Saw Ngwe Khaing, Soe Min, Lin Thu Aung, Thura Aung, Soe Thura Tun, Hiroshi Kawase, Chung-Han Chang, Yu Wang, "Updated Probabilistic Seismic Models of Myanmar", Report of Myanmar Earthquake Committee, 2018.

Seismic Microzonation at Taungthaman area, Mandalay Region

Pyi Soe Thein[1], Tint Tint Khaing[2] , Junji Kiyono[3], Tun Tun Win [4], Htay Win[5]

Abstract

Taunthaman area is located very closed to the most active dextral Sagaing Fault in Myanmar. In the historical record, several earthquakes happened in and around Mandalay, Amarapura, Innwa, Sagaing region from the beginning of the year of 1400. Even a moderately strong earthquake may cause great loss of lives and property damage. The study area is partly built on alluvial sediments which can amplify seismic ground motion. There is a need to prepare a comprehensive seismic microzonation in near future to support seismic hazard assessment. We conducted 7-sites PQWT-TC series geophysical survey to estimate the shaking intensity distribution during the earthquake. We also conducted 7-site bore holes investigation to gain a representative determination of the soil condition of subsurface structures in Taung Tha Man area. These parameters are required for seismic resistant design of structures. The adopted methodology comprises of three parts:

(i) soil modeling and estimation of depth to Engineering Bed Layer (ii) estimation of the ground motion at Engineering Bed Layer (iii) estimation of ground motion at the surface by 1D ground response analysis using Multiple Reflection Analysis (MRA) program. The soil models are prepared from geophysical survey data and shear wave velocity/ N-values. The results enabled us to estimate the site-dependent shaking characteristics of earthquake ground motion.

Keywords: Alluvial sediments, Sagaing Fault, geophysical survey, earthquake ground motion

1. Introduction

In Myanmar, earthquakes are mainly caused by the tectonic movements related to the subduction of the Indian plate beneath the Burma plate along the Andaman Islands and Rakhine-China-Naga Ranges. The Indian Plate collides with Eurasia Plate at the rate of 50 mm/yr [1], while the rate of subduction of Indian plate under Burma plate is about 36 mm/yr and the Benioff zone dips in varying degree in each segment of the subduction system. Another major active geological structure that generates the major earthquakes in Myanmar is Sagaing Fault. Others are Kyaukkyan Fault, Papun Fault, Kabaw Fault, Gwegyo Fault and West Bago Yoma Fault. Taungthaman area, Mandalay region is the famous cultural center of Myanmar and the population is about thirty thousand. There are also greater population, higher urbanization, more industrialization and many infrastructures. Actually, the study area is located very closed to the most active dextral Sagaing fault in Myanmar. An active Sagaing Fault is a fault that may have displacement within a future period of concern to humans. Identification of active Sagaing Fault requires recognizing previous displacement and constraining the age of displacement [2], [3] and [4]. An active fault is usually identified by associating it with tectonically deformed Quaternary- age materials or surface. In the historical record, several earthquakes happened in and around Mandalay, Amarapura, Innwa, Sagaing region from the beginning of the year of 1400. Even a moderately strong earthquake may cause

[1] Lecturer, Department of Geology, Yadanabon University, pyisoethein@yahoo.com
[2] M.Sc student, Department of Geology, Yadanabon University, tinttintkhaing.geol@gmail.com
[3] Graduate School of Global Environmental Studies, Kyoto University, Japan, kiyono.junji.5x@kyoto.u.ac.jp
[4] Lecturer, Department of Geology, Mandalay University, geolttw73@gmail.com
[5] Professor and Head, Department of Geology, Yadanabon University, htaywin.geol.61@gmail.com

great loss of lives and property damage. Seismic microzonation studies are generally considered as a prerequisite for the site specific risk analysis to mitigate earthquake losses or damages. The first relevant applications appeared in Myanmar at recent years [5].

In this research, the development of a high resolution near-surface Mandalay region Vs^{30} model is presented, including descriptions of the processing steps applied to the adopted SPT dataset and PQWT-TC500 geophysical data, the consideration made for the seismic microzonation mapping of the selected spatial interpolation schemes. The seismic microzonation maps are developed by using the multiple reflection analysis and empirical stochastic green function.

2. Geophysical Survey and Data Analysis

Geophysical lines are generally arranged perpendicular to the line to be constructed, can detect tectonic crushed zone on both sides of the border and its different physical characteristics, contrast is strong, crushing width, extending distinctive characteristics. There are seven sites from PQWT-TC500 geophysical instrument throughout the taungthaman area to evaluate the geotechnical properties of subsurface layers (Figure 1). The collected data each time is the data of the midpoint between two electrode data, Electrode spacing is generally 5-10 m, dot spacing is generally about 0.5-2m, electrode spacing and dot spacing must keep the same distance for one measuring line (Figure 2). The measurement and result PQWT-TC500 geophysical cross-section of the site no.1 is reported in Figure 3 and 4.

Figure 1. SRTM Satellite image with Geophysical survey Sites.

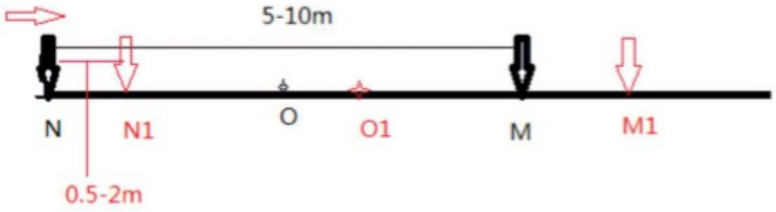

Figure 2. Sketch map of wiring method N、M are electrodes, O is Measuring point, NM=10m, dot spacing is generally about 0.5-2m (standardis1m)

Figure 3. PQWT-TC500 Geophysical measurement at site No 1, Yadanabon University [96°4'18.897" E & 21°53'31.516" N].

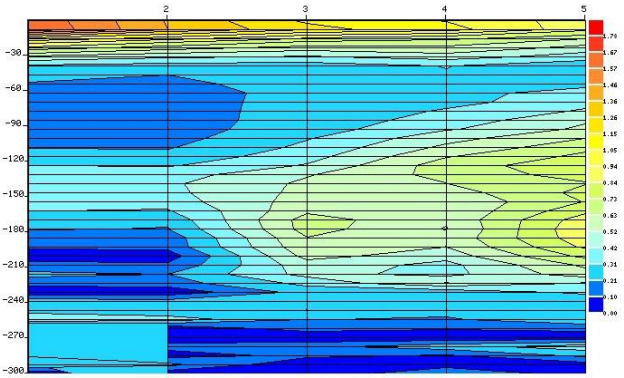

Figure 3. The result PQWT-TC500 geophysical cross-section of the site no.1

Seven borehole data were collected to evaluate the subsurface profiles and related geotechnical parameters for seismic microzonation analyses. The detailed drilling program had been carried out for subsurface investigation in taungthaman area. The SPT dataset is used to develop surfaces describing the distribution of time-averaged shear wave velocity, Vs^{30}, across the urban area in Mandalay region. Target profile depths of 5, 10, 20, 30 m were considered to allow for an assessment of the distributions of soil stiffness with depth across the region. Vs^{30} values are computed for each target depth, as Eq. (1) [6] and [7]. The evaluated subsurface profiles for each area in Mandalay region are shown in the following Figure 4.

$Vs^{30}=$ $$\frac{\sum d_i}{\sum t_i} = \frac{\sum d_i}{\sum(\frac{d_i}{vs_i})} \quad (1)$$

where v_si is shear wave velocity, d_i thickness of i layer and t_i one way travel time in i^{th} layer.

Figure 4. Example of Vs profile at Taungthaman area (SPT 1 dataset).

The MRA (Multiple Reflection Analysis) was used to calculate the transfer function, which expresses the relation between the period and the corresponding magnification factor. Calculation of predominant period by using boring data and the ground model profile is done according to the MRA. The governing equation is

$$\rho \frac{\delta^2 \mu}{\delta t^2} (2); \frac{\delta^2 \mu}{\delta z^2} + \eta \frac{\delta^3 \mu}{\delta z^2 \delta t}$$

in which μ is the displacement of horizontal S-wave (SH), Z the direction of wave propagation (up-down), *t* the time, ρ the density, *G* the shear modulus and η the coefficient of visco-elasticity. The soil damping is considered by giving the complex value to the shear modulus and solving Eq. (2). The damping constant is 5% of critical damping for each layer [8].

3. Peak Ground Acceleration

Seismic hazard models are being updated by modifying some of the seismic sources in Myanmar. In this research, the input motions were selected based on the Probabilistic PGA (Peak Ground Acceleration) (g) Map of Myanmar for 10% probability of exceedance in 50 years, for engineering bedrock condition [9]. The ground response analyses were conducted by using the assumption of vertical propagation of shear waves from the engineering bedrock to the ground surface. The seismic ground motion at EBL is estimated using Empirical

Stochastic Green Function. The surface ground motion is estimated by passing ground motion simulated at EBL through prepared soil models of each site using Multiple reflection program. The peak horizontal ground acceleration of these seismic events ranged from 0.35 g to 0.55 g. Distribution of the estimated peak ground accelerations are shown in Figure 5. The component of the shaking is NS, EW. This is the first trial to estimate the shaking and the damage under the condition of the occurrence of a future Amarapura earthquake.

Table 1. Results of Geophysical data.

Location Site	**PGA (g)**	**Ground Water**	**$Vs30$ (m/s)**
Yadanabon University	0.45-0.35	> 74	250

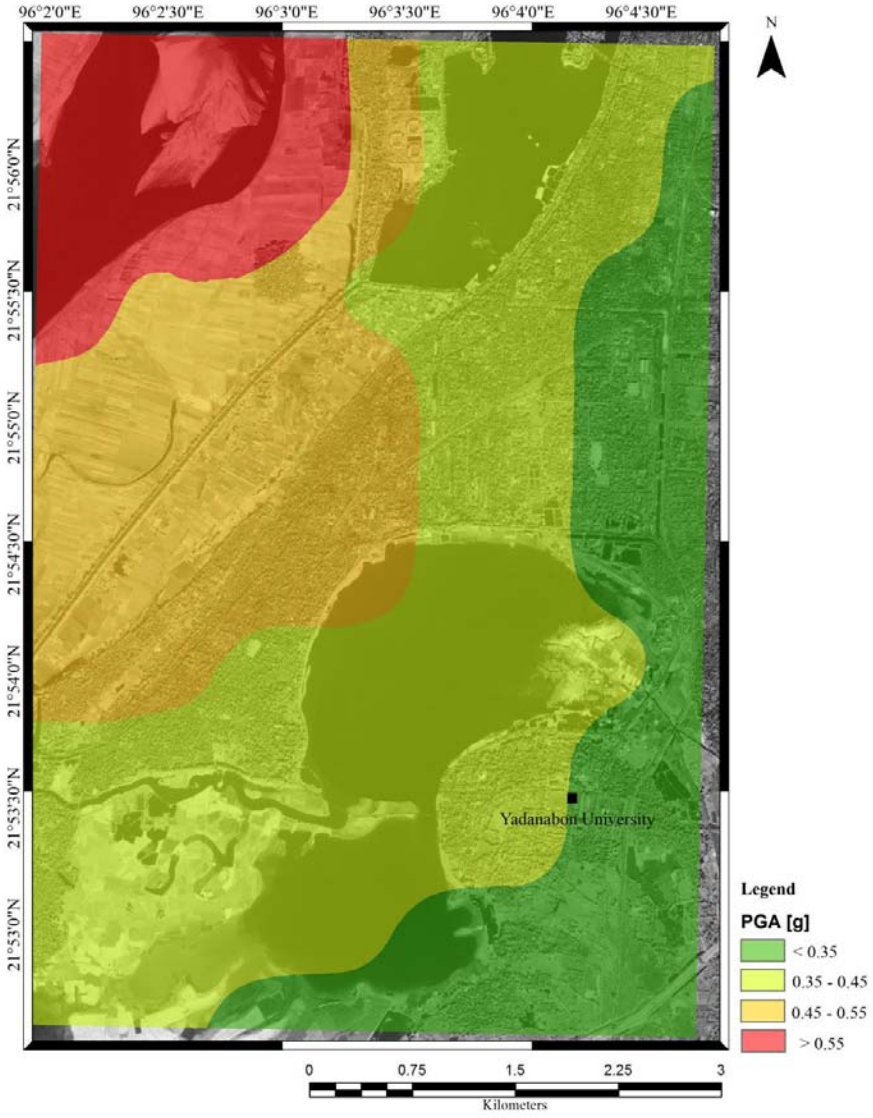

Figure 5. Estimated (PGA) map of Taungthaman area, Amarapura township, Mandalay region.

4. Conclusions

Seven sites of Standard Peneration Test (SPT) and PQWT-TC500 series ground water detection were carried out for constructing a subsurface ground model in Taungthaman area. The Kriging method can be used for the interpolation of subsurface information such as shear wave velocity and depth of irregular boundary. The shear wave velocity of the top layer is Vs ≤ 250 m/s. By combining above two-layer model and the results of geophysical observation, the author proposed the distribution of the first layer thickness of the sediment. Seismic microzonation of the Taungthaman area had predicted based on the multiple reflection analysis by using the proposed ground model. The outputs of this research would be very applicable for both engineering purpose and to identify and mitigate the seismic risk for Mandalay region, Myanmar. There are high acceleration areas appears along the dextral Sagaing Fault, especially near the epicenter. Peak acceleration becomes more than 0.45 g in some areas, which causes severe damage for buildings in high probability (Table 1).

Acknowledgements

This study was supported by the Yadanabon University, Ministry of Education. The acknowledgement is extended to Rector Dr. Maung Maung Naing, Pro-rector of Dr. Si Si Khin and Dr. Tint Moe Thu Zar, Yadanabon University for their kind permission for the submission of this research paper. We would also like to thank the Foundation Soil Investigation Group (FIG) Company for providing geotechnical and geophysical data of the Taung Tha Man area. Managing director Mr Kyaw Khant (Robust Trust Company) provided well points and geophysical data of the study area and his deserve special acknowledgement.

References

[1] GIAC, TOTAL, UNOCAL, MOGE, EcoleNormaleSuperieure, Yangon, Dagon, Mandalay, Chaing Mai and Chulalonkom Universities), "The tectonics of Myanmar", Final Report of GIAC Project 1996-1999, 2002

[2] Win Swe, "Rift-features at the Sagaing-Tagaung Ridge". Abstract, Burma Research Congr., Rangoon, 101. 1970

[3] Hla Maung, "Transcurrent movements in the Burma-Andaman Sea region". Geology 15, 911 912, 1987

[4] Myint Thein, Kyaw Tint and Aye, Ko Aung, "On the lateral displacement of the Sagaing fault" 1991, Georeports 1, 23–34.

[5] Maung Thein and Tint Lwin Swe, "Explanatory Account for Seismic Zone Map of Myanmar (Revised Version, 2005) February (Prepared under the auspices of Myanmar Earthquake Committee)", 2006, 4 p.

[6] Pyi Soe Thein, Junji Kiyono, Tun Tun Win, Than Than Nuand Day Wa Aung, "Seismic Microzonation of Mandalay City, Myanmar". Journal of Geological Resources and Engineering, David Puiblishing, 2015.

[7] Ohta, Y. and Goto, N,"Estimation of s-wave velocity in terms of characteristic indices of soil", Butsuri-Tanko, 29(4), 1976. 34-41

[8] Kiyono, J. and Suzuki, M, "Conditional Simulation of Stochastic Waves by Using Kalman Filter and Kriging

Techniques", Proc. of the 11th World Conference on Earthquake Engineering, Acapulco, Mexico, 1996. Paper No.1620.

[9] Myo Thant, Nwai Le' Ngal, Soe Thura Tun, Maung Thein, Win Swe, Than Myint, "Seismic Hazard Assessment For Myanmar", Report to Myanmar Earthquake Committee and Myanmar Geoscience Socity, 2012, P58.

Adsorptive Removal of Color from Textile Effluent Using Agricultural Wastes as Adsorbents

Nwe Nwe Aung[1], Mon Mon Aye[2], Rosy[3], Thet Thet Mon [4], Zue Zue Aung[5]

Abstract

Dyes are used in various fields such as paper, textile and plastics industries. Local dyeing houses in Amarapura discharge their dyeing wastewater into water body of Taungthaman Lake without any treatment. The color in these effluents are not biodegradable and can damage water quality. The aim of the present study is to explore the feasibility of using agricultural wastes such as rice husk, peanut husk and saw dust in the removal of color from dyeing effluents. The adsorption study was carried out by column method by choosing the most effective adsorbent from rice husk, peanut husk and sawdust. Different particle sizes and dose of adsorbents were used for study the effect of various parameter on adsorption process. The absorbances of dye containing wastewater and treated wastewater were measured by using UV-visible spectrophotometer. The λ_{max} value of dyeing wastewater was found to be 546 nm. The percent removal of red color from dyeing effluent could be calculated as 78 % by rice husk, 83 % by peanut husk and 80 % by saw dust. The pH value of effluents was measured after biosorption process and found to be 11.4 and 7.9 respectively. In addition, the removal efficiency for COD in the final effluent was found to be 78 %. The results prove that agricultural wastes, peanut husk and saw dust, are cost-effective and eco-friendly for removal of color from dyeing effluents.

1. Introduction

Textile dyes are generally made of synthetic, organic and aromatic compounds that may contain some heavy metals in their structure. These heavy metal containing aromatic compound can cause toxicity and carcinogen [1]. Wastewater discharged by the textile industry and dyeing houses are generally high in both color and such organic compounds. The presence of large amount of suspended solids, dissolved solids, high pH in the textile wastewater can cause serious environmental problems. Among then, color is the very first contaminant to be recognized in the textile dyeing wastewater [2]. A very small amount of dye in water body is highly visible and reduces penetration of light in water systems, thus causing the negative impacts on photosynthesis of aquatic plant [3]. One of the major challenges to environmental scientists is the environmental impact of textile effluent which contain residual color and some other organic contain residual color and some other organic compounds. In the last few years, environmental scientists paid great attention to the color removal from the textile effluents not only because of their potential toxicity but also mainly due to its visibility problems [4, 5].

Nowadays, various treatment methods such as adsorption, coagulation/flocculation/ precipitation [6], biological processes and ionizing/gamma radiation [7] are available for the removal of dye from textile effluent. However, most of them are expensive. Among these methods, adsorption is the most economical and effective treatment method, and so environmental scientists widely used adsorption technique for color removal from textile

[1] Lecturer, Department of Chemistry, Yadanabon University, nwenweaung748@gmail.com
[2] Assistant Lecturer, Department of Chemistry, Yadanabon University, monmon129464@gmail.com
[3] Assistant Lecturer, Department of Chemistry, Yadanabon University, rosylaphai@gmail.com
[4] Assistant Lecturer, Department of Chemistry, Yadanabon University, tthet8365@gmail.com
[5] M Sc student, Department of Chemistry, Yadanabon University, zuezueaung3333@gmail.com

effluent. Due to high cost of activated carbon, adsorption on natural materials such as sand [8], fly ash [9], orange peel and banana peel [10], sugarcane bagasse and used black tea leaves [11], rice husk [9], peanut husk [12], sawdust [13] and modified biomaterials [14-16] have received great interest. These natural adsorbents are locally available, cost-effective and ecofriendly.

The present study investigates the effective use of agricultural wastes as nonconventional and low-cost adsorbents for the removal of color from textile effluents using column method. The aim of this study was to compare the color removal efficiency of the selected agricultural wastes and to find an ecofriendly solution for the environmental problems caused by direct discharge of dyeing wastewater into water body without treatment. The effect of various parameters such as adsorbent dose, particle size of adsorbent and volume of dyeing wastewater were also investigated in this study.

2. Methods

2.1 Collection of textile wastewater

The textile wastewater sample was collected from local dyeing house located near Taungthaman Lake, Amarapura township, Mandalay Region. Sample was collected in precleaned pdyethlene bottles and placed in icebox for analysis. The collected wastewater sample for the present study was blue colored. The physicochemical parameters such as pH, electrical conductivity (EC), total dissolved solid (TDS) and chemical oxygen demand (COD) were analyzed to characterize the collected wastewater samples according to the methods prescribed in APHA [17].

2.2 Preparation of Adsorbents

The different agricultural wastes (rice husk, peanut husk and sawdust) were collected from different areas of Patheingyi Township, Mandalay Region. The biomasses were rinsed with tap water for several times to remove dust and any debris. And then they were rinsed two times with distilled water and dried in sunlight. The dried biomasses were further dried in oven for 24 hours at 60°C. The cleaned dried biomasses were ground into fine particles by grinding machine and sieved into different particles sizes. The particles sizes used in this study were 125 μm, 250 μm and 400 μm.

(a) *(b)* *(c)*

Figure 1. Adsorbents of 250 μm size (a) rice husk (b) peanut husk (c) sawdust.

2.3 Removal of color from textile effluent by column method

To choose the most effective adsorbent, three different columns having the diameter of 1cm and length of 25cm were packed with different adsorbents of 250 μm particle sizes. A piece of cotton wool was used as support at the bottom of each column. The characteristic features of the columns packed with different adsorbents were given in Table 1.

Table.1 The Characteristic features of different column packed with different adsorbent.

Adsorbent	Adsorbent dose (g)	Height of adsorbent in column (cm)	Flowrate at effluent ($mLmin^{-1}$)
Rice husk	2	3	0.3
Peanut husk	1.5	3	0.3
Saw dust	1.5	3	0.3

To remove dissolved materials and dissolved coloring substances from the adsorbents, same amount of distilled water was allowed to pass the column until clear solution was obtained. Then, all the water in the column was drained out. After that, 50 mL of dye wastewater was poured into the columns. The effluent from the column was collected at suitable time interval in different test tubes. Five fractions were collected. The absorbance of each fraction was measured by UV-visible spectrophotometer and the percent color removal for each fraction was calculated by the following equation.

$$\text{Percent color removal} = \frac{\text{inital absorbance} - \text{final absorbance}}{\text{initial absorbance}} \text{ x } 100$$

2.4 Effect of particle sizes

After choosing the best adsorbent for collected textile effluent from the dyeing house, the effect of particle size on the color removal efficiency was studied by using the adsorbent of different particle sizes such as 125 μm, 250μm and 400 μm.

2.5 Effect of adsorbent dose

After optimizing the particle size, the effect of adsorbent dose on the color removal efficiency was also studied by varying the amount of adsorbent with pre-optimized particle size. The amount of adsorbent used for this study were 2 g, 2.5 g, 3 g, 3.5 g, 4 g, 4.5 g and 5 g, respectively.

2.6 Effect of volume of wastewater

To study the influence of the volume of textile wastewater on the adsorption process, the different volumes of textile wastewater in the range of 20 ml to 200 ml were used. The column was packed with 5g of sawdust powder having the particle size of 125 μm. After removing the dissolved coloring matter by passing distilled water, 200 ml of textile wastewater was allowed to pass into the column. The flow rate was maintained at 0.3 ml min^{-1} and the eluent was collected with different test tubes at 5min time interval. The volume of each fraction was 15.0ml and totally fractions were collected.

3. Results and Discussion

To choose the adsorbent with highest color removal efficiency for each wastewater sample, screening tests were carried out. The highest color removal efficiencies of the different adsorbents were found to be 78% by rice husk, 83% by peanut husk and 90% by sawdust. From these results, it was observed that the most effective adsorbent for collected wastewater sample was sawdust and hence sawdust powder was chosen for the color removal process of the collected textile wastewater sample.

3.1 Effect of particle size

After choosing the most effective adsorbent, the effects of three different particle sizes such as 125 μm, 250 μm and 400 μm were investigated by column method. The percent color removal of each fraction collect from the column with 125 μm particle size adsorbent was shown in Table 2.

Table 2. Percent color removal by 125 μm size sawdust adsorbent.

Fraction No.	Volume of eluent (ml)	Percent color removal (%)	Average percent color removal (%)
1	10	92.93	90.09
2	10	92.87	
3	10	91.89	
4	10	90.92	
5	10	81.85	

The percent color removal was varied from 92.93% to 81.85% with the sawdust powder of 125 μm particle size and the average percent color removal was found to be 90.09%. Similarly, the sawdust adsorbent of particle sizes 250 μm and 400 μm gave the average percent color removal from collected textile wastewater at 81.85% and 64.87% respectively. The plot of percent color removal from textile wastewater against particle size is shown in Figure 2.

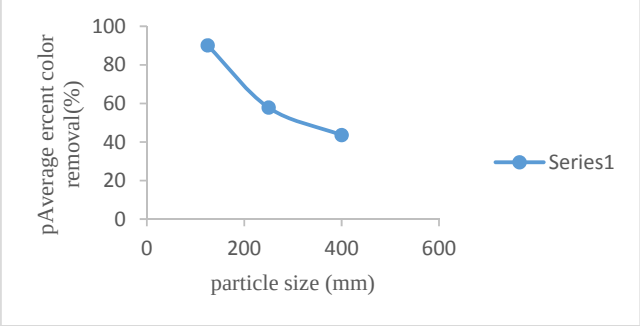

Figure 2. Optimization of particle size for color removal process

The figure reveals that the color removal efficiency of sawdust adsorbent for the collected dyeing wastewater sample decreased with increase in particle size. This phenomenon was probably due to the fact that the smaller the particle size, the greater the surface area of the adsorbent and the number of adsorption sites on the surface of the adsorbent to adsorb the dye molecules. According to the results, the particle size 125 μm of the adsorbent showed the highest color removal efficiency and was chosen for further investigations.

3.2 Effect of Adsorbent dose

After selecting the optimized particle size, the effect of adsorbent dose was studied by using various amount of sawdust powder (125 μm particle size) and flow rate of 0.3 ml min^{-1}. It was observed that the percent color removal varied from 47.75 % to 91.94 % by 5g of sawdust powder. The percent color removal of each fraction collected from the column experiment with 5g adsorbent (125μm particle size) and the average percent color removal were depicted in Table3.

Table 3. Percent color removal by different amount of sawdust powder (125 μm particle size)

Adsorbent dose (g)	Average percent color removal (%)
2	47.75
2.5	56.32
3	67.84
3.5	81.76
4	88.94
4.5	91.44
5	91.94

Figure 3 was represented the plot of adsorbent dose against the average percent color removal. From the figure, it was also observed that the color removal efficiency of sawdust powder increased with increase the amount of adsorbent. This result is probably due to the increased number of adsorption sites when the amount of adsorbent was raised. From the experimental results, 5 g of sawdust powder exhibit the highest color removal efficiency (91.94 %). Therefore, adsorbent dose (5 g) and particle size (125 μm) of sawdust powder were selected for further study.

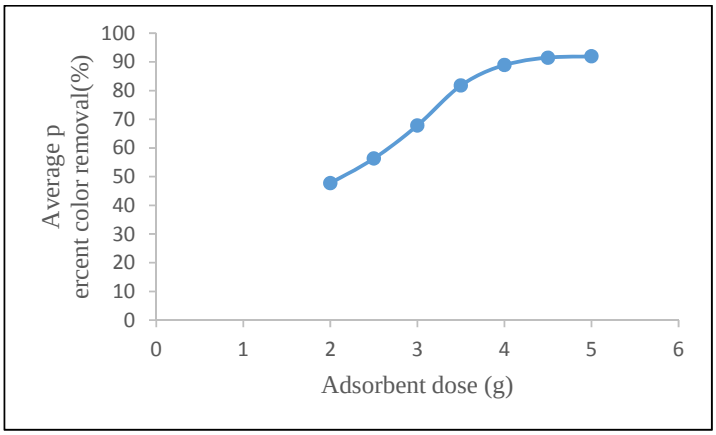

Figure 2. Optimization of adsorbent dose for color removal process

3.3 Effect of textile wastewater volume

The effect of the volume of the dyeing wastewater was shown in Figure 4. The figures pointed out that the color removal efficiency became decreased with increase in volume of textile wastewater. Therefore it can be observed that 5 g of sawdust powder (125 µm particle size) can reduce the color from the maximum volume of 160 mL textile wastewater.

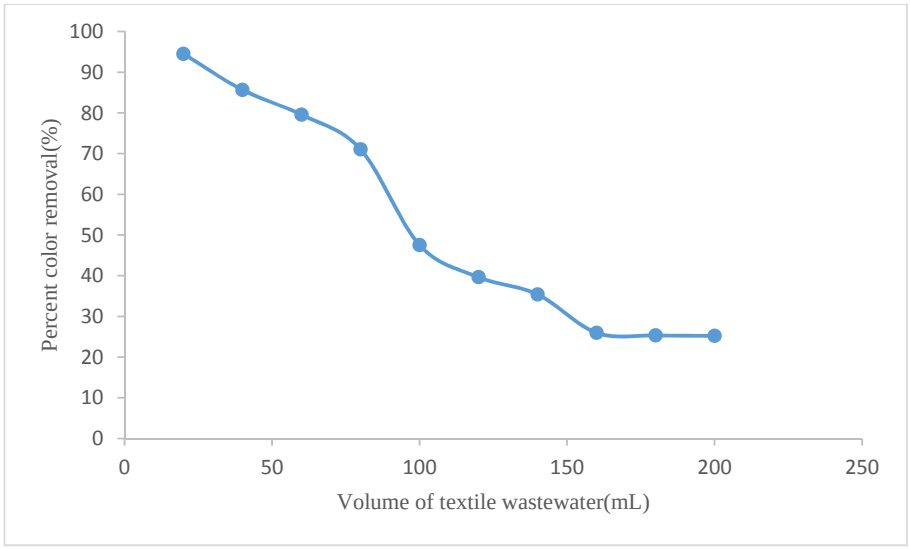

Figure 4. Effect of textile effluent volume on color removal process

3.4 Physico-chemical characterization of textile effluent

The effluent selected for the present study is dark blue color. The effluent was highly colored indicating high content of different dyes and color producing compounds. The high color may be the combined result of pH, temperature and acidic conditions that do not allow the chromophore group of dye to disintegrate during dyeing process and making the effluent highly colored.

In the present study, the pH value of dye wastewater was found to be 11.4 before adsorption and 7.8 after adsorption and was found to be within the standard discharge limit (6-9)[18]. EC values of wastewater sample reflect the content of dissolved ions in the wastewater.

TDS value of dye wastewater was determined to be 2500 mgL^{-1}. This high TDS value may be due to the fixing, bleaching and dyeing agent used in different stages of dyeing processes. The high TDS values of water are not recommended not only for drinking but also for irrigation purposes. After adsorption by sawdust powder, the TDS value of the effluent was found to be 1140 mgL^{-1}.

Before adsorption, COD of the effluent was found to be 1645.5 mgL^{-1} which is very high compared to discharge standard and reuse standard. High COD value indicate the presence of several waste such as detergents, softeners non-biodegradable chemicals such as dye fixing agents. After adsorption, COD value of the effluent was determined to be 362 mgL^{-1}. This value is still higher than the water quality standard for industrial uses and standard discharge values [19]. The results reveals that the values of pH, EC, TDS and COD decrease after adsorption of textile effluent using sawdust powder as adsorbent. This indicate that removal of color from textile effluent is effective and ecofriendly.

4. Conclusions

In this study, an attempt has been made for the removal of color from the textile wastewater by adsorption using the agricultural wastes as adsorbents. Of the three adsorbent, rice husk, peanut husk and sawdust, sawdust powder showed the highest color removal efficiency. The effects of various parameters on adsorption process such as particle size of adsorbent, adsorbent dose, and volume of textile effluent were studied. The optimum particle size was found to be 125 μm and the optimum adsorbent dose for column adsorption was 5 g. Another important finding was the decrease in color removal efficiency with increase in wastewater volume. The adsorption by column method using optimized particle size (125 μm) and adsorbent dose (5 g) exhibit the maximum color removal efficiency up to 91.94 % . Based on findings, the agricultural wastes such as sawdust was found to be useful as a low-cost, natural, abundant and effective adsorbent for the removal of color from dye wastewater.

Acknowledgements

The authors would like to thank to Dr Hlaing Hlaing Myat, Professor and Head of the department of Chemistry, Yadanabon University for the permission to carry out this research and supporting the required facilities throughout the research work. We also thanks to Professor Dr Htay Htay Win for her thoughtful suggestions which is necessary to complete this work. We also wish to thank to our colleagues for their kind and understanding helps.

References

[1] Venkatamohan S, Mamatha VVS, Karthikeyan J. Removal of color from acid and direct dyes by adsorption onto silica fumes. Fresenius Envion Bull, 1998; 7(1):51.8.

[2] Patel, H and RT Vashi, 2010 (a), Treatment of textile wastewater by adsorption and coagulation, E.J. Chemistry, 7 (4): 1468-1476.

[3] Poots V.I.P, Mckay G and Healy J, J.Water Pollut Con.F., 1978,5065), 926

[4] Robinson T, Chandran B and Nigam P, Water Res.,2002,36,2824-2830.

[5] Nigam P, Armour G, Banat IM, Singh D and Marchant R, Bioresource Technology, 2002,72,219-226.

[6] Pala A, Indian J Environ Health, 2001, 43(3), 128-134.

[7] Prieto), Fermoso J, Nae-ez Yand Del.Valle JL, Solar Energy, 2005, 79(4), 376-386.

[8] Y.Zaker, M.A Hossain, T.S.A Islam, Effect of various factors on the adsorption of methylene blue on sitt fractionated from Bijoypur soil, Bangladesh, Int. Res.J. Environment sci. 2(6), (2013) 243-250.

[9] S.De Gisi etal., Characteristics and adsorption capacities of low-cost adsorbents for wastewater treatment: a review, sustain, materials. Technol.9, 2016, 10-40.

[10] R.SiMane and V.N Bhusari, Removal of colour (dyes) from textile effluent byadsorption using orange and banana peel, International Journal of Engineering Research and Applications, Vol-2, Issues, 2012,PP-1997-2004.

[11] M.A Hossain, M.M.Ali and T.S.A Islam, Comparative adsorption of methylene blue on different low cost adsorbents by continuous column process, Int. letters of Chemistry, Physics and Astronomy, 77,2018,26-34.

[12] A.M. Etroki and F.M.N. Massoudi, The use of peanut hull for the adsorption of colour from aqueous dye solutions and dye textile effluent, Oriental Journal of Chemistry, 2011, Vol.27, 875-884.

[13] Mohammad Shafiqul Alam, Rexona Khanom, Mohmmad Arifur Raham, Removal of Congo Red Dye from Industrial Wastewater by untreated sawdust, American Journal of Environmental protection, Vol.4,No.5,2015,pp207-213. Doi:10.11648/J.ajep 20150405.12.

[14] Mane . V.S. and P.V.V Babu, Studies on the adsorption of brilliant green dye from aqueous solution onto low-cost NaOH treated sawdust. Desalination 2011,273:321-329.

[15] H.N.Bhatti, S.Sadaf and A.Aleem, Treatment of textile effluent by low-cost agricultural wastes: Batch adsorption study,The Journal of Animal and Plant Science, 2015,pp 284-289.

[16] China-Discharge Standards of water pollutants for dyeing and finishing of textile industry (GB.4278-2012), 2015.

[17] A.E.Greenberg, L.S.Clesceri and A.D. Eaton, Standard methods for the analysis of water and wastewater, 17th ed., American public Health Association(APHA), Washington DC,1992.

[18] L.V.Wilcos, Classification and use of irrigation waters, 1955, USDA Circular No.969.

The Innovation of Housebuilding Industry in Japan

Kazunobu Minami[1]

Abstract

Following my paper "Adaptable Infill for the Durable and Sustainable Japanese Housing" presented at the last year SCA Conference, the author continues the analysis of the innovations in Japanese house building and construction industry. Recent developments in housing technology has been promoting the longer life for housing and has reduced the material consumption and its environmental impacts. The adaptable infill system preserves building longer by changing its fit out according to the changes of lifestyles of the resident. The number of skilled construction workers in Japan is predicted to fall significantly in the near future. We are conducting the research and development in order to use less manpower for the site works. The use of robots on site works and the use of Artificial Intelligence and BIM in the process of design, building permission, on site construction and maintenance are the main research agenda for the expected innovation of our industry.

This paper analysis the characteristics of the past innovations in Japan and examines the key factors to foster the future innovations. The tradition of the collaborative relation among the government, academia and industry in Japan will be the most effective way to promote new innovation in the housebuilding and construction industry.

Keywords: Innovation, House building industry, Robot, AI, BIM

1. Introduction

In the previous paper "Adaptable Infill for the Durable and Sustainable Japanese Housing [1]" presented at the last year SCA Conference, the author pointed that the continuous research and development of adaptable housing in Japan from KEP, CHS (Century Housing System), KSI (Kodan Skelton Infill) to the establishment of the long fife housing law and the recent development of the zero slope gray water drainage system by the collaboration of the government, private companies and research institutions have been one of the most essential forces for the development of adaptable and sustainable housing in Japan. Based on this, the author tries to find out the necessary collaboration among public and privates sectors for the future innovation of housebuilding and building industries.

2. Methods

Sections 3-1 and 3-2 in this paper are summaries based on references [2] ~ [8] previously presented by the author. Section 3-3 is an examination based on references [9] ~ [10], which contain up-to-date information on technological development in Japan.

[1] Professor, Department of Architecture Shibaura Institute of Technology, k-minami@shibaura-it.ac.jp

3. Results and Discussion

3.1 History of the research and developments of housebuilding industry in Japan

In Japan, research and development has been carried out to improve the adaptability of multi-family dwellings and enable residents to continue living there for a longer period of time. In Japan, such housing units are often demolished after a short period of about 30 years, so efforts have been made to prolong their useful lifetimes by considering environmental and resource problems and economic efficiency.

In Japan, the Japan Housing Corporation, which is now called the Urban Renaissance Agency or UR, has been conducting joint research and development with universities and private companies under the leadership of the national government and the Ministry of Construction. In the early 1970s, their research resolved the problem of housing shortages, and since then it has been improving the quality of housing. Research and development by KEP since the late 1970s and by CHS beginning in the 1980s contributed to the KSI and to the enactment in 2009 of the Act Concerning the Promotion of Long-Life Quality Housing. Many dwellings for family use range in size from 70 to 80 square meters, requiring that they be occupied skillfully or remodeled to keep up with the growth of the children. Our research in housing adaptability is a response to these demands for such housing units in Japan.

The Act Concerning the Promotion of Long-Life Quality Housing was designed to prolong the life of housing units. This law came into effect on June 4, 2009. About 800,000 housing units have been constructed based on technical standards mandated by this law, but almost all were detached houses. Few have been condominiums. Because it must be possible to maintain and replace equipment piping of multi-family dwellings from common corridors, it is difficult for condominiums and apartments to comply with the technical guidelines, preventing the increase in the number of dwellings in compliance with the act.

Technical Guidelines have been enacted under this law. Chapter 3 stipulates ease of maintenance and renewal. Chapter 4 stipulates interior adaptability of dwellings. Vertical sewer pipes need to be easily accessible to allow replacement every couple of decades. The Piping space needs to have additional holes for future replacements.

The first condominium apartment constructed in Japan in compliance with the Act Concerning the Promotion of Long-Life Quality Housing is located in Urawa City. In order to be able to modify the layout of a dwelling, the ceiling and floor slabs of a condominium must ensure at least a vertical distance of 2,650 millimeters. The double floors are 275 millimeters thick. If this dimension is ensured, equipment piping can pass through the double floors, permitting the modification of rooms such as kitchens or bathrooms. Families can create the floor plan they desire by arranging movable storage systems.

3.2 Recent trends in technical developments for collective dwellings

Figure 1 and Figure 2 show a condominium equipped with movable storage walls and movable kitchens developed by Mitsui Real Estate and Haseko Corporation. The bathroom and toilet are installed as a single unit and cannot be moved, but other spaces can be laid out freely. The ceiling inside the room is flat and no columns or beams protrude into the rooms, so the movable storage walls can be installed anywhere without any limitations. The entire unit is double-floored, enabling the location of the kitchen to be changed. The thickness of the double

floor is 130 millimeters and the double ceiling is from 120 to 140 millimeters thick. This space is used to install equipment wiring and piping. Users create the floor plan they desire by arranging the movable storage walls. The kitchen can be relocated. Exhaust from the kitchen can be ventilated above the range to keep the air in the kitchen clean.

The other example of a recent technical development is the zero-slope drainage system. Figure 3 and Figure 4 show a new drainage system based on the siphon principle. The drainage slope is zero in order to fill the interior of the narrow 20-millimeter horizontal pipe with water. The drain pipe fills with water then it flows out under the force of gravity. If a siphonic floor drainage system is installed, the area where the kitchen can be located is greatly expanded. This new drainage system narrows drain pipes and ends the need for a slope. By reducing the height of the double floor, it removes the need for a level difference on the floor, lowering the cost of structure work.

Figure 1. Movable Kitchen System

Figure 2. Wheels for Movable Kitchen System

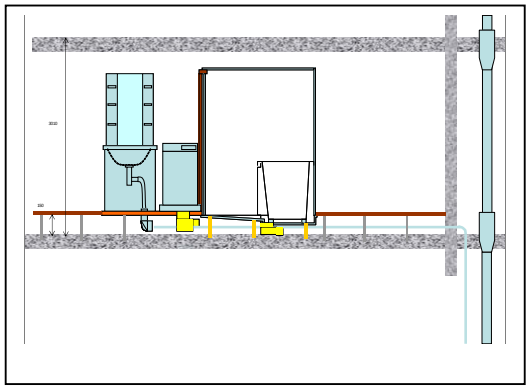

Figure 3. *Diagram of Zero-Slope Drainage System*

Figure 4. Example of Zero-Slope Drainage System

3.3 Strategy for the future technical developments and innovations for building industry

The construction industry in Japan is currently facing a severe shortage of skilled workers, and thus improving productivity is a pressing issue. The construction and housing industry in Japan has so far been improving productivity through innovative refinements to construction methods, in both reinforced concrete as well as conventional wooden structures. The construction industry, which has overcome numerous ordeals, including oil shocks and the collapse of Japan's bubble economy, will likely overcome this shortage of workers to a great

extent through application of robotics, IT (Information Technology) and AI (Artificial Intelligence).

Robotic systems for pulling construction materials have already been introduced in order to reduce the burden of on-site operations on aging workers as well as to improve productivity. Tests have also been conducted on tasking robotic systems with cleaning operations so that workers can focus exclusively on on-site operations during the day. In the near future, it may be possible for workers to commence operations from first thing in the morning thanks to robotic systems conducting cleaning operations at night. It would also likely not be very difficult to repurpose Power Assist Suits, which are used in the distribution industry among others, to be more in line with the characteristics of construction site operations.

The efforts of individual companies and on-site initiatives alone will be insufficient for achieving significant improvements in productivity. It is vital for the industry to engage with the issue collectively. When personnel related to the construction industry were interviewed, personnel in both Design Divisions and Construction Divisions said that, although the in-house inspections, client inspections and government inspections conducted at each stage throughout the construction process are necessary in ensuring construction quality, these inspections are a major time burden. In order to make inspection operations more advanced and streamlined, future developments may be in areas such as laser-based measurements, image recognition technology-based inspections, drone-based layout inspections and photography for construction records. Attaching RFIDs (Radio Frequency Identifiers) to construction materials and architectural parts will likely accelerate on-site confirmation and provide greater accuracy, and may also facilitate confirmation of concealed areas.

Government agencies also likely need to examine ways to streamline various inspection operations for the purpose of improving the productivity of the industry as a whole. For example, in the future, the ratio of existing structures that undergo repair will increase, which means that forming databases and disclosing information on previous building approvals so that clients and designers can clearly determine whether to make use of an existing structure or to rebuild during the initial stages of operational planning will likely lead to smoother project progression and increased productivity.

Utilization of BIM (Building Information Modeling) is expected to improve productivity. Initiatives are progressing in regard to building approvals that utilize BIM, such as standardizing expressions used in drawings and specifications for applications. In the near future, in addition to ensuring consistency between design drawings and application drawings, automatic confirmation will also be conducted for both stand-alone and group regulations relating to various types of area calculations, physical dividers to prevent the spread of fires, fire prevention equipment, measurements of evacuation distances, etc. And this will likely greatly reduce the amount of time necessary for building approvals and for receiving consent from the fire department. Eventually, legality will be automatically checked starting from the basic design stage, and this will likely eliminate the need to redo operations. When it comes to industrialized housing, application of type certification and manufacturer certification systems will streamline building approvals and also simplify on-site inspections. In the field of industrialized housing, which is becoming increasingly componentized, unique CAD systems have been introduced for design, production and construction, so engaging in building approvals that utilize BIM based on these systems will likely be easier than for other general structures. The field of industrialized housing could

become capable of BIM level 3 inspections at a very early stage.

The construction industry in Japan is a mature industry, and it is good at progressively improving productivity. The industry contains companies that have attempted new businesses, such as nursing care and agriculture, by applying their skilled personnel and organizational capacity to these new businesses during periods in which their existing businesses are performing favorably and without falling into 'success traps.' However, due to rapid progress in the fields of IT and AI, companies that are currently aiming to introduce robotics and AI into the construction industry are gaining more and more experience, and this could introduce 'destructive innovation' into the construction and housing industries. In the future, AI technologies will be more advanced, and in terms of architectural designs for residences in particular, this may lead direct connections between clients and production process and cause major changes in business models. In companies that provide industrialized housing, engineers from other fields who graduated from courses other than architecture will be responsible for the information technologies that form the core of production, and educational programs implemented at universities and human resource development programs conducted by companies must stay up-to-date with changes in society.

Achieving further innovation requires 'ambidextrous' administration in which managers search for new businesses while at the same time deepening existing, mature businesses*1. The textile industry in Japan succeeded in shifting its core focus into new fields. But will the constructing and housing industries, for which a drop in domestic demand is unavoidable, also be able to do the same thing?

Komatsu Ltd., a manufacturer of construction equipment, began globalization at an early stage, including entering the Chinese market, and the company has constantly created value through innovation*2, including development of ICT construction equipment, which is increasingly becoming automatized, KOMTRAX, which provides a visual representation of operation status, and SMART CONSTRUCTION, which provides higher level solution businesses. In 2017, through a joint venture with NTT Docomo, SAP Japan and OPTiM Corporation, Komatsu started LANDLOG, an IoT platform for construction sites. This is exactly what Joseph Schumpeter meant by 'new combination' between different industries. Komatsu Ltd., which had previously provided construction equipment for use at construction sites, established a position as a leading company through proactive introduction of IT. And by constructing a platform[*3] that accumulates and processes all types of construction-related data and providing access even to competitors, the company is increasingly becoming the main pillar in the construction solution business.

Even though it is presently limited to the field of civil engineering, including site preparation, etc., it may eventually expand into building construction work. Together with IT, AI and robotics companies, the general construction industry and the housing industry should continue searching for businesses that will create new social value and develop these into their core businesses in the future.

So far, growth of the Japanese economy has been supported by initiatives in which industry, academia and the government are in close cooperation. In terms of technology, further developing the housing and construction industries in Japan, which are already highly advanced, will require not only technological development and technological innovations but also restructuring of social systems to produce new value. It is thought that, in the future as well, the

key to promoting social system reforms and technological innovations in an integrated and effective way will be cooperation between government sectors in charge of policy and private sectors in charge of research and technological development – in other words, the promotion of open innovation in cooperation between industry, academia and the government.

4. Conclusions

Technological developments in the construction and housing industries in Japan during the 1970s and 1980s were promoted through participation by major companies in national technology development projects under government leadership, and these produced results. However, in terms of technological development currently in progress, it is necessary to cooperate with start-up companies in fields other than the construction industry that possess advanced technologies, including IT and robotics. In particular, it is necessary to proceed in a different way than before, including in relation to the state of government subsidies for research and development, etc. In addition, in regard to the ideal state of construction production in the future, it would be preferable to construct a vision that can be shared by society as a whole and to proceed research and development aligned with society as a whole.

Acknowledgements

The author would like to express deep gratitude to all of the researchers who provided advice regarding the writing of this paper.

References

[1] Kazunobu Minami, Adaptable Infill for the Durable and Sustainable Japanese Housing, December 6th, 2018, ORAL presentation at the Conference Strand: 1. Energy, Natural Resources and Built Environment, The 18th Science Council of Asia Conference “Role of Science for Society: Strategies towards SDGs in Asia”, Science Council of Japan (SCJ)

[2] Kazunobu Minami, Japanese Innovation in Adaptable Homes, Loose-Fit Architecture: Designing Buildings for Change AD, pp. 38-45, Willy, September 2017, Alex Lifschutz (Editor) et.al.. Profile 249 Volume 87 No 5

[3] Kazunobu Minami a, The efforts to develop longer life housing with adaptability in Japan, PROCEEDINGS pp.755-766、SBE16 Tallinn and Helsinki Conference; Build Green and Renovate Deep, 5-7 October 2016, Tallinn and Helsinki

[4] Kazunobu Minami b, The Adaptability of Long Life Housing in Japan - Case Studies of Century Housing System (CHS) -, 11th International Symposium on Architectural Interchanges in Asia (ISAIA 2016), September 21st-22nd, 2016

[5] Kazunobu Minami, Long-Term Occupancy Records and Infill Renovation of Housing Designed Based on the Century Housing System, The Future of Open Building Conference 2015, ETH Zurich, September 9-11 2015

[6] Kazunobu Minami, ANALYSES OF LONG TERM OCCUPANCY RECORDS OF PUBLIC HOUSING IN JAPAN, Architecture in the Fourth Dimension Methods + Practices for a Sustainable Building Stock, Proceedings of an International Conference of CIB W104 Open Building Implementation and CIB W110 Informal Settlements and Affordable housing, pp.287-293, November 15th -17th 2011

[7] Kazunobu Minami, The New Japanese Housing Law to Promote The Longer Life of Housing And Exaple of Changes in The Layout of Public Housing Over 40 Years In Japan, Changing Roles; New Roles,

New Challenges, pp.449-455, October 5-9,2009, Noordwijk aan Zee, The Netherlands

[8] Kazunobu Minami, A Study on the Continuous Customization of an adaptable housing by KEP System, Adaptables2006, TU/e, International Conference On Adaptable Building Structures, July,2006,Vol.1, PP.2-101～106

[9] Lead and disrupt: how to solve the innovator's dilemma, Charles A. O'Reilly III and Michael L. Tushman, Stanford Business Books, c2016, Japanese Translation by Noriko Watanabe, Feburary 2019

[10] Komatsu NEWS RELEASE No.017（2852）“DANTOTSU Value-FORWARD Together for Sustainable Growth”, April 26th 2019, https://home.komatsu/jp/press/2019/ management/1202302_1600.html , viewed May 2019

Mold and Dampness in Unplanned Urban Houses in the Hot and Humid Climate of Indonesia

Tetsu Kubota[1], Jumpei Sumi[2], Kresna Bhayu Adinugraha[3] and Usep Surahman[4]

Abstract

Many parts of Indonesian cities comprise unplanned houses, the so-called Kampongs. Most Kampong houses are small detached houses constructed by non-professional workers in densely crowded settlements. Mold and dampness are commonly seen in Kampongs particularly during the rainy season along with seasonal floods, and therefore adverse health effects, especially respiratory diseases, are suspected among residents. We investigated the mold risk using fungal detectors (n=68) and the self-reported prevalence of respiratory diseases using a questionnaire form (ATS-DLD-78) (n=599) in a typical Kampong neighborhood in the city of Bandung, Indonesia during 2018-19. Mainly due to the high humidity conditions, most houses were suffered from severe molds. Approximately 79% of the measured rooms showed a possibility of mold propagation even during the dry season, whereas more than 97% were categorized as severe conditions during the rainy season. Nevertheless, further results showed that the respondents with some symptoms of respiratory diseases tended to be exposed to a lower mold growth index compared to those without any symptoms. The respiratory diseases might be attributed to outdoor air pollutions as well.

Keywords: Mold, Dampness, Health, Tropics, Kampongs

1. Introduction

Microbial pollution involves hundreds of species of bacteria and fungi that grow indoors when sufficient moisture is available. Exposure to microbial contaminations is clinically associated with respiratory symptoms, allergies, asthma and immunological reactions [1]. The presence of many biological agents in the indoor environment is due to dampness and inadequate ventilation [1-2]. Excess moisture on almost all indoor materials leads to growth of microbes, such as mold, fungi and bacteria, which subsequently emit spores, cells, fragments and volatile organic compounds (VOCs) into indoor air [1]. Moreover, dampness initiates chemical or biological degradation of materials, which also pollutes indoor air. Dampness has therefore been suggested to be a strong, consistent indicator of risk of asthma and respiratory symptoms (e.g. cough and wheeze) [1].

Indonesia has a population of more than 150 million as of today and it is still rising particularly in the urban areas. In order to accommodate growing number of urban population, now the central government is highly promoting provisions of affordable housing. But still, many parts of Indonesian cities comprise traditional unplanned houses, the so-called Kampongs. Most Kampong houses are small detached houses constructed by non-professional workers in densely crowded settlements (Fig. 1). Mold and dampness are commonly seen in Kampongs particularly during the rainy season along with seasonal floods, and therefore adverse health effects, especially respiratory diseases, are suspected among residents. We investigated the mold risk

[1] Dr. Associate Professor, Graduate School for International Development and Cooperation, Hiroshima University; Research Institute for Human Settlement and Housing, Ministry of Public Works and Housing, tetsu@hiroshima-u.ac.jp
[2] Graduate School for International Development and Cooperation, Hiroshima University
[3] Graduate School for International Development and Cooperation, Hiroshima University
[4] Department of Architecture, Indonesia University of Education, Indonesia

using fungal detectors and the self-reported prevalence of respiratory diseases using a questionnaire form (ATS-DLD-78) in a typical Kampong neighborhood in the city of Bandung, Indonesia during 2018-19. This paper reports the results of the investigations to analyze an association between the mold risk and the prevalence of respiratory diseases.

2. Methods

A typical Kampong neighborhood, comprising 360 households, was selected in Bandung as a case study area (Fig. 1). After obtaining a consent from the head of the neighborhood association, the field measurements and interviews were conducted during the dry season (October 2018) and the rainy season (March 2019). The subjects investigated include 333 and 266 residents in dry and rainy seasons respectively for the interviews, and 34 and 34 houses for field measurement of air temperature (AT), relative humidity (RH) and mold risk.

The interviews were conducted using a questionnaire form, comprising the American Thoracic Society-Division of Lung Diseases (ATS-DLD-78) [3] and several additional questions, among others: personal attributes, building attributes, cleaning habits, window-opening behavior and smoking habits. The ATS-DLD questionnaire has been validated in many previous studies [4] and commonly used to evaluate general respiratory health. The questionnaire comprises questions for symptoms of cough, phlegm, wheezing, breathlessness, chest colds and chest illnesses. Moreover, occupational history and tobacco smoking habits were additionally asked for adults, among others.

Fungal contamination was predicted by using a fungal detector developed by Abe [5]. The fungal detector encapsulates dried fungal spores and nutrients to measure fungal index. The fungal index, defined by Abe [5], quantifies the capacity for mold growth in an environment being examined, and therefore it is considered one of the useful indices for evaluating microclimates for potential mold growth (Table 1) [6]. The mold measurements were taken at approximately 10 cm above floor in the master bedroom during the dry and rainy seasons, respectively. AT and RH were measured using a small recorder (T&D 72ui, 72wf & 73u) at the same places.

3. Results and Discussion

3.1 Profiles of Respondents

Out of the respective samples (i.e. dry season (n=333) and rainy season (n=266)), there are intersections of 77 respondents. As shown in Table 3, the average age of respondents in dry season is 34.3 years, including 16.5% of children aged 12 years old and below. The majority of respondents are classified as the income group of US$ 150-450 (monthly average). Averagely, they open windows for approximately 8-9 hours in the bedroom and 7-8.5 hours in the living room. They tend to open windows during the daytime. As shown, approximately 69% of the respondents (active; 32%, passive; 37%) are exposed to ETS during the dry season, while more than 98% (50% and 48%) are suspected during the rainy season. Moreover, more than 45% of the respondents (dust; 29%, chemical; 17%) are exposed to dust or chemical fumes during their working time, whereas more than 70% (49% and 22%) are suspected during the rainy season

Table1. Fungal index (6)

Level	Fungal index	Predicted propagation of fungi	Remarks
A	<2	No propagation	Good environment
B	2 – 5	Low possibility of propagation	There is no problem in terms of fungi, but there is a possibility of propagation of mites, which requires countermeasures. Dehumidification is recommended.
C	5 – 15	Possibility of propagation	Fungi prevention measures are recommended. Dehumidification is recommended.
D	>15	High possibility of propagation	Fungi prevention measures are required. Dehumidification is needed for living rooms and regular cleaning is needed for wet areas, such as bathroom.

Figure 1. Kampong houses in the case study area.

Table 2. Number of samples

Samples	Dry season	Rainy season	Total
Questionnaires (ATS-DLD-78)	333	266	599
Measurements (Mold risk)	34	34	68

Table 3. Profile of respondents and overview of building attributes, interior sources and perceived dampness

			Dry season	Rainy season
Personal attributes	Age [%]	Years [mean]	34.3	-
	Gender [%]	Male/ Female	45/55	47/53
	Income (US$) [%]	< 150	36.2	25.9
		150-450	43.6	62.4
		450-750	8.5	9.4
		> 750	4.3	2.4
	Window opening in bedroom	Hours	7.9	8.8
	Window opening in living room	Hours	7.0	8.5
	Smoking behavior [%]	Active	32.3	50.0
		Passive	37.0	48.3
	Work in dusty job	[%]	29.1	49.0
	Exposed to gas or chemical fumes	[%]	16.9	22.3
Health	Asthma	[%]	13.8	6.7
	Eczema	[%]	13.5	-
	Allergy	[%]	13.6	-
	Stress	[mean: 0 = no stress, 10 = very stressful]	1.5	0.9
Building attributes	Age of building	Average age [years]	39.9	41.8
	No. of windows in master bedroom [%]	0	25.9	18.5
		1	50.6	49.2
		>1	23.5	32.3
	No. of windows in living room [%]	0	34.6	22.8
		1	42.0	35.1
		>1	23.5	42.1
	HVAC system [%]	AC	5.6	8.0
		Ceiling / stand fan	50.0	-
		Exhaust fan	21.4	-
	Modification(s)	[%]	-	59.7
	Furniture (units)	Living room [mean]	3.1	-
		Bedroom [mean]	2.4	-
Dampness	Visual mold	[%]	51.3	34.1
	Mite	[%]	17.0	11.0
	Water leakage	[%]	48.3	50.6
	Smell / Odor	[%]	40.9	55.9
	Humidity [%]	0-3: (rather) dry	24.3	28.2
		4-6: neutral	45.2	43.5
		7-10: (rather) humid	30.5	28.2
Perceived IAQ	IAQ [%]	0-3: (rather) clean	35.4	42.0
		4-6: neutral	50.3	44.3
		7-10: (rather) dirty	14.4	13.6
	OAQ [%]	0-3: (rather) clean	28.7	38.6
		4-6: neutral	52.8	46.6
		7-10: (rather) dirty	18.5	14.8
	Annoyance by outdoor air pollution [%]	0-3: not annoyed	57.6	69.4
		4-6: neutral	34.3	18.7
		7-10: annoyed	8.1	11.9
Cleaning behavior	How to clean room	Sweep	95.0	98.9
		Wipe	4.2	1.1
		Vacuum cleaner	0.0	0.0
		Others	0.8	0.0
	How to dry laundries	Indoor	13.7	10.1
		Outdoor	59.8	44.9
		At veranda	9.4	30.3
		Others	17.1	14.6

The average age of buildings is about 40 years in the dry season and 42 years in the rainy season. It should be noted that approximately 26% and 35% of houses do not have any windows in the master bedroom and the living room respectively in the dry season, whereas about 19% and 23% of houses do not have them in the rainy season. Dampness is commonly seen in Kampong houses. As shown in Table 3, visual mold was reported in approximately 51% and 34% of the houses during the dry and rainy season, respectively. About 17% and 11% of the houses reported mite problems in dry and rainy season, respectively. Water leakage was reported particularly in the rain season (51%), and smell and odor were reported more in the rainy season as well (56%). Meanwhile, approximately 14% of the respondents perceived IAQ to be dirty in the both seasons. On the other hand, about 15-19% of the respondents perceived OAQ to be dirty in the two seasons. Approximately 8-12% of the respondents were annoyed by the outdoor air pollutions.

3.2 Self-reported respiratory health: ATS-DLD-78

Magnitude of symptoms on respiratory health (i.e. asthma, cough and phlegm) was evaluated through the ATS-DLD-78 questionnaire (Fig. 2). In the dry season, the percentages of those who have severe symptoms (i.e. sickness) and some degrees of symptoms account for 0.3%/16.1% (asthma), 1.9%/21.9% (cough) and 3.2%/9.6% (phlegm). The percentages are increased in the rainy season especially in persistent cough, and the percentages are 0%/7.6% (asthma), 4.0%/25.4% (cough) and 1.3%/12.7% (phlegm).

3.3 Mold risk

The measured average AT and RH (at the same places of fungal detectors) are summarized in Fig. 3. As shown, in the dry season, the outdoor AT ranges approximately from 21.3-27.3°C with an average of 24.2°C, whereas the corresponding indoor AT ranges from 23.6-26.3°C with an average of 24.9°C. In the rainy season, the outdoor AT maintains almost the same as that of the dry season (approximately 22.1-26.4°C), but indoor AT was averagely increased to approximately 24.7-26.8°C. Meanwhile, in the dry season, the outdoor RH ranges approximately from 56-100% with an average of 81%, whereas the corresponding indoor RH ranges approximately from 71 to 86%. In the rainy season, the outdoor RH is increased to 70-97%, while the indoor RH is averaged at 82%. The results clearly indicate extremely high humidity conditions in Kampong houses even in the dry season.

Mold growth was evaluated in terms of fungal indexes ranging from A to D (see Table 1). The results show that as expected, approximately 79% of the houses are classified as C or D even in the dry season, whereas more than 97% are classified as D, which shows a high possibility of propagation, in the rainy season. It should be noted that in the rainy season, more than 44% of the houses recorded the maximum fungal index of more than 70.

Fig. 5 depicts the relationship between the measured thermal conditions and the mold indexes. As shown, the mold conditions are severe particularly when the indoor RH exceeds 70%. The measured mold indexes slightly vary even when the indoor RH is more than 70% probably due to the other dampness conditions such as water leakage and floods.

3.4. Factors affecting the respiratory health

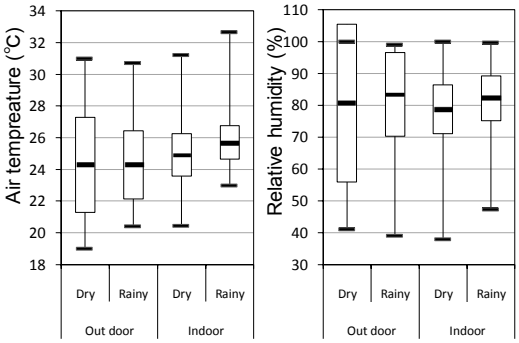

***Figure 2**. Self-reported respiratory health.*

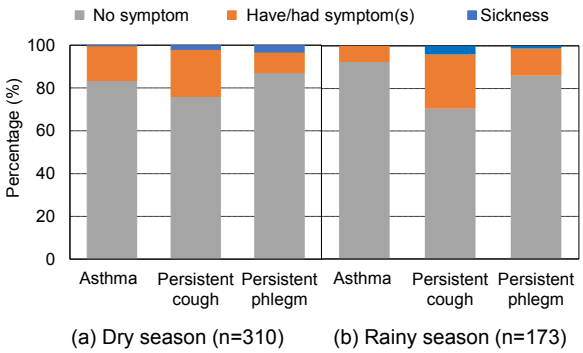

*Figure **3**. Statistical summary of outdoor and indoor AT and RH in dry and rainy season.*

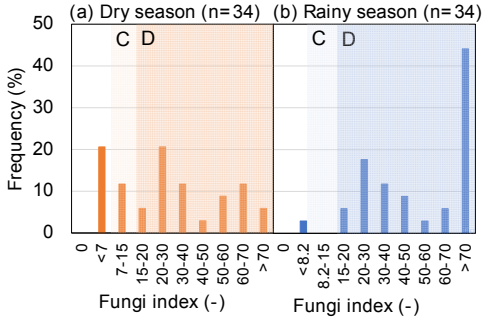

Figure 4. Measured fungal indexes in Kampong houses.

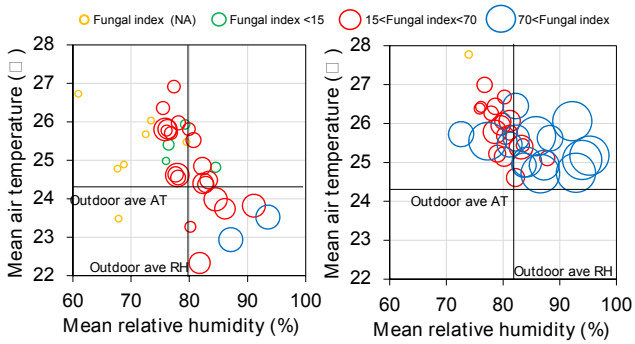

(a) Dry season (b) Rainy season

***Figure 5**. Relationship between thermal conditions and mold risk.*

Table 4. Results of correlation analysis for Respiratory health (dry season)

A: Asthma, C: Persistent cough, P: Persistent phlegm	**A**	**C**	**P**
Personal attributes			
Age group[a]	0.33	0.51	0.29
Gender[a]	0.49	0.34	0.66
Living in home [years][b]	0.09	0.35	0.66
Income[b]	0.38	0.03	0.04
Window-opening_ bedroom[b]	0.97	0.08	0.59
Window-opening_ living room[b]	0.31	0.03	0.08
Active smoking	0.18	0.84	0.47
Passive smoking	0.06	0.35	0.00
Work in dusty job	0.64	0.00	0.22
Exposed to gas or chemical fumes	0.20	0.06	0.33
Health			
Asthma[a]	0.00	0.03	0.03
Eczema[a]	0.42	0.77	0.08
Allergy[a]	0.04	0.02	0.00
Stress[b]	0.25	0.02	0.07
Building attributes			
Age of building [years][b]	0.69	0.66	0.04
No. of windows_bedroom[b]	0.37	0.26	0.60
No. of windows_living room[b]	0.40	0.61	0.07
AC[a]	0.73	0.53	0.61
Furniture living room[b]	0.30	0.94	0.32
Dampness			
Visual mold[a]	0.29	0.45	0.89
Mite[a]	0.91	0.00	0.01
Water leakage	0.42	0.00	0.09
Smell/Odor	0.42	0.55	0.01
Humidity	0.68	0.19	0.28
Perceived IAQ			
IAQ rating[b]	0.26	0.45	0.24
OAQ rating[b]	0.47	0.68	0.48
Annoyance by outdoor air pollution	0.42	0.02	0.05
Creaning behavior			
How to clean room	0.33	0.75	0.00
How to dry laundries	0.14	0.81	0.81

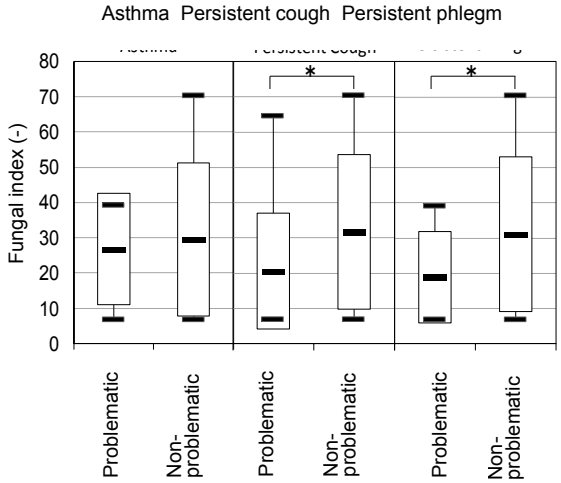

Figure 6. Measured fungal indexes by problematic/ non-problematic respiratory health groups (dry season).

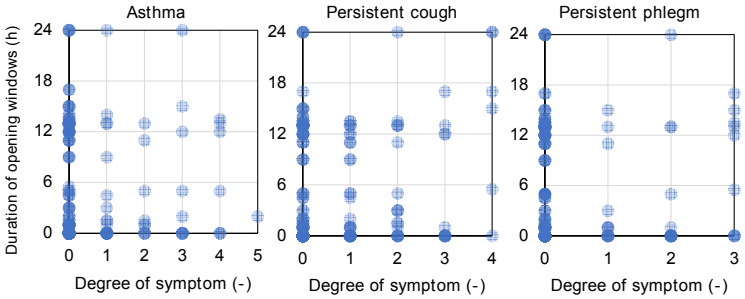

Figure 7. Relationship between duration of opening windows and respiratory health (dry season).

[a] p-value of Chi-Square-Test, [b] p-value of Spearman rho, red: Correlation is significant at the 0.01 level (2-tailed), green: Correlation is significant at the 0.05 level (2-tailed)

By taking the degrees of symptom of respiratory diseases (i.e. ATS-DLD-78) as the target variable, we conducted correlation analyses in order to determine the factors affecting the respiratory health of occupants (Table 4). As shown, the average household income is associated with respiratory health, particularly in terms of cough and phlegm. This may reflect their job occupations and basic sanitary conditions, but further analysis is required. The average duration of opening windows negatively affect the degree of asthma symptoms (the more they open windows the less the symptoms are), but it has positive associations with persistent cough and phlegm. As expected, passive smoking is associated with asthma and persistent phlegm in particular. Meanwhile, those who work in a dusty job tend to have a higher symptom of cough in particular. Previous history of asthma, allergy and stress are also associated with the current symptoms as expected. Furthermore, the age of buildings negatively associates with the phlegm symptoms, which requires further investigation.

Unlike other previous studies, visual mold does not show significant associations with respiratory health in this survey, although other dampness indicators, including mite and water leakage and smell/odor, are associated with persistent cough and/or phlegm. On the other hand, when it comes to the perceived IAQ, it is seen that those who are annoyed by the outdoor air pollutions tend to have higher degrees of persistent cough and phlegm.

We divide the samples into two groups in terms of respiratory health conditions (i.e. problematic and non-problematic groups) and compare the two groups in terms of the measured fungal indexes (Fig. 6). As shown, unexpectedly, those who have no respiratory symptoms tend to be exposed to higher fungal indexes, especially in terms of persistent cough and phlegm. Further investigations are required to clarify the reasons (e.g. it is necessary to identify the species of mold contained in the air). However, the results imply that there is a possibility that respiratory health of these Kampong residents is influenced not only by indoor mold and dampness but also, rather, by outdoor air pollutions, among others. Fig. 7 analyses the respiratory health symptoms by the average duration of opening windows. Interestingly, especially in persistent cough and phlegm, there are two modes in terms of the respiratory health symptoms. The first mode appears when the duration of opening windows is close to zero (i.e. windows are closed for 24 hours), and the second mode is observed when the duration is about 12 hours/day. The results imply that their respiratory health is influenced by the two sources (i.e. indoor sources such as mold and ETS, and outdoor sources such as traffic air pollution) respectively, depending on the window-opening conditions.

4. Conclusions

We investigated the mold risk using fungal detectors and the self-reported prevalence of respiratory diseases using ATS-DLD-78 in a typical Kampong neighborhood in the city of Bandung, Indonesia during 2018-19. The main findings from the investigations are summarized as follows:

- As expected, Kampong houses were suffered from severe mold growths. Even in the dry season, approximately 79% of the houses showed a possibility of mold propagation and 68% were considered to be a high possibility of propagation. In the rainy season, more than 97% of the houses were classified as a high possibility of propagation.
- The possibilities of propagation were mainly due to the very high humidity conditions. The outdoor RH was averaged at 83% while the corresponding indoor RH was averaged at 82% during the rainy season.
- Nevertheless, further results showed that the respondents with some symptoms of respiratory diseases tended to be exposed to lower mold growth conditions compared to those without any symptoms. On the other hand, respiratory health of occupants, particularly persistent cough and phlegm, were associated with average household income, duration of opening windows, passive smoking, working environment (dusty job), medical history such as asthma, eczema and allergy, age of buildings, dampness such as mite, water leakage and smell/odor, and annoyance by outdoor air pollution.
- The results implied that their respiratory health was influenced by the two sources (i.e. indoor sources and outdoor sources) respectively, depending on the window-opening conditions. When they close windows, indoor sources such as mold and ETS may become the main causes of prevalence of respiratory diseases. Meanwhile, if they open windows, then the indoor sources can be less influential, but the occupants are exposed to the outdoor sources more such as traffic air pollutions.

Acknowledgements

This research was supported by a grant from the Sumitomo Foundation. We also would like to sincerely thank the students in Indonesia University of Education (UPI) who supported the surveys in Bandung. We also appreciate the supports from the Laboratory for Mold Prediction in Japan.

References

[1] WHO, "WHO Guidelines for Indoor Air Quality: Dampness and Mould", WHO Regional Office for Europe, 2009.

[2] Olaf C.G. Adan, Robert A. Samson (eds), "Fundamentals of Mold Growth in Indoor Environments and Strategies for Health Living", Wageningen Academic Publishers, 2011.

[3] Ferris B.G., "Epidemiology Standardization Project (American Thoracic Society)", Am Rev Respir Dis, 1978, vol.118, pp.1-120.

[4] Hawari F.I., Obeidat N.A., Ghonimat I.M., Ayub H.S., Dawahreh S.S., "The effect of habitual waterpipe tobacco smoking on pulmonary function and exercise capacity in young healthy males: A pilot study", Respiratory Medicine, 2017, vol. 122, pp. 71-75.

[5] Abe K., "A method for numerical characterization of indoor climates by a biosensor using a xerophilic fungus", Indoor Air, 1993, vol. 3, pp. 344–348.

[6] Laboratory for Mold Prediction, "Additional Guidelines for Fungal Detector", Laboratory for Mold Prediction, Tokyo, Japan, 2004 (in Japanese) (unpublished).

Retail Site Location in Dagon Myothit (North) Township Using GIS

Khin Mi Mi Win[1] , Khin Khin Htay[2], Lae Lae Mon[3]

Abstract

The opening of a new establishment is a critical factor for firms in the retail sector. This article presents the development of a methodology for the process of selecting a retail site location that combines geographic information systems (GIS). The social, economic and environmental impacts of large-scale retail outlets on existing retail and urban systems have been extensively discussed in the planning literature. This article documents the last two decades of transformation in Dagon Myothit (North)'s market sector, which have been characterized by a more organized development of the sector than traditionally existed. Changes in the economy and related legislation prepared a base for the subsequent transformations of that decade, culminating, especially in large cities, in the development of shopping malls as alternative retail spaces to traditional markets and stores on a shopping street. This article may provide implications for urban policy and retail planning in Dagon Myothit (North) Township. The case may also be interesting for urban areas experiencing similar patterns of change and development, that is, where the globalization process in retailing and consumption-related sites began later than in other countries and observed fast-paced development.

Keywords: Retail development, Shopping mall, GIS, Urban policy

1. Introduction

Retailing is defined as the sale of goods and articles individually or in small quantities directly to the consumer, which involves selling relatively large quantities of goods, especially to retailers. Retail location analysis is an important part in site selection of a retail shop. Spatial arrangement of retail shops is one of the most important indicators in the development process of a town. The influences on the location of retail areas, they usually co-vary most closely with population density. This paper presents the development of a methodology for the process of selecting a retail site location that combines geographic information systems (GIS).

The main objectives of this research work are to assess the driving force of the emergence and spatial distribution of retail shop and to analyze the relationship between location of retail shop and urban infrastructure in Dagon Myothit (North) Township.

Dagon Myothit (North) Township is one of 12 townships of Eastern Yangon District in Yangon Region. (Figure. 2) It lies between North latitudes 16° 51′ and 16° 55′ and between East longitude 96° 10′ and 96° 14′. The area of Dagon Myothit (North) is 26.28 square kilometer (10.145 square miles) constituting 27 wards. (Figure 3)

In 2019, the total population was 196199 persons with 92774 males and 103425 females and the average population density was 7465persons per square kilometre. The population distribution in Dagon Myothit (North) is highly uneven. More people are concentrating around the main road and junction's area. East longitude 96° 10′ and 96° 14′. The area of Dagon Myothit (North) is 26.28 square

[1] Dr. Professor, Department of Geography, University of Yangon, Yangon, Myanmar khinmimiwingeog@gmail.com
[2] Department of Geography, Bago University, Bago, Myanmar kkhinhtay.geog@gmail.com
[3] Department of Geography, University of Yangon, Myanmar. laelaemon69@gmail.com

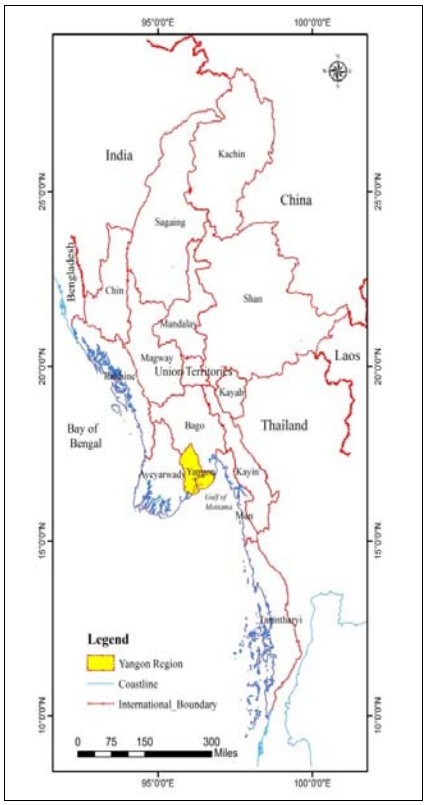

Figure 1. Location of Yangon Regions in Myanmar
Source: UTM Map of Myanmar Survey Department

Figure 2. Location of Dagon Myoyhit (North) Township
Source: Map Based on 1:50000UTM Map No.1696-01

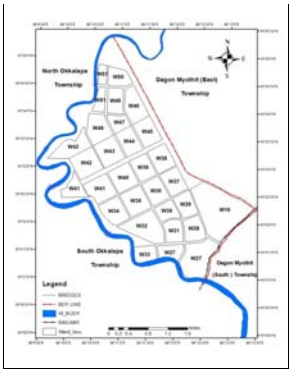

Figure 3. Location of Wards within Dagon Myothit (North) Township
Source: Township General Administrative Department

2. Method

Data processing was done from extracting geographic objects such as ward boundaries roads and streets by using based map of topographic map (1: 63360 and 1:50000) and Google earth images of geographically references data. Retail shops data from field survey (2018), using analysis of geospatial analysis and geostatistical analysis. Location of retail shop is analyzed by nearest neighbor analysis, directional distribution (Standard Deviation Ellipse) and cluster analysis (Anselin Moran I) which are used to present uneven distribution of retail shops.

3. Results and Discussion

For analysis purposes, retail shops can be divided into seven main types in Dagon Myothit (North) Township. They are (I) Food and Beverages, (II) Services, (III) Personal Goods, (IV) Building Material Shop, (V) Grocery Shop, (VI) Fabric shop and (VII) Others. (Table 1) The total number of retail shops was 727 in 2018. In survey 2018, study area of 27 wards found in total retail shop is 727 shops**.** It has 39.61 % of shop type I, 22.42% of shop type II, 15.54 % of shop type III, 7.02 % of shop type IV, 4.40 % of shop type V, 3.58 % of shop type VI and 7.43 % of shop type VII respectively. (Table 2, Figure.4) In the study area, largest retail shop type is type I of food and beverages shop. Retail shops are appears to the increasing population within a short span of time. Retailers are consideration of sold to meet the threshold of customer. Customers are

attracted the retail shops location on basis of accessibility of road side area. High accessibility area are enhances retail shops clustering pattern. Therefore, various types of retail shops were concentrated along the Pyi Htaung Su Road, Pin Lon Road, Bo Hmu Ba Htoo Road and U Wizara Road for having high population density and good accessibility. Among the various types of grocery, food and beverages shops, 75% are dynamic type and include such shops as dry goods, Monghinga and quid of betel, etc. Each of them can move and open easily in every suitable place. Therefore, food and beverages shop, and grocery shops are of footloose and hence have dispersed distribution pattern. Majority of the personal goods and fabric shops are found in linear pattern along the Pinlon Road. Building Material shops have both cluster and dispersed patterns. The building material shops selling likes sand and gravel shops are found along the Ngamoeyeik creek. Distribution pattern of services and other shops are somewhere between the clustered and dispersed pattern due to their type of function. For example, car workshop and car spa shops can be found on either side along the road. Some services like mobile phone services and beauty palor can be found in every ward. (Figure. 5)

Table1. Classification of Retail Shops

Type I	Food and Beverages	Tea shop, Coffee shop, beer station, cold and soft drink, liquor house, restaurant, Monhinga ,Shan noodle food, snack shop, chicken fried shop, rice and curry, Thai food etc,
Type II	Services	Beauty Palor, photo studio, photo copy service, clinic, car workshop, car spa service, T.V repairing service, KTV lounge, lottery shop, phone repairing service, purified drinking water service
Type III	Personal Goods Shops	Gold Smith shop, medicine store, cosmetic store, monk'robe and utensils shop, mobile shop, slipper shop
Type IV	Building Material Shop	Brick and sand shop, ceiling plate shop, timber shop, bamboo shop
Type V	Grocery Shop	Rice and edible oil shop, vegetable shop, ngapi and dried fish shop
Type VI	Fabric Shop	Textile shop, fashion shop, clothes shop
Type VII	Others	Furniture house, animal food shops, banner shop, pet shop, microfinance, floral and gift shop

Source: Field Observation (November, 2018)

Table2. Total Number of Retail Shop by Types (2018)

Types	Name	Number	%
I	Food and Beverages	288	39.61
II	Services	163	22.42
III	Personal Goods	113	15.54
IV	Building Materials	51	7.02
V	Grocery	32	4.40
I	Fabric	26	3.58
VII	Others	54	7.43
	Total	727	100

Source: Field Observation (November, 2018)

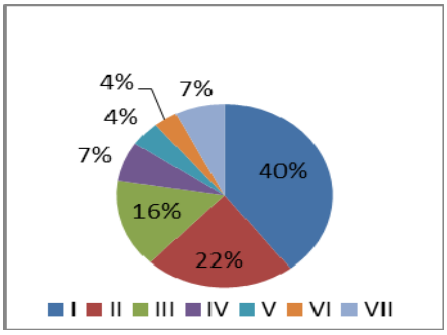

Figure 4. Total Number of Retail Shop by Types (2018)

The nearest neighbor analysis compares the observed average distances between nearest neighboring points and those of a known pattern. This test is required because a point distribution pattern is examined visually whether it is cluster or dispersed or not. It is also explained by computed R scale value. It is difficult to get exact conclusion on clustered or disperse pattern without calculating significant test to accept or reject R value. Therefore, significant test is calculated. The observed average neighbor distance, expected average neighbor distance, nearest neighbor statistics (R), and standardized Z score of the all types of retail shop are calculated to present clustered and dispersed pattern in the study area. According to nearest neighbor statistics, type I, II and III are more clustered than a random pattern since their nearest neighbor value is less than 1. It has been observed that type V is more dispersed pattern then their nearest neighbor value is more than 1. (Table.3)

Table.3 Average Nearest Neighbor Analysis

Types	**Z score**	**P Value Significant Level**	**R value**	**Distribution**
I	-9.037151	0.000000	0.721642	Clustered
II	-5.550311	0.000000	0.772756	Clustered
III	-5.546916	0.000000	0.727239	Clustered
IV	0.671261	0.502054	1.049133	Random
V	1.352297	0.000138	1.352297	Dispersed
VI	0.288505	0.772960	1.029576	Random
VII	0.504186	0.614131	1.035864	Random

Source : Field Survey and NN Analysis

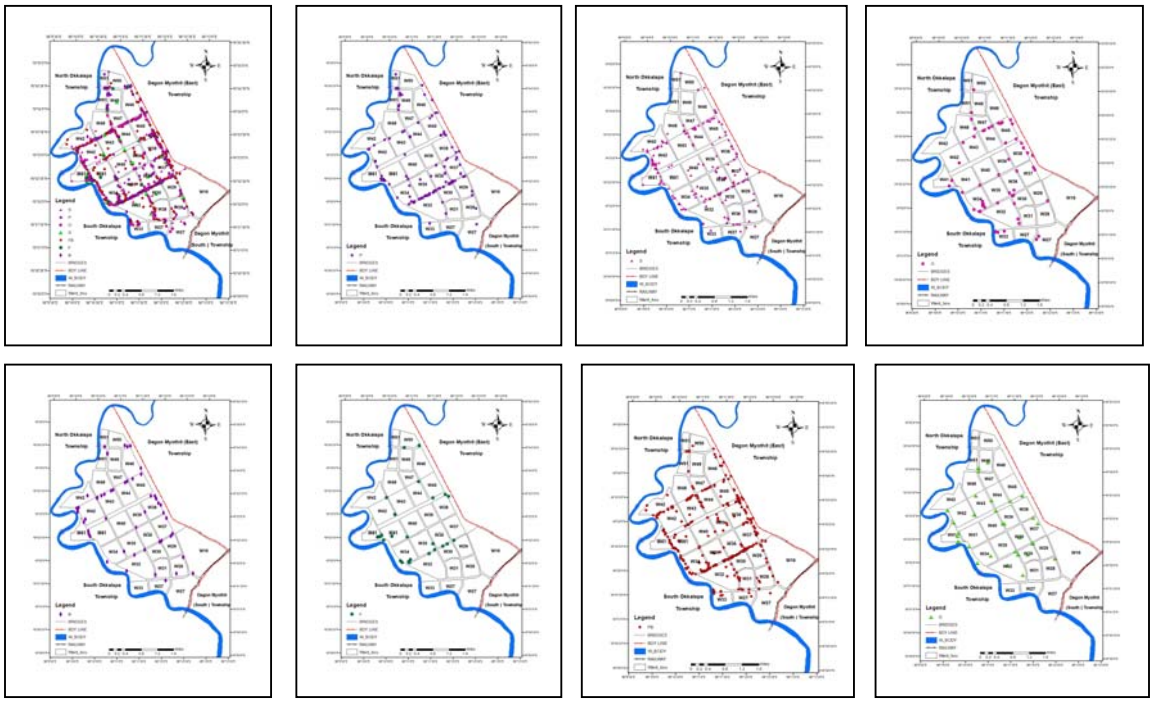

Source: Field Observation (Nov, 2018)

Figure 5. Distribution of Retail Shop by Types in Dagon Myothit (North) Township

Directional Distribution (Standard Deviational Ellipse) measures a distribution of features exhibiting a directional trend. Standard Deviational Ellipse provides information on the directional bias of their locations and also indicates the direction of urban growth. (Figure. 6) The most retail shops are found in southeast and northwest of the area. It is caused by situation of Ngamoeyeik Creek serving as northwest and southeast boundary.

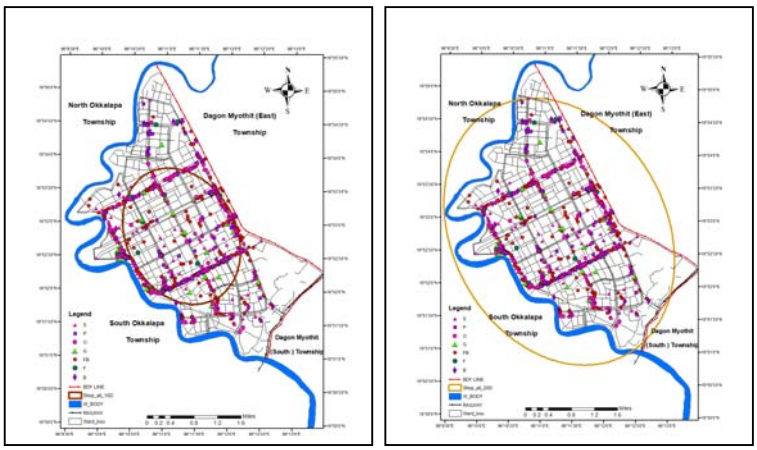

Figure 6. Directional Distribution of All Retail Shop in Dagon Myothit (North) Township

Given a set of weighted features, identifies statistically significant spatial outliers using the Anselin Local Moran's I statistic. Calculates as formula:

$$I = \frac{N\sum_{i=1}^{n}\sum_{j=1}^{n} w_{ij}(x_i - \bar{x})(x_j - \bar{x})}{(\sum_{i=1}^{n}\sum_{j=1}^{n} w_{ij})\sum_{i=1}^{n}(x_i - \bar{x})^2}$$

Where:

N is the number of observations (points or polygons)

Xi is the variable value at a particular location

Xj is the variable value at another location

Wij is a weight indexing location of i relative to j

The most common measure of Spatial Auto Correlation is used for points or polygons. It joins Count Statistic only for polygons. Use for a continuous variable (any value) and join count statistic only for binary variable (1,0)

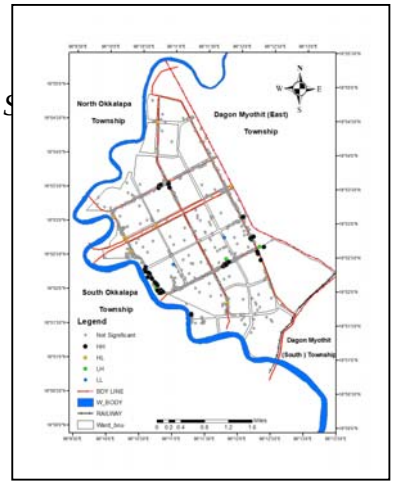

Figure 7. Anselin Local Moran's I Analysis of All Retail Shops

Table.4 Anselin Local Moran's I Analysis of All Retail

Group	Value	Number	Workers
1	HH	50	10-30
2	HL	8	5-10
3	LH	5	3-5

HH=High cluster, High Value

HL=High Cluster, Low Value

LH=Low Cluster, High Value

4. Conclusion

This paper analyzes the retail site location in Dagon Myothit (North) Township by using data obtain from Township Administrative Department and Yangon City Development Committee. To find out the relationship between retail shop and urban infrastructure like main road, Nearest Neighbor Analysis, Directional Distribution and Anselin Local Moran's I Analysis are used. According to the nearest neighbor analysis result is type I, II, III more cluster than the type V, VI and VII. As a result of directional distribution (standard deviation ellipse) of all type of 27 wards northwest and southeast direction are similar to the settlement expansion pattern and road pattern. Result of Cluster and Outlier Analysis (Anselin Local Moran's I) – U Wizara Road, Pinlon Road and Bo Hmu Ba Htoo road are high cluster value of total retail shops in Dagon Myothit (North)Township. (Z score 7.14 & P value 0.00). As a result, retail shop distribution pattern are related to the population density, road network expansion and settlement expansion

pattern. According to geospatial statistics analysis, the large numbers of retail shops are situated at both sides of main road. It shows that transportation roads really have an effect on development of retail shops in this area. Therefore retail site location, shops distribution pattern and trend are indicate the urban development processes.

Acknowledgements

I would like to express my heartfelt thanks to Professor Dr Htun Ko, Head of the Geography Department, University of Yangon for his kind permission and encouragement do this research paper.

Thanks are due to the respective authorizes Dagon Myothit (North) Township Administrative Department and the responsible persons and local people of Township for their ready help in data collection and willing responses to open talk.

References

[1] Aung Kyaw (2006):Spatial Structure of Retail Shops in Loikaw Town, Journal of Myanmar Art & Science, 2006 Vol IV, No 6 (ii)

[2] Khin Khin Htay (2015): Geostatistical Analysis on Retail shops Distribution of 13 wards and Bardo Village in Loikaw Township, Departmental Research Paper, Department of Geography, Loikaw University

[3] Lee,J. and Wong,D.W.S.(2000): Statistical Analysis with Arc View GIS. John Wiley & Son,Inc.New York

[4] Ye Wint Htut (2009): Retail Markets in Dagon Myothit (North) Township, Unpublished MRes: Paper, Submitted to the Department of Geography, Dagon University

Geospatial Analysis of Solid Waste Management in Bago City, Myanmar

Khin Khin Htay[1], Khin Mi Mi Win[2], KhinKhin Han[3], Zaw Zaw[4]

Abstract

Solid waste management of the study area is one of the basic factor to urban development planning of an area because of municipal solid waste is related the systematically collected system. This study only concerns with the urban area covering Bago City which has solid waste collection system and solid waste dump site area in the study area. The primary objective of this study is to practically apply geostatistics tools that can help to improve an evaluation of municipal solid waste for a particular area. A set of geostatistics tools has been applied to the different real data sets which were collected of solid waste form as household, market, commerce, hotel, garden and other waste. There are different methods of data analyses use in this study, which include: (1) spatial source of solid waste, (2) spatial solid waste collection systems, (3) Extend sustainable management of solid wastes, (4) Exploratory Geostatistical Data Analysis. As a result of spatial waste collection system in Bago city and spatial variation dump sites. Conclusion and recommendation of this paper are spatial management of municipal solid collected and sustainability of waste management, encourage people to think about the reduce, reuse and recycle, increase awareness raising the waste management system.

Keywords: Geospatial, Geostatistics, Municipal solid waste, Sustainable

1. Introduction

Solid waste is the useless, unwanted and discarded material resulting from day to day activities in the community. It is widespread problem in both urban and rural areas in many developed and developing countries. Solid waste management may be defined as the discipline associated with the control of generation, storage, collection, transfer, processing and disposal of solid waste. The present paper based on the study carried out on solid waste management practice in Bago City in Myanmar. Bago city is the economic development of lower Myanmar, located between 17° 14′13.59″ North latitude and 17°21′35.56″, between 96°26′15.15″ and 96°30′59.46″ East longitudes. This study was also designed and managing waste sustainably to study the composition of solid waste in Bago city. Municipal solid waste (MSW) collection and disposal is one of the major problems of urban environment in most countries worldwide today. Municipal solid waste management (MSW) solutions must be financially sustainable, technically feasible, socially, legally acceptable and environmentally friendly. Current Municipal Solid Waste Management (MSWM) system in the city of Bago is open dumping system and challenges are insufficient monitoring system, lack of people awareness, law enforcement and lack of research development facilities. In this situation, it is important to understand the current potential of environmental impact of current system in order to set up the new effective management system. Bago City has the 31 wards and central part of the city across the Yangon-Mandalay highway road. There are 53217houses in Bago city and the total population is 222309 in 2018. The average annual rainfall is 285.1 mm in 2018. In this paper, study on the geospatial analysis of municipal solid waste management and sustainable development of solid waste management system in Bago City.

[1] Dr. Associate Professor, Department of Geography, Bago University, Myanmar, kkhinhtay.geog@gmail.com
[2] Department of Geography, University of Yangon, Myanmar, khinmimimwingeog@gmail.com
[3] Professor and Head, Department of Geography, West Yangon University, Myanmar, drkhinkhinhan2013@gmail.com
[4] Assistant Lecturer, Department of Geography, Bago University, Myanmar, Zinlay23837@gmail.com

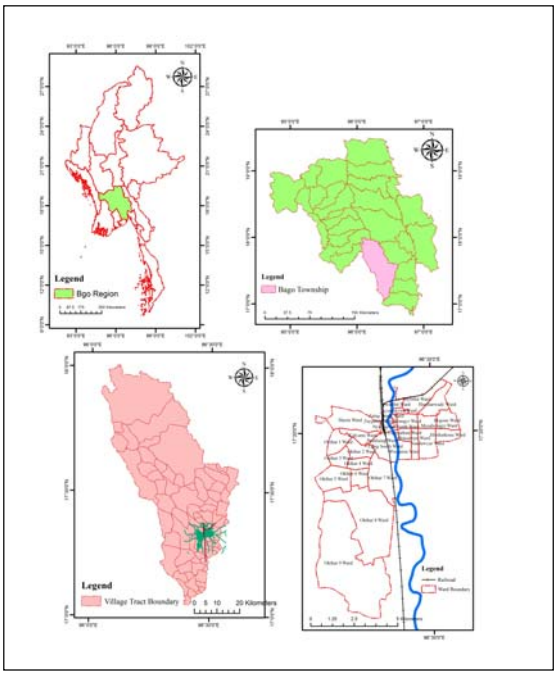

Figure 1. Location of the Study Area

Source: Based on Topographic Map (1:50000) and Google Earth Images (2017)

2. Methods

Garbage truck location data, waste collect sites data and waste collection routes data from Bago City Development Committee (BCDC) and field surveys in 2019. Methodology uses of this paper are geostatistical data analysis of the measures of Incremental spatial autocorrelation and others relevant statistical methods.

3. Results and Discussion

Solid waste can be classified into different types depending on their sources: These are (1) Municipal Solid Waste (MSW), (2) Hazardous Wastes, (3) Industrial Wastes, (4) Agricultural Wastes, (5) Bio-Medical Wastes and (6) Waste Minimization.

In this paper, examine the Municipal Solid Waste Management of the Bago City area. Municipal solid waste (MSW) management solutions must be financially sustainable, technically feasible, socially, legally acceptable and environmentally friendly. Solid waste management issue is the biggest challenge to the authorities of both small and large cities'. Municipal solid waste includes ash generated in thermal or electric power plants, sludge from wastewater treatment plants, animals' farm waste and gangue rocks from mineral extraction.

The activities associated with the management of municipal solid waste from the point of generation to final disposal can be grouped into the six functional elements. These are Waste generation, Storage, Collection, Transportation, Segregation & Processing, and Disposal. These municipal solid wastes including household kitchen waste as well as the domestic food waste from restaurants and markets consist of high lignocellulose materials that could be decomposed and exploited to produce valuable bio-products.

Solid waste management issue is the biggest challenge to the authorities of both small and large cities. Total solid waste generation is 84 tons /day in Bago city. From that solid waste

generation per person is approximately 200 gm/capita/day. Solid waste collection system are three time per day, first time of the day collected the along the Yangon-Mandalay highway road of garbage truck at 7am to 10 am. Second time of day collected the within the Wards at 10 pm to 12. The third time of day is collected the 1 pm to 3 pm. But, collected of car routes are distribute the whole wards except the Okkthar (9) Ward the southern part of City.

Plate 1. Solid Waste collection Sites in Bago City *Source: Field Survey, 2019 August*

Table 1. Sources and Types of Solid Wastes

Source	Typical waste generators	Types of solid wastes
Residential Food	Single and multifamily dwellings	wastes, paper, cardboard, plastics, textiles, eather, yard wastes, wood, glass, metals, shes, special wastes (e.g. bulky items, onsumer electronics, white goods, batteries, il, tires), and household hazardous wastes
Industrial	Light and heavy manufacturing, fabrication, construction sites, power and chemical plants	Housekeeping wastes, packaging, food wastes, construction and demolition materials, hazardous wastes, ashes, special wastes
Commercial	Stores, hotels, restaurants, markets, office buildings, etc.	Paper, cardboard, plastics, wood, food wastes, glass, metals, special wastes, hazardous wastes
Institutional	Schools, hospitals, prisons, government centers	Same as commercial
Construction and demolition	New construction sites, road repair, renovation sites, demolition of buildings	Wood, steel, concrete, dirt, etc.
Municipal services	Street cleaning, landscaping, parks, beaches, other recreational areas, water and wastewater treatment plants	Street sweepings, landscape and tree trimmings, general wastes from parks, beaches, and other recreational area, sludge
Process	Heavy and light manufacturing, refineries, chemical plants, power plants, mineral extraction and processing	Industrial process wastes, scrap materials, off specification products, slag, tailings

Source: World Bank 1999

In the Bago City, the Nearest Neighbour Analysis (NNA) result, garbage truck location pattern is the cluster pattern, Z score values is -6.22 and P value is the 0.000. According to the Nearest Neighbour Analysis (NNA) result, the whole city of garbage site location are near to the

each other's and suited the along the Bago-Yangon highway road and not suited the other parts of the Wards.

Highest population and houses of the Bago City is the Mazin Ward 23124 and 4752 house, Nantawyar Ward as 35076 and 7922 house in 2018 respectively. Mazin Ward is near to the Garbage Truck, Nantawyar Ward is not near the Garbage truck. But collected the waste by car system routes are more the Nantawyar Ward, Ponarsu Ward, Zaypaing, Nyaungwaing-south, Nyaungwaing-north, Zaing-south, Zaing-north, Hintharkone and Bokone Ward. Garbage trucks collected and collected by car of wastes are combined to the site of Sinphyukwin disposal site area. Sinphyukwin disposal site area is only the dump site, not repair the waste.

Plate 2. Classification of Solid waste in Bago City
Source : Bago City Development Committee

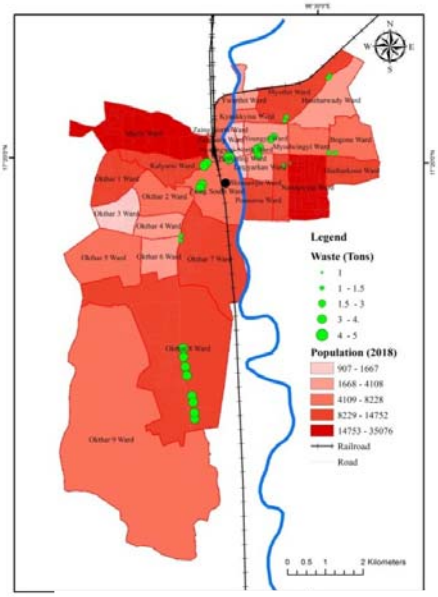

Figure 2. Garbage Truck Location and population in Wards of Bago City
Source : Data from the Bago City Development Committee and Bago Township Administrative

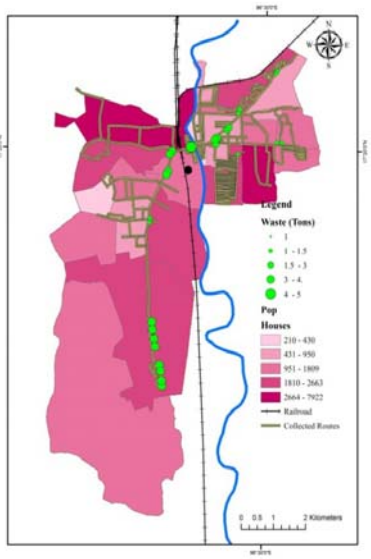

Figure 3. Solid waste collected routes and Houses of Ward in Bago City
Source: Data from the Bago City Development Committee and Bago Township Administrative Office

Measures of Incremental spatial autocorrelation for a series of distances and optionally creates a line graph of those distances and their corresponding z-scores. Z-scores reflect the intensity of spatial clustering, and statistically significant peak z-scores indicate distances where spatial processes promoting clustering are most pronounced. These peak distances are often appropriate values to use for tools with a Distance Band or Distance Radius parameter.

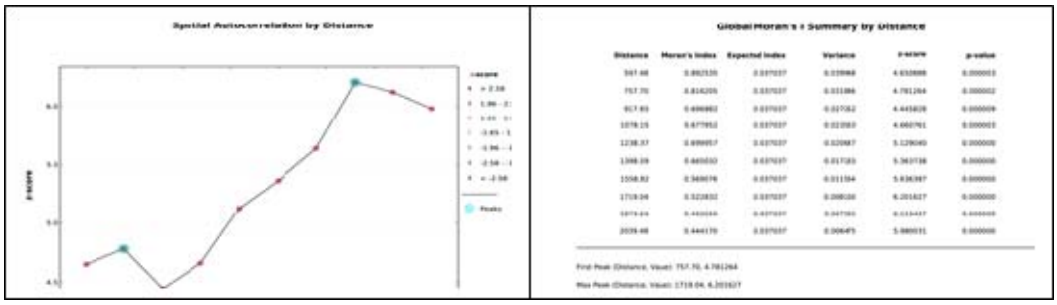

Figure 4. Spatial Autocorrelation by Distance of Garbage Truck Location and Waste tons

Source: Result of the Incremental Spatial Auto correlation

The center of the study area lies between Zaing-south and Shinsawpu Ward which is located the Yangon-Mandalay railroad. All the places of Garbage-truck location are found within the radius of 2100 meter. There are two peaks distance of garbage-truck sites and waste tons within the study area. One peak distance is about 757.70 meter and another is about 1719.04 meter away from the center Figure 5.

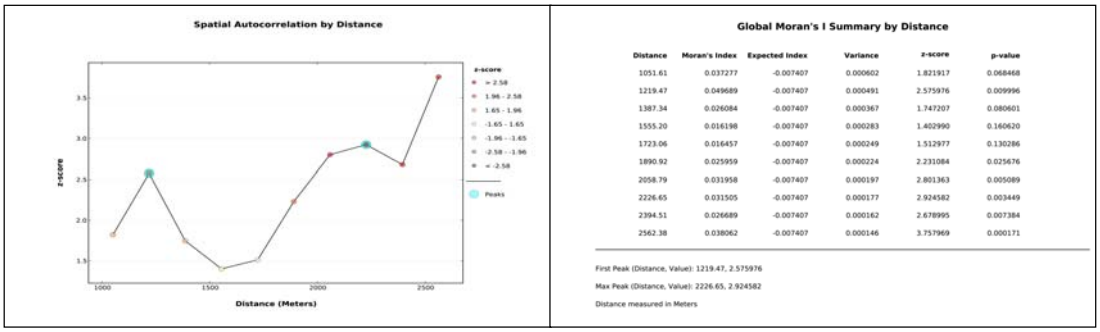

Figure 5. Spatial Autocorrelation by Distance of Solid Waste collected routes and Distance

Source: Result of the Incremental Spatial Auto correlation

The center of the study area lies between Zaing-south and Shinsawpu Ward which is located the Yangon-Mandalay railroad. All the waste collect route location is found within the radius of 2600 meter. There are two peaks distance of garbage-truck sites within the study area. One peak distance is about 1219.97 meter and another is about 2226.65 mete away from the center Figure 5. In 2017, Cooperation of Bago Municipal Development Committee and Green World Energy Co.., Ltd surveyed the waste of City area. In survey, composition Municipal Solid waste were separate of food and garden waste, plastic/rubber, glass, paper, metal, inert and textile. In this survey, food and garden waste is highest collect of 75.87 percent, the second is the plastic/rubber waste is 15.49 percent and the metal waste is lowest collect as 1.78 percent show Figure 6.

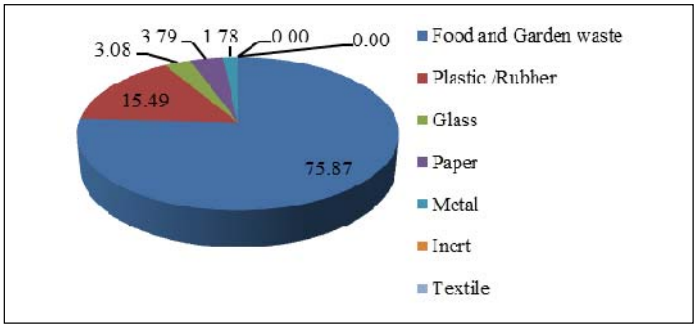

Figure 6. Composition of Municipal Solid Waste in Typical in Bago City Development Committee
Source : Data from Department of Bago Municipal

According to the 2017 survey, Bago Municipal Development Committee has municipal solid collected and sustainability of waste management encourages. It plan will be need the land area about 30 acres. Bago Municipal Development Committee is innovate the people to think about the reduce, reuse, recycle and increase awareness raising the waste management system.

4. Conclusion

The activities associated with the management of municipal solid waste from the point of generation to final disposal can be grouped into the six functional elements. There are Waste generations, Storage, Collection, Transportation, and Segregation & Processing Disposal. In Bago City, BCDC is serves as the waste storage, collection and transportation. The collected data show that the maximum proportion of refuse caused by food and garden wastes, second highest was plastic waste and the third highest was inert material. Percentage of Plastic carry bags was higher, where glass, ceramic and metals were nearly equal with each other in Bago City. As the disposal site is at 6.22 km away the City center and big and smaller vehicle are used for the transportation of solid waste. In Bago City areas: Primary collections are from households and blocks using carts or tricycles. Collectors transport the waste to local depots. Secondary collections use dumper trucks to transport waste from the depots to the disposal sites. Disposal in landfill sites typically 6-8 km from the wards in Bago City. Usually “open dump” sites but there are small engineered landfills in Bago. In the landfill area of advantages are minimizes human contact with the waste, Some potential for energy recovery, no need for separate collections and disadvantages are an expensive solution, more economical at large scale, still some risk of leachate pollution and gas emissions, Sites can be active for many decades, no potential for recycling, leachate and run off a particular problem in the rainy season. Future waste management plan of Bago City, MJT Group of Agricultural Machinery Co., Ltd will start to management of waste. In this project will start to test period at 1.9.2019 to 31.9 2019 the Leikpyarkan, Shinsawpu and Bokone Wards area. It should be done throughout the year. MJT Group plan will collected plastic waste and after renew of plastic seeds and others will make the bio-fertilize. System should be based on Environmental protection rules (reduce, recycle, reuse and recover) Public awareness, political will and public participation as essential for the successful implementation of the legal provisions and to have an integrated approach towards sustainable management of municipal solid wastes. There should be sufficient health and safety provisions for workers at all stages of waste handling. Finally, understand the amounts and composition of solid waste produced in Bago City. Appreciate Myanmar’s waste management

policy and plans. Understand the concept of "stakeholders". Identify the stakeholders involved in waste management in Myanmar people.

Acknowledgements

We would like to express our thanks to Dr Aye Aye Tun, Rector, Bago University for her permission and advice. And then our thanks are also due to Dr Yin Yin Than, Pro-Rector, Bago University for her encouragement and suggestion. I also thanks to Dr Mar Mar Khin, Professor and Head, Department of Geography, Bago University for their suggestion. Moreover, we are greatly thanks to local people in Bago Region and all teachers of Geography Department, Bago University for their help to get the data and conducted field survey.

References

[1] Ashish R et.al, Solid Waste Management – Case Study, International Journal of Research in Advent, Technology, Volume 2, Issues 1, January 2014.

[2] Kurian Joseph, Perspectives of solid waste management in India, International Symposium on the Technology and Management of the Treatment & Reuse of The Municipal Solid Waste, Shanghai, China, 2002.

[3] Hussein Abdel-Shafy, Solid waste issue: Sources, composition, disposal, recycling, and valorization, Egyptian, Journal of Petroleum- 27 (2018) 1275–1290, 2018.

[4] Gaurav K. Singh, Kunal Gupta, and Shashank Chaudhary, Solid Waste Management: Its Sources, Collection, Transportation and Recycling, International Journal of Environmental Science and Development, Vol. 5, No. 4, August 2014.

[5]Mainstreaming Integrated Solid Waste Management in Asia - Solid Waste Management Team, Integrated Solid Waste Management Plan Mandalay, Mainstreaming Integrated Solid Waste Management in Asia, 2016.

[6]Tin Min Htoo, Yoshiro HIGANO, The Environmental Impact Assessment of Current Municipal Waste Management System in Yangon City, Myanmar, Research Paper, 2016

[7]Frank Kreith, Hand Book on Solid Waste Management, The McGraw- Hill Companies, Inc. All rights reserved, Manufactured in the United States of America, 0-07-135623-1, 2002

[8]Bago City Development Committee and Green World Energy C., Ltd, Statistical Analysis Report of Solid Waste management in Bago City, Bago City Development Committee, 2017

Establishment of Sustainable Port Criteria in Myanmar

Mee Mee Soe[1], Min Han Htet[2], Khin Nawarat[3]

Abstract

Moving towards a sustainable port is a balance between the socio-economic development and protection of ecosystems. This paper attempts to establish the appropriate criteria to develop a standard for the sustainable port in Myanmar. It is based on the concrete literature reviews of sustainable principles not only from the Asia but also from all over the world for port development. After that, data collection and analysis step is performed to point out the current situations and challenges of port sector intended for sustainable future in Myanmar. Interviewing with the government agency like Port Authority and stakeholders are comprised to collect the data. Based on these local challenges facing in port industry, opinions from government authorities and stakeholders in combination with the reviews on sustainability principles, the criteria for a sustainable port which is the most promising for Myanmar are established.

Keywords: Challenges in port sector, Sustainable port criteria, Myanmar ports

1. Introduction

Sustainability is "Meeting the needs of the present without compromising the ability of future generations to meet their own needs" by Brundland Report [1]. Sustainability concept consists of environmental, economic and social dimensions and these three dimensions also referred as the triple bottom line of sustainability [2]. Ports are very complicated and combined activities of various services which have a wide range of environmental issues such as water releases, harmful emissions, waste and noise production and pollution [3, 4]. Seaports are notorious to be serious polluting industry; however, they have many opportunities for reducing emissions and pollutions [5]. Sustainability in the port industry is of growing source of fear for port authorities, policy makers, port users and local communities [6]. Therefore, sustainability is one of the important concepts for port industry and implementation of sustainable port development which satisfy economic, environmental and social dimension are intension of current and future generation. To achieve this intension, there are no exact determinations of sustainable port development criteria. To fulfil this gas in the literature, the present study aim to contribute the sustainable port criteria by analyzing the published databases in the literatures and by enquiring some experts and scholars from port related industry.

2. Literature Review

2.1 Sustainable Development – Shipping

Shipping operations interact with environment in many ways, either accidently or intentionally (Talley, 2006a) [7]. Heaver, (2006 b) reported such interactions of shipping operation with environment are generating substantial damages to natural habitats and affecting

[1] Dr, Lecturer, Department of Port and Harbour Engineering, Myanmar Maritime University, meemeesoe@gmail.com
[2] Dr Associate Professor, Department of Marine Engineering, Myanmar Maritime University, mhhtet79@gmail.com
[3] Teaching Assistant, Department of Port and Harbour Engineering, Myanmar Maritime University, khinnawarat.ph.mmu@gmail.com

maritime related economic activities such as ports[8]. Gupta et al. (2005c) studied that the environment is suffering from oil and chemical spills from ships [9]. In these aspects, Yang et al., 2013 suggested shipping firms are increasingly expected to adopt green practices to their system and process that promise environmentally friendly to the international community [10]. Cheng and Tsai (2009 a) also stated that it is a challenge for shipping firms how to perform shipping operations profitably with reducing their negative impacts on the environment [11].

The environmental impact on water quality and atmospheric pollution caused from ship operations were studied by several authors. Frankel (1987 b) included the impact of ballast water on port design and development plan [12]. Maritime operations such as bunkering may cause oil spill risks with potentially terrible impacts on beaches, food chains, sediment and fishing communities (Edoho, 2008; Idemudia and Ite, 2006c)[13,14]. Backhurst and Cole, (2000) concluded that ship operations such as anchoring may damage irreplaceable environments [15]. Gupta et al. (2005) studied various environmental impacts on surface water quality caused by ship and port discharges such as sewage, bilge, sludge, waste, oil discharges and leakages of harmful materials [9].

The emission from ships would affect the air quality in the port and surrounding areas. Zonn (2005b) studied the environmental pollution such as NOx, carbon dioxide (CO_2), sulfur dioxide (SO_2) emission caused by shipping, ports and terminals [16]. It is reported that containerships are by far the most important source of CO_2 emissions in the shipping industry (Psaraftis and Kontovas, 2009b) [17]. Walsh and Bows (2012b) studied the correlation between ship emissions and size as well as ship type [18].

Table 1 . Typical Survey Form which identify the Challenges by Activities with the important level to do the sustainable port development

(for one of challenges: Air Pollution/ Quality (emission of NO_x, SO_x, Black Carbon, PM, VOC's, etc.))

Air Pollution/ Quality (emission of NOx, SOx, Black Carbon, PM, VOC's, etc.)		Important Level				
		I	II	III	IV	V
1	By Land Use	☐	☐	☐	☐	☐
2	By Hinterland Connectivity	☐	☐	☐	☐	☐
3	By Port Structure & Port Construction	☐	☐	☐	☐	☐
4	By Shipping Vessels	☐	☐	☐	☐	☐
5	By Port Vessels	☐	☐	☐	☐	☐
6	By Port Operations	☐	☐	☐	☐	☐
7	By Cargo Handling Equipments	☐	☐	☐	☐	☐
8	By Land Traffic (Truck, Cars, etc.)	☐	☐	☐	☐	☐
9	By Bunkering	☐	☐	☐	☐	☐

Air Pollution/ Quality (emission of NOx, SOx, Black Carbon, PM, VOC's, etc.)		Important Level				
		I	II	III	IV	V
10	By Dredging	☐	☐	☐	☐	☐
11	By Fisheries	☐	☐	☐	☐	☐
12	By Recreation and Tourism	☐	☐	☐	☐	☐
13	By Cargo Storage	☐	☐	☐	☐	☐
14	By Oil and Chemical Spill	☐	☐	☐	☐	☐
15	By Ballast Water Disposal	☐	☐	☐	☐	☐

2.2 Sustainable Development – Port

Ports are considered responsible for a wider set of impacts and seek to resolve short-term views, private and public interests, and commercial and social objectives (Dooms et al., 2012c) [19]. However, (Acciaro et al., 2014a; Dinwoodie et al., 2012d) reported that port activities have adverse consequences on the environment effects [20, 21]. Puig et al., 2014b indicated that port activities would facilitate commercial and economic growth, but also likely cause deterioration of air and marine water quality in the surrounding [22]. In the year of 2015b, Wang et al., investigated port energy efficiency with financial success. They reported a framework of assessing energy efficiency of port operations on the data from public and data base. [23].

Port authorities and administration have to perform sustainable port in a satisfactory of economic demands, environmental and social activities. Daamen's (2007a) investigate port sustainable development in two different geographies to find a new typology and new interpretation of the contemporary port-city interface [24]. Abood K. A. (2007b) made a sustainability framework of New York Port with eight port operational topics such as dredging, ballast water, habitat restoration, air quality, water/energy/material conservation and waste handling [25]. In (2012e) Lam and Van de Voorde made a gap analysis for ports to formulate the concept of green and sustainable port strategy [26]. Jonathan et al. (2014b) propose a sustainable port planning model with the aid of basics of sustainability [27]. Hosseini et al. (2014c) investigated to 381 people to acquire urban sustainable development from citizens' rights point and determined most and least effected identifiers on sustainable port-city development [28]. Kutkaitis et al. (2014d) conducted interviews with practitioners of port and logistics sector to identify the criteria of sustainable port development. Hence, they prepared a set of indicators that determine different levels of sustainability of ports [29]. The decision making process of port authority using the literature review method is suggested by Martino, 2014e [30]. In Roh et al. (2016b) conducted in-depth interviews with Asian port authorities to determine the main factors that shaping sustainable port development. As a result, they identified key elements of sustainable port development from port authorities' perspective [31].

3. Method and Methodology

In this study, proposed indicators of sustainability are air pollution, water pollution, soil pollution, sediment pollution, waste, hazardous waste, noise, habitats loss and so on. The values

and limitations of those indicators have not been measured currently and have not been found in detail in the literatures. Moreover, there is a need to collect in-depth information on people's opinions, particular idea, experiences, desire, and so on. In this regards, a qualitative research technique such as structured-interview- research- methodology was conducted as a data collection (Boyce, C. and Neale, P., 2006d) [32]. For a structured interview, a set of standard, predetermined questions/survey forms are prepared for particular topics in specific orders. For the calculation of weighted values, very high important (I), high important (II), medium important (III), low important (IV) and no important (V) are set up as 5,4,3,2 and 1, respectively. For the interviews, the experts and scholars from port related industry such as Hohai University, Shanghai Maritime University, Myanmar Maritime University, Myanma Port Authority, and Department of Marine Administration in Myanmar have been asked through email using the predetermined survey forms.

4. Results and Discussions

4.1 Current Situations and Challenges

By doing the concrete literature review and discussion with the experiences of port and sustainable fields, the challenges for sustainable port development and port activities which make the challenge can be presented as shown in Table 1. By using this survey form, the opinions can be collected via emails. And then the survey data are weighted and the analysis results of important levels are organized in Table 2. This table can be easily observed by using color cells. Since water pollution/ quality by oil and chemical shows 100% in the color table, it can be clearly assumed that this challenge is the most important one to be performed in achieving the desired sustainable purposes.

The following factors are pointing out the percentage of above 80 percent. Land use, hinterland connectivity, land traffic, oil and chemical spills are the main causes of Air pollution/ quality. The three activities that causes water pollution are land use, dredging and ballast water disposal activities. The activities that causes soil pollution/ contamination are land use, hinterland connectivity and oil and chemical spills. Sediment pollution/ contamination is caused by land use and dredging activities. Waste is formed mainly by land use activities. Hazardous waste is mainly resulted from oil and chemical spills. Noise and higher energy consumption are the results of port structures construction. Land use, hinterland connectivity and land traffic causes traffic congestion. Port structures and dredging causes sedimentation in the vicinity of the port. Land use, hinterland connectivity, oil and chemical spills, ballast water disposal are the main reasons for habitat loss of marine organisms. The challenges concerning with the above mentioned activities are the second important challenges to be performed to achieve sustainable purposes.

The following activities can be performed and solved by taking time since they are 60 to 80 weighted activities. Noise and energy consumption caused by land use and sedimentation/ erosion problems are the activities which are necessary to take actions. Waste and noise resulted from hinterland connectivity should be take into account to meet the sustainable requirements. Air, water, soil and sediment pollution, waste, traffic congestion, erosion and habitat loss caused by type of port structures and construction should be considered to reduce the sustainably against situations. Air and water pollution, various waste, noise and energy consumptions are mainly caused by shipping vessels. And also, air and water pollution, hazardous waste, noise and energy consumption are caused by port vessels. Moreover, air pollution, waste, hazardous waste, noise, energy consumption and traffic congestion are mainly caused by port operations.

The challenges caused by Cargo handling equipment, land traffic, bunkering, dredging , fishery, recreation and tourism, cargo storage, oil and chemical spills, ballast water disposal etc. can be observed in the following color map according to their important level as shown in Table 2.

Table 2. Results of Important level of Activities and Challenges Relationship for Sustainable Port Development

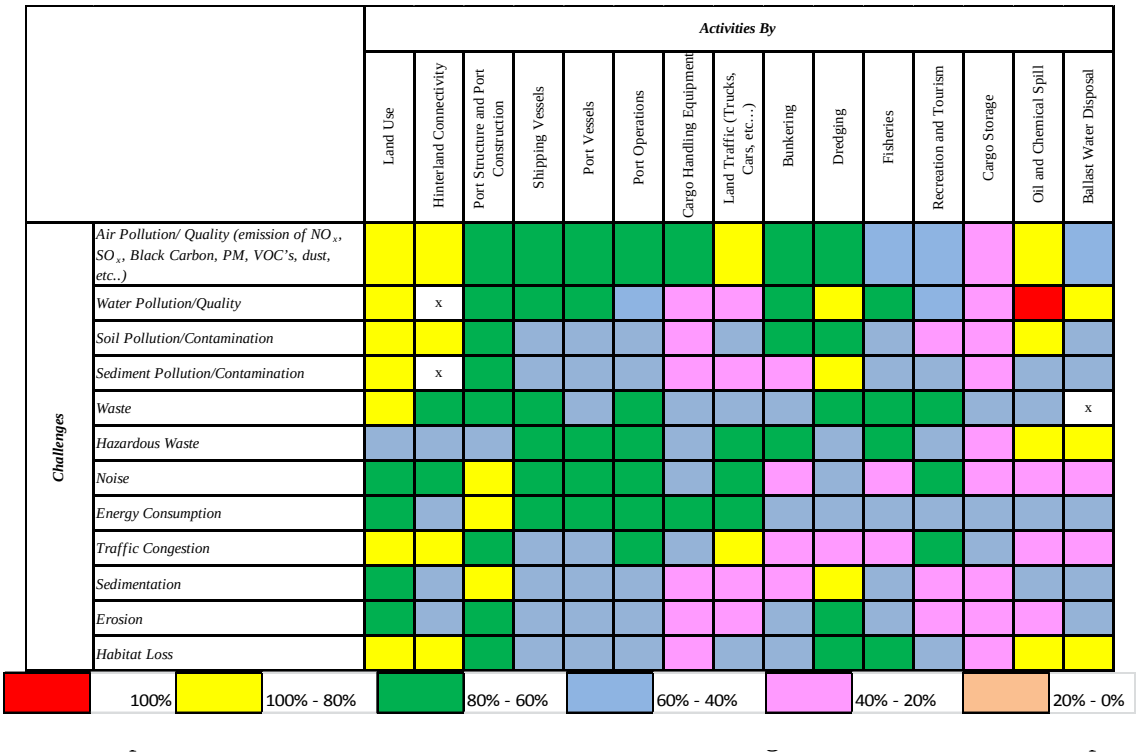

4.2 Sustainable Criteria For Myanmar Port Development

Proposed sustainable criteria based on the review of the guidelines of international ports and the analysis of the port operation experience and challenges with Local Port Authority and stakeholders are listed as follows:

Land use mainly causes pollution and waste. It can also happen traffic congestion, energy consumption, noise, and habitat loss. Effectiveness of existing ports should be promoted with the sustainable practices instead of building a new one. If a new port has to be propose in order to meet the country requirement, a well-made feasibility study should be prepared to choose the location which is the least environmental damage one. Public space and habitat conservation desire should be added in port area planning for the health, recreation and the nature. Port stakeholders' meeting should be held with well-prepared port master plan to decide the land use and local people participation should also be emphasized.

Mode of transport connecting the ports with industrial zone, downtown area and other hubs, etc. should be carefully analyzed in order to avoid the traffic congestion. Transport connectivity plan is vitally needed with the suitable mode of transport. Especially rail transport

network should be arranged with the collaboration of related sectors. So that, the consequences such as time-consuming, feel tired, fuel energy loss and risk of accidents between containers, regular-size cars, slow moving vehicles and people, etc. of uncomfortable transport system can be avoided. Furthermore, Myanmar's inland waterways should be more encouraged doing the investment for cargo and container transportation. This method is cost-effective and it can be reduced the traffic congestion and energy consumption. For the existing ports, current transportation network should be requested to submit and if necessary, appropriate modifications for better network should be done under the charge of the government with the full effort of port owners.

Erosion and sedimentation conditions in water area caused by existing jetty and port structures should be analyzed and informed to the corresponding authorized body. Also the proposed solution to these observed problems should be attached during the inform process. Erosion and sedimentation estimation must be perform before constructing a new structure. The technologies and designs which coincide best to the sustainable requirements should be used during the whole construction process. Sustainable codes for design and construction are also necessary to establish.

Shipping and port vessel causes pollution and waste, energy consumption and noise. The type and size of allowable shipping vessels should be according to the international sustainable criteria. The shipping vessels should follow the rules and regulations which are established according to the international standards. Strict monitoring and actions should be taken for the enforcement of rules and regulations.

Noise and air pollution caused by port operation in port area should be assessed by using monitoring devices. The methods using in the port facilities should coincide with the sustainable needs. Renewable resources such as solar, wind and tidal energy should be replaced in the conventional resources. LED technology should be replaced in lighting inside the port area. Light reduction equipment should be used to reduce annoyance to the nearby residential area [33].

In practice, cargo handling equipment consume large amount of energy. Replacing smart and green cargo handling equipment in port operation can not only reduce the energy consumption but also protect the environment and increase the cost efficiency [34].

Air pollution, traffic congestion, noise and energy consumption can be reduced by establishing good driving practices and applying well trained drivers in land traffic.

Transfer procedures among vessels, bunker stations, bunker vessels, terminal and trucks should be well defined and followed to avoid the pollution and hazardous waste.

In Myanmar, the energy consumption for maintenance dredging works is very large. Dredging is also a major issue to be considered in achieving sustainable requirements. To reduce the energy consumption in dredging works, the location of the deep sea ports should be proposed to an area where dredging works are not necessary. Even if necessary, the proposed site should be chosen wisely where the dredged material can be reused. If disposal of dredged material is unavoidable, the disposal site should be analyzed and allocate carefully.

Since fishery can affect health and environment, good management is required in these fishery ports. Good fishing practice and management should be launched for the reduction of waste. Warning and taking action by using severe penalty system can be used to reduce waste

and noise caused by recreation and tourism. Ballast water disposal can cause the habitat loss of marine organisms. Taking actions in enforcing the existing laws can enhance the protection of the species. If oil and chemical spills occurred, air and water pollution and the habitat loss of marine organisms can happened in serious condition. Therefore, the rules and regulations concerning with oil and chemical spills should be establish precisely and accurately. And also even when spills happened, taking action effectively and removing in a very quick manner should be performed to avoid the unnecessary circumstances.

5. Conclusion

In this paper, we have tried to point out the sustainable challenges by port activities intended for Myanmar ports. The literature was concretely reviewed to identify the activities and challenges. And then the important level of challenges was collected with surveying the experiencers and specialist of port and sustainable fields and it can be seen the colour table to analyze easily. . Later this can be done the large scale for sustainable purpose with more activities and challenges. It was found that land use, hinterland connectivity, are the main activities for sustainable challenges and also port structure and construction, dredging, oil and chemical spill, ballast water disposal cause the challenges This paper proposed some sustainable criteria in accordance of challenges of Myanmar ports such as effective land use, Inland water way transport, Ship size and type limitation, enforcement of rules and regulations.

Acknowledgements

This paper is the first step of our proposing the sustainable criteria for Myanmar port sector and we would like to thank Dr. Tao Aifeng, Dr. Mu Mu Han, Dr. Myo Nyein Aye, Mr. Ye Naing for supporting of their valuable experience.

References

[1] Brundtland, G. H., United Nations,1987a.

[2] Sislian, L., Jaegler, A. and Cariou. P., “Research in Transportation Business & Management,”2016a, 19, 19-26.

[3] Hakam, M. H., “Journal of Service science and Management,” 2015a, 8(01), 14.

[4] Darbra, R. M., “Marine pollution bulletin,” 2005, 50.8: 866-874.

[5] Broesterhuizen, E. F. M., Vellinga, T., Docters van Leeuwen, L., Zwakhals, J. W., Taneja, P. and Nijdam, M. Cesun2012, 2012a.

[6] Acciaro, M., Ghiara, H. and Cusano, M.I., Energy Policy, 2014, 71, 4-12.

[7] Talley, W.K., “Port performance: an economic perspective,” in Brooks, M. R. and Cullinane, K. (eds.), Devolution, Port Governance and Port Performance, Amsterdam: Elsevier Ltd., 2006a, pp. 499-516.

[8] Heaver, T., “The evolution and challenges of port economics,” in Brooks, M.R. and Cullinane, K. (eds.), Devolution, Port Governance and Port Performance, Amsterdam: Elsevier Ltd., 2006b, pp. 11-41.

[9] Gupta, A.K., Gupta, S.K. and Patil, R.S., “Environmental management plan for port and harbor”, Clean Technologies and Environmental Policy, 2005a, Vol. 7, No. 2, pp. pp. 133-141.

[10] Yang, C.S., Lu, C.S., Haider, J.J. and Marlow, P.B. , “The effect of green supply chain management on green performance and firm competitiveness in the context of container shipping Taiwan,” Transportation Research Part E, 2013, Vol. 5, pp. 55-73.

[11] Cheng, Y.H. and Tsai, Y.L., "Factors influencing shippers to use multiple country consolidation services in international distribution centers," International Journal of Production Economics, 2009a, Vol. 122, No. 1, pp. 78-88.

[12] Frankel, E.G., Port planning and development, New York: John Wiley & Sons Inc., 1987b.

[13] Edoho, F.M., "Oil transnational corporations: corporate social responsibility and environmental sustainability," Corporate Social Responsibility and Environmental Management, 2008, Vol. 14, No. 4, pp. 210-222.

[14] Idemudia, U. and Ite, U.E., "Corporate-community relations in Nigeria's oil industry: Challenges and imperatives," Corporate Social Responsibility and Environmental Management, 2006c, Vol. 13, No. 4, pp. 194-206.

[15] Backhurst, M.K. and Cole, R.G., "Biological impacts of boating at Kawau Island, north-eastern New Zealand," Journal of Environmental Management, 2000, Vol. 60, No. 3, pp. 239-251.

[16] Zonn, I., "Environmental issues of the Caspian," in Kostianoy, A. and Kosarev, A. (Eds.) The Caspian Sea Environment, Berlin: Springer, 2005b, pp. 223-242.

[17] Psaraftis, H.N. and Kontovas, C.A., "CO2 emission statistics for the world commercial fleet," WMU Journal of Maritime Affairs, 2009b, Vol. 8, No. 1, pp. 1-25.

[18] Walsh, C. and Bows, A., "Size matters: Exploring the importance of vessel characteristics to inform estimates of shipping emissions," Applied Energy, 2012b, Vol. 98, pp. 128-137.

[19] Dooms, M., Verbeke, A. and Haezendonck, E., "Stakeholder management and path dependence in large-scale transport infrastructure development: the port of Antwerp case (1960-2010)," Journal of Transport Geography, 2012c, Vol. 27, pp. 14-25.

[20] Acciaro, M., Vanelslander T., Sys, C., Ferrari, C., Roumboutsos, A., Giulliano, G., Lam, J.S.L. and Kapros, S., "Environmental sustainability in seaports: a framework for successful innovation," Maritime Policy & Management, 2014a, Vol. 41, No. 5, pp. 480-500.

[21] Dinwoodie, J., Truck, S., Knowles, H., Benhin, J. and Sansom, M., "Sustainable development of maritime operations in port," Business Strategy and the Environment, 2012d, Vol. 21(2), p.111-126.

[22] Puig, M., Wooldridge, C. and Darbra, R.M., "Identification and selection of Environmental Performance Indicators for sustainable port development," Marine Pollution Bulletin, 2014b, Vol. 81, No. 1, pp. 124-130.

[23] Wang, H., Huo, D. and Ortiz. J., Open Journal of Social Sciences, 2015b,3(05), 28.

[24] Daamen. T., In ENHR-conference, 2007a,25-28..

[25] Abood, K. A., In Ports 2007: 30 Years of Sharing Ideas: 2007b,1977-2007.

[26] Lam, J. S. L. and E. Van de Voorde. International Forum on Shipping, Ports and Airports (IFSPA), 2012e, 27-30.

[27] Jonathan, Y. C. E., Kader, A. S. A., Bin Ahmad, Z., Mokhtar, I., "Green and sustainable port project planning: paradigm shift for an integrated container handling system expansion,"2014b.

[28] Hosseini, S. A., Amozad, H. and Mafi, M.K., "European Online Journal of Natural and Social Sciences," 2014c, 3(3), 810.

[29] Kutkaitis, A., Šimanskiené, L.and Burgis, D., "Scientific Papers of the University of Pardubice," Series D, Faculty of Economics & Administration, 2014d, 21(30).

[30] De Martino M., "In Advanced Engineering Forum Trans Tech Publications," 2014e, 11, 87-95.

[31] S. Roh, V.V. Thai and Y.D. Wong. The Asian Journal of Shipping and Logistics, 2016b, 32(2), 107-118.

[32] Boyce, C. & Neale, P., "Conducting in-depth Interviews: A Guide for Designing and Conducting In-Depth Interviews", Pathfinder International Tool Series, 2006d.

[33] Dalwon Kang & Sihyun Kim, "Conceptual Model Development of Sustainability Practices: The Case of Port Operations for Collaboration and Governance", December 2017, 9(12):2333

[34] Jasmine Siu Lee Lam, 'Smart and green cargo handling equipment for port sustainable energy management", October 2018

Effective Control of Hybrid Solar-Hydro Renewable Energy System

Wut Hmone Oo [1], Khin Mar Win [2], Hla Htay Win[3]

Abstract

This research presents the control system of prototype hybrid power driven by two sources of renewable energy which purpose is to provide the continuous electrical power using solar-hydro renewable energy system without causing the environmental pollution. The voltage generated from the solar panel and waPter mill will be stored on a large battery by two different modes, real time mode and switching mode. The real time clock module is used to control the real time data from solar phase during the daytime and a hydro phase is used at night. The solar voltage is recognized as the first priority charging mode from 8:00 a.m. to 5:00 p.m. and the hydro charging mode will start working after solar charging time. Since the availability of voltage from solar and water sources depends on the weather condition, the switching mode needs to be manually changed in the hybrid control system. The hybrid system operates only with higher power source by reading the voltage firstly and then switching the voltage given by higher power plant. The system is constructed with a programmable microcontroller development board, voltage divider circuits, real time clock module, a few input switches and charging control circuit.

Keywords: solar energy, hydro power, hybrid control system, renewable energy sources

1. Introduction

Nowadays, pollution is one of the most serious problems in the world. The best way of reducing CO_2 emission is to use clean source of electrical energy produced from renewable energy. Among these renewable sources, hydroelectric power and solar power are the two most common sources for generating electricity for rural areas. However, these energy sources greatly depend on weather conditions and possess inherited intermittent nature. So, hybrid system, one of the complex control systems due to integration of two or more renewable energy, becomes a solution to those limited conditions [1]. The power generation capacity of hybrid system is more than the power generation capacity of the individual system. The major advantage of solar-hydro hybrid energy system is that when used together, reduces the cost of supplying electricity [2]. In solar-hydro hybrid system, solar panel directly converts solar radiation into electrical energy and hydroelectric system is the process of generating electrical energy by converting kinetic energy of water into mechanical work to turn the turbine [3]. This hybrid power system is suitable for remote places. Rural areas need generation in the form of hybrid power system [4].The scope of the hybrid renewable power system is very high and it is very advantageous for both rural and urban areas [5]. In Myanmar, especially in Tanintharyi Region which lies on the southern part of Myanmar in North Latitude 13° and East Longitude 98°45´, fifth largest region in Myanmar, majority of rural areas are still lack of electricity. Therefore, candles and oil lamps are still being used in those areas. The photograph of the map of Tanintharyi Region is expressed in figure 1 and it is the best location for generating renewable energy such as solar energy from sunlight, and hydro power from water resources. As per annual data recorded from regional department of meteorology and hydrology, both the rainfall (inches) and the sunshine hours in Tanintharyi region is the higher and longer than those in other cities in Myanmar. The Monthly maximum

[1] Department of Physics, Dawei University, Myanmar, hmone1390@gmail.com, +959422203725
[2] Engineering Physics Department, Mandalay Technological University, Myanmar, drkhinmarwin@gmail.com
[3] Department of Physics, University of Bago, Myanmar, hlahtayphy2016@gmail.com

rainfall, Average monthly rainfall, monthly maximum sunshine and average monthly maximum sunshine are illustrated in figures 2-5. So, the effective control of hybrid system is one of the main advantages for rural areas in this region and can provide a good solution for those areas, villages nearby the rivers, streams, mountain, waterfall, and under sufficient sunshine. Furthermore, the system can solve the demand of electricity in regional problem successfully.

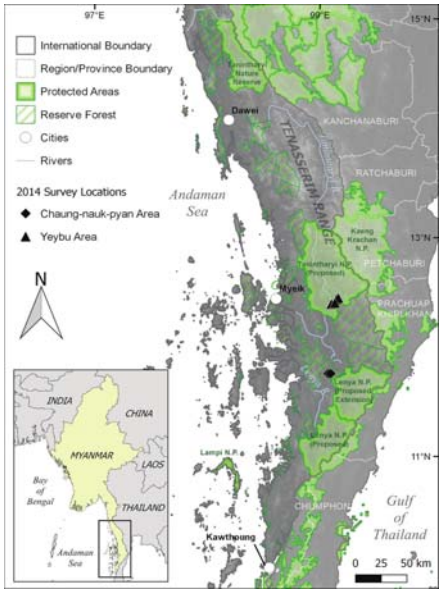

Figure 1. Map of Tanintharyi Region Myanmar [www.researchgate.net]

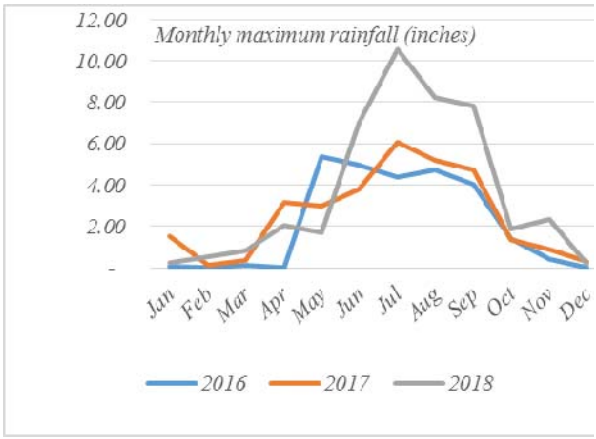

Figure 2. Monthly maximum rainfall

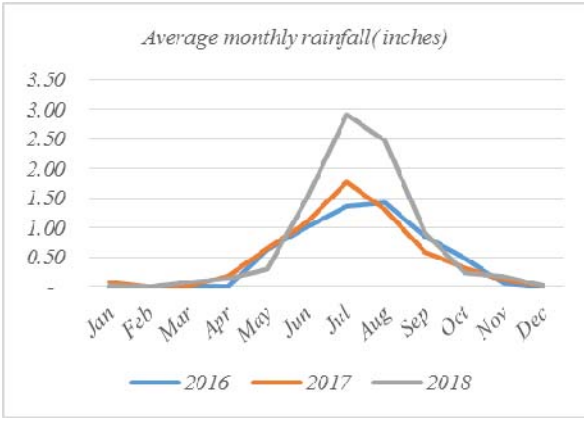

Figure 3. Average monthly rainfall

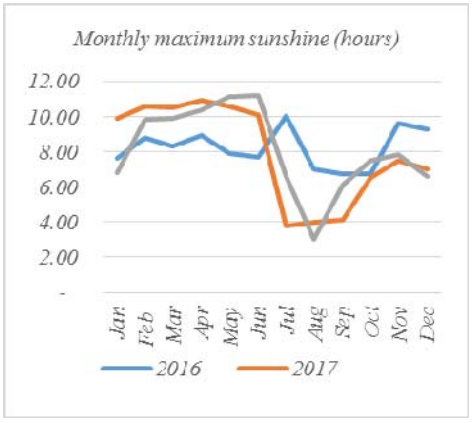

Figure 4. Monthly maximum sunshine

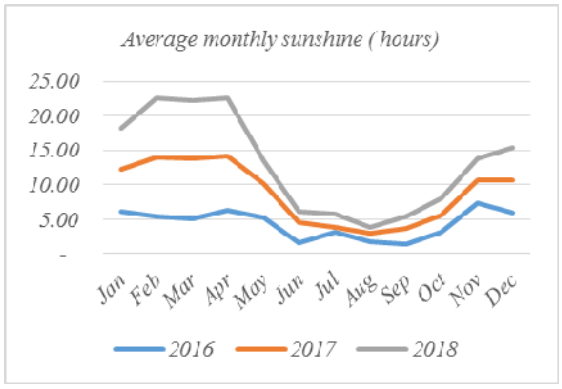

Figure 5. Average monthly maximum sunshine

2. Design and Simulation of Hybrid Power Control System

2.1 Circuit Simulation

The Proteus 8.1 software is a Printed Circuit Board (PCB) design software integrated with the simulation of the circuit design. The main purpose to design with Proteus software is to get the optimum circuit diagram. In this research the circuit design consists of eleven main parts**;** an 8-bit programmable microcontroller (ATmega328p), a crystal oscillator, an alphanumeric liquid crystal LCD display, a few control input switches, a real time clock module, three voltage divider circuits that are used to divide the output voltages of solar plant, hydro plant and storage battery, transistors, relays driver circuits, storage battery, a 5V regulated power supply circuit and a charge controller units. The control system operates together with the two different power plants, charging controller circuit, inverter circuit and storage units. The basic structure of the hybrid system is illustrated with a block diagram in figure 6. The complete schematic diagram of hybrid solar-hydro control system is shown in figure 7.

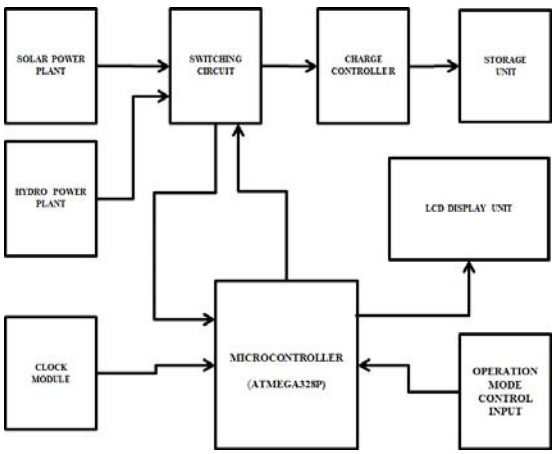

Figure 6. Block diagram of the hybrid solar-hydro power control system

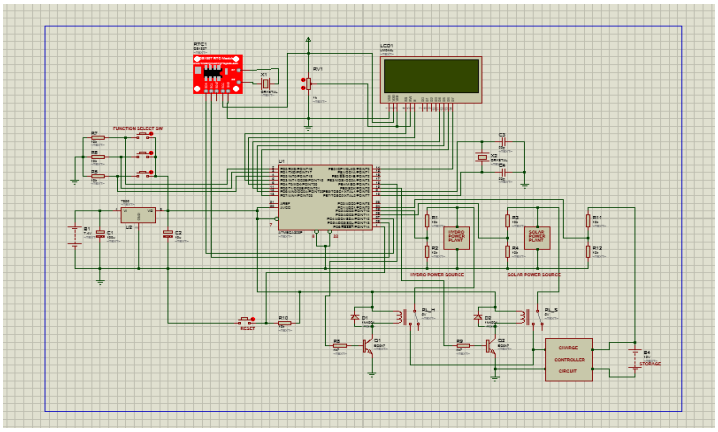

Figure 7. Complete schematic diagram of hybrid power control circuit

2.2 Controller Circuit

The microcontroller is an 8-bit microcontroller and it is Atmega328p. The microcontroller itself cannot operate to run the operation of the circuit; therefore, a program code was created and uploaded into the memory ROM of microcontroller before building the circuit. The program coding was created by using Arduino IDE software. In this circuit design, the program memory in microcontroller cannot execute each instruction without an external clock circuit. In this case, a 16MHz crystal oscillator is connected with the two pins of microcontroller. A real time clock module circuit is included in this circuit design to control the hybrid power system according to the real time data. The real time data can differentiate both day or night and seasonal periods of month within a year. For the experimental process, it is required to create two different circuit boards to complete the prototype design for hybrid power control system since the design of circuit is very complex and consisting of numerous components. The circuits are known as controller circuit and switching circuit. The control circuit consists of four pairs of green terminals, two on the upper edge and other two on the right edge of the circuit. The first terminal on the upper edge is to connect with the solar power plant. The second green terminal is to connect with the hydro power plant. The first green terminal on the right is to connect with battery storage. The second green terminal is to connect with the charge controller circuit. Moreover, there are three voltage divider circuits with three trimmer resistors which are used to divide the voltage of solar power plant, hydro power plant and battery voltages. The control sketch is written in c programming language and the flow chart of the hybrid power control system is as shown in figure 8.

2.3 Switching Circuit

There are two relays and relay driver circuits. Each of the relays cannot be directly operated with a microcontroller since it is a coil device. Therefore, the relays are used to switch the connection between the storage battery and power plants. The common pin of each relays are connected with the solar plant and hydro plant. The normally open pins of relays are connected with the storage battery. There are three control switches on the circuit, and they are wired as active high input switches. They are connected with the three digital pins on the microcontroller. In the moment, only one input switch is used and it is to change the operation mode between real time control (RT CON) and higher voltage control (HV CON). Completely installed and ready to

test circuit board is shown in figure 9 and default operating condition and voltage displays in figure 10.

2.4 Operation of Hybrid Power Control System

The whole circuit will operate with two 3.7V Li-ion batteries. It is not a suitable power supply for the microcontroller and LCD display, real time clock module and relays on the circuit. Therefore, a 5V regulator IC (7805) is utilized to become Vcc voltage level to 5V. When the power supply on/off switch is pressed, the LCD display illuminated the data of clock on the first line. Each voltage level is going to be illuminated on the LCD displays. But the actual maximum input of analog voltage to the microcontroller was limited to 5V. If it is higher than 5V, the microcontroller may damage. Therefore, voltage divider circuits are used in the design. The real time clock function operation is very useful and the system operation can be automatically made by predefined periods. In this design, the default mode operation for hybrid power control system is "RT CON". The operation period predefined for the solar power plant is within a period starting from 8:00 to 17:00 hours. In the display photo as shown in figure the clock is 20 hour, and it is greater than17 hours predefined period, therefore the operation of hydro power plant will be operated. The operation system is predefined for hydro power plant after solar charging time. In this case, the switching on power plant is display on the screen "Hy_P_ON" (hydro power on). If the time is between 8:00 and 17:00, the system will change the solar power plant automatically. In this case, the switching on power plant is display on the screen as "S_P_ON" (solar power on). In switching circuit, voltage divider circuits with blue trimmer resistors are used to divide the input voltages of solar power plant, hydro power plant, and battery voltage terminals.

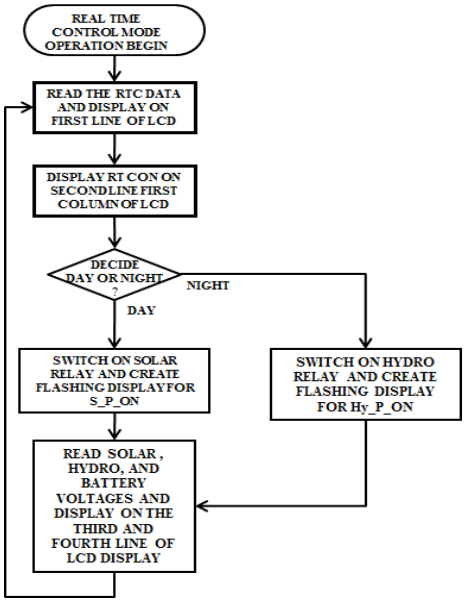

Figure 8. Flow chart of the hybrid power control system

Figure 9. The photograph of the hybrid power control circuit

Figure 10. Default operating condition and voltage display

Figure 11. Calibration of solar power plant voltage

Figure 12. Calibration of hydropower plant voltage

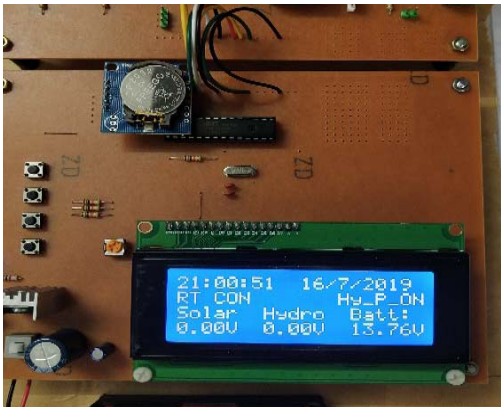

Figure 13. Calibration of storage battery voltage

Figure 14. The selection of operation mode for HV CON

3. Results and Discussion

The solar-hydro hybrid power control system is constructed and the operations have been tested for several times for different results. The hybrid control system is based on ATMEGA328 microcontroller. Moreover, there are two types of relay control pins, relay for hydro power plant and relay for solar power plant. If the power output of solar power plant is higher than input from the other power plant, then the solar relay will operate. If the power output of hydro power plant is higher than input from the other power plant, then the hydro relay will operate. The voltages of each power plant and battery shows 0V, since no power plant and battery are connected on the switching circuit. Therefore, before connecting with any power plants, a variable power supply is

connected instead of solar power plant. Then, the variable power supply is switched on and checks the result display screen on the voltage position of solar power plant. Figure 11 shows the calibration of output solar power voltage plant in hybrid energy system. If the voltage difference between the display of variable power supply and constructed circuit is not equal, it can be adjusted by slowly turning the trimmer resistor with a small flat screw driver. Similarly, the variable power supply is connected on other remaining terminal inputs and calibrated as shown in figure 12 and 13 respectively. The simulation carries out nearly 10 hours between 8:00 and 17:00 hours in a sunny day. In addition, the two power plants are combined with a microcontroller and manage for real time control (RT CON) and higher voltage control (HV CON).So to be able to use effectively higher power source, the manual selection of either “HV CON” from “RT CON” operation mode or “RT CON” from “HV CON” operation mode is required after reading the voltage level. The press of mode switch toggle the two operation mode as shown in figure 14.The availability of the electricity in Tanintharyi Region is only 10.7% and the lowest in Myanmar. According to the results of the proposed research and the above data information shown in the chart, the rainy season is about 6 months and monthly maximum and average rainfall are 10.55 inches and 2.91 inches respectively as shown in figure 2 and figure 3 . Except the rainy period, it is sunny over the course of the year.Monthly maximum and average sunshine are 11.2 hours and 8.48 hours as shown in figure 4 and figure 5.Therefore, the hybrid power control system can be the most suitable hybrid system to solve the lack of electricity and provide continuous power generation in Tanintharyi region especially for rural areas.

4. Conclusions

The use of hybrid power control system is the most effective and efficient ways of generating electrical power. The designed system is intended to reduce the cost of supplying electricity and to solve the power requirement in rural community. Single source system provides discrete power if the source is faced disable conditions. The solar-hydro hybrid system can be used in any region that has the sufficient solar radiation and sufficient kinetic energy of water flow. In such region, the condition of solar power and hydro power will be power complement of each other when the seasonal and variations of the weather condition occur. According to the annual results of weather station of Tanintharyi region figures 2-5, solar-hydro hybrid system should be used rather than other renewable energy generating system. Hybrid system will be able to provide the continuous power generating processes along the coastal region and for sustainable development. Although the system designed is made to be flawless, sudden unexpected changes on weather conditions may arise problem states. But the causes of problem state are negligible comparing with its overall advantages.

Acknowledgements

I would like to express my profound thanks to Professor Dr San San Aye, Head of Department of Physics, and Professor Dr Khin Swe Oo, Department of Physics, Dawei University, for their kind permission to carry out this work. Special thanks are Dr Thiri Khin, Lecturer, Department of Physics, Dawei University, for encouragement and help during this work.

References

Binayak Bhandari, Shiva Raj Poudel, Kyung-Tae. Lee, and Sung-Hoon Ahn, "Mathematical modeling of hybrid renewable energy system: A review on small hydro-solar wind power generation", 2014, Vol.1, pp.157-173.

Bhushan. D. Agarkar and Shivprakash B. Brave, "A review on hybrid solar/ wind/hydro power generation system", 2016, vol.4, pp.188-191.

G. Joga Rao and S.K Shrivastava, "Modeling and implementation of hybrid solar-hydro renewable energy systems", 2016, Vol.3, pp.63-69.

G.Lakshmi,P.V.V. Rama rao, Y.R. Palleswari,"Power Management of Hybrid Renewable Energy System by Frequency Deviation Control",2014,Vol.10,pp.243-251.

Diksha.A. Shinde, "Power quality improvement by solar –hydro hybrid system", 2016, (IJIRST), Vol.3, pp-234-236.

Kavitha Sirasain and S.Y. Kamdi, "Solar wind hydro hybrid energy system simulation", 2013, (IJSCE) Vol.2, pp.500-503.

B.Murali Mohan, S. Muqthiar Ali and P.Manohar, "Designing and control of isolated wind-hydro hybrid system with BEES", 2014, Vol.10, pp.64-70.

Hassan Moghbelli, Hamid Toliyat, Haitham Abu-Rub, "A green hybrid power plant using photovoltaic and wind energy with power quality improvement in Qatar",2011, American Society for Engineering Education, pp-2-14.

Source: MOEE web site: http://www.moee.gov.mm/en/ignite/page/80)

Applying High Performance Seismic Structures to All Asian Countries

Tsutomu Komuro[1], Yozo Shinozaki [2] and Akira Wada[3]

Abstract

In 1868, Japan began importing science and technology from Europe and the USA, which have little experience with severe earthquake disasters. This was the beginning of great changes in Japan's civilization, culture and politics. Over time, vast cities with tremendous numbers of buildings, such as Tokyo, Osaka and Nagoya, became the centers of modern Japanese life. Although Japanese society has always been concerned about earthquakes, people focused more on economic growth during the modernization process than on protecting mega-cities from possible natural disasters. Other Asian countries also have a similar pattern of development.Seismic design codes focus on saving human life, not only in Japan but also in other Asian countries, the USA and some European countries. Regulations generally allow for plastic deformation of building structures in large earthquakes. Under such design standards, it is not necessary to ensure that buildings can continue being used after a major earthquake. However, if too many buildings – governmental, office, factory and residential – become unusable in an earthquake, a city cannot survive and certainly cannot be described as resilient. As society becomes more dense, high-potential and excessively rational, we must develop more reliable structures using current technologies of seismic isolation and passive earthquake control. We would like to introduce some beautiful new buildings constructed with high-performance seismic structural systems to other Asian countries and for Sustainable Development Goals (SDGs).

Keywords: Seismic Design, Human life, Business Continuity, Seismic Isolation, Response Control

1. Introduction

Through the experience of earthquakes over history, the seismic design sections of Japan's building standards law have been continually revised. A new seismic design method enforced in 1981 is the current design code. The basic principle of this code is to limit structural damage to within an allowable range in the case of small and medium earthquakes, while severe damage (plastic deformation) is allowed in the case major earthquakes. The purpose is to prevent buildings from collapsing with the primary purpose of protecting human life. In the 1995 Hyogoken-Nanbu Earthquake (the Kobe Earthquake), many buildings were severely damaged, as shown in Figures 1 and 2. However, damage to buildings designed by the 1981 seismic design code tended to be less than to older buildings, so engineers and bureaucrats believed that the principle of the code was effective. However, the 1981 seismic design code alone is not sufficient from the viewpoint of maintenance or early recovery of building function and the seismic resilience of mega-cities **[1]**.

[1] Dr. Member, Architectural Institute of Japan, Taisei Corporation, komuro@arch.taisei.co.jp
[2] Member, Architectural Institute of Japan, Taisei Corporation, sinozaki@arch.taisei.co.jp
[3] Member, Science Council of Japan, Professor Emeritus, Tokyo Institute of Technology, ada@akira-wada.com

Figure 1. Pancake crushing of Kobe city hall

Figure 2. Building damage scene in Kobe

Since 1995, major earthquakes have occurred in many places in Japan and damage to actual building structures has been reduced. In particular, it has been found that damage to buildings with seismic-isolation structures or response-controlled structures is very small. However, there have been cases where damage to the finish, and to interior fittings, of buildings designed by the current design code but lacking such advanced seismic technologies has had a significant impact on business continuity after an earthquake.

In this paper, we report on several large earthquakes that have occurred in Japan since 1995 and on the behavior of certain buildings. We describe advanced technologies, such as seismic-isolation and damage-controlled structures, that have helped minimize earthquake damage.

2. Nursing Home Facility Hit by Earthquake in 2004

During the period October to November 2004, a series of earthquakes took place about 80km south of Niigata city in Japan's Chuetsu region. The main shock, named the 2004 Mid-Niigata Prefecture Earthquake, occurred on October 23. The magnitude was estimated at M_{JMA}6.8 by the Japan Meteorological Agency (JMA). On the JMA scale of seismic intensity, the earthquake reached level 6+ to 7, which indicate extremely strong motion. Many aftershocks including some of M6 class followed the main shock. The Fire and Disaster Management Agency reported that there were 48 people killed and 634 seriously injured, with 3,181 completely buildings destroyed and 13,531 heavily damaged in Niigata Prefecture.

The nursing home shown in Figure 3 is a five-story reinforced concrete building with a seismic isolation system [2]. It is located in Ojiya city and is about 7 km from the epicenter of the main shock (as shown in Figure 4). This facility was planned in 1995, just after the Hyogo-ken Nanbu Earthquake that seriously damaged many buildings in Kobe city. Considering that damage, the decision was made that the facility should be able to maintain its function as a medical service facility in the case of a major earthquake. Therefore, a seismic isolation system was adopted as the main structural design feature for reducing earthquake damage.

Figure 3. Overview of nursing home

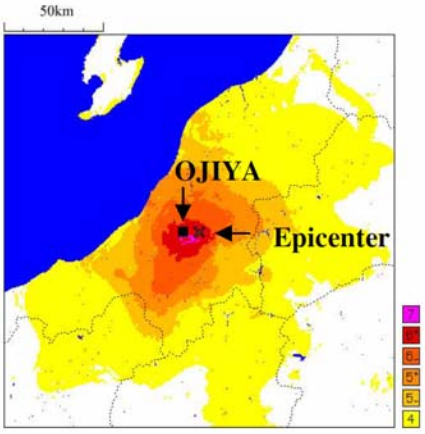

Figure 4. Map of main shock intensity on JMA scale

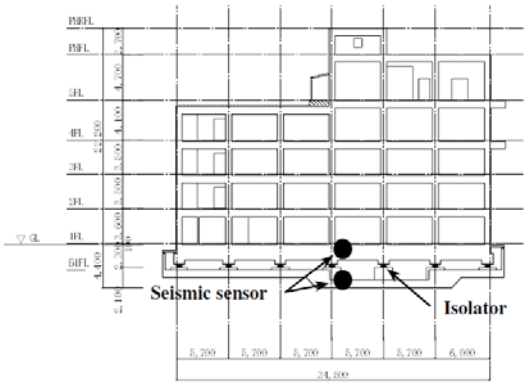

Figure 5. Structural section

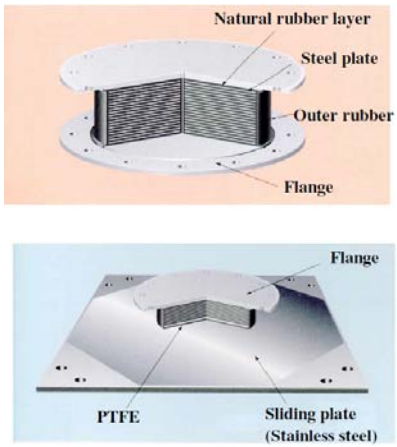

Figure 6. Isolators

(Upper: rubber bearing, lower: slide bearing)

A structural section of the building is shown in Figure 5. The isolation devices (isolators) are installed beneath the first floor. The building is supported by the isolators, 18 sets of rubber bearings and 21 sets of slide bearings. As shown in Figure 6, the rubber bearing consists of thin layers of natural rubber bonded to steel plates and the slide bearing consists of a 3-layer high-damping rubber bearing with a PTFE sliding surface in contact with polished stainless steel.

A field survey of the building was carried out after the main shock. No damage was identified to the exterior wall tiles or the structural members of the building. As Figure 7 shows, there was no falling of objects to the floor. In contrast, some of the wooden houses adjacent to the facility suffered damage and a concrete block wall belonging to a house next door collapsed. The photograph in Figure 8 shows how furniture and household items were thrown around in a building in the neighboring area, giving an indication of the severity of the seismic motion. Taken together, Figures 7 and 8 show the overwhelming difference that a seismic isolation system can make.

Figure 7. Cupboard on 1st floor of the facility after the main shock

Figure 8. Room in neighboring building

3. 2011 Great East Japan Earthquake and Seismic Retrofit of High-rise Building

On March 11 of 2011, a huge earthquake hit the Tohoku district forming the north-eastern part of Japan's main island (the 2011 Off the Pacific Coast of Tohoku Earthquake M_w9.0 (on the moment magnitude scale), sometimes called the 2011 Great East Japan Earthquake). Approximately 16,000 people died and 3,000 people remain missing, mainly due to the tsunami. Figure 9 shows the seismic intensity of this event on the JMA scale [3]. The ground motion was felt across almost the whole of Japan. Figure10 shows a building that toppled in the tsunami. The tsunami-induced meltdowns at Fukushima Daiichi Nuclear Power Plants shocked people around the world while liquefaction in the bay area of Chiba prefecture caused major difficulties to the people living in the region. Buildings were badly shaken, not only in east Japan but also far from the epicenter. High-rise buildings in Tokyo, Osaka and Nagoya experienced strong, long-period motion for several minutes and some residents and office workers in these buildings were quite frightened.

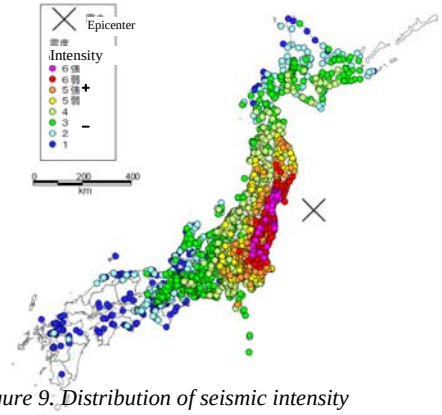

Figure 9. Distribution of seismic intensity of 2011 Great East Japan Earthquake [3]

Figure 10. Building toppled by the tsunami

In 2009, special oil dampers were developed as seismic damage control devices for the retrofitting of old high-rise buildings. They were fitted to an existing 54-story office building (Shinjuku Center Building, as shown in Figure 11, completed in 1979 and located in Shinjuku ward, Tokyo) to suppress vibration during long-period earthquake ground motion [4]. Twelve oil dampers with a deformation-dependent damping characteristic (shown in Figure 12) were fitted on every floor between the 15th and the 39th, for a total of 288 dampers. These floors were

selected because dynamic analysis showed that the story drift and the cumulative plastic deformation ratio of the steel reinforcing bars were relatively large in this range of floors.

The seismic response of the building was recorded in the 2011 Great East Japan Earthquake. Later, simulation analyses were conducted to estimate the performance of the dampers in controlling motion. This modeling work clarified that damping was improved and the response was reduced by 20% as compared to the building without dampers. Figure 13 shows (a) the simulated relative displacement between the roof and the ground floor and (b) the simulated acceleration at the top floor with and without the dampers. The maximum displacement at top floor was 76.4cm without the dampers and this was reduced to 60.8cm with the dampers (the actual observed displacement was 54.2cm). This indicates that the dampers reduced displacement by 20%. The maximum acceleration was 220.3 cm/sec^2 without the dampers and 184.1 cm/sec^2 with them (and the actual observed value was 161.3 cm/sec^2), also about a 20% reduction. This confirmed the value of the seismic retrofitting of this super high-rise building and the analytical results are in good agreement with the observed motion record.

Figure 11. Shinjuku Center Building

Figure 12. Installed oil damper

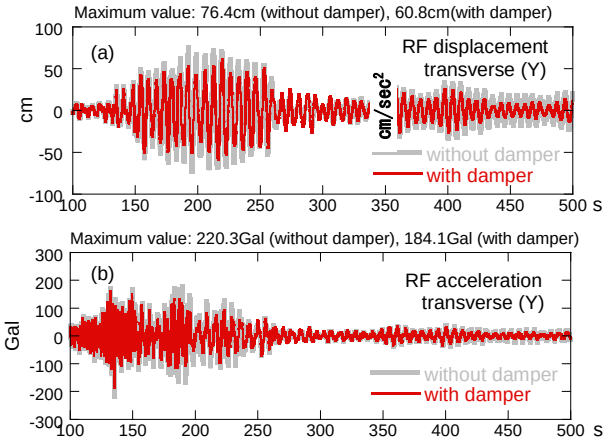

Figure 13. Comparison of simulated response waveforms with/without dampers

3.1 2016 Kumamoto Earthquake and Semiconductor Factory

A series of earthquakes hit the middle of the island of Kyusyu beginning on April 14, 2016, centering on Kumamoto Prefecture, where major damage occurred (the 2016 Kumamoto earthquake, shown in Figures 14[5] and 15). Among the series of events, two major earthquakes occurred at 21:26 on April 14 (foreshock $M_{JMA}6.5$) and at 01:25 on April 16 (main shock $M_{JMA}7.3$). This was the first time in Japan that a seismic intensity of 7 had been recorded twice within two days. The earthquakes caused severe damage not only to the structures of buildings, but also to the contents and the finish (non-structural elements) of buildings and to lifeline in the area.

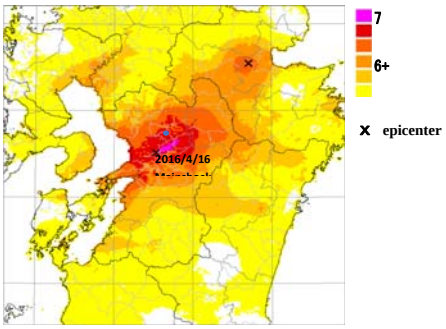

Figure 14. Distribution of seismic intensity of 2016 Kumamoto Earthquake (Main Shock) [5]

Figure 15. Damaged Kumamoto castle

Kumamoto prefecture is home to many factories, including manufacturing facilities for semiconductors. Semiconductor plants include equipment that is sensitive to vibration and also clean rooms that must remain airtight, so they are relatively fragile in the face of a large earthquake. A large earthquake might cause operations to be halted, which leads to opportunity loss. Opportunity losses for semiconductor manufacturers are large and in some cases may exceed actual material losses.

A semiconductor factory (shown in Figure 16) consisting of two buildings of steel structure in Kikuyou town, Kumamoto prefecture, is located 12km away from the epicenter of the main shock. These buildings were designed according to the current seismic design code. The structure, finish and contents of the factory were severely damaged by, principally, the main shock, but there were no injuries or deaths [6]. Brace buckling, bolt fractures and failure of structural member connections were observed. Figure 17 shows the structural damage at the point where the column bases meet the foundation. Figures 18 and 19 show the damage to the finish and to the factory equipment.

Due to the severe damage caused by the main shock, operations at the factory were halted. Full production on all lines resumed by the end of July, about three months after the earthquake. The impact on operating income from the Kumamoto earthquake was estimated at more than 50 billion yen, of which opportunity losses account for about 60%. If recovery could have been hastened, the opportunity losses would have been minimized.

Figure 16. View of factory [6]

Figure 17. Damage to connection of column bases and foundation [6]

Figure 18. Collapse of automatic conveyor rail [6]

Figure 19. Damaged clean room [6]

Figures 16 to 19, Source: Sony Semiconductor Manufacturing

4. Conclusion

Numerous earthquakes, including especially the 2011 Great East Japan Earthquake, have taught us that our goal in seismic design for severe ground motion should evolve from simply the protection of human life to the combined protection of life + property conservation + maintenance of functionality. In other words, we can say our aim should be “resilience”, which is a hot topic these days.

Japan has long made efforts to deliver high seismic performance through the user of seismic isolation and response control technologies. The devices and systems that support these technologies have been improved and have become more reliable and cheaper than in the past. We are now in a position to apply these technologies to a variety of building types in all the countries of Asia for the benefit of the next generation.

References

[1] Wada, A., “From prologue to epilogue in solutions for seismic resilience of mega-city”, Structural Engineering Frontier Conference, March 18-19 2015, Tokyo Institute of Technology, Yokohama, Japan, pp. 323-335.

[2] Komuro, T., Kawamoto, S., Tamari, M., Fukuyama, H., and Iiba, M., “Performance of seismic isolated building under strong earthquakes”, 5th World Conference on Structural Control and Monitoring, 2010

[3] The Headquarters for Earthquake Research Promotion, https://www.jishin.go.jp/main/oshirase/20110311_sanriku-oki.htm, 5 Oct. 2019

[4] Aono, H., Hosozawa, O., Shinozaki, Y., and Kimura, Y., “Seismic retrofit of high-rise building against the long-period ground motions”, 10th U.S. National Conference on Earthquake Engineering Frontiers of Earthquake Engineering, July 21-25, 2014

[5] JapanMeteorological Agency, https://www.data.jma.go.jp/svd/eqev/ data/2016_04_14_kumamoto/ index.html, 5 Oct. 2019

[6] Ito, T., Damages and recovery processes of major semiconductor manufacturers following the Kumamoto earthquake (in Japanese), Matsuyama University Journal, Vol. 29, 2017, pp. 65-96.

Analysis of Some Heavy Metals Concentrations in Muscle Tissue of Three Fish Species and environs, Thanlwin River Segment of Mon State

Yee Yee Win[1] et al

Abstract

The present study was conducted in two different study sites situated on the Thanlwin segment and its tributaries of Mon state. Study period lasted from February 2018 to January 2019. Fish, water and sediment samples were collected seasonally in the study sites. Element concentrations of As, Pb and Cd in extracts were determined by using Flame Atomic Absorption Spectrophotometry (FAAS) (Perkin Elmer AA Analyst 800 and Winlab – 32 s oftware) at University Research Center (URC) in University of Yangon. Concentration of As, Pb and Cd on muscle tissues of three study fish species (*Lates calcarifer*, *Otolithoides pama* and *Polynemus paradiseus*) were analyzed in the study period. Heavy metal concentrations in muscle tissues of all study fish species were below WHO limit. Concentration of As in **water** of study site I in rainy and winter seasons as well as those of study site II in all seasons were found to higher than the WHO limitation. As concentration in **sediment** of study site I in all seasons as well as those of study site II in summer and winter seasons were found to higher than the WHO limitation. In the study site, positive **relationships** between size of fish and heavy metal concentrations were found in *L. calcarifer* while those were negative in *O. pama* and no relation in *P. paradiseus* at study site I. In site II, positive relationships between size of fish and As and Pb concentrations in *L. calcarifer*, As in *O. pama* and Pb and Cd in *P. paradiseus* were observed. However, heavy metal concentrations in muscle tissues of study fish species were not over the WHO MPL. Thus, study fishes from the study area are generally safe for human consumption.

Keyword: fish, arsenic, lead, cadmium, muscle tissue, sediment, water

1. Introduction

Heavy metals are environmentally ubiquitous, readily dissolved and transported by water and readily taken up by aquatic organisms (Alam *et al*., 2002). Fishes are often at the top of aquatic food chain in water ecosystems and fish living in the polluted water may accumulate toxic trace metals (Mansour, and Sidky, 2002).

It is well known that fish, as a regular constituent of the human diet, can represent a dangerous source of certain heavy metals. The discharge of wastewater and industrial effluents whether treated or not can be regarded a constant pollution source that dominate water quality. Water quality parameters can produce an improved understanding of the environmental situation and assist policy makers to design priorities for sustainable water management (Hung *et al*., 2010).

The degree of water quality is determined by the content of physical, chemical and biological parameters available in it. Association between two parameters may cause to increase or decrease in the concentration of others. In this study, concentrations of three metals (arsenic, lead and cadmium) in the three fish species because these fish species have been consumed as food by local people. Water and sediments from Thanlwin river segment of Mon State environs were determined. The muscle is the section of fish that is consumed by human. It is required to verify whether contaminants like heavy metals are within the recommended limits for human consumption. Therefore the metal content in the muscle was analyzed in the present study.

[1] Lecturer, Department of zoology, Mawlamyine University. Myanmar, yeewynn1@gmail.com
2. Kay Lwin Tun 3. Min Thu Aung 4.Cho Cho Thin

Especially, the mean concentrations of test metals were evaluated in terms of international guidelines.

Therefore, present study was chosen to conduct in order to know the following objectives.

- to find out seasonal variation of heavy metals concentration (As, Pb, Cd,) in muscle tissue of study fish species
- to monitor the toxic metals (As, Pb, Cd) concentration in aquatic environs (water and sediment) of the study fish sites
- to investigate relationship between size of fish and metal concentrations in muscle tissue of fish

2. Materials and Methods

The present study will be conducted in two different study sites (Ngan Tae village and Kyauk Tan village) situated on the Thanlwin River segment and its tributaries of Mon states. Ngan Tae village (Lat 16º 28' N and Long, 97º 39' E) and Kyauk Tan village (Lat 16º 24' N and Long, 97º 36' E) were designated as the study site I and II, respectively. Study period lasted from January to December 2018. *Lates calcarifer*, *Otolithoides pama* and *Polynemus paradiseus*,, water and sediment samples were collected monthly in fish landing depots of the study sites. At least seven samples from each fish species were collected. Total length and body weight of specimens were measured. They were dissected using stainless steel scalpels and forceps. A part of the muscle (dorsal muscle) was removed and weighted. Samples were put into an oven (90 ºC) and dried to reach constant weight. After that they were stored at low temperature until digestion. Digestion of the samples carried out according to dry method by using furnace (Model-L-3383).

Element concentrations of As, Pb and Cd in extracts were determined by using Flame Atomic Absorption Spectrophotometry (FAAS) (Perkin Elmer AA Analyst 800 and Winlab-32 software) at Universities Research Center (URC) in University of Yangon. Test results were compared with maximum permissible limit (MPL) designated by WHO.

Functional relationship between size of fish and heavy metal concentrations were analyzed by using regression method with the following formula

$Y = a + bX$

a = Y intercept

b = slope of the line

r = regression coefficient

Fig. 1. Map of the study sites

Cement Factory (near Ngan Tae village)
(site I) Hind view

Industrial Zone (near Kyauk Tan village)
(site II) Hind view

Plate 1. Environs of the study sites

Lates calcarifer

Otolithoides pama

Polynemus paradiseus

Plate 2. Study fish species

3. Results

Seasonal variation of As concentration in muscle tissue of *Lates calcarifer* collected from study site I was -6.296mg/L in rainy season > -6.837 mg/L in summer season > -9.985 mg/L in winter season. Similar results were observed in study site II. As concentration in muscle tissue of *Otolithoides pama* and *Polynemus paradiseus* was summer > rainy season > winter season. As concentration in muscle tissues of three study fish species which collected from study site II were higher than that of study site I in summer season (Table 2).

Lead concentration in muscle tissue of *Lates calcarifer* collected from study site I was -0.873 mg/L in summer season > -0.928mg/L in rainy season > -0.959mg/L in winter season. Similar results were observed in study site II. The same conditions of Pb concentration were found in muscle tissue of *Otolithoides pama* and *Polynemus paradiseus.* However, Pb concentration in muscle tissues of three study fish species which collected from study site II were higher than that of study site I in summer season (Table 2).

Cadmium concentration in muscle tissue of *Lates calcarifer* at rainy season (0.007mg/L) was higher than those of summer season 0.009 mg/L) and winter season (-0.01mg/L) in study site I. Similar results were observed in study site II. The same conditions of Cd concentration were found in muscle tissue of *Otolithoides pama* and *Polynemus paradiseus.* However, Cd concentration in muscle tissues of *Lates calcarifer, Otolithoides pama* and *Polynemus paradiseus* which collected from study site II were higher than that of study site I (Table 2).

Arsenic concentration in water and sediment at winter season (1.003mg/L in water and 74.64mg/L in sediment) was higher than those of rainy season (0.134mg/L in water and 26.43mg/L in sediment) and Summer season (-0.326mg/L in water and 99.36mg/L in sediment)

in study site I. Similar results were observed in study site II. However, As concentrations in water which collected from study site II was higher than that of study site I although As concentrations in sediment which collected from study site I was higher than that of study site II (Table 3, 4).

Lead concentration in water at winter season (1.003mg/L in water and 74.64mg/L in sediment) was higher than those of rainy season (0.134mg/L in water and 26.43mg/L in sediment) and summer season (- 0.326 mg/L in water) but summer season was the most higher (99.36 in sediment) in study site I. Similar results were observed in study site II. However, Pb concentrations in water and sediment which collected from study site I were higher than that of study site II in summer season (Table 3, 4).

Cadmium concentration in water and sediment at rainy season (-0.005mg/L in water and 0.02mg/L in sediment) was higher than those of summer season (-0.011mg/L in water and 0.025mg/L in sediment) and winter season (-0.008mg/L in water and 0.029mg/L in sediment) in study site I. Similar results were observed in study site II. However, Cd concentrations in water and sediment which collected from study site I were higher than that of study site II in summer season (Table 3, 4).

WHO maximum permissible limit of As, Pb and Cd in muscle tissue of fish are 0.01 mg/L, 1 mg/L and 0.2 mg/L, respectively. Concentrations of As, Pb and Cd in muscle tissues of study three fish species were not found over the maximum levels permitted by WHO (Table 2).

Positive relationships between length of fish and concentrations of As ($y = 0.380x – 16.67$, $r = 0.868$), Pb ($y= 0.009x - 1.135$, $r = 0.955$) and Cd ($y = 0.002x - 0.049$, $r = 0.959$) were found in *L. calcarifer* while those were negative in *O. pama* ($y = -1.543x +33.13$, $r = 0.740$), Pb ($y= -0.020x – 0.380$, $r = 0.828$) and Cd ($y = -0.003x + 0.091$, $r = 0.530$) and no relation in *P. paradiseus* ($y = -0.094x – 3.426$, $r = 0.045$), Pb ($y= -0.010x – 0.765$, $r = 0.232$) and Cd ($y = 0.001x - 0.021$, $r = 0.161$) at study site I (Table 5). Similar results were observed between body weight of fish and metal concentrations (Table 5).

In the study site II, positive relationships between size of fish and As and Pb concentrations in *L. calcarifer*, As in *O. pama* and Pb and Cd in *P. paradiseus* were observed (Table10, 11).

Table 1. Mean total length and body weight of fish for seasonal analysis of metal concentration in site I and site II

Study area	Species	Summer		Rainy		Winter	
		TL(cm)	Weight(g)	TL(cm)	Weight(g)	TL(cm)	Weight(g)
Site I	*Lates calcarifer*	18.7 ± 2.71	78.4 ± 39.3	27.7 ± 2.32	263.1 ± 52.46	23.3 ± 1.08	191.4 ± 35.5
	Otolithiodes pama	26.7 ± 0.37	137.1 ± 6.21	24.58 ± 1.57	102.2 ± 20.92	26.58 ± 1.4	127.3 ± 3.97
	Polynemus paradiseus	16.2 ± 0.71	24.73 ± 2.67	16.22 ± 0.67	25.33 ± 3.3	17.78 ± 0.97	4.39 ± 5.46
Site II	*Lates calcarifer*	18.5 ± 2.3	82.5 ± 42	18.7 ± 1.86	94.82 ± 34.05	27.8 ± 3.97	225.4 ± 22.05
	Otolithiodes pama	20.3 ± 0.55	57.05 ± 5.02	21.67 ± 0.37	64.22 ± 5.53	24.83 ± 1.28	96.42 ± 13.13
	Polynemus paradiseus	16.3 ± 1.42	25.06 ± 7.6	18.38 ± 0.7	46.23 ± 10.2	15.06 ± 0.8	20.33 ± 2.82

MPL = Maximun permissible limit

Table 2. Variation of heavy metals concentration (mg/L) in studied species at two different study sites

Species	**Element**	**Site I**			**Site II**			**MPL**
		Summer	**Rainy**	**Winter**	**Summer**	**Rainy**	**Winter**	
Lates calcarifer	As	-6.837	-6.296	-9.985	-6.296	-6.051	-10.24	0.26
	Pb	-0.873	-0.928	-0.959	-0.769	-0.799	-0.843	1
	Cd	0.009	0.007	-0.01	0.019	0.01	0.011	0.2
Otolithiodes pama	As	-4.872	-6.207	-9.637	-6.67	-5.255	-6.17	0.26
	Pb	-0.893	-0.917	-0.952	-0.788	-0.818	-0.859	1
	Cd	0.008	0.008	-0.005	0.023	0.011	0.011	0.2
Polynemus paradiseus	As	-3.379	-5.112	-6.55	-7.221	-4.431	-5.196	0.26
	Pb	-0.902	-0.96	-0.984	-0.785	-0.829	-0.862	1
	Cd	0.006	0.001	-0.008	0.022	0.008	0.013	0.2

MPL = Maximun permissible limit

Table 3. Variation of metal concentrations in water of two different study sites at Thanlwin River

Sr No.	Elements	Site I			Site II			MPL
		Summer	Rainy	Winter	Summer	Rainy	Winter	
1	Arsenic	-0.326	**0.134**	**1.003**	**0.329**	**0.356**	**0.978**	0.01
2	Lead	-0.445	-0.487	-0.518	-0.537	-0.57	-0.599	0.01
3	Cadmium	-0.011	-0.005	-0.008	-0.013	-0.016	-0.022	0.003

Table 4. Variation of metal concentrations in sediment of two different study sites at Thanlwin River

Sr No.	Elements	Site I			Site II			MPL		
		Summer	Rainy	Winter	Summer	Rainy	Winter	TEC	MEC	PEC
1	Arsenic	99.36	26.43	74.64	43.54	0.235	**29.75**	9.8	21.4	33
2	Lead	-0.514	-0.467	-0.477	-0.549	-0.572	-0.507	36	83	130
3	Cadmium	0.025	0.02	0.029	0.023	0.023	0.028	0.99	3	5

MPL = Maximun permissible limit

TEC = Threshold effect concentration

MEC = Midpoint effect concentration

PEC = Portable effect concentration

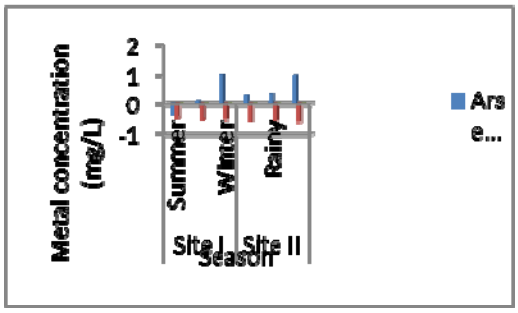

Fig. 2. Variation of metal concentrations in water of two different study sites at Thanlwin River

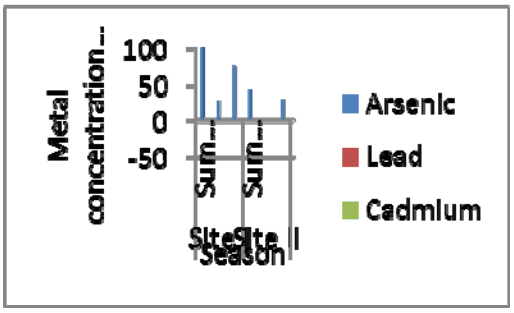

Fig. 3. Variation of metal concentrations in sediment of two different study sites at Thanlwin River

Table.5.Relationship between body length(cm) and weight(g) of fish and heavy metal concentrations in muscle tissue of fish at study site I and Site II

Species	Heavy	Site I				Site II			
		Length		Weight		Len		Weig	
		Linear equation	Remark	Linear equation	Remark	Linear equation	Remark	Linear equation	Remark
Lates calcarifer	As	y=0.380x-16.67 R^2=0.753 r=0.868	Positive relation	y=0.018x-10.98 R^2=0.743 r=0.862	Positive relation	=0.247x-12.9 ^{2}=0.313 =0.559	Positive relation	y=0.0018x-9.952 R^2=0.369 r=0.607	Positive relation
	Pb	y=0.009x-1.135 R^2=0.912 r=0.955	Positive relation	Y=0.000x-0.999 R^2=0.919 r=0.959	Positive relation	=47.24x-1305 ^{2}R=0.266 =0.516	Positive relation	Y=3.474x-747.8 R^2R=0.320 r=0.566	Positive relation
	Cd	Y=0.002x-0.049 R^2R=0.919 r=0.959	Positive relation	Y=0.000x-0.017 R^2R=0.913 r=0.956	Positive relation	=-0.000x=0.0024 ^{2}R=0.324 =0.569	Negative relation	y=-3E-05x+0.017 R^2R=0.270 r=0.520	Negative relation
Otolithoides pama	As	y=-1.543x+33.13 R^2=0.548 r=0.740	Negative relation	y=-0.0120x-7.766 R^2=0.773 r=0.879	Negative relation	=0.247x-11.54 ^{2}=0.635 =0.979	Positive relation	y=0.029x-8.177 R^2=0.746 r=0.864	Positive relation
	Pb	y=-0.020x-0.380 R^2=0.685 r=0.828	Negative relation	y=-0.0001x-0.731 R^2=0.879 r=0.938	Negative relation	=0.005x-0.949 ^{2}=0.138 =0.371	No relation	y=0.000x-0.853 R^2=0.066 r=0.257	No relation
	Cd	y=-0.003x+0.091 R^2=0.281 r=0.530	Negative relation	y=-0.000x+0.040 R^2=0.514 r=0.717	Negative relation	=-0.000x+0.030 ^{2}=0.052 =0.228	No relation	y=-0.000x+0.023 R^2=0.118 r=0.344	No relation
Polynemus paradiseus	As	y=-0.094x-3.426 R^2=0.002 r=0.045	No relation	y=-0.120x=7.766 R^2=0.773 r=0.879	Negative relation	=-0.850x+8.479 ^{2}=o.989 =0.994	Negative relation	y=0.029x-8.177 R^2=0.746 r=0.864	Positive relation
	Pb	y=-0.010x-0.765 R^2=0.054 r=0.323	No relation	y=-0.001x-0.909 R^2=0.031 r-0.176	No relation	=0.015x-1.086 ^{2}=0.473 =0.688	Positive relation	y=0.002x-0.895 R^2=0.668 r=0.817	Positive relation
	Cd	y=0.001x-0.021 R^2=0.026 r=0.161	No relation	y=-0.000x-0.008 R^2=0.047 r=0.217	No relation	=0.004x-0.055 ^{2}=0.999 =0.999	Positive relation tion	y=0.000x-0.001 R^2=0.965 r=0.982	Positive relation

Discussion

Toxic metals are very harmful because of their potential to absorb, accumulate and concentrate in different body parts. Heavy metals, such as As, Pb and Cd are dangerous for human health because of their accumulation properties in the body parts (Tressou *et al*., 2004). Metals bioaccumulation through aquatic food webs to fish, human and other piscivorous animals are environmental and human health concern (Dehn *et al*., 2006).

Arsenic is released in the environment through natural processes such as weathering, and may circulate in natural ecosystems for long time (Mol *et al*., 2010).Toxic effects appear when arsenic is ingested in excess for long periods resulting in cancer, cutaneous malignancies, etc.Lead is toxic metal and non-essential element for human body as it causes a rise in blood

pressure, kidney damage and miscarriage (Kiran *et al*., 20111).Cadmium injures the kidney, poor reproductive capacity, hypertension, tumors and hepatic dysfunction.

Khin Thida Kyaw (2008) stated that in the Daydaye Thilawar fisheries, seasonal variation of toxic metals (As, Pb and Cd) concentration in three fish species were higher in summer and rainy season than those of winter. However, Cho Cho Thin (2017) stated that the concentration level of As in muscle tissues of fish in Ayeyawady River segment of Salay environ were found over the WHO limit but Khin Myint Mar(2011) studied that the concentration of heavy metals in studied species were lower than WHO limit. Thus, present findings were not agreed with the findings of above authors and potential danger may not be occurred for the consumption of study fish species from the present study area.

In the present study, arsenic, concentration in water of study site I in rainy and winter seasons as well as those of study site II in all seasons were found to higher than the WHO limitation. In the present study, arsenic, concentration in sediment of study site I in all seasons as well as those of study site II in summer and winter seasons were found to higher than the WHO limitation. Arvind (2002) also stated that metal content of fish increases with the increment of metal level in water, sediment and food organism. Present findings were agreed with the findings and potential danger may be occurred for water and sediment. In the present study, concentrations of As, Pb and Cd in muscle tissues of three study fish species which collected from study site I and II were not over the MPL recommended by WHO. However, near the study sites, cement factory, machine cleaning workshop and industrial zone were established in 2014. The accumulation trend of As was approximately summer> winter>rainy. The elevation of these metals accumulation in this study may be due to industrial and sewage wastes. Therefore, As in fish will be expected over the MPL in the future study.

In the present study, positive relationships between size of fish and heavy metal concentrations were found in *L. calcarifer* while those were negative in *O. pama* and no relation in *P. paradiseus* at study site I. In the study site II, positive relationships between size of fish and As and Pb concentrations in *L. calcarifer*,As in *O. pama* and Pb and Cd in *P. paradiseus* were observed. However, heavy metal concentrations in muscle tissues of study fish species were not over the WHO MPL. Thus, study fishes from the study area are generally safe for human consumption.

Acknowledgements

I am greatly indebted to Dr Thida Lay Thwe Professor/Head and Dr Aye Mi San Professor. My profound gratitude goes to Dr Kay Lwin Tun, Professor, Department of Zoology, Yangon University and Dr Min Thu Aung, Professor, Department of Zoology, University of Pathein, for their kind support, guidance and supervision.

References

Alam, M. G. M., Tanaka, A., Allinson, G., Laurenson, L. J. B., Stagnitu, F., Snow, E. T., "A comparison of trace element concentrations in cultured and wild carp (*Cyprinus carpio*) of Lake Kasumigaura, Japan. *Ecotox. Environ."* 2012. *Safe*., 53:348-354.

Arvind, K., "*Ecology of polluted waters"*, A. P. H Publishing Corporation, New Delhi. 2002.

Cho Cho "Thin, Relation of some essential and Toxic elements Ayeyawady on different feeding types of some freshwater fishes along the Ayeyawady River segment, Salay Environs". *PhD Thesis*, Department of Zoology, University of Yangon. 2017

Dehn L.A.,Follman E. H., Thomas D. L.,Sheffield G.G., Rosa C., Duffyl.K.,O.Harat.M., "Trophic relationships in an Arctic food web and implication for trace metal transfer". Science of the Environment. 2006. 362,103.

Hung, H., Kallenborn, R., Breivik, K., Su, Y., Brorström-Lundén, E., Olafsdottir, K., Thorlacius, J. M., Leppänen, S., Bossi, R., Skov, H., Manø, S., Patton, G. W., Stern, G., Sverko, E., Fellin., "Atmospheric monitoring of organic pollutants in the Arctic under the Arctic Monitoring and Assessment Programme". *Sci Total Environ* Kiran, 2010. 408: 2854-2873.

Khin Thida Kyaw, "Analytical studies on toxic metals (A, Cd, Pb, and Hg) concentrations in Nga-dan (*Pangasius pangasius)*, Ka-kadit (*Lates calcarifer)*, and Nga-yant (*Channa striata*) samples", *PhD Thesis*. Department of Chemistry, University of Yangon. 2008. 61-104 pp.

Khin Myint Mar, "Uptake of heavy metals and its relationship to feeding habit of selected fish species in Ayeyawady River, Mandalay and Magway segments", *PhD Thesis*. Department of Zoology, University of Mandalay. 2011.

Kiran, Y. K., Mir, A. K., Rabia, N., Mamoona, M., Hina, F., Nighat, S., Tasmia, B., Ammarah, K., "Element content analysis of plants of genus *Ficus* using actomic absorption spectrometer". *African Journal of Pharmacy and Pharmacology* 5 2011. (3): 317-321.

Mansour. S. A., Sidky, M. M., "Ecotoxicological studies 3. Heavy metals contaminating water and fish from Fayoum Governorate, Egypt". *Food Chemistry*, 2002. 78(1):15-22.

Mol ,O, Ozden and S.A. Oymak. Turkish J. Fish. Aqua. Sci., "Determination of Heavy Metals in Fish Tissues, Water and Sediment from Epe and Badagry Lagoons, Lagos, Nigeria",2010. 10:209-213,

Tressou J., Crepet A., Bertail P., Feinberg M.H.., Leblanc J. Ch., Probalistic exposure assessment to food chemicals based on extreme value theory. "Application to heavy metal from fish and sea products". Food and Chemical Toxicology. 2004. 42,1349.

Analysis of Elemental Concentration in Kye Pè (*Plukenetia volubilis* L.) Samples by Using WDXRF Technique

Khin Shwe Tint[1]

Abstract

In this research work, we have been analyzed the concentration elements in three kinds of samples which are fruits (M1), leaves (M2) and stems (M3) for KyePè or Sacha Inchi plant. The concentration elements in these samples were determined by using WDXRF (wavelength dispersive X-rays fluorescence) technique. All measurements have been done in drying condition. According to the experimental results, eighteen elements are contained in fruits sample and stems samples, seventeen elements are contained in leaves samples. These elements are Magnesium (Mg), Aluminum (Al), Silicon (Si), Phosphorus (P), Sulfur (S), Chlorine (Cl), Potassium (K), Calcium (Ca), Titanium (Ti), Vanadium (V), Manganese (Mn), Iron (Fe), Nickel (Ni), Copper (Cu), Zinc (Zn), Rubidium (Rb), Strontium (Sr) and Lead (Pb) elements in fruits sample (M1) and stems sample (M3) and then Nickel (Ni) is not contain in leaves sample (M2). The concentration of Silicon (Si) is large in leave (M2) samples. The concentration of Potassium (K), Calcium (Ca) and Magnesium (Mg) are largest in this research samples. The concentration element in Kye Pè can be prevented diabetes, hypertension, cancer cell and heart disease. Health benefits of Kye Pè include improving digestion, aiding in weight loss, managing diabetes and stimulating cognition. Kye Pè plant is a medicinal plant.

Keywords: WDXRF technique, elemental concentration, Kye Pè plant.

1. Introduction

Everybody, human health is very important. If everybody has good health, everybody will make everything. Nowadays, people would like to use fresh air, clean water, hygienic food and good medicine for health but human activities are causing harm. Plants are not only the major source of energy-rich foods in our societies, but are also an indispensable source of vitamin and other substances promoting healthy growth. They have played an important role in traditional medicine in Myanmar since ancient time. Human health, natural safeguard and minimizing the damages of human activities to Earth are the environmental study today. The aim of this research is to analysis of the concentration of elements in Sacha inchi or Kye Pè samples by using WDXRF (wavelength dispersive X-rays fluorescence) technique. We have collected the fruits, leaves and stems of Sacha inchi or Kye Pè plant. These samples were collected from KyunHla village, Myittha Township, Mandalay Region.

2. Experimental Procedure

2.1 Sample Collection

In this research, we analyzed the three samples in Sacha inchi or Kye Pè plant samples by using WDXRF. We collected three samples which are fruits, leaves and stems. To analysis the elemental concentration of these samples, they were sent to Department of Chemistry, Yadanabon University. The concentrations of elements contained in three samples were analyzed by WDXRF technique.

[1] Dr. Lecturer, Department of Physics, Yadanabon University, Myanmar, physdrshwe@gmail.com

Sample Preparation

Sample preparation is very important process to experiment. In the first step, three samples were dried under the shade of any roof. These samples were ground in order to get fine powders. The lists of sample are shown in Table (1).

Table 1. The list of samples.

Local Name	Kye Pè
English Name	Sacha inchi, sacha peanut
Scientific Name	*Plukenetia volubilis L*
Family Name	Euphorbiaceaes
First sample code	M1 (fruits)
Second sample code	M2 (leaves)
Third sample code	M3 (stems)

The characters of three samples are shown in Figure 1 to Figure 4.

Figure 1. The Kye Pè plants from Myittha Township, KyunHla village, Mandalay region.

Figure 2. The photograph of dried fruits (M1) and fine powder in Kye Pè plant.

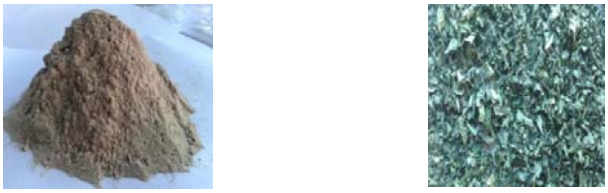

Figure 3. The photograph of dried leaves (M2) and fine powder in Kye Pè plant.

Figure 4. The photograph of dried cortices (M3) and fine powder in Kye Pè plant

These powders were sent to Experimental Laboratory, Department of Chemistry, Yadanabon University. Sample preparation is important in the WDXRF analysis because it is required to get flat, smooth and homogeneous samples for best results. To obtain reliable results in X-ray emission spectrometry, proper sampling is taken and sample storage and sample preparation prior to measurement are conducted. Then hydraulic press machine and a 32 mm diameter die set including a die body, base and two polished metal disks were used for pellet sample in our research work. Prior to pelletizing all parts of the die set was carefully cleaned with methylated spirit to prevent contamination. Initially each sample was weighed using digital balance to obtain the needed amount (5g). Binding agent is added to form stable pellet of the samples. Therefore, binder (1g) was added to the samples (5g) and they were mixed to homogenize with each other. After that weighed sample were poured into the die set (mould) and pressed with 25 tons for 15 minutes by using hydraulic press machine. The pellet was then removed from the die set, taking care not to creak it in the process. After getting the pellet, each of these samples is weighed again and whose weight is exactly 5g is used in this experiment. In making pressed pellets for each sample, these samples were weighted by using the digital balance. The density of each pellet is 0.2 gcm^{-3}.X-ray fluorescence technique is a multi-elemental quantities determination and it can provide concentration of many elements contained in the sample by a single measurement. Three samples were analyzed by using energy dispersive X-ray fluorescence system. All of the pellet samples were analyzed 600 sec for four secondary targets system and the measurement of atmosphere is helium purge. It is used 50 kV bias voltage and tube current is automatically adjusted by hardware. The analyzed range is 0-50 keV. The X-ray spectrum is analyzed with the help of computer to obtain the concentration of each element in the sample. This research was done with WDXRF technique in Experimental Laboratory, Department of Chemistry, Yadanabon. The wavelength dispersive spectrometer is usually coupled with a SEM imaging system and requires dedicated instruments designated by electron microprobe micro-analyzer (EPMA). The spectrometer uses diffraction to sort by wavelength the characteristic. X-rays emitted by the sample. The X-rays are selected using analytical crystals with specific lattice spacing positioned at specific θ angles. Only the wavelengths that satisfy Bragg's law are allowed to pass on the detector. The analytical crystals are bent in order to focus the X-ray beam on the sample and on the detector. These are situated in the Rowland circle to maximize the collection efficiency of the spectrometer. The function of diffraction is shown in Figure (5).

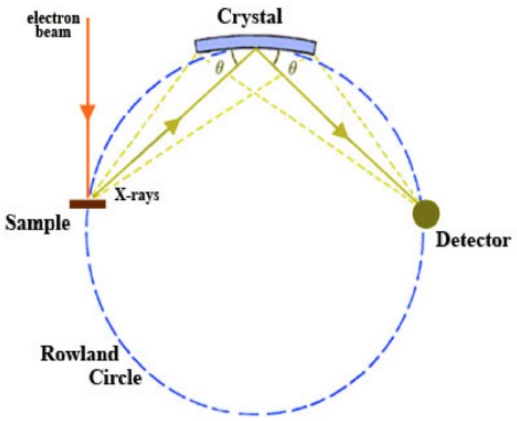

Figure 5. The function of diffraction in WDXRF technique

Each element produces a unique set of characteristic X-rays when bombarded with electros. Each X-ray will have a specific energy and wavelength. Wavelength dispersive spectrometers (WDS) sort the X-rays based on their λ. WDS system use X-ray diffraction as the means by which they separate X-rays. The spectrometer consists of the crystal and diffract will enter the detector. An X-ray photon will diffract, depending on its wavelength, the orientation of the crystal and the crystal's lattice spacing. Only X-ray of a given wavelength will enter the detector at a given time. To measure X-rays of another wavelength, the crystal and the detector are moved to a new position. Since a specific WD spectrometer can measure only one X-ray wavelength at a time. It is important that a WDXRF system has an array of spectrometers in order to work efficiency. Electron microprobes typically have up to five elements simultaneously. Each spectrometer typically has between two and four analyzing crystals, each with a different lattice spacing, because each type of crystal can diffract only a given wavelength. WDXRF requires standard reference materials in concentrations similar to the materials to investigate and is typically used for quantitative spot analysis. The composition of unknown samples is determined by comparing the intensities obtained from studied samples with those from the reference standard materials.

3. Results and Discussion

In this research work, three samples of fruits (M1), leaves (M2) and stems (M3) for *Plukenetia volubilis L.* or Kye Pè or Sacha Inchi were analyzed with WDXRF (wavelength dispersive X-rays fluorescence)technique in the Experimental Laboratory, Department of Chemistry, Yadanabon University. Elemental concentrations of sample contained in the three samples were measured by WDXRF technique and their results are expressed in Table (2). The graphs of these samples are shown in Figure (6).

The concentration of elements was analyzed for three samples. The three samples are M1, M2 and M3. The concentration of elements for three samples is shown in Table (3). According to the experimental results, the sample of fruit (M1) is contained eighteen kinds of elements. They are Magnesium (Mg), Aluminum (Al), Silicon (Si), Phosphorus (P), Sulfur (S), Chlorine (Cl), Potassium (K), Calcium (Ca), Titanium (Ti), Vanadium (V), Manganese (Mn), Iron (Fe), Nickel (Ni), Copper (Cu), Zinc (Zn), Rubidium (Rb), Strontium (Sr) and Lead (Pb) elements. According to the experimental results, Lead (Pb) element is minimum concentration. The samples of leaf (M2) are contained seventeen kinds of elements. According to the experimental results, Bromine (Br) element is very small concentration. The samples of stem (M3) are contained eighteen kinds of elements. They are Magnesium (Mg), Silicon (Si), Aluminum (Al), Phosphorus (P), Sulfur (S), Chlorine (Cl), Potassium (K), Calcium (Ca), Vanadium (V), Copper (Cu), Zinc (Zn), Bromine (Br), Rubidium(Rb), Manganese (Mn), Titanium (Ti), Iron (Fe), Strontium (Sr) and Lead (Pb) elements. According to the experimental results, the concentration of Bromine (Br) element is very small in M3 samples.

Table (2) The comparison of elemental concentration in M1, M2 and M3 samples.

Symbol	Concentration (ppm)			Symbol	Concentration (ppm)		
	M1	**M2**	**M3**		**M1**	**M2**	**M3**
K	42800.00	43200.00	53700.00	Zn	39.00	42.00	36.00
Ca	8290.00	54600.00	21500.00	Ti	24.00	93.00	50.00
Mg	3700.00	4400.00	5400.00	Mn	23.00	86.00	39.00
P	3120.00	2660.00	3160.00	Cu	20.00	23.00	17.00
S	2680.00	4090.00	1840.00	Sr	17.00	139.00	50.00
Si	1450.00	32200.00	2940.00	Rb	10.00	7.00	10.00
Al	655.00	1450.00	1140.00	V	3.00	-	4.00
Cl	203.00	377.00	390.00	Ni	3.00	-	-
Fe	173.00	462.00	245.00	Pb	2.00	4.00	4.00

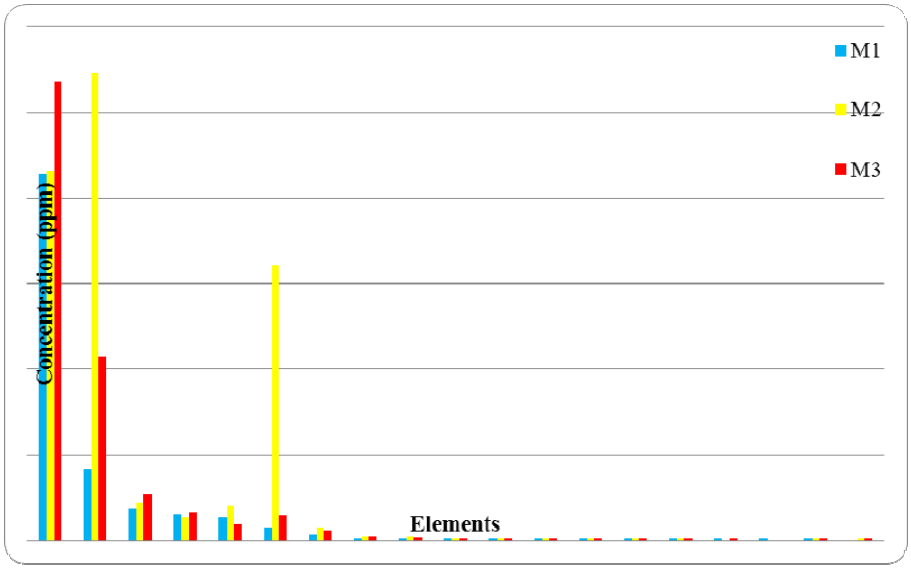

Figure 6. The experimental results of elemental concentration in M1, M2 and M3 samples.

4. Conclusion

According to the experimental result, the concentration of potassium (K) is larger in sample M3 than M2 and M1. The potassium is highest concentration in M3. This element is needed for many essential process including enzyme activation photosynthesis. Potassium is one of the seven essential macrominerals. Potassium (K) participates actively in the maintenance of the cardiac rhythm. High levels of potassium in the blood have been linked to pressure, heart and kidney disorders, and other health problems.

The concentration of calcium (Ca) measured in M1 is small and measured in M2 is larger than M3. Calcium is the main constituent of the skeleton, bone and dental health and important for regulating many vital cellular activities such as nerve and muscle function and lowers the blood pressure. The concentration of magnesium (Mg) measured in M3 is large and measured in

M2 and M1 is small. Magnesium is essential for both plant and animal growth and health. Magnesium is also included in some remedies for heartburn and upset stomach due to acid indigestion. The concentration of phosphorus (P) measured in M1 and M3 is large and measured in M2 is small. Phosphorus is required in most of the body's bio-chemical process including cell growth and converting food to energy is also required for metabolism of fats and carbohydrate to produce energy. The main function of P is to bind with calcium to make healthy teeth and bones.

It is also necessary for the synthesis of protein for repair and growth of tissue and cells. Other key functions help the body to utilize vitamin B complex and support proper nerve and muscle functioning, maintaining, calcium balance and preventing high blood calcium levels. The concentration of sulfur (S) measured is larger in sample M2 than M1 and M3 is smaller than M1. This element aids the liver in bile secretion and maintains oxygen balance for proper brain function and is involving in the clotting of blood. It assists in the fight against bacterial infection by disinfecting the blood helping the body resist bacterial, and protecting. The concentration of Iron (Fe) measured in M1 and M3 is smaller than M2. This element is an essential element for human beings and animals and component of hemoglobin. It facilitates the oxidation of carbohydrates, protein and fat to control body weight, which is very important factor in diabetes.

The concentration of Lead (Pb) measured in three samples is very small. Lead is a useful and common metal that has been used by humans for thousands of years. Lead in the body is distributed to the brain, liver, kidney and bones. It accumulates over time. Lead in bone is released into blood during pregnancy and becomes a source of exposure to the developing fetus. The concentration of Potassium (K), Calcium (Ca) and Magnesium (Mg) are largest in this research sample. The concentration element in Kye Pè can be prevented diabetes, hypertension, cancer cell and heart disease. Health benefits of Kye Pè include improving digestion, aiding in weight loss, managing diabetes and stimulating cognition. Kye Pè plant is a medicinal plant.

Acknowledgements

I would like to express my heartful thanks to Dr Mg Mg Naing, Rector, Dr Tint Moe Thuzar and Dr Si Si Khin, Pro-Rector of Yadanabon University for giving permission and encouragement. I wish to express my gratitude of Professor Dr.Yi Yi Myint, Head of Physics Department, Yadanabon University, for her valuable advice in this research work.I am also grateful to Professor Dr May Thida Win, Physics Department, Yadanabon University, for her advice and suggestions.

References

[1] Guillen, MariaD*et al.,* "Characterization of SachaInchi (*Plukenetia Volubilis L.*) Oil by FTIR spectroscopy and LH NMR.Comparison with Linseed Oil".Journal of the American Oil Chemists' Society. 80(8): 755-762, (2003).

[2] Hla Hla Than, Dr., "Analysis of Traditional Medicine", University of Yangon (2000).

Hufstader. Chris. "Looking to SachaInchi for their Future". Oxfam Exchange, (2009).

[3] Ministry of Health, Department of Trditional Medicine, "Collection of Commonly Used Herbal Plants" (1982).

[4] L. friberg*et al*., "Handbook on the Toxicology of metals" Elsever, Amsterdan (1979).

[5] Win Myint, Dr., "A Study on Combined Effects of TMF-27 and TMF-35 on Plants with Type 2 Diabetes Mllitus", University of Trditional Medicine, Mandalay (2012).

Importance of Soil Moisture Balance and Soil texture in Yields of Crop: A Case Study of Thayetlaypin Village Tract in Magway Township

Hlaing Myo Myo Htay[1], Win Win Maw[2], Si Si Wai[3], Hnin Khaing Aye[4]

Abstract

Climate, soil moisture and soil texture interact with each other for crops growth. The main issue is crop yield deterioration in Magway Township. It is necessary to know the nature of soil water in the area for future utilization in agriculture. The aim of this research is to investigate the effect of soil moisture balance and texture on crop yields of Magway Township. Soil moisture balance was calculated by CW Thornthwaite method to estimate the balance of soil water in the soil. Soil water content is controlled by the soil texture. Soil texture was analyzed by biker method. Soil textural class is determined by USDA soil textural triangle, 1987. The main types of soil texture are sandy loam, loamy sand and sandy soil. The relative yields of sesame and groundnut are 25.67% and 78.38% respectively. Soil moisture deficiency is 538.10 mm/month in 2018. According to the ratio of evapotranspiration and rainfall, the study area needs the water supply or rain fall. The variables can effectively explain the yield together with other variables as correlation. As a result, the yields of sesame and groundnut related to these soil properties but not significantly.

Keywords: soil moisture balance, soil texture, crop yields

1. Introduction

The soil moisture budget refers to water in the soil as moisture, as it is the term most commonly used by scientists who study the subject from the agronomist‘s point of view. A fundamental concept of physical geography is that the availability of water to plants and animals is more important in the environment than precipitation itself (Fundamental of physical geography). Field capacity of a given soil depends largely on its texture. Soil texture influences on the availability of water to the plant. Soil texture also impacts organic matter levels; organic matter breaks down faster in sandy soil than in fine texture soil (www.ristormwatersolutions.). Soil texture is composition of size of soil particles that is sand, silt, clay. Soil texture can be classified by the percentage of sand, silt and clay into loam, silty loam, loamy sand, sandy loam, silty clay loam, etc. (www.ristormwatersolution.org). The importance of soil texture determines different methods and management decisions in cultivation. There are also subclass in sand and silt. Sand is divided into very coarse sand, coarse sand, medium sand, fine sand and very fine sand (USDA, 1987). Density of soil porosity, water holding capacity, organic matter content and susceptibility to erosion are controlled by soil texture (Daji et al 1996; Biswas and Mukherjee, 1994). Sandy soil is suitable for maize, groundnut potato and grapes (USDA,1987). The relationship between crop yield and soil is very complex and depends on complex interaction between physical and chemical properties of soil and other external natural factors’(Sys et al,1991). The soil quality should be tested before cultivation; does soil have problems? Does the crop need water? How much should you apply? Therefore, soil analysis is very important for to farmers. In this paper, soil texture, moisture and basic analysis of soil properties such as pH, and

[1] Dr., Professor, Department of Geography, University of Magway, Myanmar, myomyo67.hh39@gmail.com
[2] Assistant Lecturer, Department of Geography, University of Magway, Myanmar, winwinmaw.mdy.24@gmail.com
[3] Assistant Lecturer, Department of Geography, University of Magway, Myanmar, sisiwai.mdy.26@gmail.com
[4] Dr., Lecturer, Department of Geography, University of Magway, Myanmar, ,hninkhineaye@gmail.com

organic matter were studied preliminarily for suitable crops cultivation and also to sustain the crop productivity base on moisture conditions.

Aim and Objectives

The aim of this paper is to investigate the effect of soil moisture balance and texture on crop yields of Magway Township. The objectives are as follows:

1. To measure the ratio between precipitation and evapotranspiration
2. To analyze the soil moisture budget
3. To determine the soil textural categories and
4. To find out the relationship between soil properties and crop yields

2. Materials and Methods

This research was done based on the primary data. The soil samples were collected by grid method in field area. With the sample collection, land owners were interviewed in detail as well as their suggestions regarding crop yield. Selection of study area, literature survey, and selection of soil samples location in grid methods have been done before going to the field. Soil texture has been tested by biker method in study room. Soil moisture balance was analyzed by CW Thornthwaite method. After that soil test data are plotted on map by GIS 10.0.The estimation of evaporation was used by Penman coefficient equation.Finally, interpretation and analyzing was done by using MS-Excel 2007.

2.1 Study Area

Magway Township is one of the significant oil crops areas in Central Myanmar. Sesame and groundnut are predominantly cultivated crops in this area. The Thatyetlaypin village tract consisting of the oil pots in Magway Township was chosen as a case study to explore relation between the soil texture, moisture and crops. The study area is located at between latitude 19 ^{0} 45′ North and latitude 20 ^{0} 21′ North and between longitude 94 ^{0} 54′ East and longitude 96^{0}18′ East. The total area is 11007acres on which 5142 acres is cultivable land, actually in Thatyetlaypin Village Tract.

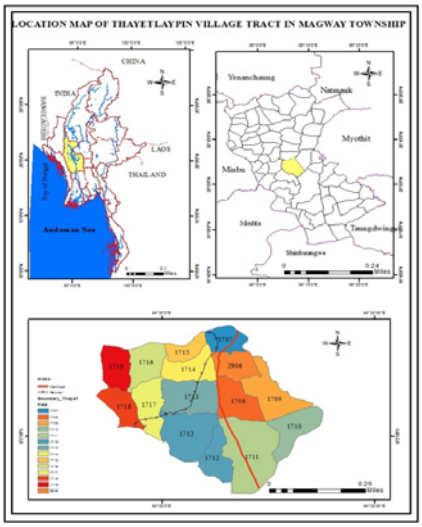

Figure 1. Thatyetlaypin Village Tract.

3. Results and Discussions

3.1 Relationship between precipitation and evapotranspiration

Potential evapotranspiration is a maximum water loss and it measures the moisture demand for regions, (CW Thornthwaite, 1948) and also the ratio of precipitation to potential evapotranspiration. This ratio may be less than 0.1 for these regions; water must be supplied at potential rate. The ratio of precipitation to evapotranspiration ranges from 0.2 to 0.6, again indicating a need for irrigation water in crop production. The range is from 0.8 to 1.6, indicating a rather well balanced situation and in some cases, water surplus. In the study area, the ratio of precipitation to evapotranspiration lying within 0.8 to 1.6, indicates rather well balanced situation and in some cases, water surplus.

3.2 Soil moisture budget analyze in study area

The annual water budget of the soil concerned with the storage of water in soil, runoff and deficiency for plant growth. The basic soil moisture balance equation is as follows: P=E+G+R (CW Thorn Thwaite, 1948) Where P = Precipitation, E = Evapotranspiration, G = Change in soil moisture storage, R = Runoff. The water balance has been calculated the water balance for each month singly and for the year as a whole. As a result, precipitation varies are less than actual evapotranspiration value. In this case, very high potential evapotranspiration is occurred. When Ep (Potential Evapotranspiration) exceed P (precipitation), the plant must draw up moisture stored in the soil as an attempt to sustain as rapid growth as possible at all time. P is measurable in small amount in most months. The values of Ep are always larger. Consequently soil moisture deficiency (D) prevails throughout all months of the year although the storage of moisture is larger than 300 mm. Therefore, crops thrive without irrigation and yields are high in some years.(Table-1)

Table (1) The equation of Soil moisture budget analysis of study area

Rainfall	AET	G(-)	G(+)	R	PET	D=PET-AET
91.95	46.66		45.29		66.66	20
0	58.22	-58.22			83.18	24.95
0	80.3	-80.3			114.72	34.42
6.1	89.78	-83.68			128.26	38.48
172.97	96.11		76.86		137.3	41.19
491.99	84.83		77.07	330.09	121.18	36.35
99.06	87.17	11.89			124.53	37.36
182.12	83.24		98.88		118.92	35.68
15	80.39	-65.39			114.84	34.45
117.1	69.57	47.53	17.71		99.39	29.82
0	54.71	-54.71			78.15	23.45
15	47.93	-32.93			68.46	20.54
1191.29	878.9	-315.81	315.81	330.09	1255.58	376.67

Source: Meteorology and Hydrology Department, Magway Region

3.3 Soil textural classes of study area

According to the experimental results, soil textural classes were determined by the ratio of sand silt and clay. In the study area, the soil textural class is moderately coarse textures are loamy sand, sandy loam and sand respectively. The common names are sandy soils and texture are coarse texture .Size of grain size is involved in the group of 2-0.05 mm (USDA 1987). In the study area, sandy loam 70%, loamy sand 20%, sand texture 10 % is occurred. Spatial distribution of Soil texture classes were shown in figure(2).The result show that the loamy sand contains 87.5% of sand, silt 8.3 %and clay 4.2%. The sandy loam types contains sand 68%,silt 21% and clay 11%.

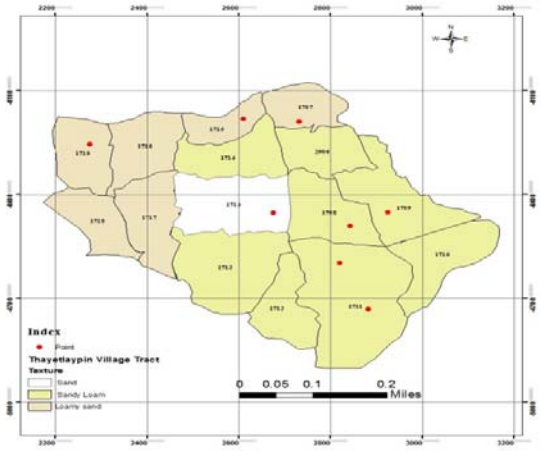

Figure 2. Spatial distributions of soil texture classes of study area

3.4 Soil water content

The soil water content is the amount of water held in the soil at any given time. Average water content for various soils textural classes are shown with organic carbon, pH and humus in table (3). According to table 3, soil water holding capacity was observed with soil texture. The correlation coefficient(r) between the percent of sand content in soil samples and water holding capacity(WHC) is positive correlation (r= 0.54).It is 74% significantly. Moreover, the correlation between clay content in soil samples and WHC is assessed by regression method .The correlation value is (r= 0.59). The relation of silt content in soil samples and WHC is positive correlation (r= 0.47).So, Soil texture controls the water holding capacity. Furthermore, the organic matter carbon is very low and low value in the study area. There are positive correlation between organic carbon and WHC (r=0.02). So, the study area is not sufficient in organic carbon in the soil. Organic matters retain the soil moisture. So it is suggested that providing the soil organic matter increases the soil water holding capacity.

Table (3) Soil Water holding capacity and properties of soil with texture in study area

Soil texture	field capacity	available water	organic carbon	PH	Humus
sandy loam	21	12	0.3	7.29	0.47
loamy sand	19	11	1.4	8.0	2.5
sandy loam	21	12	0.3	6.3	0.5
sandy loam	21	12	0.4	6.5	0.6
sandy loam	21	12	0.4	6.7	0.6
sandy loam	21	12	0.3	6.5	0.6
sandy loam	21	12	0.3	6.7	0.5
loamy sand	19	11	1.4	8.0	2.4
sandy	12	7	0.3	8.0	2.5
sandy loam	21	12	0.2	6.3	0.6

Source: USDA (1987) and field data

3.5 The relative crop yields

The sesame and groundnut yields were collected from each sample field. Therefore, The potential of crop production cannot be equaled in actual because of other factors. Therefore, raw yield data (survey) was calculated by relative crop yield (pp.435,Katalin Jushos, Szilard Szaabo, and Marta Ladanyi, September,2015). The data were calculated by using the relative yield of each crop as follows: $RY_p = Y_p / Y_{max}$ RY_p is the relative yield of plot *p*(a value between 0 and 1), Y_p = the yield of plot p (t/h^{-1}), Y_{max} = maximum yield the total research site over all plots (t/h^{-1}).According to the indices of yield, the relative yield of sesame is less than the relative yield of groundnut. The largest yields of sesame and groundnut indices value are 1, 1 are found in sandy loam type respectively. The yield variability of sesame and groundnut are 63.17% and 27.84%. Table (4) shows the Indices of crop relative yield of plot. As a result, the sandy loam type and sandy soil are more suitable for sesame crop and for groundnut.

Table (4) Indices of crop relative yield of plot

sample soil type	yields/Acres sesame	Yield /Acres groundnut	Relative Yield (Sesame)	Relative yield (Groundnut)
sandy loam	8	6	1	0.60
loamy sand	6	4	0.8	0.40
sandy loam	5	8	0.6	0.80
sandy loam	6	6	0.8	0.60
loamy sand	6.7	5.3	0.8	0.53
sandy loam	6	8	0.8	0.8
sandy loam	6	5	0.8	0.50
loamy sand	4.4	5.4	0.6	0.54
sand	5	10	0.6	1.00
sandy loam	5	4	0.7	0.64

Sources; Field survey

3.6 An analysis of importance of Soil properties on crop yields

Based on the soil moisture balance and soil texture, soil water, field capacity, organic, pH, humus is studied for the crop yields. These factors were analyzed by regression analysis method. As a result, the relative of sesame yield / acres are relations the available water in soil due to the r value=0.47, as well as significant level p=0.16(84%). Similarly, the yields of groundnut were observed with percent of water available in the soil, it is also correlated to the available of water in soil due to the significant level 0.07(93%). In the analysis of oil crop relationship, field capacity and yields of sesame are correlations due to the correlation coefficient r=0.47. Moreover, the confident level is 0.16(84%).The relationship between groundnut and field capacity were occurred significantly by p value is 0.08(91%).Furthermore, the relation between sesame yields and the percent of sand content in the soil samples were observed due to the coefficient correlation r=0.58. Moreover the relationship between sesame and pH value is very strong correlation (r=0.92).However, the relationship between pH in the samples and groundnut yields is very weak(r=0.26).The pH value also is correlation significantly with the humus in the sample soil due to the r value (r=0.91). All these variables are also controlled by soil texture. Therefore, the others factors have to consider for the increase of crop yields.

4. Conclusion

According to the relationship between precipitation and evapotranspiration, the value of ratio is indicating to the good water balance situation for plant growth in the study area. Whereas the conditions of moisture balance, the crop can grow without irrigation because of the storage of moisture larger than 300 mm. Furthermore, the common type of soil is sandy soil and the basic soil classes are sandy loam, loamy sand and sandy soil. Soil texture classes are more suitable for in sesame and groundnut. The basic type of soil textural classes determines the water for plant growth. As a result, the yields of sesame and groundnut are related to these physical and chemical properties but it is not significantly related. However, the soil moisture, texture and properties are not only important but also need to test before crop cultivation for soil quality. Therefore, it is suggested that other external factors have to be considered in the crop cultivations.

Acknowledgements

We deeply indebted to Dr Khin Maung Oo, Rector of University of Magway, for his kind permission to do this research. We also thank to Dr Khin Myo Myo Chun, (Professor and Head, Department of geography, University of Magway) for her recommendation. Finally, we acknowledge to Science Council of Asia and all respectable teachers for call paper and encouragement.

References

[1] Maurice Amooh,Kwame Nkrumoh ,University of Science and Technology, Effects of Soil Texture and Organic matter in Evaporative loss of soil moisture, August, 2015.

[2] Surinda Jalota and Seven authors,Punjab Agriculture University, Soil Texture, Climate and Management effect on plant growth, grain yield and water use by rainfed maize-wheat cropping system: field and simulation study.

[3] Katain Jushos, Szilard Szaabo,and Marta Ladanyi, Influence of soil Properties on Crop Yield: a multivariate statistical approach. September,2015

[4] Kshudiram Chakraborty& Biswranjan Mistri, Importance of soil texture in sustenance of agriculture: A study in Burdwan-I C.D Block, Burdwam, West Bengal,Vol XXINo1 Jan, 2015,ISSN 0973-7642

[5] T.N.Nath,Int.J.chem.sci.: Soil Texture and Total Organic Matter content and Its Influences on Soil Water Holding Capacity of Some Selected Tea Growing Soils in Sivasagar District of Assam,India,12(4),2014,1419-1429,ISSN 0972-768X,www.sadgurupublication.com,

[6] Zachary M.Easton, Assistance Professor and Extension Specialist,Virginia Cooperative Extension,Virginia Tec.Virginia University, Soil and Soil Water Relationships ,PSE-194P,

Operation Models of Mini-Grid in Myanmar: The Case of Shan State

Kensuke Yamaguchi[1], Hiroshi Komikado[2]

Abstract

In Myanmar, rural electrification by mini-grids is necessary for its balanced development. This paper examines the effectiveness of each operation model in conflict areas in Shan State. There are four operation models: utility-operator; private-operator; community; and hybrid model. First, focus group interviews were conducted to sample representative cases of each model. Next, a survey was conducted on each operator about energy capacity, energy resources, tariff, owner, and maintenance. Finally, semi-structured interviews were conducted on members of the Parliament and the state assembly and the chief of the ward. Three main points were found out: (i) When the private enterprise operates, the tariff can be reduced through the economy of scale. But the private have low incentives to enter conflict areas. (ii) When the local leader is responsible, people enjoy relatively cheap electricity with stable supply, which eventually benefits anti-government armed forces. (iii) When the community both constructs and operates, the tariff is highest due to its high initial cost, which widens inequality in the community. In the conflict areas, a hybrid model—mini-grids initially built by governments, then transferred to communities—is most feasible. To scale up this model, a rural development fund is recommended to subsidize initial costs.

Keywords: Rural electrification, Mini-grid, Operation model, Rural Development Fund, Myanmar

1. Introduction

In Myanmar, there is an unbalanced situation in the use of electricity between urban and rural areas. People living in urban areas enjoy electricity with heavily subsidized tariff, while people in rural areas face much higher tariff, and often do not have access to electricity. Since the beginning of the rule by Burmese people in 1948, ethnic minorities, most of whom live in rural areas, have increasingly suffered from this unfair situation. As a consequence, severe poverty still remains among minorities while the urban development is rapid.

As a counter, lots of ethnic groups formed armed forces and they began incidents with the national army. Electrification in rural areas is essential to correct the gap among ethnic groups and achieve balanced development over the nation (Noah and Yamaguchi, 2017; Yamaguchi et al., 2018ab; Yamaguchi, 2019). Especially in conflict areas, expansion of the national grid has a huge risk, and then the development of mini-grids has its significance for electrification. This paper examines the effectiveness of each operation model of mini-grids in Shan State with contentious conflicts area.

2. Methods

There are several key issues for mini-grids, such as who should manage and own them. As the initial and running costs of mini-grids are far larger than the cost of a small power management system such as SHS, their business sustainability needs to be considered carefully (ERIA, 2018; GNESD, 2014; Seguin, 2014). An analysis using the business operator model

[1] Project Assistant Professor, Institute of Future Initiatives, The University of Tokyo, yamaguchi@ifi.u-tokyo.ac.jp; +81-(0)3-5841-0933
[2] Research Assistant, Institute of Future Initiatives, The University of Tokyo, komikadohiroshi@gmail.com

gives an effective view of the discussion (Safdar, 2017). Focusing on operators of mini-grids makes it possible to analyze the structure of the business, the flow of funds, among others. Although there is no universal solution for electrification by mini- grids, an appropriate business model can be chosen based on the advantages and disadvantages for business operators, and the situations where mini-grids are introduced. There are four models of mini-grids operators: Utility operator model; Private operator model; Community model; Hybrid model (European Union Energy Initiative Partnership Dialogue Facility, 2014; Shirley, 2018). Based on the advantages and disadvantages mentioned in previous papers, mini-grids in Shan State are analyzed in this paper.

Data used in the analysis were collected from the field survey conducted by authors from October to December in 2018. There were three surveys in the field survey. The first survey is focus group interviews with five informants on Shan State, including a member of Kachin Democratic Party, members and an advisor of Union Parliament. It was conducted to sample six representative towns with mini-grids in Shan State, considering the operator model of operators of mini-grids. The second is a questionnaire survey on each operator of the six representative town to collect basic information, such as tariff, energy capacity, energy resources, owner, and people in charge of maintenance. The third is semi-structured interviews with 12 stakeholders related to each mini-grid, including members of the Parliament, members of a state assembly, and the chief of the ward. It was conducted to collect information about the advantages and disadvantages of each model to clarify detail information of each case.

3. Results and Discussion

First, focus group interviews picked up six representative cases of mini-grid. Real names and locations of the cases are not used to protect personal information and the towns are re-named Town A, Town B, Town C, Town D, Town E, and Town F. It was clarified that the six representative cases can be divided into four models. Private Operator Model (Private enterprise); Private Operator Model (Local leaders and armed ethnic groups); Community Model; Hybrid Model (Community transfer). Unlike the previous paper, it was clarified that there was no utility-operator model, but that private-operator model can be divided into two models: Private enterprise; Local leaders and armed ethnic groups.

Basic information of each case and model, such as tariff and energy capacity, was clarified by the questionnaire survey. Table 1 summarizes the result. Information about scale (Energy capacity), tariff, operator, owner, and maintenance are described in each case.

Table1. Mini-grid in Shan State, Myanmar

Private	Private enterprise	Town B	6,300 kW	Illumination: MMK100/kWh Industry:	Private enterprise	Four stockholders	Private enterprise
		Town E	20 MW	MMK65/kWh	Private enterprise	Private enterprise, government	Private enterprise
	Local leader	Town C	640 kW	MMK35/kWh	Private enterprise	Armed ethnic group	Private enterprise
		Town F	75 and 65 kW	MMK500 /bulb	Private enterprise	Local leader	Private enterprise
Community	Community burden	Town D	160 kW	MMK100–200/kWh	Community (government loan)	Community	Community
Hybrid	Community transfer	Town A	5 kW	MMK1000 /month	From DRD to Community	Community	Community

Source: Based on interviews conducted by authors

Private Operator Model (Private enterprise) is observed in Town B and Tow E. Private companies contract with the government to invest and manage the business In Town B, private companies and residents are communicating each other and both are satisfied. However, in rural areas, residents are dissatisfied with electricity charges because they do not know the pricing system. Private Operator Model (Local leaders and armed ethnic groups) is observed in Town C and Town F, where armed forces are involved in electricity distribution. Armed groups invest in a power generator for electricity supply as company shareholders. The private company by the armed forces that set up the system is given overall control by the local government and taxes are paid to the federal government. In some cases, the community is involved in system administration because the armed forces are closely related to the community.

Community Model is observed in Town D, and the government provides loans to residents for an initial investment. The mini-grid is owned by the community and is managed by several residents. The initial cost is borne by the residents. Hybrid Model (Community transfer) is observed in Town A, allowing low-cost operation by the community. The initial cost of the mini-grid was borne by government agencies and foreign funds, and its operation will be handed over to the community. Japan International Cooperation System transfers human resources to the community through the Department of Rural Development (DRD). The community owns and manages the mini-grid. This system is expected to reduce electricity costs because it only recovers the lowest operational costs.

As a result, the following three points became clear. First, as the private operator model, not only private companies but also local leaders are often business operators. When the operators are private enterprises, the average energy capacity is ten times bigger than that of other models. On the other hand, if the operator is a local leader, the tariff is cheaper than other

models, but the owner is an anti-government army. Second, the tariff of the Community Model was from three to five times than that of other models. Third, as the Hybrid Model (Community transfer), transfers of mini-grid facilities from the Department of Rural Development to communities are observed. In this model, energy capacity is much smaller than that of other models.

Based on the results, an appropriate model of mini-grids is discussed for rural electrification. If the private enterprise is responsible for an operation of mini-grid, there is an advantage that the economy of scale can be pursued and the price can be reduced. On the other hand, these private-sector businesses have low incentives to enter areas with frequent conflicts and poor purchasing power because there is a possibility that they cannot recover their cost. Then, areas, where the private enterprise wants to introduce mini-grids, are limited and, that is, Private Operator Model (Private enterprise) is limited in scale. If the local leader is responsible for operation, people may be able to receive power supply at a cheap price, but there is a concern that it will be a source of anti- government armed forces. In other words, the patron-client relationship in local politics is strengthened through the mini-grids. Conflicts between armed ethnic forces and the national force will happen more often and they will be more serious. Private Operator Model (Local leaders and armed ethnic groups) will be deepen the gap between people in urban areas and in rural areas, which is originally planned to be solved. When the community takes charge of construction and operation, mini-grids have high initial costs, which leads to high prices. There is a possibility that the people with purchasing power and the people without it will be divided. Moreover, the transfer of knowledge about construction and operation of mini-grid is another challenge for replication of mini-grids with Community Model.

Based on the discussion above, a hybrid model can be expected to be an efficient solution for electrification in conflict areas where purchasing power is often scarce because it will reduce risks for private enterprises to enter the mini-grid business, because it will not be a resource for anti-governmental armed forces, and it gives all residents an access to electricity with relatively low tariff.

4. Conclusions

This paper examines the effectiveness of each model of the Shan state mini-grid. Rural electrification is expected to correct the disparity between ethnic groups and achieve balanced development across the country. Particularly in conflict areas, the expansion of the national grid presents significant risks, and the development of mini-grids is very important for electrification. Analyses employed the framework of business operator model to discuss the appropriate model. Data was collected from a field survey conducted by the author in 2018. There were three surveys: focus group interview, questionnaire survey, and semi-structured interview. The survey clarified the mini-grids in Shan State can be classified into four models and details of each models. Considering each advantages and disadvantages and current situation in Myanmar, Hybrid model (Community transfer) is appropriate for replications of mini-grids because there is a possibility that Hybrid model can solve the problems the other models have.

Finally, following three points are proposed to promote replications of mini-grids of

Hybrid model (Community transfer). First, if DRD is in charge of construction, scalability is limited. Therefore, it is highly expected to leave some of constructions to private enterprises, but, at the same time, a public subsidy needs to be provided so that they can recovered cost by operation for a fixed period. Second, a fund under on the village development law, which is about to be approved, can be utilized for such subsidies. For example, a gasoline tax may be collected to make the fund managed sustainably. Third, it is better for DRD to carry out electrification within the Ministry of Electricity and Energy with not only on-grid but also off-grid electrification, although it is currently in charge of only off-grid solutions and oversees the above-mentioned village development law. Carrying out the proposals above, mini-grid developments with the electric power company model, which was not seen this time, can be expected.

1. Recommendations

To secure government support in a significant scale, a public financing mechanism such as fund is needed.

Where a banking sector is not mature in a country such as Myanmar, fund mechanism is important to achieve a certain multi-year target. Currently, a rural development law legalizing rural development fund is in its final deliberation. As the law articulates that the fund can be used for rural infrastructure such as electrification, it is reasonable and realistic to utilize this fund mechanism to support mini-grids by community.

The source for the fund could be secured as an ear-marked tax system such as gasoline tax.

The initial cost of the mini-grid is required to be subsidized, especially for this community model. The current public support for one project by DRD is around 0.18mil USD. As the Minister of MOEE states, 2,000 villages need mini-grid solution in peripheral regions. A rough calculation shows around 360 million USD to achieve mini-grid targets in conflict-prone areas. Referring to the case in Thailand (i.e. Energy Conservation Fund, ENCON Fund), a petroleum tax is one of the feasible options. Assuming the surging transportation usage in urban areas, imposing an approximately 5% tax rate both on gasoline and on diesel is sufficient as this fund source.

A certain institutional reform among relevant line-ministries is favored to diffuse mini-grid systems in a large scale.

Currently, Ministry of Energy and Electricity (MOEE) is in charge of on-grid electrification while Ministry of Agriculture and Livelihood (MoALI) conducts the off- grid electrification projects such as the “60-20-20” program. As MoALI is not an “energy” Ministry, the program remains at a small scale. To expand the scale and integrate off-grid systems with on-grid ones, an institutional reform between MOEE and MoALI is required for deeper integration and coordination. Ultimately, an integrated policy and planning bodies such as National Energy Management Committee (NEMC) as under the previous government is required with more authority.

Acknowledgements

The authors thank Myo Zaw Shein and Mitasu Company for its research assistance, anonymous reviewers, and seminar participants at Yangon Technical University and the University of Tokyo for useful comments. This research was partially supported by the Ministry of Education, Science, Sports and Culture, Grant-in-Aid for Research Activity Start-up (17H06582, Kensuke Yamaguchi). The authors also gratefully acknowledge financial support from the Economic Research Institute for ASEAN and East Asia (ERIA).

References

[1] ERIA, “Electricity futures in the Greater Mekong Sub region: Towards sustainability, inclusive development, and conflict resolution”, ERIA, 2018

[2] European Union Energy Initiative Partnership Dialogue Facility, “Mini-grid Policy

Toolkit”, European Union Energy Initiative Partnership Dialogue Facility, 2014

[3] GNESD, “Renewable energy-based rural electrification: The mini-grid experience from India”, GNESD, 2014

[4] Yamaguchi, K., “Why economic sanctions in Myanmar is a bad idea”, PacNet: Pacific Forum CSIS, 2019

[5] Yamaguchi, K., Kittner, N., Del-barrio, D., Yoshikawa, H., and Kammen, D., “Energy for Peace in Myanmar: a sustainable and inclusive strategy”, Myanmar Times, 2018a (Burmese)

[6] Yamaguchi, K., Kittner, N., and Yoshikawa, H., “Energy for Peace: ミャンマーにおける水力ダム開発”, エネルギー・資源, 39(4), 247-251, 2018b (Japanese)

[7] Kittner, N., and Yamaguchi, K., “Hydropower threatens peace in Myanmar -- but it

doesn't have to”, Nikkei Asian Review, 2017

[8] Safdar, T., “Business models for mini-grids”, Smart Villages, 2017

[9] Seguin Robert, “Economic feasibility of rural electrification projects”, In Side Event at the High-Level Meeting of the Africa-EU Energy Partner- ship. Addis Ababa, 2014 [10] Shirley, R., “Fact Sheet: Mini-Grids in India: Mini-Grid Finance and Business Models”, Power for All, 2018.

Health Risk Assessment of Soil and Water Pollution near Public Dug Wells along Shwe-Ta-Chaung Creek in Mandalay City

Aye Myat Mon[1]

Abstract

The objective of this research is to determine the environmental pollution in the four public dug wells located adjacent to the Shwe-Ta-Chaung Creek in Tanpawaddy Quarter, Mandalay, Myanmar. Four water samples from four dug wells, named Yarma, Coco-plant, Cow Lake and Salty Water along the creek were examined with Public Health Laboratory to determine the contamination of surface associated with waste water. The water chemical analysis reports for twelve water quality posts of measurement in Coco-plant and Salty Water dug wells are chemically potable and the other two dug wells are chemically unpotable. Eight soil samples near each dug well and relevant creek were determined with Rigaku EDXRF spectrometer to estimate the elemental pollution in the soil. Modified degrees of contamination and pollution load index for soil pollution were analyzed. The water supply wells are impacted by contamination associated with waste water. Soil around Yarma Dug Well and Salty Water Dug Well are more polluted than the other two dug well regions along the creek.

Keywords: Yarma Dug Well, Coco-plant Dug Well, Cow Lake Dug Well, Salty Water Dug Well, Shwe-Ta-Chaung Creek

1. Introduction

The quality of the water in the wells can impact human health even if it is not consumed, due to the contamination of surfaces with chemicals or pathogenic microorganisms through improper installation of wells, or being in close proximity to sources of pollution such as sewage or lands fills. The main ways a home has access to water is either through a municipal water supply from a major city or through wells. Wells exist in two forms, dug wells and tube wells. It is hypothesized that the sewage migrates through the soil and will decrease the water quality of the groundwater. Soil pollution as part of land degradation is caused by the presence of human-made chemicals or other alteration in the natural soil environment. It is typically caused by industrial activity, agricultural chemicals, or improper disposal or waste. Soil Pollution can have a number of harmful effects on ecosystems and human, plants and animal health. Health consequences from exposure to soil contamination vary greatly depending on pollutant type. Industrial or man-made concentrations of naturally occurring substances, such as nitrate and ammonia associated with livestock manure form agricultural operations, have also been identified as health hazards in soil and groundwater.

It is suspected that the waste water from the Shwe-Ta-Chaung Creek may be contaminating the dug wells degrading the water quality. Thus, this research is to determine the impact of the creek on environment near four public dug wells by the analysis of four water samples and eight soil samples collected at four sites next to the creek during the dry season in 2018.

[1] Dr Lecturer, Department of Physics, Banmaw University, Myanmar, ammon37@gmail.com,+9592017813

2. Materials and Methods

2.1 Description of Research Area

Yarma Dug Well (W_1), Coco-plant Dug Well (W_2), Cow Lake Dug Well (W_3) and Salty Water Dug Well (W_4) are located in the Tanpawaddy, Chanmyatharsi Township, Mandalay district, Myanmar and situated beside Mandalay-Sagaing-Shwebo Road.

2.2 Sample Location (Sampling Site), Collection and Preparation

Yarma Dug Well (W_1), Coco-plant Dug Well (W_2), Cow Lake Dug Well (W_3) and Salty Water Dug Well (W_4) were constructed over 100 years ago. The well-bases of four wells are about 30 feet, 9.5 feet, 45 feet and 36.5 feet away from the creek during the dry season. A garbage area is about 75 feet, 15 feet, 95 feet and 65 feet away from each well-base. The diameter of the four wells are 6.5 feet, 4.9 feet , 4 feet and 4 feet .The thickness of the four wells are 1.5 feet, 10 inches, 11 inches and 10 inches which are constructed with a brick lining. The heights of their well bases are 1.5 feet, 5 inches, 9 inches and 1 foot above the ground. The depth to water from the top of the four wells casing are 20.5 feet, 17 feet, 21 feet and 19 feet in March 2018. The widths of the creek near the four wells are about 25 ft, 25ft, 20 ft and 22 ft. Raw sewage from downtown Mandalay flows into the creek. The creek adjacent to W_1 and W_2 are not lined by concrete. Waste water is in direct contact with the ground in the creek. The creek adjacent to W_3 and W_4 are lined by concrete. Waste water is not in direct contact with the ground in the creek. W_1 region is located adjacent to the rubbish filter site along the creek. There is vegetation between W_4 and the creek. The photographs of the four dug wells beside the Shwe-Ta-Chaung Creek are shown in Figure 1, 2, 3 and 4. Photograph of location map of eight research sites in Tanpawaddy Township, Mandalay is represented in Figure 5.

Four water samples were collected with one litre bottle each from the four wells during period in March, 2018. Eight soil samples were collected from the creek at the same time. The sample codes for eight soil samples are listed in Table 1. These soil samples from eight research sites were each collected with two inches in diameter PVC pipe which is one feet long. The small trashes in these samples were cleaned and dried under the room temperature. And then it is needed to grind the soil powdered samples and to get very fine powders. The soil powder samples were passed through 325 mesh sieve of the samples. After getting very fine powder, the sample was weighted nearly 5g. Sample preparation is an important role in X Ray Fluorescence (XRF) measurement.

2.3 Public Health Laboratory, Ministry of Health and Sports

The water quality parameters (Appearance, Colour, Turbity, pH value, Total Solids, Total Hardness, Total Alkalinity, Ca, Mg, Cl, SO_4 and Fe) in four water samples of Yarma Dug Well (W_1),Coco-plant Dug Well (W_2), Cow Lake Dug Well (W_3)and Salty Water Dug Well (W_4) were tested at Public Health Laboratory, Ministry of Health and Sports, Mandalay.

Experimental Procedure for Rigaku X-ray Spectrometer

The EDXRF machine (Rigaku) at the University Research Centre, Taunggyi University is used for determination of elemental concentration in the sample of interest.

Contamination Factor (CF) and Modified Degree of Contamination (mC_d)

The level of metal contamination was expressed by the contamination status of sediment in the current research. CF and mC_d were calculated according to the equation described as

$$CF = \frac{MC}{BC} \qquad \text{and} \qquad mC_d = \frac{1}{N}\sum_{i=1}^{N} CF$$

.

Pollution Load Index (PLI)

Pollution Load Index (PLI) was used to evaluate the extent of pollution by metals in the environment.

$$PLI = (CF_1 \times CF_2 \times CF_3 \times ..... \times CF_n)^{1/n}$$

where n is the number of metals and CF is the contamination factor.

.

Figure.1 Yarma Dug Well beside the creek

Figure.2 Coco-plant Dug Well beside the creek

Figure.3 Cow Lake Dug Well beside the creek

Figure.4 Salty Water Dug Well beside the creek

Figure.5 Location Map of four dug wells in Tanpawaddy Township,Mandalay District,Myanmar

Table.1 Sample Codes for eight soil samples

Sample Code	Soil Samples
S_1W_1	Soil sample near Yarma Dug Well (W_1)
S_1C_1	Soil sample adjacent to Shwe -Ta- Chaung Creek around W_1
S_2W_2	Soil sample near Coco-plant Dug Well (W_2)
S_2C_2	Soil sample adjacent to Shwe -Ta- Chaung Creek around W_2
S_3W_3	Soil sample near Cow Lake Dug Well (W_3)
S_3C_3	Soil sample adjacent to Shwe-Ta-Chaung Creek around W_3
S_4W_4	Soil sample near Salty Water Dug Well (W_4)
S_4C_4	Soil sample adjacent to Shwe-Ta-Chaung Creek around W_4

3. Results and Discussions

The water chemical analysis for twelve water quality posts of measurement in four dug wells are listed in Table 2.Total solids and total alkalinity are greater than maximum permissible level in W_1 and W_3.Other parameters are under the maximum permissible level. The remarks of water chemical analysis report for W_1 and W_3 are chemically unpotable and W_2 and W_4 are chemically potable. The depth to water from the top of the well casing of W_1 and W_3 are greater than the other two dug wells. The water from the four dug wells is now used for taking baths, washing clothes and cleaning dishes. It is not used for drinking purpose now.

Modified Degree of contamination (mC_d) and pollution load index (PLI) of metal contaminates in soil pollution near four dug wells were calculated in Table 3. The comparison of mC_d for soil pollution near four dug wells is shown in Figure 6. The comparison of mC_d for soil pollution in the bank of the creek near four dug wells is also shown in figure 7. Figure 8 gives the comparison of PLI for soil pollution near four dug wells. Figure 9 gives the comparison of PLI for soil pollution in the bank of the creek near four dug wells. The mC_d for soil near W_1 and in the bank of the creek near W_1 is moderate degree of contamination. The mC_d results for soil near W_2 is moderate degree of contamination and in the bank of the creek near W_2 is low degree of contamination. The result of mC_d for soil near W_3 and in the bank of the creek near W_3 is very low degree of contamination. The mC_d results for soil near W_4 is very low degree of contamination and in the bank of the creek near W_4 is very high degree of contamination.

Pollution Load indices (PLI) for soil near the four dug wells are moderately polluted and would indicate deterioration of site quality. The PLI for soil in the bank of the creek near W_1, W_2 and W_3 are moderately polluted and near W_4 is strongly polluted. The PLI for soil in the bank of the creek near the four dug wells would indicate deterioration of site quality. Although the creek near Yarma Dug Well (W_1) and Coco-plant Dug Well (W_2) are not lined by concrete and the creek near Cow Lake Dug Well (W_3) and Salty Water Dug Well (W_4) are lined by concrete.

According to the results, soil around W_1 and W_4 are more polluted than the other two dug well regions along Shwe-Ta-Chaung Creek. There is more pollution at Yarma Dug Well (W_1) because there are many trash and garbage near in it. And there are many cash crop eugenia trees near the Salty Water Dug Well (W_4). Therefore, there are heavy pollutions because of fertilizer insecticide from the plantations adjacent to creek around W_4 region.

Table.2 Water chemical analysis in four dug wells

No.	**Parameter**	**W_1**	**W_2**	**W_3**	**W_4**	**Maximum Permissible Level [WHO]**	**Unit**
1	Appearance	Slightly Turbid	Slightly Turbid	Clear	Slightly Turbid	-	-
2	Colour (Platinum, Cobolot Scale)	7	6	6	6	50	Units
3	Turbidity (Silcoda Scale Unit)	-	-	-	-	25	NTU
4	PH value	7.1	7.1	7.3	7.3	6.5 to 9.2	-
5	Total Solids	1571	1109	1808	1109	1500	mg/l
6	Total Hardness (as $CaCO_3$)	310	270	230	260	500	mg/l
7	Total Alkalinity (as $CaCO_3$)	1105	715	1495	780	950	mg/l
8	Calcium as Ca	112	80	84	96	200	mg/l
9	Magnesium as Mg	7	17	5	5	150	mg/l
10	Chloride as Cl	140	100	120	60	600	mg/l
11	Sulphate as SO_4	147	147	49	118	400	mg/l
12	Total Iron as Fe	Nil	Nil	0.01	Nil	1	mg/l

Table.3 Modified Degree of Contamination (mC_d) and Pollution Load Index (PLI) for soil pollution near four dug wells

Sample Location	S_1W_1	S_1C_1	S_2W_2	S_2C_2	S_3W_3	S_3C_3	S_4W_4	S_4C_4
mC_d	3.128	2.713	2.530	1.994	1.447	1.279	1.363	11.362
PLI	1.879	1.941	1.743	1.845	1.397	1.256	1.340	3.045

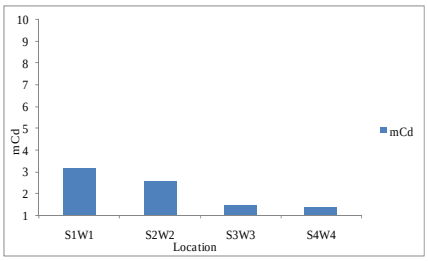

Figure.6 Comparison of mC_d for soil pollution

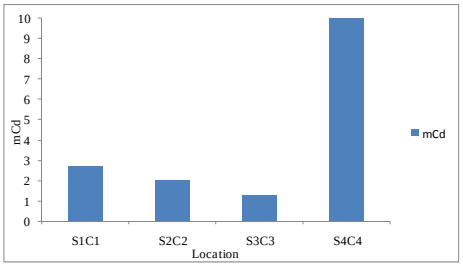

Figure.7 Comparison of mC_d for soil pollution in the bank of the creek near four dug wells

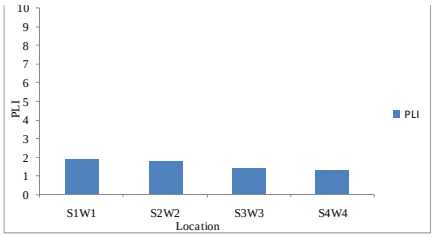

Figure.8 Comparison of PLI for soil pollution near four dug wells

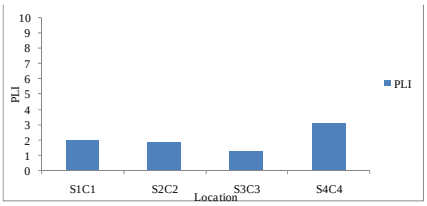

Figure.9 Comparisons of PLI for soil pollution

4. Conclusion

It is indicated that the water supply wells are impacted by contamination associated with waste water. It is recommended that the municipality declare a policy to reduce the pollution and educate the public to have a cleaner environment. The water in Coco-plant (W_2) and Salty Water (W_4) dug wells for twelve water quality posts of measurement are chemically potable and the other two dug wells are chemically unpotable. Soil around Yarma Dug Well (W_1) and Salty Water Dug Well (W_4) are more polluted than the other two dug well regions along Shwe-Ta-Chaung Creek. The pollution around Yarma Dug Well (W_1) is due to garbage landfills. The pollution around Salty Water Dug Well (W_4) is due to excessive fertilizers and pesticides used in agriculture. The waste water creek should be reconstructed with appropriate protection. Humans and animals should not use the wells located near the waste water canal for any purpose. To protect public welfare, safety and health, the water from public dug wells located beside Shwe-Ta-Chaung Creek should not be used long-term.

Acknowledgements

First and foremost I would like to express my gratitude to Dr Aung Kyaw Tin , Rector of Banmaw University, for his kind permission to carry out this work. I am also grateful to Professor Dr Than Than Lwin, Head of Physics Department, Banmaw University for her valuable suggestions.

References

[1] Angelidis T.N,(1997), Water Air Soil Pollution, pp 99-179

[2] Foster S.D & P.J Chilton, (2004), Hydrogeology Journal, pp12-15

[3] Lawrence A R et al., (2000), Hydrogeology Journal, pp 8- 564

[4] Lorna Fewtrell, (2004), Environmental Health Perspectives, Vol. 112,pp 1371-1374

Health Risk Assessment of Heavy Metals via Consumption of Vegetables

Me Me Nyunt[1]

Abstract

Vegetables are an important part of a healthy and balanced diet. They could be contaminated by heavy metals in many ways. Health risk assessment is a very good technique to regard heavy metal contamination in vegetables. The main objective of this paper is to estimate the risk to human health by heavy metals (Mn, Fe, Cu, Zn, Sr and Pb) through the intake of five common vegetables (lettuce, mustard, radish, roselle and water spinach) grown near the drain in Taungthaman lake at Amarapura township by using indexes for vegetables. The elemental concentrations of samples were checked by EDXRF method. Then the indexes for vegetables were calculated. The condition of risk is determined by health risk index (HRI). If the HRI value is less than one, there will be no observed risk. An index more than one is considered as not safe for human health. According to the calculated results, all analyzed vegetable samples except water spinach were not found to cause any risk to the consumer. Water spinach had greatest potential to pose health risk to the consumers. It may be due to the higher absorptivity of heavy metals than the other samples because of its soft and spongy stem.

Keywords: Vegetables, Contamination, Heavy Metals, EDXRF, Indexes for Vegetables

1. Introduction

Vegetables are widely used as food due to their high nutrition values and are edible plants or parts of a plant; they are herbaceous plants whose parts are eaten as supporting food or main dishes. The nutrient content of different types of vegetables varies considerably. Human beings are encouraged to consume more vegetables and fruits due to their richness in vitamins, minerals, fibers and anti-oxidative effects. The fruits and vegetables are important components of a healthy diet and their consumption could prevent a wide range of diseases. However, plants take up metals by absorbing them from contaminated soil as well as from deposits on parts of the plants exposed to the air from polluted environments.

Heavy metals are generally used to describe chemical elements with a specific gravity that is at least 5 times the specific gravity of water. Heavy metals such as manganese (Mn), iron (Fe), copper (Cu) and zinc (Zn) are essential in plant nutrition, however many heavy metals do not play a significant role in the plant physiology. Plants cultivated in polluted environments can accumulate these toxic metals at a high concentration causing serious risks to human health when consumed. Moreover potentially harmful metal contents in soils may come not only from the bedrock itself, but also from the anthropogenic sources like liquid or solid waste deposits, agricultural inputs, fallout of industrial and urban emissions. The use of polluted soils mainly results in decrease the growth of vegetables. Moreover, the heavy metals in soil reduce the yield of vegetables because of disturbing the metabolic processes of plants. Heavy metals contamination is a major problem of our environment and they are also one of major contaminating agents of our food supply. This problem is receiving more and more attention all over the world.

[1] Dr. Lecturer, Department of Physics, Yadanabon University, Myanmar. memeamarapura@gmail.com

Human health are directly affected through intake of vegetables grown in polluted soils. Since heavy metals in the nutrient cycle have seriously threatened health and environmental integrity, more research work is still needed to be done on all species of vegetables grown and consumed. Thus this study was designed to assess the level of some heavy metals (Mn, Fe, Cu, Zn, Sr and Pb) in five vegetable samples (lettuce, mustard, radish, roselle and water spinach) grown near the drain in Taungthaman lake, Amarapura.

2. Methods

2.1 Collection and Preparation of Vegetables

In the present work, the vegetable samples had been collected from the fields near the drain of Taungthamanlake during the period in December 2018. The field is located in the east part of Taungthamanlake of Amarapura Township in Myanmar. To grow the plants, the farmers use the water in drain. The water in the drain is mixed with rainwater, water from the river and the waste water of industries. The industries from the industrial zone used to discard their waste products into the drain. The photograph of the sampling area is shown in *Figure 1*.

The five vegetable samples collected are lettuce, mustard, radish, roselle and water spinach shown in *Figure 2 (a)*. After collecting, the freshly vegetable samples were washed with tap water thoroughly to remove the attached dust particles, soil, unicellular algae, etc. Then they were washed with distilled water. The washed vegetables were passed through filter papers to remove surface water. After that the edible parts were chopped into small pieces. All wet vegetable samples were dried with natural air in room temperature and the drying process was continued until the constant weight had been obtained as shown *Figure 2 (b)*. The dry pieces of samples were crushed into powder using a porcelain mortar and pestle. Then, powder samples were passed through the mesh to get homogeneous powder. The resulting powder samples shown in *Figure 2 (c)* were kept in air tight polythene packet before being taken to the laboratory for metal analyses.

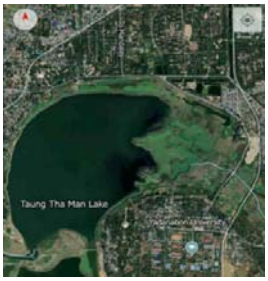

Figure 1. Photograph of sampling area

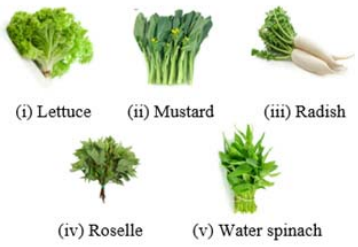

(a)

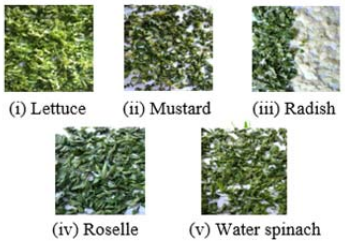

(b)

(c)

Figure2(a.) Photographs of analyzed samples, (b) Sample preparation for fresh condition, (c) Sample preparation for dry and powder condition

2.2 Health risk assessment

Food safety is a major public concern worldwide. The index for food and foodstuff are required to know the information about heavy metal concentration in food products and their dietary intake is very important for assessing their risk to human health. There are many indexes for food and foodstuff according to the field of the study area. In this work, the three indexes associated for food and foodstuff will be discussed, these indexes are (i) the metal pollution index MPI, (ii) daily intake for metal DIM and (iiii) health risk index HRI.

2.3 Metal pollution index (MPI)

Metal pollution index is one of the indexes associated to food and foodstuff which is to determine overall trace elements concentrations in different foodstuff analyzed. This index is obtained by calculating the mean concentration of all the metals in different foodstuff as follow.

$$\text{Metal Pollution Index MPI (mg/kg)} = (Cf_1 \times Cf_2 \times ... \times Cf_n)^{1/n} \quad (1)$$

Where Cf_n = concentration of n^{th} metal in a given foodstuff

Metal pollution index is suggested to be a reliable and precise method for metal pollution monitoring of wastewater irrigation areas. Leafy vegetables are found to contain higher MPI value than which are may be due to the uptake of higher amount of heavy metal available from polluted soil.

2.4 Daily intake of metal (DIM)

The potential health risks of heavy metal consumption through vegetables were assessed based on the daily intake of metal (DIM) and health risk index (HRI). To averagely estimate the daily metal loading into the body system of a specified body weight of a consumer, the daily intake of metal was calculated based on the formula below:

$$\text{Daily Intake of Metal} = \frac{C_{metal} \times C_{factor} \times Con \times EF \times ED}{B_w \times AT} \quad (2)$$

Where C_{metal} = the concentration of heavy metal in vegetable (mg/kg)

C_{factor} = conversion factor from fresh to dry vegetable weight = 0.085

Con = daily average consumption of vegetable in the region (kg person^{-1} day^{-1})

EF = exposure frequency (37 days/year)

ED = exposure duration (65 years, equivalent to the average lifespan)

AT = average time (ED × 365 days/year)

B_w= average body mass of the consumer (kg/person)

The average daily vegetable intakes for a person vary according to locality and their life style. For this present work, the average daily vegetable intake of adult for lettuce and roselle were considered to be 0.165 kg person^{-1} day^{-1}and that for mustard, radish and water spinach were to be 0.345kg person^{-1}day^{-1}(expressed as fresh weight). The average body weight was taken as 70kg for adults according to the World Health Organization (WHO 1993).

Health Risk Index (HRI)

Health risk index HRI is the ratio of daily intake of metal DIM to the reference dose RD, and it is defined as the maximum tolerable daily intake of a specific metal that does not result in any harmful health effects. If the value of HRI less than one, the exposed local population (consumers) is said to be safe and if greater than one indicating that there is a potential risk associated with that metal and not safe for human health. The health risk index HRI was calculated by using the following equation

$$\text{Health Risk Index HRI} = \frac{\text{Daily intake of metal DIM}}{\text{reference dose RD}} \qquad (3)$$

3. Results and Discussion

3.1 Results for metal pollution index: The EDXRF measurement of the vegetable samples gives the elemental concentration of the metal in each sample. The detectable percentage forms of the concentration for each sample have been transformed into the form of milligram per kilogram (mg/kg) scale. The metal pollution index (MPI) for each sample has been calculated by using equation (1). The calculated result of metal pollution index was shown in Table 1.

Table 1. Metal pollution indexes for vegetable samples

Sample	Number of elements (n)	MPI values (mg/kg)
Lettuce	21	447.127
Mustard	23	664.449
Radish	23	485.671
Roselle	21	622.901
Water Spinach	23	3992.254

Results for daily intake of metal : The concentrations of some heavy metals: Mn, Fe, Cu, Zn, Sr and Pb were presented in Table 2. Concentration of heavy metals were in the increasing order: Fe>Zn>Cu>Mn,Sr>Pb. The daily intake of metal (DIM) for a person has been calculated by using equation (2). For DIM calculation, heavy metal concentration, the conversion factor from fresh vegetable to dry vegetable, the daily average consumption of vegetable, exposure frequency, exposure duration, average time and the average body weight were used. In calculation, daily intakes of vegetable per person for lettuce and roselle were used as 0.165 kg and that for mustard, radish and water spinach were 0.345 kg for fresh condition. The average body weight of a person was taken as 70kg for adults according to World Health Organization (WHO, 1993). In this present work, the daily intakes of metal indexes were estimated for six heavy metals. The calculated result data of DIM values for all samples was shown in Table 3. The DIM values of Fe are the highest and that of Pb are least in all samples.

Table 2. Heavy metal concentrations in vegetable samples

Elements	**Heavy Metal concentration (mg/kg)**				
	Lettuce	**Mustard**	**Radish**	**Roselle**	**Water Spinach**
Mn	117	180	150	216	25100
Fe	1050	2410	1830	3170	152000
Cu	173	761	724	797	49000
Zn	305	988	778	814	54400
Sr	134	281	135	169	4190
Pb	23	51	65	63	2500

Table 3. Daily intake of metal (DIM) values for vegetable samples

Elements	**Daily intake of metal (DIM) values (mg/kg/day)**				
	Lettuce	**Mustard**	**Radish**	**Roselle**	**Water Spinach**
Mn	0.0024	0.0077	0.0064	0.0043	1.0659
Fe	0.0214	0.1023	0.0777	0.0644	6.4549
Cu	0.0035	0.0323	0.0307	0.0162	2.0809
Zn	0.0062	0.0420	0.0330	0.0166	2.3102
Sr	0.0027	0.0119	0.0057	0.0034	0.1780
Pb	0.0005	0.0021	0.0028	0.0013	0.1062

Results for health risk index : By using daily intake of metals (DIM) and reference oral dose for each metal, the important index called the health risk index (HRI) can be calculated by applying equation (3). The oral reference dose values for analyzed heavy metals Mn, Fe, Cu, Zn, Sr and Pb are 0.014, 0.7, 0.04, 0.3, 0.6 and 0.004mg kg^{-1} day^{-1}respectively. If the HRI value is less than one, there will be no observed risk. An index more than one is considered as not safe for human health. The calculated result data of HRI values were shown in Table 4. According to these results, HRI value of water spinach is greater than one for almost all heavy metals except strontium.

Table 4. Health risk index (HRI) values for vegetable samples

Elements	Health risk index (HRI) values				
	Lettuce	**Mustard**	**Radish**	**Roselle**	**Water Spinach**
Mn	0.1697	0.5460	0.4550	0.3134	76.1368
Fe	0.0304	0.1462	0.1110	0.0919	9.2213
Cu	0.0879	0.8079	0.7687	0.4047	52.0217
Zn	0.0206	0.1399	0.1102	0.0551	7.7006
Sr	0.0045	0.0199	0.0057	0.0057	0.2966
Pb	0.1168	0.5415	0.0028	0.3199	26.5417

3.2 Discussion

In the present research, five kinds of vegetable samples have been observed. In these samples, lettuce, mustard, roselle and water spinach are the types of leaf vegetables and radish is the type of storage root vegetable. According to Table (1), water spinach and mustard have the highest MPI value while lettuce has the lowest MPI value among the samples. Higher MPI of water spinach and mustard suggests that these vegetables may cause more human health risk due to higher accumulation of heavy metals in the edible portion. Therefore, the leaf vegetable is found to contain higher MPI value than the other types of vegetable which may be due to the uptake of higher amount of heavy metals available from soil and photosynthesis process takes place in the leaf.

To assess the health risk associated with heavy metal contamination of plants grown locally, estimated exposure of tested vegetables (daily intake of metal) and risk index were calculated. The health risk index results showed that Mn, Fe, Cu, Zn and Pb in water spinach had greatest potential to pose health risk to the consumers. It may be due to the higher absorptivity of heavy metals than the other samples because of its soft and spongy stem. The HRI values for analyzed heavy metals in other samples are lower than one. Therefore, it can be said that all analyzed vegetable samples except water spinach were not found to cause any risk to the consumer in the present study.

4. Conclusion

The higher health risk index of heavy metals in water spinach also suggests that there may be potential for human health risk due to consumption. Therefore, it can be concluded that consumption of foodstuff with elevated levels of heavy metals may lead to high level of accumulation in the body causing related health disorders. Long term consumption of heavy metal contamination may be leading to health risk of consumers. Moreover, waste water irrigation for vegetables should be discouraged as it serves as the major route for heavy metal accumulation in vegetables. Further research has to be carried out of determine the concentration of heavy metals in this environment.

Acknowledgements

I would like to express thanks to my students, HninPwintWai and WahWahNaing, atDepartment of Physics, Yadanabon University for theirhelpsin collecting the samples to do this research work.

I would like to express gratitude to my colleagues at the Department of Physics, Taunggyi University for their helps in checking the EDXRF results.

References

[1] Chauhan, G. and Prof. Chauhann, U. K.,"Human health risk assessment of heavy metals via dietary intake of vegetables grown in wastewater irrigated area of Rewa, India", International Journal of Science and Research Publication, Volume 4, Issue 9, September 2014

[2]Duruibe, J. O., Ogwuegbu, M. O. C and Egwurugwa, J. N., "Heavy metal pollution and human biotoxic effects", International Journal of Physical Science Vol. (2), May 2007

[3] Ramteke, S., Sahu, B. L., Dahariya, N. S., Patel, K. S., Blazhev, B. and Matin, L., "Heavy metal contamination of Vegetables", Journal of Environmental Protection, 2016

[4] Singh, A., Sharma, R. K., Agrawal, M. and Marshall, F. M., "Health risk assessment of heavy metals via dietary intake of foodstuffs from the wastewater irrigated site of a dry tropical area of India", Food and Chemical Toxicology, 2010

[5] Adedokun, Aderinola Hannah; Njoku, Kelechi Longinus; Akinola, ModupeOlatunde; Adesuyi, Adeola Alex; Jolaoso, AnuoluwapoOmosileola "Potential human health risk assessment of heavy metals intake via consumption of some leafy vegetables obtained from four market in Lagos Metropolis, Nigeria", J. Appl. Sci. Environ. Manage. Vol (20), Sept. 2016

PC-Based Ultrasound Object Detection System

Aung Naing Oo[1] , Mar Mar Cho[2]

Abstract

To determine the presence of object and to search the object when it moves from its initial position, the object detection system by using ultrasound transducers is constructed. The PIC microcontroller (PIC16F628A) is programmed to generate the required driving clock frequency for ultrasound transmitter (T40-16). The echo sent back from the detected object is received by the ultrasound receiver (R40-16). Then, the received echo pulse is amplified and transformed into digital signal by dual audio operational amplifier (LM833) and low power dual voltage comparators (LM393). Three receiver modules are constructed to sense the movement of the object. The receiver which accepts the echo sent back from the object is identified. The CMOS quad 2-input NAND schmitt triggers (CD4093B) is used to produce the proper logic level of signal receiver which receives the echo. The camera takes the picture of the object and sends to the monitor via VLC media player software. The stepper motor performs the movement of the constructed system either clockwise or counter clockwise direction. The operation of the system is controlled by the written program in Visual C Sharp programming language.

Keywords: PIC microcontroller, ultrasound transmitter, ultrasound receiver, Visual C Sharp programming language.

1. Introduction

Ultrasonic waves are mechanical waves that consist of oscillations or vibrations of the atomic or particles of a substance about the equilibrium positions of these particles. Ultrasonic waves behave essentially the same as audible sound waves. They can propagate in an elastic medium, which can be solid, liquid or gaseous, but not in a vacuum.

To find a barrier in the path or to avoid from the obstacles, ultrasonic transducers are used to detect the presence of object. In this work, 40 kHz driver circuit is constructed by PIC microcontroller (PIC16F628A). This frequency is sent to the ultrasonic transmitter circuits. The ultrasonic transmitter (T40-16) produces the ultrasound. When the transmitted ultrasound detects the object, echo is appeared. The ultrasonic receiver (R40-16) accepts the echo that falls on to it. The signal is amplified by dual audio operational amplifier (LM833). The amplified signal is sent to the low power dual voltage comparators (LM393) to be free from the noise interference. After that the output voltage from LM393 is changed to digital logic level of HIGH or LOW corresponding on the existence of object or not. Then, the logic level is sent to the personal computer via line printer terminal. The written program controls the operation of stepper motor depending on the logic level sent along the line printer terminal. The PC camera mounted on the circuit board sends the photographs of objects that lie in front of it. These photographs are shown on the monitor.

2. PIC Microcontroller

A microcontroller is an inexpensive single-chip computer. The PIC16F628A is 18-pin flash-based member of the versatile PIC microcontroller. It is complementary metal oxide semiconductor and has high performance. It employs an advanced RISC architecture. The

[1] Dr. Lecturer, Department of Physics, Yadanabon University
[2] Dr. Lecturer, Department of Physics, Yadanabon University

PIC16F628A has enhanced core features, eight-level deep stack, and multiple internal and external interrupt sources. The separate instruction and data buses of the Harvard architecture allow a 14-bit wide instruction word with the separate 8-bit wide data. The two-stage instruction pipeline allows all instructions to execute in a single-cycle, except for program branches. A total of 35 instructions are available, complemented by a large register set. Fig. (1) shows the photograph and pin diagram of PIC16F628A microcontroller.

Figure1. The photograph and pin diagram of PIC16F628A microcontroller

2.1 Ultrasonic Transducer (TR40-16)

The T40-16 and R40-16 are matched pair ultrasonic transmitter and receiver respectively operated at 40 kHz center frequency. This transducer utilizes the piezoelectric properties of engineering ceramic that provides high sound pressure and high sensitivity. Fig. (2) shows the photograph of ultrasonic transducer (TR40-16).

Figure2. Photograph of ultrasonic transducer (TR40-16)

2.2 Stepper Motor

A stepper motor is an electromechanical device which converts electrical pulses into discrete mechanical movements. The shaft or spindle of a stepper motor rotates in discrete step increments when electrical command pulses are applied to it in the proper sequence. The motor rotation has several direct relationships to these applied input pulses. The sequence of the applied pulses is directly related to the direction of motor shafts rotation. The speed of the motor shafts rotation is directly related to the frequency of the input pulses and the length of rotation is directly related to the number of input pulses applied. The photograph of stepper motor is shown in Fig. (3).

Figure 3. Photograph of stepper motor

2.3 Design and Construction

To find the barrier in path or to know the disappearance of the object, object detection systems are constructed. In these systems, infrared sensor or ultrasonic transducers are used. This work is intended to detect an object which is placed in front of the detector. In this work, ultrasonic transducers are used to detect the object.

The block diagram of the constructed system is shown in Fig. (4). The system is composed of seven main parts. They are power supply unit, oscillator unit, ultrasonic transmitter unit, ultrasonic receiver unit, level comparator unit, interfacing unit and stepper motor control unit.

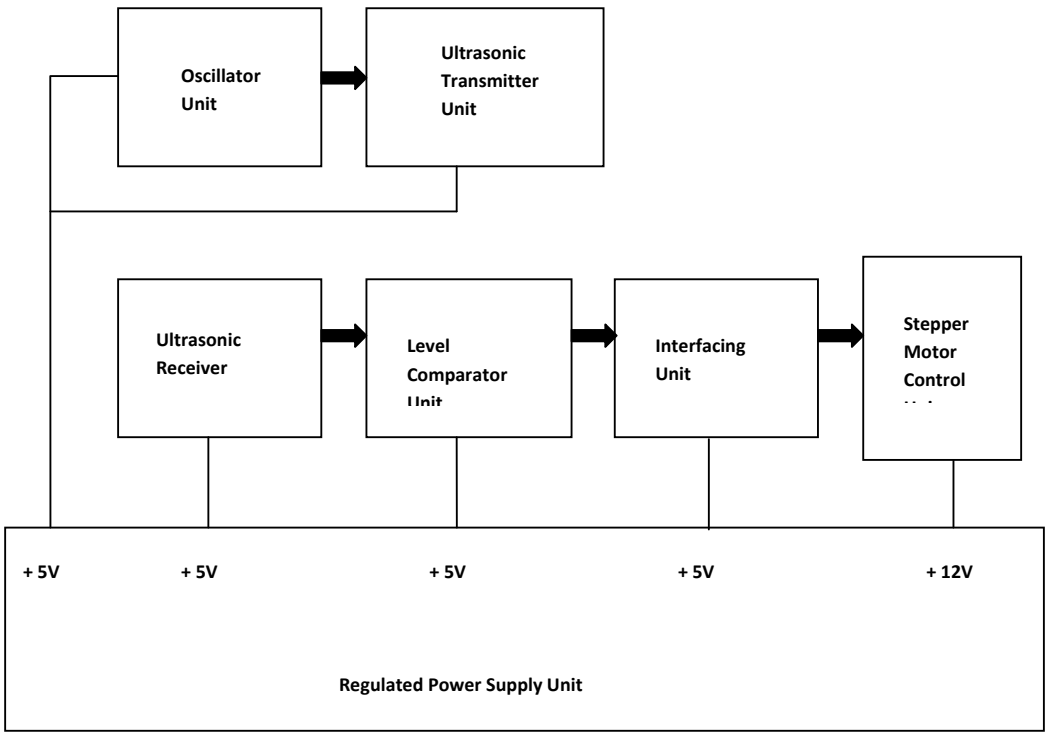

Figure 4. Block diagram of the constructed system

The oscillator circuit composed of PIC microcontroller (PIC16F628A) is used to generate the required driving clock frequency. The ultrasonic transmitter unit and ultrasonic receiver unit are constructed by using ultrasonic transmitter (T40-16) and ultrasonic receiver (R40-16). To get the noise free voltage level, level comparator circuits are constructed by using low power dual voltage comparators (LM393). For interfacing with the personal computer, the interfacing circuit using CMOS quad 2-input NAND schmitt triggers (CD4093B) is also attached. When the object is disappeared, the transducer units are needed to rotate either in clockwise or counter clockwise direction in searching the object. Therefore, stepper motor control circuit is also constructed. To show the object on the monitor, a camera is also fixed in this system. Fig. (5) shows the ultrasonic transmitter and receiver transducers array.

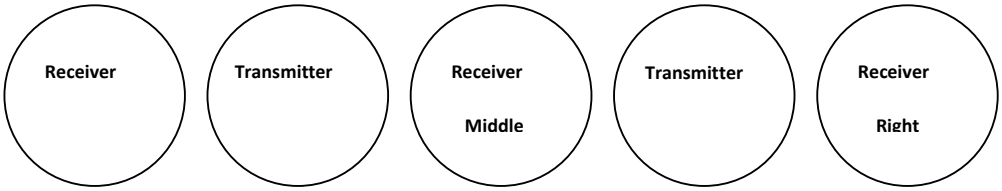

Figure 5. The ultrasonic transmitter and receiver transducers array

3. Results and Discussion

The oscillator produces the required clock frequency. The ultrasonic transmitter (T40-16) uses this frequency and sends out the ultrasound. When the ultrasound hits the object, the echo is appeared. This echo is received by the ultrasonic receiver circuit and sent to the personal computer. The written program determines the presence of object. If there is no object, no echo is appeared. Since there are three receivers for middle, left and right positions, the movement of the object from its initial position can be known. The written program also drives the stepper motor to rotate in clockwise or counter clockwise direction until the system finds the object. The function of the constructed system is shown in Fig. (6).

The photograph of constructed circuit is shown in Fig. (7). Fig. (8) shows the complete circuit diagram of the constructed circuit.

Ultrasonic Receiver			**Stepper Motor Rotation**
Left	**Middle**	**Right**	
OFF	ON	OFF	Stationary (No Rotation)
ON	OFF	OFF	Counter Clockwise Rotation
OFF	OFF	ON	Clockwise Rotation

Figure 6. The function of the constructed system

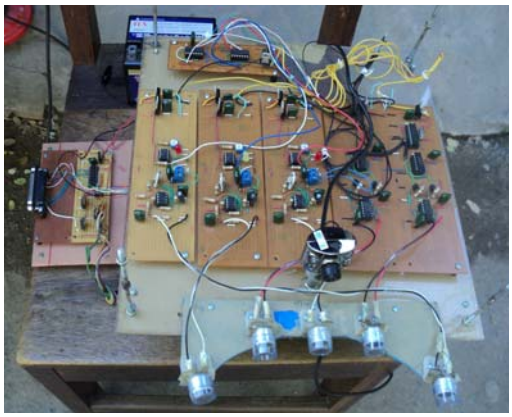

Figure 7. Photograph of constructed circuit

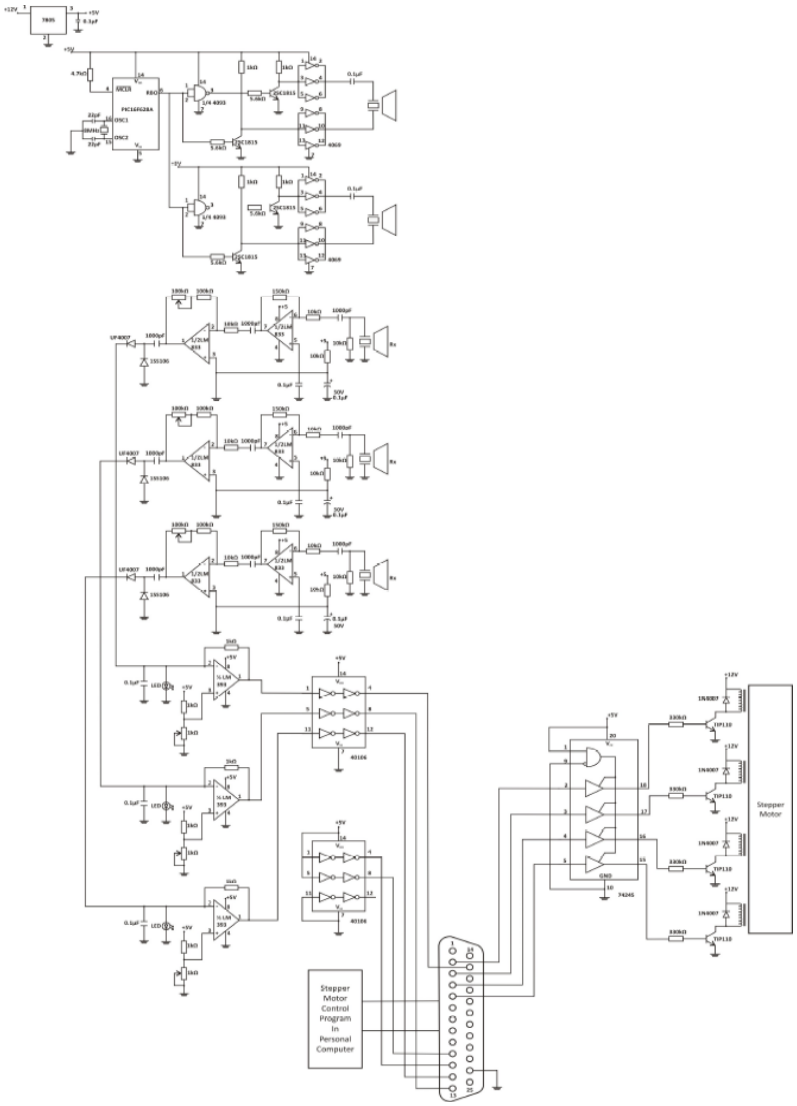

Figure 8. Complete circuit diagram of the constructed circuit

4. Conclusion

In this work, three ultrasonic receivers (R40-16) are used to detect the movement of object. Each ultrasonic receiver is needed to get the noise free echo for the exact object location. So, the voltage gain from dual audio operational amplifier (LM833) is limited even though the operational amplifier has very high open loop gain. Therefore, the constructed work is effective in detecting the object in short range.

Circuit design and programming for PIC microcontroller and personal computer is also very important in carrying out this work. The enhancement of knowledge of application of PIC microcontroller, interfacing with the personal computer is the great advantage of this work.

Acknowledgements

We would like to express our gratitude to Dr Maung Maung Naing, Rector, Dr Si Si Khin, Pro-Rector and Dr Tin Moe Thuzar, Pro-Rector of Yadanabon University for their suggestion and permission to perform this project work. We would also like to express our great thanks to Dr Yi Yi Myint, Professor (Head of the Department), Dr May Thida Win, Professor and all the teachers and staff from the Department of Physics, Yadanabon University for their help and discussion throughout this research work.

References

[1] J. David N. Cheeke, “Fundamentals and Applications of Ultrasonic Waves”, CRC Press LLC, United States of America (2002).

[2] Parallax Inc., “Detect Distance With The Ping))) Ultrasonic Sensor”, http://www.parallax.com (2005).

[3] Waitrony, “Ultrasonic Transducer (TR40-16)”, http://www.ic-on-line.cn (2003).

[4] R. A Penfold, “Easy PC Interfacing”, Bernard Babani Ltd., England (1995).

[5] S. Mueller, “Upgrading and Repairing PCs”, 14th Edition, Que, Indiana (2003).

[6] J. Iovine, “PIC Microcontroller Project Book”, McGraw-Hill, New York (2000).

[7] Microchip Technology Inc., “PIC16F627A/628A/648A Data Sheet”, United States of America (2004).

[8] Stmicroelectronics, “LM393”, http://www.st.com (2011).

[9] National Semiconductor Corporation, “LM7805”, http://www.national.com (2006).

[10] National Semiconductor Corporation, “LM833”, United States of America (1995).

[11] Texas Instruments, “CD4093B”, Dallas (2003).

[12] Philips Semiconductors, “HEF40106B”, http://www.datasheetcatalog.com (1995).

[13] Texas Instruments, “SN74LS245A”, Dallas (2003).

Green Synthesis and Characterization of Chitosan-Copper Nanoparticle Used as Antimicrobial and Antitumor Activities

Aung Than Htwe[1], Thinzar Nu[2], Cho Cho[3]

Abstract

This work is an attempt to aim to synthesize, characterize and apply of eco-friendly green synthesized copper - chitosan nanoparticles (Cu-NPs). In this work the environmentally friendly synthesis of stable Cu chitosan NPs through green route with chitosan as a stabilizer and or reducing agent was synthesized. The synthesized copper nanoparticles were confirmed by the change of colour after addition of chitosan into the Copper (II) sulphate solution. The biosynthesized CuNPs were characterized by using UV-Vis, Fourier Transform Infrared (FTIR), X-ray diffraction analysis (XRD) and Scanning Electron Microscopy (SEM). Average crystalline size of the nanoparticles was estimated from the Debye- Scherrer's equation. The antimicrobial activity of the nanoparticles were investigated using six microorganisms of interest, including *Staphylococcus aureus, Bacillus subtilis, Pseudomonas aeruginosa, Bacillus pumilus, E-coli and Candida albicans*. The effect of a chitosan medium on growth of the microorganism was studied, and this was found to influence growth rate. The antitumor activities of the synthesized CuNPs were investigated by Potato Crown Gall teat and these activities were found to be within 5-7 days by the dose of 0.05, 0.1 and 0.15 g of CuNPs. Finally, the present study provided to full fill the scientific evidence, become a new trend to save and reduce environmental pollution and safety in bactericidal, wound healing and other medical applications.

Keywords: Chitosan, Cu-NPs nanoparticles, antimicrobial activity, antitumor activity

1. Introduction

Bacterial and fungus infection is a problem in all over the world. So this chitosan-copper nanoparticles (CuNPs) is to solve and reduce this problem.

Metal nanoparticles have attracted considerable attention in many fields, such as catalysis, optoelectronics, photovoltaic technology, information storage, environmental technology, engineering, biosensors development, medicine, and so on [1]. Among nanomaterials, nanoparticles have been contributing to the progress in this field. In particular, therapies using nanoparticles have widely been achieved for the treatments of cancer, diabetes, allergy, infection and inflammation [2]. Generally, metallic nanoparticles show antibacterial and antifungal activity, even though there are environmental and human safety concerns regarding the release and consumption of metal nanoparticles which are yet to be explored. Excessive release of silver, for example, causes environmental pollution which in turn makes silver harmful to human and animals. An excess of copper in the human body leads to generation of the most damaging radicals, such as the hydroxyl radical [3]. Nanomaterials are widely used in various technological applications viz. refrigeration systems, medical imaging, drug targeting and other biological applications, and catalysis [4].

[1] Dr Assistant Lecturer, Department of Chemistry, University of Yangon, Myanmar, e-mail: aungthanhtwe76@gmail.com

[2] Associate Professor, Department of Chemistry, University of Yangon,Myanmar, e-mail: thinzarnu50@gmail.com

[3] Professor, Department of Chemistry, University of Yangon, Myanmar, e-mail: chocho.urc@gmail.com

Environmentally friendly solvents, reducing agents are used with enormous potential as part of a responsible green approach for the development of nanotechnology. Biocompatible and nontoxic polymers (e.g. chitosan) as a reducing and stabilizing agent of metal nanoparticles is suggested [1]. Copper nanoparticles (CuNPs), due to their excellent physical and chemical properties and low cost for preparation, have been of great interest [5].

Chitosan is a natural product derived from chitin, a polysaccharide present in the exoskeletons of shellfish such as shrimps and crabs. It is a cationic polysaccharide composed of β-(1-4)-linked D-glucosamine and N-acetyl-D glucosamine units. Environmental-friendly material with many superior properties with momentous amounts of amine and hydroxyl groups that can be easily engineered [6]. The antimicrobial action is influenced by intrinsic factors such as the type of chitosan, the degree of chitosan polymerization, the host, the natural nutrient constituency, the chemical or nutrient composition of the substrates or both, and the environmental conditions (e.g. substract water activity or moisture or both) [7]. The NPs generated are strongly attached to the chitosan due to the chemical bond between the electron rich nitrogen present in the amino groups of the polymer and copper. The use of biopolymer as capping and or reducing agents represents an environmentally friendly alternative to hazardous organic solvents [8].

The present work deals with environmentally friendly synthesis of stable chitosan-copper nanoparticles through green route with chitosan as a stabilizer and or reducing agent. The synthesized NPs were characterized by UV-Visible spectrometry, SEM, and XRD. Their antimicrobial properties were tested using microorganism such as fungi, algae and some bacteria. Finally, antitumor activities were investigated.

2. Methods

2.1 Synthesis of Chitosan-Copper Nanoparticles (CuNPs)

In a typical one-step synthesis, 50 mL of 1 % (w/v) chitosan solution was prepared by using 1 g of chitosan(CS) was dissolved in 100 mL of 1 % acetic acid solution. 50 mL of 1 % CS solution and 25 mL of 0.05 M $CuSO_4.5H_2O$ were then mixed and stirred on magnetic stirrer at 80 °C for 12 h till the reaction was completed. After 12 h the colloid was centrifuged at 7,000 rpm for 20 mins to separate particles from suspension. The precipitate was re-suspended in acetone (90%, v/v) and the centrifugation was repeated three times to remove unreacted reagents. Finally, the precipitate was dissolved in water, dried under vacuum overnight and stored.

2.2 Characterization of Cu NPs

UV-visible spectra were recorded using a Shimadzu UV-Vis1800 Spectrophotometer for the confirmation of NP formation. The structural features of Cu-Chitosan NPs were performed in a PerKinElmer GX system FT IR spectrometer in a range from 400 to 4000 cm^{-1}. The size and morphology of the Cu-Chitosan NPs were examined by SEM (JEOL model JSM 5610 LV scanning microscope). X-ray diffraction studies were performed with an X-ray diffractometer (Rigaku Ultima III XRD) with Cu Kα1 radiation to determine the structure of a sample. The X-ray source was operated at 40 kV and 40 mA. Diffraction intensity was measured in the reflection mode at a scanning rate of 2°/min for 2θ=10-70°.

2.3 Determination of Antimicrobial Activity

The CuNPs was tested with *Bacillus subtilis, staphylococcus aureus, Pseudomonus aeruginosa, Bacillus pumalis, Candida albican and E. coil* species to investigate the nature of antimicrobial activity. After preparing the bacteriological media, the dried films were placed on the agar with flamed forceps and gently pressed down to ensure proper contact. The plates were incubated immediately or within 30 min after incubation [9, 10]. After overnight incubation at 37 ºC, the results are shown in Table 1 and Figure 1.

2.4 Screening of Antitumor Activity by Potato Crown Gall Test or Potato Disc Assay

Tumor producing bacteria, *Agrobacterium tumefacien*, was used in this study. All of these strains have been maintained as solid slants under refrigerator. For inoculation of potato discs, 48 h broth cultures containing $5\times 10^7 - 5\times 10^9$ cell/mL were used. *Agrobacterium tumefaciens* strain was cultured on Luria-Bertani (LB) agar medium which was prepared by dissolving a mixture of yeast extract (1 g), peptone (1 g), NaCl (0.5 g) and agar (2 g) in distilled water (100 mL). Single colony was transferred into LB broth and incubated at 30 °C for 48 hours in the shake. Six to seven loops of bacterial suspensions (1.0×10^9 cfu) were transferred into sterilized phosphate buffer saline (PBS) and this was used during antitumor assay inoculums. The antitumor activity was examined by observation of tumor produced or not.

3. Results and Discussion

The formation of Cu-NPs was observed in a series of colour changes. The addition of Cu^{2+} solution to CS solution resulted in the appearance of a light blue which indicates the formation of a $[Cu (CS)]^{2+}$ (aq) complex figure 1. The reduction of metal ion is one of the most convenient and promising synthetic approaches to obtain metallic nanoparticles with relatively inexpensive setups. Cu-NPs are very difficult to obtain by simple reduction of copper salts in aqueous solution where copper is oxidized to CuO and Cu_2O [6].

chitosan solution | *$CuSO_4.5H_2O$ (aq)* | *$[Cu(CS)]^{2+}$* | *[Cu(CS)]NPs*

Figure 1: Photographs of the sample at the different stages of synthesis showing colour variations

3.1 UV-visible Spectrophotometric Analysis

The observation of the absorption spectra of different aliquots overtime containing copper sulphate (50 mM) in chitosan (0.75% w/v) showed major peak in the range 500-600 nm , thus revealing the formation of Cu-NPs. The colloidal Cu-NPs prepared at 12 h at 70 °C showed a characteristic single absorption peak at 536 nm (Figure 1), which indicates the decrease of reactants Cu^{2+} ions in the presence of chitosan to the formation of large amount of monodisperse NPs. The present finding was in agreement with the blue shift of the surface plasmon resonance

(SPR) of the metallic NPs with their decreasing size. Nanosized Cu particles exhibited a SPR at around 500-600 nm. This shows that copper ions was added to the chitosan solution. This is to indicate that Cu^{2+} ions are attached to chitosan macromolecules by electrostatic interactions. The electron-rich oxygen atoms of polar hydroxyl and ether groups of chitosan are responsible to interact with electropositive metal cations. It has been reported that chitosan acts as a controller of nucleation as well as a stabilizer [8].

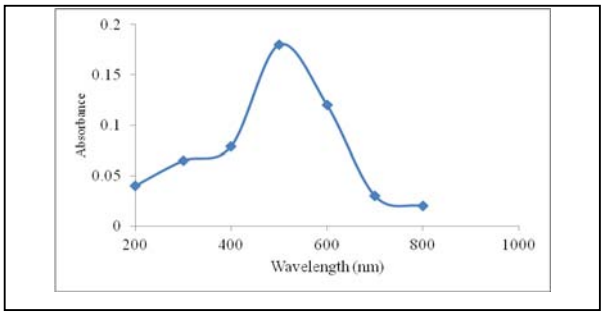

Figure 2: UV- visible spectrum of synthesized copper-chitosan nanoparticle

3.2 FTIR Analysis

FTIR analysis was conducted to determine the molecular interactions between chitosan and the synthesized NPs. The chitosan spectrum in figure 3(b) illustrates an amide I C = O vibration band at 1633.94 cm^{-1}. The spectrum also dhows transmissions at 3303.19 cm^{-1} assigned to the overlap of O-H and N-H stretching vibrations, 1633.94 cm^{-1} and 1537.88 cm^{-1} to -NH_2 bending, 1336.57 cm^{-1} to C-H bending and 1064.11 cm^{-1} to -C-O skeletal stretching. A similar trend was observed in CuNPs spectrum (figure 3(c)). For instance, a general decrease in band with a blue shift was noticed (from 1633.94 to 1632.60, 1537.88 to1531.25 and 1064.11 to 1063.68 cm^{-1}). The peak at 611.7 cm^{-1} evidence the interaction between CuNPs and CS media which indicates a reaction between the CuNPs surface, and the CS amino and hydroxyl group [3, 11].

The experiments described above indicate the importance of chitosan in the performed synthesis. Chitosan, as a biopolymer, has a significant content of primary amines and hydroxyl groups and possess a strong affinity towards metal ions, which are incorporated by simple chelation by ion exchange, thereby making it an excellent support for nucleation of Cu-NPs. The generation of $[Cu\ (CS)]^{2+}$ complexes in solution enables metal ion reduction. From these results, it can be envisaged that the biopolymer plays an important role as polymeric capping agent (Stabilizer) [1].

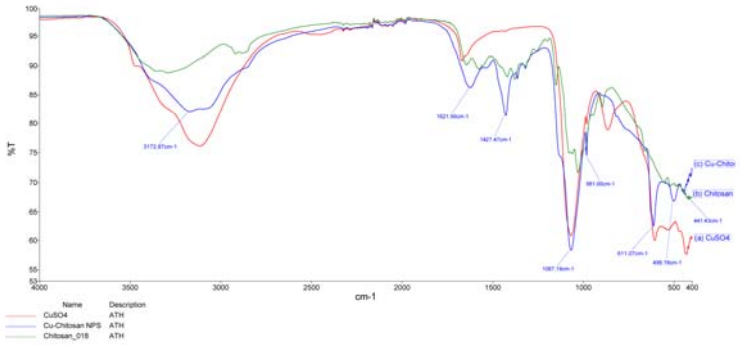

Figure 3. FT IR Spectrum of synthesized copper-chitosan nanoparticle

3.3 Powder X-ray Diffraction Analysis

The solid state or crystallinity of the synthesized CuNPs was characterized by X-ray diffractometry. The XRD diffractogram of the CuNPs are shown in figure 4. The XRD pattern for CuNPs exhibited two crystalline peaks at 2θ angles of 36.628 ° and 50.141° respectively. The prominent diffraction peaks observed are indexed to (111) and (200) reflections. This confirms that the resultant nanoparticles are face centered cubic (fcc) of metal nanoparticles. The highest intense peak for fcc materials is generally (111) reflection and this was observed in the synthesized nanoparticles. These planes observed were compared with the standard powder diffraction card of JCPDS copper file No. 78-0428 and copper X-ray diffraction reference No. 85-1326. The absence of any noticeable peaks in the pattern resulting from the sample suggests that the sample is free from impurities such as CuO and Cu_2O. The average crystalline size of the CuNPs obtained was estimated to be in the range of 28.221 nm using Debye-Scherrer equation is given as: $D = \frac{K\lambda}{\beta \cos\theta}$, where D is the mean nanoparticles diameter (Particle size), K is a constant with value 0.94, λ is the wavelength of X-ray (0.154), β is full width at half maximum and θ is the differential angle [12].

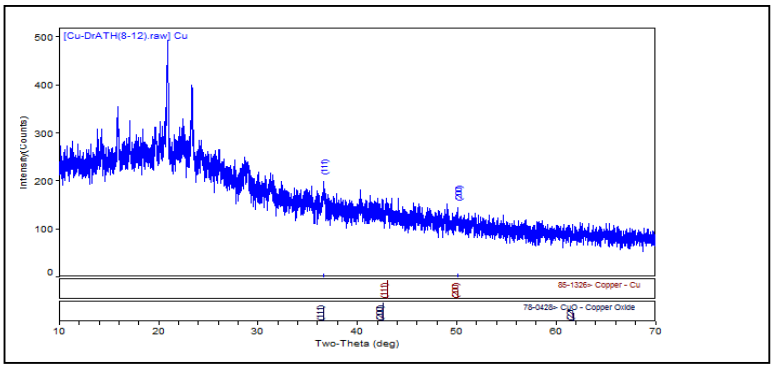

Figure 4. XRD diffractogram of synthesized copper-chitosan nanoparticle in chitosan media

3.4 SEM

The surface morphology of synthesized CuNPs was examined and the thickness of these particles was determined by JEOL scanning electron microscopy. The thickness was approximately 10 μm. The micrograph of the cross-section surface structure of CuNPs was shown in figure 5. From the micrographs the CuNPs found to be made up of the slightly

aggregated due to the absence of strong surface protecting ligands and found to be irregular in shape.

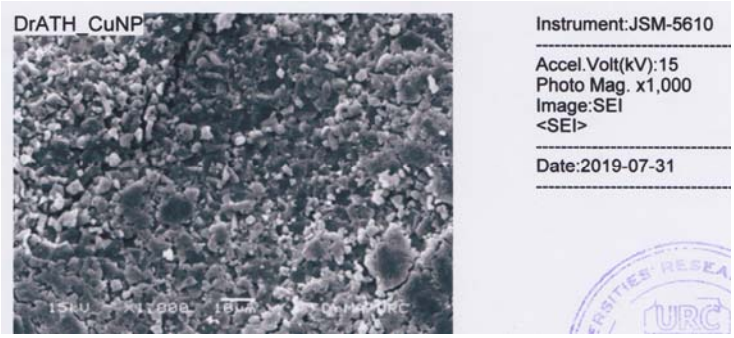

Figure 5. SEM micrograph of synthesized copper-chitosan nanoparticle

3.5 Antimicrobial Activity of CuNPs

Antimicrobial activity of CuNPs are shown in Table 1. Tested organisms were *Bacillus subtitles*, *Staphylococcus aurous*, *Pseudomonas aeruginosa*, *Bacillus pumalis*, *Candida albican* and *E.Coli*. As seen in figure 6, antimicrobial test of CuNPs was used the agar medium cultivation. According to the experimental results, the prepared CuNPs was really effective to antimicrobial activity. The cell wall is more exposed to nanoparticles through the outer bacterial membrane. The unique high surface to volume ratio of CuNPs enables them to interact with the bacterial cell membrane through its surface, which leads to the death of the bacterium. Therefore, the size of the nanoparticles is important for antimicrobial activity [3]. It was observed that CuNPs was bactericidal and fungicidal against both gram-positive and gram-negative bacteria and fungus.

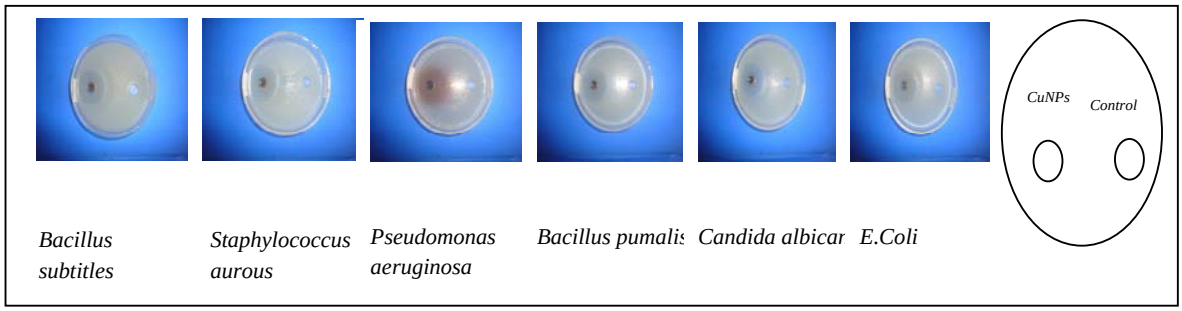

Figure 6. Antimicrobial activities of synthesized copper-chitosan nanoparticle

Table 1. Antimicrobial Activity of CuNPs by Agar Disc Diffusion Method

Sample	***Microorganism***					
	Bacillus subtilis	***Staphylococcus aureus***	***Pseudomonas aeruginosa***	***Bacillus pumilus***	***Candida albican***	***E-coil***
CuNPs	25 mm (+++)	20 mm (+++)	13 mm (+)	16 mm (++)	23 mm (+++)	21 mm (+++)

Agar well 10 mm, 10 mm-14 mm (+), 15 mm-19 mm (++), 20 mm above (+++)

3.6 Antitumor Activity of CuNPs

The antitumor activity of CuNPs was investigated by using PCG test with bacterium *A. tumefaciens*. For inoculation of the potato disc, 48 h broth cultures containing 5× 10^9 cells/mL were used. The tested sample was dissolved in DMSO, diluted and mixed with the bacterial culture for inoculated on the cleaned and sterilized potato discs, and incubated for 7 days at room temperature. After that, the tumors were appeared on potato disc and checked by staining the knob with Lugol's (I_2-KI) solution. In the control the formation of while knob were on the blue background indicated the presence of tumors cell because there is no protein in tumor cells. The tested sample did not form any tumors on the potato discs and its surface remained blue. Form this experiment, it was found that CuNPs was not significantly inhibited the formation of tumor cell with the dose of 0.1, 0.2 and 0.3 g/disc. These results are shown in Table 2 and figure 7.

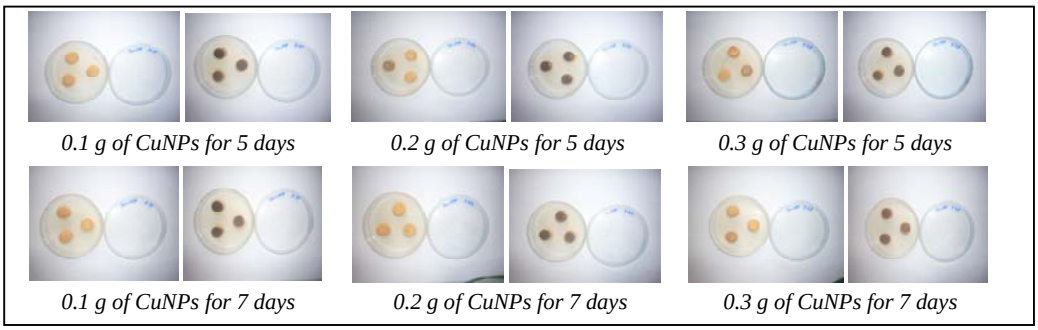

Table 2. Antitumor activity of CuNPs

sample	**Days**	**Concentration/disc (mg)**		
		0.1 g	**0.2 g**	**0.3 g**
CuNPs	**5**	+	+	+
	7	+	+	+
Control	++			

Tumor inhibition:

(++) = non activity

(+) = less activity

4. Conclusion

The present study indicates that of CuNPs with a size of 28.22 nm have been successfully synthesized in the presence of a biowaste polymer chitosan. The synthesized NPs were characterized by UV-Vis, FTIR, XRD and SEM analyses. From FTIR analysis, the peaks of the CuNPs are attributed to N-H, O-H, C=O, C-O, C-OH, CH and Cu-O stretching and bending vibrations. The average crystalline size of CuNPs nanoparticle is 28.22 nm and agglomerate porous and crystalline nature. The chitosan plays the main role of chelating with metal ions. The synthesized CuNPs exhibited good antimicrobial and antitumor activity. The present synthetic method represents a simple, convenient, cost-effective and environmental-friendly. The main contribution of the present work producing chitosan-copper nanoparticles could promote to a certain extent of sustainable development and foster innovation toward and may be used for pharmaceutical and biomedical application.

Acknowledgements

The authors feel indebted to Professor and Head Dr. Ni Ni Than, Department of Chemistry, University of Yangon, Yangon, Myanmar, for his stimulating suggestions. I would like to express my deepest gratitude to Science Council of Asia (SCA) and Myanmar Academy of Arts and Science for this conference.

References

[1] Katarzyna Tokarek, Jose L Hueso, Piotr Kustrowski, Grazyna Stochel, Agnieszka Kyziol, "Green synthesis of chitosan-stabilized copper nanoparticles", European Journal of Inorganic Chemistry, 2013, vol.28, pp. 4940-4947.

[2] Sachiko Kaihara Nitta, Keiji Numata, "Biopolymer-based nanoparticles for drug/gene delivery and tissue engineering", International Journal of Molecular Science, 2013, vol. 14, pp. 1629-1654.

[3] Muhammad Sani Usman, Mohamed Ezzat EI Zowalaty, Kamyar Shameli, Norhazlin Zainuddin, Mohamed Salama and Nor Azowa Ibrahim, "Synthesis, characterization, and antimicrobial properties of copper nanoparticles", International Journal of Nanomedicine, 2013, vol. 8, pp. 4467-4479.

[4] Marimuthu Nidhin, Ramasamy Indumathy, Kalarical Janardhanan Sreeram, Balachandran Unni Nair, "Synthesis of iron oxide nanoparticles of narrow size distribution on polysaccharide templates" , Bulletin of Materials Science, 2008, vol. 31(1), pp. 93–96.

[5] Muhammad Sani Usman, Nor Azowa Ibrahim, Kamyar Shameli, Norhazlin Zainuddi, Wan Md Wan Yunus, "Copper nanoparticles mediated by chitosan: synthesis and characterization via chemical methods", Molecules, 2012, vol. 17, pp. 14928-14936.(DOI: 10 3390/molecules 171214928)

[6] Kaushik Mallick, Mike J. Witcomb, Mike S. Scurrell, "In Situ synthesis of copper nanoparticles and poly (o-toluidine): a metal-polymer composite material", European Polymer Journal, 2006, vol. 42, pp. 670-675.

[7] Entsar I. Rabea, Mohamed E. T. Badawy, Christian V. Stevens, Guy Smagghe and Walter Steurbaut, "Chitosan as antimicrobial agent: Applications and Mode of Action", Biomacromolecules, 2003, vol. 4 (6), pp. 1457-1465.

[8] Appu Manikandan and Muthukrishnan Sathiyabama, "Green synthesis of copper-chitosan nanoparticles and study of its antibacterial activity", Journal of Nanomedicine & Nanotechnology, 2015, vol. **6**(1), pp. 1-5. (DOI: 10.4172/2157-7439.1000251)

[9] Norashikin Mat Zain, Andrew G. F. Stapley, Gilbert Shama, "Green synthesis of silver and copper nanoparticles using ascorbic acid and chitosan for antimicrobial applications", Carbohydrate Polymers, 2014, vol. 112, pp. 195-202.

[10] Aung Than Htwe, Sandar Tun, Khin Aye May, Kyaw Myo Naing, "Studies on preparation, characterization and application of pH-sensitive biodegradable chitosan-polyvinyl alcohol hydrogel", Jour. Myan. Acad. Arts & Sc., 2013, vol. XI (1), pp. 127-140.

[11] Thi My Dung, Thi Thu Tuyet Le, Eric Fribourg-Blanc, Mau Chien Dang, "The influence of solvents and surfactants on the preparation of copper nanoparticles by a chemical reduction method", Advances in Natural Science: Nanoscience and Nanotechnoloty, 2011, vol. 2, pp. 1-7.

[12] Krithiga N, Jayachitra A. Synthesis of copper nanoparticle by chemical method and analysis, its significant antibacterial activity. International Journal for Research in Applied Sciences and Biotechnology, 2014, vol. 1(1), pp.22-27.

Determination of Ion Occupation Model in Spinel Lettice

Aye Aye Thant[1], Thet Phyu Phyu Naing[2]

Abstract

Ferrite materials have exploited for a number of extensive applications in non-reciprocal devices at microwave frequencies. Ferrite samples with the chemical composition $Ni(Gd_xFe_{1-x})_2O_4$ (x = 0.0125, 0.0250, 0.0375 and 0.0500) were prepared by Conventional Ceramic Method. By introducing a relatively small amount of Gd^{3+} ions instead of Fe^{3+} ions, the crystallization of these dopants in the mother system was investigated. The structural analyses were performed via X-ray diffraction (XRD) and Scanning Electron Microscope (SEM). The partial substitution of Gd^{3+} ions in the place of Fe^{3+} ions was confirmed by the decrease in the lattice parameter with the Gd^{3+} concentration. The formation of small crystallite and grains are responsible for the increase of coercivity with Gd^{3+} ion substitution. The model of ion occupation among the available tetrahedral (A) and octahedral (B) sites of spinel was estimated by the obtained magnetic moment per unit cell and the Bohr magneton of each ion in the lattice according to spin quantization.

Keywords: nickel ferrite, Gd^{3+} ion, conventional, coercivity, ion occupation

1. Introduction

Spinel ferrite in general and magnesium-manganese in particular have extensive applications in construction of non-reciprocal devices at microwave frequencies [1]. Ferrimagnetic cation substituted spinal ferrites are technologically versatile materials [2]. The interesting physical and chemical properties of ferrospinels arise from their ability to distribute the cations among the available tetrahedral (A) and octahedral (B) sites [3]. The addition of trivalent ions in ferrites influences the electric and magnetic properties of the system; density, crystallite size, grain size, residual macrostress and initial permeability [4], [5]. The rare earth oxides are becoming the promising additives for the improvement ferrite properties [6], [7]. In the case of advanced functional materials, doping with small concentration of rare earth is a well-known versatile way to tune the desirable physical properties of ferrites not only because of the lanthanide contraction which induces monotonic change of ionic radii, but also because of the different stable oxidation states and the periodical variation in magnetic moments coming from the sequential filling of electrons in their 4f shells [8]. To date very few literature is available reporting the effect of rare earth atom on the properties of ferrite. In this background, nickel ferrite doped with gadolinium ions was prepared by conventional ceramic technique to provide an accurate understanding of the changes caused by the substitution.

2. Materials and Methods

Specimens of the Gd doped Ni ferrites, Ni $(Gd_xFe_{1-x})_2O_4$, where x = 0.0125, 0.0250, 0.0375 and 0.0500, were grounded in an Agate mortar for 4 h. The mixture was pre-sintered at 1000 ºC for 4 h with heating rate of 20 ºC /min, and cooled to room temperature with the same rate. The mixture was ground with an Agate mortar for 1 h. A few drops of PVA binder were added to the powder and the powder was pressed into pellets by uniaxial hydraulic press at a pressure of 150MPa. The final sintering was performed at 1100 ºC for 10 h with the heating rate

[1] Dr. Professor, Department of Physics, University of Yangon, Myanmar, ayeayethant@uy.edu.mm
[2] Yangon, Myanmar, thetzin18@gmail.com

of 20 ºC/min. The pellets were well polished for further characterizations. The phase formation of the sintered ferrite pellet was checked using XRD. The morphology of the samples was examined by using SEM. The magnetic properties were also measured and the model of ion occupation among the available tetrahedral (A) and octahedral (B) sites of spinel was estimated in this work.

3. Results and Discussion

3.1 Structural Analysis by XRD

After preparing Gd doped Nickel Ferrite, Ni $(Gd_xFe_{1-x})_2$ O_4, by Conventional Ceramic Method, the structural characteristics of these samples were analyzed by XRD method. The XRD patterns of the samples with compositions (x = 0.000 and 0.0125) show the formation of single phase cubic spinel while the samples with (x =0.025, 0.0375 and 0.0500) involved a secondary phase at around 2θ value of 32º in addition to spinal phase as shown in Figure 1. Among the XRD patterns of the samples with gadolinium (Gd) dopants, only the sample with compositions (x = 0.0125) exhibited single phase cubic structure while the samples with (x =0.025, 0.0375 and 0.0500) involved a secondary phase at around 2θ value of 32º in addition to spinal phase.

According to the literature, the secondary phase may be identified as $GdFeO_3$ phase. The initial sample $NiFe_2O_4$ is inverse spinel and Gd^{3+} ions preferentially occupy the B-sites. It was estimated from the present study that the Gd^{3+} ions preferentially occupy the B-sites at Gd concentration x > 0.0125 while small fraction of it also entered into the A-sites.

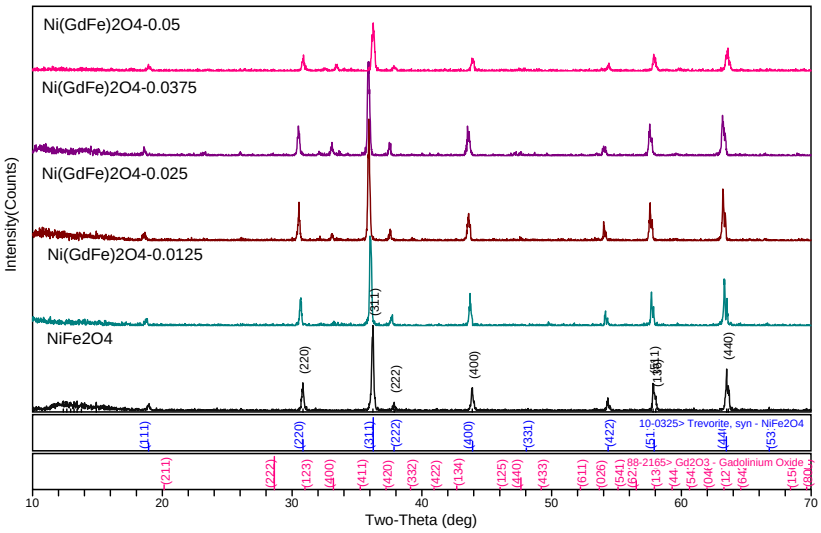

Figure 1. XRD patterns of $Ni(Gd_xFe_{1-x})_2O_4$, where x = 0.0125, 0.0250, 0.0375 and 0.0500.

3.2 Estimation of Lattice Parameter and Crystallite Size

The values of lattice constant were determined from the XRD data and presented in Table 1. The lattice constant slightly increases with increase in Gd-content. The increase of the lattice constants with increasing Gd concentration is strongly related to the relative ionic radius of Fe^{3+} and Gd^{3+} ions. The ionic radius of Fe^{3+} (0.64 Å) is smaller than that of Gd^{3+} (0.94 Å). It shows the increase of the crystalline lattice parameters. If the ionic radius of the impurity ion is larger

than that of the displaced ion, the lattice expends and the lattice constant increases. However, the lattice parameter again decreased with the Gd concentration x=0.0500 which is the largest value in this system. This observation again confirms the partial substitution of Gd ions in the place of Fe ions. The crystallite size was calculated from the XRD peak broadening of the (311) peak using Scherrer formula and presented in Table 1. It is observed that the crystallite size increased with the substitution of small amount of Gd^{3+} ions in $NiFe_2O_4$. However, the size became smaller with the increase in Gd dopants beyond x=0.0250. This may be due to the presence of secondary phase in the samples with larger amount of dopants. Moreover, the broad peaks in XRD patterns are due to fine crystallite size of the ferrite particles. The crystallite sizes of Ni $(Gd_xFe_{1-x})_2\ O_4$ were found to be in the range of 41 to 32 nm.

3.3 Structural Analysis by SEM

SEM investigations was conducted mainly on sample surfaces to obtain information with respect to grain morphology and bonding characteristics. SEM micrographs of Ni $(Gd_xFe_{1-x})_2\ O_4$ samples are shown in Figure 2. As shown in SEM micrographs, the grains are found to be in spherical shape. However, the grains become smaller and the pores between the necks of the grains become bigger with increasing Gd^{3+} ions substitutions. It reveals that the average grain size ranges from 1.07 μm to 1.66 μm for sintering at 1100 ºC.

Table 1**.** Lattice parameter, crystallite size as a function of the concentration of Gadolinium

Gd content (x)	**Ferrite**	**Lattice constant (nm)**	**Crystallite size (nm)**	**Average grain size (μm)**
0.0000	$Ni\,Fe_2O_4$	8.21	33.39	2.783
0.0125	$Ni(Gd_{0.0125}\,Fe_{0.9875})_2O_4$	8.26	32.64	2.466
0.0250	$Ni(Gd_{0.0250}\,Fe_{0.9750})_2O_4$	8.28	40.73	2.425
0.0375	$Ni(Gd_{0.0375}\,Fe_{0.9625})_2O_4$	8.29	33.74	2.183
0. 0500	$Ni(Gd_{0.0500}\,Fe_{0.9500})_2O_4$	8.21	34.37	2.151

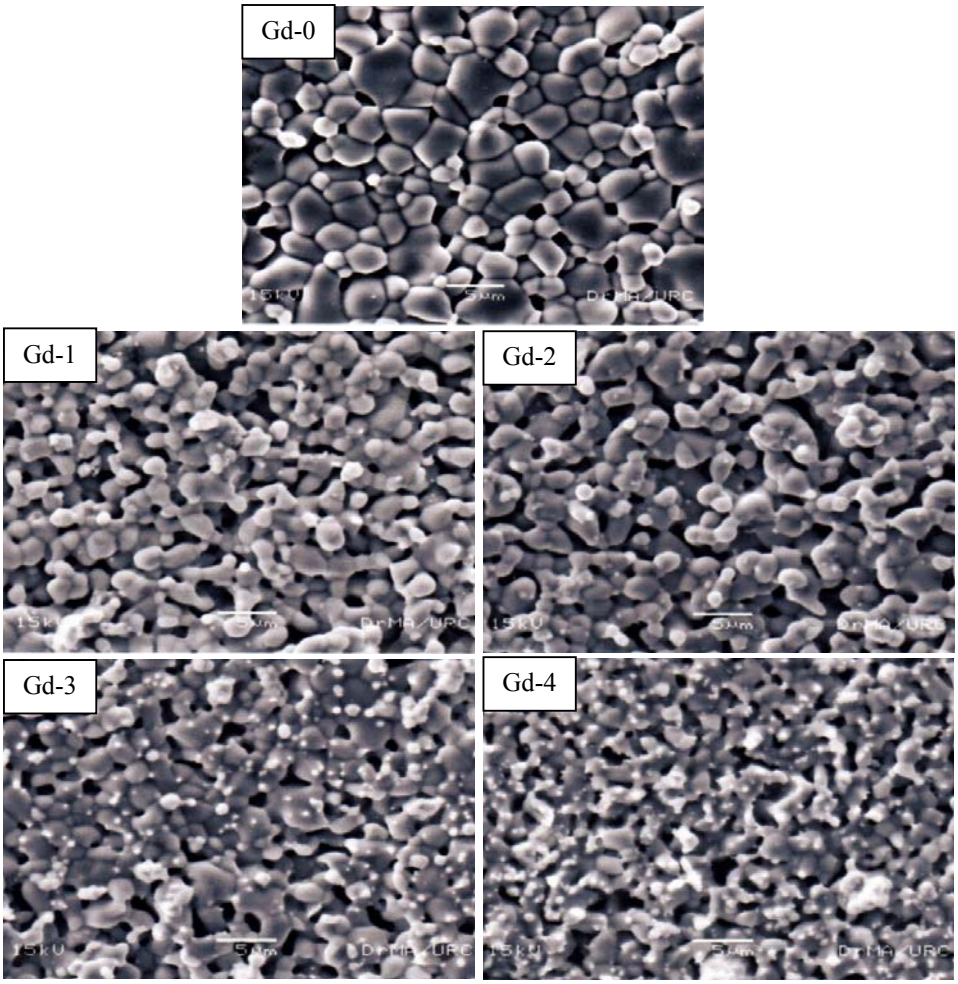

Figure 2. SEM micrographs of $Ni(Gd_xFe_{1-x})_2O_4$, x = 0.0000 (Gd-0), 0.0125 (Gd-1), 0.0250 (Gd-2), 0.0375 (Gd-3) and 0.0500 (Gd-4)

3.4 Analysis on Magnetic Hysteresis Loop

The most interesting characteristics in ferrite are the behavior of mixed ferrites with different non-magnetic ion concentrations. As the values of magnetization can be conveniently varied by suitable substitution, Gd^{3+} ions were substituted for Fe^{3+} ions in $NiFe_2O_4$ and the magnetizations were obtained for different compositions. The hysteresis loops Ni $(Gd_xFe_{1-x})_2$ O_4 are shown in Figure 3. From the hysteresis loops, the coercivity (H_c), saturation magnetization (M_s), magnetic moment (n_B) and remnant flux density (B_r) of the samples were calculated and presented in Table 2.

The increase in Gd^{3+} ion concentration leads saturation magnetization and saturation moment to be decreased. Gd^{3+} ion with ionic radius of 0.94 Å may prefer to occupy B site while Ni ions with ionic radius of 0.78 Å may enter both A site and B site. Since the resultant magnetization is the difference of B site magnetization and A site magnetization, the decrease in saturation magnetic moment pointed out that the magnetization resulted from the simultaneous increase of Gd^{3+} ion and decrease of Fe ions in B site is smaller than that from the decrease of Ni

ions and increase of Fe ions in A site. H_c shows an increase with increasing Gd^{3+} ions substitution. One important effect on H_c is the microstructural behavior. Therefore, the formation of small crystallite and grains are responsible for the increase of coercivity with Gd^{3+} ion substitution.

Table 2. Coercivity (Hc), the residual flux density (Br), saturation magnetization (Ms) and magnetic moment (nB) of $Ni(Gd_xFe_{1-x})_2O_4$

Gd contents (x)	Coercivity, H_c (O_e)	Saturation flux density, B_s (Gauss)	Residual flux density, B_r (Gauss)	Saturation magnetization, M_s (emu/g)	Magnetic moment, n_B (μB)
0.0000	5.90	893.19	803.87	70.64	2.9647
0.0125	9.56	738.45	521.26	58.03	2.4618
0.0250	12.12	617.82	376.06	48.22	2.0267
0.0375	14.20	551.26	413.45	42.75	1.8527
0.0500	14.81	403.50	238.43	30.94	1.3549

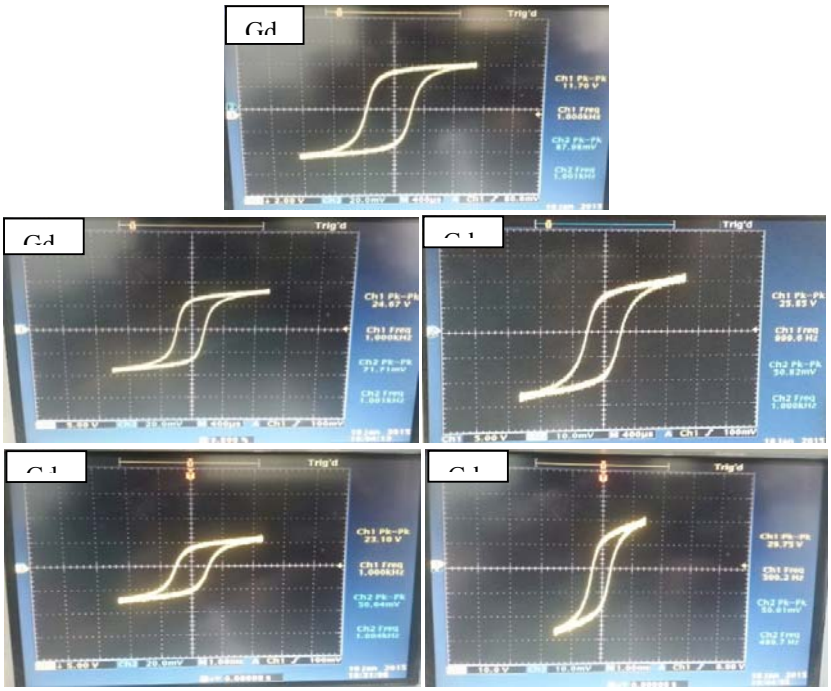

Figure 3. Hysteresis loops of $Ni(Gd_xFe_{1-x})_2O_4$, x = 0.0000 (Gd-0), 0.0125 (Gd-1), 0.0250 (Gd-2), 0.0375 (Gd-3) and 0.0500 (Gd-4)

3.5 Ion Occupation in Ni $(Gd_xFe_{1-x})_2O_4$

It is generally known that the divalent ions are generally larger than the trivalent ions. This is because the larger charge in the trivalent ion produces greater electrostatic attraction and so pulls the outer orbit inward. In the unit cell of the spinel lattice, the radius of octahedral site is apparently larger than that of the tetrahedral site. Particularly, in $NiFe_2O_4$ ferrite, the tetrahedral site has a radius of 0.57 Å and octahedral site has a radius of 0.73 Å. Therefore, it would be reasonable to suggest that the trivalent ions, Fe^{3+} prefer to go into the tetrahedral A-sites while the divalent Ni^{2+} and Gd^{3+} ions into the octahedral B-sites.

The most interesting characteristic in this study is the behavior of cation distribution in the mixed ferrites. Based on the site preference of ions, the crystal structure of spinel and the reported work on the distribution of $NiFe_2O_4$, a model of ion occupation in Gd doped $NiFe_2O_4$, Ni $(Gd_xFe_{1-x})_2O_4$, is proposed in this work.

For $NiFe_2O_4$ spinel lattice,

$$(Ni^{2+}{}_{\delta}\ Fe^{3+}{}_{1-\delta})_{A\text{-site}}\ [Ni^{2+}{}_{1-\delta}\ Fe^{3+}{}_{1+\delta}]_{\ B\text{-site}}O_4$$

where δ = the mole of the Ni^{2+} ions. On the other hand, for the Ni $(Gd_xFe_{1-x)2}\ O_4$ spinel lattice, the model for cation distribution is proposed as:

$$(Ni^{2+}{}_{y+\delta}\ Fe^{3+}{}_{1-x-\delta})_{\ A\text{-site}}\ [Ni^{2+}{}_{1-y-\delta}\ Fe^{3+}{}_{1-x+\delta}Gd^{3+}{}_{2x}]_{\ B\text{-site}}O_4$$

The magnetic moment of a unit cell of Ni $(Gd_xFe_{1-x})_2\ O_4$ferrite was calculated by using the following equation.

$$n_B = [m_{Ni}\,(1\text{-}y\text{-}\delta) + m_{Fe}\,(1\text{-}x +\delta) + m_{Gd}\,2x]_B - [m_{Ni}\,(y+\delta) + m_{Fe}\,(1\text{-}x\text{-}\delta)]_{\ A}$$

The net magnetic moment of Gd^{3+} ion (61 electrons in the electronic shells); m_{Gd} is 7 μ_B, that of Ni^{2+} ion (26 electrons in the electronic shells); m_{Ni} is 2 μ_B and Fe^{3+} ion (23 electrons in the electronic shells); m_{Fe} is 5 μ_B.

This proposal is supported by the resultant magnetization of the Gd doped nickel ferrite samples which has been observed in hysteresis measurement. According to the above estimation, the added Ni^{2+} ions replaced Fe^{3+} ions in A-sites while Gd^{3+} ions replaced Ni^{2+} ions in B sites preferably as simplified in Table 4.

Table 4. Occupation of cations in $Ni(Gd_xFe_{1-x})_2O_4$

Ferrite	A-site	B-site
$NiFe_2O_4$	$Ni^{2+}{}_{0.16}\ Fe^{3+}{}_{0.84}$	$Ni^{2+}{}_{0.84}\ Fe^{3+}{}_{1.16}$
$Ni(Gd_{0.0125}Fe_{0.9875})_2O_4$	$Ni^{2+}{}_{0.71447}\ Fe^{3+}{}_{0.67303}$	$Ni^{2+}{}_{0.28553}$ $Fe^{3+}{}_{1.30197}$ $Gd^{3+}{}_{0.0250}$
$Ni(Gd_{0.0250}Fe_{0.9750})_2O_4$	$Ni^{2+}{}_{0.61279}\ Fe^{3+}{}_{0.76221}$	$Ni^{2+}{}_{0.38721}$ $Fe^{3+}{}_{1.18779}$ $Gd^{3+}{}_{0.0500}$
$Ni(Gd_{0.0375}Fe_{0.96250})_2O_4$	$Ni^{2+}{}_{0.55462}\ Fe^{3+}{}_{0.80788}$	$Ni^{2+}{}_{0.44538}$ $Fe^{3+}{}_{1.11712}$ $Gd^{3+}{}_{0.0750}$
$Ni(Gd_{0.0500}Fe_{0.9500})_2O_4$	$Ni^{2+}{}_{0.44249}\ Fe^{3+}{}_{0.90751}$	$Ni^{2+}{}_{0.55751}$ $Fe^{3+}{}_{0.99249}$ $Gd^{3+}{}_{0.1000}$

4. Conclusion

The Ni $(Gd_xFe_{1-x})_2O_4$ (x= 0.0000, 0.0125, 0.0250, 0.0375, 0.0500) spinel ferrite system was synthesized successfully using Conventional Ceramic method. The XRD analysis confirmed that all Gd^{3+} substituted ferrite was obtained a single spinel phase in the range of x=0.0000-0.0125. The lattice parameter showed an increase with Gd^{3+} substitution until x = 0.0375 and decrease up to x=0.0500, because of the formation of the secondary phase of $GdFeO_3$. However, the particle size decreases with increase of Gd^{3+} content due to hindrance of grain boundary mobility. The saturation magnetization decreased and coercivity H_c increased with increasing Gd^{3+} ions substitution due to the formation of small crystallite and grains with Gd ion substitution. Importantly, a model of ion occupation in Ni $(Gd_xFe_{1-x})_2O_4$ was estimated by the obtained magnetic moment per unit cell and the Bohr magneton of each ion in the lattice according to spin quantization.

Acknowledgements

The authors are grateful to the Department of Physics and Universities' Research Centre, University of Yangon for the supports with research facilities.

References

[1] Anjana Dogra, M. Singh and Ravi Kumar, "50MeV Li^{+3} ion irradiation induced modifications in dielectric properties of Al^{+3} substituted Mg-Mn ferrite", Nucl. Instr. and Meth. B, 2003, vol. 207, pp. 296-300.

[2] S K Sharma, Ravi Kumar, Shalendra Kumar, M Knobel, C T Meneses, V V Siva Kumar, V R Reddy, M Singh and C G Lee, "Role of interparticle interactions on the magnetic behavior of $Mg_{0.95}Mn_{0.05}Fe_2O_4$ ferrite nanoparticles", J. Phys.: Condens. Matter, 2008, vol. 20, pp. 235214.

[3] A. A. Pandit, A. R. Shitre, D. R. Shengule and K. M. Jadhav, "Magnetic and dielectric properties of $Mg_{1+x}Mn_xFe_{2-2x}O_4$ ferrite system" J. Mater. Sci., 2005, vol. 40, pp. 423-428.

[4] Mohd Hashim, SS Meena, RK Kotnala, Sagar E Shirsath, Aashis S Roy, Ameena Parveen, Pramod Bhatt, Shalendra Kumar, RB Jotania, Ravi Kumar, "Study of structural, electrical and magnetic properties of Cr doped Ni–Mg ferrite nanoparticle", Journal of Alloys and Compounds, 2014, vol. 602, pp. 150-156.

[5] M Singh, SP Sud, "Controlling the properties of magnesium–manganese ferrites", Mater. Sci. Engng. B, 2001, vol. 83, pp. 180.

[6] Balwinder Kaur, Monita Bhat, F. Licci, Ravi Kumar, S.D. Kulkarni, P.A. Joy, K.K. Bamzai and P.N. Kotru, "Modifications in magnetic anisotropy of M-type strontium hexaferrite crystals by swift heavy ion, irradiation", J. Magn. Magn. Mater, 2006, vol. 305, pp. 392.

[7] M Hashim, SS Meena, RK Kotnala, SE Shirsath, AS Roy, A Parveen, "Study of structural, electrical and magnetic properties of Cr doped Ni–Mg ferrite nanoparticle", Journal of Alloys and Compounds, 2014, vol. 602, pp. 150-156.

[8] Pardavi-Horvalh M., "Microwave applications of soft ferrites" J. Magn. Magn. Mater., 2000, vol. 171(83), pp. 215-216.

A Study on Structural Properties and Biological Response of HAP/β-TCP

Nay Win Tun[1], Win Kyaw[2], Aye Aye Thant[3]

Abstract

Hydroxyapatite ($Ca_{10}(PO_4)_6(OH)_2$) is used in many biomedical applications including bone graft and joint replacements. Due to its structural and chemical similarities to human bone mineral and teeth, HAP promotes growth of bone tissue directly on its surface. In this research, hydroxyapatite was prepared by precipitation method to provide an accurate understanding of the behavior of biphasic biomaterials with hydroxyapatite (HAP) and beta-tricalcium phosphate (β-TCP). Raw materials of calcium sulphate dihydrate ($CaSO_4.2H_2O$, or Gypsum) and di-ammonium hydrogen phosphate ($(NH_4)_2HPO_4$) solution were used as the starting materials to synthesize high purity hydroxyapatite in the first step. The effect of reaction temperature on conversion efficiencies of gypsum to HAP and reaction kinetics were investigated. After calcination at 1000 ℃, HAP ($Ca_{10}(PO_4)_6(OH)_2$) converted partially into beta-tricalcium phosphate (β-TCP, $Ca_3(PO_4)_2$). Fourier Transform Infrared Spectroscopy (FTIR) analysis clearly revealed the presence of various vibrational modes corresponding to phosphate and hydroxyl groups. Besides porosity were measured at different sintering temperatures, the theoretical density was calculated from X- Rays Diffraction (XRD) results. Finally, the bone bonding ability was evaluated by examining the formation of the new apatite layer on the surface after immersing in Simulated Body Fluid (SBF).

Keywords: calcium sulphate, HAP,βTCP, FTIR, XRD, SBF

1. Introduction

Among all biomaterials, hydroxyapatite; the mineral component of hard tissues in vertebrates, is the most biocompatible material able to be used in clinical applications of conservation and restoration because of its excellent features such as biocompatibility and bioactivity. Hydroxyapatite shows excellent biocompatibility not only with hard tissue but also with soft tissue [1]. This material is capable of integrating biologically when directly implanted into a bone defect; furthermore, it produces no harmful effect on the immune system and features of an osteoconductive behavior. Tricalcium phosphate is also one of the most important biomaterials based on phosphates, currently recognized as ceramic material that significantly simulates the mineralogical structure of bone. β-TCP is found to be resorbable in vivo with new bone growth replacing the implanted β-TCP. Theoretically, resorbable β-TCP is an ideal implant material [2].

2. Materials and Methods

2.1 Experimental Procedure

Laboratory grade gypsum ($CaSO_4.2H_2O$) was used for starting material to synthesize hydroxyapatite (HAP) in the first stage. HAP synthesized from gypsum powder was achieved by precipitation method at 90 ℃. This reaction conversion was achieved according to the reaction below.

$$10CaSO_4.2H_2O + 6(NH_4)_2\,HPO_4 \rightarrow Ca_{10}(PO_4)_6(OH)_2 + 6(NH_4)_2SO_4 + 4H_2SO_4 + 18H_2O$$

1.6 M of gypsum solution was prepared with 11.5 g of gypsum and 40 ml of deionized water. Then the gypsum solution was mixed with 40 ml of 1 M - $(NH_4)_2HPO_4$ solution in conical flask with water bath at the reaction temperature of 90° with magnetic stirring. The reaction time was lasted for 4 hours. At the end of the reaction period, the solid products were washed with DI-

[1] Department of Physics, Dagon University, naywinhtun747@gmail.com
[2] Department of Physics, Pyay University, wkyaw08@gmail.com
[3] Department of Physics, University of Yangon, ayeayethant@uy.edu.mm

water for 5 times and filtered to eliminate any water soluble remains. After washing, the solid residue was put in drying oven operating at 75 ℃ for 24 hours. Again, the dry powder was heat-treated at 500 ℃, 800 ℃, 1000 ℃, 1100 ℃ and 1150 ℃ for 2 hours each in a furnace. The HAP phase was formed at 500 ℃ and 800 ℃ for 2 hours. However, HAP converts into β-tricalcium phosphate (β-TCP) at 1000 ℃ and beyond. After sintering 1200 ℃ of HAP/β-TCP pellet partially converts into biphasic HAP/α-TCP. The α-TCP is brittle and more soluble than HAP and β-TCP. Therefore, this research focuses on biphasic HAP/β-TCP.

3. Results and Discussion

3.1. Formation of Dentures with HAP, HAP/β-TCP and β-TCP

Titanium-Chromium alloy was used as base of the denture. Bricera vacuum porcelain body A-3 from Brident Inc, USA was placed above the base. Then, HAP, HAP/β-TCP and β-TCP powder which were mixed with DI water was placed above the porcelain layer as enamel. The heat-treatment was conducted into the Automatic Programmable Vacuum Porcelain Furnace at 930 ℃ for 15 minutes. The denture obtained by using this method is shown in Figure 1.

Figure 1. The formation of dentures with HAP, HAP/β-TCP and β-TCP at different calcination temperatures.

3.2. Bioactivity Test

The bone-bonding ability of a material is often evaluated by examining the ability of apatite to form on its surface in a Simulated Body Fluid (SBF) with ion concentrations nearly equal to those of human blood plasma. Haemo-A (Aeonmed Co., Ltd) was mixed with Haemo-B (Aeonmed Co., Ltd) in 1:1.2 ratio to form Simulated Body Fluid (SBF). This solution was mixed with DI water in 1:32.8 ratio. Each of this solution (5 ml) was put into 25 ml of three glass beakers. HAP, HAP/β-TCP and β-TCP pellets were put into the SBF solution in each beaker. The beakers were put into an incubator and set the temperature at 37 ℃ for 14 days. Then, the pellets were dried in desiccator for 2 days. These dried pellets were analyzed by SEM. SEM micrographs obtained from pellets before SBF test and after SBF test were compared.

3.3. Analysis on Molecular Vibration by FTIR

The FTIR analysis strongly supports the XRD result in this work. FTIR spectroscopy has been performed in order to investigate the functional groups presented in hydroxyapatite synthesized by precipitation method. The functional groups present in hydroxyapatite clearly revealed the presence of various vibrational modes corresponding to phosphate and hydroxyl groups. Chemical groups with vibration bands are confirmed by the FTIR transmission bands of synthesized HAP and β-TCP.

In HAP and β-TCP, PO_4^{3-} group formed intensive IR absorption bands at 502 cm^{-1} and at 1000 – 1100 cm^{-1}. Adsorbed water band was relatively wide, from 3600 to 2600 cm^{-1} indicating the symmetric stretching and asymmetric stretching vibrations of water. In FTIR spectra of HAP and β-TCP, the characteristic absorption bands at 3435 and 3428 cm^{-1} were attributed to υ_3 mode (asymmetric stretching) of water. The bands at 900-1200 cm^{-1} were the stretching mode of PO_4^{3-} group. The sharp peaks at 608 and 677 cm^{-1} represented the vibrational peaks υ_4 mode of PO_4^{3-}

in both HAP and β-TCP. The characteristic bands due to vibration of PO_4^{3-} group appeared at 595, 604, 606, 608, 615 and 677 cm^{-1}. Five IR bands were detected peaking at 2132, 2133, 2135 and 2137 cm^{-1} for soluble CO_2 (gas) in the ceramic materials. The peaks at 2137 cm^{-1} were formed at the two calcination temperatures at 500 ℃ and 800 ℃. FTIR results are similar to the literature data [3].

Figures 2 shows the FTIR results obtained at different calcination temperatures. All spectra show the characteristic band of adsorbed water, hydroxyl and phosphate species. The peaks in the spectrum and their association to respective chemical groups are summarized in Table 1.

3.4. Porosity Measurement

The values of apparent porosity of HAP, HAP/β-TCP and β-TCP at different sintering temperatures were estimated by the equations using Archimedes' method and are shown in Table 2. In this study, for three different sintering temperatures, the porosity of sintered pellets rapidly increased to the highest percentage, 63.63% when sintered at 1200 ℃ compared to other temperatures.

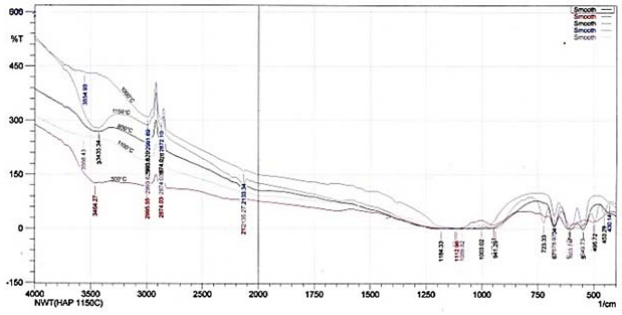

Figure 2. The FTIR spectra of HAP, HAP/ β-TCP and β-TCP prepared at different calcination temperatures of 500 ℃, 800 ℃,1000 ℃, 1100 ℃ and 1150 ℃

Table 1. The FTIR transmission bands of HAP, HAP/ β-TCP and β-TCP at calcination temperatures of 500 ℃, 800 ℃, 1000 ℃, 1100 ℃ and 1150 ℃

Chemical Group	Transmission Band (cm-1)					Vibrational Mode (cm^{-1})
	500 ℃	800 ℃	1000 ℃	1100 ℃	1150 ℃	
PO_4^{3-}	949	941	ND	ND	ND	υ_1 Symmetric Stretching
	502	453 496	430 550	ND	ND	υ_2 Bending
	1113	1003 1184	1090	1090	1119	υ_3 Dipole
	606 677	615 677 723	615 677	595 604 679	595 608 677	υ_4 Polarization

Chemical Group	Transmission Band (cm-1) 500 ℃	800 ℃	1000 ℃	1100 ℃	1150 ℃	Vibrational Mode (cm^{-1})
H-O-H	2874	2870	2872	2874	2874	υ_1 Symmetric Stretching
	2996	2994	2992	2994	2994	
	ND	ND	ND	ND	ND	υ_2 Bending
	3464	3435	3555	3568	3428	υ_3 Asymmetric Stretching
CO_2	2137	2137	2133	2135	2132	

ND= Non Detected

Table 2. The variation of Apparent Porosity and Theoretical Density of HAP, HAP/β-TCP and β-TCP at three different sintering Temperatures

Sintered Temperature (℃)	Dry Weight, D (g)	Soaked Weight, W (g)	Suspended Weight, S (g)	Apparent Porosity (%)	Theoretical Density (g/cm3)
900	1.63	1.78	1.42	41.66	3.38
1100	1.58	1.72	1.45	51.85	3.17
1200	1.23	1.30	1.19	63.63	3.23

3.5. Apatite Formation in Simulated Body Fluid (SBF)

The SEM images for the pellets before and after immersing in SBF are presented in Figures 3 to 5. It is worth to note that the morphology of the pellets immersed in SBF was changed distinctly. As seen in the SEM images the formation of apatite layers on each surface of HAP, HAP/β-TCP and β-TCP pellets was confirmed by the difference in the surface texture of the sample. Importantly, the β-TCP exhibited the faster rate of formation of apatite layer compared to the pure HAP and biphasic HAP/β-TCP. Based on the SEM analysis, β-TCP seemed to have better bioactivity than HAP in this work. The apatite layer formed on the surface of the HAP, HAP/β-TCP and β-TCP can bond to living bone. Therefore, the HAP, HAP/β-TCP and β-TCP prepared in this research have potential biomaterials which can be applied for bone replacement.

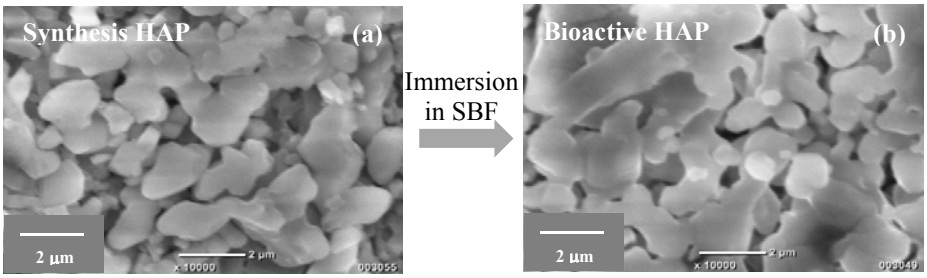

Figure 3. SEM micrographs of HAP pellets at the calcination temperature of 900 ℃ in 10 K × magnification (a) before and (b) after immersion in SBF.

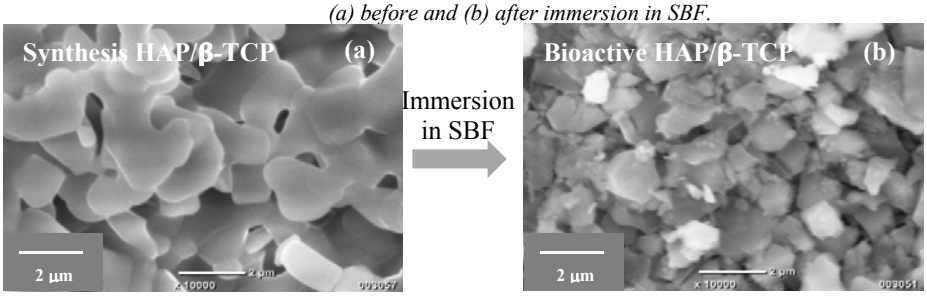

Figure 4. SEM micrographs of HAP/β-TCP pellets at the calcination temperature of 1100 ℃ in 10 K × magnification(a) before and (b) after immersion in SBF.

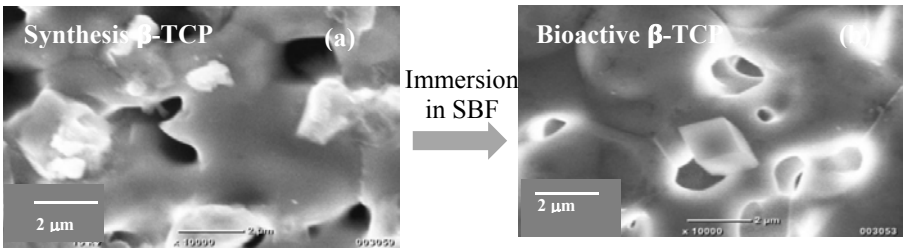

Figure 5. SEM micrographs of β-TCP pellets at the calcination temperature of 1200 □ in 10 K × magnification (a)before and (b) after immersion in SBF

4. Conclusion

Hydroxyapatite, $Ca_{10}(PO_4)_6(OH)_2$ was prepared from gypsum by precipitation method. The raw materials were well characterized prior to the preparation of HAP. A single phase structure of HAP from gypsum was successfully formed via the precipitation method after heat-treated at 500 ℃ and 800 ℃ for 2 hours. It is worth to note that some parts of HAP converted to β-TCP phases after heat-treated at 1000 ℃ for 2 hours. It is interesting to note that transformation to β-TCP started by calcination at 1000 ℃ and the transformation rate increased with increase in temperature. FTIR data clearly revealed the presence of various vibrational modes corresponding to phosphate and hydroxyl groups. The porosity of sintered pellets rapidly increased to the highest percentage, 63.63% when sintered at 1200 ℃ compared to other temperatures. The SBF soaking results revealed that all the studied materials are biologically active which confirmed its application as bone in living things.

Acknowledgements

The authors are grateful to the Department of Physics and Universities' Research Centre, University of Yangon for the supports with research facilities.

References

[1] Angelescu, N., Ungureanu, D.N., Anghelina F.V. "Synthesis and Characteristic of Hydroxyapatite Obtained in Different Experimental Conditions", 2011, Valahia University of Targoviste, Romania.

[2] Bahman Mirhadi, Bahman Mehdikhani , Nayereh Askari, "Sintering effects on the hardness of β-TCP", Journal of Ceramic Processing Research, 2012, vol. 13, No.4.

[3] Maisara S.M. Arsad, Pat M.Lee, Lee Kong Hung, "Synthesis and Characterization of Hydroxyapatite Nanoparticles and β-TCP Particles", 2011, IPCBEE vol.7.

[4] Hitachi High-Tech Science Corporation, "Thermal Analysis of Gypsum", 1985, Tokyo, TA No.22.

[5] Kim, S.R., Lee, J.H., Riu, D.H., Jung, S.J., Lee, Y.J., Chung, S.C., Kim, Y.H., "Synthesis of Si, Mg substituted hydroxyapatite and their sintering behaviors", Biomaterials, 2003, vol. 24, pp. 1389-1398.

[6] Kannan,S., Lemos,I.A.F., Rocha, J.H.G., Ferreira, J.M.F. "Synthesis and characterization of magnesium substituted biphasic mixtures of controlled hydroxyapatite/beta-tricalcium phosphate ratios", 2005, Department of Ceramics and Glass Engineering, University of Aveiro, Portugal.

[7] Onur Rauf Bingöl, Caner Durucan, "Hydrothermal Synthesis of Hydroxyapatite from Calcium Sulfate Hemihydrate", 2011, Department of Metallurgical and Materials Engineering, Middle East Technical University, Ankara, Turkey.

[8] Orlovskii, V.P. et al., "Hydroxyapatite and Hydroxyapatite-Based Ceramics", Inorganic Materials, 2002, vol. 38.

Characterization & Morphological Analysis of Nanostructured Material Images by Image Processing

Khin Khin Win[1], Zin Min Tun[2], Zin Min Myat[3], Thidar Pyone[4] Thazin Khaing[5]

Abstract

This paper aims to analyse and characterize the nanostructured material images obtained from SEM (Scanning Electron Microscopy) technique at the morphological aspect. State-of-the-art techniques for these purposes are complex and complicated given the variability of the different image acquisition modalities, different synthesis parameters and material composition. Image processing is a potential tool to characterize and analyse the properties of nanoscale images in terms of data acquisition, pre-processing, filtering, classification, surface morphology, particle size, porosity measurement which is enable to use in many areas. The morphological analysis of nanoscale images is an important research area in Materials Science to characterize their properties for many applications in the area of materials science and solid state physics. This work has carried out the characterization and morphological analysis of titanium dioxide (TiO_2) nanostructured material images at different temperatures by utilizing the image processing methods. The results show that current approach is capable of characterizing complex morphological characteristics of the subtle nanostructured SEM images. The analysis of nanostructured materials is easy to perform for well-behaved samples which have been described using simple functions of existing MatLab software packages (R2019b). This paper compares and presents the results of previous works. It is found that the present work can be able to perform more efficient and effective methods to analyse and characterize the nanostructured material images. Moreover, this research work is enabling to address the issues and challenges of nanostructured materials image characterization and analysis.

Keywords: SEM (Scanning Electron Microscopy), pre-processing, edge detection, morphology,

1. Introduction

This paper aims to address some problems and state-of-the-art techniques encountered in image processing for material analysis and design. Current methods for this purpose are a complex task given the variability of the different image acquisition modalities, different synthesis parameters and material composition. This paper presents an overview of techniques that have been and are currently developed to address this diversity of problems, such as segmentation, texture analysis, multi scale and directional features extraction, stochastic models and rendering, among others. Finally, it provides references to enter the issues, challenges and opportunities in materials characterization for Nanostructured Material Images.

1.1 Scanning Electron Microscope (SEM)[1]

The Scanning Electron Microscope (SEM) is a tool for visualizing the surface of solid samples, with a resolution (depending on the application) that can approach 1nm. Energy-dispersive X-ray analysis can be used to analyze volumes with dimensions of around 1 micron with a sensitivity of about 0.2wt%, while back-scattered electron imaging allows the

[1] Dr, Professor & Head, Department of Physics, University of Yangon, khinkhinwin@uy.edu.mm
[2] Dr, Assistant Lecturer, Department of Physics, West University of Yangon
[3] Dr. Assistant Lecturer, Department of Physics, University of Yangon
[4] PhD Candidate, Lecturer, Department of Physics, University of Yangon,
[5] PhD Candidate, Assistant Lecturer, Department of Physics, Bamaw University,

visualization of regions of different composition. Crystallographic orientation and structure can be examined using electron backscatter diffraction (EBSD) analysis, though sample preparation requirements for this technique are very stringent and limit the number of samples that can be studied in this way.

In principle, the SEM generates a primary focused electron beam in a vacuum chamber and raster scans the beam over a sample surface. The incident primary electrons interact with the atoms in the surface of the sample. Some of the primary electrons excite the sample to emit secondary electrons while some are being scattered back. A secondary electron detector or a backscattered electron detector collects and converts the secondary electrons or the back scattered electrons into high resolution images.

Secondary electrons are emitted by atoms near the surface of a sample material when their electrons become excited and have sufficient energy to escape the sample surface. Secondary electrons carry information about morphology and surface topography of the sample. The contrast is dominated by the so-called edge effect: more secondary electron can leave the sample at edges for reduced material retardation and adsorption and thus can lead to increased brightness.

A highly sensitive backscatter electron detector captures composition, topography, and shadow images. Elements of higher atomic number will backscatter electrons more strongly than those of lower atomic numbers. Backscatter imaging allows for improved image contrast for compositional images as well as topographical images. Therefore, backscatter detectors are used to detect areas of varying chemical compositions. Backscattered electron imaging of nonconductive, uncoated samples shows composition by contrast; higher atomic number regions are brighter, while lower atomic number regions are darker.

1.2. Nano structured materials images and Features

The possibility of designing, analysing and modelling materials from images (or generally two- or three dimensional modalities) reveals important contributions in this area. As mentioned, the appearance of nano structured materials images changes significantly with imaging processing techniques, the scale of analysis, image qualities and settings, physical properties and sample preparation methods of materials. Understanding these aspects turns out to be crucial for material analysis and modelling. In particular, we face challenges regarding the characterization of the physical assembly process of materials, the formation process of images, of imaging techniques interacting with materials (geometry, transmission, illumination, reflection, scattering). Answering these questions is important to separate the material appearance from its intrinsic morphology and properties. This paper aims to report on issues from image feature extraction to image simulation with the challenges and emerging trends in material analysis and modelling that are likely to pose challenges to image processing, through the diversity of types of materials, acquisition techniques and applications. Most likely traditional such as human vision-based interpretation of materials image can be misleading, as illustrated in Figure 1. Fully taking into account physical properties and laws is at the heart of successful image analysis in material science.

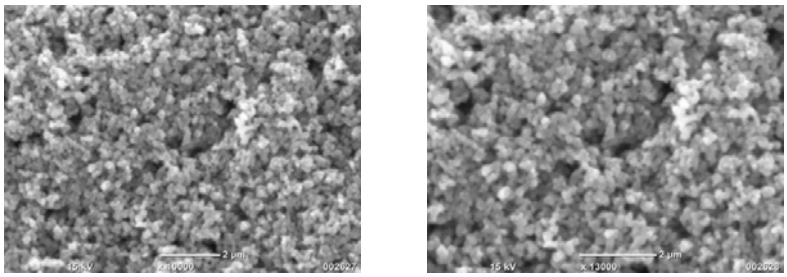

Figure 1 Images at 400℃ *and* 500℃ *temperature treatment*

2. Methods and Outputs

Figures 2 represent a sample of images acquired and problems for material analysis. It illustrates the cracks (black), partially filled pores (rounded dark grey shapes with white spots) and zeolite inclusions (scattered or aggregated white dots) in a neutral substrate. Its characteristics relate to the efficiency of a spherical catalyst used in refining for the conversion of hydrocarbons into chemical products. Such images raise different problems at different scales of observations, from isolated objects to scattered phases, requiring different segmentation tools. Figure 3 results from optical microscopy. The thickness of the crusts may be measured by electron probe microanalysis. It directly correlates with catalyst activity. Resorting to image processing techniques to automate the measurement of crust thickness avoids invasive probe techniques, and hastens the conception of new catalysts. It can use local orientation estimates for 2D and 3D texture segmentation. The goal is to infer bounds on the effective properties of materials by dealing with three-dimensional, computational microstructure simulations. It combines a multiscale approach with homogenization techniques. The same goal is pursued in the nanometric scale that illustrates a mixture of a crystalline and an amorphous material. The periodicity of the first one, and the lack of long-term regularity of the second one, drives the use of local Fourier attributes.

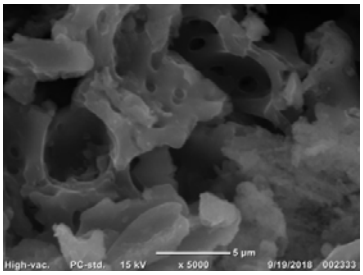

Figure 2 Sample acquired image

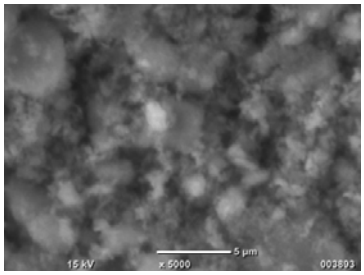

Figure 3 Sample Image from Optical Microscopy

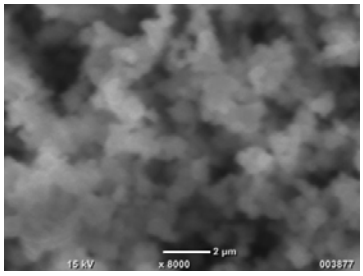

Figure 4 CaTiO3 Image at 1100℃

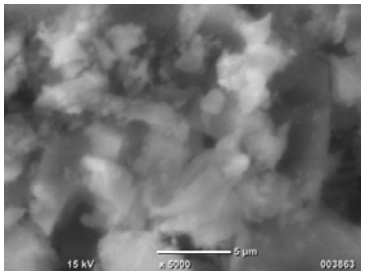

*Figure 5 SiO2 Image at 8*00℃

3. Image processing: issues and challenges

Classical approaches and techniques may define a relatively standard work-flow for image processing in materials science. It includes the following steps: Image acquisition or reconstruction Depending on the resolution of interest, different equipments may be used, for instance optical microscopes (mm-µm), scanning electron microscopes or SEM (µm) and transmission electron microscopes or TEM (nm-˚A) for 2D acquisitions. Turning to 3D acquisitions, one observes a frequent use of X-ray tomography (mm-µm) and electronic tomography (nm) based on TEM projections. Some techniques deal with the reconstruction of surface topography [20].

Enhancement and filtering: This step (Fig. 2, with bilateral filtering) relates to image improvement from a noise level or homogeneity point-of-view. One is primarily interested in noise filtering techniques permitting only minimal modifications in the structures of interest, or drift or background correction. Techniques for artifact corrections, specific to the acquisition process, include for instance ring artifact suppression (X-ray tomography), sample impregnation or encasement in colourless resin (causing effects akin to cast shadows), mechanical or ionic surface polishing.

Segmentation: This step encompassing dimensionality reduction, classification and model fitting, simplifies rich images into a few meaningful intensities or components. It aims at the recovery of the border of the objects of interest. When the colour intensity level is directly related to object properties (topography, like in secondary electron SEM, or chemical structure, like in back-scattered electron SEM), global histogram segmentation methods (inter-class variance maximization, entropy, Expectation-Maximization) are complemented by criterion-based segmentation (object length, surface, tortuosity). This combination permits the elimination of non conform or non interesting elements, sometimes mere residuals of a previous processing sequence. For images whose intensity is less directly related to properties, extraction of local morphology or contours may be performed using global optimization approaches such as geodesic active contours and regions, maximum flows approaches and/or mathematical morphology operations such as top-hat filtering or watershed transformations. Analysis Image structures can be described without an explicit segmentation of the objects of interest using multi scale image representations based on morphological decompositions or wavelet-based multi scale representations. Once simplified, objects of interest may be characterized by numbers, shapes and spatial distribution among others. Stereology, stochastic modelling (spatial moments, such as the covariance, and spatial distributions) and the use of distance functions (inter-object, geodesic length, tortuosity) provide the main sources of algorithms. Multi-modality It involves image regularization and segmentation of multi-modal/multichannel/multi scale images acquired from the same samples. In order to deal with this kind of data, some pre-processing steps such as registration, denoising and image fusion are required. In addition to extract relevant information from complex data sets integrating various acquisition techniques, it is useful to use dimensionally reduction techniques, from classical PCA to modern nonlinear manifold learning.

Microstructure stochastic modelling: This step (with 3D modelling from 2D images) may use input characteristic data either from segmentation or analysis. It consists in estimating a stochastic, geometric model (Boolean random functions, reaction-diffusion or dilution models, dead leaves tessellations), representing the microstructure of the observed material. It serves the purposes of inferring the potential 3D structure from 2D cuts, or of obtaining structure variations

through model parameter modifications, hence of “numerical material by design”. Finally, this step may even replace the segmentation step, when individual objects can not, or need not, be individualized.

Segmentation and analysis are sometimes merged. “Texture approaches” aim at extracting image characteristics without resorting to individual or excessively precise object separation. Morphological metrics are extracted, with the help of 2D/3D models. Machine learning techniques are also emerging, typically to automate supervised/unsupervised classification problems. Meaningful characteristics may be enriched by combining or merging different acquisition techniques. Acquisitions may consider different scales of observation (multiscale fusion approaches), or different modalities (multi-modal fusion approaches), or both. Such techniques, very common in medical or satellite imaging, are increasingly being used in materials design, combining for instance topographic and physico-chemical information (via secondary electron and back-scattered SEM or Energy-Dispersive Spectroscopy). With 3D or 3D+time imaging [9], an important effort is dedicated to processing performance, especially algorithm acceleration. Materials science processing work-flows are increasingly carried out, with reduced cost, with CPU/GPU optimization. For instance, tomographic reconstruction is typically now faster than acquisition. Similar performance increases are being pursued with filtering or segmentation techniques, toward integrated high-throughput materials science and engineering.

4. Conclusions

Among the challenges proposed before, and the ones recently exposed in [9], we retain the attention on the following four:

• multi-step: to produce a complete pipe-line or work-flow of image analyses and simulations, from sample acquisition to the estimation of physical properties;

• data-flow: to manage raw and simulated data and acceleration of the aforementioned work-flows from high throughput screening of materials with ever increasing amounts of numerical information;

• multi-modality (or synergy): to employ as much as possible the potentialities to retrieve information on materials from different acquisition sources, with novel fusion/combination techniques improving characterization or providing access to novel properties;

• reverse engineering: to help in computational material design, by orienting the synthesis or manufacturing process of novel materials, desired or predicted (e.g. graphene).

A successful application of more standard image processing thus requires a better integration of known techniques, as well as the deployment of image analysis not used in materials science yet, with the new challenges raised by its variety of data and physical models.

Acknowledgements

Author would like to thank all concerns from Ministry of Education (MOE), Department of Higher Education (MOE), Myanmar Academy of Arts & Science (MAAS), Science Council of Asia and Japan Science Council (JSC) for their permission, supporting and all round assisting to carry out this paper.

References

[1] R. E. Hummel, “Understanding Materials Science: History, Properties, Applications”, Springer, 2nd edition, 2004.

[2] J. A. Mathews, “The steel age—1876 to 1926,” Ind. Eng. Chem., vol. 18, no. 9, pp. 913–914, 1926.

[3] P. Ball, Madeto Measure: NewMaterialsforthe21stCentury, PrincetonUniversity Press, 1999.

[4] Y. Br´echet, “Materials science: from materials discovered by chance to made-tomeasure materials,” Coll`ege de France, 2013.

[5] J. P. Davim and C. A. Charitidis, Eds., “Nanocomposites: materials, manufacturing, and engineering, Advanced Composites”, Walter De Gruyter, Berlin Boston, 2013.

[6] Y. Liu and X. Zhang, “Met materials: a new frontier of science and technology,” Chem. Soc. Rev., vol. 40, no. 5, pp. 2494, 2011.

[7] J. W. Gibbs, “On the equilibrium of heterogeneous substances”, Trans. Connect. Acad. Arts Sci., vol. III, pp. 108–248 and 343–524, 1875 to 1878.

[8] L.Wojnar, “Image analysis. Applications in materials engineering”, CRCPress,1999.

[9] I. M. Robertson, C. A. Schuh, J. S. Vetrano, N. D. Browning, D. P. Field, D. J. Jensen, M. K. Miller, I. Baker, D. C. Dunand, R. Dunin-Borkowski, B. Kabius, T.Kelly,S.Lozano-Perez,A.Misra,G.S.Rohrer,A.D.Rollett,M.L.Taheri,G.B. Thompson, M. Uchic, X.-L. Wang, and G. Was, “Towards an integrated materials characterization toolbox,” J. Mater. Res., vol. 26, no. 11, pp. 1341–1383, Jun 2011.

[10] D. Salomon and G. Motta, Handbook of Data Compression, Springer, 2009.

[11] B. K. Gunturk and X. Li, Eds., “Image Restoration: Fundamentals and Advances, Digital Imaging and Computer Vision”, CRC Press, 2012.

[12] J. Chanussot, C. Collet, and K. Chehdi, Eds., Multivariate Image Processing, ISTE Ltd and John Wiley & Sons Inc., 2009.

[13] J. Ohser and K. Schladitz, “3D Images of Materials Structures: Processing and Analysis”, Wiley-VCH, 2009.

[14] A.Depeursinge,A.Foncubierta-Rodriguez,D.VanDeVille, and H.M¨uller, “Three dimensional solid texture analysis in biomedical imaging: Review and opportunities,” Med. Image Anal., vol. 18, no. 1, pp. 176–196, 2014.

[15] H. H. Bauschke, R. S. Burachik, P. L. Combettes, V. Elser, D. R. Luke, and H. Wolkowicz, Eds., “Fixed-Point Algorithms for Inverse Problems in Science and Engineering”, Springer, 2011.

[16] M.L. Comer and E.J.Delp, “The EM/MPM algorithm for segmentation of textured images: analysis and further experimental results,” IEEE Trans. Image Process .,vol. 9, no. 10, pp. 1731–1744, 2000.

[17] C. Chaux, A. Jezierska, J.-C. Pesquet, and H. Talbot, “A spatial regularization approach for vector quantization,” J. Math. Imaging Vis., vol. 41, no. 1-2, pp. 23–38, 2011.

[18] C. Park, J. Z. Huang, J. X. Ji, and Y. Ding, “Segmentation, inference and classification of partially overlapping nanoparticles,” IEEE Trans. Patt. Anal. Mach. Int.,vol. 35, no. 3, pp. 669–681, 2013.

[19] M. Petrou and P. G. Sevilla, Image processing: dealing with texture, John Wiley & Sons, Ltd, 2006.

[20] R. Leach, Ed., “Characterisation of Areal Surface Texture”, Springer, 2013.

[21]S. T. Ali, J.-P. Antoine, and J.-P. Gazeau, “Multidimensional Wavelets and Generalizations”, pp. 411–456, Theoretical and Mathematical Physics. Springer-Verlag, Aug. 2014.

[22] S. Torquato,“Random Heterogeneous Materials: Microstructure and Macroscopic Properties”, Springer, 2002.

Formation of Calcium Hydroxide ($Ca(OH)_2$) Nanorods for CO_2 Adsorption

Nwe Ni Hlaing[1], Srimala Sreekantan[2], Hirofumi Hinode[3], Winarto Kurniawan[4],

Aye Aye Thant[5]

Abstract

Carbon dioxide (CO_2) is one of the major contributors to the global warming and climate change. Hence, mitigate towards the emission of CO_2 into an atmosphere, various types of adsorbents were reported. Recent years, nanostructured calcium hydroxide ($Ca(OH)_2$) has been proposed as a potential calcium oxide (CaO) based adsorbent for CO_2 adsorption. In this study, $Ca(OH)_2$ samples were synthesized via simple precipitation method by using cetyltrimethyl ammonium bromide (CTAB) as a surfactant. The effect of CTAB concentration (0.01-0.03 mol) on the structure and morphology of synthetic $Ca(OH)_2$ samples were investigated by X-ray diffraction and field emission scanning electron microscopy (FESEM). From XRD and FESEM results, the formation of $Ca(OH)_2$ nanorods with an average diameter of 80-100 nm was observed at 0.03 mol of CTAB. The CO_2 adsorption capacities of CaO derived from synthetic $Ca(OH)_2$ samples were studied by thermogravimetric analysis (TGA). The TGA results demonstrated that CaO derived from $Ca(OH)_2$ nanorods exhibited CO_2 adsorption capacity of 0.75 g-CO_2/g-adsorbent which was higher than those of CaO derived from irregular and hexagonal shapes $Ca(OH)_2$ samples synthesized at 0.01 and 0.02 mol of CTAB, respectively.

Keywords: calcium hydroxide, nanorods, carbon dioxide, adsorption capacity, XRD, TGA

1. Introduction

Mitigate towards the emission of carbon dioxide (CO_2) from the combustion of fossil fuel burning has been worldwide concerns due to their adverse effect towards the heath of mankind and environment. Carbon dioxide capture, utilization and storage (CCUS) technology is a reasonable technology that prevents the release of large quantities of CO_2 into the atmosphere by capturing CO_2 and transporting it to where it can be useful. The first step of CCUS technology is carbon dioxide capturing process and hence, researches are focused on the investigation of materials and techniques which can capture large amount of CO_2 [1,2].

Among numerous gas separation technologies which have been attempted to capture CO_2 from flue gas, adsorption using solid materials is one the most promising methods due to some advantages of solid adsorbents including low energy requirement, cost advantage, and the ability to use over a wide range of temperatures and pressures. Different solid adsorbents including metal organic frameworks (MOFs), grapheme organic frameworks (GOFs), zeolites, activated carbons, clays, calcium oxide, etc have different capability to adsorb CO_2 and cyclic stabilities. Among various materials, calcium oxide (CaO) based adsorbent is one of the promising material

[1] Department of Physics, Taunggyi University, 06013, Taunggyi, Myanmar, nwenihlaing76@gmail.com
[2] School of Materials and Mineral Resources Engineering, Engineering Campus, Universiti Sains Malaysia, 14300 Nibong Tebal, Penang,
[3] Department of Transdiciplinary Science and Technology, School of Environment and Society, Tokyo Institute of Technology, 2-12-1 Ookayama, Meguro-ku, Tokyo, Japan
[4] Department of Transdiciplinary Science and Technology, School of Environment and Society, Tokyo Institute of Technology, 2-12-1 Ookayama, Meguro-ku, Tokyo, Japan
[5] Department of Physics, University of Yangon, 11041 Kamayut, Yangon, Myanmar

because of the advantages such as high CO_2 adsorption capacity, low material cost and reversible carbonation/calcination cycles [2,3].

Calcium hydroxide ($Ca(OH)_2$) is one of the materials that can be used as CaO-based adsorbent for the capture of CO_2 because of its excellent properties such as high reactivity and fast reactions [4,5]. Some researchers synthesized $Ca(OH)_2$ by various methods including water-in-oil (W/O) microemulsions [6], sonochemical [7], hydrogen plasma-metal reaction [8] and wet chemical method [9]. However, some of these methods require high temperature or complicated equipment [6-8]. Therefore, the development of a simple method with low-temperature is highly desirable for the synthesis of $Ca(OH)_2$.

Recent years, high aspect ratio one dimensional (1D) nanostructures including nanowires, nanorods, and nanotubes have attracted attention owing to their chemical, mechanical, electrical, and optical properties and their promising applications in in different types of applications. Up to now, a variety of synthetic approaches including precipitation, hydrothermal, solvothermal, spray pyrolysis, thermal hydrolysis and sol-gel methods have been developed to synthesize one dimensional nanostructures [10-12].

In this study, $Ca(OH)_2$ nanostructures were synthesized by a simple precipitation method using calcium acetate hydrate as calcium (Ca) source. The formation of $Ca(OH)_2$ nanorods were studied by varying the concentration of cetyltrimethyl ammonium bromide (CTAB). The obtained samples were characterized by X-ray diffraction (XRD) and scanning electron microscopy (SEM). The CO_2 adsorption capacities of the synthetic $Ca(OH)_2$ nanostructures were investigated by thermogravimetric analysis (TGA).

2. Methods

A 0.01 mol of cetyltrimethyl ammonium bromide, CTAB (Merck) was added to the 0.16 mol of sodium hydroxide, NaOH (Aldrich) aqueous solution. This solution was stirred for 30 min. A 0.02 mol of calcium acetate hydrate, $Ca(CH_3COO)_2.H_2O$ (Merck) was dissolved in 100 ml distilled water and then dropped slowly into the previously stirred solution. This mixed solution was heated to 40°C and vigorously stirred for 30 min. White precipitates were formed and subsequently centrifuged and then dried in an oven at 70°C for 24 hours. The same procedures were performed for preparing other samples with different moles of CTAB (0.02-0.03).

The obtained samples were characterized by X-ray diffraction (XRD) with a Bruker AXS D8 Advance X-Ray Diffractometer and field emission scanning electron microscopy (FESEM, Carl Zeiss SUPRA 35 VP). The thermal behaviors and CO_2 adsorption capacities of CaO derived from synthetic $Ca(OH)_2$ samples were studied by a Rigaku thermogravimetry-differential thermal analysis (TG-DTA) apparatus with Thermoplus 2 software. A small amount of $Ca(OH)_2$ sample (~ 6.5 mg) was placed in a platinum crucible and heated from room temperature to 700°C at a heating rate of 10°C/min under 100% N_2 gas flow. After that, carbonation process was performed for 30 min under 100% CO_2 gas flow. The constant gas flow rate for CO_2 and N_2 was 40 ml/min. The CO_2 adsorption capacity was calculated by using the following equation.

$$CO_2 \text{ Adsorption Capacity} = \frac{W_n - W_i}{W_i}$$

where, W_n is the weight of the carbonated sample after carbonation process and W_i is the initial weight of the calcined sample.

3. Results and Discussion

Figure 1(a-c) shows the XRD patterns of the synthetic samples obtained by a simple precipitation method. All the major diffraction peaks could be indexed to the hexagonal structure $Ca(OH)_2$ (calcium hydroxide) phase, according to the standard data (JCPDS No. 78-0135). The peaks at 2θ value of 28°, 34°, 47°, 50°, and 54° were corresponded to the reflection from (100), (011), (012), (110) and (111) planes of $Ca(OH)_2$ phase, respectively. Moreover, minor diffraction peaks belong to the calcite ($CaCO_3$,) phase with rhombohedral structure (JCPDS No. 05-0586) were also observed.

In the XRD pattern of $Ca(OH)_2$ sample prepared with 0.01 mol of CTAB (Figure 1(a)), the high intensity diffraction peak was found at 2θ value of 29° which was corresponded to the reflection from (104) plane of calcite phase. In the XRD patterns of $Ca(OH)_2$ samples prepared with 0.02 mol and 0.03 mol of CTAB, the intensities of the characteristic diffraction peaks of calcite (at 2θ value of 29°) decreased. On the other hand, the intensity of characteristic diffraction peak of $Ca(OH)_2$ phase at 2θ=34° increased. The results showed that the concentration of CTAB influenced the contents of calcite phase in the synthetic $Ca(OH)_2$ samples.

The crystallite sizes of $Ca(OH)_2$ samples were calculated by well-known Scherrer's equation ($D = k\,\lambda/\beta \cos\theta$), where D is crystallite, k is Scherrer's constant (typically between 0.85 and 0.99), λ is the wavelength of the incident X-rays, θ is the angle of diffraction and β is full width at half maximum (FWHM). The calculated crystallite sizes of $Ca(OH)_2$ samples prepared with 0.01 mol, 0.02 mol and 0.03 mol of CTAB were 42.07 nm, 45.54 nm and 56.04 nm, respectively. The results showed that the crystallite size and crystallinity increased with increasing the concentration of CTAB.

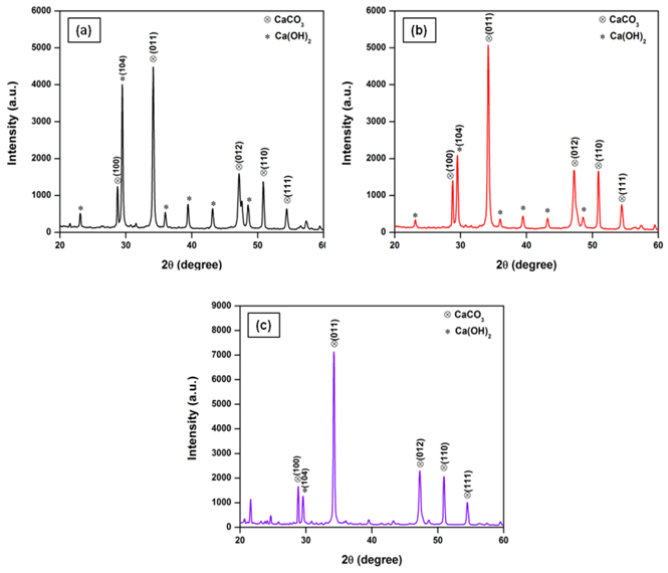

Figure 1. XRD patterns of calcium hydroxide samples synthesized with (a) 0.01 mol, (b) 0.02 mol and (c) 0.03 mol of CTAB

Figure 2(a-c) displays the FESEM images of synthetic $Ca(OH)_2$ samples prepared with 0.01 mol, 0.02 mol and 0.03 mol of CTAB. In the FESEM image of $Ca(OH)_2$ sample prepared with 0.01 mol of CTAB (Figure 2(a)), irregular shaped and irregular sized micro/nano particles were observed. When CTAB was increased to 0.02 mol, micro/nano hexagonal plates with non uniform sizes were seen in Figure 2(b). With 0.03 mol of CTAB, the formation of $Ca(OH)_2$ nanorods with an average diameter of 80-100 nm was observed (Figure 2(c)). FESEM images revealed that the concentration of CTAB played a critical role to control the formation of $Ca(OH)_2$ nanorods.

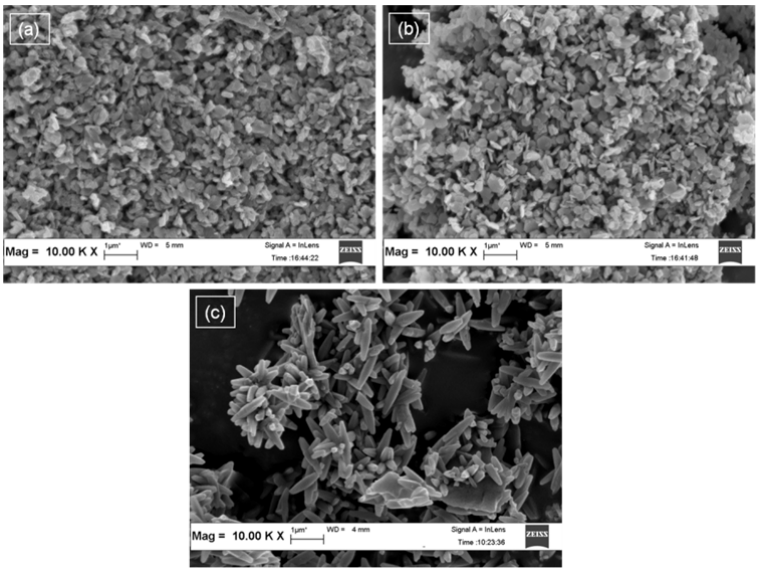

Figure 2. FESEM images of calcium hydroxide samples synthesized with (a) 0.01 mol, (b) 0.02 mol and (c) 0.03 mol of CTAB

TG/DTA analysis was carried out to examine the conversion process of synthetic $Ca(OH)_2$ sample during calcination process. Figure 3(a-b) shows the TG and DTA curves of synthetic $Ca(OH)_2$ sample prepared with 0.03 mol of CTAB. Three weight-loss steps were observed in the TGA curve shown in Figure 3(a). The first step occurring in the temperature range from 50°C to 300°C was attributed to the physical water evaporation of $Ca(OH)_2$ sample. The second step between 360°C and 460°C was ascribed to the chemical dehydration of $Ca(OH)_2$, which are confirmed by the sharp endothermic peak at 430°C in DTA curve (Figure 3(b)). The weight loss of this step was about 20%. The third step between 550°C and 680°C was attributed to the decomposition of $CaCO_3$. The weight loss 6% in this step was consistent with the XRD result shown in Figure 1(c), indicating that calcite was a minor phase.

The synthetic $Ca(OH)_2$ samples were used as calcium oxide (CaO) based adsorbents for carbon dioxide (CO_2) adsorption. The CO_2 adsorption capacities of CaO derived from synthetic $Ca(OH)_2$ samples were determined by TGA. Figure 4(a) shows the TGA profile of two consecutive carbonation/calcination cycles of CaO derived from synthetic $Ca(OH)_2$ sample prepared with 0.03 mol of CTAB in weight percentage. When synthetic $Ca(OH)_2$ sample was heated from room temperature to 700°C under 100% N_2 gas, dehydration of $Ca(OH)_2$ and decomposition of $CaCO_3$ were observed. Then, the temperature was maintained at 700°C for 6 min to ensure complete decomposition of $CaCO_3$ to CaO. After that, the reaction atmosphere was

switched to 100% CO_2, the carbonation reaction of CaO took place to form the carbonated $CaCO_3$. This step was followed by the next calcination reaction whereby the carbonated $CaCO_3$ converted to CaO under 100% N_2 gas.

The CO_2 adsorption capacities of CaO obtained from synthetic $Ca(OH)_2$ samples prepared with 0.01 mol, 0.02 mol and 0.03 mol of CTAB were calculated from the TGA profile. The calculated results are presented in Table 1 and Figure 4(b). As seen in Table 1 and Figure 4(b), CO_2 adsorption capacities of CaO derived from $Ca(OH)_2$ samples increased with increasing of CTAB concentration. In comparison with CaO derived from irregular-shaped and hexagonal-shaped $Ca(OH)_2$ samples prepared with 0.01 mol and 0.02 mol of CTAB, the capacity of CaO derived from one dimensional (1D) nanorods $Ca(OH)_2$ sample prepared with 0.03 mol of CTAB after 1st cycle was higher (0.75 g-CO_2/g-adsorbent), which approached to the theoretical adsorption capacity of CaO (0.78 g-CO_2/g-adsorbent).

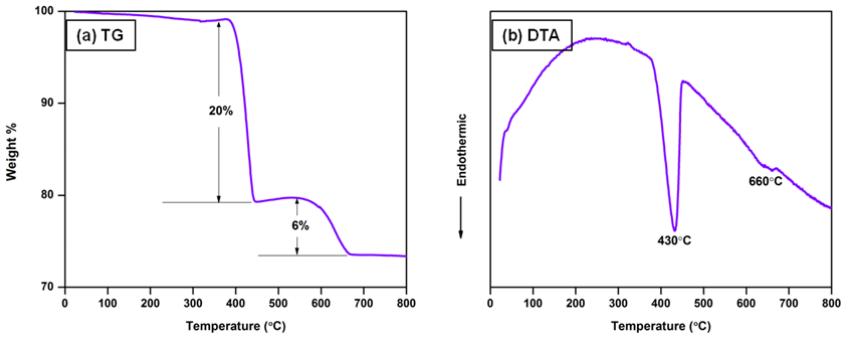

Figure 3. (a) TG and (b) DTA curves of calcium hydroxide sample synthesized with 0.03 mol of CTAB

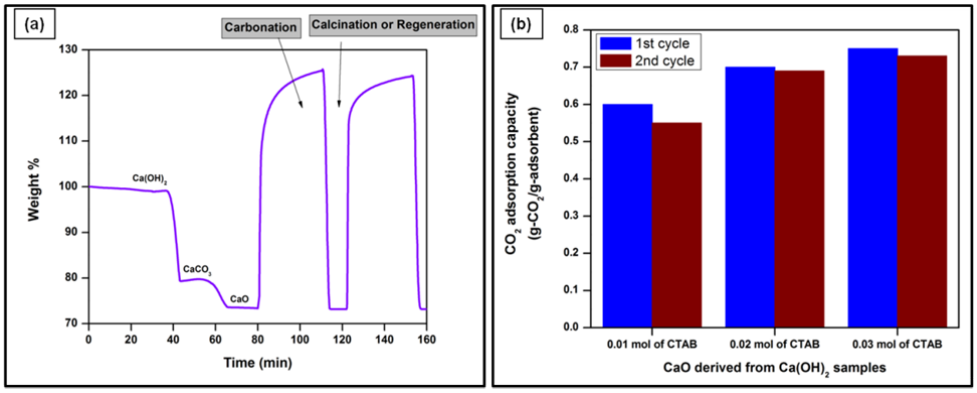

Figure 4. (a) TGA profile $Ca(OH)_2$ sample synthesized with 0.03 mol of CTAB and

(b) CO_2 adsorption capacity of CaO derived from $Ca(OH)_2$ samples

Table 1. CO_2 adsorption capacities of CaO derived from $Ca(OH)_2$ samples

No	Sample	CO_2 adsorption capacity (g-CO_2/g-adsorbent)	
		First cycle	Second cycle
1	CaO derived from $Ca(OH)_2$ sample prepared with 0.01 mol of CTAB	0.60	0.55
2	CaO derived from $Ca(OH)_2$ sample prepared with 0.02 mol of CTAB	0.70	0.69
3	CaO derived from $Ca(OH)_2$ sample prepared with 0.03 mol of CTAB	0.75	0.73

4. Conclusion

In this study, nanostructured calcium hydroxide ($Ca(OH)_2$) samples were synthesized via a simple precipitation method at the temperature 40°C by varying the concentration of cetyltrimethyl ammonium bromide (CTAB). The formation of one dimensional $Ca(OH)_2$ nanorods was investigated. FESEM images exhibited that $Ca(OH)_2$ samples synthesized with 0.01 mol of CTAB resulted in irregular shaped and sized micro/nano particles, with 0.02 mol of CTAB resulted in micro/nano hexagonal plates with non uniform sizes, with 0.03 mol of CTAB resulted in nanorods with an average diameter of 80-100 nm, respectively. Based on FESEM images, it could be concluded that the concentration of CTAB played a critical role to control the formation of $Ca(OH)_2$ nanorods. The TGA results showed that the CO_2 adsorption capacity of CaO derived from synthetic $Ca(OH)_2$ nanorods sample (0.75 g-CO_2/g-adsorbent) was higher than those of CaO derived from irregular and hexagonal shapes $Ca(OH)_2$ samples.

Acknowledgements

The authors thank the AUN/SEED Net Project under the Grant no. 304/6050219 and JICA for financial support and greatly acknowledge to Universiti Sains Malaysia and Tokyo Institute of Technology for facility support. The authors are grateful to Dr Mu Mu Myint, Rector and Dr Win Win Ei, Pro-Rectors, Taunggyi University for their permission to submit this paper. The authors grateful to Dr Khin Khin Htoot, Head of Department of Physics and Professor Dr Nwe Nwe San, Department of Physics, Taunggyi University for encouragement to submit this paper.

References

[1] Luís Quesada Carballo, María del Rosario Perez, David Cantador Fernández, Alvaro Caballero Amores, and José María Fernández Rodríguez , "Optimum particle size of treated calcites for CO_2 capture in a power plant", Materials, 2019, vol.12, pp.1-17.

[2] Muhammad Awais Naeem, Andac Armutlulu, Qasim Imtiaz, Felix Donat, Robin Schäublin, Agnieszka Kierzkowska and Christoph R. Müller, "Optimization of the structural characteristics of CaO and its effective stabilization yield high-capacity CO_2 sorbents", Nature communications, 2018, 9:2408, pp.1-11.

[3] Qiang Wang, Jizhong Luo, Ziyi Zhong and Armando Borgna, "CO_2 capture by solid adsorbents and their applications: current status and new trends", Energy Environ. Sci, 2011, vol.4, pp. 42-55.

[4] Chiung-Fang Liu, Shin-Min Shih, and Tsai-Bang Huang, "Effect of SO_2 on the reaction of calcium hydroxide with CO_2 at low temperatures", Ind. Eng. Chem. Res. 2010, vol.49, pp.9052-9057.

[5] Wu, S.F, T. H. Beum, J. I. Yang, and J. N. Kim, "Properties of Ca-base CO_2 sorbent using $Ca(OH)_2$ as precursor", Ind. Eng. Chem. Res, 2007, vol. 46, pp. 7896-7899.

[6] Nanni, A. and L. Dei, "$Ca(OH)_2$ nanoparticles from W/O microemulsions", Langmuir, 2002, vol.19, pp. 933-938.

[7] Amin Alavi, M. and A. Morsali, "Ultrasonic-assisted synthesis of $Ca(OH)_2$ and CaO nanostructures", Journal of Experimental Nanoscience, 2010, vol. 5, pp. 93-105.

[8] Tong Liu, Yarong Zhu, Xuanzhou Zhang, Tongwen Zhang, Tao Zhang, Xingguo Li, "Synthesis and characterization of calcium hydroxide nanoparticles by hydrogen plasma-metal reaction method", Materials Letters, 2010, vol. 64, pp. 2575-2577.

[9] Rodriguez-Navarro, C, A. Suzuki, and E. Ruiz-Agudo, "Alcohol dispersions of calcium hydroxide nanoparticles for stone conservation", Langmuir, 2013, vol. 29, pp. 11457-11470.

[10] Yanlong Xing and Petra S. Dittrich, "One-dimensional nanostructures: microfluidic-based synthesis, alignment and integration towards functional sensing devices", Sensors, 2018, vol.18:134, pp.1-21.

[11] Maithri Tharmavaram, Deepak Rawtani and Gaurav Pandey, "Fabrication routes for one-dimensional nanostructures via block copolymers", Nano Convergence, 2017, vol. 4:12, pp.1-13.

[12] Rui Chen, Zuoshan Wang, Qingqing Zhou, Juan Lu and Min Zheng, "A template-free microwave synthesis of one-dimensional Cu_2O nanowires with desired photocatalytic property", Materials, 2018, vol.11: 1843, pp.1-11.

The Updated Probabilistic Seismic Models 2018 for Mitigation of Seismic Risks in Myanmar

Myo Thant[1], Maung Thein[2]

Abstract

The seismic hazard assessment of Myanmar was firstly carried out by Gorshkov (1959), and the seismic hazard model was then continuously updated by Mg Thein in 1985 and 2001, and Maung Thein et al. in 2003 and 2005. All of those seismic hazard models based on the previous major events, it means that the models were developed by using deterministic seismic hazard assessment (DSHA) methodology. The seismic hazard maps and information are very important for a country in seismic risk reduction processes. In recent years, all of the scientists accept that only deterministic seismic hazard model is not sufficient for conducting the seismic risk reduction processes, and the seismic hazard models constructed by using probabilistic seismic hazard assessment (PSHA) method. Therefore, the probabilistic seismic hazard maps of Myanmar were developed in 2012 by Myo Thant et al. In developing those maps, the seismic sources are modeled as areal seismic sources for the subduction zone domain of Indian-Australia Plate beneath Burma Plate, in the west of country and the collision zone domain of Indian-Australia Plate and Eurasia Plate, in the north-west. Moreover, the Eastern Highland region is also modeled as the areal seismic sources due to the unavailability of the sufficient fault parameters, even though there are several strike-slip faults in that region (e.g. Moemeik Fault, Nampon Fault, Shweli Fault, Kyaukme Fault, and Nam Ma Fault, etc.). The 2012 seismic sources were remodeled especially the areal seismic sources of subduction and collision zones, and Eastern Highland, and the new probabilistic hazard models are proposed for Myanmar in 2018. In those models, the seismic hazard calculations are for 10% and 2% probability of exceedances in 50 years as the previous one. The resulted seismic hazard maps of Myanmar are peak ground acceleration (PGA) maps, spectral acceleration (SA) maps for the period 0.2 s and 1.0 s, and peak ground velocity (PGV) maps. In this work, we try to understand the seismic risk of Myanmar based on the available demographic and other related information, and the modified seismic hazard models, especially for the major cities as Yangon, Mandalay, Sagaing, Bago, etc. Moreover, we also make the seismic hazard model for 10% probability of exceedance in 50 years simple to understand by public for self-realization of risk condition, and the public can prepare themselves for seismic risk reduction purposes.

Keywords: probabilistic seismic hazard maps, peak ground acceleration, spectral acceleration, peak ground velocity, seismic risk reduction.

1. Introduction

Myanmar is the earthquake disaster prone country since it lies along one of the major earthquake belts of the world, Alpide earthquake belt. With respect to the tectonics of the country, the convergence of Indian-Australia Plate in the south with the Eurasia Plate in north is the major cause of the earthquakes in Myanmar and surrounding regions. The crustal faults present in Myanmar can be assumed due to this tectonic process. One of the major active faults is the right-lateral, strike-slip, Sagaing Fault passing through near or on the major cities of Myanmar such as Naypyitaw, Yangon, Mandalay, Bago, and Sagaing, etc. The others are Kabaw Fault, Mrauk-U Fault, Gwegyo Fault, West Bago Yoma Fault in central and western parts of Myanmar; Lashio

[1] Dr Professor, Department of Geology, University of Yangon, myothant05@gmail.com
[2] Dr Professor, Ret., Department of Geology, University of Yangon

Fault in the Eastern Highland; NW-SE trending Three Pagodas Fault, and Papun Fault in Tanintharyi Region. From the point of view of earthquake experiences, the country has experienced several large earthquakes such as 1839 Ava (Innwa) Earthquake, 1912 Maymyo Earthquake, 1929 Swa Earthquake, 1930 Bago Earthquake, 1930 Phyu Earthquake, 1956 Sagaing Earthquake, 1991 Tagaung Earthquake, etc. Among them th deadliest and the most damaged events are 1930 Bago Earthquake originated from Sagaing Fault, which struck on May 5 with the magnitude of 7.3 M, causing 550 deaths and several buildings were damaged in Bago and Yangon, while the other is 1839 Ava (Innwa) event that caused 400 casualties in Innwa and surrounding areas with several buildings damages especially pagodas, and monasteries. The most recent events are 2011 Tarlay Earthquake, 2012 Thabeikkyin Earthquake, 2016 Chauk Earthquake and 2017 Taikkyi Earthquake.

It can, therefore, be clearly seen that earthquake disaster of Myanmar is quite high, and the earthquake disaster mitigation processes are required to continuously carry out. Among those processes, the seismic hazard assessment is the essential and initial step. Therefore, seismic hazard assessments had been carrying out since eighteen century, e.g. Gorshkov (1959) [1], Mg Thein (1985, 2001) [2, 3], and Maung Thein et al. (2003, 2005)[4,5] based on the deterministic methodology. In 2012, Myo Thant et al. [6] carried out seismic hazard assessment of Myanmar by using the probabilistic seismic hazard assessment (PSHA) approach, then they modified in 2018 again.

2. Probabilistic Seismic Hazard Assessment Methodology and Applied Data

The methodology used in the seismic hazard assessment of Myanmar by Myo Thant et al. (2018) is probabilistic seismic hazard analysis defined by Cornell (1968) [7], and the basic steps are briefly described as four steps (Reiter, 1990; Cramer, 1996) [8, 9]. The earthquake sources identification is the first step of the method, in which the seismic sources are identified as being of uniform earthquake potential throughout the sources that can be range from planar faults to large seismotectonic provinces. The second step is definition of seismicity recurrence characteristics for each seismic source, by earthquake recurrence relationship giving the chance of an earthquake of a given size to happen in the source during a specific period of time, considering all of the upper limits of earthquakes. The simple earthquake recurrence relationship is Log N= a - bM, in which N is the cumulative number of earthquakes of a given magnitude or larger that can be expected to happened during a specified time period; a and b are the constants of earthquake occurrence, M is the earthquake magnitude, normally moment magnitude. Estimation of the earthquake effect is the step, and the attenuation of ground motion expected from the earthquakes in different magnitude range with distance, mostly represented nowadays by means of ground motion prediction equations. The last step is determining the seismic hazard at the site, i.e. the probability that the ground motion parameter (for example: ground acceleration, ground velocity and spectral acceleration) will be exceeded during a specified time period is calculated by considering the uncertainties in spatial and temporal earthquake occurrences, earthquake size, and ground motion prediction, etc.

The data and information applied in the seismic hazard calculation are the combined information of seismic sources model (2012) and the modified 2016 seismic sources model, and the seismicity information (Figure 1). The seismic sources are modeled as areal seismic sources for the subduction zone domain of Indian-Australia Plate beneath Burma Plate, in the west of country and the collision zone domain of Indian-Australia Plate and Eurasia Plate, in the north-

west. Moreover, the Eastern Highland region is also modeled as the areal seismic sources due to the unavailability of the sufficient fault parameters, even though there are several strike-slip faults in that region (e.g. Moemeik Fault, Nampon Fault, Shweli Fault, Kyaukme Fault, and Nam Ma Fault, etc.). The 2012 seismic sources were remodeled especially the areal seismic sources of subduction and collision zones, and Eastern Highland, and the new probabilistic hazard models are proposed for Myanmar in 2018.

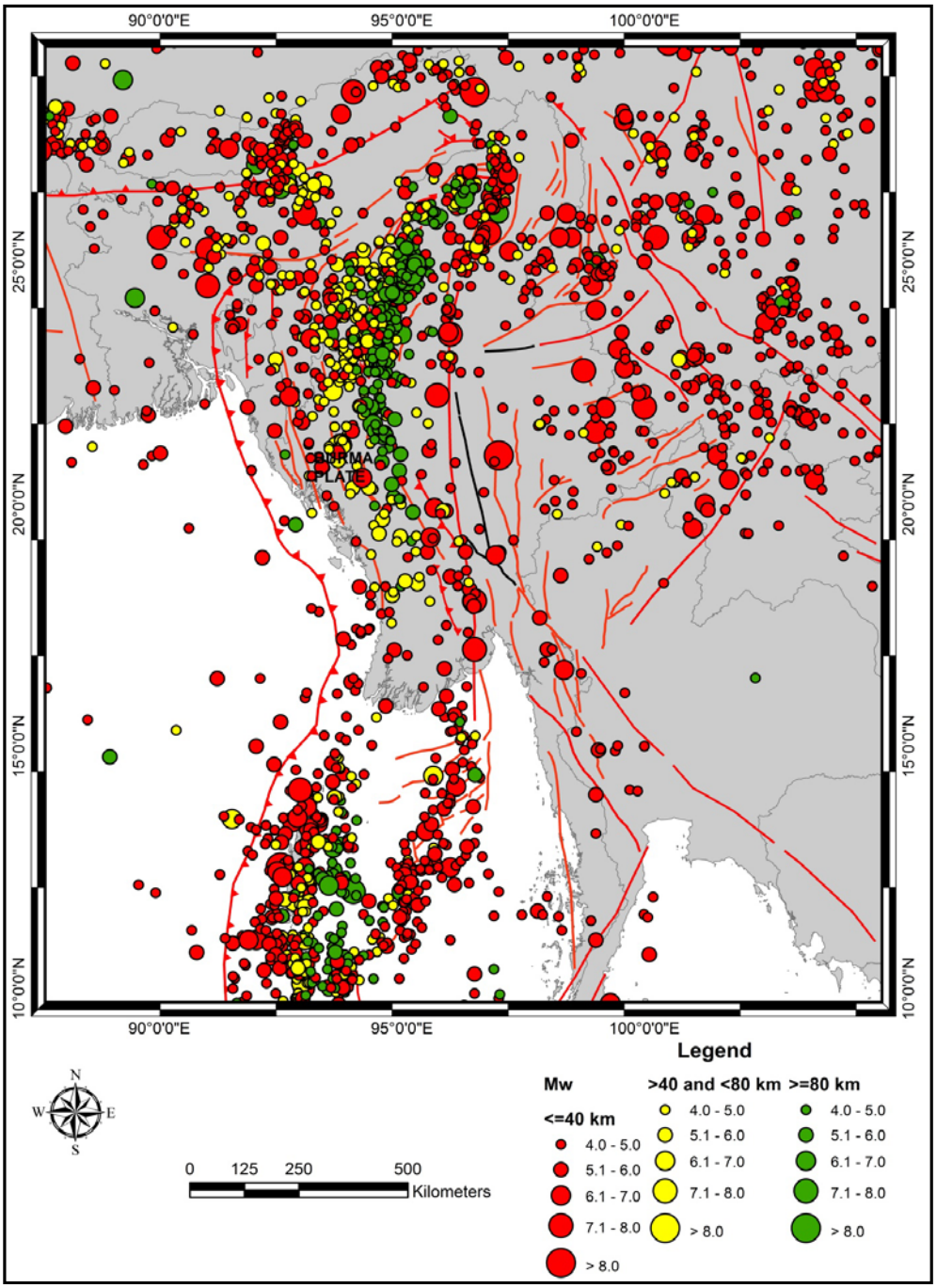

Figure 1. Map presenting the seismicity of Myanmar region (ISC earthquake catalog, 2011) after declustering.

3. Results and Discussion

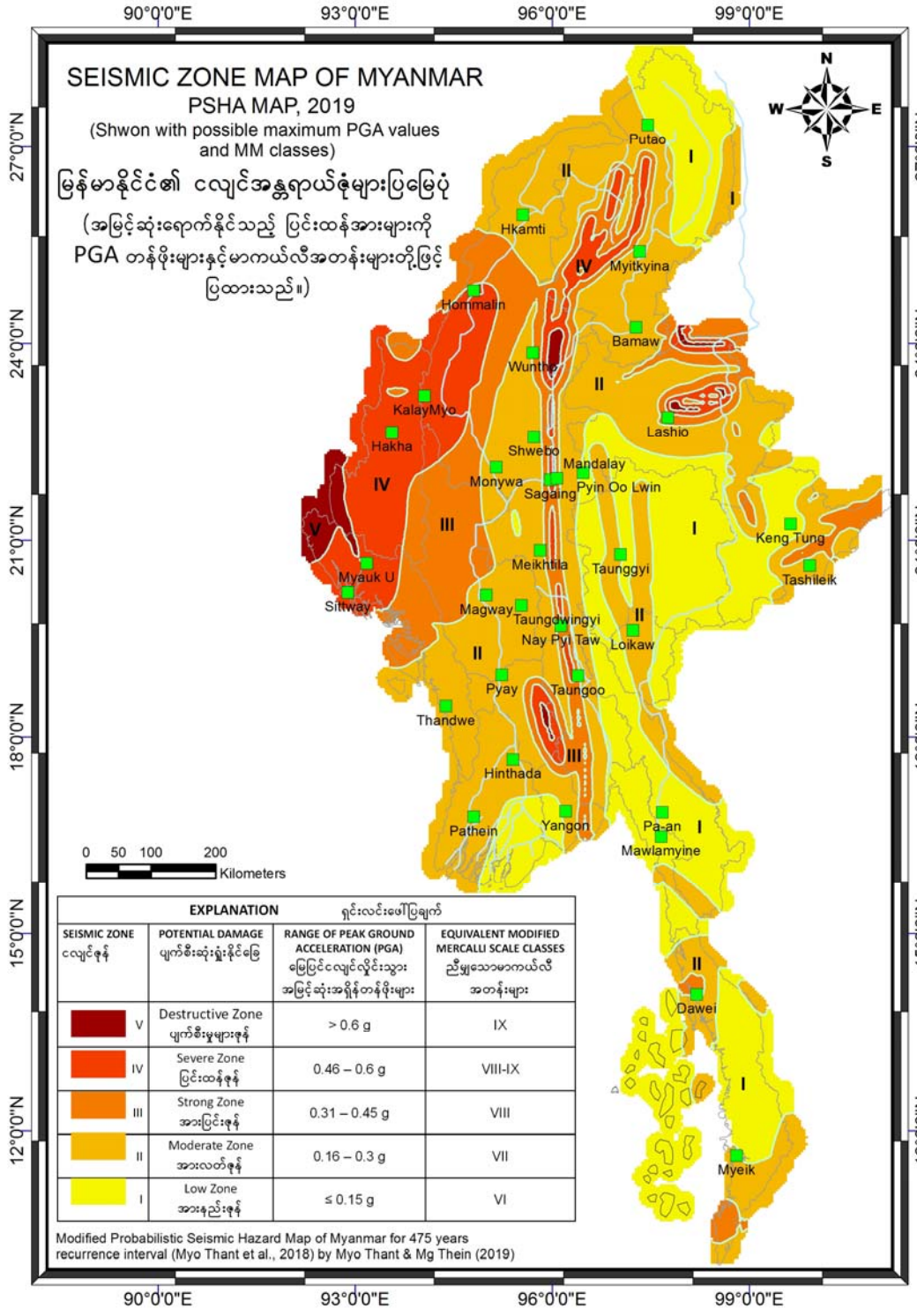

Figure 2. Seismic zone map of Myanmar, modified probabilistic seismic hazard map of Myanmar for 475 years recurrence interval (Myo Thant et al., 2018) by Myo Thant and Mg Thein (2019)

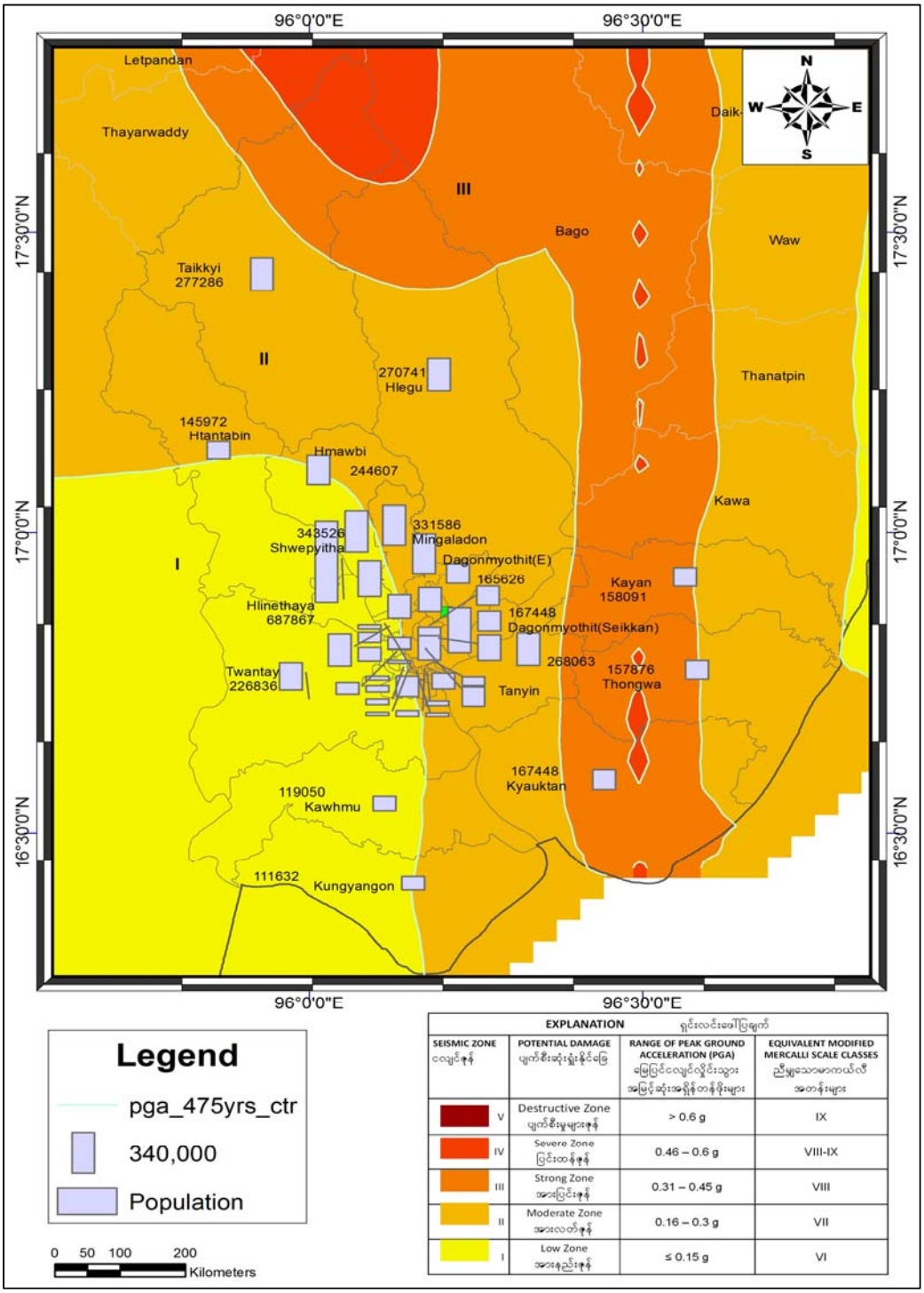

Figure 3. Seismic zone map of Yangon Region, modified probabilistic seismic hazard map of Myanmar for 475 years recurrence interval (Myo Thant et al., 2018) by Myo Thant and Mg Thein (2019)

Myo Thant et al. (2018) [10] constructed the probabilistic hazard maps of Myanmar for 10% and 2% probability of exceedance in 50 years and seismic hazards are illustrated in terms of peak ground acceleration (PGA), peak ground velocity (PGV), and spectral acceleration at the periods of 0.2 s and 1.0 s. In here, we modified the seismic hazard map for 10% probability of exceedance in 50 years (Figure 2) and the seismic hazards are presented by dividing different

zones in terms of peak ground acceleration (PGA), Modified Mercalli (MM) scale and potential damages. Five seismic zones are identified based on the range of PGA in which Seismic Zone I comprises Low Zone of Potential Damage with PGA value of ≤ 0.15 g and MM scale of VI; Seismic Zone II as Moderate Potential Zone with PGA range of 0.16 -0.3 g and MM scale VII, Zone III as Strong Potential Damage Zone with PGA range 0.31 – 0.45 g; Zone IV as Severe Potential Damage Zone with PGA range of 0.46 – 0.6 g and MM scale VIII-IX; and Seismic Zone V as Destructive Zone with PGA range ≥ 0.6 g and MM scale IX (Figure 2). The western part of Myanmar as northern Rakhine, Chin, northern Magway, western Sagaing are located in Seismic Zone III, IV and V. Four major regions/states as Yangon, Bago, Mandalay, Kachin also occur in Zone III, IV and V. Most of the major cities such as Mandalay, Sagaing, Naypyitaw, Bago, Taungoo, and Wuntho correspond to the seismic zones of III and IV while the city Yangon belongs to seismic zone of II. However, it should be noted that this seismic zone map is probabilistic seismic hazard map of 10% probability of exceedance in 50 years (475 years recurrence interval) and the site condition is considered as the bedrock. If the reference seismic hazard is for 2% probability of exceedance in 50 years (2475 years recurrence interval) and the site conditions are considered based on the soil properties, the hazard values will be higher than the present one and the hazard distributed areas will also be wider.

With regards to Yagon Region, The central and eastern part of the region belongs to the seismic zones of Zone II to III and some are of Seismic Zone IV such as Thongwa and Kyaukktan, Tanyin, Taikkyi and Hlegu Townships. Based on the population of Yangon City, Most of the high populated townships, e.g. Dagonmyothit (S), Myaukokkalar, Mingaladon, Thakeda, Thingankyun, Dagonmyothit (N), Dagonmyothit (Seikkan), Dagonmyothit (E) Tamwe, Taungokkalar, comprise of Seismic Zone II. As mentioned previously, This also bases on the seismic hazard information of 10% probability of exceedance in 50 years and bedrock condition, if the hazard information based on 2% probability of exceedance in 50 years and the detailed soil condition, the seismic hazard will be higher and the area of distribution will be wider.

The seismic hazard assessment plays an important role for earthquake disaster mitigation processes that will include application in seismic resistance design calculation (for engineering purposes, the seismic zone factor will be included in National Building Code), land-use plan, seismic risk assessment, and other mitigation purposes. Moreover, the public must understand the seismic risk condition of their buildings and areas, the development of seismic zone map by translation the estimated seismic hazard is therefore very important, especially for the public. Based on these information, they can carry out earthquake disaster preparing processes and the concerned ministries, departments and organizations can also use for various purposes.

References

[1] Gorshkov, G. P. "Problems of Seismotectonics and Seismicity – Zoning of the Territory of the Union of Burma". (Mineographed Manuscript), 1959.

[2] Maung Thein. "Mitigation of Earthquake Hazards in Myanmar (in Myanmar Language)", Working People Daily, 18 Nov., 1985.

[3] Maung Thein. "Mitigation of Earthquake Hazard in Myanmar (in Myanmar Language)", Jour. Myan. Acad. Tech., Vol. 1., No. 2, P. 124 – 134.

[4] Maung Thein, Tint Lwin Swe and Tin Htay Mu. "Seismic Zone Map of Myanmar", With an Explanatory Note (9 pg.), 2003.

[5] Maung Thein and Tint Lwin Swe. "The Seismic Zone Map of Myanmar", Myanmar Earthquake Committee, Myanmar Engineer Society, 2005.

[6] Myo Thant, Nwai Le' Ngal, Soe Thura Tun, Maung Thein, Win Swe, Than Myint**.** "Seismic Hazard Assessment For Myanmar**",** Report to Myanmar Earthquake Committee and Myanmar Geoscience Socity, P58., 2012.

[7] Cornell, C. A. "Engineering Seismic Risk Analysis", Bulletin of the Seismological Society of America, Vol. 58, 1583-1606, 1968.

[8] Reiter, L., "Earthquake Hazard Analysis- Issues and Insights", Columbia University Press, New York, 254pp., 1990.

[9] Kramer, S. L. "Geotechnical Earthquake Engineering", Prentice-Hall International Series in Civil Engineering and Engineering Mechanics, 653 pp., 1996.

[10] Myo Thant, Saw Ngwe Khaing, Soe Min, Lin Thu Aung, Thura Aung, Soe Thura Tun, Hiroshi Kawase, Chung-Han Chang, Yu Wang, "Updated Probabilistic Seismic Models of Myanmar", Report of Myanmar Earthquake Committee, 2018.

Seismic Microzonation at Taungthaman area, Mandalay Region

Pyi Soe Thein[1], Tint Tint Khaing[2] , Junji Kiyono[3], Tun Tun Win [4], Htay Win[5]

Abstract

Taunthaman area is located very closed to the most active dextral Sagaing Fault in Myanmar. In the historical record, several earthquakes happened in and around Mandalay, Amarapura, Innwa, Sagaing region from the beginning of the year of 1400. Even a moderately strong earthquake may cause great loss of lives and property damage. The study area is partly built on alluvial sediments which can amplify seismic ground motion. There is a need to prepare a comprehensive seismic microzonation in near future to support seismic hazard assessment. We conducted 7-sites PQWT-TC series geophysical survey to estimate the shaking intensity distribution during the earthquake. We also conducted 7-site bore holes investigation to gain a representative determination of the soil condition of subsurface structures in Taung Tha Man area. These parameters are required for seismic resistant design of structures. The adopted methodology comprises of three parts:

(i) soil modeling and estimation of depth to Engineering Bed Layer (ii) estimation of the ground motion at Engineering Bed Layer (iii) estimation of ground motion at the surface by 1D ground response analysis using Multiple Reflection Analysis (MRA) program. The soil models are prepared from geophysical survey data and shear wave velocity/ N-values. The results enabled us to estimate the site-dependent shaking characteristics of earthquake ground motion.

Keywords: Alluvial sediments, Sagaing Fault, geophysical survey, earthquake ground motion

1. Introduction

In Myanmar, earthquakes are mainly caused by the tectonic movements related to the subduction of the Indian plate beneath the Burma plate along the Andaman Islands and Rakhine-China-Naga Ranges. The Indian Plate collides with Eurasia Plate at the rate of 50 mm/yr [1], while the rate of subduction of Indian plate under Burma plate is about 36 mm/yr and the Benioff zone dips in varying degree in each segment of the subduction system. Another major active geological structure that generates the major earthquakes in Myanmar is Sagaing Fault. Others are Kyaukkyan Fault, Papun Fault, Kabaw Fault, Gwegyo Fault and West Bago Yoma Fault. Taungthaman area, Mandalay region is the famous cultural center of Myanmar and the population is about thirty thousand. There are also greater population, higher urbanization, more industrialization and many infrastructures. Actually, the study area is located very closed to the most active dextral Sagaing fault in Myanmar. An active Sagaing Fault is a fault that may have displacement within a future period of concern to humans. Identification of active Sagaing Fault requires recognizing previous displacement and constraining the age of displacement [2], [3] and [4]. An active fault is usually identified by associating it with tectonically deformed Quaternary- age materials or surface. In the historical record, several earthquakes happened in and around Mandalay, Amarapura, Innwa, Sagaing region from the beginning of the year of 1400. Even a moderately strong earthquake may cause

[1] Lecturer, Department of Geology, Yadanabon University, pyisoethein@yahoo.com
[2] M.Sc student, Department of Geology, Yadanabon University, tinttintkhaing.geol@gmail.com
[3] Graduate School of Global Environmental Studies, Kyoto University, Japan, kiyono.junji.5x@kyoto.u.ac.jp
[4] Lecturer, Department of Geology, Mandalay University, geolttw73@gmail.com
[5] Professor and Head, Department of Geology, Yadanabon University, htaywin.geol.61@gmail.com

great loss of lives and property damage. Seismic microzonation studies are generally considered as a prerequisite for the site specific risk analysis to mitigate earthquake losses or damages. The first relevant applications appeared in Myanmar at recent years [5].

In this research, the development of a high resolution near-surface Mandalay region Vs^{30} model is presented, including descriptions of the processing steps applied to the adopted SPT dataset and PQWT-TC500 geophysical data, the consideration made for the seismic microzonation mapping of the selected spatial interpolation schemes. The seismic microzonation maps are developed by using the multiple reflection analysis and empirical stochastic green function.

2. Geophysical Survey and Data Analysis

Geophysical lines are generally arranged perpendicular to the line to be constructed, can detect tectonic crushed zone on both sides of the border and its different physical characteristics, contrast is strong, crushing width, extending distinctive characteristics. There are seven sites from PQWT-TC500 geophysical instrument throughout the taungthaman area to evaluate the geotechnical properties of subsurface layers (Figure 1). The collected data each time is the data of the midpoint between two electrode data, Electrode spacing is generally 5-10 m, dot spacing is generally about 0.5-2m, electrode spacing and dot spacing must keep the same distance for one measuring line (Figure 2). The measurement and result PQWT-TC500 geophysical cross-section of the site no.1 is reported in Figure 3 and 4.

Figure 1. SRTM Satellite image with Geophysical survey Sites.

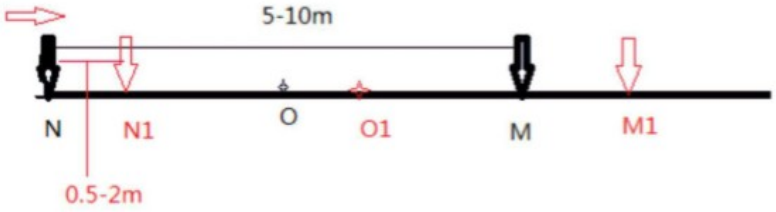

Figure 2. Sketch map of wiring method N、M are electrodes, O is Measuring point, NM=10m, dot spacing is generally about 0.5-2m (standardis1m)

Figure 3. PQWT-TC500 Geophysical measurement at site No 1, Yadanabon University [96°4'18.897" E & 21°53'31.516" N].

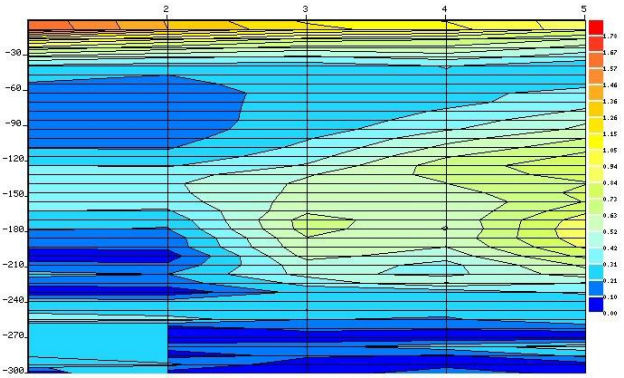

Figure 3. The result PQWT-TC500 geophysical cross-section of the site no.1

Seven borehole data were collected to evaluate the subsurface profiles and related geotechnical parameters for seismic microzonation analyses. The detailed drilling program had been carried out for subsurface investigation in taungthaman area. The SPT dataset is used to develop surfaces describing the distribution of time-averaged shear wave velocity, Vs^{30}, across the urban area in Mandalay region. Target profile depths of 5, 10, 20, 30 m were considered to allow for an assessment of the distributions of soil stiffness with depth across the region. Vs^{30} values are computed for each target depth, as Eq. (1) [6] and [7]. The evaluated subsurface profiles for each area in Mandalay region are shown in the following Figure 4.

$Vs^{30}=$ $$\frac{\sum d_i}{\sum t_i} = \frac{\sum d_i}{\sum(\frac{d_i}{vs_i})} \quad (1)$$

where v_si is shear wave velocity, d_i thickness of i layer and t_i one way travel time in i^{th} layer.

Figure 4. Example of Vs profile at Taungthaman area (SPT 1 dataset).

The MRA (Multiple Reflection Analysis) was used to calculate the transfer function, which expresses the relation between the period and the corresponding magnification factor. Calculation of predominant period by using boring data and the ground model profile is done according to the MRA. The governing equation is

$$\rho \frac{\delta^2 \mu}{\delta t^2} (2); \frac{\delta^2 \mu}{\delta z^2} + \eta \frac{\delta^3 \mu}{\delta z^2 \delta t}$$

in which μ is the displacement of horizontal S-wave (SH), Z the direction of wave propagation (up-down), *t* the time, ρ the density, *G* the shear modulus and η the coefficient of visco-elasticity. The soil damping is considered by giving the complex value to the shear modulus and solving Eq. (2). The damping constant is 5% of critical damping for each layer [8].

3. Peak Ground Acceleration

Seismic hazard models are being updated by modifying some of the seismic sources in Myanmar. In this research, the input motions were selected based on the Probabilistic PGA (Peak Ground Acceleration) (g) Map of Myanmar for 10% probability of exceedance in 50 years, for engineering bedrock condition [9]. The ground response analyses were conducted by using the assumption of vertical propagation of shear waves from the engineering bedrock to the ground surface. The seismic ground motion at EBL is estimated using Empirical

Stochastic Green Function. The surface ground motion is estimated by passing ground motion simulated at EBL through prepared soil models of each site using Multiple reflection program. The peak horizontal ground acceleration of these seismic events ranged from 0.35 g to 0.55 g. Distribution of the estimated peak ground accelerations are shown in Figure 5. The component of the shaking is NS, EW. This is the first trial to estimate the shaking and the damage under the condition of the occurrence of a future Amarapura earthquake.

Table 1. Results of Geophysical data.

Location Site	**PGA (g)**	**Ground Water**	**$Vs30$ (m/s)**
Yadanabon University	0.45-0.35	> 74	250

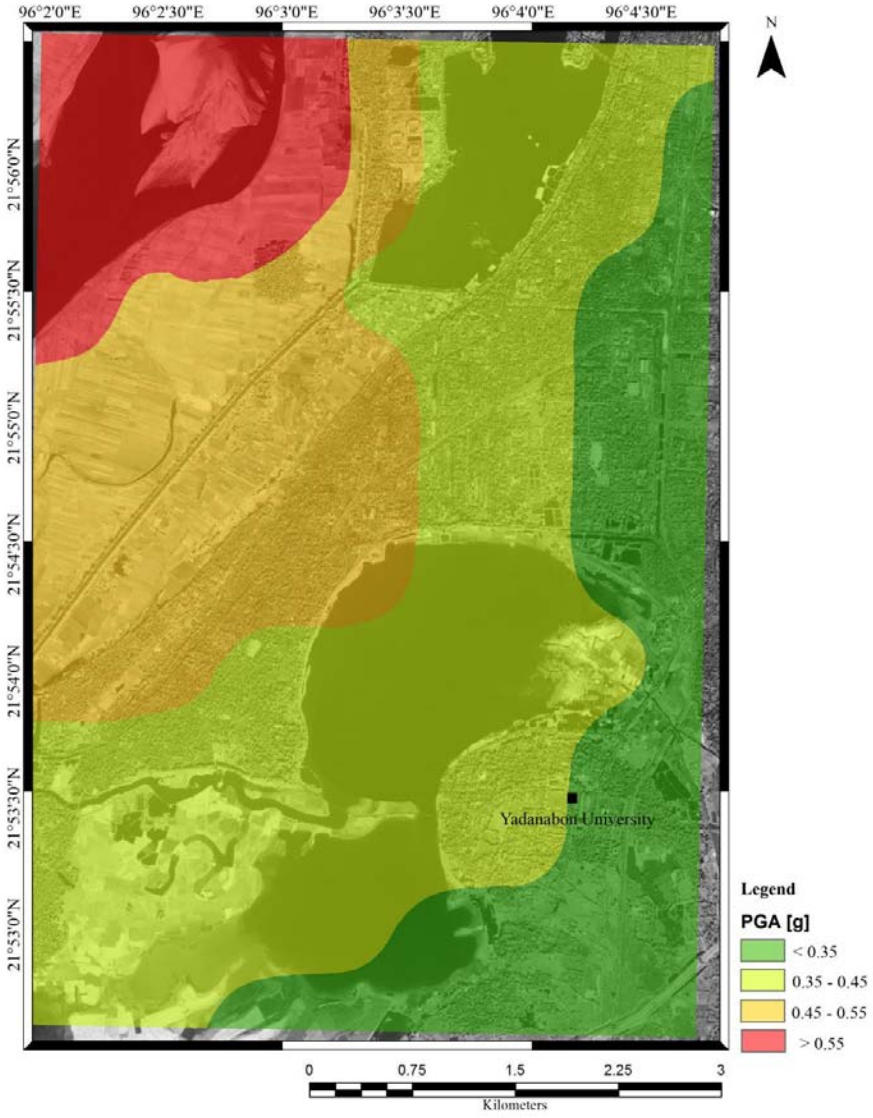

Figure 5. Estimated (PGA) map of Taungthaman area, Amarapura township, Mandalay region.

4. Conclusions

Seven sites of Standard Peneration Test (SPT) and PQWT-TC500 series ground water detection were carried out for constructing a subsurface ground model in Taungthaman area. The Kriging method can be used for the interpolation of subsurface information such as shear wave velocity and depth of irregular boundary. The shear wave velocity of the top layer is Vs ≤ 250 m/s. By combining above two-layer model and the results of geophysical observation, the author proposed the distribution of the first layer thickness of the sediment. Seismic microzonation of the Taungthaman area had predicted based on the multiple reflection analysis by using the proposed ground model. The outputs of this research would be very applicable for both engineering purpose and to identify and mitigate the seismic risk for Mandalay region, Myanmar. There are high acceleration areas appears along the dextral Sagaing Fault, especially near the epicenter. Peak acceleration becomes more than 0.45 g in some areas, which causes severe damage for buildings in high probability (Table 1).

Acknowledgements

This study was supported by the Yadanabon University, Ministry of Education. The acknowledgement is extended to Rector Dr. Maung Maung Naing, Pro-rector of Dr. Si Si Khin and Dr. Tint Moe Thu Zar, Yadanabon University for their kind permission for the submission of this research paper. We would also like to thank the Foundation Soil Investigation Group (FIG) Company for providing geotechnical and geophysical data of the Taung Tha Man area. Managing director Mr Kyaw Khant (Robust Trust Company) provided well points and geophysical data of the study area and his deserve special acknowledgement.

References

[1] GIAC, TOTAL, UNOCAL, MOGE, EcoleNormaleSuperieure, Yangon, Dagon, Mandalay, Chaing Mai and Chulalonkom Universities), "The tectonics of Myanmar", Final Report of GIAC Project 1996-1999, 2002

[2] Win Swe, "Rift-features at the Sagaing-Tagaung Ridge". Abstract, Burma Research Congr., Rangoon, 101. 1970

[3] Hla Maung, "Transcurrent movements in the Burma-Andaman Sea region". Geology 15, 911 912, 1987

[4] Myint Thein, Kyaw Tint and Aye, Ko Aung, "On the lateral displacement of the Sagaing fault" 1991, Georeports 1, 23–34.

[5] Maung Thein and Tint Lwin Swe, "Explanatory Account for Seismic Zone Map of Myanmar (Revised Version, 2005) February (Prepared under the auspices of Myanmar Earthquake Committee)", 2006, 4 p.

[6] Pyi Soe Thein, Junji Kiyono, Tun Tun Win, Than Than Nuand Day Wa Aung, "Seismic Microzonation of Mandalay City, Myanmar". Journal of Geological Resources and Engineering, David Puiblishing, 2015.

[7] Ohta, Y. and Goto, N,"Estimation of s-wave velocity in terms of characteristic indices of soil", Butsuri-Tanko, 29(4), 1976. 34-41

[8] Kiyono, J. and Suzuki, M, "Conditional Simulation of Stochastic Waves by Using Kalman Filter and Kriging

Techniques", Proc. of the 11th World Conference on Earthquake Engineering, Acapulco, Mexico, 1996. Paper No.1620.

[9] Myo Thant, Nwai Le' Ngal, Soe Thura Tun, Maung Thein, Win Swe, Than Myint, "Seismic Hazard Assessment For Myanmar", Report to Myanmar Earthquake Committee and Myanmar Geoscience Socity, 2012, P58.

Adsorptive Removal of Color from Textile Effluent Using Agricultural Wastes as Adsorbents

Nwe Nwe Aung[1], Mon Mon Aye[2], Rosy[3], Thet Thet Mon [4], Zue Zue Aung[5]

Abstract

Dyes are used in various fields such as paper, textile and plastics industries. Local dyeing houses in Amarapura discharge their dyeing wastewater into water body of Taungthaman Lake without any treatment. The color in these effluents are not biodegradable and can damage water quality. The aim of the present study is to explore the feasibility of using agricultural wastes such as rice husk, peanut husk and saw dust in the removal of color from dyeing effluents. The adsorption study was carried out by column method by choosing the most effective adsorbent from rice husk, peanut husk and sawdust. Different particle sizes and dose of adsorbents were used for study the effect of various parameter on adsorption process. The absorbances of dye containing wastewater and treated wastewater were measured by using UV-visible spectrophotometer. The λ_{max} value of dyeing wastewater was found to be 546 nm. The percent removal of red color from dyeing effluent could be calculated as 78 % by rice husk, 83 % by peanut husk and 80 % by saw dust. The pH value of effluents was measured after biosorption process and found to be 11.4 and 7.9 respectively. In addition, the removal efficiency for COD in the final effluent was found to be 78 %. The results prove that agricultural wastes, peanut husk and saw dust, are cost-effective and eco-friendly for removal of color from dyeing effluents.

1. Introduction

Textile dyes are generally made of synthetic, organic and aromatic compounds that may contain some heavy metals in their structure. These heavy metal containing aromatic compound can cause toxicity and carcinogen [1]. Wastewater discharged by the textile industry and dyeing houses are generally high in both color and such organic compounds. The presence of large amount of suspended solids, dissolved solids, high pH in the textile wastewater can cause serious environmental problems. Among then, color is the very first contaminant to be recognized in the textile dyeing wastewater [2]. A very small amount of dye in water body is highly visible and reduces penetration of light in water systems, thus causing the negative impacts on photosynthesis of aquatic plant [3]. One of the major challenges to environmental scientists is the environmental impact of textile effluent which contain residual color and some other organic contain residual color and some other organic compounds. In the last few years, environmental scientists paid great attention to the color removal from the textile effluents not only because of their potential toxicity but also mainly due to its visibility problems [4, 5].

Nowadays, various treatment methods such as adsorption, coagulation/flocculation/ precipitation [6], biological processes and ionizing/gamma radiation [7] are available for the removal of dye from textile effluent. However, most of them are expensive. Among these methods, adsorption is the most economical and effective treatment method, and so environmental scientists widely used adsorption technique for color removal from textile

[1] Lecturer, Department of Chemistry, Yadanabon University, nwenweaung748@gmail.com
[2] Assistant Lecturer, Department of Chemistry, Yadanabon University, monmon129464@gmail.com
[3] Assistant Lecturer, Department of Chemistry, Yadanabon University, rosylaphai@gmail.com
[4] Assistant Lecturer, Department of Chemistry, Yadanabon University, tthet8365@gmail.com
[5] M Sc student, Department of Chemistry, Yadanabon University, zuezueaung3333@gmail.com

effluent. Due to high cost of activated carbon, adsorption on natural materials such as sand [8], fly ash [9], orange peel and banana peel [10], sugarcane bagasse and used black tea leaves [11], rice husk [9], peanut husk [12], sawdust [13] and modified biomaterials [14-16] have received great interest. These natural adsorbents are locally available, cost-effective and ecofriendly.

The present study investigates the effective use of agricultural wastes as nonconventional and low-cost adsorbents for the removal of color from textile effluents using column method. The aim of this study was to compare the color removal efficiency of the selected agricultural wastes and to find an ecofriendly solution for the environmental problems caused by direct discharge of dyeing wastewater into water body without treatment. The effect of various parameters such as adsorbent dose, particle size of adsorbent and volume of dyeing wastewater were also investigated in this study.

2. Methods

2.1 Collection of textile wastewater

The textile wastewater sample was collected from local dyeing house located near Taungthaman Lake, Amarapura township, Mandalay Region. Sample was collected in precleaned pdyethlene bottles and placed in icebox for analysis. The collected wastewater sample for the present study was blue colored. The physicochemical parameters such as pH, electrical conductivity (EC), total dissolved solid (TDS) and chemical oxygen demand (COD) were analyzed to characterize the collected wastewater samples according to the methods prescribed in APHA [17].

2.2 Preparation of Adsorbents

The different agricultural wastes (rice husk, peanut husk and sawdust) were collected from different areas of Patheingyi Township, Mandalay Region. The biomasses were rinsed with tap water for several times to remove dust and any debris. And then they were rinsed two times with distilled water and dried in sunlight. The dried biomasses were further dried in oven for 24 hours at 60°C. The cleaned dried biomasses were ground into fine particles by grinding machine and sieved into different particles sizes. The particles sizes used in this study were 125 μm, 250 μm and 400 μm.

(a) *(b)* *(c)*

Figure 1. Adsorbents of 250 μm size (a) rice husk (b) peanut husk (c) sawdust.

2.3 Removal of color from textile effluent by column method

To choose the most effective adsorbent, three different columns having the diameter of 1cm and length of 25cm were packed with different adsorbents of 250 μm particle sizes. A piece of cotton wool was used as support at the bottom of each column. The characteristic features of the columns packed with different adsorbents were given in Table 1.

Table.1 The Characteristic features of different column packed with different adsorbent.

Adsorbent	Adsorbent dose (g)	Height of adsorbent in column (cm)	Flowrate at effluent ($mLmin^{-1}$)
Rice husk	2	3	0.3
Peanut husk	1.5	3	0.3
Saw dust	1.5	3	0.3

To remove dissolved materials and dissolved coloring substances from the adsorbents, same amount of distilled water was allowed to pass the column until clear solution was obtained. Then, all the water in the column was drained out. After that, 50 mL of dye wastewater was poured into the columns. The effluent from the column was collected at suitable time interval in different test tubes. Five fractions were collected. The absorbance of each fraction was measured by UV-visible spectrophotometer and the percent color removal for each fraction was calculated by the following equation.

$$\text{Percent color removal} = \frac{\text{inital absorbance} - \text{final absorbance}}{\text{initial absorbance}} \text{ x } 100$$

2.4 Effect of particle sizes

After choosing the best adsorbent for collected textile effluent from the dyeing house, the effect of particle size on the color removal efficiency was studied by using the adsorbent of different particle sizes such as 125 μm, 250μm and 400 μm.

2.5 Effect of adsorbent dose

After optimizing the particle size, the effect of adsorbent dose on the color removal efficiency was also studied by varying the amount of adsorbent with pre-optimized particle size. The amount of adsorbent used for this study were 2 g, 2.5 g, 3 g, 3.5 g, 4 g, 4.5 g and 5 g, respectively.

2.6 Effect of volume of wastewater

To study the influence of the volume of textile wastewater on the adsorption process, the different volumes of textile wastewater in the range of 20 ml to 200 ml were used. The column was packed with 5g of sawdust powder having the particle size of 125 μm. After removing the dissolved coloring matter by passing distilled water, 200 ml of textile wastewater was allowed to pass into the column. The flow rate was maintained at 0.3 ml min^{-1} and the eluent was collected with different test tubes at 5min time interval. The volume of each fraction was 15.0ml and totally fractions were collected.

3. Results and Discussion

To choose the adsorbent with highest color removal efficiency for each wastewater sample, screening tests were carried out. The highest color removal efficiencies of the different adsorbents were found to be 78% by rice husk, 83% by peanut husk and 90% by sawdust. From these results, it was observed that the most effective adsorbent for collected wastewater sample was sawdust and hence sawdust powder was chosen for the color removal process of the collected textile wastewater sample.

3.1 Effect of particle size

After choosing the most effective adsorbent, the effects of three different particle sizes such as 125 μm, 250 μm and 400 μm were investigated by column method. The percent color removal of each fraction collect from the column with 125 μm particle size adsorbent was shown in Table 2.

Table 2. Percent color removal by 125 μm size sawdust adsorbent.

Fraction No.	Volume of eluent (ml)	Percent color removal (%)	Average percent color removal (%)
1	10	92.93	90.09
2	10	92.87	
3	10	91.89	
4	10	90.92	
5	10	81.85	

The percent color removal was varied from 92.93% to 81.85% with the sawdust powder of 125 μm particle size and the average percent color removal was found to be 90.09%. Similarly, the sawdust adsorbent of particle sizes 250 μm and 400 μm gave the average percent color removal from collected textile wastewater at 81.85% and 64.87% respectively. The plot of percent color removal from textile wastewater against particle size is shown in Figure 2.

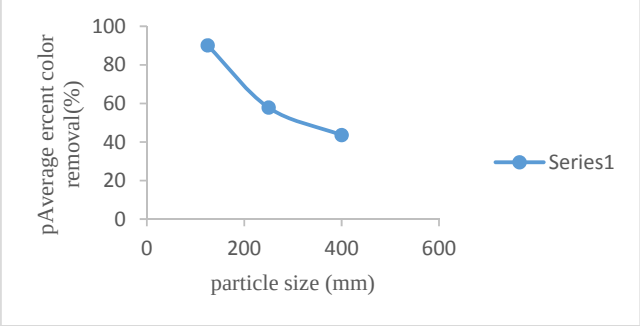

Figure 2. Optimization of particle size for color removal process

The figure reveals that the color removal efficiency of sawdust adsorbent for the collected dyeing wastewater sample decreased with increase in particle size. This phenomenon was probably due to the fact that the smaller the particle size, the greater the surface area of the adsorbent and the number of adsorption sites on the surface of the adsorbent to adsorb the dye molecules. According to the results, the particle size 125 μm of the adsorbent showed the highest color removal efficiency and was chosen for further investigations.

3.2 Effect of Adsorbent dose

After selecting the optimized particle size, the effect of adsorbent dose was studied by using various amount of sawdust powder (125 μm particle size) and flow rate of 0.3 ml min^{-1}. It was observed that the percent color removal varied from 47.75 % to 91.94 % by 5g of sawdust powder. The percent color removal of each fraction collected from the column experiment with 5g adsorbent (125μm particle size) and the average percent color removal were depicted in Table3.

Table 3. Percent color removal by different amount of sawdust powder (125 μm particle size)

Adsorbent dose (g)	Average percent color removal (%)
2	47.75
2.5	56.32
3	67.84
3.5	81.76
4	88.94
4.5	91.44
5	91.94

Figure 3 was represented the plot of adsorbent dose against the average percent color removal. From the figure, it was also observed that the color removal efficiency of sawdust powder increased with increase the amount of adsorbent. This result is probably due to the increased number of adsorption sites when the amount of adsorbent was raised. From the experimental results, 5 g of sawdust powder exhibit the highest color removal efficiency (91.94 %). Therefore, adsorbent dose (5 g) and particle size (125 μm) of sawdust powder were selected for further study.

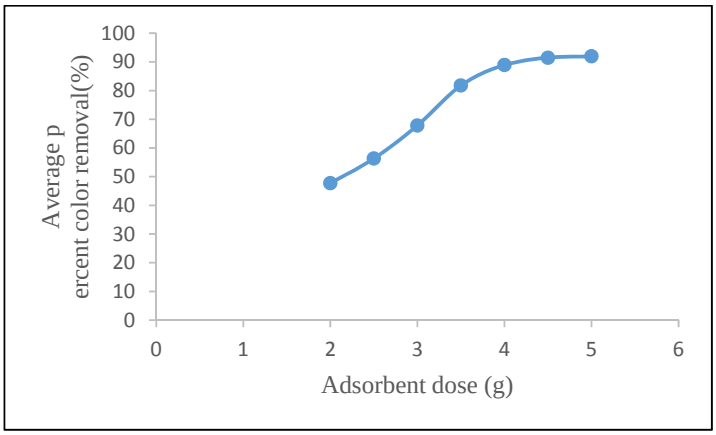

Figure 2. Optimization of adsorbent dose for color removal process

3.3 Effect of textile wastewater volume

The effect of the volume of the dyeing wastewater was shown in Figure 4. The figures pointed out that the color removal efficiency became decreased with increase in volume of textile wastewater. Therefore it can be observed that 5 g of sawdust powder (125 µm particle size) can reduce the color from the maximum volume of 160 mL textile wastewater.

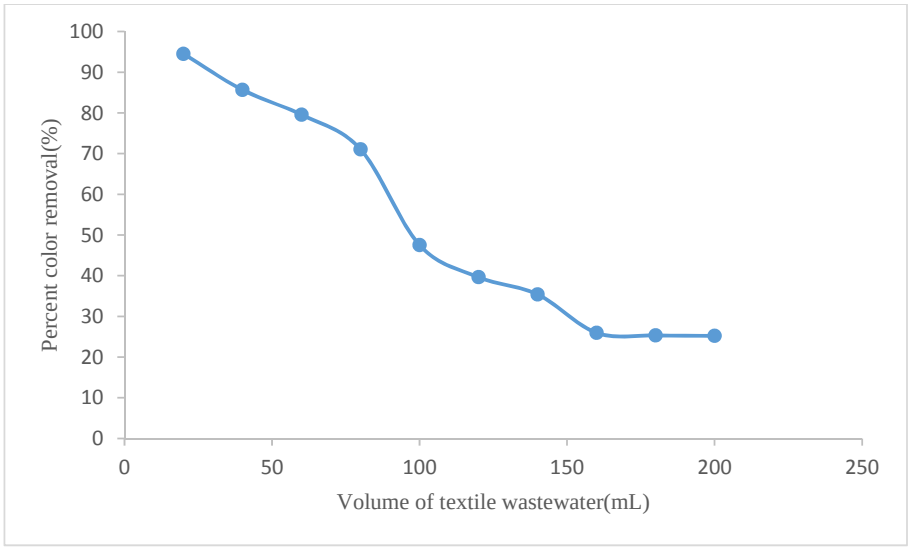

Figure 4. Effect of textile effluent volume on color removal process

3.4 Physico-chemical characterization of textile effluent

The effluent selected for the present study is dark blue color. The effluent was highly colored indicating high content of different dyes and color producing compounds. The high color may be the combined result of pH, temperature and acidic conditions that do not allow the chromophore group of dye to disintegrate during dyeing process and making the effluent highly colored.

In the present study, the pH value of dye wastewater was found to be 11.4 before adsorption and 7.8 after adsorption and was found to be within the standard discharge limit (6-9)[18]. EC values of wastewater sample reflect the content of dissolved ions in the wastewater.

TDS value of dye wastewater was determined to be 2500 mgL^{-1}. This high TDS value may be due to the fixing, bleaching and dyeing agent used in different stages of dyeing processes. The high TDS values of water are not recommended not only for drinking but also for irrigation purposes. After adsorption by sawdust powder, the TDS value of the effluent was found to be 1140 mgL^{-1}.

Before adsorption, COD of the effluent was found to be 1645.5 mgL^{-1} which is very high compared to discharge standard and reuse standard. High COD value indicate the presence of several waste such as detergents, softeners non-biodegradable chemicals such as dye fixing agents. After adsorption, COD value of the effluent was determined to be 362 mgL^{-1}. This value is still higher than the water quality standard for industrial uses and standard discharge values [19]. The results reveals that the values of pH, EC, TDS and COD decrease after adsorption of textile effluent using sawdust powder as adsorbent. This indicate that removal of color from textile effluent is effective and ecofriendly.

4. Conclusions

In this study, an attempt has been made for the removal of color from the textile wastewater by adsorption using the agricultural wastes as adsorbents. Of the three adsorbent, rice husk, peanut husk and sawdust, sawdust powder showed the highest color removal efficiency. The effects of various parameters on adsorption process such as particle size of adsorbent, adsorbent dose, and volume of textile effluent were studied. The optimum particle size was found to be 125 μm and the optimum adsorbent dose for column adsorption was 5 g. Another important finding was the decrease in color removal efficiency with increase in wastewater volume. The adsorption by column method using optimized particle size (125 μm) and adsorbent dose (5 g) exhibit the maximum color removal efficiency up to 91.94 % . Based on findings, the agricultural wastes such as sawdust was found to be useful as a low-cost, natural, abundant and effective adsorbent for the removal of color from dye wastewater.

Acknowledgements

The authors would like to thank to Dr Hlaing Hlaing Myat, Professor and Head of the department of Chemistry, Yadanabon University for the permission to carry out this research and supporting the required facilities throughout the research work. We also thanks to Professor Dr Htay Htay Win for her thoughtful suggestions which is necessary to complete this work. We also wish to thank to our colleagues for their kind and understanding helps.

References

[1] Venkatamohan S, Mamatha VVS, Karthikeyan J. Removal of color from acid and direct dyes by adsorption onto silica fumes. Fresenius Envion Bull, 1998; 7(1):51.8.

[2] Patel, H and RT Vashi, 2010 (a), Treatment of textile wastewater by adsorption and coagulation, E.J. Chemistry, 7 (4): 1468-1476.

[3] Poots V.I.P, Mckay G and Healy J, J.Water Pollut Con.F., 1978,5065), 926

[4] Robinson T, Chandran B and Nigam P, Water Res.,2002,36,2824-2830.

[5] Nigam P, Armour G, Banat IM, Singh D and Marchant R, Bioresource Technology, 2002,72,219-226.

[6] Pala A, Indian J Environ Health, 2001, 43(3), 128-134.

[7] Prieto), Fermoso J, Nae-ez Yand Del.Valle JL, Solar Energy, 2005, 79(4), 376-386.

[8] Y.Zaker, M.A Hossain, T.S.A Islam, Effect of various factors on the adsorption of methylene blue on sitt fractionated from Bijoypur soil, Bangladesh, Int. Res.J. Environment sci. 2(6), (2013) 243-250.

[9] S.De Gisi etal., Characteristics and adsorption capacities of low-cost adsorbents for wastewater treatment: a review, sustain, materials. Technol.9, 2016, 10-40.

[10] R.SiMane and V.N Bhusari, Removal of colour (dyes) from textile effluent byadsorption using orange and banana peel, International Journal of Engineering Research and Applications, Vol-2, Issues, 2012,PP-1997-2004.

[11] M.A Hossain, M.M.Ali and T.S.A Islam, Comparative adsorption of methylene blue on different low cost adsorbents by continuous column process, Int. letters of Chemistry, Physics and Astronomy, 77,2018,26-34.

[12] A.M. Etroki and F.M.N. Massoudi, The use of peanut hull for the adsorption of colour from aqueous dye solutions and dye textile effluent, Oriental Journal of Chemistry, 2011, Vol.27, 875-884.

[13] Mohammad Shafiqul Alam, Rexona Khanom, Mohmmad Arifur Raham, Removal of Congo Red Dye from Industrial Wastewater by untreated sawdust, American Journal of Environmental protection, Vol.4,No.5,2015,pp207-213. Doi:10.11648/J.ajep 20150405.12.

[14] Mane . V.S. and P.V.V Babu, Studies on the adsorption of brilliant green dye from aqueous solution onto low-cost NaOH treated sawdust. Desalination 2011,273:321-329.

[15] H.N.Bhatti, S.Sadaf and A.Aleem, Treatment of textile effluent by low-cost agricultural wastes: Batch adsorption study,The Journal of Animal and Plant Science, 2015,pp 284-289.

[16] China-Discharge Standards of water pollutants for dyeing and finishing of textile industry (GB.4278-2012), 2015.

[17] A.E.Greenberg, L.S.Clesceri and A.D. Eaton, Standard methods for the analysis of water and wastewater, 17th ed., American public Health Association(APHA), Washington DC,1992.

[18] L.V.Wilcos, Classification and use of irrigation waters, 1955, USDA Circular No.969.